ASAM 8

2023
NOVOSIBIRSK

The 8th Asian Symposium on Advanced Materials

# Book of Abstracts

2023

**Boreskov Institute of Catalysis**
**Siberian Branch of the Russian Academy of Sciences**

# ASAM-8

## The 8th Asian Symposium on Advanced Materials

July 3 – 7, 2023

Novosibirsk, Russia

# BOOK OF ABSTRACTS

Novosibirsk − 2023

УДК 620.22+544.47+ 615+504.75
ББК 30.3+24.54+52.8+20.18
А82

А82 **ASAM-8**
**The 8th Asian Symposium on Advanced Materials**
Book of Abstracts (July 3 – 7, 2023, Novosibirsk, Russia)
[Electronic resource] / eds.: Prof. A.A. Vedyagin, Prof. A.M. Volodin, Prof. Yu.V. Shubin, Dr. M.O. Kazakov, Dr. M.S. Melgunov, Dr. D.A. Shlyapin
– Novosibirsk : Boreskov institute of Catalysis SB RAS, 2023.
– ISBN 978-5-906376-49-7
– URL: http://conf.ict.nsc.ru/asam8/en

В надзаг.:
Boreskov Institute of Catalysis
Siberian Branch of the Russian Academy of Sciences

Сборник включает тезисы пленарных, ключевых и приглашенных лекций, устных и стендовых докладов.
Основные темы научной программы симпозиума:
I. Синтез и структура современных материалов
II. Биоматериалы и бионанокомпозиты
III. Применение

The collection includes abstracts of plenary, keynote and invited lectures, oral and poster presentations.
The main topics of the Symposium scientific program are:

I. Synthesis and Structure of Advanced Materials
II. Biomaterials and Bionanocomposites
III. Applications

УДК 620.22+544.47+ 615+504.75
ББК 30.3+24.54+52.8+20.18

ISBN 978-5-906376-49-7 

## ORGANIZER

Boreskov Institute of Catalysis,
Novosibirsk, Russia

## SUPPORTED BY

Siberian Branch of the Russian Academy of Sciences,
Novosibirsk, Russia

## SYMPOSIUM PARTNERS

LABTEST RCC

МТЕОН – ООО НТЦ «ЭМТИОН»

## INTERNATIONAL ADVISORY COMMITTEE

### Symposium Chair

**Prof. Valerii Bukhtiyarov**, Boreskov Institute of Catalysis, Novosibirsk, Russia

**Prof. Li-Jen Chen**, National Taiwan University, Taipei, Taiwan

**Prof. Ildoo Chung**, Pusan National University, Busan, Republic of Korea

**Prof. Jian Ping Gong**, Hokkaido University, Sapporo, Japan

**Prof. Chang-Sik Ha**, Pusan National University, Busan, Republic of Korea

**Prof.Toyoko Imae**, National Taiwan University of Science & Technology, Taipei, Taiwan

**Prof. Alexei Khokhlov**, Lomonosov Moscow State University, Moscow, Russia

**Prof. Yury Kulchin**, Institute of Automation and Control Processes, Vladivostok, Russia

**Prof. Sang-Young Lee**, Yonsei University, Seoul, Republic of Korea

**Prof. Nguyen Quang Liem**, Vietnam Academy of Science and Technology, Hanoi, Vietnam

**Prof. Valentin Parmon**, Siberian Branch of the Russian Academy of Sciences, Novosibirsk, Russia

**Prof. Yury Shchipunov**, Institute of Chemistry, Far East Branch, Russian Academy of Sciences, Vladivostok, Russia

**Prof. Atsushi Takahara**, Kyushu University, Fukuoka, Japan

**Prof. Supason Wanichwecharungruang**, Chulalongkorn University, Bangkok, Thailand

**Prof. Limin Wu**, Fudan University, Shanghai, China

**Prof. Dongyuan Zhao**, Fudan University, Shanghai, China

# ORGANIZING COMMITTEE

**Chair**

**Prof. Aleksey Vedyagin**, Boreskov Institute of Catalysis, Novosibirsk, Russia

**Vice chair**

**Dr. Maksim Kazakov**, Boreskov Institute of Catalysis, Novosibirsk, Russia

**Prof. Yury Shubin**, Nikolaev Institute of Inorganic Chemistry SB RAS, Novosibirsk, Russia

**Prof. Alexander Volodin**, Boreskov Institute of Catalysis, Novosibirsk, Russia

**Dr. Maksim Melgunov**, Boreskov Institute of Catalysis, Novosibirsk, Russia

**Dr. Dmitry Shlyapin**, Center of New Chemical Technologies BIC, Omsk, Russia

**Sofia Afonnikova**, Boreskov Institute of Catalysis, Novosibirsk, Russia

**Arina Potylitsyna**, Boreskov Institute of Catalysis, Novosibirsk, Russia

**Grigory Veselov**, Boreskov Institute of Catalysis, Novosibirsk, Russia

**Daria Almaeva**, Boreskov Institute of Catalysis, Novosibirsk, Russia

**Eva Kazakova**, Boreskov Institute of Catalysis, Novosibirsk, Russia

**Artem Krivonogov**, Boreskov Institute of Catalysis, Novosibirsk, Russia

**Marina Suvorova**, Boreskov Institute of Catalysis, Novosibirsk, Russia

**SECRETARY**

**Svetlana Logunova**, Boreskov Institute of Catalysis, Novosibirsk, Russia

# Plenary Lectures

**PL-1 ÷ PL-4**

## PL-1

# Polyimides and/or Their Hybrid Films for Tailor-Made Applications

Chang-Sik Ha
*School of Chemical Engineering, Pusan National University, Busan 46241, Korea*
*csha@pnu.edu*

Polyimides (PIs) are quite well-known high performance polymers with outstanding properties including high thermal stability and good mechanical properties, which make them suitable for applications in many high-tech fields, such as automotive, electronics, and aerospace industry. However, aromatic PI films exhibit a poor optical transmittance with yellow or dark brown color that is originated from the formation of charge transfer{CT} complexes between the electron donor diamine and the electron acceptor dianhydride in the main backbone. The poor optical transparency is one of the great disadvantages for microelectronics and optoelectronic application. Thus, the development of colorless and transparent PIs has been one of hot topics in the microelectronic and electrooptic devices industries. Recently, the development of PIs with low dielectric constant and low moisture uptake has also been another important issue in PI industries according to the fast growth of wireless mobile communication industries. Take such important issues in PI industries into consideration, our research was devoted to the tailor-made applications of PIs and/or their hybrid films in organic light-emitting devices (OLEDs), flexible substrates, and flexible sensing skin, etc.[1-4]

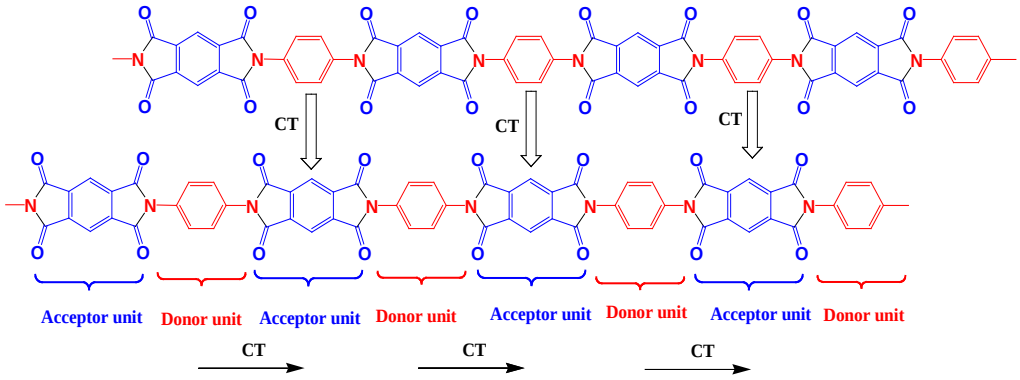


***Fig. 1.*** *Chain sequence of wholly aromatic PI (pyromellitic diahydride(PMDA)/p-phenylene diamine(PDA) PI) and intra- and intermolecular CT interactions [3].*

**Acknowledgement:** The work was supported by the National Research Foundation of Korea (NRF) Grant funded by the Ministry of Science and ICT, Korea (2021R1I1A3060098).

**References:**

[1] D.J. Liaw, K.L. Wang, Y.C. Huang, K.R. Lee, J.Y Lai, C.S. Ha, Prog. Polym. Sci. 37 (7) (2012) 907.
[2] P.K. Tapaswi, M.C. Choi, K.M. Jeong, S. Ando C.S. Ha, Macromolecules 48(11) (2015) 3462.
[3] P.K. Tapaswi, C.S. Ha, Macromol. Chem. Phys. 220 (2019) 1800313 (1-33).
[4] T. Cai, Y.Z. Yan, Y. Park, T. Lee, D. Peng, Y. Liu, C.S. Ha, K.C. Kim, ACS Appl. Polym. Mater. 3 (2021) 2461.
[5] J.S. Lee, Y.Z. Yan, S.S. Park, S. Ahn, C.S.Ha, Polymers 14 (2022) 4504.

## PL-2

# Nanoporous Materials for Energy and Environment

Vinu A.
*School of Chemical Engineering, Pusan National University, Busan 46241, Korea*
*Global Innovative Center for Advanced Nanomaterials (GICAN), The University of Newcastle, Newcastle Callaghan, Australia*

## PL-3

# Novel Electrode Materials for Metal-Ion Batteries

Antipov E.V.
*Lomonosov Moscow State University, Moscow, 119991, Russia*
*Skolkovo Institute of Science and Technology (Skoltech), Moscow 121205, Russia*
*evgeny.antipov@gmail.com*

Ninety percent of the energy produced today come from fossil fuels. Rapid consumption of these energy sources makes dramatically negative impact on our future due to ecological damage and climate change. In this sense the development of the environmentally benign renewable energy sources capable to replace fossil fuels and concurrently efficient large energy storage devices requires no justification. Li-ion batteries (LIBs) have been originally developed for portable electronic devices, but nowadays new application niches are envisaged in electric vehicles and stationary grid-scale energy storages. However, LIBs may be not fully adopted for these applications. The geographical scarcity and excessive demand for Li resources intensifies the development of alternative sustainable technologies based on vastly accessible materials, namely Na- and K- ion batteries.

The Na/K-based oxides and polyanion materials of transition metals are scrutinized as cathodes for these batteries aiming to enhance the specific energy, durability and rate capability. Whereas the layered oxides display greater volumetric energy density, the polyanion materials usually exhibit better cycling and thermal stability and higher C-rate capabilities due to covalently bonded structural frameworks. The polyanion compounds reveal an extra dimension in their crystal chemistry, which significantly extends the playground for designing materials with superior electrochemical performance. Further advantages are expected from the synergistic effect of combining different anions (such as $(XO_4)^{p-}$ and $F^-$) in the anion sublattice.

An overview of the research on novel phosphates and fluoride-phosphates as prospective electrode materials for the Na/K-ion batteries will be presented with a special emphasis on the interrelation between composition, synthesis conditions, crystal structure and electrochemical properties of the materials intended for practical applications.

**Acknowledgement:** This work was supported by the Russian Science Foundation, grant No. 17-73-30006.

## PL-4

# Interfacial Oriented Assembly of Hierarchical-Pore Functional Mesoporous Materials from Monomicelles

Dongyuan Zhao
*Department of Chemistry, Laboratory of Advanced Materials, Faculty of Chemistry and Materials, Fudan University, Shanghai 200433, China*
*dyzhao@fudan.edu.cn*

Functional mesoporous materials are a class of porous solids with pore size of 2-50 nm. They not only possess unique properties such as a high specific surface area, a large pore size and volume, and pore uniformity control, but also have excellent optical, electrical and magnetic properties of inorganic functional nanoparticles. Therefore, multilevel functional mesoporous materials have broad application prospects in many fields such as catalysis, adsorption, separation and biomedicine. In this paper, we mainly review the recent advances in the synthesis of multilevel functional mesoporous materials by oriented assembly controlled by interfacial assembly of surfactant monomicelles. Based on the core idea of interface assembly regulation, we developed a series of new methods for the synthesis of multilevel structural and functional mesoporous materials, including confined micro-emulsion confinement self-assembly, liquid-liquid bi-phase synthesis, evaporation-driven oriented/aggregation assembly, anisotropic growth method, interface driven orientation arrangement, interfacial dynamic migration strategy *etc.* By using these new synthesis approaches, a family of novel mesoporous nanomaterials with one-level and multi-level architectures can be nationally designed and well synthesized, such as core-shell, yolk-shell, multi-shell, 2D film structures for silica, $TiO_2$, carbon spheres, 3D mesoporous bouquet-posy-like $TiO_2$ multi-level superstructures and asymmetric Janus, single-hole hollow structure, nano-thermometer, multipods nanostructure, hemispheres, streamlined nanotadpoles *etc.*. These novel mesoporous materials not only have unique and uniform morphology, but also have controllable mesoscopic pore structure, high specific surface area, large pore volume and open pore. It is because of their unique structure and function that these materials show a very good application prospect in biomedicine and other fields.

**References:**

[1] *Nat. Rev. Mater.*, **2016**, 1, 16023; *Acc. Chem. Res.*, **2019**, 52, 2928; *Nat. Rev. Mater.*, **2019**, 4, 775. *Chem. Rev.* **2021,** *121,* 14349−14429.
[2] *Angew. Chem. Int. Ed.,* **2020**, *59, 17676; J. Am. Chem. Soc.,* **2020**, *142, 20359; Nat. Mater.* **2020,** *19, 203-211; Nat. Commun.,* **2021**, *12, 2973; Nano Lett.,* **2021**, *21, 6071; Adv. Mater.,* **2021**, *33, 2100820; J. Am. Chem. Soc.,* **2021**, *143, 14097–14105; Chem.* **2021**, *7, 1020-1032; Sci. Adv.* **2021**, *7, eabi7403b. Sci. Adv.* **2022**, *8, eabo0283; Angew Chem Int. Ed.,* **2022,** *61, e202211307; J. Am. Chem. Soc.* **2022**, *144, 3892-3901; Science Adv.* **2022**, *8, eabq2356; J. Am. Chem. Soc.* **2022**, *144, 11767; Nature Commun.* **2022**, *3, 6136; J. Am. Chem. Soc.* **2022**, *144, 15754-15763.*

# Keynote Lectures

**KL-1 ÷ KL-7**

## KL-1

# Polysaccharides and Polyphenols as Structure-Directing and Functionalizing Constituents of Bionanocomposites

Postnova I.V.[1,2], Shchipunov Y.A.[1]
*1 – Institute of Chemistry, Far-East Department, Vladivostok, 690022, Russia*
*2 – Far-Eastern Federal University, 690922 Vladivostok, Russia*
*YAS@ich.dvo.ru*

Bionanocomposites are materials consisting of biopolymers and inorganic nanoparticles. The sol-gel method is one of the main approaches to fabricate them. However, when using the traditional precursor, tetraethoxysilane or TEOS, one needs to add an acid/alkali and organic solvent, as well as heat for catalysis and acceleration of the processes. This results in protein denaturation, precipitation of polysaccharides or oxidation of polyphenols.

Precursor compatibility with biopolymer is improved if alcohol residues in TEOS are exchanged for ethylene glycol. The latter, which is issued after the hydrolysis, does not denature or precipitate biopolymers. Furthermore, both proteins and polysaccharides, in turn, accelerate the hydrolysis reaction, including neutral solutions. This makes it possible to perform the sol-gel synthesis at a high rate over the entire pH range.

Biopolymers in sol-gel synthesis act as a template, determining the structure of the formed silica and functionalizing it. The features of the processes, structure, properties and functional characteristics of the resulting bionanocomposites are considered.

It is shown that polysaccharides, acting as a template, regulate the porosity of materials. They also bring different functional groups and confer biological activity. The silica formed causes cross-linking of macromolecules, which leads to gelation in the case of polysaccharides that do not have the ability to form hydrogels. Silica coating is also used to control the hydrophilicity/hydrophobicity and enhance the mechanical strength of the polysaccharide structures.

Proteins whose conformation depends on the pH of the solution make it possible to control the structure of bionanocomposites over a wide range by simple acidification/alkalization. The immobilization of enzymes under optimal conditions for them, are not dictated by the sol-gel process, led to the development of biocatalysts that could not be obtained by other methods or using the TEOS.

Recently, polyphenols like tannic acid have been applied as a template regulating porosity and functional component of bionanocomposites. It provided the means of preparing optically transparent monolithic silica with uniformly sized 2–4 nm pores. Gold and silver nanoparticles were synthesized by using polyphenols as reducing agents. These bionanocomposites possessed localized surface plasmon resonance and high catalytic activity.

**Acknowledgement:** This work was partially supported by the Russian Science Foundation (grant No. 22-13-00337).

## KL-2

# Charge Modulation for Photocatalytic $CO_2$ Conversion

Liqiang Jing
*Key Lab of Functional Inorganic Materials Chemistry (MOE), School of Chemistry and Materials Science, Heilongjiang University, Harbin City 150080, China*
*Jinglq@hlju.edu.cn.*

Photocatalysis as a new advanced technique is one of most potential methods for energy production and environmental remediation in the future. It is highly desired to greatly enhance the photogenerated charge separation for efficient $CO_2$ conversion by photocatalysis. In recent years, two strategies have been successfully developed to modulate the charge separation based on the main scientific questions as follows. Firstly, the introduced proper-level-energy platform by controllably modifying metal phthalocyanine and constructing single-metal atom could accept the excited electrons from the narrow-bandgap g-$C_3N_4$, so as to prolong the carrier lifetime and thereby improve the visible-light-driven catalytic activities for $CO_2$ conversion. Secondly, novel narrow-bandgap oxide-based Z-scheme heterojunctional nanocomposites as wide-visible-light-driven photocatalysts have been designed and fabricated by using metal-organic coordination aggregates like phthalocyanine and metal organic frame for efficient $CO_2$ conversion, especially with the rationally introduced co-catalysts for promoting charge-induced reactions. Meanwhile, the mechanism insights have been explored in details by developing effective time-resolved (in-situ) photophysical techniques to investigate charge dynamics. These works will provide feasible routes to improve the photocatalysis for $CO_2$ conversion and energy production.

**Acknowledgements:** This work was supported by the National Natural Science Foundation of China (grant U1805255 and U2102211).

**References:**

[1] J. Bian, F. Q. Bai*, J. W. Tang*, L. Q. Jing*, et al. Angew. Chem. Int. Ed. 2019, 58, 10873.
[2] X. Y. Chu, Y. Qu, L. L. Bai*, Z. D. Yang*, L. Q. Jing*, et al. Adv. Sci. 2020, 2001543(10).
[3] Y. Y. Wang, Y. Qu, L. L. Bai*, L. Q. Jing*, H. G. Fu*, et al. Adv. Mater. 2021, 2105482 (10).
[4] J. Bian, F. Q. Bai*, J. W. Tang*, L. Q. Jing*, et al. Angew. Chem. Int. Ed. 2021, 60, 2.
[5] J. N. Feng, J. Bian*, L. L. Bai*, L. Q. Jing*, et al. Appl. Catal. B, 2021, 295, 120260.
[6] L. N. Zhao, L. L. Bai*, Y. X. Li*, L. Q. Jing*, et al. Adv. Mater. 2022, 34, 2205303(10).
[7] D. H. Hu, L. J. Song, Y. Qu*, L. Q. Jing*, et al. Chem. Eng. J. 2022, 440, 135786 (10).
[8] Y. Liu, J. H. Sun, L. L. Bai*, J. W. Tang*, L. Q. Jing*, et al. Nat. Commun. 2023, 14, 1457.
[9] B. H. Qu, Y. Qu*, B. Zheng*, L. Q. Jing*, et al. Adv. Mater. 2023, 2211575.
[10] L. Sun, J. Bian*, J. W. Tang*, L. Q. Jing*, et al. Adv. Mater. 2023, 202300064.

## KL-3

# Catalytic Growth of Carbon Nanomaterials as a Tool for Designing Novel Nanostructured Catalysts

Mishakov I.V.
*Boreskov Institute of Catalysis, Novosibirsk, Russia*
*mishakov@catalysis.ru*

The metallic alloyed Ni- and Co-based catalysts (often containing such precious metals as Pt and Pd) supported on nanostructured carbon substrates are demanded in different areas of heterogeneous catalysis. Among the diverse types of carbon nanomaterials, the carbon nanofibers (CNFs) are currently of particular interest because of the unique combination of their physical and chemical properties [1]. In the case of Ni-M and Co-M alloys, the same active component can be used for the synthesis of CNF material via catalytic chemical vapor deposition technique (CCVD). After the carbon filaments are grown, the catalytic Ni(Co)-M alloyed particles turn to be embedded into the structure of resulted CNFs (Fig. 1), thus providing catalyst with almost absolute resistance to sintering.

One of the most promising “one-stage” approaches to synthesize Ni(Co)-M/CNF catalysts is based on utilizing the metal dusting (or carbon erosion, CE) phenomenon. Carbon erosion is known as spontaneous degradation (disintegration) of bulk metals (Fe, Co, Ni) and their alloys in carburizing atmosphere at 400-800°C [2]. On the other hand, CE results in the emergence of supported catalytic system, which is represented by a number of dispersed active particles formed as a result of exposure to the reaction medium [3-5]. The phenomenon of controlled carbon erosion provides researchers with extensive opportunities in the field of targeted synthesis of carbon nanomaterials [6], supported catalysts [3, 5] and hybrid composite materials [7, 8]. By adjusting the composition and properties of the precursor alloy, it is possible to direct the process of its disintegration driven by CE along the way of creating carbon nanomaterials with the desired morphological and structural characteristics.

The TEM images of active metallic particles resulted from the disintegration of the bulk Ni-Pd alloy can be seen in Fig. 1.

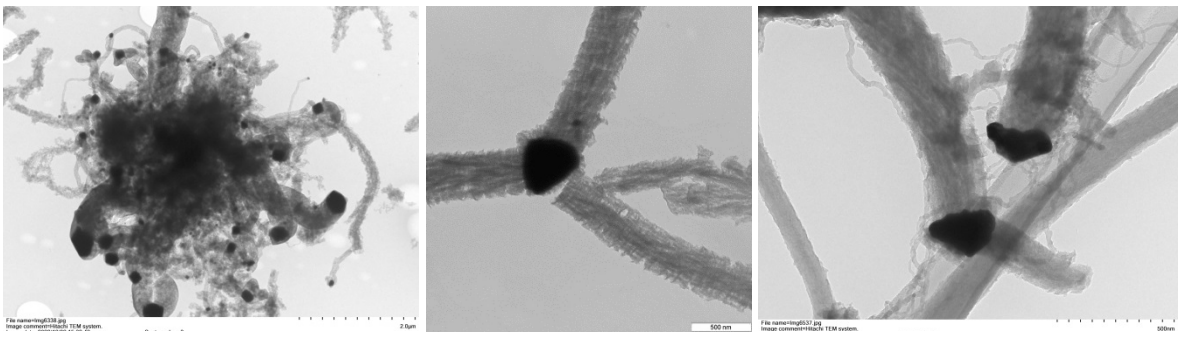

*Fig.1. TEM images of the active particles (Ni-Pd) embedded into the structure of carbon nanofibers. Samples were fabricated via carbon erosion of bulk Ni-Pd alloys (10-25% Pd) at 600°C using different carbon precursors: (a) – $C_2HCl_3/H_2$; (b) – $C_2H_4Cl_2/H_2$; (c) – $C_2H_4/H_2$.*

## KL-3

The choice of a carbon source to grow CNF is almost unlimited (various hydrocarbons including the chlorinated ones, etc.), which provides researchers with wide opportunities to tune the structural features of the resulted carbon nanomaterials.

In this report, the systematization of works carried out in the field of carbon erosion used as a targeted way to synthesize carbon nanomaterials and related composites will be given. The recent results of the team concerning to developing methods for the synthesis of nano-porous and microdispersed alloys based on nickel (Ni-M) and cobalt (Co-M), to be then used as precursors to catalysts for the CNF synthesis, will be presented. Three different preparative approaches to synthesize starting alloys will be compared: i) *thermolysis of multicomponent precursors* (TMCP); ii) *mechanochemical alloying of metals* (MCA); iii) *electric explosion of wires* (EEW). The results of the study on effect of the nature and concentration of the second metal (M = Cu, Pd, Pt, W etc.) in composition of Ni-M and Co-M alloys on the rate of CE, the catalytic activity of the forming particles and the structural features of the resulting carbon nanomaterial will be also discussed. In addition, the prospective of using 4-6-component (high-entropy) alloys as precursors for the preparation CNF-based supported catalysts will be demonstrated.

The report will also demonstrate the most promising areas of practical application of synthesized carbon nanomaterials as well as supported Ni(Co)-M/CNF catalysts. Prospects for the use of CNF as adsorbents for the purification of water from chloroaromatic compounds, catalyst carriers for electrochemical processes, and modifying additives in various composite materials will be highlighted.

**Acknowledgement:** This work was financially supported by the Russian Science Foundation [project No. 22-13-00406].

**References:**

[1] Sun L.L., Li B., Zhao Y. et al., Nanotechnology 21 (2010) 305702.
[2] Grabke H. J. Mater Corros 54 (2003) 736.
[3] Afonnikova S. D., Popov A. A., et al., Materials 15 (2022) 7456.
[4] Ozerova A. M., Potylitsyna A.R., Y.I. Bauman et al. Materials. 15 (2022) 8414.
[5] Popov A. A., Afonnikova S. D., et al. Catalysts 13 (2023) 599:1-18.
[6] Chang C. H., Tsai H. Y., Tsai W. T. J. Phys. Chem. C 112 (2008) 20143.
[7] Pacheco Benito S., Lefferts L. Carbon 48 (2010) 2862.
[8] Hashempour M., Vicenzo A., F. Zhao, et al. Carbon 63 (2013) 330.

## KL-4

# Exploring Binder Chemistry for High-Energy Li Battery Cathodes

Sang-Young Lee
*Department of Chemical and Biomolecular Engineering, Yonsei University, Seoul, Korea*
*syleek@yonsei.ac.kr*

Achieving high-energy-density Li batteries is of paramount importance in facilitating the advent of smart energy era. Major research approaches implemented to achieve this goal have focused on the synthesis and modification of electrode active materials and electrolytes. Along with these materials-based works, much attention should be devoted to designing high-areal-capacity (leading to high-energy-density) electrodes as a facile and scalable architectural strategy. Notable benefits of high-C/A electrodes include the increase in the cell energy density without the synthesis of new electrode active materials and the simplification of cell configurations by reducing electrode layer numbers. To achieve high areal-capacity electrodes (= areal-mass-loading × specific capacity of electrode active materials), the areal-mass-loading should be maximized while stably maintaining the specific capacity of electrode active materials. However, due to the involvement of thick electrodes (physical issue) and the nonuniform charge transfer throughout the electrodes (electrochemical issue), conventional electrodes cannot achieve this requirement. A formidable challenge facing the high-areal-mass-loading electrodes is the inhomogeneous redox reaction in their through-thickness direction, which is mainly affected by the electrode binders. Therefore, exploring binder chemistry that is compatible with commercial slurry-cast electrode fabrication is urgently needed to develop practically scalable high-areal-capacity electrodes.

In this talk, I present a class of practical electrode design based on coupled ion/electron transport phenomena, with a focus on binder chemistry. This approach includes the heteronanomat skeletons, amphiphilic bottlebrush polymeric binders, and cationic polymeric binders. Particularly, the cationic polymer binders suppressed the solvent-drying-induced crack evolution of electrodes and improved the dispersion state of electrode components owing to its surface charge-driven electrostatic repulsion and mechanical toughness, thus enabling the fabrication of high-mass-loading electrodes (reaching 96 mg $cm^{-2}$) with uniform topologies. This new binder chemistry strategy decribed herein opens a new route toward scalable high-mass-loading electrodes with redox homogeneity in the through-thickness direction, which lie far beyond those achievable with previously reported electrode sheets based on conventional neutral binders .

## KL-4


***Fig**. Schematic of the amphiphilic bottlebrush polymeric (BBP) binders for scalable high-areal-capacity Li battery cathodes.*

**Acknowledgement:** This work was supported by the Basic Science Research Program (2021R1A2B5B03001615) through the Natioanl Research Foundation of Korea (NRF).

**References:**

[1] Sang-Young Lee *et.al.*, "Amphiphilic Bottlebrush Polymeric Binders for High-Mass-Loading Cathodes in Lithium-Ion Batteries", *Adv. Energy Mater*. **2021**, 2021021109.
[2] Sang-Young Lee *et.al.*, "Redox-homogeneous, gel electrolyte-embedded high-mass-loading cathodes for high-energy lithium metal batteries", *Nature Commun*. **2022**, 13, 2541.

## KL-5

# How Advanced Transmission Electron Microscopy Can Contribute to Battery Research?

Abakumov A.M.
*Skolkovo Institute of Science and Technology, Moscow, Russia*
*a.abakumov@skoltech.ru*

The design and improvement of the cathode materials for Li-ion batteries requires detailed knowledge on the crystal structure at different charge/discharge states and comprehensive understanding of the processes occurring at the nanoscale or even atomic scale level, as many electrode materials demonstrate highly inhomogeneous non-equilibrium behaviour. Advanced transmission electron microscopy (TEM) is by far the most suitable and direct tool to look at the materials down to atomic scale. Recent progress in the quantitative electron diffraction methods and aberration-corrected scanning TEM imaging will be illustrated here with the examples of atomic structure investigation of various cathode materials. Electron diffraction tomography provides quantitative diffraction data enabling reliable structure solution and refinement from extremely small crystallites, typically smaller than 1 $\mu m^3$. Aberration-corrected scanning transmission electron microscopy (STEM) delivers local information with sub-Å resolution (Fig. 1). Employing various STEM techniques for visualization of cation migration, metal clustering, anion-anion bonding, oxygen vacancies will be exemplified with layered oxide cathode materials. Observations are supported with local chemistry assessment with spatially-resolved energy-dispersive X-ray analysis and electron energy loss spectroscopy.

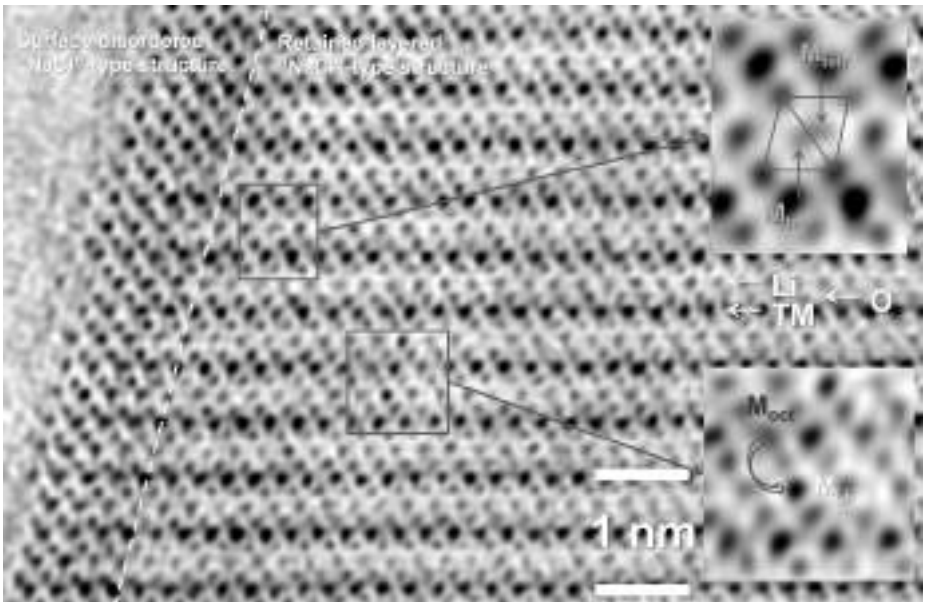


*Fig.1. [010] ABF-STEM image of Li-rich NMC after discharge. Dashed line marks the near-surface layer with pronounced Li/M antisite disorder.*

**Acknowledgement:** This work was supported by the Russian Science Foundation, grant 23-73-30003.

## KL-6

# Optically Active Carbon Dot-Based Hybrids for Practical Applications

Krivoshapkina E.F.
*EnergyLab, ITMO University, St. Petersburg, Russia*
*kef@scamt-itmo.ru*

Today, biopolymers have elicited significant attention in the scientific community due to their highly desirable properties, namely their abundance, renewability, biodegradability, biocompatibility, and low toxicity. Biopolymers are also highly modifiable due to the presence of hydroxyl, carboxyl, and carbonyl groups within their structure, which allow them to interact with various functional groups through variability of chemical modifications [1]. These surface functional groups can also act as point carbon sources for the synthesis of carbon dots (C-dots) directly on the biopolymer surface, resulting in the formation of optically active hybrids, in which the biopolymers also act as supports, with excellent sensory properties [2]. As such, these functional C-dot-based hybrids have found several useful applications across various industries.

Several studies have shown that various factors can influence C-dot optical properties, including doping with different heteroatoms, suspension in different solvents, size, presence of surface functional groups, and irradiation with different excitation wavelengths, resulting in different coloured and intensity fluorescence. A very good example is a temperature indicator incorporated into intelligent food packaging for monitoring ambient temperature in cold chain logistics [3]. This indicator used the solvatochromic properties of a C-dot/cellulose hybrid suspended in dimethyl sulfoxide (DMSO) and water along with the significant variations in temperature for DMSO/water mixtures with various compositions to indicate if temperature-sensitive food were exposed to undesired temperatures.

C-dots have also been shown to be particularly sensitive to the presence of heavy metal ions; therefore, they can be used in heavy metal ion detection. Other studies have shown that biopolymers form matrices that can be used in ion sequestration [4]; thus, C-dot/biopolymer hybrids can be used in the detection and removal of heavy metal ions from water. One such example is a reusable C-dot/chitin hybrid used in the detection and adsorption of cobalt and chromium ions [5]. The presence of chromium and cobalt ions were confirmed by quenching of C-dot fluorescence, and adsorption isotherms indicated that the hybrid had good adsorption capacity for chromium and cobalt ions, which were weakly adsorbed unto its surface and were readily removed, suggesting high cyclability. Preliminary results show that C-dot/cellulose hybrids can be used for the detection of rare earth metals.

Most usefully, due to the cytocompatibility and sensitive properties of C-dots as well as the cytobiocompatibility and high cellular uptake of biopolymers [2,6], C-dot/biopolymers have also shown immense potential for application in the biomedical industry, particularly in wound healing. Thus far, C-dot/spider silk hybrids have been used as dressings and sutures,

respectively, that indicate when they need to be changed, prevent bacterial infection, and promote rapid wound healing by acting as frameworks for tissue regeneration [7].

**Acknowledgement:** work was supported by state task № FSER-2022-0002 within the framework of the Russian Ministry of Science and Higher Education “Science and Universities” National Project.

**References:**

[1] G. Li, H. Liu, T. Li, J. Wang, Mater. Sci. Eng. C 32 (2012) 627.
[2] M. Chekini, E. Prince, L. Zhao, H. Mundoor, I. I. Smalyukh, E. Kumacheva, Adv. Opt. Mater. 8(4) (2020) 1901911.
[3] A. Navrotskaya, D. Aleksandrova, M. Chekini, I. Yakavets, S. Kheiri, E. Krivoshapkina, E. Kumacheva, ACS Nano. 16(6) (2022) 8641-8650.
[4] G. B. D’Souza, A. Kumar, S. V Kamath, A. S. Maraddi, S. K. Nataraj, Chem. Eng. J. 443 (2022) 136462.
[5] T.S. Ngo, C.T. Tracey, A.G. Navrotskaya, A.V. Bukhtiyarov, P.V. Krivoshapkin, E.F. Krivoshapkina, Carbohydrate Polymers. 304 (2023) 120471.
[6] M. Ghirardello, J. Ramos-Soriano, M. C. Galan, Nanomaterials. 11(8) (2021) 1877.
[7] E.S. Maltseva, V.O. Nikolaeva, A.M. Savin, M.Y. Dobryakov, E.I. Koshel, P.V. Krivoshapkin, E.F. Krivoshapkina, ACS Biomater. Sci. Eng. 8(8) (2022) 3310–3319.

## KL-7

# Novel Synthetic Techniques for Catalyst Design for Sensing and Energy Applications

Il-Doo Kim
*Department of Materials Science and Engineering, KAIST, Daejeon, Korea*
*idkim@kaist.ac.kr*

Electrocatalysts play a crucial role in the fields of sensors, energy, and the environment. Research on the synthesis and application of catalysts with various shapes, sizes, and compositions is currently underway. Our research team is actively engaged in the synthesis of single-atom catalysts, bimetallic, high-entropy alloy, and polyelemental alloy catalysts, as well as the development of sensors and Li-air batteries. Particularly, we have been conducting interesting research on catalyst design using the Joule heating process and photo-induced optical sintering process for novel catalysts design. The Joule heating process is a technique for producing multi-metal catalysts-decorated conducting carbon fibers. The photo-induced process utilizes a xenon flash lamp to rapidly produce multi-metal catalysts within a few tens of milliseconds. Another interesting catalyst design technique that has recently received significant attention is the exsolution catalyst synthesis method. This technique involves the exsolving of elements doped within the lattice of oxide support to the surface of a material via a reduction heat treatment process. The catalyst is strongly anchored to the oxide support, providing excellent durability. In this presentation, we will also introduce the exsolution process as a new catalyst synthesis method. In this presentation, we will discuss and introduce our new catalyst synthesis techniques and methods for designing high-efficiency chemical sensors through catalyst design.

# Invited Lectures

**IL-I 1 ÷IL-I-3**

**IL-II-1 ÷ IL-II-3**

**IL-III-1 ÷ IL-III-3**

## IL-I-1

# Physical Production of Clusters and their Catalytic Activity

Toyoko Imae
*Graduate Institute of Applied Science and Technology,*
*National Taiwan University of Science and Technology, Taipei 10607, Taiwan*
*imae@mail.ntust.edu.tw*

Metal clusters have received plenty of attention in nanotechnology due to exert the quantum confinement effect, divide the continuous density of state into the highest occupied molecular orbital and the lowest unoccupied molecular orbital energy levels, and lead to the size-dependent fluorescence property. Different from theoretical estimation of cluster characters, the synthesis of clusters is a relatively scarce field even now because of their instability in medium. Here we report the novel synthesis procedure of metal clusters using high-intensity femtosecond pulse laser irradiation technique, which is a simple and efficient bottom-up physical procedure without adding any reducing agent, because this water radiolysis method self-produces the reducer and the reaction can finalize within a few minutes to produce clusters in a metal precursor solution.

The method produced gold clusters with average sizes of 0.6 to 1.6 nm after femtosecond pulse laser irradiation for 1 to 3 min, where hydrated electron reacts as a reducer [1]. As the irradiation is continued longer, plasmonic nanoparticles with larger sizes were produced. Both clusters and plasmonic nanoparticles exhibited fluorescence, indicating a quantum property, though it is not usually expected from conventional plasmonic gold nanoparticles. When gold precursor ions were incorporated in zeolitic imidazolate framework-8 (ZIF-8) as a holder before synthesis of gold cluster, the gold cluster-encapsulated ZIF-8 was prepared. Then Au cluster in ZIF-8 has shown good catalytic property on the reduction of 4-nitrophenol within 4 min.

The water radiolysis by femtosecond pulse laser irradiation generates species of hydrated electron ($e^-_{aq}$), hydrogen radical ($H^\bullet$), hydroxyl radical ($OH^\bullet$), and hydrogen ion ($H_3O^+$), and these species play a role as reductant or oxidant on metal precursor ions. For instance, gold, silver, and platinum precursor ions were reduced by $e^-_{aq}$ to be metals, but zinc and copper precursor ions were oxidized by $OH^\bullet$ and produced metal oxides. Thus, the femtosecond pulse laser irradiation to Zn and Cu ions produced ZnO and CuO clusters, respectively [2,3]. Such clusters could work well for photocatalytic degradation of formaldehyde and $CO_2$ gas, respectively.

Thus, we could demonstrate that femtosecond pulse laser irradiation can work on both reduction and oxidation of metal ions and form metal and metal oxide, respectively. The produced clusters with size of around 1 nm or less have quantum properties and act excellent catalytic performance within the reaction time of a few min to 15 min

**References:**

[1] T. Imae, A. Rahmawati, A.M. Berhe, M.A. Kebede, ACS Applied Nano Mater. 5 (2022) 16842-16852.
[2] G.F. Gemeda, W.-J. Hwang, T. Imae; Y.-W. Yen, J. Coll. Int. Sci. 614 (2022) 310-321.
[3] M.B. Getahun, E.B. Santiko, T. Imae, C.-L. Chiang, Y.-G. Lin, Appl. Surface Sci. 604 (2022) 154515.

## IL-I-2

# Remodelling Double Network Hydrogels by Force Triggered Polymerization

Jian Ping Gong

*[12]Faculty of Advanced Life Science, [2]WPI-ICReDD, Hokkaido University, Sapporo, Hokkaido, Japan*
*gong@sci.hokudai.ac.jp*

Biological tissues are dynamic, open systems in which structural transformations to adapt to the surrounding environment are constantly occurring through metabolic processes. For example, skeletal muscles hypertrophy and strengthen due to repeated mechanical exercise. The exertion destroys the fibril structure, whereas the nutrition (amino acids) supply and constructive chemical reactions grows new muscle. By contrast, synthetic materials are static, closed systems, with no structural reconstruction and substance exchange with surroundings. Usually, repetitive mechanical loading leads to damage and even failure of materials.

Herein, we present a principle for creating metabolic-like hydrogels that self-grow and strengthen by repetitive mechanical stimuli [Matsuda, et al., Science, 2019]. We show that the double-network hydrogels exhibit sustained strength increase along with size increase under repetitive loading in monomer (nutrition) solution. This metabolic-like phenomenon of double network hydrogels is through a repetitive structural destruction and reconstruction of the brittle network by mechanochemical transduction. This remodelling mechanism endows the hydrogels to achieve new functions at specific time and position triggered by mechanical stimuli. This work might inspire new strategies for developing self-adaptable and sustainable materials.

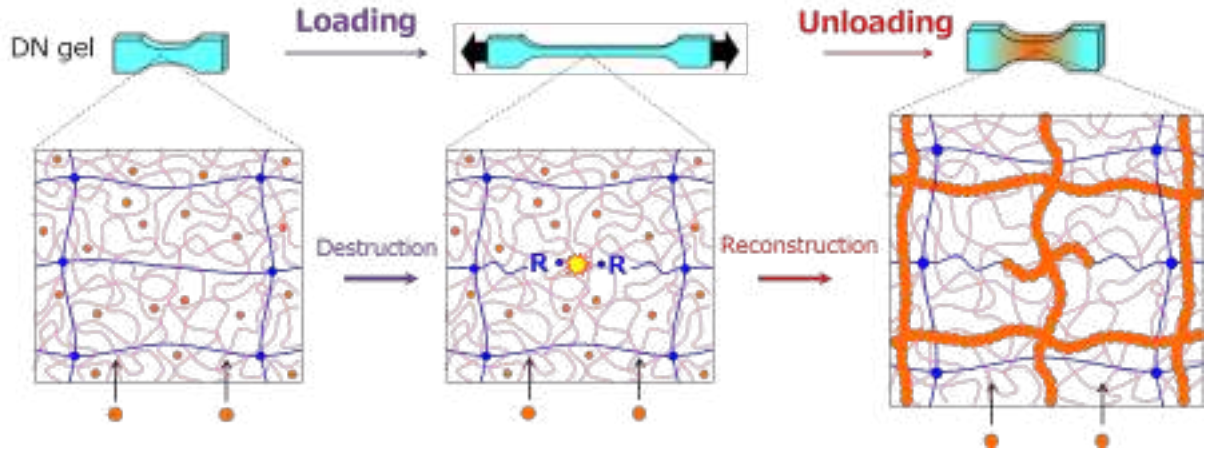

## IL-I-3

# Single-Atom Alloy Pd-Based Catalysts: Characterization and Catalytic Performance in Liquid-Phase and Gas-Phase Selective Alkyne Hydrogenation

Mashkovsky I.S.[1], Bukhtiyarov A.V.[2], Markov P.V.[1], Melnikov D.P.[1], Stakheev A.Yu.[1]
*1 – Zelinsky Institute of Organic Chemistry, Moscow, Russia*
*2 – Boreskov Institute of Catalysis, Novosibirsk, Russia*
*st@ioc.ac.ru*

Single atom alloy (SAA) catalysts attract increasing attention due to uniform structure of active sites and superior selectivity in a number of catalytic reactions [1-2]. In this lecture we will focus on the preparation, characterization, and the catalytic performance of $Pd_1Ag/Al_2O_3$ SAA catalysts. Several critical issues will be addressed:

1) Preparation and characterisation of SAA catalyst. How can we confirm the formation of single-atom $Pd_1$ sites on the surface of $Pd_1Ag$ alloy nanoparticles?
2) How much Ag do we need to isolate $Pd_1$ sites from each other? Stability of single atom $Pd_1$ sites upon adsorption of strongly bound molecules.
3) Catalytic performance of $Pd_1Ag$ SAA in gas-phase hydrogenation of acetylene in ethylene and liquid-phase hydrogenation of substituted alkynes. Possible reaction pathways. Influence of Pd/Ag ratio on the activity/selectivity parameters.
4) Can $Pd_1Ag$ SAA activity be improved without sacrificing selectivity?
5) Industrial application of SAA catalysts. "Egg-shell" $Pd_1Ag/Al_2O_3$ in acetylene hydrogenation.

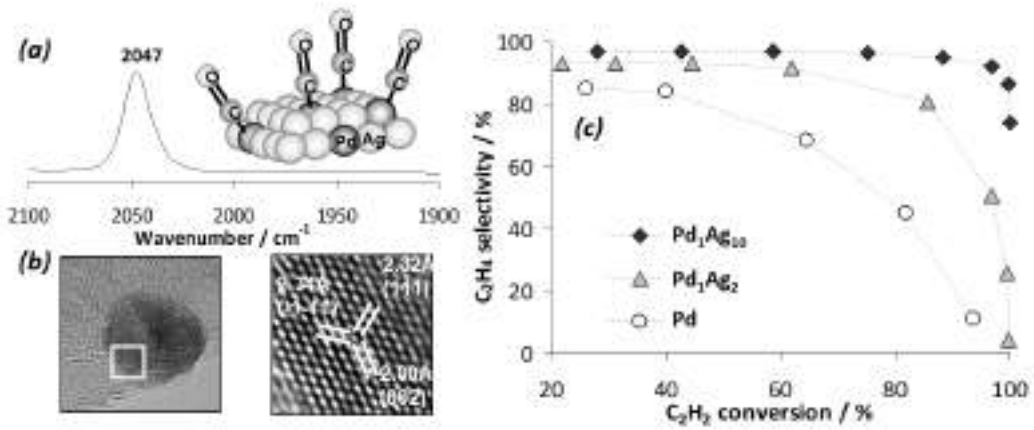


*Fig. 1. CO-DRIFT spectrum of $Pd_1Ag_{10}$ SAA catalyst (a); HRTEM image of $Pd_1Ag_{10}$ nanoparticle (b); catalytic performance of SAA-$Pd_1Ag_{10}$, bimetallic $Pd_1Ag_2$ and monometallic Pd-catalysts in gas-phase hydrogenation of acetylene ($C_2H_2$: $H_2$ :$C_2H_4$:=1:5:100, 1bar) (c).*

**Acknowledgement:** This work was supported by the Russian Science Foundation, Grant No. 23-13-00301.

**References:**

[1] R.T. Hannagan, G. Giannakakis, M. Flytzani-Stephanopoulos, E.C.H. Sykes, Chem. Rev. 120 (2020) 1204493.
[2] A.V. Rassolov, I.S. Mashkovsky, A.Yu. Stakheev et al., Nanomaterials 11 (2021) 3286.

## IL-II-1

# Trans-Synaptic Nose-to-Brain Transport of Nanoparticles and Its Modulation by Odor, Aging, and Diseases

Moshkin M.P., Romashchenko A.V.
*The Federal Research Center Institute of Cytology and Genetics, SB RAS, Academician Lavrentiev Avenue, 10, 630090, Novosibirsk, Russia*
*mmp@bionet.nsc.ru*

Nanoparticles (NPs) can be transported via the nose-to-brain (N2B) route. Nonetheless, quantitative data on their spatiotemporal dynamics and regulation of the N2B transport are largely lacking. We surveyed metal oxide/hydroxide NPs as MRI contrasts for quantitative N2B tracking. NPs containing divalent transition metals were the only ones capable of N2B transmission. Using T1-weighted (T1W) magnetic resonance imaging (MRI), we showed that $Mn_3O_4$-NPs were readily engulfed by olfactory receptor neurons (ORNs) without disrupting olfactory sensing, and we mapped their N2B trajectory. Within neurons, the $Mn_3O_4$-NPs were localized to the cytosol, mitochondria, and vesicles, and moved at mixed fast and slow axonal transport velocities intra- and extra-vesicularly through ORNs. The NPs' axonal transport required neuronal activity and microtubule integrity. The $Mn_3O_4$-NPs were trans-synaptically transmitted through at least four synapses across the olfactory tract. Trans-synaptic transmission of the NPs was dependent on N-type Ca2+ channels and NMDA receptors but blocked by GABA receptor activation. A five-parameter Weibull signal increase/decrease model fitted to the T1W MRI data allowed for estimating kinetic parameters of $Mn_3O_4$-NP accumulation/elimination. Absolute and relative accumulation rates, but not elimination, correlated negatively with the number of synapses from ORNs, indicating a coupling of the NPs' N2B transport with spontaneous neuronal activity. Accordingly, olfactory stimuli (2,5-dimethylpyrazine and acetophenone) significantly modulated and rerouted the $Mn_3O_4$-NP N2B transport odor specifically. Finally, the NPs' trans-synaptic transmission was impaired by aging and the onset of Parkinson's disease. These data suggest new approaches to diagnostics, functional neuroimaging, and controlling N2B drug delivery.

## IL-II-2

# Designing Intelligent Materials from Anisotropic Rubbers: Liquid Crystal Elastomers in Action

Suk-kyun Ahn
*Department of Polymer Science and Engineering, Pusan National University, Busan, Korea*
*skahn@pusan.ac.kr*

The intelligent materials that can interact with the environment, regulate their actions, and even learn from input signals is crucial for the advancement of various applications, including artificial skins, smart clothing, and soft robotics. While liquid crystals (LCs) have traditionally been used as key materials for flat panel displays, they can also offer intelligent and useful properties when incorporated into various polymeric forms. In this talk, I will focus on liquid crystal elastomers (LCEs), which are loosely crosslinked polymer networks that combine the elastic properties of rubber with the anisotropic properties of LCs. Unlike other monolithic materials, the multifunctionality and stimuli-responsivity of LCEs can be pre-programmed by directing molecular orientation, making them promising materials for soft actuators and sensors. By judiciously designing the molecular structure of LCEs, we demonstrate 4D printable hygroscopic LCE actuators and reprogrammable artificial muscles.

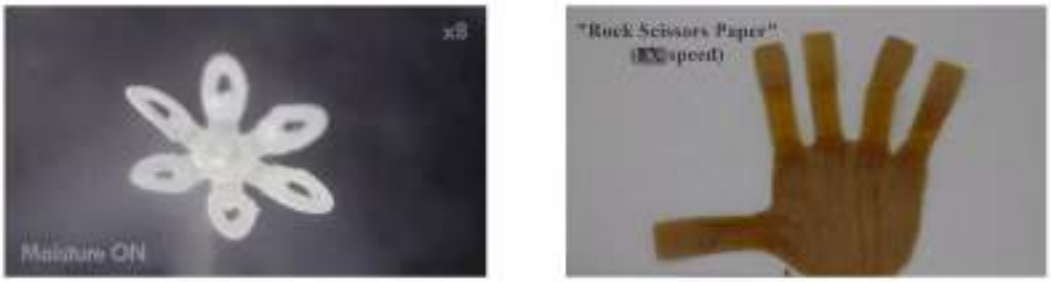


*Fig. 1. Liquid crystal elastomer-based hygroscopic actuator (left) and artificial muscle (right)*

**Acknowledgement:** This work was supported by the National Research Foundation (NRF), Korea by the Korean Government, Ministry of Science and ICT (MSIT) (2019R1C1C1006048).

**References:**

[1] K. Kim, Y. Guo, J. Bae, S. Choi, H. Y. Song, S. Park, K. Hyun, S.-K. Ahn, "4D Printing of Hygroscopic Liquid Crystal Elastomer Actuators" Small, **2021**, 2100910.
[2] J-H. Lee, J. Bae, J. H. Hwang, M-Y. Choi, Y. S. Kim, S. Park, J-H. Na, D-G. Kim and S-k. Ahn, Adv. Funct. Mater. **2022**, 32, 2110360.

## IL-II-3

# Recewnt Development of Starch-Based Materials

Mao Yang[1], Mahafooj Alee[1], Jun Fu[2], Long Yu[1,2]
*1 – Centre for Polymers from Renewable Resources, SFSE, SCUT, Guangzhou, China*
*2 – Institute of Chemistry, Henan Academy of Sciences, Zhengzhou,China*
*felyu@scut.edu.cn*

The development and production of biodegradable materials from renewable resources have been spurred by oil shortages and the growing interest in easing the environmental burden of petro-chemically derived polymers. Currently more and more countries have introduced regulations and lows of banning disposable plastics. Starches offer a very attractive low-cost base for new biodegradable polymers due to their low material cost and ability to be processed with conventional plastic processing equipment. During the quick development of bio-based materials recently, starch-based materials face both challenges and opportunities. Various conventional processing techniques such as extrusion, injection compression moulding, and casting, as well as some new techniques such as reactive extrusion, have been adapted for processing starch-based polymers. On other hand, the study of the unique microstructures of different starches and their multiphase transitions during thermal processing have increased fundamental knowledge of polymeric science, in particular to understand the structure–processing–property relationships in polymers. In this presentation, I will introduce our recent research on starch-based materials, including both scientific achievement and commercial applications [1-7]. Fig.1 shows various developed and commercialized starch-based products.

*Figure 1. Photos of starch-based materials*

**Acknowledgement:** Authors would like to acknowledge the financial fund from National Natural Science Foundation of China (CN) (22178124, 32272340).

**References:**

[1] L. Meng; S. Li; et al., ACS Sust. Chem. & Eng., 2019, 7, 9506.
[2] L. Meng; H. Liu,; H. Yu; Q. Duan; et al., Ind Crops and Products 2019, 134, 43.
[3] A. Ali, Y. Chen, H. Liu, L. Yu, et al., Inter. J. Bio. Macrom., 2019, 129, 1120.
[4] X. Ge, L. Yu, Z. Liu, H. Liu, et al., Inter. J. Bio. Macrom., 2019, 125,370.
[5] Q.Duan, L. Meng, H. Liu, L. Yu, K. Lu, S. Khalid, L. Chen, J. Polym. Envi., 2018, 27(1), 158.
[6] Q. Duan, Z.i Zhu, Y. Chen, et al., ACS Sust. Chem. & Eng., 2022. online.
[7] M. Alee, Q. Duan, Y. Chen, H. Liu, Jet al., ACS Sust. Chem. & Eng., 2021, 11960.

## IL-III-1

# Well-Defined Porous Biodegradable/Thermoresponsive Microspheres

Ildoo Chung
*Department of Polymer Science and Engineering,*
*Pusan National University, Busan 46241, Korea*
*idchung@pusan.ac.kr*

Aliphatic polyesters such as polycaprolactone (PCL) and polylactide (PLA), endowed with semicrystallinity and degradability, has been widely used as a scaffold in tissue engineering, drug delivery systems, packaging and biomedical applications, due to its controlled biodegradability, biocompatibility, and good physical properties. Our work focuses on the successful polymerization of methyl vinyl ketone onto PCL/PLA via RAFT followed by the formation of their biodegradable microspheres that were made porous by UV irradiation.

Porous biodegradable microspheres were fabricated by successful RAFT polymerization of methyl vinyl ketone (MVK) onto PCL and PLA, which was first synthesized by ring opening polymerization of lactide followed by an oil/water emulsion-evaporation method, then finally photodegradation of PMVK blocks by UV irradiation.

For photodegradation by UV light under dried condition, the molecular weight of triblock copolymer was decreased gradually with UV irradiation time, reaching close to that of macro-CTA, meaning that 90% of PMVK block was photodegraded after 24 h of UV irradiation. The morphology of microspheres was spherical with smooth surfaces before UV irradiation (Fig. 1(upper)). Microspheres fabricated only from PCL homopolymers could also retain their smooth surface after UV irradiation (Fig. 1a (bottom)). However, those from PCL-PMVK and PCL-PLA-PMVK block copolymers had rough surfaces and porous structures after UV irradiation due to the photodegradation of PMVK blocks as a porous template [Fig. 1b and c (bottom)]. The porosity and shape of the microspheres and shape of microspheres were dependent on the PMVK contents and size of microspheres.

Well-defined biodegradable PCL-PLA-PMVK triblock copolymers were successfully synthesized by ring-opening and RAFT polymerization. Linear increase in molecular weight and narrow polydispersities of the triblock copolymers are clear indications of a controlled polymerization mechanism. Porous microspheres were fabricated by the O/W emulsion-evaporation method followed by the photodegradation of PMVK blocks by UV irradiation. Our findings pave the way to novel methods for direct templating fabrication of porous polymers by removing template blocks by UV light.

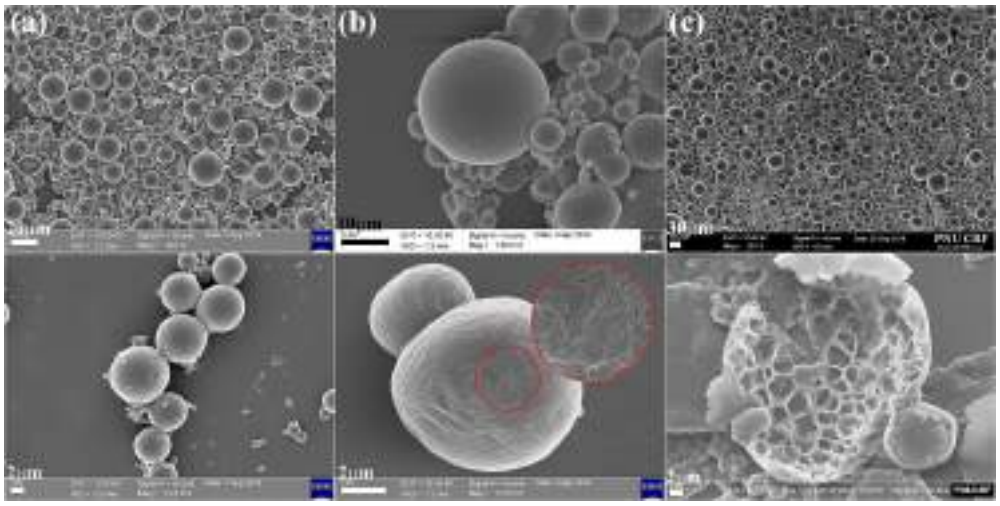


*Figure 1. SEM images of microspheres before (upper) and after (bottom) UV irradiation. (a) PCL, (b) and (c) PCL-PMVK triblock copolymer [PMVK contents, (b) 16%, (c) 45%].*

**Acknowledgement:** This work was supported by the Technology Innovation Program (20011422) funded by Ministry of Trade, Industry & Energy (MOTIE, Korea).

**References:**

[1] T. Kim, S. Lee, S.-Y. Park, and I. Chung, Polymers, 13, 3964 (2021).
[2] T. Kim, J. Mays and I. Chung, Polymer, 158, 198 (2018).

## IL-III-2

# Amorphous Nanostructures: Fabrication, Properties, and Applications in Catalysis and Energy Storage

Gurevich S.A.
*Ioffe Institute, St. Petersburg, Russia*
*gurevich@quantel.ioffe.ru*

Amorphous nanostructures, due to the specifics of their structural organization, can have very unusual and useful properties. In this report we consider structures of two types, consisting of amorphous metal nanoparticles and formed from sub-nanometer carbon clusters, which are characterized by the absence of a regular arrangement of atoms. Such structures were fabricated within the framework of a single technology of pulsed laser deposition.

Amorphous metal nanoparticles of various metals, including Pt, Pd, Ni, Co, Cu, etc., were produced in vacuum by pulsed laser ablation of pure metal targets. The particles were formed under extremely rapid cooling, charging, and decay of metal microdroplets ejected from the target surface under laser illumination (we call this process as “laser electrodispersion” or LED). Small particle sizes, from 2 to 5 nm, depending on the type of metal, as well as rapid particle forming process guarantee the absence of crystallization centers in them, due to which the resulting particles are amorphous. The relative dispersion of particle sizes usually does not exceed 20%. One of important and useful property of the amorphous metal nanoparticles produced by LED is their high stability with respect to coagulation, so that the particles retain their size and shape even in direct contact with each other, such as in relatively thick coatings.

The developed LED technology was used for the manufacture of catalysts comprising amorphous metal nanoparticles deposited on the surface of granular carriers. In these catalysts the metal load was usually within 0.01 and 0.001 wt%. With such a low metal content, the catalysts have exceptionally high specific activity, which is orders of magnitude higher than the activity of common nanostructure catalysts. In some cases, these catalysts were superior in terms of selectivity and long-term stability. We believe that the above features are due to two factors. First is the amorphous nature of the particles and second is specific for LED particle arrangement on the support surface. In the case of a porous carrier, LED technology ensures that the particles are deposited predominantly on the “outer” surface of the carrier, while the particles do not penetrate into deep and narrow pores. This ensures better contact of the active phase of the catalyst with the reagents in comparison with catalysts obtained by impregnation. High specific activity of catalysts is especially in demand when expensive noble metals are used as the active phase of the catalyst. Performance advantage of LED catalysts has been repeatedly observed in various processes, including hydrogenation, oxidation, isomerization, addition, etc. Some examples of high performance of our catalysts in such processes are discussed in the report.

Further, the features of the process of pulsed laser deposition of carbon are discussed. In this process, sub-nanometer carbon clusters are produced containing up to several tens of carbon atoms. The mechanism of formation of these clusters is the condensation of carbon vapors occurring in a rapidly expanding and rapidly cooling laser plasma that appears at the surface of a carbon target during each laser pulse. The random stacking of the clusters in course of their deposition on a substrate forms a very peculiar amorphous material, which we call "cluster carbon". Among the very unusual properties of this material are its high conductivity (weak and linear temperature dependence of conductivity), exceptionally high hardness and chemical stability. Direct experiments as well as detailed quantum chemical calculations have shown another unique property, namely, as-made cluster carbon is in a metastable state and has a significant excess internal energy, up to 1 eV per atom.

When thin films of cluster carbon were first fabricated, we find that this material has rather surprising electrochemical characteristics - specific capacity for lithium accumulation is over 600 mAh/g and this value only slightly decreases under very fast charge-discharge by high current, up to 200C, and this high capacity retains for more than 10,000 charge-discharge cycles! Having this encouraging result, the “bulk” cluster material in the form of a powder (with a particle size of about 10 μm) was produced and used to fabricate anode electrodes of lithium-ion batteries (LIB). In this way anode electrodes with a specific capacity up to 10 mA/cm2 were made, and samples of lithium-ion batteries (in the form of “pouch”) with a capacity of 10 Ah and a specific energy of more than 200 Wh/kg were fabricated. When operating at charge-discharge current of 3C (charge-discharge for 20 minutes), the life span of these batteries was more than 5,000 cycles. It is also shown that the manufactured samples of LIB can work successfully at low temperatures, down to -40 C. These results are at the leading edge of world-wide LIB technologies.

Thus, by several examples we show that amorphous nanostructures produced from different materials with different sizes of amorphous particles may demonstrate very interesting and useful properties. In some way amorphous nanostructures can be considered as separate class of functional materials promising efficient solutions in different areas including catalysis and energy storage.

**Acknowledgement:** The discussed results were obtained by a team of researchers from the Ioffe Institute (partly within the state task No. 0040-2019-0010) in cooperation with the team from Chemistry Department of Lomonosov MSU (catalysis) and with HC Carbon SuperCap LLC (carbon material).

## IL-III-3

# Porous Carbon Materials from Available Resources as Adsorbents and Catalyst Supports

Belskaya O.B.
*Center of New Chemical Technologies BIC, Boreskov Institute of Catalysis, Omsk, Russia*
*obelska@ihcp.ru*

Obtaining carbon materials is currently one of the most developing areas of science and technology. The progress of methods for synthesis and subsequent modification make it possible to provide such materials with desired properties. Expanding the range of use, as well as following the strategy of sustainable development, dictate directions with the widening of sources for obtaining carbon materials, including the use of natural, recycled, low-grade raw materials. The synthesis of specific carbon materials using polyvinyl chloride (PVC), pyrolysis products of hydrocarbon gases and heavy oil products as carbon precursors will be considered and possible directions for their use will be proposed.

PVC is the fourth largest polymer product in the world, and the expansion of its scope makes PVC waste disposal an urgent problem. The impossibility of using thermal-oxidative and high-temperature methods, leading to the formation of highly toxic substances (polyaromatic compounds, dioxins), initiates the development of safe processing methods. A scheme for the production of carbon materials is proposed, including the formation of polyvinylene chains during the dehydrochlorination of PVC molecules, low-temperature carbonization of polyvinylenes and high-temperature activation. Approaches of PVC dehydrochlorination in polar solvents medium and under mechanical activation conditions are considered, with varying the nature of the dehydrochlorinating agent. The introduction of nitrogen, sulphur and metal (Fe, Co, or Ni) containing additives into a reaction mixture for the dehydrochlorination makes it possible to obtain porous carbon materials with heteroatoms, and metal particles incorporated into a graphite like carbon matrix. The possibility of obtaining carbon-carbon composite materials with a controlled porous space by embedding graphite oxide, reduced graphite oxide or nanoglobular carbon into a PVC-based carbon matrix is shown. Such materials can be used to create adsorbents and catalysts and have the potential to be used in energy storage systems. The hydrogenating activity of Pd/C(PVC) catalysts has been demonstrated in the conversion of styrene, nitrobenzene, chlorobenzene, acetophenone.

Carbon foams (CF) with an interconnected three-dimensional graphite structure, resistance to aggressive compounds and high temperatures, and a large external surface attract great attention in many fields, such as the chemical and construction industries, aircraft engineering, rocket science, mechanical engineering, medicine, and others. Various methods and raw materials are used in the production of CF, including blowing carbon precursors followed by carbonization, template carbonization of carbon precursors, compression of exfoliated graphite, and others. This paper proposes a method for producing

carbon foam with a cellular openwork structure using a propane-butane gas mixture as a raw material. The method includes two stages: decomposition of gaseous hydrocarbon feedstock to liquid pyrolysis products (LPP) with mesophase properties and their subsequent foaming at high temperature. The paper presents the results of the LPP mesophase precursor study, ideas about the process of CF formation, as well as data on CF structure. Based on the knowledge of the composition of the carbon foam precursor, the possibility of synthesizing CF of the same structure from technical products containing condensed aromatic hydrocarbons is shown in order to make the synthesis more technologically advanced and increase the yield of the target carbon material. To solve this problem, various mixtures were prepared from catalytic heavy gas oil, coke-chemical and pyrolysis resins, coal tar pitch to obtain the required combination of hydrocarbons. Approaches have been developed to increase the strength of the openwork material and change its morphology by fixing pyrocarbon particles on the CF surface. The resulting carbon foams have a high chemical and thermal stability and can be used in adsorption-catalytic technologies. Methods for fixing palladium particles from $Pd_2(dba)_3$ and polyhydroxo complexes on the surface of CF have been proposed; the catalysts were tested in the hydrogenation of acetylene to ethylene, which requires a short contact time. The resulting carbon foams have a density of 0.02-0.04 g/cm$^3$ and have high thermal stability in an oxidizing environment up to 550°C. This makes it possible to consider CF as an absorbent for collecting oil and light oil products from the water surface, a feature of the absorbent is a rather high capacity (20 g of oil/g of absorbent) in combination with the possibility of its oxidative regeneration.

**Acknowledgement:** This work was supported by the Ministry of Science and Higher Education of the Russian Federation within the governmental order for Boreskov Institute of Catalysis (project AAAA-A21-121011490008-3).

# Symposium Remarks

## SR-1 ÷SR-2

## SR-1

# Asian Symposium on Advanced Materials: Scientometric Trajectory

Vedyagin A.A., Zibareva I.V.
*Boreskov Institute of Catalysis, Siberian Branch of the Russian Academy of Sciences, 630090 Novosibirsk, Russia*
*vedyagin@catalysis.ru*

Since 2007, *Asian Symposium on Advanced Materials (ASAM)* is steadily expanding regular international event uniting specialists in chemistry, physics, and materials sciences including biomaterials. Actually, the *ASAM* reveals global character and contributes much into contemporary scholarly communications.

| ***ASAM*** | **Chrono and Geolocation** | **General Topics** | **Number of Sections** |
|---|---|---|---|
| *ASAM-1* | 2007, Vladivostok, Russia | Chemistry; physics; biology | 1 |
| *ASAM-2* | 2009, Shanghai, China | Chemistry of functional materials | 3 |
| *ASAM-3* | 2011, Fukuoka, Japan | Chemistry and physics of soft interfaces, nanosystems, and novel materials; biomimetics; synchrotron radiation | 1 |
| *ASAM-4* | 2013, Taipei, Taiwan | Chemistry, physics, and biomedicine of functional and novel materials | 5 |
| *ASAM-5* | 2015, Pusan, Korea | Chemistry, physics, and biomedicine of functional and novel materials | 6 |
| *ASAM-6* | 2017, Hanoi, Vietnam | Fundamental science of materials; materials on energy, environmental and biomedical sciences | 2 |
| *ASAM-7* | 2019, Beijing, China | Porous, functional, biomedical materials; materials for energy and optoelectronics | 6 |
| *ASAM-8* | 2013, Novosibirsk, Russia | Chemistry; biomaterials; applications | 3 |

Traditionally, the *ASAM* proceeds, and will proceed, in the in-person form – despite current criticism of the form with numerous online-informational, environmental, financial, etc. arguments (e. g. [1]). Taking those into account, and saving once retrieved scientometric information upon the *ASAM* (this and future work), a special database is planned for the ASAM with 2007+ retrospective to be based on the *SciAct*–like platform [2].

| ***ASAM*** | **Contributions** | | | | | |
|---|---|---|---|---|---|---|
| | plenary | invited | oral | keynote | poster | total |
| *ASAM-1* | 1 | 21 | 14 | 1 | 55 | 92 |
| *ASAM-2* | 4 | 39 | 34 | 26 | 67 | 170 |
| *ASAM-3* | 6 | 26 | 57 | - | 115 | 204 |
| *ASAM-4* | 4 | 25 | 46 | 7 | 70 | 152 |
| *ASAM-5* | 5 | 19 | 11 | 5 | 74 | 114 |
| *ASAM-6* | 4 | 18 | 35 | 15 | 127 | 199 |
| *ASAM-7* | 6 | 14 | 12 | 13 | 57 | 102 |
| *ASAM-8* | 4 | 10 | 123 | 7 | 170 | 314 |

| ***ASAM*** | **Countries** | |
|---|---|---|
| | number | contributions by countries [a] |
| *ASAM-1* | 6 | Russia 56; Japan, Korea 5; China, Taiwan 2; India 1 |
| *ASAM-2* | 13 | China 68; Russia 10; Japan, Korea 4; Singapore, Germany, Spain 3; Thailand, Italy, Lithuania, Pakistan, Switzerland 1 |
| *ASAM-3* | 10 | Japan 54; Korea 14; Russia 6; Taiwan 5; China 4; USA 2; France, Germany, United Kingdom, Singapore 1 |
| *ASAM-4* | 10 | Japan 36; Taiwan 16; China 10; Korea 7; USA, France 2; Thailand, India, Australia, Israel 1 |
| *ASAM-5* | 10 | Japan 9; Russia 8; Korea 7; Taiwan 4; China 3; Vietnam, Thailand, France, Spain 2; USA 1 |
| *ASAM-6* | 13 | Vietnam 32; Taiwan 9; Japan, Korea 8; Russia 6; China 4; Thailand, Brunei, Egypt, USA, Germany, Spain, United Kingdom 1 |
| *ASAM-7* | 7 | China 27; Korea 8; Russia 4; Japan 3; Taiwan, USA 2; Vietnam 1 |
| *ASAM-8* | 5 | Russia 123; Korea 10; China 6; Australia, Algeria, Taiwan, Japan 1 |

[a] Without posters.

**Acknowledgement:** This work was supported by the Ministry of Science and Higher Education of the Russian Federation within the governmental order for Boreskov Institute of Catalysis (project AAAA-A21-121011390054-1).

**References:**

[1] S. Sarabipour, A. Khan, Y. F. S. Seah, A. D. Mwakilili, F. M. Mutoki, P. J. Sáez, B. Schwessinger, H. J. Debat, T. Mestanovic, *Nature Human Behaviour*. 5 (2021) 296. DOI: 10.1038/s41562-021-01067-y
[2] B. L. Alperin, I. V. Zibareva, A. A. Vedyagin, *ASAM-8 Book of Abstracts*.

## SR-2

# The Conference Database for *ASAM*

Alperin B.L., Zibareva I.V., Vedyagin A.A.
*Boreskov Institute of Catalysis, Siberian Branch of the Russian Academy of Sciences,*
*630090 Novosibirsk, Russia*
*alperin@catalysis.ru*

Nowadays, there are many suggestions under discussion in academic community towards changing scientific meetings for the better [1]. One of them deals with a creation of specialized online databases containing information not only upon conferences' scholarly output but also upon their participants – speakers and attendees, together with additional data embracing personal identifiers, affiliations, geolocations, genders, career-stage statistics, etc. The ultimate goal of such undertakings can be creating a central database affording key sustainability and equity considerations of conferences and enabling researchers to identify the most beneficial gatherings.

We believe that once obtained scholarly information must not be lost. Meanwhile, a search of scientometric information upon the *Asian Symposium on Advanced Materials (ASAM*; eight events since 2007) revealed a rather big number of problems [2]. Particularly, some sites of previous *ASAM*s were out of operation, and *ASAM*s materials such as *Books of Abstracts*, *Circulars*, *Programs*, etc., were inaccessible even as printed copies. These findings support an idea of special databases focused on scientific meetings and allowing multipurpose analysis of relevant unique information. In the case of *ASAM*, such database is designed as a module of the *SciAct* CRIS system of the *Boreskov Institute of Catalysis, i.e.,* a web application written in *PHP* scripting language based on *Symfony 6* framework with *Doctrine ORM* with *MariaDB* using for data storage. The *SciAct* has multiple interfaces for data editing and viewing, e. g. *Administrator* interface – for full access to data: administrator can create, edit, view, delete, and approve data items; *User* interface – user (who is not identical with administrator) can create, view, and send data for approvement; *Public* interface – any visitor can view certain data with filtering and sorting [3].

The basic elements of the *ASAM* database are as follows: Conference Title; Conference Chrono and Geolocation; Organizers (International Advisory Committee, Local Committee); General Topics and Themed Sections; Contribution Title and Summary; Contribution URL; Contribution type (plenary, invited, keynote, oral, poster, online); Contribution Author(s) with speaker highlighted; Authors' affiliations; and obviously Book of Abstracts, Program and other useful materials (e. g. Proceedings Chairs). Particularly, the *ASAM* database data scheme for Conferences is as follows:

[Conference report] → [Conference] → [Country]

[Conference report] → [Author's description] → [Author]

[Conference report] → [Affiliation description] → [Organisation] → [Country]

## SR-2

A role of Conferences' reports in scholarly communication is very important (at least, as precursors of further journals' articles) [4], and Conferences' reports are the main entities for any Conference database. They relate to other entities, such as Conference, Author description, Affiliation description, having, in turn, their own relations, e. g. Conference → Country. The Author's description is an intermediate entity with full author information in the context of current Conference report: Authors' order (position in the Authors' line), Authors' original names and initials, Authors' affiliations, and link to Author entity.

Such treatment of the relevant entities provides necessary flexibility of analytical queries, e.g. counting number of plenary speakers featuring target affiliations can be done with a single SQL query. Furthermore, Conference report entity is linked to other scholarly activity items: Theses, Funding sources, Publications, etc. These links allow creating a full story of the specific research from Conference report to eventual journal article.

**Acknowledgement:** This work was supported by the Ministry of Science and Higher Education of the Russian Federation within the State Assignment for Boreskov Institute of Catalysis (project AAAA-A21-121011390054-1).

**References:**

[1] S. Sarabipour, A. Khan, Y. F. S. Seah, A. D. Mwakilili, F. M. Mutoki, P. J. Sáez, B. Schwessinger, H. J. Debat, T. Mestanovic, *Nature Human Behaviour*. 5 (2021) 296. DOI: 10.1038/s41562-021-01067-y
[2] A. A. Vedyagin, I. V. Zibareva, *ASAM-8 Book of Abstracts*.
[3] *SciAct*: CRIS system of Boreskov Institute of Catalysis. URL:https://sciact.catalysis.ru/en/public
[4] M. C. Drott, *J. Am. Soc. Inform. Sci.* 46 (1995), 299. DOI: 10.1002/(SICI)1097-4571(199505)46:4<299::AID-ASI6>3.0.CO;2-0

# Oral Presentations

## I. Synthesis and Structure of Advanced Materials

**OP-IA-1 ÷OP-IA-37**

**OP-IB-1 ÷OP-IB-22**

**OP-IC-1 ÷OP-IC-12**

## II. Biomaterials and Bionanocomposites

**OP-II-1 ÷ OP-II-15**

## III. Applications

**OP-III-1 ÷ OP-III-37**

## OP-IA-01

# Spark Plasma Sintering of Nb/$Ti_3Al(Si)C_2$ Nanolaminated Composites

Abdulmenova A.V., Krotkevich D.G., Mingazova Y.R., Kashkarov E.B.
*Tomsk Polytechnic University, Tomsk, Russia*
*ava75@tpu.ru*

**Introduction.** MAX-phases and composites based on them represent a relatively new class of nanolaminated materials described by the general formula $M_{n+1}AX_n$, where M – transition metal, A – IIIA or IVA metal of periodic table, X – C or N, n=1–3 [1]. They have unique properties of metals and ceramics such as high melting point, low density, corrosion resistance, high thermal and electrical conductivity. Despite their high strength properties at high temperatures, their application is limited due to their macroscopic brittleness at low temperatures because of the absence of plastic deformation [2]. Therefore, it is necessary to develop a method of toughening ceramic composites. One way is to reinforce the material through the formation of solid solution MAX-phases by substitution of atoms, formation of secondary phases after sintering, reinforcement with short or continuous fibers. Another way is to create metal-ceramic layered composites. In order to obtain such composites an approach based on the use of preceramic papers with MAX-phase powder filler and metal foils made of ductile niobium has been proposed. Spark plasma sintering was used to reduce the interaction between metal and ceramic layers, providing high-speed synthesis of dense composites [3]. The aim of this work is to obtain nanolaminated metal-ceramic composites based on Nb/$Ti_3(Al,Si)C_2$ at different sintering duration.

**Materials and methods.** The feedstock is a multilayer material with alternating layers of preceramic papers based on the $Ti_3Al(Si)C_2$ (TAC) MAX-phase and Nb metal foils. The preceramic sheets were fabricated using a dynamic sheet former machine. The prepared paper sheets had the following composition: 7.3 wt.% cellulose fibers, 87 wt.% $Ti_3Al_{0,75}Si_{0,25}C_2$ powder, 3 wt.% $Al_2O_3$ powder, 2.7 wt.% retention additives. Nb foils were stacked through each TAC layer so that the total number of layers was 21 and the outer layers were TAC layers. Sintering of the prepared stacks was carried out using Advanced Technology SPS 10-4 at T=1250 °C, P=5 MPa for 3, 10 and 20 min. The microstructure and elemental composition of the sintered samples were studied by scanning electron microscopy (SEM) using Tescan Vega 3 microscope equipped with an energy dispersive X-ray spectroscopy (EDS) attachment.

**Results.** Figure 1a shows the elemental mapping image of the cross-section of the nanolaminated composite. It can be seen alternating ceramic layers formed from preceramic papers and Nb metal layers. A reaction layer is formed at the metal/ceramic interface. The formation of this layer is caused by the mutual diffusion of MAX-phase elements (mainly Al and Si) and Nb. Small iron impurities were also found in the ceramic and reaction layers. It can

be explained by the presence of this element in the initial powder used for the fabrication of the preceramic papers.

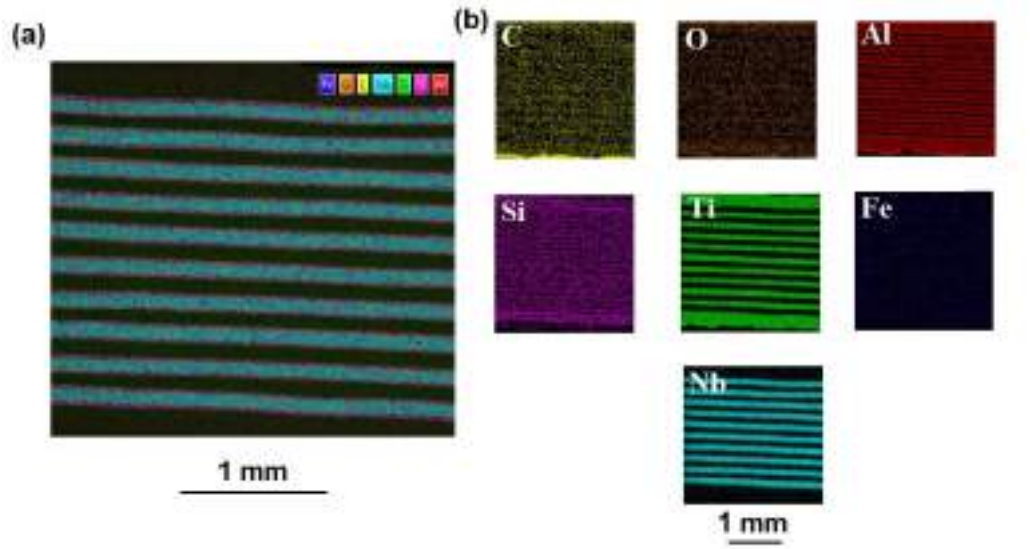


*Fig. 1. Typical SEM image with colored elemental distribution (a) and EDS maps for individual elements (b)*

As a result of sintering at different durations, reaction layers of various thicknesses are formed (Fig. 2): 26 ± 2 μm (3 min), 30 ± 3 μm (10 min), 38 ± 5 μm (20 min). Thus, as the sintering time of the composites increases, the thickness of the reaction zones increases.

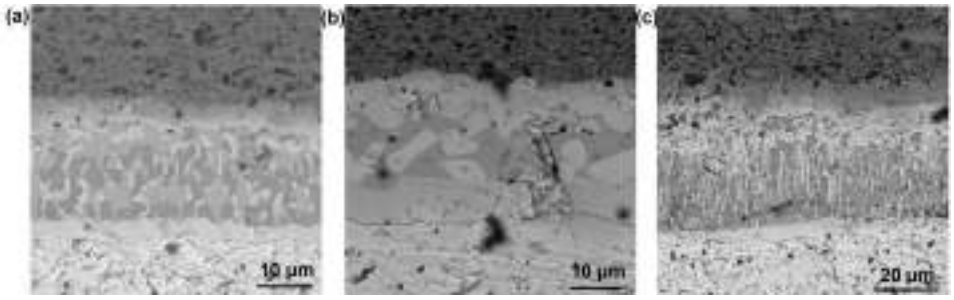


*Fig. 2. SEM images of cross-sections of reaction layers of nanolaminated composites at sintering times of 3 min (a), 10 min (b), 20 min (c)*

**Conclusion.** New metal/ceramic nanolaminated composites Nb/$Ti_3Al(Si)C_2$ have been obtained by spark plasma sintering. It is shown that due to sintering, mutual diffusion occurs between metal layers of Nb and ceramic layers based on $Ti_3Al(Si)C_2$ , as a result of which a diffusion layer enriched with Nb, Al and Si is formed. The effect on the mechanical behaviour of increasing the thickness of the reaction layers with increasing sintering time should be investigated.

**Acknowledgement:** This work was supported by a grant from the President of the Russian Federation (Project No. MK-1048.2022.4).

**References:**

[1] M. W. Barsoum, J. Ceram. Sci. Technol. (2013) 299.
[2] X. Fan,X. Yin, Adv. Compos. Hybrid Mater. 1 (2018) 685.
[3] D. G. Krotkevich, E. B. Kashkarov, M. S. Syrtanov, T. L. Murashkina, A.M. Lider, S. Schmiedeke, N. Travitzky, Ceram. Int. 47 (2021) 12221.

## PP-IA-02

# $CeO_2$-$ZrO_2$-$MnO_x$ Composites for Oxidative Purification of Exhaust Gas

Grabchenko M.V., Chernykh M.V., Mikheeva N.N., Savel'eva A.S., Dorofeeva N.V., Mamontov G.V., Salaev M.A.
*Tomsk State University, Tomsk, Russia*
*marygra@mail.ru*

Atmospheric air pollution by CO, particulate matter (especially, soot) and VOCs is a global environmental challenge, and the development of ways to reduce emissions of harmful substances by industrial enterprises and motor vehicles has been and remains an urgent task. The most effective and promising way to solve this problem is the low-temperature catalytic oxidation of harmful compounds to $CO_2$ and water [1,2]. A significant part of the studied low-temperature oxidation catalysts comprise compositions based on noble metals (Pd, Pt, Au, Rh) deposited on oxide supports. However, the use of such catalysts for applied challenges is complicated due to their high cost. Mixed oxide systems have attracted particular interest as they feature no noble metals in the composition becoming less expensive, possess a relatively high surface area and stability to particle aggregation at high-temperatures due to the effects of composite components [3]. Thus, the present work is focused on designing $CeO_2$-$ZrO_2$-$MnO_x$ composites and study of the effect of the composition and preparation method on the structure of oxide systems and catalytic properties in CO oxidation and soot combustion.

The ternary $CeO_2$-$ZrO_2$-$MnO_x$ composites with different Ce/Zr/Mn molar ratios were synthesized using citrate and template (with CTAB or propionic acid) methods. The physical-chemical properties of the prepared composites were studied using low-temperature $N_2$ adsorption/desorption, XRF, XRD, Raman spectroscopy, temperature-programmed reduction with hydrogen, etc. The catalytic activity of the prepared catalysts was evaluated in CO oxidation and soot combustion.

The composites obtained feature high catalytic performance caused by increased oxygen mobility and phase defectiveness ensured by the formation of the corresponding mixed oxide phases and interphase boundaries. The revealed relationships between the method of composite synthesis, conditions of thermal treatment, physical-chemical properties and catalytic performance are discussed.

**Acknowledgement:** The work was supported by the Russian Science Foundation grant № 23-73-00109, https://rscf.ru/project/23-73-00109/.

**References:**

[1] M.V. Grabchenko, N.N. Mikheeva, G.V. Mamontov, M.A. Salaev, L.F. Liotta, O.V. Vodyankina, Catalysts 8 (2018), 285.
[2] M.V. Grabchenko, G.V. Mamontov, V.I. Zaikovskii, V. La Parola, L.F. Liotta, O.V. Vodyankina, Appl. Catal. B: Environ.260 (2020), 118148.
[3] P. Yao, J. He, X. Jiang, Y. Jiao, J. Wang & Y. Chen, J. Energy Inst. 93 (2020) 774.

## OP-IA-03

# Organic Cations Improve the Properties of $MoS_2$-Based Hybrid Materials by Enhancing of 1T Phase Stability

Goloveshkin A.S., Lenenko N.D., Ushakov I.E., Golub A.S.
*A.N. Nesmeyanov Institute of Organoelement Compounds, Moscow, Russia*
*golov-1@mail.ru*

Molybdenum disulfide is a well-known 2D material highly demanded in various fields due to excellent physicochemical properties provided by its polymorphic modifications with trigonal prismatic (2H) and octahedral (1T) polyhedron. The latter modification is in demand for constructing the photothermal materials, electrocatalysts and energy storage devices. However, 1T-$MoS_2$ polymorph suffers from structural instability, tending to transform to the stable 2H-$MoS_2$ on heating or ageing. Stabilization of 1T-$MoS_2$ may help to expand application potential of this material and thus merits much attention.

To address the problem of 1T-$MoS_2$ stability, the inorganic-organic layered compounds containing regularly alternating layers of 1T-$MoS_2$ and organic cationic molecules have been synthesized. The guest molecules capable of binding to $MoS_2$ layers and participating in noncovalent interactions with them have been used. Special attention has been paid to the systems containing bioactive molecules as, for instance, quaternary ammonium antiseptic Miramistin [1]. The structures of the synthesized hybrid compounds have been solved by modeling their powder diffraction patterns followed by quantum-chemical optimization of the structural models [2]. The obtained structural data allowed us to reveal the effect of nanorelief of the $MoS_2$ sheet surface on disposition of organic species in the interlayer space of $MoS_2$ as well as to determine and quantify the various noncovalent interactions established between the organic guest and $MoS_2$, including CH···S, NH···S and π···S ones [1-4].

The noncovalent guest-$MoS_2$ interactions was found to enhance structural stability of 1T-$MoS_2$ sheets as evidenced by spectral and thermal behavior studies [4-5]. The influence of structure stabilization on photothermal and electrocatalytic properties of materials is discussed.

**Acknowledgement:** This work was supported by the Russian Science Foundation (grant 22-23-00225).

**References:**

[1] A.S. Goloveshkin, N.D. Lenenko, A.V. Naumkin, A.S. Golub, Molecules, 28 (2023) 1702
[2] A.S. Goloveshkin, N.D. Lenenko, V.I. Zaikovskii et al., RSC Adv. 5 (2015) 19206
[3] I.E. Ushakov, N.D. Lenenko, A.S. Goloveshkin et al., CrystEngComm 24 (2022) 639
[4] A.S. Goloveshkin, N.D. Lenenko, A.V. Naumkin et al., ChemNanoMat, 7 (2021) 447
[5] A.S. Goloveshkin, N.D. Lenenko, M.I. Buzin et al, Int. J. Hydrogen Energy, 48 (2023) 10555

## OP-IA-04

# Genesis and Structural Properties of $(Ce_{1-x}Al_x)_{0.8}Ni_{0.2}O_y$ Materials for Hydrogen Production through Methane Reforming Processes

Matus E.V.[1,2], Kuznetsova I.O.[1,2], Sukhova O.B.[1], Ismagilov I.Z.[1], Ushakov V.A.[1], Stonkus O.A.[1], Kapishnikov A.V.[1], Kerzhentsev M.A.[1], Ismagilov Z.R.[1,3]

*1 – Boreskov Institute of Catalysis, Novosibirsk, Russia*

*2 – Novosibirsk State Technical University, Novosibirsk, Russia*

*3 – Federal Research Center of Coal and Coal Chemistry, Kemerovo, Russia*

*matus@catalysis.ru*

Solid solutions based on cerium oxide are successfully used as supports, promoters, and catalyst precursors [1–3]. Doping the ceria by aliovalent ($Ni^{2+}$, $Mg^{2+}$, $Gd^{3+}$, $La^{3+}$, $Al^{3+}$), isovalent ($Zr^{4+}$, $Si^{4+}$, $Ti^{4+}$) or aliovalent/isovalent ($Pr^{3+/4+}$, $Tb^{3+/4+}$, $Mn^{2+/3+/4+}$) dopants provide directed regulation of crystal structure and morphology, thermal stability, surface basicity, concentration of oxygen vacancies and mobility of oxygen. As a consequence, the functional properties of the $CeO_2$-based solid solution are finely tuned, making it a very convenient nanomaterial. The search for new compositions of materials and methods for their synthesis to obtain catalysts with improved anti-coking and anti-sintering properties is topical.

This work is devoted to synthesis and studying the genesis and structural properties of $(Ce_{1-x}Al_x)_{0.8}Ni_{0.2}O_y$ (x = 0, 0.2, 0.5, 0.8) materials for hydrogen production through methane reforming processes. The oxides were obtained by a modified Pechini method followed by heat treatment under various conditions (gas medium: inert, oxidizing, reducing; temperature 300–900°C). The materials were characterized using X-ray fluorescence analysis, thermal analysis, $N_2$ adsorption, ex situ and in situ X-ray diffraction, Raman spectroscopy, high-resolution transmission electron microscopy, scanning electron microscopy, EDX analysis and temperature-programmed hydrogen reduction and tested in autothermal reforming of $CH_4$ and steam/$CO_2$ reforming of $CH_4$ reactions to produce $H_2$.

In was shown that solid solutions based on the cubic structure of cerium dioxide with a very fine crystallite size were formed after calcination in oxygen at 300–700°C. Both $Ni^{2+}$ and $Al^{3+}$ cations were inserted into the structure of cerium dioxide that led to a significant decrease in the size of crystallites (11→2.8 nm at x 0→0.5), an increase in the defectiveness of the material, and the formation of oxygen vacancies. Traces of highly dispersed NiO species were also formed. An increase in the calcination temperature of $(Ce_{1-x}Al_x)_{0.8}Ni_{0.2}O_y$ to 900°C leads to the destruction of the solid solution and the formation of a three-phase system, including cerium dioxide, nickel oxide, and a solid solution based on the spinel structure of aluminum oxide. The fraction of NiO increases with decreasing x. After treatment of solid solution in reducing medium at 600–800°C, exsolution from fluorite structure and reduction of $Ni^{2+}$

cations occur with formation of $Ni^o$ particles with 2–15 nm in size. The Ce-Al-O solid solution is retained only partially, aluminum oxide crystallites appear.

The optimal composition of the catalyst was chosen: $(Ce_{0.8}Al_{0.2})_{0.8}Ni_{0.2}O_y$ sample provides the highest $H_2$ yield (65% in ATR of $CH_4$ and 95% in steam/$CO_2$ reforming of $CH_4$ at 800°C) and stability against coking.

**Acknowledgement:** This work was supported by the Ministry of Science and Higher Education of the Russian Federation within the governmental order for the Boreskov Institute of Catalysis (project AAAA-A21-121011490008-3).

**References:**

[1] M. Boaro, S. Colussi, A. Trovarelli, Front. Chem. 7 (2019) 28.
[2] E.V. Matus, S.D. Vasil'ev, I.Z. Ismagilov, V.A. Ushakov, M.A. Kerzhentsev, Z.R. Ismagilov, Chem. Sustain. Develop. 28 (2020) 403.
[3] L. Pino, C. Italiano, M. Lagana, A. Vita, V. Recupero, Catal. Sci. Technol. 10 (2020) 2652.

## OP-IA-05

# Size-Dependence of the Properties of Metal Nanoparticles: A Computational Density Functional Study

Laletina S.S.[1,2], Yudanov I.V.[2,3]

*1 – Institute of Chemistry and Chemical Technology SB RAS, Federal Research Center "Krasnoyarsk Science Center SB RAS", Krasnoyarsk, Russia*

*2 – Federal Research Center "G.K. Boreskov Institute of Catalysis SB RAS", Novosibirsk, Russia*

*3 – Institute of Solid State Chemistry and Mechanochemistry SB RAS, Novosibirsk, Russia*

*shkulepo@rambler.ru*

Size and shape of metal nanoparticles (NPs) determine their properties including the chemical activity. A detailed understanding if and how the reactivity of such NPs scales with size is crucial for the rational design of new nanosized catalysts with enhanced catalytic properties [1,2].

Using DFT calculations, the size dependence of CO adsorption as a probe was studied on $Pt_n$ clusters with n = 38−314 atoms. These computational results suggest the transition to a pronounced higher (compared to single-crystal) adsorption activity occurs for Pt NPs of size about 200 atoms (Fig. 1). To elucidate the structural effects connected to low-coordinated sites on particle edges and vertexes the concept of generalized coordination numbers was adapted to include of second coordination sphere [2].

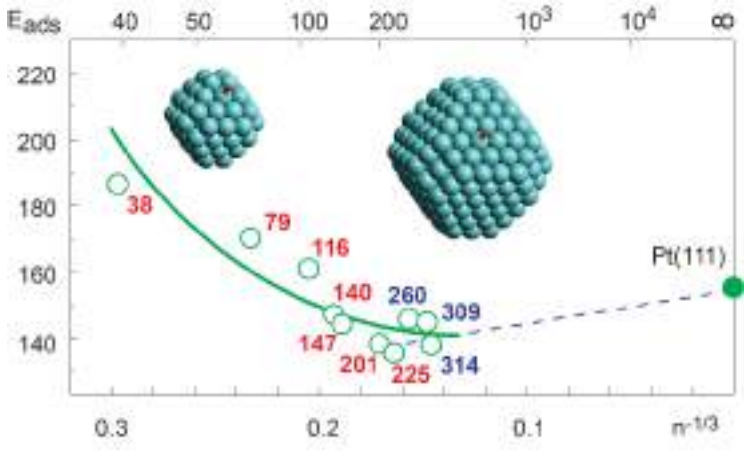


*Fig. 1. CO adsorption energies on the (111) terrace of Pt nanoparticles with n = 38-314 atoms and on the ideal Pt(111) surface. The NPs in the non-scaled region are colored red, and ones in the scaled area are colored blue.*

Further, the size and structure effects on Pt nanoparticles were studied using methanol dehydrogenation as a model surface reaction [3]. The effect of cluster morphology is manifested by higher adsorption energy of $COH_x$ intermediates on vertexes and edges of model nanoparticles compared to the close-packed terraces (Fig. 2). Moreover, due to the size effect, adsorption sites of $Pt_{79}$ nanoparticles (1.2 nm in diameter) exhibit considerably higher adsorption activity than the same sites of $Pt_{201}$ (1.7 nm). Thus, particles with a size of about 1 nm are shown to be more active compared to particles with a size of more 2 nm due to the

superposition of two effects: (i) higher surface fraction of low-coordinated adsorption sites, and (ii) higher activity of these sites.

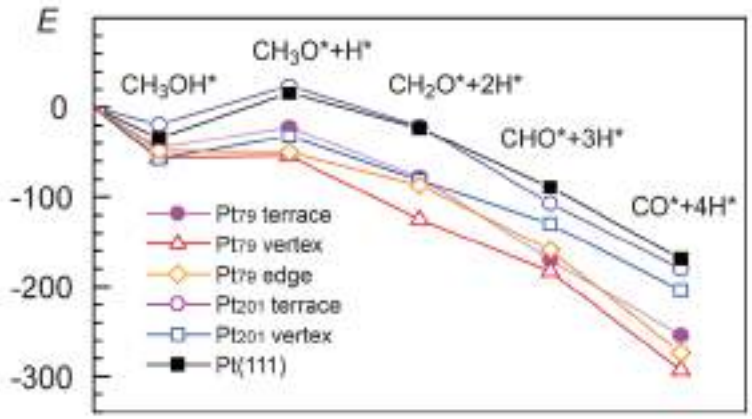


*Fig. 2. Energies of elementary reaction steps of methanol dehydrogenation (in kJ·mol$^{-1}$) on the regular Pt(111) surface and different sites of $Pt_{79}$ and $Pt_{201}$ NPs.*

Metal nanoparticles by their catalytic properties can differ from bulk metals. Therefore, we studied geometric deformations of metal nanoparticles $M_{201}$ (M = Ag, Au, Pd, Pt, Rh, and Ir) upon a relaxation and lattice contraction. Our results show that Pt and Au are unique, because they exhibit a larger structural deformation than other metals, which is pronounced for particles of less than 200 atoms. Ir and Rh are rigid and not malleable. While Ag and Pd possess intermediate elastic and plastic properties among the noble metals under study. The structural deformations induced by relaxation of the surface atoms stabilizes the nanoparticles and thus reduces the catalytic activity.

**Acknowledgement:** This work was performed within the framework of the State budget project 0287-2021-0012 for Institute of Chemistry and Chemical Technology of SB RAS.

We gratefully acknowledge access to the following computational resources: the Siberian Supercomputer Center (www.sscc.icmmg.nsc.ru), the Supercomputing Center of Novosibirsk State University (http://nusc.nsu.ru) and The Joint Supercomputer Center of the Russian Academy of Sciences (www.jscc.ru).

**References:**

[1] I. V. Yudanov, A. Genest, S. Schauermann, H. J. Freund, & N. Rösch. Nano Lett. 12(4) (2012) 2134.
[2] S. S. Laletina, M. Mamatkulov, E. A. Shor, V. V. Kaichev, A. Genest, I. V. Yudanov, & N. Rösch. J. Phys. Chem. C 121(32) (2017) 17371.
[3] S. S. Laletina, M. Mamatkulov, A. M. Shor, E. A. Shor, V. V. Kaichev, & I. V. Yudanov. Nanoscale 14 (2022) 4145.

## OP-IA-06

# Synthesis of Magnetically Recovered Co and Co@Pt Catalysts by Galvanic Replacement Method for Hydrolysis of $NaBH_4$

Ozerova A.M., Komova O.V., Prosvirin I.P., Bulavchenko O.A., Netskina O.V.
*Boreskov Institute of Catalysis, Novosibirsk, Russia*
*ozerova@catalysis.ru*

Due to the widespread use of mobile technology, small energy devices based on fuel cells are now being developed. Their operation requires compact hydrogen storage and generation systems. Sodium borohydride ($NaBH_4$) is one of the most promising hydrogen-generating materials due to its high hydrogen content (10.8 wt% or 112 $kg \cdot m^{-3}$), commercial availability, storage stability, and high water solubility (14.5 $mol \cdot L^{-1}$ at 25 °C) [1]. Its catalytic hydrolysis provides controllable and safe $H_2$ evolution in a wide temperature range (40…+60 °C).

$$NaBH4 + 4H2O \rightarrow NaB(OH)4 + 4H2\uparrow \quad \Delta H298K = 299\ kJ/mol$$

There is an intense search for active and stable catalysts for this process. Cobalt is given main focus because of its high catalytic activity and an acceptable price [2]. This study is devoted to the synthesis of magnetically recovered cobalt-based catalysts by the galvanic replacement method using aluminium micropowder as a template. This method has been actively investigated for catalyst preparation in recent times [3]. However, almost no studies on its use in the synthesis of catalysts for the hydrolysis of $NaBH_4$ have been published.

In the first stage, the galvanic replacement conditions for preparing cobalt-based catalysts were optimized. $Co(acac)_3$ was shown to be more promising as a cobalt precursor than $CoCl_2$ and $CoSO_4$. And in ethanol solutions, higher-activity catalysts are formed than in aqueous solutions. Sonication significantly reduces synthesis time. According to elemental analysis, XRD, and SEM, the particles formed have an average size of 45 μm and are composed of an aluminium core covered by a metallic cobalt (hcp) shell with a thickness of ~3 μm (Fig. 1). It was shown that treatment of catalysts with NaOH solution allows one to remove aluminium residues and produce hollow shells of metallic cobalt (Fig. 1). This enabled an increase in catalytic activity of 1,8 times [4].

To improve catalytic properties, the hollow cobalt micro-shells were modified with a platinum layer through galvanic replacement in $H_2PtCl_6$ aqueous solution. XRD and SEM revealed a uniform $Pt^0$ distribution on the surface of cobalt (Fig. 1). The catalysts' magnetic properties make their separation from the reaction medium by magnet and subsequent reuse simple. It was also shown that Pt improves the stability of cobalt catalysts during storage. The addition of just 0,2 at% of Pt increases the catalytic activity by 1,6 times. The next addition of up to 19 at% of Pt leads to a linear activity increase of up to 5,2 times. The impacts of further increasing the platinum concentration are not as significant [4].

Synthesized catalysts provide stable hydrogen generation in reusability tests. $Pt_{0,2}Co_{99,8}$ shows an increase in catalytic activity of 34% after 10 cycles of testing in $NaBH_4$ hydrolysis and

washing off the deposited reaction by-products from the catalyst surface with $H_2O$. XPS data indicate that this is related to the activation catalysts under the action of $NaBH_4$ *in situ* with the formation of a highly active cobalt-boron-containing species [4].

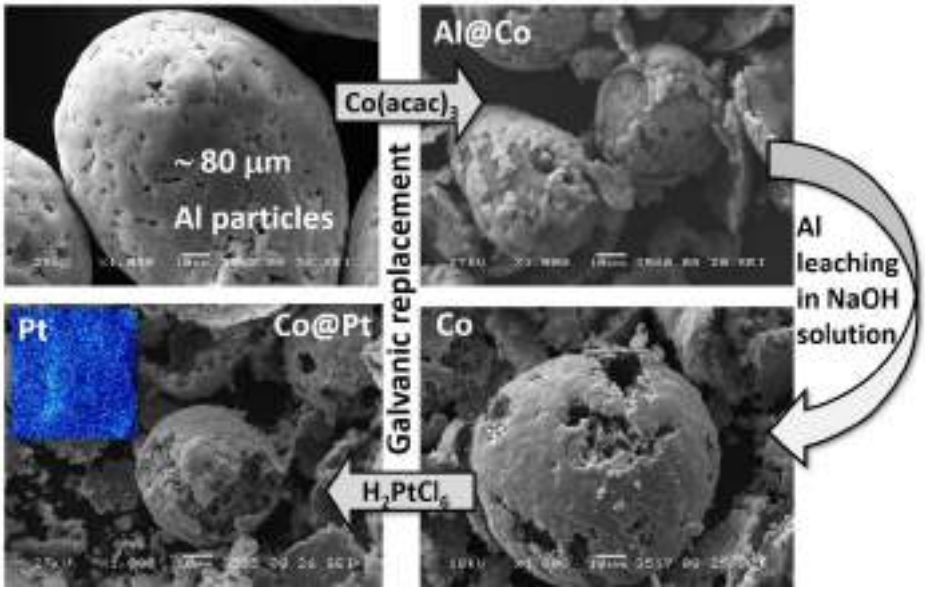


*Fig. 1. SEM images of initial aluminium powder and synthesized cobalt and platinum-cobalt catalysts.*

**Acknowledgement:** This work was supported by the Ministry of Science and Higher Education of the Russian Federation within the governmental order for Boreskov Institute of Catalysis, project AAAAA21- 121011390006-0.

**References:**

[1] H.N. Abdelhamid, Int. J. Hydrogen Energy 46 (2021) 726.
[2] V.I. Simagina, A.M. Ozerova, O.V. Komova, O.V. Netskina, Catalysts 11 (2021) 1.
[3] A.G.M. Da Silva, T.S. Rodrigues, S.J. Haigh, P.H.C. Camargo, Chem. Commun. 53 (2017) 7135.
[4] A.M. Ozerova, A.A. Skobelkina, V.I. Simagina, O.V. Komova, I.P. Prosvirin, O.A. Bulavchenko, I.L. Lipatnikova, O.V. Netskina, Materials 15 (2022) 3010.

## OP-IA-07

# Structural Features and Reduction – Induced Structural Evolution of $Pt/Ce_{0.75}Zr_{0.25}O_2$ Catalyst for Water Gas Shift Reaction

Pakharukova V.P., Potemkin D.I., Stonkus O.A., Saraev A.A., Gorlova A.M, Gladky A.Y.
*Boreskov Institute of Catalysis, Novosibirsk, Russia*
*verapakh@catalysis.ru*

Water–gas shift (WGS) reaction has received a great attention during the last years due to development fuel cell technology and need for CO removal from synthesis - gas. Ceria-based platinum catalysts are known as some of the most active in WGS [1, 2]. A high efficiency has been ascribed to the ability of the ceria – based supports to be easily and reversibly reduced as well as to stabilize fine Pt species. Despite a large number of studies on the activity of such catalysts, there is little information about their structural organization and structure of Pt species. High dispersion of Pt species complicates their structural diagnostics.

This work was devoted to comprehensive study on structural organization of $Pt/Ce_{0.75}Zr_{0.25}O_2$ (5 wt.% Pt) catalyst. A wide range of methods for structure diagnostics were used: X-ray diffraction (XRD) studies, atomic pair distribution function (PDF) analysis and high resolution electron microscopy (HRTEM) studies. The structural evolution of the catalyst at standard activation in $H_2$ atmosphere was studied by in situ XRD, pseudo in situ X-ray photoelectron spectroscopy (XPS) and results were correlated with the data of $H_2$-TPR study.

The HRTEM data showed that the catalyst contains platinum-containing clusters of 0.5 -1 nm in size as well as atomic - scale Pt species. PDF analysis was used to probe atomic arrangement in the Pt species. The PDF results revealed formation of oxide clusters with structure similar to PtO oxide and existence of metal-support interaction (MSI) with fixation Pt ions in the square planar oxygen coordination on the (100) $Ce_{0.75}Zr_{0.25}O_2$ facet. Similar MSI was recently reported for Pt-$CeO_2$ catalysts obtained by coprecipitation [3].The formation of metallic $Pt^0$ particles was detected in the catalyst treated under $H_2$ atmosphere or WGS reaction conditions. Pseudo in-situ XPS, in-situ XRD and $H_2$-TPR studies of the catalyst during its heating under $H_2$ atmosphere revealed that platinum oxide clusters are easily reduced at low temperatures (25 -75$^o$C). Formation of metallic $Pt^0$ particles was shown to induce partial reduction of $Ce_{0.75}Zr_{0.25}O_2$ oxide via hydrogen spillover. The revealed MSI and synergism of redox properties of the $Pt/Ce_{0.75}Zr_{0.25}O_2$ system is believed to have significant impact on the catalytic performance in WGS reaction.

**Acknowledgement:** This work was supported by the Russian Science Foundation, grant 21-73-20075.

**References:**

[1] T. Bunluesin, R.J. Gorte, G.W. Graham, Appl. Catal. B Environ. 15 (1998) 107.
[2] C.I. Vignatti, M.S.Avila, C.R. Apesteguía, T.F. Garetto, Catal. Today 171 (2011) 297.
[3] E.A. Derevyannikova, T.Y. Kardash, A.I Stadnichenko, O.A.Stonkus, E.M. Slavinskaya, V.A. Svetlichnyi, A.I. Boronin, J. Phys. Chem. C 123 (2019) 1320.

## OP-IA-08

# Primary Alcohols as Hydrogen Donors in Ni-Catalyzed Transfer Hydrogenation

Philippov A.A., Nesterov N.S., Chibiryaev A.M., Martyanov O.N.
*Boreskov Institute of Catalysis, Novosibirsk, Russia*
*philippov@catalysis.ru*

Transfer hydrogenation (TH) is considered as one of the most promising alternative way of conventional hydrogenation. This method does not require using of molecular hydrogen which is replaced with small organic molecules, for example, lower aliphatic alcohols. These donors can be relatively easily produced from biomass [1], whereas, $H_2$ is mostly obtained from fossil resources [2]. Thus, TH significantly decreases environmental and technological risks specific for conventional hydrogenation. Our study discusses H-donor activity of $C_1$-$C_4$ alcohols in catalytic and catalyst-free TH of aromatic and oxygen-containing molecules.

Among many heterogeneous catalysts using in TH, Ni-based systems occupy the wide niche. Metal nickel nanoparticles demonstrate average activity compared to the noble metals, at the same time, price of Ni is much lower that makes this metal promising catalyst in the bulk processes, such as biomass or oil conversion [3,4]. Literature data show that heterogeneous Ni-based catalysts demonstrate excellent results in TH of secondary alcohols as H-donors [5,6], whereas, primary alcohols often remain low active or even inactive [5]. To understand this difference, which was not discussed in details in literature, we paid key attention to TH of primary alcohols over the different Ni catalysts, such as Raney nickel [7], supported Ni nanoparticles prepared by the deposition-precipitation [8] and the precipitation in supercritical antisolvent methods [9].

It has been demonstrated that the primary and secondary alcohols show comparable donor activity in catalyst-free TH with carbonyl compounds (Figure 1) [7,8], however, the reaction proceeds under hard conditions in sub- and supercritical alcohols. The catalyst addition results in faster transformations and higher activity of the secondary alcohols compared to the primary isomers. These results are in good accordance with the known literature data showing negative influence of primary alcohols on the performance of Ni-based catalyst in TH [3,5]. The samples of the catalysts before and after reaction were characterized with many physicochemical methods. It was found that using of the secondary alcohols almost does not affect catalyst properties. At the same time, after the experiments with MeOH, EtOH and 1-PrOH formation of nickel carbide was observed. This phase formation significantly decreases the catalyst performance because nickel carbide blocks metal nickel, which presence on the catalyst surface plays a crucial role in TH.

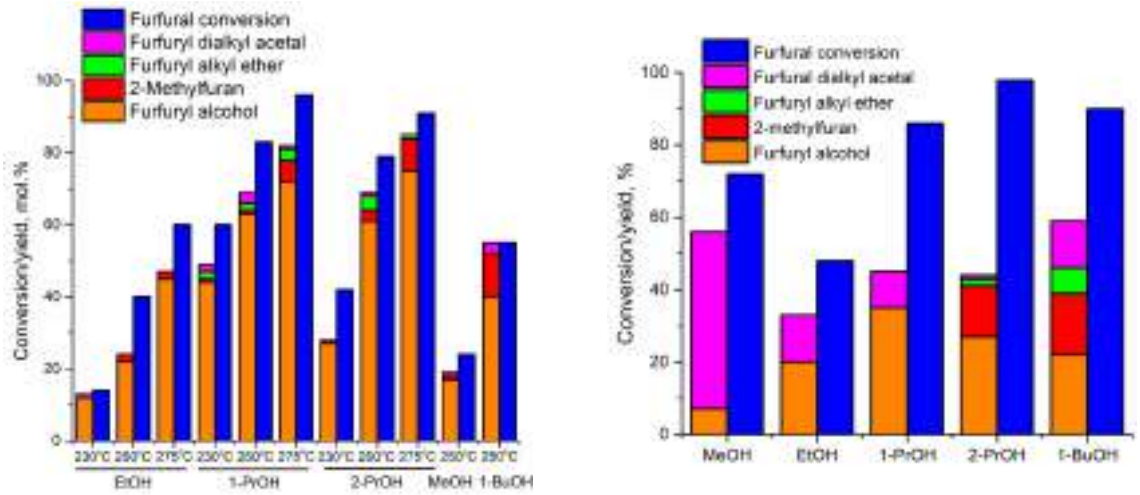


*Fig. 1. Transfer hydrogenation of furfural with $C_1$-$C_4$ alcohols under catalyst-free (left) and Ni/γ-$Al_2O_3$ catalyzed (right) conditions.*

**Acknowledgement:** This work was supported by the Russian Science Foundation, grant 21-13-00065.

**References:**

[1] T. Schubert, Bioprod. Biorefining (2020), 14, 845–878.
[2] B.C.R. Ewan, R.W.K. Allen, Int. J. Hydrogen Energy (2005), 30, 809–819.
[3] M.J. Gilkey, B. Xu, ACS Catal. (2016), 6, 1420–1436.
[4] S.S. Bello, C. Wang, M. Zhang, H. Gao, Z. Han, L. Shi, F. Su, G. Xu, (2021), 35, 10998–11016.
[5] X. Wang, R. Rinaldi, Energy Environ. Sci. (2012), 5.
[6] H. Shafaghat, Y.F. Tsang, J.K. Jeon, J.M. Kim, Y. Kim, S. Kim, Y.K. Park, Chem. Eng. J. (2020), 382, 122912.
[7] A.A. Philippov, A.M. Chibiryaev, O.N. Martyanov, J. Supercrit. Fluids (2019), 145, 162–168.
[8] A.A. Philippov, V.M. Anufrieva, V.P. Pakharukova, O.N. Martyanov, J. Supercrit. Fluids (2023), 193, 105815.
[9] A.A. Philippov, N.S. Nesterov, V.P. Pakharukova, O.N. Martyanov, Appl. Catal. A Gen. (2022), 643, 118792.

## OP-IA-09

# Ways of Dark $TiO_2$ Modification by Copper Nanoparticles to Increase Photocatalytic Activity in the Hydrogen Generation Reaction

Reutova O.A., Pimenov A.D., Fakhrutdinova E.D., Goncharova D.A., Kharlamova T.S., Svetlichnyi V.A., Vodyankina O.V.
*Tomsk State University, Tomsk, Russia*
*reutovaolesya@mail.ru*

Titanium dioxide is a well-known semiconductor, which is widely used for photocatalytic water and air purification, hydrogen generation, and also in solar cells. [1,2]. The widespread use of $TiO_2$ as a photocatalyst is due to its low toxicity, chemical and thermal stability and resistance to photocorrosion. The disadvantages of $TiO_2$ are its low quantum efficiency, as well as a relatively large band gap value (~3.2 eV), which limits absorption in the visible range, requires improving. The first drawback is overcome by obtaining nanosized particles (NPs), as well as by increasing the defective states in the structure. Defective states also leads to an increase in absorption in the visible region of the spectrum. It is possible to additionally increase the absorption range of materials based on $TiO_2$ by creating heterostructures with narrow-gap semiconductors. Previously, we have obtained highly defective dark $TiO_2$ via pulsed laser ablation (PLA) in water. The material has shown increased activity in the processes of decomposition of the dye Rhodamine B, phenol, and antibacterial properties [3]. When doped with platinum, it has shown high efficiency of hydrogen generation [4].

This work is devoted to the development of approaches for modifying dark $TiO_2$ with copper NPs, as an alternative to expensive noble metals, to increase its photocatalytic activity.

The first approach was based on doping with copper cations to create additional acceptor impurities in the structure of dark $TiO_2$. For this, individual colloids Ti_$H_2O$ and Cu_$H_2O$ were obtained by PLA of Ti (99,99%) and Cu (99,95%) metal targets in distilled water with using a Nd:YAG laser ($\lambda_{las}$ = 1064 nm, $E_{puls}$ = 150 mJ, $\tau_{puls}$ = 7 ns, f = 20 Hz). The colloids were mixed in a certain mass ratio, followed by ultrasonic treatment. Next, the colloids were dried and powders were annealed at a temperature of 400°C (sample with 0.5 wt % Cu-$TiO_2$). The second approach consisted in creating a type II heterojunction between semiconductors with different types of conductivity - dark $TiO_2$ (n-type) and $Cu_2O$ (p-type). For this, individual colloids were obtained by PLA method were dried. Dark $TiO_2$ powder obtained was annealed at 400°C ($TiO_2$ sample). Then, $TiO_2$ and uncalcined $Cu_2O$ powders were mixed and activated by grinding in an agate mortar (sample 0.5 wt.% $Cu_2O$-$TiO_2$). The resulting samples were characterized by X-ray diffraction, low temperature nitrogen, UV-vis spectroscopy.

Both modified materials consisting of a mixture of titanium dioxide modifications: anatase, rutile and brookite. Anatase is the dominant phase (~85%). No phases of Cu metal NPs and its oxides were detected in XRD. It is assumed that during doping, copper cations are able to introduce is introduced into the crystal lattice of $TiO_2$, since $Cu^+$ and $Ti^{4+}$ have close ionic radii [5,6]. When creating the heterostructure, the $Cu_2O$ phase was not detected, since

the amount of introduced oxide is 0.5 wt. % less sensitivity of the XRD method. The data of low-temperature nitrogen adsorption showed that, upon doping, the specific surface area of the sample is 105 $m^2/g$, and after mechanical activation, it is 90 $m^2/g$, respectively.

Figure 1a shows the absorption spectra of the obtained materials in comparison with the initial dark $TiO_2$. Doping with $Cu^+$ does not lead to significant changes in the absorption, while the creation of a heterostructure increases the absorption in the visible region of the spectrum due to the absorption of $Cu_2O$.

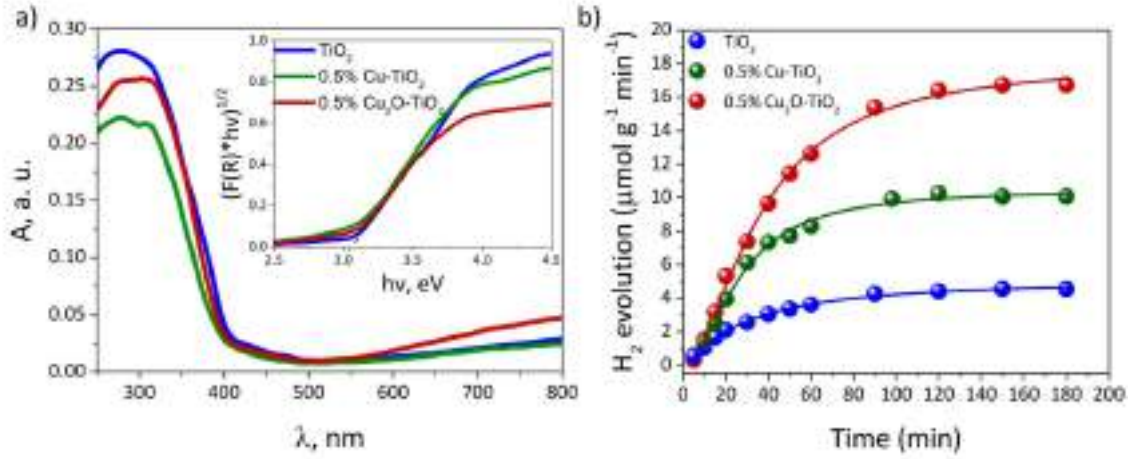


*Fig. 1. Results of (a) UV-vis spectroscopy and (b) photocatalytic hydrogen generation.*

The photocatalytic activity of the materials was studied in the hydrogen generation reaction (HER) in the presence of glycerol (20 wt.%) as a sacrificial reagent in a flow reactor under LED irradiation ($\lambda_{fl}$=375 nm). Doping with copper leads to an increase in hydrogen evolution by 2 times in comparison with the activity of the initial dark $TiO_2$, and the creation of a type II heterostructure by 4 times (Figure 1b). The results of the study showed that copper nanoparticles exhibit an activity close to that of platinum in the reaction of photocatalytic generation of hydrogen.

**Acknowledgement:** This work was supported by the Russian Science Foundation, grant 19-73-30026, https://rscf.ru/project/19-73-30026.

**References:**

[1] Z. Li, S. Wang, J. Wu, W. Zhou, 156 (2022) 111980.
[2] H. Mao, F. Zhang, M. Du, L. Dai, Y. Qian, H. Pang, Ceram. Int. 47 (2021) 25177–25200.
[3] E. Fakhrutdinova, A. Shabalina, M. Gerasimova, A. Nemoykina, O. Vodyankina, V. Svetlichnyi, Mater., 13 (2020) 2054.
[5] E. Fakhrutdinova, O. Reutova, L. Maliy, T. Kharlamova, O. Vodyankina, V. Svetlichnyi, Mater., 15 (2022) 7413.
[5] Q. Hu, J. Huang, G. Li, Y. Jiang, H. Lan, W. Guo, Y. Cao, Appl. Surf. Sci., 382 (2016) 170-177.
[5] M. O. Segovia-Guzmán, M. Román-Aguirre, J. Y. Verde-Gomez, V. H. Collins-Martínez, G. Zaragoza-Galán, V. H. Ramos-Sánchez, Cat. Today, 349 (2020) 88-97.

## OP-IA-10

# Specifics of Particles Morphology and Structural-Phase Properties of Nanostructured FePt and CoPt

Zakharov Yu.A.[1], Popova A.N.[1], Pugachev V.M.[1,2], Zakharov N.S.[1], Tikhonova I.N.[1], Russakov D.M.[1], Dodonov V.G.[1], Yakubik D.G[1,2], Ivanova N.V.[2], Lobanov A.A.[2], Sadykova L.R.[1]

*1 – Federal Research Center of Coal and Coal Chemistry SB RAS, Kemerovo, Russia*

*2 – Kemerovo State University, Kemerovo, Russia*

*ZakharovYA@iccms.sbras.ru*

The synthesis and study of the properties of FePt and CoPt nanosized and nanostructured systems (MePt) is one of the well-known "flashpoints" in the materials' science of bimetallic nanoalloys, because of the complexity of the phase diagram (PhD) of these systems and the great differences in the reduction potential of components (fundamental aspect) on the one side, and as well as the uniqueness of the magnetic characteristics of intermetallic compounds (IC) of equimatomic compositions with a highly ordered structure $L1_0$, which determines their high prospects in nanomagnetic engineering, magneto-optics, when creating media with ultrahigh information recording density (practical aspect), on the other hand.

To solve these problems, we used a set of methods of X-ray diffractometry (SAXS, XRD, including in situ at elevated temperatures, with precise determination of lattice parameters and determination of phase compositions based on it), microscopy (SEM, TEM HR and SAED), thermal analysis (coupled with differential scanning calorimetry, quadrupole mass spectrometry of volatile decomposition products), stripping voltammetry, adsorption and temperature-programmed oxidation of samples. In addition, we involve the calculation of the different structures nanoclusters stability by the method of molecular dynamics.

We found several non-trivial specifics of morphology and structural-phase properties in the work result, such as: 1) blockiness and core-shell type structures of nanocrystals of solid solutions rich in Pt, 2) the existence of upper limits of solubility (ULS) of Fe and Co in Pt during the synthesis of nanosystems and when they heated, 3) formation of two types of nanophases undetectable by X-ray diffraction, namely solid solutions rich in Me and (or) IC (Me3Pt) in case when Me concentrations are higher than the ULS and when they heated; 4) the formation of several types of different compositions of bi-phase regions when MePt nanosystems heated. Based on the results of experiments, models of these effects and processes are proposed.

As a result, we've developed a generalized scheme of the formation of intermetallic compounds that correspond to the phase diagram when MePt systems heated, including those that are practically relevant intermetallic compounds of equiatomic composition with a tetragonal structure L10.

The study was carried out using the equipment of the Kemerovo Regional Center for Collective Use of FRC CCC SB RAS as part of the state task of FRC CCC SB RAS 2021 - 2023 (number EGISU 121031500211-9).

## OP-IA-11

# Synthesis of Nanoparticles and their Modification in Solutions of Anionic Surfactants for Obtaining Stable Dispersions

Zelentsov D.O.[1], Petrova Yu.Yu.[1], Korobkin A.V.[1], Ivanova A.A.[1,2], Cheremisin A.N.[1,2], Shanenkov I.I.[3,4], Sivkov A.A.[4]

*1 – Surgut State University, Surgut, Russia*

*2 – Skolkovo Institute of Science and Technology, Moscow, Russia*

*3 – Tyumen State University, Tyumen, Russia*

*4 – Tomsk Polytechnic University, Tomsk, Russia*

*zelentsov_do@surgu.ru*

Chemical enhanced oil recovery (cEOR) methods are actively applied for the development of unconventional hydrocarbon reservoirs, which are characterized by a high temperature and ultra-low permeability. In the past decades, mixtures of nanoparticles (NPs) and surfactants are attracting researchers' interest from around the world for cEOR development. Nanoparticles modified with surfactants are able to adsorb at the oil-water interface, resulting in interfacial tension (IFT) reduction. In addition, these composites can change the wettability of the reservoir rocks from hydrophobic (oil-wet) to hydrophilic (water-wet), which leads to oil recovery increase [1]. Moreover, the stability of NPs is significantly higher than that of surfactants at higher temperatures and salinities [2]. Therefore, the purpose of this work was to obtain modified NPs with an anionic surfactant that will be stable under typical reservoir conditions, and then to study its main properties.

In the present work, we used $SiO_2$ and $TiO_2$ NPs (Sigma-Aldrich); $Al_2O_3$ synthesized by sol-gel method [3]; β-$Bi_2O_3$ obtained by thermal decomposition of $BiC_2H_4(OH)$ [4]; graphite-like carbon materials (CM) obtained by plasma plasma treatment of asphaltenes [5]; and NPs obtained by plasmodynamic synthesis [6]: $TiO_2$, $Al_2O_3$ and iron oxide mixture. Sodium dodecyl sulfate (SDS, PanReac) was used as an anionic surfactant.

Modification of $SiO_2$ and $TiO_2$ nanoparticles (Sigma-Aldrich) was performed in nonmicellar (5 mmol/L) and micellar (10 and 50 mmol/L) SDS solutions. The obtained samples were separated from solution by centrifugation and characterized by FT-IR spectroscopy, differential thermal analysis (DTA) and X-ray fluorescence analysis (XRF). The stability of dispersions of modified NPs in water as well as $SiO_2$ sols was studied by laser diffraction, tensiometry, dynamic light scattering (DLS) and electrophoretic light scattering (ELS). To select nanoparticles, the stability of their dispersions in water and 5, 10, and 50 mmol/L SDS solutions was studied by laser diffraction. The effect of pH on the aggregation of $TiO_2$-NPs in SDS solution was investigated by DLS and ELS using phosphate buffer for 4.5-9.0 pH, $H_3PO_4$ solutions for pH<4.0 and NaOH solutions for pH>9.0.

The characterization of the modified nanoparticles (NPs-SDS) by FT-IR spectroscopy, DTA and XRD showed that adsorption of SDS increased with increasing surfactant concentration in the $TiO_2$-NPs dispersion and decreased in the $SiO_2$-NPs dispersion. This can be explained by

the different charge density on the NPs surface. Laser diffraction and DLS showed that with the increase of SDS concentration in the nanoparticle modification solution from 5 to 50 mmol/L, the size of the aggregates increased, which can be explained by hydrophobic interactions of SDS molecules adsorbed on the NPs surface. The interfacial tension at the dispersion of NPs-SDS/*n*-decane interface measured by the rotating drop method also increased. The zeta potential of the investigated sols and NPs-SDS dispersions characterized their low stability, which was consistent with the particle size distribution and interfacial tension. Consequently, $TiO_2$-NPs-SDS tended to aggregate and form low stable dispersions. $SiO_2$-NPs in SDS solutions form more stable sols, but after separation and drying, $SiO_2$-NPs-SDS re-disperses poorly.

Therefore, it is crucial to select nanoparticles forming stable sols in the presence of SDS. The stabilizing effect of SDS micellar solutions in dispersions of β-$Bi_2O_3$, CM and $TiO_2$, obtained by plasmodynamic synthesis (average size of nanoparticle aggregates from 0.5 to 6.0 μm, respectively) was found, which is promising for research of nano-surfactant composites and their use in cEOR.

A study of the effect of pH on the NPs aggregation by DLS showed that small aggregates (up to 225 nm) are formed at 5-7 pH. In strongly acidic (pH<2.0) and strongly alkaline (pH>11.0) media, the size of nanoparticles aggregates increase (up to 900 nm). It was shown by the ELS that 0.01 wt.% aqueous dispersions of $TiO_2$-NPs had a zeta potential of less than -30 mV over a wide range of 4-12 pH, which characterized them as stable. Meanwhile, the dispersions of nanoparticles in SDS solutions showed high stability even in an acidic pH<4.0 environment.

Thus, the β-$Bi_2O_3$ and $TiO_2$ nanoparticles obtained by plasmodynamic synthesis as well as graphite-like carbon materials obtained by plasma treatment of asphaltenes were selected in this work as the most promising for use in cEOR for low-permeability reservoirs. It was shown that $TiO_2$-NPs at 5-7 pH form stable nanosols, which can be used for their subsequent modification in anionic surfactant solutions.

**Acknowledgement:** This work was supported by the Government of the Khanty-Mansi Autonomous Okrug - Yugra (order from 04.09.2020 № 10-P-1308) and the Russian Science Foundation (№ 22-13-20016, https://rscf.ru/project/22-13-20016/).

**References:**

[1] M. Almahfood, B. Bai, J. Pet. Sci. Eng. 171 (2018) 14.
[2] A.E. Bayat, R. Junin, A. Samsuri et al., Energy Fuels 28 (2014) 11.
[3] A. Khazaei, S. Nazari, G. Karimi et al., Int. J. Nanosci. Nanotechnol. 12 (2016) 7.
[4] K.V. Mishchenko, K.B. Gerasimov, Y.M. Yukhin, Mater. Today Proc. 25 (2020) 3.
[5] A.Ya. Pak, P.V. Povalyaev, E.V. Franzina et al., Bull. TPU. Geo Assets Eng. 333 (2022) 12.
[6] A. Sivkov, Y. Vympina, A. Ivashutenko et al., Ceram. Int. 48 (2022) 11.

## OP-IA-12

# Soft Modification of La-Based Perovskite Crystalline Structure and its Influence on Catalytic Activity in Methane Oxidation

Gerasimov E.Yu.[1], Kapishnikov A.V.[1,2], Smal E.A.[1], Simonov M.N.[1]
*1 – Boreskov Institute of Catalysis, Novosibirsk, Russia*
*2 – Novosibirsk State University, Novosibirsk, Russia*
*gerasimov@catalysis.ru*

Solid solutions with a perovskite structure with the general formula $ABO_3$ are intensively studied due to the structural features of the crystal lattice, which makes it quite easy to embed various chemical elements into its structure. For example, lanthanum–based materials at high temperatures have mixed ionic and electronic conductivity and can be used in high-temperature electrochemical devices. Solid solutions based on $LaMnO_3$ can be used as catalysts for gas purification processes, including in reactions of complete oxidation of light hydrocarbons.

The catalytic properties of the solid solutions strongly depend on the synthesis methods and the degree of cations substitution. For example, an enhancement of the Ca2+ cations content increases the mobility of O2- anions in the system, which positively affects the catalytic activity of samples, but reduces their thermal and structural stability.

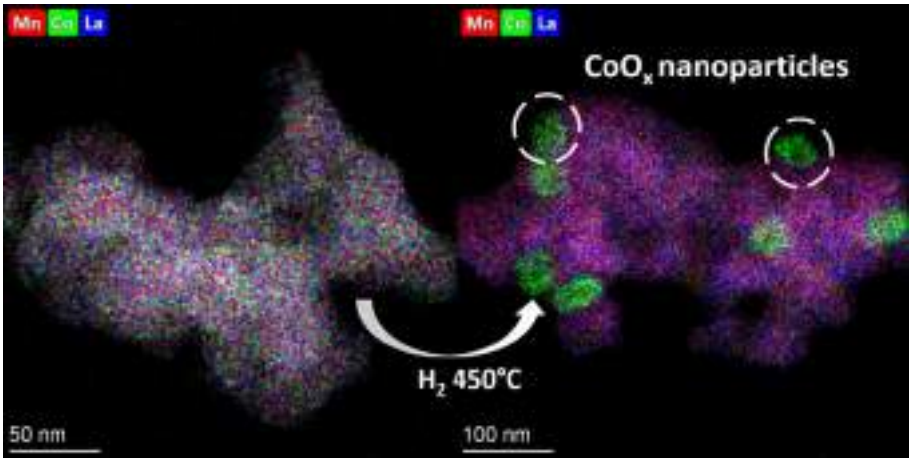


*Fig. 1. EDX mapping of perovskite particles before and after modification in hydrogen*

On the other hand, the presence of transition metal oxide nanoparticles on the surface of the perovskite phase can significantly increase the catalytic activity in methane decomposition reactions. However, at high temperatures, the sintering process of these nanoparticles is possible. One of the ways to prevent sintering of these oxides on the surface of the perovskite phase is to form these nanoparticles from the perovskite structure.

The purpose of this work was to study the processes of allocation of transition metal cations on the surface of particles directly from the perovskite phase as well as the determination of the influence of the perovskite modified structure on the reaction of complete oxidation of methane.

**Acknowledgement:** This work was supported by the Russian Science Foundation, grant 23-23-00535.

## OP-IA-13

# Effect of Pore Size on the Activity of an Immobilized Enzyme in Mesoporous Magnetic Silica

Sulman A.M.[1], Tikhonov B.B.[1], Grebennikova O.V.[1], Sidorov A.I.[1], Stadolnikova P.Yu.[1], Doluda V.Yu.[1], Molchanov V.P.[1], Matveeva V.G.[1,2]

*1 – Tver State Technical University, Tver, Russia*

*2 – Tver State University, Tver, Russia*

*matveeva@science.tver.ru*

Immobilized enzymes (native enzymes fixed on/in solid supports) received considerable attention in the field of biocatalysis due to improved thermostability and easier separation of the catalysts as well as possible repeated use [1, 2]. As supports for immobilized enzymes, porous materials such as mesoporous silicas play an important role, allowing for larger enzyme loading than solid or microporous supports, variation of pores sizes, a more robust reaction temperature and pressure range compared to native enzymes, etc. [3, 4].

In our preceding work, it was established that an impregnation of mesoporous silica (6 nm pores) with Fe(III) nitrate followed by thermal decomposition at 200 ◦C in the presence of ethylene glycol results in the formation of magnetite (Fe3O4) NPs in the silica pores [5]. The structure of magnetite NPs was unambiguously validated by X-ray powder diffraction (showing spinel) and X-ray photoelectron spectroscopy (showing magnetite). Such a magnetic support was utilized for stabilization of catalytic NPs or a covalent attachment of GOx [5]. The focus of the work presented here is to study the influence of the pore size of mesoporous magnetic silica on loading of GOx and its activity after immobilization on the amino functionalized silica surface via glutaraldehyde linkage. Moreover, the idea here is to compare pores which cannot accommodate GOx because they are too small (~6 nm) with those, whose size is dramatically larger than the GOx hydrodynamic diameter (7.6 nm), i.e., ~15 nm (Scheme 1).

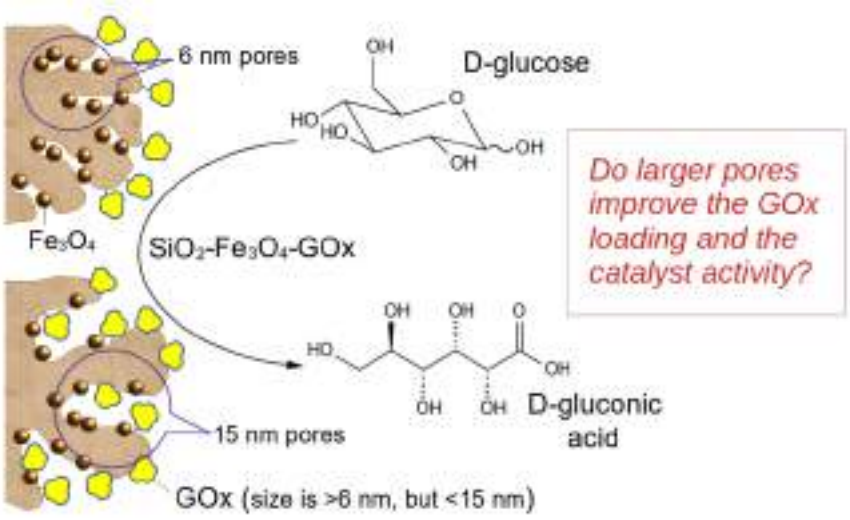


*Fig. 1. Schematic representation of the magnetic biocatalysts based on mesoporous silica with 6 nm and 15 nm pores and of the reaction they catalyzed*

## OP-IA-13

We synthesized two magnetically recoverable biocatalysts based on mesoporous silica with 6 nm and 15 nm pores to study the influence of a pore size on the enzyme loading and biocatalytic activity of 6 nm-$SiO_2$-$Fe_3O_4$-GOx and 15 nm-$SiO_2$-$Fe_3O_4$-GOx. The choice of silica supports with the above pores was determined by size of GOx, whose hydrodynamic diameter is 7.6 nm. Thus, in the case of the 6 nm-$SiO_2$ support, enzyme molecules can be located only outside the pores, while in the case of 15 nm-$SiO_2$, the GOx molecules can be immobilized inside the pores presumably without loss of conformation integrity. This results in several crucial outcomes for 15 nm-$SiO_2$-$Fe_3O_4$, such as the higher loading capacity, remarkable relative activity as well as its excellent stability in the repeated use. These factors combined with facile magnetic separation and commercially available parent silica supports make this biocatalyst promising for successful commercialization.

**Acknowledgement:** This work was supported by the Russian Science Foundation, project 21-19-00192.

**References:**

[1] Arsalan A., Younus H. Int J Biol Macromol. 118 (2018) 1833.
[2] Bilal M., Ashraf S.S., Ferreira L.F.R., Cui J., Lou W.-Y., Franco M., Iqbal H.M.N. Int. J. Biol. Macromol. 162 (2020) 1906.
[3] Mokhtar N.F., Rahman R.N.Z.R.A., Noor N.D.M., Shariff F.M., Ali M.S.M. Catalysts 10 (2020) 744.
[4] Zhao F., Zhang H., Zhang Z., Liang Y. Microporous Mesoporous Mater. 323 (2021) 111227.
[5] Jaquish R., Reilly A.K., Lawson B.P., Golikova E., Sulman A.M., Stein B.D., Lakina N.V., Tkachenko O.P., Sulman E.M., Matveeva V.G., Bronstein L.M. Int. J. Biol. Macromol. 120 (2018) 896.

## OP-IA-14

# Spin-Coating of Thin Graphene Oxide Films from Multicomponent Dispersions

Komarov I.A.[1,2], Danilov E.A.[1]
*1 - JSC Research Institute «Graphite», Moscow, Russia*
*2 - GraphApta LLC, Moscow Region, Russia*
*master_kom@mail.ru*

Carbon nanomaterials, especially graphene derivatives that include graphene oxide (GO) and reduced graphene oxide (rGO) are very promising materials for different applications in flexible electronics [1], chemical and biological sensors [2], drug delivery platforms [3] etc. Highly uniform thin films can be formed on polymer substrates via different methods but spin-coating [4] and spray coating [5] are one of the most perspective for at least small batch production. The significant problem for both abovementioned methods is the poor wettability of polymer substrates by commercially available GO suspensions that are usually water based. This limitation can be overcome by mechanical or plasma pre-treatment, but in case of need of nanometer-thick films those cannot be applied. On the other hand, wettability can be improved by the dispersion's properties themselves.

In the current study, we tried to introduce additional organic components to the water-based GO suspension. According to the data obtained from [6], GO can form long-time stable dispersions in some organic solvents (besides water) like dimethylformamide (DMF), N-methylpyrrolidone (NMP). On the other hand, it is known that dimethylacetamide (DMA) is a good dispersion media for functionalised carbon nanotubes [7]. For the multicomponent mixed dispersion media we used such components as DMA and Tamiya lacquer thinner (ethyleneglycol, butylglycol, methylisobutylketone) (LT) at different concentrations and ratio. We investigated wettability of these multicomponent dispersions (fig.1) analysed such properties of spin-coated films as morphology, transparency, and Raman and IR spectra.

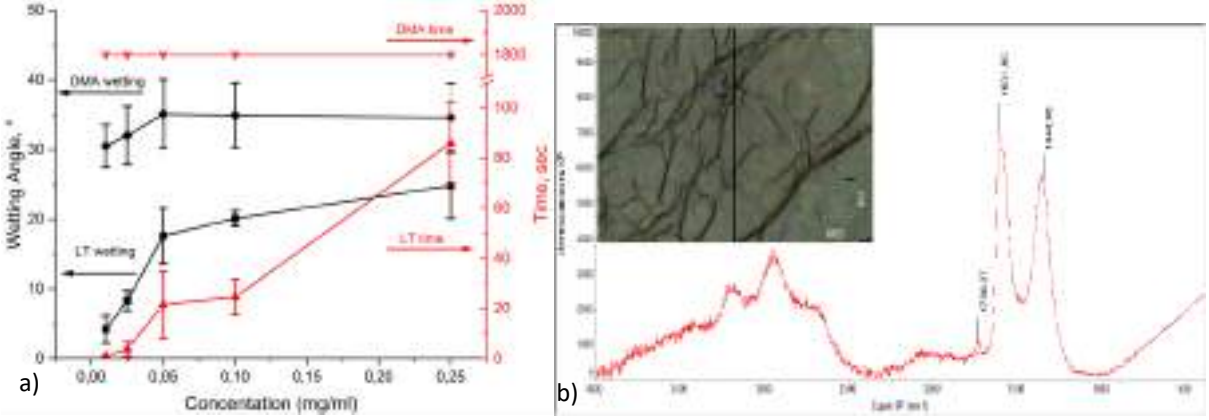


*Fig. 1. Dependence of wetting angle and drying time on the type of the additional component and GO concentration (a); Raman spectra and morphology of deposited GO films.*

Dependence of wetting angle on the additional organic component of the dispersion, GO concentration and drying time is shown in the figure 1a. Initial GO water suspension wetting angle was found as 41,6 °. From these data, one can see that dispersion with LT as additional component has two shoulders with approximate linear dependence of wetting angle (under and above 0,05 mg/ml concentration). Drying time on the concentration dependence can be approximated with linear function. This result, on the one hand, means that we reached basic goal to reduce wetting angle. On the other hand, drying time is relatively low and less than typical time of s[in-coating process. This mean that LT as additional component will be perspective for spray coating of large area GO films.

Dispersion with DMA on the contrary did not show strong dependence of the wetting angle or time on the GO concentration. This mixture also showed decrease in wetting angle, but the decrease is much lower than in case of LT. We suppose that in case of DMA addition the dispersion properties are primarily affected by water. Low reduction of wetting angle and drying time in range of tenth minutes confirm the abovementioned fact. Drying time in range of tenth of minutes means that DMA-containing dispersion will be better for spin-coating deposition due to the characteristic time of spin-coating process (few minutes). Drying time in the case of DMA addition is at least 15 times more than in case of LT.

Analysis of morphology images and Raman spectra (fig. 1b) shows that concentration of GO under the 0,05 mg/ml leads to the island-type film formation. Difference is that in case of LT we observe islands as mixture of many small flakes, whereas in case of DMA islands are relatively large individual multilayered GO flakes. Over the 0,05 mg/ml concentration films are uniform. Raman spectra and band ratio are classic for thin GO films [8]. This result was also confirmed by morphology observations on SEM.

In this work, we showed the possibility to decrease and control wetting angle on GO suspension/PET interface by adding organic components to the commercially available GO water-based suspension. We found out that addition of the dilutant for enamel paints (LT) leads to the formation of highly volatile dispersion that will be perspective for spray coating. Addition of DMA leads to the formation of much lower volatile dispersion that may be efficiently used for spin-coating deposition due to the at least 15 times larger drying time and relatively low wetting angle.

**References:**

[1] Gilshteyn E. P et al. ACS Appl. Mater. Interfaces. 2019, 11, 27327–27334.
[2] Freddi S et al. Advanced Healthcare Materials. 2020, 9, 2000377.
[3] Oliveira A.M.L. et al. Nanomaterials. 2022, 12, 1149.
[4] Nguyen A.N. et al. Spin Coating and Micro-Patterning Optimization of Composite Thin Films Based on PVDF. Materials. 2020, 13, 1342.
[5] Struchkov N.S. et al. Fullerenes Nanotubes and Carbon Nanostructures. 2020, 28, 214-220.
[6] Konios D et al. Journal of Colloid and Interface Science. 2014, 430, 108-112.
[7] Komarov I. A. et al. Biomedical Engineering. 2018, 51, 377-380.
[8] Jiang-Bin Wu et al. Chem. Soc. Rev. 2018, 47, 1822.

## OP-IA-15

# Molecular Engineering of Exchangeable Liquid Crystal Elastomers toward Body-Temperature Shape-Morphing Materials

Lee J.-H.[1], Kim D.-G.[2], Ahn S.-k.[1]

*1 – School of Chemical Engineering, Pusan National Univ., Busan, Korea*

*2 – Advanced Materials Division, Korea Research Institute of Chemical Technology, Daejeon, Korea*

*jin-hyeong@pusan.ac.kr*

Liquid crystal elastomers (LCEs) combine both the anisotropic properties of rod-like mesogens and a loosely cross-linked polymer network. Acting together, molecularly aligned LCEs can exhibit unique properties, such as muscle-like contraction along the liquid crystal director upon heating above nematic-isotropic transition temperature. Thus, LCEs are being widely adopted for novel engineering applications such as soft robotics, biomedical devices, and sensors.[1] In this study, we synthesized dynamically cross-linked LCEs capable of reprocessing and reprogramming, namely “exchangeable LCEs (xLCEs)”, by incorporating oligo(ether-thiourea) as crosslinkers. In particular, the impact of molecular structure and composition of LCE building blocks on the physical properties of the xLCEs was investigated. A structure-property relationship of xLCEs was developed, and an effective modulation in a broad range of actuation temperature (30-70 °C) which encompassing body heat temperature was demonstrated.

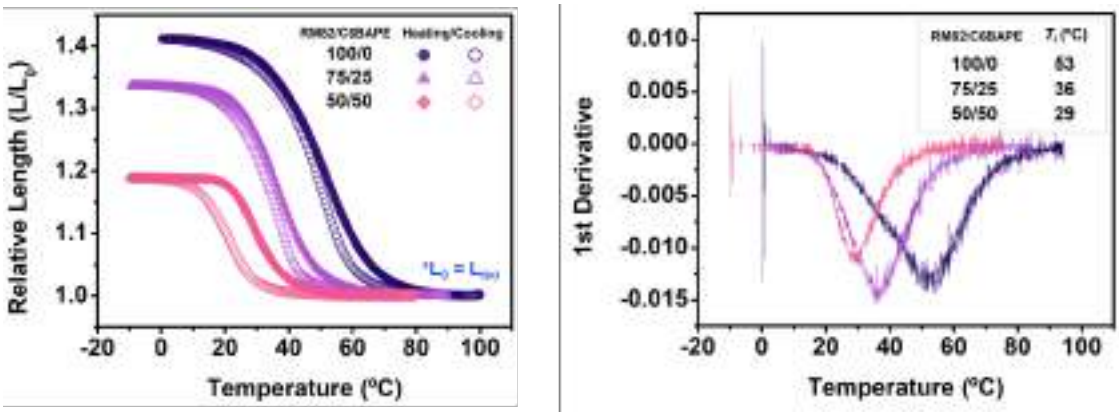


*Fig. 1. Isostress actuation results (left) and derivative of actuation length (right) for variable composition of LCEs.*

**Acknowledgement:** This work was supported by Basic Science Research Program and by BK21 Four program through the National Research Foundation funded by the Ministry of Education.

**References:**

[1] K. M. Herbert, H. E. Fowler, J. M. McCracken, K. R. Schlafmann, J. A. Koch, and T. J. White. Nat. Rev. Mater. 7 (2022) 23-83.

## OP-IA-16

# Synthesis and Characterization of PVDF-CFO Composite Films

Vorontsov P.A., Salnikov V.D., Ershov P.A., Omelyanchik A.S., Rodionova V.V.
*Immanuel Kant Baltic Federal University, Kaliningrad, Russia*
*pavel.voroncov.a@gmail.com*

Multiferroics can exhibit segmentelectricity, ferromagnetism, segment elasticity, and ferrothoroidal properties for a single phase. The coexistence of at least two ferroic properties, such as ferroelectric and ferromagnetic, in a composite magnetoelectric (ME) structure, has attracted attention because of the potency of such devices in various applications such as sensors, transducers, multistate memory devices, switching, and filters [1].

Among electroactive polymers, PVDF is a semi-crystalline polymer that has five crystalline phases: α, β, γ, δ, ε. The β-phase has a trans-conformation (TTT), where fluorine and hydrogen atoms are on opposite sides of the polymer chain structure. This structure exhibits the total characteristics of a nonzero dipole moment. The β-phase includes electroactive properties of the polymer and exhibits segmentelectric, piezoelectric, pyroelectric properties [1].

In this work, composite films of different thicknesses were fabricated and oha-characterized in terms of their structural, morphological, and magnetic properties. The PVDF-CFO composite films were synthesized by the doctor blade method and characterized by various methods including X-ray diffraction (XRD), Raman spectroscopy (RAMAN), scanning electron microscopy (SEM), scanning atomic force microscopy, and vibrating sample magnetometry analysis.

Cobalt ferrite nanoparticles were synthesized by the hydrothermal method. The hydrothermal method allows controlling the size of CoFe2O4 particles only by adjusting the reaction time at low temperatures, which is also vital for obtaining appropriate values of saturation magnetization M s and coercivity H c for its practical application [2].

The results of investigations of synthesized composite films showed the successful synthesis of composite films with a uniform dispersion of CoFe2O4 particles in the PVDF matrix. Moreover, the composite films showed improved magnetization and thermal stability compared to pure PVDF films, making them suitable for potential applications in magnetic sensors, energy harvesting devices, and magnetic storage devices. Also, composite films of polyvinylidene fluoride (PVDF) and cobalt ferrite (CFO) have ferromagnetic and piezoelectric properties, which makes them attractive for various biomedical applications, including biosensors, drug delivery, and tissue engineering.

**References:**

[1] Koç, M., Dönmez, Ç.E.D., Paralı, L. et al. Piezoelectric and magnetoelectric evaluations on PVDF/CoFe2O4 based flexible nanogenerators for energy harvesting applications. J Mater Sci: Mater Electron 33, 8048–8064 (2022). https://doi.org/10.1007/s10854-022-07956-w
[2] Liu, M., Lu, M., Wang, L. et al. Mössbauer study on the magnetic properties and cation distribution of CoFe2O4 nanoparticles synthesized by hydrothermal method. J Mater Sci 51, 5487–5492 (2016). https://doi.org/10.1007/s10853-016-9853-3

## OP-IA-17

# Dynamic- and Mechanical-Damping in Liquid Crystal Elastomers with Slidable Polyrotaxane Network

Choi S.[1], Seo J.-H.[2], Ahn S.-k.[1]

*1 – School of Chemical Engineering, Pusan National University, Busan, Korea*

*2 – Department of Materials Science and Engineering, Korea University, Seoul, Korea*

*sbchoi@pusan.ac.kr*

A new class of liquid crystal elastomer (LCE) incorporating polyrotaxane-based slidable cross-linkers (PR-LCE) was synthesized for the first time [1]. In particular, we investigated the damping performance of the PR-LCEs using dynamic and mechanical energy dissipation method. Interestingly, both the soft elasticity and mechanical damping of the PR-LCE were considerably enhanced compared to conventional LCEs without PR crosslinkers [2]. In addition, it was revealed that the number of cyclodextrin (CD) rings could be a useful molecular handle to further improve the damping properties of PR-LCEs. The unique energy dissipation behavior of LCE with slidable cross-links can be useful for developing high-performance sound absorbing materials as well as antivibrating apparatus [3].

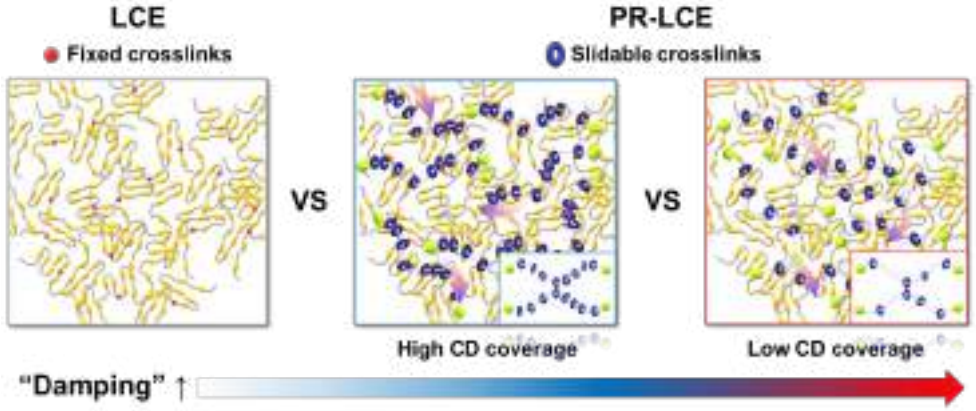


*Fig. 1. Schematic of slide-ring effect for LCE incorporating PR crosslinker*

**Acknowledgement:** This work was supported by Basic Science Research Program through the National Research Foundation of Korea (NRF) funded by the Ministry of Education, grant 2022R1A6A3A13073709.

**References:**

[1] S. Choi, ACS Appl. Mater. Interfaces 14 (2022) 32486.
[2] S. Y. Zheng, Macromolecules 52 (2019) 6748.
[3] C. Luo, ACS Appl. Mater. Interfaces 13 (2021) 12698.

## OP-IA-18

# Advances in the Analysis of the Materials Porous Structure by Means of the Machine Learning Methods

Ivanov A.D., Mel'gunov M.S.
*Boreskov Institute of Catalysis, Novosibirsk, Russia*
*max@catalysis.ru*

One of the tasks of machine learning (MO) is to provide a tool that allows transfer of the routine of analyzing numerical data characterizing physical phenomena to a computer, leaving the researcher time for scientific interpretation and significantly facilitating it. This approach is especially useful in physico-chemical methods, for which different variants of interpretation are possible. A characteristic example is nitrogen porometry, a widely known method that allows calculating from the same physical data such important parameters as specific surface area, dispersion, pore volume and their size distribution in different ways. The choice of a specific calculation method today lies entirely on the individual, while relevant recommendations have long been formulated [1], the strict application of which would make such a choice unambiguous and automatic, i.e. reduce the influence of the subjective factor.

By this contribution, we discuss examples of the application of trained neural networks in nitrogen porometry. We show the possibility of calculating adsorption isotherms for cylindrical and slit-shaped pores of arbitrary size based on a training set of model isotherms calculated within the framework of the theory of the nonlocal density functional (NLDFT) [2,3]. Due to a number of reasons, including the weak possibility of parallelization, the exact calculation of one isotherm on modern computers can take up to several days. At the same time, a neural network trained on a fairly representative set of such pre-calculated isotherms for different pore sizes transfers the task to the  in real time calculation mode. A set of model isotherms can be used to construct integral isotherms corresponding to model materials with a given pore size distribution. In turn, a set of integral isotherms can be used to train a neural network to detect, for example, the presence of micropores (pores smaller than 2 nm). To date, such detection significantly depends on the user's preferences to use one or another traditional method of data analysis. Another example is the determination of the type of capillary–condensation hysteresis loop (CCHL), which allows for the correct choice of the method for calculating pore size distributions [4]. Figure 1 shows the goodness of the prediction of the type of CCHL accumulated using the set of ~800 unique $N_2$ (77K) adsorption isotherms.

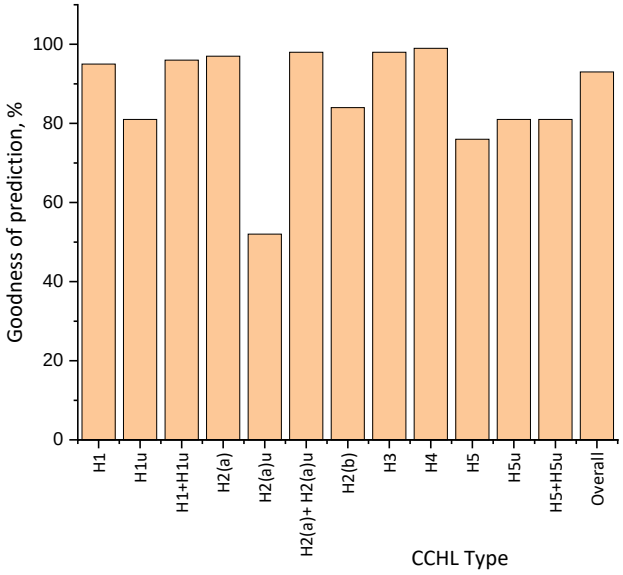


*Fig. 1. Goodness of prediction of the type of capillary–condensation hysteresis loop by means of the ML algorithm trained over ~800 unique $N_2$ (77K) adsorption isotherms [4].*

All the constructed neural networks have been tested on model and real data and show good applicability in terms of accuracy of prediction of target parameters and dependencies.

**Acknowledgement:** This work was supported by the Ministry of Science and Higher Education of the Russian Federation, grant *AAAA-A21-121011390054–1* for BIC.

**References:**

[1] Thommes, M., Kaneko, K., Neimark, A.V. et al //Pure Appl. Chem. 2015. V.87. P. 1051–1069.
[2] Ravikovitch, P.I., Neimark, A.V. // Langmuir. 2006. V.22. P.11171–11179.
[3] Neimark, A.V., Lin, Y., Ravikovitch, P.I., et al // Carbon. 2009. V.47. P. 1617–1628.
[4] Mel'gunov M.S. //Adsorption. 2023. doi: 10.1007/s10450-022-00369-5.

## OP-IA-19

# Electrochemical and Mechanical Properties of the Composite "PLGA/CaP/Ti" Scaffolds for Targeted Drug Delivery

Komarova E.G.[1], Kazantseva E.A.[1,2], Prosolov K.A.[1], Luginin N.A.[1], Uvarkin P.V.[1], Tolkacheva T.V.[1]

*1 – Institute of Strength Physics and Materials Science SB RAS, Tomsk, Russia*

*2 – Tomsk State University, Tomsk, Russia*

*katerina@ispms.ru*

The work focused on studying the corrosion resistance, adhesion-cohesion strength, microhardness, and Young's modulus of multilevel "PLGA/CaP/Ti" 3D-scaffolds as drug delivery systems. The two-stage technology for manufacturing 3D-scaffolds included: at the first stage, deposition of a calcium phosphate (CaP) coating by the hybrid ultrasound-assisted micro-arc oxidation method (UMAOH) on a titanium substrate [1]. At the second stage, the layer-by-layer self-assembled dip-coating of the samples in 5, 8, and 10% polylactic acid/glycolic acid copolymer 50/50 (PLGA) solutions.

Electrochemical corrosion tests showed that the unmodified CaP coatings had high corrosion resistance. Their corrosion currents ($I_{corr}$) were 228.2 and 355 nA/cm$^2$ in 0.9% NaCl and phosphate-buffered saline (PBS) solutions, respectively. Coating modification with 5, 8, and 10% PLGA led to an extreme reduction of the corrosion current below 1 nA/cm$^2$ in both solutions. Other characteristics of corrosion resistance, such as electrochemical impedance |Z| and polarization resistance ($R_p$), were significantly increased for the PLGA/CaP coatings compared to unmodified CaP coatings. Polarization resistance in both environments varied in the ranges of 0.17 – 0.32 MΩ·cm$^2$ and 17.78 – 261.72 MΩ·cm$^2$ for the unmodified CaP and composite PLGA/CaP coatings, respectively. The extreme increase in corrosion resistance of the PLGA/CaP coatings may be due to changes in their chemical and phase compositions, morphology, and related properties. Previously [2], we found that the UMAOH CaP coatings were characterized by high internal porosity of 39%, high surface porosity of 28%, thickness in the range of 50 – 50 µm, and surface roughness Ra of 3.0 – 4.0 µm. Increase in concentration of PLGA during modification led to an increase in the PLGA/CaP layer thickness up to 65 µm, a decrease in Ra down to 2.2 µm, and a decrease in porosity.

Corrosion studies showed a monotonous increase in the mass loss of the samples up to 0.9 and 1.7% after their exposure in 0.9% NaCl and PBS solutions, respectively, at 37 °C for 21 days. It should be noted that the mass loss of the samples did not have statistically significant differences between the unmodified and 5 – 10% PLGA-modified CaP coatings.

The results of the scratch test indicate the critical load which is characterizing the initial cohesion fracture (Lc1) to be higher for PLGA/CaP coatings (1.2 N) compared to unmodified CaP coatings (0.5 N). Moreover, the PLGA modification of the CaP coatings also led to a significant increase in their critical load characterizing the initial adhesion fracture (Lc2). For CaP coatings, Lc2 did not exceed 6.7 N, whereas for 5, 8, and 10% PLGA-modified CaP coatings,

it increased up to 13.9, 22.0, and 22.5 N, respectively. However, PLGA modification did not affect the critical load Lc3 at which complete detachment of CaP and CaP/PLGA coatings from the substrate occurred, which was found to be 30.6 N.

As orthogonal test for determination of the adhesion strength of the composite coatings to the substrate, the pull-off adhesion method was used. The adhesion strength was calculated using the formula: A = F/S, where F is the breakout force and S is the area of the detached coating. It was shown that the failure of the unmodified CaP and 5% PLGA/CaP coatings occurred according to the adhesion-cohesion type. At the same time, the 8 – 10% PLGA/CaP coatings broke off according to the cohesion type at the interface between PLGA and CaP layers. A linear decrease in adhesion-cohesion strength was recorded from 20.1 ± 1.6 MPa to 9.8 ± 0.8 MPa with an increasing concentration of PLGA.

Nanoindentation using the Berkovich indenter under a maximum load of 20 mN performed on the UMAOH CaP coating cross-section showed that its microhardness was equal to 4.3 ± 1.0 GPa, while the reduced Young's modulus was equal to 56.9 ± 9.5 GPa.

In conclusion, the developed composite system "PLGA/CaP/Ti" was characterized by high corrosion resistance, linear and slow degradation of the soluble components of the system in saline solutions (excluding the possibility of burst-like growth in the solution pH), and good mechanical properties.

**Acknowledgement:** This work was supported by the Russian Science Foundation, Grant 21-73-10265, https://rscf.ru/project/21-73-10265/.

**References:**

[1] K.A. Prosolov, E.G. Komarova, E.A. Kazantseva, A.S. Lozhkomoev, S.O. Kazantsev, O.V. Bakina, M.V. Mishina, A.P. Zima, S.V. Krivoshchekov, I.A. Khlusov, Y.P. Sharkeev, Materials 45 (2022) 4643.
[2] E.G. Komarova, E.A. Kazantseva, K.A. Prosolov, A.S. Lozhkomoev, S.O. Kazantsev, AIP Conf. Proc. (2023).

## OP-IA-20

# Ionic Mobility in the Composite (Ionic Liquids)@MOF Electrolytes Probed by Solid State NMR

Khudozhitkov A.E.[1], Veselovskaya J.V.[1], Ludwig R.[3], Kolokolov D.I.[1,2]
*1 – Boreskov Institute of Catalysis, Novosibirsk, Russia*
*2 – Novosibirsk State University, Novosibirsk, Russia*
*3 – University of Rostock, Rostock , Germany*
*kdi@catalysis.ru*

The current strategy for a sustainable development dictates the technological shift towards wider use of electric power storage and transfer systems, which motivates the development of new electrolytes. These advanced electrolytes, used in hydrogen fuel cells or Li-ion batteries, are subject to strict ecological restrictions such as being free from volatile compounds and the risk of leakage. In this sense, the solid electrolytes are preferable. In the same time, these materials have to be good conductors with high ionic mobility. One of ways to unite these concurrent requirements is to use a composite electrolyte based on ionic liquids confined in ordered porous host matrices, such as the metal-organic frameworks. Recent advances[1-2] have shown the high potential and the versatility of this strategy. In particular, the composite electrolytes show high conductivities even at low temperatures, which is believed to be due to the absence of a sharp liquid-solid phase transition and thus higher ionic mobility when in pores. However, up to now no microscopic measurements of the actual dynamics in confinement was reported. Herein we report the first case study of the microscopic molecular mobility of the Protic Ionic Liquids (PILs) confined within the MOF pore. We apply solid state $^{2}H$ NMR to probe mobility of the $[(C_nH_{2n+1})ND_3]^+[TFSI]^-$ (n=4-10) PILs within the MIL-100 (Al) MOF. We relate the molecular mobility of the confined PILs with the ionic conductivity of the composite. Finally, we show how the PILs mobility and ionic conductivity depends from the steric size of the cations hydrocarbon alkyl-chain.

**Acknowledgement:** This work has been supported by the Russian Science Foundation (grant № 21-13-00047)

**References:**

[1] Yoshida, Y.; Fujie, K.; Lim, D.-W.; Ikeda, R.; Kitagawa, H., *Angew. Chem., Int. Ed.* **2019,** *58* (32), 10909-10913.
[2] Huang, W.-H.; Li, X.-M.; Yang, X.-F.; Zhang, X.-X.; Wang, H.-H.; Wang, H., *Materials Chemistry Frontiers* **2021,** *5* (9), 3593-3613.

## OP-IA-21

# Sol-Gel Synthesis of Nanostructured Ni-Ce-Mg-O Ternary Systems

Veselov G.B., Stoyanovskii V.O., Afonnikova S.D., Vedyagin A.A.
*Boreskov Institute of Catalysis, Novosibirsk, Russia*
*g.veselov@catalysis.ru*

Nanostructured MgO-based systems find application in many industrially important processes as adsorbents and catalysts. In particular, Ni/MgO systems are known as active, stable, and cheap catalysts for the dry reforming of methane [1]. As usual, such catalysts are prepared by the reduction of corresponding oxides. The formation of $Ni_xMg_{1-x}O$ solid solution allows for obtaining highly dispersed Ni nanoparticles. In addition, $CO_2$ conversion is enhanced by the presence of basic sites on the MgO surface. The addition of $CeO_2$ was shown to increase the dispersion of Ni species, improve the reducibility, and inhibit coke formation. Therefore, the development of an efficient method for the preparation of MgO-based systems is an actual task.

In the present work, three-component Ni-Ce-Mg-O systems were synthesized via a sol-gel approach [2-3]. Aqueous solutions of cerium and nickel nitrates were introduced at the stage of hydrolysis of magnesium methoxide, which allowed for avoiding the use of organic precursors. This simplified approach was proposed in our group previously [3]. Thermal gravimetric analysis showed that the decomposition of both precursors occurs within the same temperature range as the decomposition of the magnesium hydroxide matrix. The obtained samples were labeled as Ni(x)Ce(y), where x and y are weight percentages of NiO and $CeO_2$ in the sample.

The physicochemical properties of the Ni-Ce-Mg-O systems were studied by a number of characterization techniques. The presence of $CeO_2$ resulted in a slight decrease in specific surface area and affected the morphology of the samples. Investigation of the samples by Raman and UV-vis spectroscopies allowed confirming that the substitution of $Ce^{4+}$ with $Ni^{2+}$ in the ceria lattice takes place. No significant interaction between $CeO_2$ and MgO was registered by these methods. In the XRD patterns of the Ni-Ce-Mg-O systems, the reflections assigned to $CeO_2$ and MgO are present (Fig. 1a). Amazingly, no shift of the MgO reflex to higher angles, expected due to the formation of $Ni_xMg_{1-x}O$ solid solutions, was observed. However, the formation of such solid solutions was confirmed by means of $H_2$-TPR and UV-vis spectroscopy. According to TEM data, nanosized $CeO_2$ particles are located on the surface of the $Ni_xMg_{1-x}O$ crystallites (Fig. 1b, 1c).

The catalytic activity of the Ni-Ce-Mg-O samples was examined in a model reaction of CO oxidation under prompt thermal aging conditions. The ternary systems demonstrated better activity than binary samples containing either NiO or $CeO_2$. In addition, ternary systems retained better activity after the high-temperature thermal aging. As is highlighted in previous works by other authors, the interactions at the NiO-$CeO_2$ interface play a decisive role in CO oxidation [4]. In the case of Ni-Ce-Mg-O, $CeO_2$ is present in a form of nanosized crystallites,

which allows contacting them with individual surface $Ni^{2+}$ ions and small NiO particles, thus resulting in increased activity in CO oxidation.

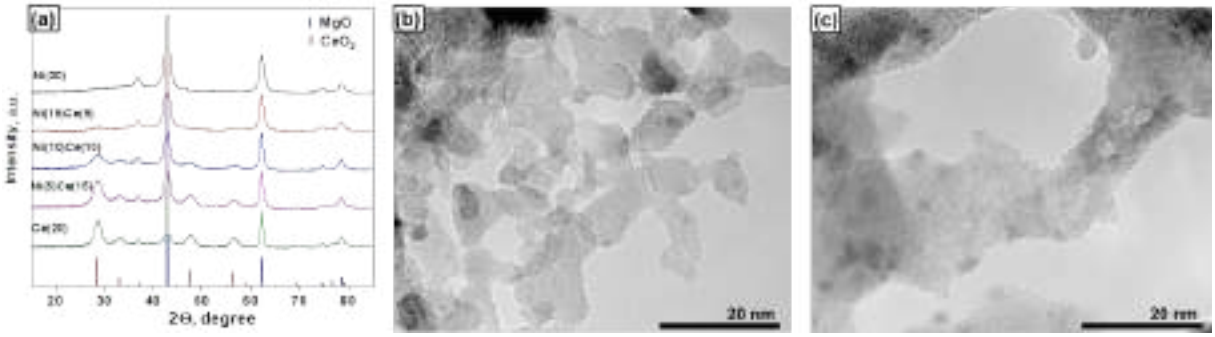


*Fig. 1. XRD patterns for the Ni-Ce-Mg-O samples (a).*
*TEM images of the samples: (b) Ni(10)Ce(10); (c) Ce(20).*

Finally, the Ni-Ce-Mg-O systems were used for the decomposition of hydrocarbons with the formation of nanostructured carbon. Two types of carbon nanofibers (CNF) were obtained on the Ni(15)Ce(5) and Ni(20) catalysts: hollow-centered fishbone-type nanofibers of 30 – 50 nm in diameter; and thin nanofibers less than 10 nm in diameter (Fig. 2). When the $CeO_2$ concentration was 10 wt.% and higher, the carbon formation was suppressed and the yield of CNF was insignificant. This indicates that the use of $CeO_2$-doped systems may be beneficial when carbon formation is the main reason for the catalyst deactivation.

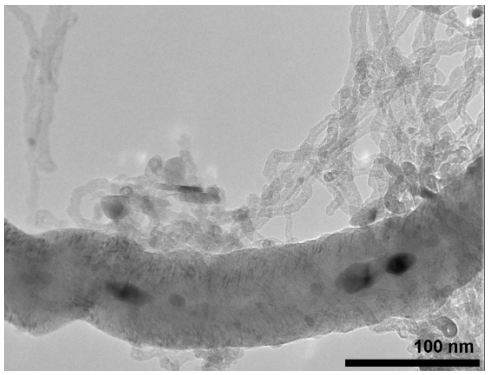


*Fig. 2. TEM image of the carbon product obtained via decomposition of ethylene over the Ni(15)Ce(5) sample at 600 °C.*

**Acknowledgment:** This work was supported by the Ministry of Science and Higher Education of the Russian Federation [project No. AAAA-A21-121011390054-1]. Characterization of the samples was performed using the equipment of the Center of Collective Use “National Center of Catalysts Research”.

**References:**

[1] Z. Zuo et al., ACS Catal. 8 (2018) 9821-9835.
[2] G.B. Veselov et al., Materials 13 (2020) 4404.
[3] A.A. Vedyagin et al., J. Sol-gel Sci. Technol. 82 (2017) 611-619.
[4] W. Zou et al., RSC Adv. 5 (2015) 98335-98343.

## OP-IA-22

# Impact of Microgel's Structure on its Functional Group's Mobility and Availability

Sergeev A.V.[1,2], Rudyak V.Yu.[2], Samodelkin R.A.[2], Fatikhova A.V.[2], Kozhunova E.Yu.[2], Chertovich A.V.[1,2], Khokhlov A.R.[2]

*1 – Semenov Federal Research Center for Chemical Physics, Moscow, 119991, Russia*

*2 – Faculty of Physics, Lomonosov Moscow State University, Moscow, 119991, Russia*

*sergeev@polly.phys.msu.ru*

Microgel is a unique modifiable polymer system which can be employed as a carrier for various useful functional groups. The attached functional groups can bear charges further employed in the formation of polyelectrolyte complexes; act as antibacterial and antiseptic substance; serve as a conjugation site for a number of target molecules. Microgels enriched with redox-active functional groups (e.g. TEMPO) is a promising catholyte/anolyte material for all-organic redox flow batteries [1]. That allows to have small viscosity at high volume concentration and the micrometer-scale size of the microgels enables application of cheap membranes. Of course, the question of spatial availability of the functional groups is of high importance for practical applications.

We performed coarse grained molecular dynamics (MD) simulation in order to investigate spatial distribution and motion of functional groups within the microgel particle. The microgel models used in this work were generated via simulation of the precipitation polymerization process from a dilute solution of initial components, which results in realistic microgel structure [2]. Systems with different structure were obtained by varying the concentration of the crosslinker, reactivity ratios and solvent quality. The mobility of functional groups was assessed through tracing the spatial area swept by the individual bids, particularly its average radius $R_{sweep}$. The mobility of functional groups does not correlate directly with the density of a microgel. Higher crosslinker concentration systematically reduces the $R_{sweep}$ value, i.e. shrinks the volume which a single functional group can diffuse. However, partial collapse does not result in the same effect: some surface-located functional groups even increase its availability area.

The simulation results were used to estimate the fraction of distributed functional groups which are available for reactions with large external objects, like electrode surface. Also, the model of functional groups with interchange reactions was studied, simulating electron transfer between redox-active functional groups. A minimum functional group concentration was evaluated to cover the whole microgel volume depending on its structure and solvents quality.

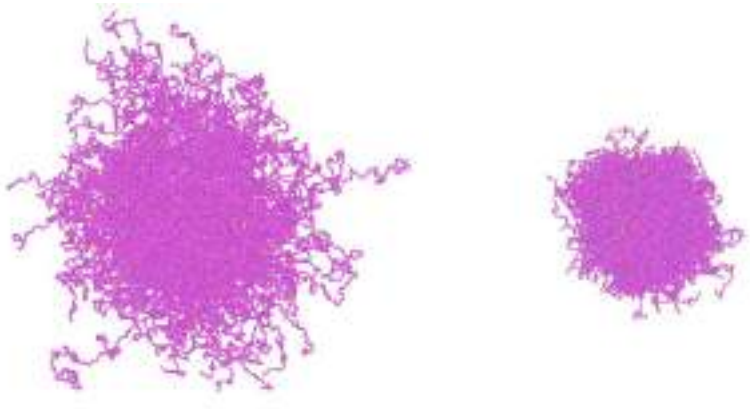

*Fig. 1. Modelled microgels with different crosslinker content: 1% (left) and 4%(right).*

**Acknowledgement:** This work was supported by the Russian Science Foundation, grant 22-13-00115.

**References:**

[1] E. Yu. Kozhunova, N. A. Gvozdik, et.al. J. Phys. Chem. Lett. 11 (2020) 10561.
[2] V.Y. Rudyak, E.Y. Kozhunova, A. V. Chertovich, Sci. Rep. 9 (2019) 13052.

## OP-IA-23

# Multiple Hydrogen Bonded Polymer Binders for High-Capacity Si Anode

Anjali Nagapadi Preman, Suk-kyun Ahn
*School of Chemical Engineering, Pusan National University, Busan 46241, Korea*
*anjaligcm94@gmail.com*

Silicon has been acknowledged as a promising anode material for lithium-ion batteries due to its high theoretical capacity. However, a significant volume change of the silicon during charge/discharge deteriorates the electrode performance in the long run [1]. A potential way to solve this problem is to develop polymer binders that can maintain the electrode morphology and conduction pathways for several cycles [2]. Herein, we synthesized a series of random copolymer binders integrating acrylic acid and butyl carbamate groups that can provide multiple hydrogen bonding. The self-healing properties of the carbamate group was exploited by controlling the molar composition of the copolymer and the effect of the various properties of binder on the long-term cycling stability of Si anodes was systematically investigated. Interestingly, the cycling properties of Si anodes made from these binders showed a stronger dependency on the composition of the binder. This study sheds light on the design principles of polymer binders to extend the lifetime of Si anodes.

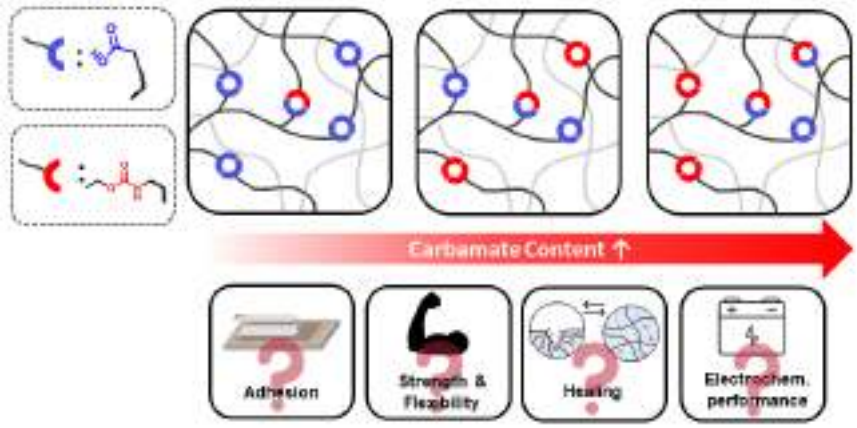


*Fig. 1. Schematic representation of the various H-bonding interactions in the binder in proportion to the carbamate content and the properties that are influenced by the carbamate content.*

**Acknowledgement:** This work was supported by the 2021 BK21 FOUR Program of Pusan National University.

**References:**

[1] T. Kwon, Chem. Soc. Rev. 47 (2018) 2145.
[2] A. N. Preman, J. Mater. Chem. A 8 (2020) 25548.

## OP-IA-24

# Electron Diffusion Induced Valley Hall Effect and Nonlinear Galvanodiffusive Transport in Hexagonal 2D Dirac Monolayer Materials

Snegirev A.V.[1,2], Kovalev V.M.[1,3], Entin M.V.[1]
*1 – Rzhanov Institute of Semiconductor Physics,*
*Siberian Branch of the Russian Academy of Sciences, Novosibirsk 630090, Russia*
*2 – Novosibirsk State University, Novosibirsk 630090, Russia*
*3 - Novosibirsk State Technical University, Novosibirsk 630073, Russia*
*komrad.snegirev2017@gmail.com*

Recently, considerable interest has been attracted to the study of the properties of two-dimensional semiconductors, such as transition metal dichalcogenides (TMD). They have unique optical properties that can be applied in optoelectronics. Their unusual band structure contains pairs of electron and hole valleys split by a strong spin-orbit interaction, which has a decisive influence on the transport properties of TMDs. As a result, the charge carriers have an additional, valley degree of freedom. Optical excitation by circularly polarized light can lead to nonequilibrium occupation of valleys. Due to the large distance in the pulse space, the valley number becomes a well-preserved quantity that can determine the transport properties of the material.

This work is devoted to the theoretical study of electronic transport effects in TMD monolayers due to the inhomogeneous distribution of the charge carriers concentration. The latter can be achieved, for example, by ununiform irradiation of the sample or by injection of electrons from other materials.

In the first part of the work, the process of anisotropic scattering of charge carriers on point impurities (skew scattering) is considered, as a result of which a current component which are transverse to the concentration gradient appears. The transverse component of the diffusion tensor is calculated and analyzed. The result is qualitatively similar to the valley Hall effect with the replacement of the components of the electric field by the corresponding gradients of charge carriers concentration.

In the second part of the work, isotropic scattering on point and coulomb impurities is considered. It is shown that as a result of taking into account the trigonal warping of zones, current corrections quadratic in concentration gradients appear. The components of nonlinear diffusion tensors associated with the trigonal spectrum in the valleys, as well as mixed components due to the concentration gradient and the electric field, were calculated and analyzed in the first order of magnitude of the corrugation of the zones. The result is qualitatively similar to the photovoltaic effect. In addition, currents due to the second derivatives of the concentration in coordinates are found.

## OP-IA-25

# The Halide-Modified Materials Based on g-$C_3N_4$ for Photocatalytic Hydrogen Production and Photocurrent Generation under Visible Light

Markovskaya D.V., Zhurenok A.V., Potapenko K.O., Sidorenko N.D., Kozlova E.A.
*Boreskov Institute of Catalysis, Novosibirsk, Russia*
*madiva@catalysis.ru*

Graphitic carbon nitride is known to be a universal material for various applications due to its layered structure and high stability [1]. Moreover, g-$C_3N_4$ is a semiconductor with sensitivity to visible light and may convert the light energy to chemical or electrical ones. These properties allow using carbon nitride both in the photocatalytic reactions such as hydrogen production and the photocurrent generation [2]. Unfortunately, their applications are restricted by high recombination rates and low surface area. These characteristics may be improved using different synthesis methods in which the chemical and textural structures are modified. The chemical structure is often changed by non-metals doping. The halogens demonstrated the maximum effect due to high differences in the electronegativity [2]. Nowadays, the fluorine-doped materials are completely studied, while other halogens as the dopants were described in a limited number of papers. The increase in the surface area may be achieved using template method. The combination of these two strategies – the template method and the modification with halogens – is in the particular interest.

The photocatalysts were prepared by the following way: melamine and D-glucose was dissolved in water and kept in the autoclave for 12 h at 180 °C. After that, the mixture of melamine and the corresponding ammonium halide was calcined at 550 °C for 2 h [3]. Before the photocatalytic tests, 1 wt. % of Pt was deposited on all photocatalysts. The obtained samples were labeled as 1% Pt/y-X, where y was the weight content of $NH_4X$ added at the second stage, X was Cl, Br, or I. The samples were characterized by a set of methods including X-ray diffraction (XRD), diffuse reflectance spectroscopy, the BET-method, transition electron microscopy, scanning electron microscopy with elemental mapping, thermal gravimetric analysis (TGA), X-ray photoelectron spectroscopy (XPS), cycling voltammetry, and impedance spectroscopy. The photocatalytic hydrogen evolution was studied in the basic solution of triethanolamine. The photoelectrochemical measurements were conducted in 1 M $Na_2S_n$ + 0.1 M NaCl. The light source in both cases was 425-LED.

The XRD, XPS, and TGA analyses proved the formation of modified graphitic carbon nitride in the case of ammonium chloride, ammonium iodide, and ammonium bromide (if y > 50). The addition of ammonium halide to melamine led to improving the surface area and pore volume of the samples. The maximum values were obtained for the photocatalyst 1% Pt/50-I. All prepared samples were found to be sensitive to visible light. The elemental mapping showed that carbon, nitrogen, platinum, and halogen were evenly distributed onto the surface. The weight content of halogens was small and did not exceed 0.3%. Fig. 1 revealed that the photocatalytic experiments demonstrated the domed dependency for the 1% Pt/y-Cl and 1%

Pt/I-y samples. It was due to the formation of the modified photocatalysts with an additional energetic level in their band gap structures when the dopants were added. The increase in the reaction rate was assisted with improving the charge separation which was realized with the additional energetic level. However, further growth of the dopant amount led to the enhancement of the recombination rate and decrease in the catalytic activity. For 1% Pt/y-Br samples, the modification of bromine was observed only if y was over 50. The reaction rate has grown with the increase of ammonium bromide amount. The same dependences were observed for the photoelectrochemical target parameters such as short-circuit current density, electron lifetime, and amount of charge carriers.

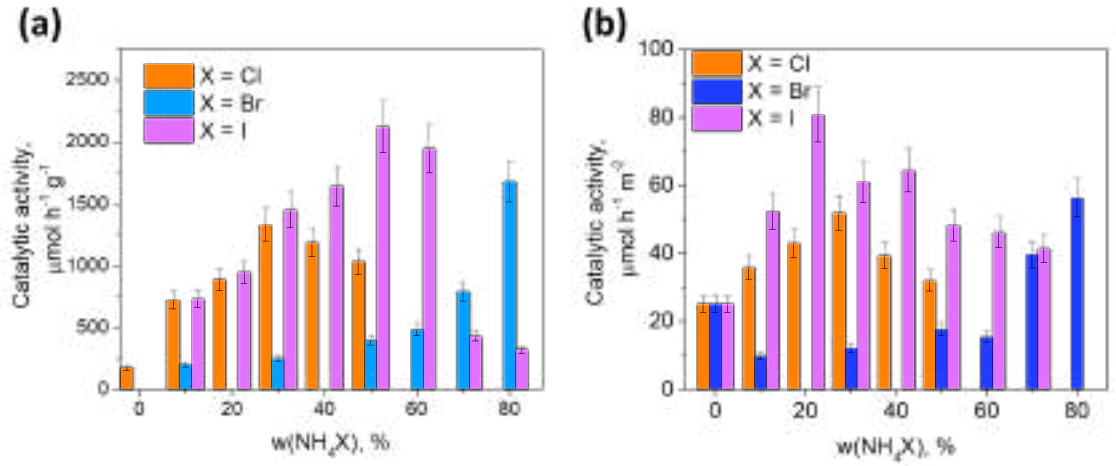


*Fig. 1. The catalytic activity of the prepared samples a) normalized by the catalyst mass; b) normalized by the catalyst surface.*

To sum up, the modified graphitic carbon nitride prepared by the two-stage technique was active in the photocatalytic hydrogen production and the photocurrent generation due to its surface area and changes in the electronic structure. The maximum catalytic activity was 2.1 mmol $h^{-1}$ $g^{-1}$ over 1% Pt/50-I, the highest photocurrent density was 2.69 mA/$cm^2$ obtained by 1% Pt/80-Br. These values exceeded the same for carbon nitride prepared by the calcination of melamine without any additional treatment in 35 and 54 times, respectively.

**Acknowledgement:** This work was supported by the grant of President of Russian Federation, grant MK-2133.2022.1.3.

**References:**

[1] E.A. Kozlova, V.N. Parmon, Russ. Chem. Rev. 86(2017) 870.
[2] S. Patnaik, D.P. Sahoo, K. Parida, Carbon 172(2021) 682.
[3] A.V. Zhurenok, T.V. Larina, D.V. Markovskaya, S.V. Cherepanova, E.A. Mel'gunova, E.A. Kozlova, Mendeleev. Commun. 31(2021) 157.

## OP-IA-26

# Heterostructured Materials for Photochemical Solar Energy Conversion: Basic Approaches

Emeline A.V., Rudakova A.V., Murashkina A.A.
*Laboratory "Photoactive Nanocomposite Materials", Saint Petersburg State University, Saint Petersburg, Russia*
*alexei.emeline@spbu.ru*

Heterogeneous photocatalysis and photoelectrochemistry represent two major trends in the photochemical conversion of solar energy into highly energetic chemical products, the so-called solar fuels. Two major challenges in these two areas are the higher photoactivity and the broader spectral sensitivity of photoactive materials toward the visible spectral range to transform increased fraction of solar light into increased quantity of solar fuels. However, requirements for higher activity and spectral sensitivity to visible light contrast each other for single-phase photoactive materials. This difficulty can be overcome combining narrow bandgap semiconductors into heterostructures to increase the driving force and make them sufficiently capable of carrying out both redox half-reactions. These concepts ultimately lead to creating novel heterostructured photoactive materials, which have recently become the leading trend in developing heterogeneous systems for the photochemical conversion of solar energy.

Heterostructured materials consist of at least two different, well-manifested phases of their components. The increase of the overall photoactivity of heterostructured materials is caused either by such kinetic factors as a decrease in recombination efficiency and an increase in charge carrier concentration of the corresponding components of the heterostructures owing to charge separation at the heterojunction (type II heterostructure; Fig. 1), or by an increase of the driving force (thermodynamic factor) of the heterostructured material for reduction/oxidation reactions compared to its separate components (Z-scheme heterostructure; Fig. 1). Consequently, type II and Z-scheme heterostructures are the dominating systems in photochemical solar energy conversions.

In general, type II heterostructures can absorb light in the visible spectral range when narrow bandgap semiconductors are used to form the heterostructures. However, the redox ability of such systems is less than the redox abilities of each individual components of the heterostructures (Fig. 1). In other words, a type II heterostructured system is capable of driving photochemical processes with redox potentials smaller than what each single semiconductor component of the heterostructure can do. As a result, such systems may be inefficient to complete the whole redox cycle in most desired photochemical redox processes such as, for example, water splitting or reduction of CO2 to produce solar fuels. At the same time, charge separation in type II heterostructures can promote the kinetic factors for one of the half-reactions of a redox cycle: either reduction or oxidation, making type II

heterostructures a prospective candidate for the fabrication of either a photocathode or a photoanode.

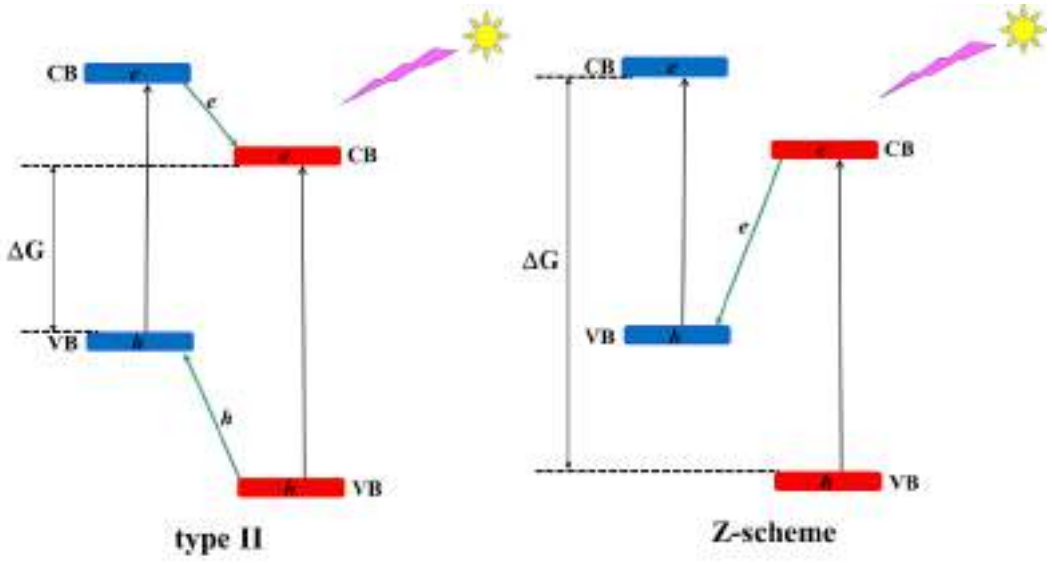


*Fig. 1. Schematic presentation of the charge separation mechanisms in heterostructures (type II – left, Z-scheme – right)*

In recent years, Z-scheme type heterostructures have become a major focus of research dealing with the photochemical conversion of solar energy because of the thermodynamic advantages provided by the Z-scheme. Indeed, should a direct Z-scheme be truly created, the difference in redox potentials becomes significantly larger than the redox potentials of either component of the heterostructures, so that such heterostructures can drive the photochemical processes with a greater free energy |ΔG| to complete the redox cycles of the desired reactions. In addition, the charge separation at the Z-scheme heterojunction results in an increase of the favourable kinetic factor. Thus, Z-scheme type heterostructured photoactive materials formed by narrow bandgap semiconductors that absorb the visible part of solar light are the most promising heterostructured systems for the photochemical conversion of solar energy as demonstrated in several studies.

In our presentation we discuss the possible pathways to create effective heterostructured materials for realization of Z-scheme mechanism considering their spatial geometry, thermodynamic, kinetic and spectral behaviour of heterostructured materials with regards to the target photoelectrochemical processes for solar energy conversion.

**Acknowledgement:** This work was supported by the Russian Science Foundation, grant 22-13-00155.

## OP-IA-27

# Functional Materials for Protonic Ceramic Fuel Cells Powered by Ammonia

Stroeva A.Y.[1], Borisov V.A.[2], Ichetovkin Z.N.[1], Fedorova Z.A.[3], Shlyapin D.A.[2], Snytnikov P.V.[3], Kuzmin A.V.[1]

*1 – Vyatka State University, Kirov, Russia*

*2 – Center of New Chemical Technologies BIC, Boreskov Institute of Catalysis SB RAS, Omsk, Russia*

*3 – Boreskov Institute of Catalysis, Novosibirsk, Russia*

*bva13011986@gmail.com*

Ammonia, within the framework of the hydrogen economy concept, is considered as one of the promising carriers of hydrogen due to its high volumetric energy density, a developed production system and a well-functioning transportation and storage system. A promising direction for the development of alternative energy is the development of protonic ceramic fuel cells (PCFC) [1], effectively operating in medium-temperature conditions (500-800 ° C) and the possibility of using not only hydrogen, but also ammonia as an energy carrier. Direct decomposition of ammonia on PCFC electrodes requires the use of Ru, Ni or Co as catalysts applied directly to the electrode surface. Among oxide materials, barium cerate-zirconates [2] and lanthanum scandates [3] have the highest proton conductivity, and the latter are more stable in the presence of water vapor, acidic oxides of CO and CO2 and/or other carbon- or sulfur-containing components. The introduction of cobalt cations into the composition of lanthanum scandate makes it possible to create electrode materials that, in addition to electrochemical activity, also have catalytic activity in the direct decomposition of ammonia.

The purpose of this work is to synthesize and study the physicochemical properties of composite materials based on $La_{0.9}Sr_{0.1}Sc_{0.9}Co_{0.1}O_{3-\delta}$ (LSSC10), $La_{0.9}Sr_{0.1}CoO_{3-\delta}$ (LSC) and $Ru/CeZrO_x$ for PCFC powered by ammonia.

Citrate-nitrate synthesis of individual materials LSSC10 and LSC was performed in the work. Composite materials based on these oxides are obtained by solid-phase mixing with different percentages of individual phases, followed by pressing and sintering at 1200 ° C. The obtained individual and composite materials were examined by XRD, SEM and dilatometry methods. It was shown by the XRD method that materials with a perovskite-type structure were obtained. The microstructure and elemental composition of the surface demonstrate a uniform distribution of cations. Dilatometric measurements have shown that composite materials are compatible with lanthanum scandate-based electrolytes. It has been found that an increase in the concentration of lanthanum cobaltite in the composition of the composite causes an increase in the conductivity of the material. The catalytic properties of the synthesized materials were studied in the decomposition reaction of ammonia at atmospheric pressure in the temperature range 500-700 °C and the WHSV of ammonia – 60.000 $mlNH_3 \cdot gcat^{-1} \cdot h^{-1}$. It was found that LSSC10-LSC composites demonstrate high activity in the decomposition of ammonia at a process temperature of 700 ° C. As one of the ways to reduce

the operating temperature of ammonia PCFC, the activity in the decomposition of ammonia of $Ru/CeZrO_x$ catalysts prepared on the basis of commercial oxide supports that can be used in PCFC as a coating for electrodes was investigated. The main advantage of these catalysts is that these same supports are used for automotive exhaust gases afterburning and are therefore produced by tons. According to the XRD and IR spectroscopy methods, the supports are substitutional solid solutions based on cerium oxide. The specific surface areas of supports and catalysts are close and amount to 71-89 $m^2/g$. As shown by the TEM and XRD methods, the particle sizes of the supports do not exceed 11 nm. According to TEM data, the sizes of ruthenium particles do not exceed 1.3 nm. It has been established that the activity of these catalysts already at 500 ° C and WHSV 60.000 ml $NH_3 \cdot gcat^{-1} \cdot h^{-1}$ can exceed 40 mmol $H_2/(g_{cat} \cdot min)$ with ammonia conversion of 63%. Under the same conditions at a temperature of 550 °C ammonia conversion exceeds 99%. It is shown that the activity of the $Ru/CeZrO_x$ catalyst in the process of ammonia decomposition remains stable for 20 hours.

**Acknowledgement:** This work was supported by the Ministry of Science and Higher Education of the Russian Federation within the governmental order for Boreskov Institute of Catalysis (project AAAA-A21-121011390009-1).

**References:**

[1] E. Fabbri, D. Pergolesi, E. Traversa, Chem. Soc. Rev. 39 (2010) 4356.
[2] D. Medvedev, A. Murashkina, E. Pikalova, A. Demin, A. Podias, P. Tsiakaras, Prog. Mater. Sci. 60 (2014) 76.
[3] M. Plekhanov, A. Kuzmin, E. Tropin, D. Korolev, M. Ananyev, J. Power Sources. 44 (2020) 227476.

## OP-IA-28

# Contact Angles between Crude Oil and Brine on Minerals in Reservoir Conditions Studied with Molecular Dynamics Simulations

Khovental P.A.[1], Kopanichuk I.[1], Kevorkyants R.[2], Vishnyakov A.[3,4]
*1 – Skolkovo Institute of Science and Technology, Moscow, Russia*
*2 – Hong Kong Quantum AI Lab, The University of Hong Kong, HKSAR, China*
*3 – Moscow State University, Department of Physics, Moscow, Russia*
*4 – Krestov Institute of Solution Chemistry (RAS), Ivanovo, Russia*
*petr.khovental@skoltech.ru*

Contact angle at water—oil—solid contact line determine the wettability and permeability of porous materials. They are easy to measure at ambient conditions, but measurements of the contact angle dependence on multiple factors at adverse conditions (such as reservoir conditions during oil recovery) are very expensive to measure, especially when large number of parameters (oil composition, temperature, pressure, salinity) nned to be considered. In this work we present results of molecular simulations of contact angles at oil—brine—quartz contact line using the models carefully fitted to experimental data.The most stable surface of alpha-quartz(001) was chosen is considered with varying degree of hydroxylation. Special attention is paid to the density of the fluids which should correspond to particular bulk systems and the algorithms of the contact angle calculation form molecular configuration. An example calculation is shown in Figure 1.

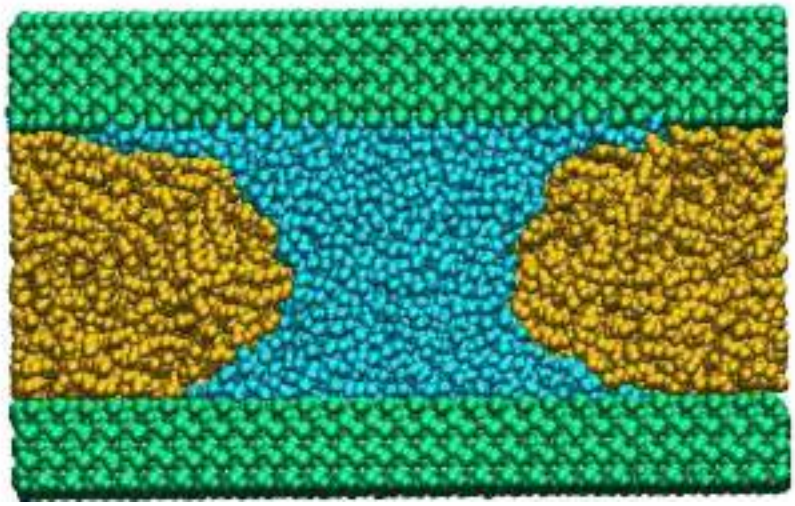

*Fig. 1. Example of contact angle. The quartz is green, decane is blue, water is orange.*

During the calculations, the influence of temperature, pressure, salinity, degree of aromatization and amount of methane in oil on the contact angle of the oil-brine-quartz system was investigated. The dependence of the contact angle on temperature is shown in figure 2.

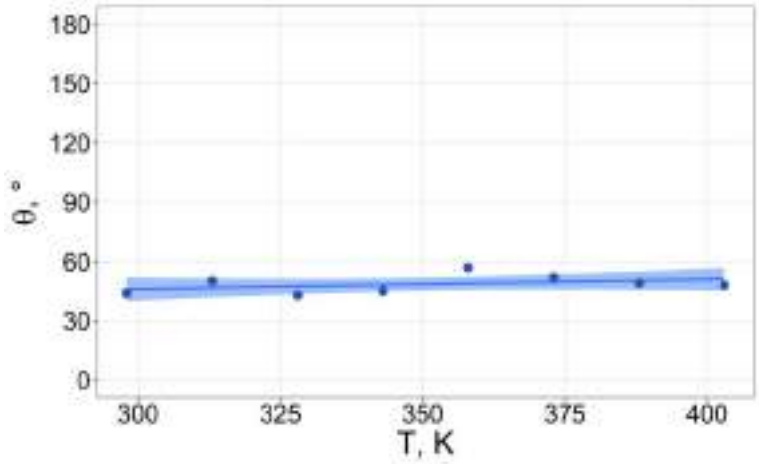


*Fig. 2. Dependence of the contact angle in the oil-brine-quartz system on temperature*

The contact angle increases with increasing temperature. This correlates well with the experimental data showing decreasing interfacial tension with increasing temperature. In this work, a model for calculating the contact angle in the oil-salt-mineral system was created and the main dependencies were determined.

## OP-IA-29

# Growth of Polymolybdate Scintillating Crystals by the Low-Thermal-Gradient Czochralski Technique

Grigorieva V.D.[1,2], Kremlev A.D.[1,2], Shlegel V.N.[1]
*1 – Nikolaev Institute of Inorganic Chemistry, Novosibirsk, Russia*
*2 – Novosibirsk State University, Novosibirsk, Russia*
*grigoryeva@niic.nsc.ru*

Neutrinoless double beta decay (0v2β decay) process is considered the most probable to happen on the molybdenum-100 nucleus. Thus, molybdate-based crystalline scintillators are of great interest for large-scale neutrino search projects. The extreme rarity of double beta decay (for the Mo-100 nucleus - $10^{28}$ years) imposes the strictest requirements on molybdate crystal scintillators used in projects. In addition to the general requirements for scintillators - high optical quality, luminescence intensity, light output, energy resolution, the material must also contain a minimum amount of impurities and have an ultra-low radiation background.

The low-thermal-gradient modification of Czochralski technique (LTG Cz) developed at NIIC SB RAS is a unique technology for obtaining large oxide crystals of high optical quality in bulk volume. LTG Cz has significant structural differences from the conventional Czochralski technique resulting in temperature gradients being reduced by two orders of magnitude to values less than 1 deg/cm. Thus, the processes of volatilization of the melt components are suppressed, the loss of expensive isotopically enriched molybdenum-100 during growth process is prevented, the number of thermoelastic stresses and defects in growing crystal is reduced.

Based on literature data, alkali metal polymolybdates $M^{+1}_xMo_yO_z$ are not hygroscopic, have a higher density and molybdenum content per unit volume than already developed molybdate scintillator $Li_2MoO_4$ [1, 2]. The study of the phase diagrams of $Li_2O$-$MoO_3$, $Na_2O$-$MoO_3$ and $Cs_2O$-$MoO_3$ showed that intermediate compounds $M_xMo_yO_z$ melt congruently at temperatures below 1000 °C, thus, they fit into the paradigm of LTG Cz crystal growth.

Fig. 1. $Li_xMo_yO_z$ crystal grown by LTG Cz technique

**Acknowledgement:** This work was supported by the Russian Science Foundation, grant 23-23-10068.

**References:**

[1] H.J. Kim, I.R. Pandey, A. Khan, J.K. Son, M.H. Lee, Y.D. Kim, Cryst. Res. Technol. 54 (2019) 1900079.
[2] S.Gossé, C.Guéneau , S.Bordier , S.Schuller, A.Laplace, J.Rogez, Proced. Mat. Sci. 7 (2014) 79–86

## OP-IA-30

# Testing of New Solvents for $CaMO_4$ (M=Mo,W) Crystal Growth

Khramtsova D.M.[1,2], Kuznetsov A.B.[2], Kokh A.E.[2], Kokh K.A.[2]
*1 – Novosibirsk State University, Novosibirsk, Russia*
*2 – Sobolev Institute of Geology and Mineralogy, Novosibirsk, Russia*
*d.khramtsova@g.nsu.ru*

Molybdates and tungstates are promising materials for optical applications due to thier thermal and luminescence properties. There are many unexplored parts in the phase diagrams like $MWO_4$-$MMoO_4$ (M = alkaline earth metal) or more difficult - $Na^+/Sr^{2+}||MoO_4^{2-}/WO_4^{2-}$. For instance, the $CaMoO_4$-$CaWO_4$ system is studied fragmentary during solid state synthesis of photoluminescence matrices.

Calcium tungstate ($CaWO_4$) and molybdate ($CaMoO_4$) are an important member of scheelite structure family as well as $PbMoO_4$, $PbWO_4$, $YLiF_4$, and high-pressure phases of $TbVO_4$ and $DyVO_4$. These compounds are highly promising as scintillating crystals for the low-temperature direct dark matter search experiments CRESST-II and EURECA [1]. Massive bulk crystals (about several hundreds grams) can be grown by the Czochralski technique. However, growth from melt of $CaMoO_4$ and $CaWO_4$ crystals is accompanied by evaporation of $MoO_3$ and $WO_3$ [2]. In addition, $CaMoO_4$ grown in air atmosphere have colored defects correlating to $Mo^{6+}$ - $Mo^{5+}$ reduction. However, transparency can be restored by annealing at 1250°C with oxygen. Another way to produce the transparent crystals is the growth from solution at lower temperatures. By using LiCl flux as low starting growth temperature as 550°C was reached [3]. An alternative is hydrothermal method. However, this method is usually used for synthesis of microcrystallites [4], but no data was found on bulk crystals.

In this work, the mixtures of $Li_2WO_4$-LiF, $Li_2MoO_4$-LiF, $Na_2WO_4$-NaF and $Na_2MoO_4$-NaF [5] were tested as solvents for crystal growth of $CaWO_4$ и $CaMoO_4$ at temperature below 1000°C. Sturctural features and compositions were studied by XRD analysis and scanning electron microscope (EDS SEM). Raman spectra and and luminescence were also studied.

**Acknowledgement:** This work was supported by state assignment of IGM SB RAS.

**References:**

[1] Andreas Erb., Jean-Co Lanfranchibc. Growth of high-purity scintillating CaWO4 single crystals for the low-temperature direct dark matter search experiments CRESST-II and EURECA/ CrystEngComm – 2013, 15, 2301.
[2] Linwen J., Zhenhai W., Hogbing C. Thermal annealing effects on the lumiscence and scintillation properties of $CaMoO_4$ single crystal grown by Brigman method/Journal of alloys and compounds – 2018, vol. 734, pp. 179-187
[3] Satish K. Arora, Naresh M. Batra, and G. s. Trivikrama. Flux Growth of Calcium Molybdate Single Crystals/ Communications of the American Ceramic SocieQ - J. Am. Ceram. Soc., 68 [9] C-240-C-241 (1985)
[4] Yan Z., Yanyan W., Dan Q., Xin L., Yun W., Mengjiao L., Daojiang G., , Jian B., Guangliang X. Hydrothermal Synthesis and Photoluminescence Properties of $Ca(MoO_4)_x(WO_4)_{(1-x)}$ Microcrystallines/ Advanced Materials Research Vols. 652-654 (2013) pp 599-606
[5] S.Jusrud, O.J.Kleppa. Thermodynamics of charge-unsymmetrical anion mixtures. II. The liquid systems AF-$A_2MoO_4$ and AF-$A_2WO_4$/Acta Chemica Scandinavica A –1981 – p.669-678

## OP-IA-31

# Crystallization of Cristobalite in Sodium Borosilicate Glass in the Presence of Chromium

Konon M.[1], Polyakova I.[1], Saratovskii A.[1,2], Danilovich D.[2], Anfimova I.[1]
*1 – Institute of Silicate Chemistry, RAS, St. Petersburg, Russia*
*2 – St. Petersburg State Institute of Technology (Technical University), St. Petersburg, Russia*
*marina-konon@mail.ru*

Chromium-containing glasses are useful materials for energy storage devices, tunable solid-state lasers, protective screens from X-ray and gamma radiation, etc. [1] Chromium oxide (III) is a well-known nucleating agent that causes crystallization in glass, which could be a hindrance to the practical application of chromium containing glasses. This work aimed to investigate the crystallization of cristobalite in $Cr_2O_3$-containing sodium borosilicate glass depending on heat treatment conditions, using XRD, DTA, SEM, EPR, and XPS methods.

Glass with composition (mol %) $6Na_2O \cdot 22B_2O_3 \cdot 70SiO_2 \cdot 2Cr_2O_3$ was synthesized using conventional melting at 1450-1480°C with the subsequent annealing in the muffle furnace. After annealing, the glass was also heat treated at 550 °C for 24-96 h, and at 700°C for 2 h. A separate quenching experiment was carried out, where the glass melt was poured into an ice-cold water bath.

According to XRD results, the crystalline phase of eskolaite ($Cr_2O_3$, PDF-2: 85-0869) forms in the samples with all thermal histories including quenching (Fig. 1, *a*). After heat treatments at 550 °C for 24 and 48 h, a very weak main peak of cristobalite (82–1410) appears at 21.9°. An increase in the duration of the heat treatment to 96 h leads to an increase in the intensity of this peak by more than 30 times, as well as to the manifestation of other weak peaks of cristobalite. Cristobalite also forms at 700°C, but the peak at the XRD pattern is less intense than the one at 550°C, 96 h. Quenched sample's XRD pattern shows no sign of cristobalite.

SEM studies showed that during heat treatment at 550 °C for 24-96 h the phase-separated structure with interpenetrating phases is formed. Starting at 72 h duration of heat treatment, spherulitic inclusions with an average size of ~5-6 μm are formed (Fig. 1, *b*), which can be attributed to cristobalite [2]. Photomicrographs taken in contrast mode by average atomic number reveal chromium-containing inclusions ~1.3 μm in size, which are predominantly observed in the center of spherulite formations (Fig. 1, *b*).

An "influx" occurs at the main peak of cristobalite from the side of small angles on the XRD pattern for the sample heat treated at 550°C for 96 h (Fig. 1, *a*). As the duration of isothermal exposure increases, the intensity of $Cr_2O_3$ peaks decreases. This can be interpreted as follows. Cristobalite is the main crystalline phase of silica under atmospheric pressure. It is distinguished by high purity, and the solubility of other chemical elements (mainly alkalis) is very low. When foreign elements enter cristobalite, polytypism is observed, which is a partial change in the stacking of one of the crystallographic layers, in which the alternation of the cristobalite type is replaced by the alternation of the tridymite type - a crystal structure that

is much more capacious in terms of accepting impurities [3]. The appearance of the “influx” at the foot of the main cristobalite peak from the side of small angles indicates polytypism. In this case, the intensity of the $Cr_2O_3$ peaks decreases compared to the samples kept at 550°C for a shorter time; therefore, it can be assumed that its atoms are partially incorporated in the layers of “tridymite”.

*(a)* *(b)*

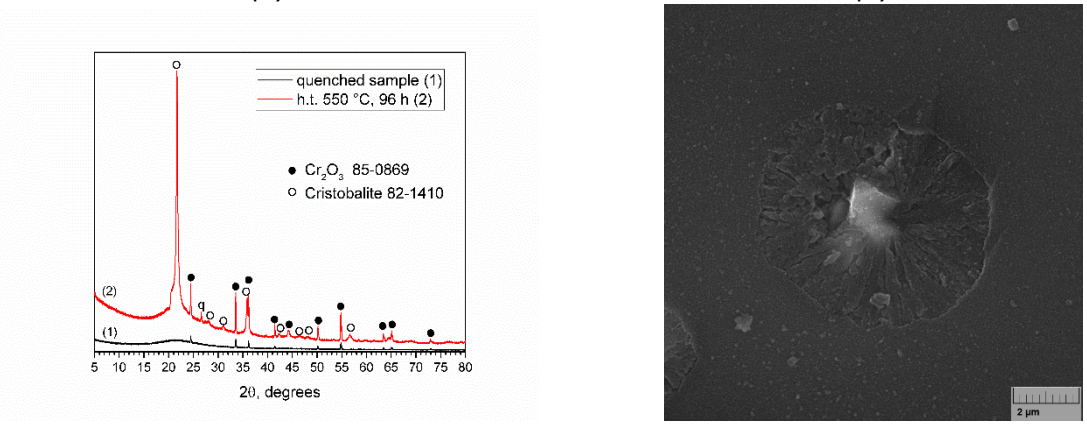


*Fig. 1. (a) XRD patterns for the quenched sample and the heat treated at 550°C for 96 h. (b) SEM image of glass sample heat treated at 550 °C for 72 h.*

The DTA results suggest that the crystallization of the $Cr_2O_3$ and $SiO_2$ phases occurs in the low-viscosity boron-rich phase.

EPR spectra of the investigated glass samples demonstrate a narrow resonance line with a g-factor of 1.98, which has an asymmetric shape, and several wide resonance bands with g=4.27 and g=2.06. Paramagnetic resonance was also observed in the region of g=4.27 and g=2.06 in chromium-free glass, suggesting that the signal with g=4.27 is associated with the presence of contaminants in the mixture. The most probable impurity may be iron, which gives an EPR signal in this area [4]. The signal with g=1.98 can be attributed to the paramagnetic state of chromium, namely, to the presence of isolated $Cr^{3+}$ ions in distorted octahedral coordination, as evidenced by the asymmetric shape of this line [5].

**Acknowledgement:** The study was supported by the Russian Science Foundation, grant 22-73-00086, (https://rscf.ru/en/project/22-73-00086/), and was carried out using the equipment of the engineering center of St. Petersburg State Institute of Technology.

**References:**

[1] M. Yu. Konon, I. G. Polyakova, A.S. Saratovskii, D. P. Danilovich, I. N. Anfimova., Glass Phys Chem. 49 (2023) 199.
[2] R. C. Breneman, J. W. Halloran, J. Am. Ceram. Soc. 97 (2014) 2272.
[3] L. I. Gorogotskaya, B. M. Mitsyuk. Горогоцкая Л. И., Мицюк Б. М. Physicochemical transformations of silica under conditions of metamorphism. Naukova Dumka, Kte. 1980. 236. (in Russian)
[4] G. O. Karapetyan, S. G. Lunter, D. M. Yudin, Optika I Spektroskopiya. 14 (1963) 700.
[5] A. Aboukaïs, L.D. Bogomolova, E. Cattaruzza [*et al*], Optical Materials. 22 (2003) 177.

## OP-IA-32

# Steam-Assisted Crystallized Fe-Silicalite-1 Nanocrystals as Heterogeneous Fenton Catalyst

Bragina A.A.[1], Babina K.A.[1,2], Parkhomchuk E.V.[1,2]
*1 – Boreskov Institute of Catalysis, Novosibirsk, Russia*
*2 – Novosibirsk State University, Novosibirsk, Russia*
*bragina@catalysis.ru*

Fenton system is one of the most safety and effective way to remove low-concentrated organic pollutants from water. Despite of high efficiency, traditional homogeneous Fenton system has a number of disadvantages, such as narrow pH reaction range, low efficiency of $H_2O_2$ consumption, binding Fe ions into complexes and difficulties of the catalyst separation from the reaction mixture. Heterogeneous catalysts based on zeolites permit to overcome limitations mentioned above [1].

However, heterogeneous Fenton system based on traditional Fe-silicalite-1 microcrystals has some limitations for large organic molecules oxidation. MFI structure type zeolite micropores diameter is 0.55 nm. Their availability is too low for large molecules in the absence wider pores. Since the active centers (Fe oxohydroxocomplexes) are located in mesopores inside the crystals where OH-radicals with a mean free path of 6 nm are generated, diffusion limitations lead to reduce the efficiency of using $H_2O_2$ because of the occurrence of a side reaction decomposition of $H_2O_2$ to $O_2$ and $H_2O$. Fe-silicalite-1 nanosized crystal using permits to solve this problem.

Preparation of nanosized zeolite crystals is difficult to implement because of centrifugation difficulties and large synthesis period for conventional hydrothermal method. One of the materials science topical problems is the development of synthesis methods for preparation nanosized zeolite crystals. Thereby, recently the dry-gel conversion zeolite crystallization was developed to solve conventional hydrothermal synthesis of nanocrystalline zeolites problems. Steam-assisted crystallization zeolite synthesis technique consist in following steps. There are initial gel preparation for the zeolite synthesis, its drying and

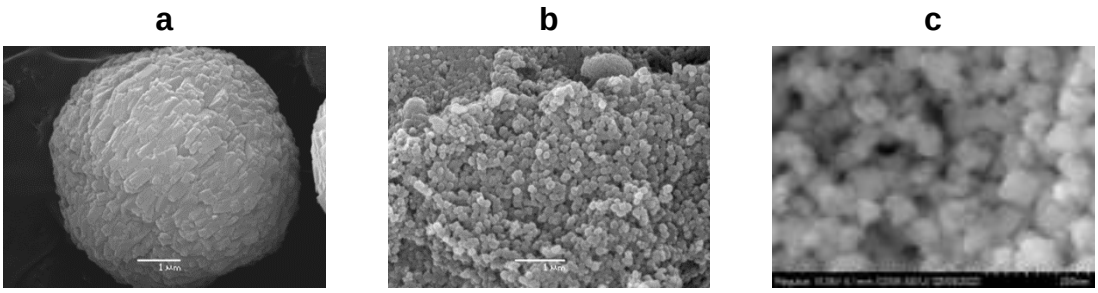


*Fig. 1. SEM images of calcined and activated Fe-silicalite-1 samples: m-FeZ (a), h-FeZ (b) and n-FeZ-1 (c).*

grinding and subsequent zeolite crystallization into autoclave in the presence water and/or volatile template.

In our work three different types of heterogeneous Fenton catalysts have been obtained. They are Fe-silicalite-1 5 μm microcrystals, hierarchically porous Fe-silicalite-1 consisting of 100-200 nm crystals synthesized using polystyrene latex as a template and steam-assisted crystallized Fe-silicalite-1 30-50 nm crystals (Fig. 1).

In case of steam-assisted Fe-silicalite-1 crystallization, the method of introducing Fe source into reaction mixture has been varied, namely in case of n-FeZ-1 Fe introducing step was carried out after aging the initial gel, as for n-FeZ-2 Fe introducing step was carried out before aging the initial gel and for n-FeZ-3 aging step wasn't performed. These samples have high surface area values (from 441 to 501 $m^2/g$), high mesoporous volume (maximum volume reaches to 0.66 $cm^3/g$ which forms 85% from overall pore volume). Synthesized Fe-silicalite-1 catalysts and homogeneous Fenton system have been compared in total oxidation by $H_2O_2$ of model ethanol molecule.

Table 1. Comparison of catalytic performance of different Fenton-type catalysts.

| | $W_{max}(CO_2)$, $10^{-7}$ mol/min | $W_{max}(O_2)$, $10^{-5}$ mol/min | $W_{max}(O_2)/W_{max}(CO_2)$ | Maximal mineralization degree, % |
|---|---|---|---|---|
| $Fe(NO_3)_3$ | 3.77 | 20.9 | 554 | 42 |
| m-FeZ | 2.06 | 3.58 | 174 | 50 |
| h-FeZ | 2.07 | 2.51 | 121 | 60 |
| n-FeZ-1 | 1.67 | 1.56 | 93 | **>75** |
| n-FeZ-2 | 1.61 | 1.61 | 100 | 70 |
| n-FeZ-3 | 1.53 | 1.59 | 104 | 62 |

Results presented in Table 1 demonstrate catalytic characteristics of used catalysts such as maximal rates of $CO_2$ and $O_2$ evolution and its ratio and maximal ethanol mineralization degree. It should be mentioned that the most efficient using $H_2O_2$ and increasing ethanol mineralization degree are observed with rates ratio decrease. n-FeZ-1 demonstrates higher catalytic efficiency in spite of lowest activity of $H_2O_2$ consumption. It is due to n-FeZ-1 texture properties such as enhanced surface area, high pore volume which provide favorable reactants diffusion. It has been shown that zeolites obtained by steam-assisted crystallization are the most effective in the ethanol oxidation by $H_2O_2$.

**References:**

[1] K.A. Sashkina, V.S. Labko, N.A. Rudina, V.N. Parmon, E.V. Parkhomchuk, J. Catal. 299 (2013) 44-52

## OP-IA-33

# The Fluorite-Like $LiLn_4Mo_3O_{15}F$ (Ln = La-Dy) Ceramics: Synthesis and Properties

Orlova E.I.[1,2], Kharitonova E.P.[1,2], Voronkova V.I.[1]
*1 – Lomonosov Moscow State University, Faculty of Physics, Moscow, Russia*
*2 – Shubnikov Institute of Crystallography of Federal Scientific Research Centre 'Crystallography and Photonics' of Russian Academy of Sciences Moscow, Russia*
*agapova@polly.phys.msu.ru*

Cubic rare earth molybdates with a variable oxygen stoichiometry $Ln_5Mo_3O_{16+\delta}$ (Ln = La–Gd; Sp. gr. *Pn*–3*n*) [1, 2] are promising materials – potential new anode materials for solid oxide fuel cells operating in the middle temperature range [3, 4]. These compounds are mixed oxygen-electron conductors (MIEC), the conductivity of which reaches $10^{-2}$ S/cm at 700°C [3]. The interstitial conductivity of such materials is very sensitive to the oxygen content (δ) that can be varied under reducing conditions or by heterovalent doping without any changes in the compound structure. The effect of the cation-anion codoping of $Ln_5Mo_3O_{16+\delta}$ (Ln = La-Dy) family, in particular with lithium and fluorine, on the physical properties of the compounds is of special interest.

Polycrystalline samples of $LiLn_4Mo_3O_{15}F$ (Ln = La-Dy) compounds, so called oxyfluorides, were synthesized in evacuated sealed quartz ampoules or in air. The firing temperatures for the ceramics were 650 - 700°C, the firing time was 12 - 24 h, depending on the composition. The samples were characterized by X-ray phase analysis (XRD), scanning electron microscopy, thermogravimetry (TG), differential scanning calorimetry (DSC), thermomechanical analysis (TMA), impedance spectroscopy in dry and humid atmosphere.

According to XRD data, the obtained $LiLn_4Mo_3O_{15}F$ (Ln = La-Eu) oxyfluorides are isostructural to fluorite-like compounds of the $Ln_5Mo_3O_{16+\delta}$ family. It is shown that the replacement of the rare earth cation with lithium and oxygen with fluorine leads to the appearance of a reversible phase transition accompanied by a jump in anionic conductivity by several orders of magnitude for all F-containing samples. The maximum conductivity value for fluorinated lithium molybdates riches $10^{-2}$ S/cm at 700°C. The oxyfluorides with large rare earth cations absorb water and exhibit proton-conducting properties in a humid environment. With decreasing Ln radius, the compounds lose their ability to hydration and proton transfer.

**Acknowledgement:** This work was supported by the Russian Science Foundation, grant 23-12-00221.

**References:**

[1] P.H. Hubert, C. R. Acad. Sc. Paris. 3-4 (1975) 475.
[2] P. Faurie, Bull. Soc. Chim. Fr. (1971) 3865.
[3] M. Tsai, M. Greenblatt, W.H. McCarroll, Chem. Matter. 1 (1989) 253.
[4] Istomin, S.Ya., Kotova, A.I., Lyskov, N.V. et.al, Russ. J. Inorg. Chem. 63 (2018) 1291.

## OP-IA-34

# The Mechanisms of Microstructure Formation in Ti-6Al-4V Titanium Alloy Produced by Wire-Feed Electron Beam Additive Manufacturing

Panin A.V., Kazachenok M.S., Perevalova O.B., Martynov S.A.
*Institute of Strength Physics and Materials Science SB RAS, Tomsk, Russia*
*pav@ispms.ru*

Wire-feed additive manufacturing for low-cost, near-net-shape industrial production of large metallic components and repair of metallic materials is currently a subject of great interest and development. The notable advantages of wire feed technology are high deposition rates, reduced material waste and ease of use of the 3D printer. The distinguishing feature of wire-feed electron beam additive manufacturing (EBAM) is also that the process is conducted within a high-vacuum environment. Consequently, EBAM opens up broad prospects for production of reactive materials such as titanium alloys which are widely used in many industrial applications. The main drawbacks of wire-feed EBAM are poor surface finish of the components, residual stresses, distortions and non-equilibrium microstructure of additive manufactured materials in the as-built state due to excessive heat input, the high solidification rates and temperature gradient.

In the present study, the material for investigations was the rectangular Ti-6Al-4V bars obtained by wire-feed EBAM setup developed in ISPMS SB RAS (Tomsk, Russia). The methods of optical, scanning electron and transmission electron microscopy as well as electron backscatter diffraction, differential scanning calorimetry and X-ray diffraction analysis gained insights into the mechanisms of surface finish and microstructure formation of Ti-6Al-4V parts during EBAM process. It was shown that the microstructure of EBAM Ti-6Al-4V samples consists of columnar primary β grains containing crystals of packet and lamellar $\alpha/\alpha'$ phases. The concentration of alloying elements in the $\alpha/\alpha'$ and β phases of titanium alloys is measured by energy-dispersive analysis. The effect of alloying elements on the lattice parameters of the $\alpha/\alpha'$ phase of the samples is demonstrated.

It was shown that the microstructure of the EBAM Ti–6Al–4V samples is characterized by the concentration inhomogeneity of vanadium due to the partial decomposition of the martensitic α' phase during 3D printing. The latter explains the presence of local regions where the vanadium content is significantly greater than its maximum solubility in the α phase in the α/α' laths. As a result, α' → α'' transformations can develop in the highly destorted regions of the α/α'-Ti lattice, in places enriched with vanadium.

The microstructure and mechanical properties of Ti-6Al-4V samples produced using different strategies of 3D printing were discussed.

**Acknowledgement:** This work was supported by the Russian Science Foundation, grant 21-19-00795.

## OP-IA-35

# A Novel Route to Produce Titanium Matrix Composites Strengthened with Titanium Carbide Particles

Pribytkov G.A., Baranovskiy A.V., Korthova V.V., Firsina I.A.
*Institute of Strength Physics and Materials Sciences, Tomsk, Russia*
*gapribyt@mail.ru*

High strength titanium alloys are produced by dopping with different metal additives (aluminium, vanadium, etc.). The dopants dissolve in titanium lattice resulting in solid solution strengthening. Another way to increase the titanium alloys strength is dopping of titanium with non-metallic elements (carbon, boron, silicon). In this case strengthening effect occurs due to disperse hard particles of refractory compounds (carbide, boride silicide) forming in the reaction of titanium with the non-metallic dopants. A suitable combination of strength and plasticity have titanium matrix composites strengthened with disperse carbide particles of submicron or nano- size. We have offered a novel production route of titanium matrix composites with titanium carbide hardening based on intensive mechanical treatment of titanium powder in hydrocarbon liquids (ethanol, heptane, toluene and so on) media. It is known [1,2], that hydrocarbon molecules destruction occurs in the course of titanium powder treatment in ball planetary mill. Released carbon and hydrogen incorporate into titanium resulting in carbide and carbohydride particles formation on the consequent heating. Volume fraction of strengthening phases can be regulated changing MA duration (fig. 1). Depending on the treatment duration an extent of hydrocarbon destruction increases resulting in carbon and hydrogen concentration rise in the reactionary volume.

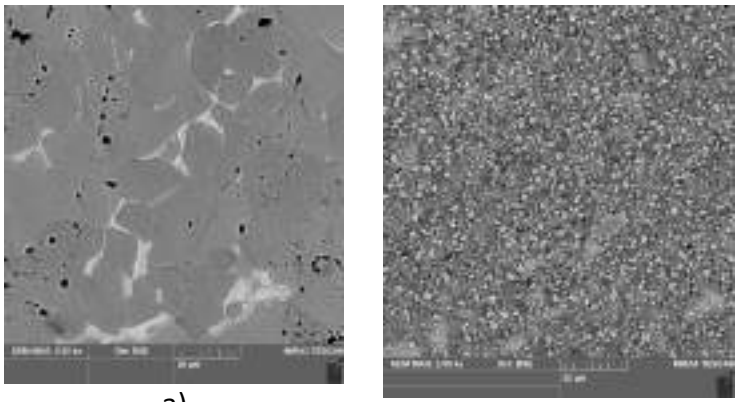

a) b)

*Fig. 1. Microstructure of hot compacted titanium powders mechanoactivated in ethanol media for: a)- 5 min, b)-30 min. Annealed in vacuum 870 C for 120 min.*

**Acknowledgement:** This work was carried out within the framework of the state task of the ISPMS SB RAS, project number FWRW-2021-0005

**References:**

[1] T. S. Suzuki and M. Nagumo. Scripta metallurgica and materialia, **32** (1995) pp. 1215-1220.
[2] G.A. Dorofeev, V.I. Lad'yanov, A.N. Lubnin, V.V. Mukhgalin, O.M. Kanunnikova, S.S. Mikhailova, V.V. Aksenova. Int.J. of Hydrogen Energy 39 (2014) pp. 9690-9699

## PP-IA-36

# On the Synthesis of Molybdenum - Carbide Powder by the Reaction of Molybdenum with Hexane

Kolosov V.N., Miroshnichenko M.N.
*Tananaev Institute of Chemistry-Subdivision of the Federal Research Centre "Kola Science Centre of the Russian Academy of Sciences", Russian Academy of Sciences, Apatity, Russia*
*v.kolosov@ksc.ru*

Molybdenum carbide $Mo_2C$ has electronic and catalytic properties similar to noble metals, but is more resistant to catalytic poisons and sintering. This makes it a potential substitute for expensive and scarce noble metals [1]. One of the common ways to obtain molybdenum carbide powder is temperature-programmed reactions (TPR), which occur when hydrocarbon gases pass through a precursor at a slow heating rate [2]. The precursor is usually a metal or its oxide. The disadvantage of TPR is that in order to obtain reproducible characteristics of the final product, many process parameters must be controlled. In addition, combustible explosive gases must be used. Previously, the possibility of synthesizing tungsten carbide and tantalum carbide by carburizing the powders of these metals by pyrolysis products of an organic liquid, hexane ($C_6H_{14}$) was shown [3, 4]. In relation to the synthesis of carbides by the TPR method, the method is simpler and safer.

The purpose of this work is to study the possibility of synthesizing molybdenum carbide by carburizing molybdenum powder with hexane pyrolysis products.

Magnesium-thermal powders of molybdenum [5] and $C_6H_{14}$ ("pure") were used as reagents. The schematic diagram of the experimental setup is shown in Fig. 1. It is a quartz tube-reactor 4, in which a quartz boat with metal powder 6 is placed. An inert gas (argon "high-frequency"), carrying hexane vapor to the reaction zone, is supplied from a cylinder through pipeline 2.

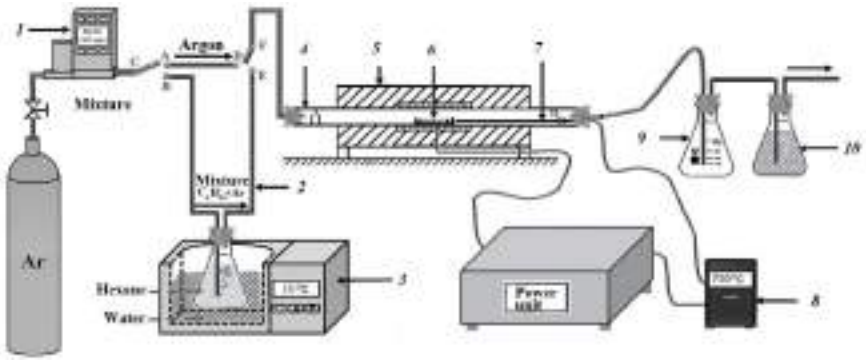


*Fig1. Scheme of the experimental setup: 1 – rotameter, 2 – hexane pipeline, 3 – thermostat for hexane, 4 – reactor tube, 5 – furnace, 6 – quartz crucible, 7 – thermocouple, 8 – thermodat, 9 – buffer tank, 10 – water lock.*

The carburization process was carried out at a temperature (T) of 650-900 °C for a time (t) of 1-3 hours. The temperature of $C_6H_{14}$ was maintained at 10.0±0.3 °C. Here, the partial pressure of its vapor was 10.0 ± 0.2 kPa. The phase composition of the reaction products was

determined on a SHIMADZU XRD-6000 diffractometer ($CuK_\alpha$ - radiation). Using a Micromeritics TriStar II 3020 instrument, the specific surface area was measured by the adsorption static BET method and porosity parameters were measured by the BJH method. The average size of molybdenum carbide crystallites (d) was estimated using the Scherrer formula. At high temperatures during the gasification process, hexane can be split into hydrocarbon gases such as methane ($CH_4$), ethylene ($C_2H_4$), ethane ($C_2H_6$), propane ($C_3H_8$) and butane ($C_4H_{10}$) [3], which will be direct sources of carbon in carbidization process.

In the temperature range of 650–900°C, using hydrocarbon gases formed during the pyrolysis of hexane as a carbon source, the possibility of obtaining powders of molybdenum carbide $Mo_2C$ with an orthorhombic (Pmna) crystal structure was shown (Fig. 2). The lattice parameters of the carbide are respectively: a=0.4748 nm, b=0.6012 nm, c=0.5212 nm (measurement error ± 0.0005 nm).

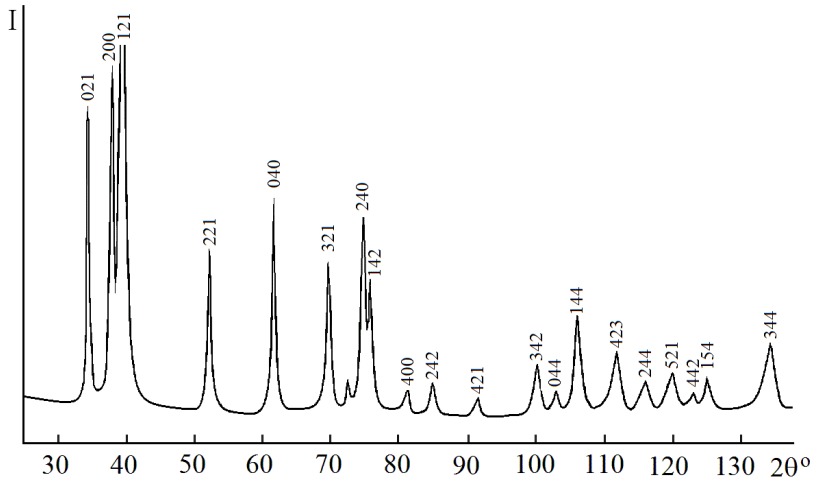


*Fig1. X-ray diffraction pattern $Mo_2C$. Reaction conditions: T = 750°C, t = 2 h.*

The specific surface area of the powders is in the range of 9-21 $m^2/g$. The average sizes of crystallites of tantalum carbides, determined by the X-ray method, are at the level of 15-24 nm. The adsorption curves of the powders of tantalum carbides correspond to the type IV according to the classification of the International Union of Pure and Applied Chemistry (IUPAC). They are distinguished by the presence of a hysteresis loop and are characteristic for materials with a mesoporous structure.

**References:**

[1] Y.Maa, G.Guan, X.Hao et al., Renewable and Sustainable Energy Reviews, 75 (2017) 1101.
[2] A. Hanif, T. Xiao, A.P.E. York et al., Chem. Mater., 14 (2002) 1009.
[3] G. Singla, K. Singh, O.P. Pandey, , Int. J. Hydrog. Energy 40 (2015) 5628
[4] Seon-Min Hwang, Ji-Won Hong, Yong-Ho Park, Dong-Won Lee, Materials, 15 (2022) 7510.
[5] V.N. Kolosov, M.N. Miroshnichenko, V.M. Orlov, Inorg. Mater., 53 (2017) 1058

## OP-IA-37

# Generation of 2D Micro Patterns Using Laser-Induced Shockwave

Junwoo Park, Jaejun Lee
*Department of Polymer Science and Engineering, Pusan National University, Busan, Republic of Korea*
*Jlee-pse@pusan.ac.kr*

A setup that employs laser-driven spallation uses shockwaves to separate thin surface films by generating tensile force at the interface between a substrate and the film. [1] This technique enables the investigation of delamination phenomenon under high strain rates ($> 10^6$ $s^{-1}$) stress loading. [2] However, the delaminated area results in irregular shapes due to uncontrolled spatial shockwave pressure, which limits its applicability in the production of well-aligned structures that are widely used in various fields, such as microelectronics and the biochip industry. We introduce a novel approach that employs spatially regulated pressure of shockwave to create 2D micro/nano surface patterns. We harness the delamination of a polystyrene spherical particle monolayer on polydimethylsiloxane (PDMS) to visualize local delamination, and we report different delamination trends of polystyrene particles by varying particle diameters from 0.5 to 2 μm. The demonstration of 2D spatial pattern requires interparticle attraction, where we tune the attraction using a thin surface coating of poly(vinyl alcohol). By adjusting the laser spot size and shape with a shadow mask, we can spatially regulate shockwave pressures to produce programmed spallation patterns. Our findings highlight the advantages of using shockwave in 2D micro pattern making.

**Acknowledgement:** This project was supported by National Research Foundation of Korea, ICT(2021M3F6A1085855), development of shockwave protective composite materials.

**References:**

[1] Wang, J.; Weaver, R. L.; Sottos, N. R. A parametric study of laser induced thin film spallation. Experimental Mechanics 2002, 42 (1), 74-83.
[2] Grady, M. E.; Geubelle, P. H.; Braun, P. V.; Sottos, N. R. Molecular Tailoring of Interfacial Failure. Langmuir 2014, 30 (37), 11096-11102.

## OP-IB-01

# In-Situ Studies of Fractal Microstructure in Nanocarbon-Polymer Composites

Artyukov I.A.[1], Bellucci S.[2], Levin V.M.[3], Morokov E.S.[3], Petronyuk Yu.S.[3]

*1 – P.N. Lebedev Physical Institute, Russian Academy of Sciences, Moscow, Russia*

*2 – National Frascati Laboratory, National Institute of Nuclear Physics, Rome, Italy*

*3 – N.M. Emanuel Institute of Biochemical Physics, Russian Academy of Sciences, Moscow, Russia*

*levin1943@gmail.com*

Polymer nanocomposites have been considered for long time as prospective materials with promising physical properties – mechanical, thermal, electrical ones. The origin of the exclusive characteristics should be a uniform distribution of nano-reinforcement over the polymer matrix volume. It is proposed that a minimal weight content of nano-reinforcement is required to form a continuous cluster of nanoparticles to provide enhanced properties of the composite material comparing with the pristine polymer. But in practice the problem of extraordinary mechanical characteristics has still remained to be unsolved. One of the most probable sources of small efficiency of nano-reinforcing is aggregation of nanoparticles into fractal conglomerates dispersed in the polymer matrix volume. Nanoparticle aggregation and fractal nature of nano-reinforcement in polymer nanocomposites has been initially demonstrated indirectly from data on the slope of scattering efficiency curves obtained in ultra-small-angle X-ray and neutron scattering (USAXS and USANS) experiments. But it is of great interest to investigate directly the volume microstructure inside polymer nanocomposites basing on the concept of its fractal nature. Such an investigation makes it possible to observe a real reinforcement distribution in the composite interior, to reveal structural peculiarities for distinct technological processes of polymer-nanocarbon composite production, and to study real processes of irreversible deformation and destruction of polymer nanocomposite under mechanical loading. Among the contemporary high-resolution visualization techniques only two ones - the X-ray computed microtomography (μ-CT) and the scanning impulse acoustic microscopy (SIAM); could be applied for non-destructive assessment of nanocomposite microstructure and studying dynamics of microstructural changes under loading.

The paper presents results of application of the both methods for observing the bulk microstructure of epoxy composites with diverse types of nanocarbon reinforcement – graphite nanoplates (GNP), carbon nanoflakes (CNF) and nanotubes (CNT). The applied techniques demonstrate different levels of micron resolution, but application of two techniques with different imaging principles and contrast mechanisms provides reliability in interpretation of the observed microstructures. Both acoustic and X-ray images demonstrate complicated structure being formed by extensive (several tens of micrometers) inclusions that

are formed by nanoparticle fractal aggregates enclosed in air shells. Such aerogel inclusions are seen as bright spots in the both types of internal microstructure images. In the acoustical

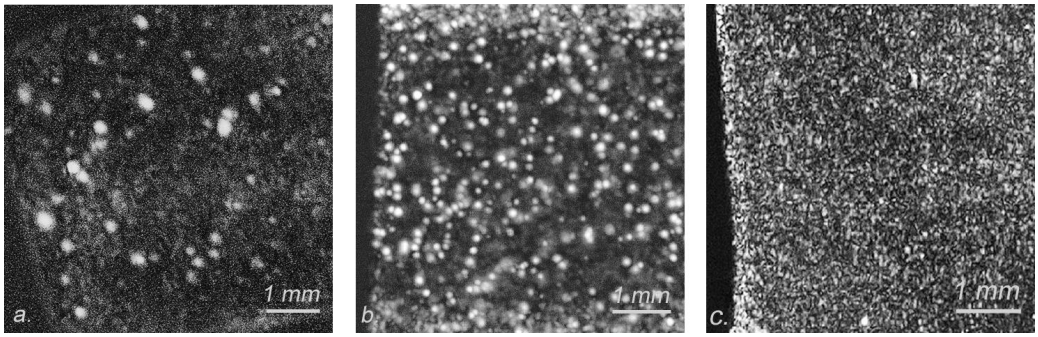


***Fig.1**. Acoustic imaging of carbon-epoxy nanocomposite with different contents and types of nanofiller at the depth of 0.5 mm within nano-composite specimens: (a) epoxy+1.5 wt% CNF; (b) epoxy+0.75 wt% GNP; (c) epoxy+0.1 wt%.CNT*

images bright regions are caused by the total reflection of probe focused ultrasound at the epoxy-air interfaces. In the X-ray images occurrence of bright regions results from small X-ray absorption inside aerogel fractal inclusions. So, the key problem of realization of exceptional physical properties in polymer nanocomposites is wetting of nano-reinforcement by matrix polymer resins. Both acoustical microscopy and X-ray microtomography are efficient techniques for assessment of a level nano-reinforcement dispersibility in nanocomposites.

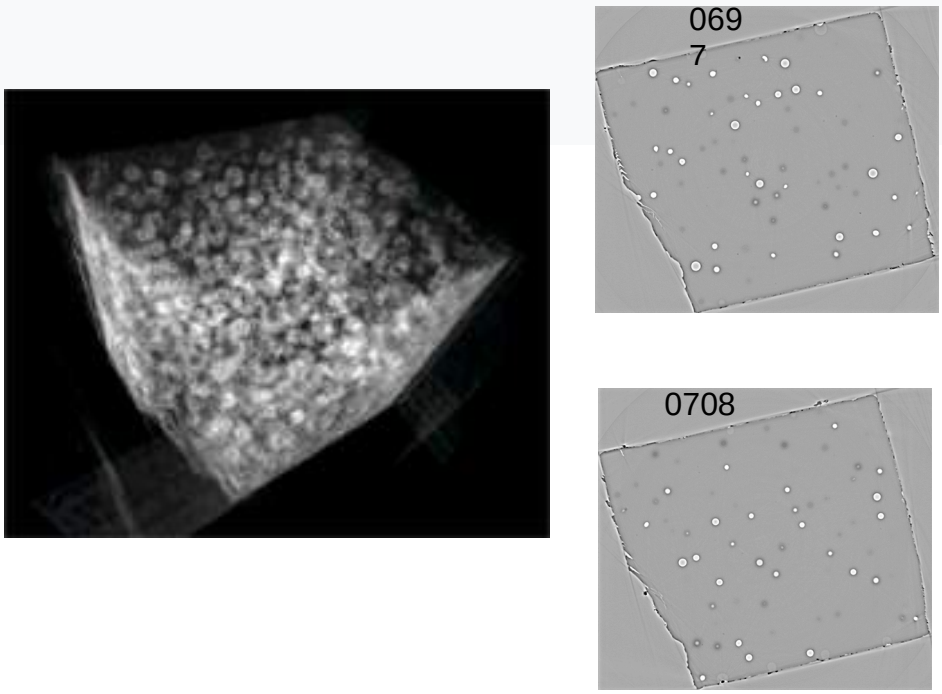


*Fig.2. X-ray µ-CT images of bulk microstructure inside the epoxy+0.1 wt%.CNT specimen, On the right -3D rendering of the specimen interior. Numerous inclusions are seen; they are nano-particle fractal agglomerates enclosed in air shell (aerogel inclusions). On the left – slices in near sections; aerogel inclusions are seen as white and dark circles.*

## OP-IB-02

# Investigation of the Change in the Structure of MWCNT-Si Composites during Heat Treatment

Zavorin A.V.[1,2], Moseenkov S.I.[1], Kuznetsov V.L.[1], Selytin A.G.[3], Ishchenko A.V.[1]
*1 – Boreskov Institute of Catalysis, Novosibirsk, Russia*
*2 – Novosibirsk State University, Novosibirsk, Russia*
*3 – Synchrotron radiation facility SKIF, Boreskov Institute of Catalysis, Novosibirsk, Russia*
*zavorin@catalysis.ru*

Multi-walled carbon nanotubes (MWCNTs) have unique physical and chemical properties (structural, mechanical, and electrical), which makes them one of the main materials for nanotechnologies. At present, due to their unique properties, MWCNTs are used as a reinforcing component in various composite and functional materials that can be used in various fields of human life [1,2]. One of the possible practical applications of MWCNTs is their use as a reinforcing component of ceramic materials. The introduction of MWCNTs into the composition of ceramics makes it possible to increase the crack resistance, strength, and achieve the appearance of electrical conductivity of such modified materials [3]. As a rule, the change in the properties of composites is associated with the intergranular modification of the composite. The most important aspect in creating composites with nanotubes is the nature of the interface between the components of the ceramic matrix and the MWCNT surface, since it is this interface that determines the main properties of the composite (strength and electrical properties). When MWCNTs are introduced into ceramics using high-temperature treatments, their morphology and electrical properties can be preserved, as well as their transformation into high-strength carbides, which increase the strength of the ceramic matrix. An example is the synthesis of high-strength ceramics based on boron carbide, where silicon carbide particles formed from MWCNTs provide an increase in the bending strength of the initial ceramic by 1.5 times, up to 585 MPa [4].

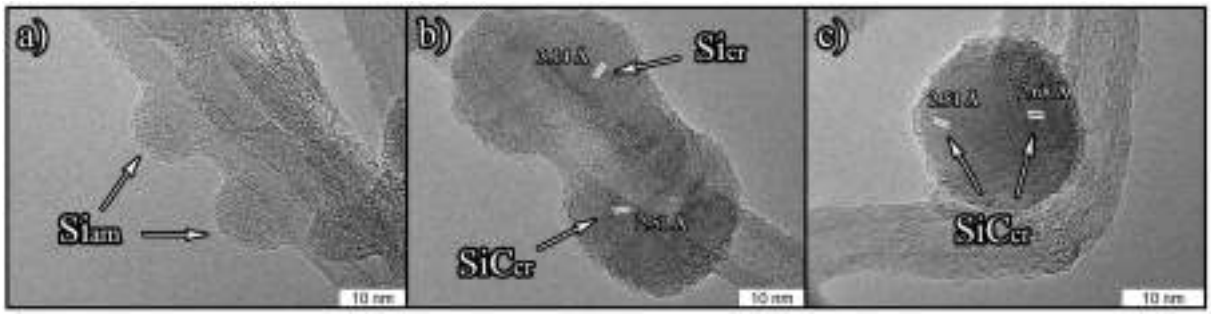


*Fig. 1. a – initial MWCNT-Si composite; b – MWCNT-SiC-1040°C composite; c – composite MWCNT-SiC-1350°C.*

The purpose of this work was to study the transformation of the structure of MWCNT-Si composites obtained by gas-phase deposition of silicon on the surface of during heat treatment in the temperature range of 700–1350°C and a pressure of $10^{-6}$ mbar.

## OP-IB-02

*Ex situ* Raman spectroscopy, TEM, and XRD have been used to study the processes occurring at the multi-walled carbon nanotube/silicon interfaces (MWCNT/Si) during heat treatment at temperature range 700–1350°C. MWCNT-Si composites contain highly dispersed silicon particles deposited on the surface of MWCNTs by the CVD method. The *in situ* XRD method was used to study the kinetics and estimate the activation energy of the process of silicon carbide formation during the interaction of silicon particles with the MWCNTs surface.

**Acknowledgement:** This work was supported by the Ministry of Science and Higher Education of the Russian Federation within the governmental order for Boreskov Institute of Catalysis (project AAAA-A21-121011390054-1). The studies were carried out using facilities of the shared research center "National center of investigation of catalysts" at Boreskov Institute of Catalysis. The work was done at the shared research center SSTRC on the basis of the VEPP-4 - VEPP-2000 complex at BINP SB RAS.

**References:**

[1] Rathinavel, S.; Priyadharshini, K.; Panda, D. A Review on Carbon Nanotube: An Overview of Synthesis, Properties, Functionalization, Characterization, and the Application. *Materials Science and Engineering: B* **2021**, *268*, 115095, doi:10.1016/j.mseb.2021.115095.
[2] Ferreira, F.V.; Franceschi, W.; Menezes, B.R.C.; Biagioni, A.F.; Coutinho, A.R.; Cividanes, L.S. Synthesis, Characterization, and Applications of Carbon Nanotubes. In *Carbon-Based Nanofillers and Their Rubber Nanocomposites*; Elsevier, 2019; pp. 1–45 ISBN 978-0-12-813248-7.
[3] Samal, S.S.; Bal, S. Carbon Nanotube Reinforced Ceramic Matrix Composites- A Review. *JMMCE* **2008**, *07*, 355–370, doi:10.4236/jmmce.2008.74028.
[4] Karagedov, G.R.; Shutilov, R.A.; Kolesov, B.A.; Kuznetsov, V.L. The Effect of Carbon Nanotubes Introduction on the Mechanical Properties of Reaction Bonded Boron Carbide Ceramics. *Journal of the European Ceramic Society* **2021**, *41*, 5782–5790, doi:10.1016/j.jeurceramsoc.2021.05.014.

## OP-IB-03

# Modifying Effect of Carbon Nanofibers on Polyethylene Depending on their Synthesis Condition

Fedorov A.L.[1], Petukhova E.S.[1], Argunova A.G.[1], Afonnikova S.D.[2], Potylitsina A.R.[2,3], Bauman Yu.I.[2,3], Mishakov I.V.[2,3]

*1 – Institute of Oil and Gas Problems of the SB of the RAS, Yakutsk, Russia*

*2 – Boreskov Institute of Catalysis, Novosibirsk, Russia*

*3 – National Technology Initiative Hydrogen Research Center of Boreskov Institute of Catalysis, Novosibirsk, Russia*

*gelvirb@mail.ru*

The development of technologies aimed to processing of natural gas and associated petroleum gas is of high interest for Russian Federation. One of the advanced approaches is based on catalytic pyrolysis of $C_1$-$C_4$ hydrocarbons to produce hydrogen (free from $CO_x$ admixtures) and carbon nanofibers (CNFs). A simple and versatile method to synthesize Ni-Cu alloys serving as a catalyst for processing of light hydrocarbons has been recently proposed in Boreskov Institute of Catalysis [1, 2]. On the other side, the microdispersed Ni-M alloys (where M = Mo, W etc.) can be effectively applied for catalytic decomposition of polychlorinated hydrocarbons (trichloroethylene, TCE) usually present in composition of industrial organochlorine wastes, with the production of CNFs characterized by the unique segmented structure [3]. Addition of the N-containing co-reagent (i.e., acetonitrile) into the reaction mixture can be used to obtain the N-functionalized carbon nanofibers in one stage [4]. The selected TEM images of the produced carbon nanofibers with different structure obtained via catalytic pyrolysis of both unsubstituted and chlorinated $C_2$ hydrocarbons are presented in Figure 1.

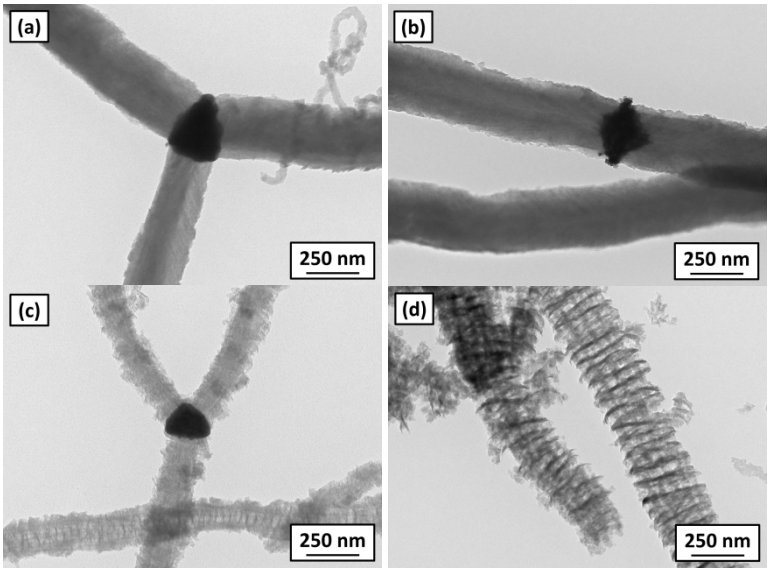


*Figure 1. The TEM micrographs of carbon nanofibers obtained by decomposition of (a,b) $C_2H_4$ over a Ni-Cu catalyst at 550 °C, (c) $C_2HCl_3$ over a Ni-W catalyst at 550 °C, (d) $C_2HCl_3$ + $CH_3CN$ over a Ni-Mo-W catalyst at 600 °C*

The search novel effective areas for application of the produced carbon nanofibers (including N- and C-functionalized ones) is recognized as the important direction of the materials science [5]. The Institute of Oil and Gas Problems has recently proposed to use CNFs as modifying additives for the low-pressure polyethylene (PE) (PE2NT11, Kazanorgsintez PJSC). CNFs obtained under different synthetic conditions (Fig. 1) were introduced into PE in amount of 0.5, 1, and 3 wt.%. It was shown that the CNF synthesis conditions (duration, nature of raw material), as well as their textural characteristics, have a significant effect on the properties of resulted polyethylene composites. An improvement in the deformation-strength properties was revealed for samples containing CNFs produced from $C_2H_4$. Tensile strength increased up to 24%, yield strength – up to 10%, elastic modulus – up to 20%, whereas the elongation at break and at yield strength remained at the level of the neat PE. At the same time, it was found that the use of CNFs characterized by the presence of polar atoms (N, Cl) leads to a significant decrease in the mechanical characteristics of the material. The reason of the fact observed may be in the high polarity of the surface of such N- and Cl-functionalized CNF materials, which reduces the adhesion at the polymer matrix/filler interface.

Thus, for obtaining the PE composites with an improved level of performance, it is recommended to introduce carbon nanofibers produced by the pyrolysis of $C_2$ hydrocarbons, at a concentration of no more than 1 wt.%; the duration of CNF synthesis should be around 20–40 min.

**Acknowledgement:** This work was supported by the State Task of the Ministry of Science and Higher Education of the Russian Federation No. 122011100162-9, FWRS-2021-0004, using the scientific equipment of the Center for Collective Use of the Federal Research Center “Yakutsk Science Center SB RAS” (grant 13.ЦКП.21.0016).

**References:**

[1] I.V. Mishakov, S.D. Afonnikova, Y.I. Bauman, Y.V. Shubin, M.V. Trenikhin, A.N. Serkova, A.A. Vedyagin, Kinetics and Catalysis. 63 (2022) 97.
[2] S.D. Afonnikova, I.V. Mishakov, Y.I. Bauman, M.V. Trenikhin, Y.V. Shubin, A.N. Serkova, A.A. Vedyagin, Top. Catal. 2023. DOI: 10.1007/s11244-022-01739-7
[3] A.R. Potylitsyna, Y.V. Rudneva, Y.I. Bauman, P.E. Plyusnin, V.O. Stoyanovskii, E.Y. Gerasimov, A.A. Vedyagin, Y.V. Shubin, I.V. Mishakov, Materials. 16 (2023) 845:1.
[4] A.R. Potylitsyna, I.V. Mishakov, Y.I. Bauman, L.S. Kibis, Y.V. Shubin, M.N. Volochaev, M.S. Melgunov, A.A. Vedyagin, Reaction Kinetics, Mechanisms and Catalysis. 135 (2022) 1387.
[5] D. Yadav, F. Amin, A. Ehrmann, Eur. Polym. J. 138 (2020) 109963.

## OP-IB-04

# Development and Characterization of Carbon–Silica Composite Materials and Their Study for Preparing Heterogeneous Catalysts for the Enzymatic Low-Temperature Synthesis of Esters

Kovalenko G.A., Perminova L.V., Moseenkov S.I., Serkova A.N., Salanov A.N., Kuznetsov V.L.
*Boreskov Institute of Catalysis, Novosibirsk, Russia*
*galina@catalysis.ru*

Carbon-silica composite materials (CSCMs) differing in the relative content of carbon component – in the form of multiwalled carbon nanotubes (MWCNTs), and silica component – in the form of xerogel of silicon dioxide ($SiO_2$), have been prepared by the following methods: *(1)* the impregnation according to moisture capacity of MWCNTs with silica sol and *(2)* the treatment of oxidized MWNTs with tetraethoxysilane following by subsequent hydrolysis and polycondensation [1]. After an appropriate heat treatment, the composites have been studied by various physicochemical methods, such as nitrogen porosimetry, scanning and high-resolution electron microscopy (SEM and HRTEM), XRF-analysis, thermal analysis.

It has been found that the physicochemical properties of the CSCMs differed significantly depending on their chemical composition, namely, the mass ratio of MWCNTs and $SiO_2$ [1]. Firstly, with an increase in the $SiO_2$ content, the texture of CSCMs has changed: the specific surface area ($S_{sp.BET}$, $m^2/g$) increased, the total pore volume ($V_\Sigma$, cc/g) and average pore diameter (D, nm) decreased. The maximum pore diameter in 25–35 nm was observed at silica content of 10±2 wt %, the minimum pore diameter in 7–9 nm – at 56±2 wt % of $SiO_2$. The change in texture occurred due to thermal cracking of amorphous silica sol particles deposited in the pores between interlacing MWCNTs (Fig. 1a). In the HRTEM image not only the primary round silica sol particles (ca. 10 nm in size) were observed, but also elongated filaments of carbon nanotubes bundled together, each individual MWCNT measuring approx. 20 nm in diameter The SEM image (Fig. 1b) confirmed that carbon nanotubes which were not encapsulated (or immured) inside $SiO_2$ conglomerates were chaotically interlaced.

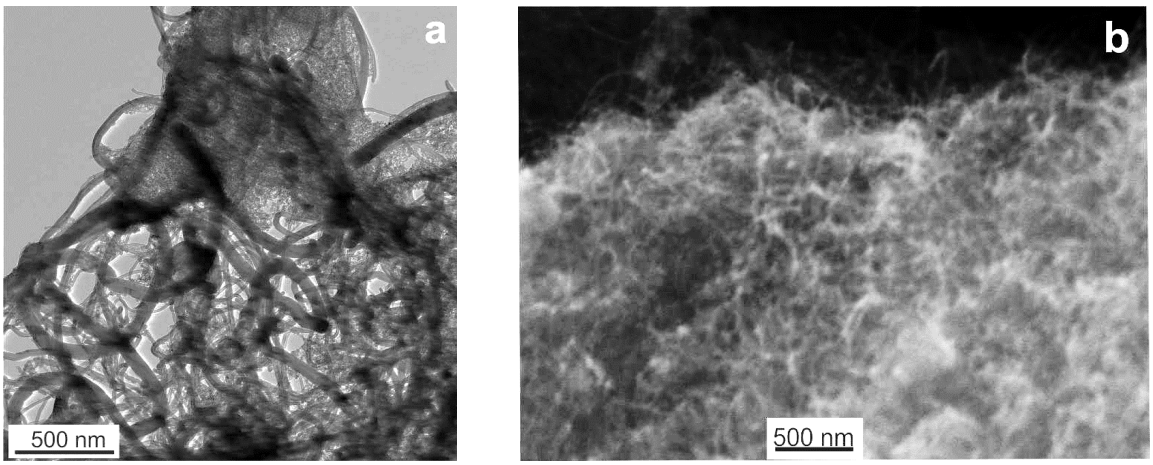


*Fig.1. HRTEM (a) and SEM (b) images of CSCMs prepared by method (1) and having a similar silica content, equal to 25 wt.% and 28 wt.% of $SiO_2$, respectively*

It has been found that an increase in the silica content led to a monotonic increase in the carbon burnout temperature from 610–630 to 670–690°C determined by thermal analysis. Hence, the thermal stability of the composites was higher than that of initial and oxidized MWCNTs. The electric conductivity of CSCMs decreased linearly with the increase of dielectric silica content till to 58 wt% of $SiO_2$ [1]. The deterioration of conductivity was observed in the entire studied pressure range (20–140 MPa), apparently due to blocking the appearance of new contacts between MWCNTs encapsulated in $SiO_2$-containing conglomerates.

The carbon-silica composite materials have been studied as adsorbing supports for preparing heterogeneous biocatalysts (BCs) for the low-temperature enzymatic synthesis of esters. The enzyme activity of BCs was measured in the esterification of heptanoic acid ($C_7$) with butanol ($C_4$) in an organic solvent (hexane) at 20-22$^o$C and 1 bar. It has shown that the adsorption value toward active component – recombinant lipase r*Pichia*/lip, and the esterifying activity of prepared biocatalysts monotonically decreased with an increase in the silica content in the CSCMs. At the maximum content of $SiO_2$ (58 wt %), the lipase adsorption values and biocatalytic activities decreased by a factor of 2–2.5 and 2.5–7, respectively. These parameters changed due to a decrease in the proportion of MWCNTs not encapsulated inside $SiO_2$-conglomerates, on the surface of which lipase was actually adsorbed since the adsorption of the enzyme on silica was insignificant. Based on analysis of all obtained results, the conclusion was made that the molecules of lipase r*Pichia*/lip may be consider as testing adsorbate for assessing the specific surface area of an individual carbon component. So, in CSCMs with a carbon content of 80±7 and 40±1 wt % of MWCNTs, respectively, only half (½) and one fifth (⅕) of the total surface area of the composite material, equal to 180 ± 20 $m^2/g$, were formed by non-immured MWCNTs.

**Acknowledgement:** This work was supported by the Ministry of Science and Higher Education of the Russian Federation under a state task to Boreskov Institute of Catalysis of the Siberian Branch of the Russian Academy of Sciences (project no. AAAA-A21-121011390007-7).

**References:**

[1] G.A. Kovalenko, L.V. Perminova, V.V. Goidin, A.V. Zavorin, S.I. Moseenkov, V.L. Kuznetsov, Catal. Kinetics. 64 (2023) 201.

## OP-IB-05

# Investigation of the Structure and Morphology of Coal Pitches

Popova A.N., Nikitin A.P., Sozinov S.A., Gavrilyuk O.M., Ismagilov Z.R.
*FRC of Coal and Coal Chemistry SB RAS, Kemerovo, Russia*
*h991@yandex.ru*

The creation of high-tech carbon functional materials, including high-quality carbon fiber from pitches of various nature, is relevant. Coal pitch (CP) is the most valuable product of metallurgical coke production and, due to its physico-chemical features of composition and properties, is promising for obtaining both high-quality carbon fiber and needle coke of "super premium" quality.

The phase composition and the main structural characteristics of the CP have been studied by X-ray diffraction methods. It is shown that in order to evaluate the structural characteristics of the studied samples, it is optimal to decompose the reflection reflection profiles from the corresponding crystallographic planes into 2 components corresponding to carbon phases with significantly different characteristics. The carbon phases have a turbostratic structure.

The Raman spectroscopy method revealed the regularities of the formation of the molecular structure of the CP. The main elements of the Raman spectra of the CP are the D- and G-bands. To describe the structural features of the CP, the value of the ratio of their intensities ($I_D/I_G$) was chosen, which shows the measure of the disorder of the carbon frame, so the relative content of defective and defect-free structures. As additional characteristics, the calculated fraction of edge defects included in graphite-like crystallites and the tangent of the baseline slope angle in the region of the first scattering strand were taken into account. A smaller number of defect-free graphite-like structures reduces the thermal conductivity from the surface deep into the sample, therefore, a higher softening temperature can be expected for such samples, compared with less defective samples.

The SEM method shows that the shape of particles and the morphology of the CP and their surfaces are characteristic of amorphous bodies: particles do not have a definite shape, and their surface has the structure of a melted body (there are no sharp boundaries, there are surges on the surface). CP particles are a two-phase system with an amorphous matrix in which inclusions of another phase are dispersed in the form of clusters of spherical particles with sizes from fractions of a micron to several microns. A higher reflectivity of spherical particles with respect to electrons was also found, which may be explained by a higher degree of their crystallinity in comparison with the matrix.

**Acknowledgement:** The research was carried out at the expense of the grant of the Russian Science Foundation No. 22-13-00042 https://rscf.ru/project/22-13-00042/

## OP-IB-06

# Comparative Study of Group Properties of Three Varieties of Coal Pitches

Ismagilov Z.R., Gavrilyuk O.M., Nikitin A.P.
*FRC of Coal and Coal Chemistry SB RAS, Kemerovo, Russia*
*o.m.gavriljuk@mail.ru*

The paper studies the characteristics of samples of coal pitches made of coal tar from various manufacturers. The main parameters characterizing the properties of coal pitch are determined.

As an object of research, samples of coal pitches (CP) obtained by dispersing coal tar from various manufacturers of JSC "EVRAZ", Novokuznetsk (CP 1 and CP 2) and JSC "Altai-Coke", Zarinsk (CP 3) were used.

Fractional analysis of the coal tar (CT) was performed by overclocking in the temperature range of 25-400 ° C on the ARN-Lab-3 device. As a result of the dispersal of resin samples provided from each manufacturer, four fractions with boiling points < 210, 210-300, 300-360 and > 360 °C were obtained [1]. The obtained separation results are shown in Table 1.

Table 1. Fractional composition during distillation of the studied CT samples

| Sample | Composition of CT, % by weight | | | |
|---|---|---|---|---|
| | Light + phenolic | Naphthalene + absorbent | Anthracene | CP (>360°C) |
| CT 1 | 1,2 | 10,2 | 5,5 | 83,1 |
| CT 2 | 1,0 | 9,8 | 2,0 | 87,2 |
| CT 3 | 0,7 | 12,0 | 7,2 | 80,1 |

The obtained samples of CP are characterized by the following main parameters (Table 2).

Table 2. Main characteristics of CP

| № | Indicator | CP 1 | CP 2 | CP 3 |
|---|---|---|---|---|
| 1 | Softening temperature, °C | 71,5 | 76,5 | 71,5 |
| 2 | Yield of volatile substances, *X*, % | 54,3 | 53,1 | 61,1 |
| 3 | Ash content, % | 0,1 | 0,1 | 0,2 |
| 4 | The content of insoluble substances: | | | |
| | in quinoline | 10,3 | 12,9 | 4,5 |
| | in toluene | 32,2 | 33,3 | 25,8 |

The obtained CP were divided into fractions by sequential dissolution in toluene, hexane, and quinoline, with distillation of the corresponding extracts on a rotary evaporator IKA RV10 basic. Solid precipitates of α, α1 fractions on the filter were washed with toluene and hexane

and dried at 69 ° and 110 ° C, respectively. The fractional composition of the sands is presented in Table 3.

Table 3. Fractional composition of CP

| № п/п | | CP 1 | CP 2 | CP 3 |
|---|---|---|---|---|
| | Fraction content, % (by weight) | | | |
| 1. | *α*- fraction, % | 29,19 | 29,58 | 24,68 |
| 2. | $\alpha_1$- fraction, % | 9,34 | 11,45 | 4,3 |
| 3. | *γ*- fraction, % | 25,39 | 26,11 | 36,19 |
| 4. | *β*- fraction, % | 36,08 | 32,8 | 34,83 |

As a result of the work, the properties of the obtained CP and their group components, which differ in their characteristics, are investigated.

**Acknowledgement:** Исследование выполнено за счет гранта Российского научного фонда № 22-13-00042, https://rscf.ru/project/22-13-00042/

**References:**

[1] Ismagilov Z. R., Gavrilyuk O. M. Comparative studies of industrial samples of coal tar // Bulletin of the Kuzbass State Technical University. 2022. No. 5(153). pp. 22-29.

## OP-IB-07

# Effects of Ag Doping on the Structure and Electromagnetic Properties of Ag/MWCNT-PMMA Composite

Golubtsov G.V.[1,2], Selyutin A.G.[1], Ishchenko A.V.[1,2], Gorokhov G.V.[3], Misiyuk P.Y.[3], Valynets N.I.[3], Kazakova M.A.[1]

*1 – Boreskov Institute of Catalysis SB RAS, Lavrentieva 5, Novosibirsk 630090, Russia*

*2 – Novosibirsk State University, Pirogova 2, Novosibirsk 630090, Russia*

*3 – Institute for Nuclear Problems Belarusian State University, Bobruiskaya str. 11, Minsk, 220006, Belarus*

*ggv@catalysis.ru*

The development of shielding material to decrease the negative impact of electromagnetic interference (EMI) is a research hotspot. In this regard, conductive composites based on polymers and multi-walled carbon nanotubes (MWCNTs) show great potential. MWCNTs have significant advantages when used as conductive fillers for polymer composites due to their structural, mechanical, and electrical properties. In addition, the shielding characteristics of polymer composite materials can be enhanced by adjusting their electrical conductivity, permittivity, and permeability by selecting appropriate fillers and controlling their distribution in the composite.

In this study, we propose an efficient strategy for the synthesis of Ag/multi-walled carbon nanotubes-polymethylmethacrylate (Ag/MWCNT-PMMA) composites, which consists in modifying the oxidized MWCNT structure with various amounts of Ag nanoparticles by impregnation and subsequent distribution of the obtained Ag/MWCNT-Ox hybrids in a PMMA matrix by coagulation precipitation. HRTEM and XRD show that Ag particles in Ag/MWCNT-Ox samples are present in the form of two ensembles corresponding to larger and smaller particles located on the surface and in the internal channels of MWCNT-Ox, respectively (Fig. 1 (a)). Two series of Ag/MWCNT-PMMA samples were obtained with varying Ag content from 0.2 to 2.5 wt.% and MWCNT content before and after the percolation threshold - 4 and 10 wt.%, respectively.

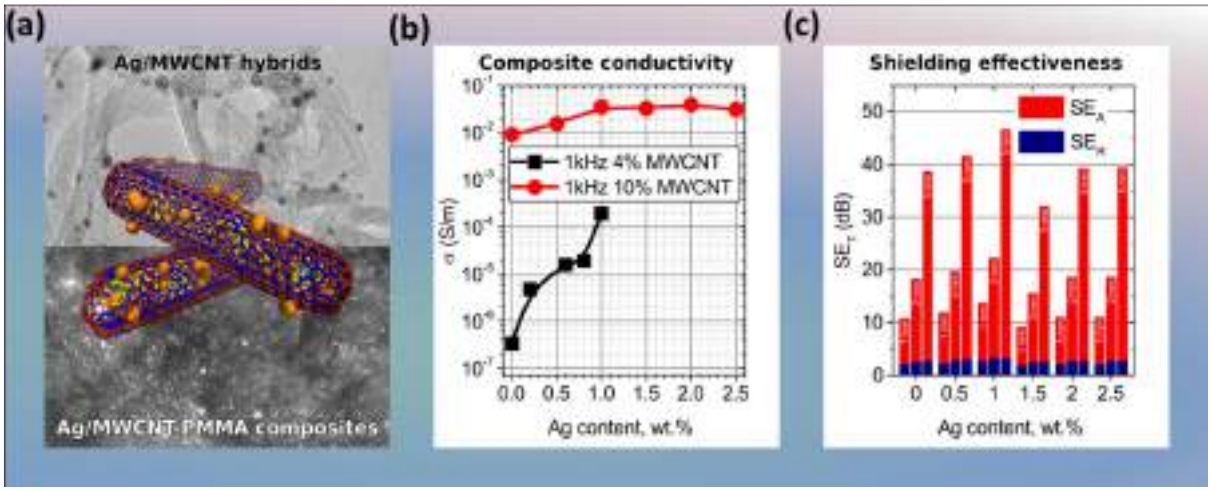


*Fig. 1. Typical TEM and SEM inages of Ag/MWCNT hybrids and Ag/MWCNT-PMMA composites (a), Electrical conductivity of Ag/MWCNT-PMMA composites with MWCNTs content - 4 and 10 wt.% at a frequency of 1 kHz (b), Concentration dependences of shielding efficiency $SE_T$ at 30 GHz for Ag/MWCNT-PMMA composites with MWCNT content of 10 wt.% at various thickness (c).*

The study of the electrical conductivity in the frequency range of 100 Hz–1 MHz showed that for the first composite series with an MWCNT content of 4 wt.%, the introduction of even a small Ag amount (0.2 wt.%) leads to a decrease in the percolation threshold in a three-component system (Fig. 1 (b)). In the case of Ag/MWCNT-PMMA samples containing 10 wt.% of MWCNT, the introduction of Ag up to 1 wt.% leads to a monotonic increase in conductivity within one order of magnitude (Fig. 1 (b)). A study of the electromagnetic properties demonstrated that Ag/MWCNT-PMMA composites exhibit high shielding efficiency for incident radiation in the frequency range of 26-37 GHz (Fig. 1 (c)). Thus, Ag/MWCNT-PMMA composites have broad application prospects in the field of electromagnetic compatibility and also as a basis for the fabrication of metamaterials with desired characteristics.

**Acknowledgement:** This work was funded by RFBR and BRFBR, project numbers 20-53-04008 and F21PM-022, respectively.

## OP-IB-08

# Hybrid Graphite/Nanodiamond Carbon Nanoparticles as a Model Filler for Polymer Composite Materials

Kurkin T.S.[1], Lebedev O.V.[1], Gatin A.K.[2], Golubev E.K.[1], Vasiliev A.L.[3], Ozerin A.N.[1]

*1 – Enikolopov Institute of Synthetic Polymer Materials Russian Academy of Sciences, Moscow, Russia*

*2 – N. N. Semenov Federal Research Center for Chemical Physics Russian Academy of Sciences, Moscow, Russia*

*3 – Federal Scientific Research Center "Crystallography and Photonics" Russian Academy of Sciences, Moscow, Russia*

*t.kurkin@gmail.com*

Detonation nanodiamond soot (NDS) is an affordable type of nanofiller with a unique set of characteristics [1]. This uniqueness comes from the hybrid graphite/nanodiamond structure of NDS powder. NDS is obtained at the post-detonation stage of the nanodiamond (ND) synthesis process, preceding the stage of NDs purification from non-diamond carbon. This significantly reduces the cost of NDS, making it an affordable alternative to the pure NDs. Considering that NDS can contain a high amount of non-diamond carbon, such as graphite, it is possible to obtain electrically conductive polymer composites modified with NDS. By using NDS powders of different synthesis it is be possible to control characteristics of the polymer composites modified with NDS. For instance, it is possible to differently enhance adhesion strength of polymer fiber/epoxy matrix as a result of its modification by NDS of various synthesis [2].

In this work, the results of a complex investigation of structure and properties of NDS of different synthesis are presented. Particularly, 3 NDS systems were studied, each of them being obtained under different detonation conditions.

Size distribution of NDS particles, dispersed in different liquid media, was investigated using dynamic light scattering and laser diffraction analysis methods. From the obtained data, as well as the results of zeta-potential measurements, it was concluded that NDS primary particles tend to aggregate/agglomerate into aggregates/agglomerates of a certain size independently of the medium they are dispersed in, or for how long they are kept in that medium. This feature makes NDS a good model object for the research of properties of composite materials since it allows to reduce the effect of polymer matrix type on the overall properties of the composites.

Additional data was obtained using scanning electron microscopy, scanning tunneling microscopy, atomic force microscopy, X-ray diffraction, and Raman spectroscopy. It was demonstrated that in NDS the spherical ND particles are densely packed into strong-coupled aggregates surrounded by graphite nanoribbons [3]. Examples of the obtained microscopy results, as well as the dependencies of specific resistance of NDS powders of different synthesis on their volume fraction, are presented in Fig. 1. X-ray diffraction analysis estimated the volume fraction of NDs in NDS as ~45 vol.%, 30 vol.% and 14 vol.% for each studied NDS

system, simultaneously showing that the graphite is not defective, which was confirmed with the electron diffraction method.

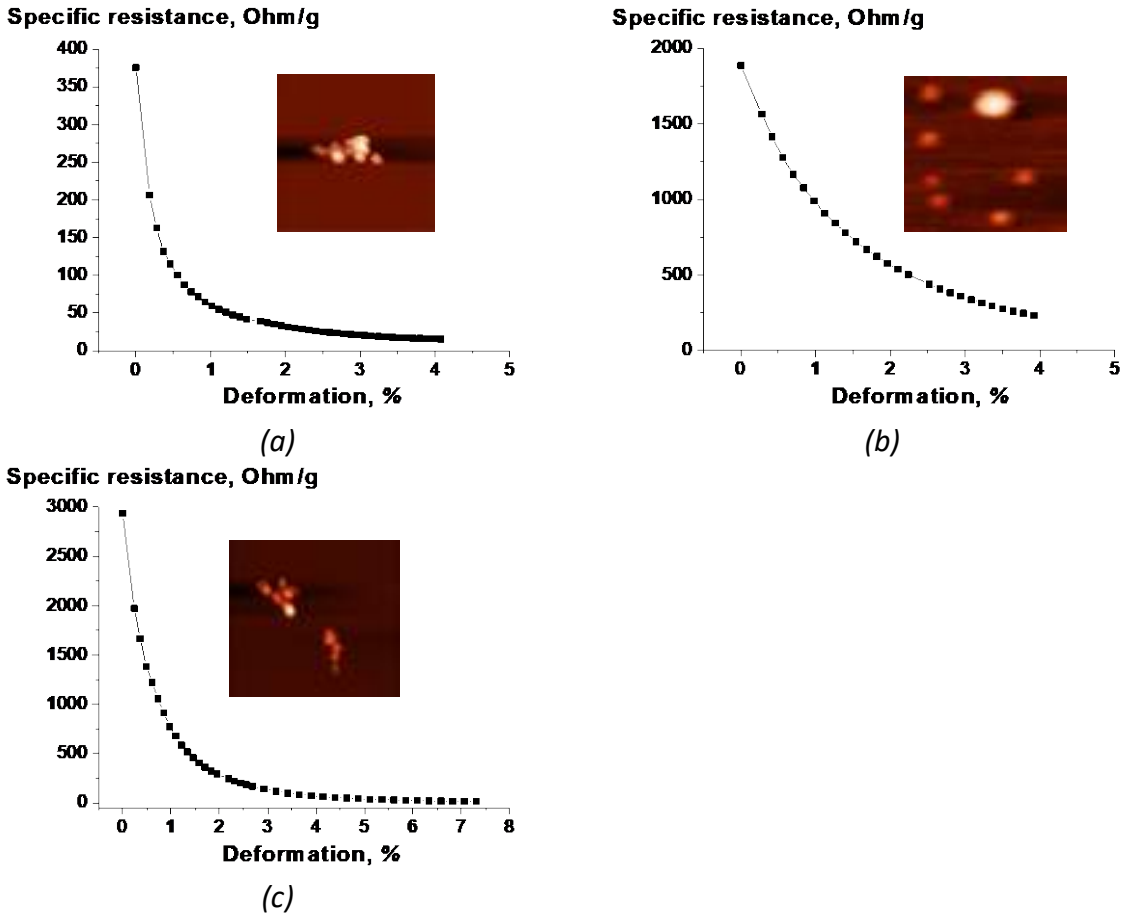


*Fig. 1. Specific resistance of NDS powder measured under compression, with NDS graphite/nanodiamond volume ratio being (a) 0.55/0.45, (b) 0.30/0.70 and (c) 0.14/0.86. For each graphite/nanodiamond powder the corresponding AFM images are provided.*

Composited based on UHMWPE and PP and filled with different NDS particles were studied. It was demonstrated that this structure of NDS allows to efficiently use NDS as a filler for polymer composites to increase polymer characteristics such as electrical conductivity or tribological characteristics, similarly to conventionally applied fillers such as carbon black. It was observed that the properties of the nanocomposites, such as mechanical, tribological, and electrophysical characteristics, strongly depend on the type of the NDS used.

**Acknowledgement:** The reported study was funded by RSF according to the research project № 22-13-00359.

**References:**

[1] V.Yu. Dolmatov, A.N. Ozerin, I.I. Kulakova, O.O. Bochechka, N.M. Lapchuk, V. Myllymäki and A. Vehanen, Russ. Chem. Rev. 89 12 (2020) 1428 – 1462.
[2] T.S. Kurkin, A.N. Ozerin, E.P. Tikunova, A.S. Kechek'yan, E.K. Golubev, A.K. Berkovich, V.Yu. Dolmatov, Nanotechnologies in Russia 10 (2015) 878 – 887.
[3] A.V. Alaferdov, O.V. Lebedev, U.F.S. Roggero, H.E. Hernandez-Figueroa, S.V.G. Nista, G.M. Trindade, Y.A. Danilov, A.N. Ozerin and S.A. Moshkalev, Results Mater. 15 (2022) 100298.

## OP-IB-09

# Fluorinated Carbon Nanotubes Incorporated into the Active Layer of Organic Photovoltaic Cells

Uvarov M.N.[1], Kobeleva E.S.[1], Kravets N.V.[1], Ponomarev S.A.[2], Gurova O.A.[3], Okotrub A.V.[3], Kazantzev M.S.[4], Degtyarenko K.M.[5], Kulik L.V.[1]

*1 – V.V. Voevodsky Institute of Chemical Kinetics and Combustion, Siberian Branch of the Russian Academy of Sciences, Novosibirsk, Russia*

*2 – A.V. Rzhanov Institute of Semiconductor Physics, Siberian Branch of the Russian Academy of Sciences, Novosibirsk, Russia*

*3 – A.V. Nikolaev Institute of Inorganic Chemistry, Siberian Branch of the Russian Academy of Sciences, Novosibirsk, Russia*

*4 – N.N. Vorozhtsov Novosibirsk Institute of Organic Chemistry, Siberian Branch of the Russian Academy of Sciences, Novosibirsk, Russia*

*5 – Siberian Physico-Technical Institute, Tomsk State University, Tomsk, Russia*

*uvarov@kinetics.nsc.ru*

Two types of single-walled carbon nanotubes (SWCNTs, TUBALL® (OCSiAl) and Super purified plasma tubes (Nanointegris Inc.)) were fluorinated, dispersed by submicron length, characterized and tested as non-volatile additive to the active layer of polymer/fullerene organic photovoltaic cells [1]. The absence of big SWCNT aggregates was revealed by atomic force microscopy. The absence of metallic SWCNTs is confirmed by optical spectra of fluorinated SWCNT dispersions. Reproducible increase of the main performance parameters of the photovoltaic cells (short circuit current, open circuit voltage, fill factor and power conversion efficiency) was obtained upon admixing small amount of fluorinated SWCNTs (less than 1 % weight) into the polymer/fullerene active layer, with either P3HT or PCDTBT donor and either $PC_{60}BM$ or $PC_{70}BM$ acceptor for both direct and inverted photovoltaic device architectures. Since effective charge mobility did not change upon fluorinated SWCNT admixture, the improvement of photovoltaic cell performance is not related to SWCNT-induced modification of the electronic structure of the active layer components or charge transfer via fluorinated SWCNTs. Presumably, the origin of this improvements is geometric optimization of the active layer morphology (improving connectivity of donor and acceptor domains) by fluorinated SWCNTs due to their high aspect ratio.

**Acknowledgement:** This work was supported by the Russian Science Foundation, grant 23-73-00072.

**References:**

[1] Kobeleva, E.S.; Uvarov, M.N.; Kravets, N.V.; Ponomarev, S.A.; Gurova, O.A.; Okotrub, A.V.; Kazantzev, M.S.; Degtyarenko, K.M.; Kulik, L.V. Fluorinated Carbon Nanotubes as Non-volatile Additive to the Active Layer of Polymer/Fullerene Solar Cells, Fuller. Nanotub. Carbon Nanostructures **2023**, DOI: 10.1080/1536383X.2023.2179618

## OP-IB-10

# Comparison of the Kinetics of Chemical Reactions during the Detonation of a Pure Explosive and One Modified with Nanotubes

Satonkina N.P.[1,2], Ershov A.P.[1], Kashkarov A.O.[1], Rubtsov I.A.[1], Kuzminykh A.A.[2]
*1 – Lavrentyev Institute of Hydrodynamics, SB RAS, 630090, Novosibirsk, Russia*
*2 – Novosibirsk State University, 630090, Novosibirsk, Russia*
*snp@hydro.nsc.ru*

It is well known that the sensitivity of an explosive charge is determined not only by the type of explosive, but also by its structure. So, with a decrease in the grain size, an increase in the shock wave sensitivity and a decrease in the critical diameter at bulk density are observed. A change in the charge structure of TNT can be achieved using various manufacturing methods, as well as by modifying the addition of an inert substance.

In the present work, we studied the effect of an additive to the TNT charge on the detonation of the resulting mixture; single-walled carbon nanotubes were used as an additive. The choice of the method for modifying explosives is determined by the unique properties of nanotubes, which have high strength, conductivity, and thermal conductivity [1]. Previously, explosives with the addition of similar carbon nanotubes were studied in [2]. The pressed high-density RDX charge detonated at a rate higher than for a similar charge of pure RDX.

The procedure for preparing a mixture of TNT + 0.5% nanotubes is similar to that described in [2]. During the condensation process, the explosive is deposited on the nanotubes contained in the solution. An interesting feature of the resulting substance is mixing at the submicron level. The resulting material is shown in Figure 1 on the right, on the left is a photo of a pure substance.

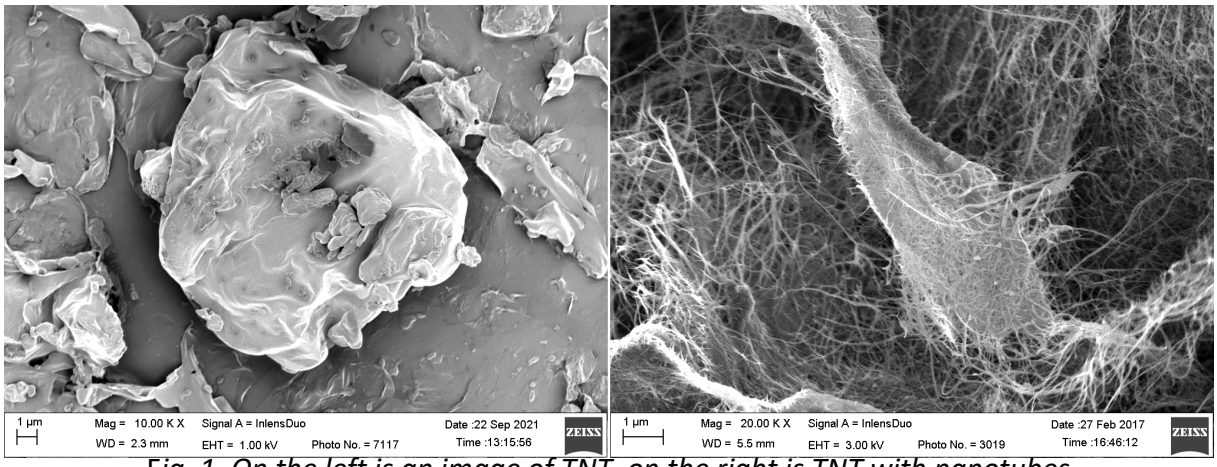


*Fig. 1. On the left is an image of TNT, on the right is TNT with nanotubes*

Comparison of experimental data on the detonation of charges with a similar density of pure TNT and with the addition of nanotubes shows an increase in the detonation velocity for the mixture, which is equivalent to an intensification of the chemical reaction due to an increase in the concentration of hot spots.

**References:**

[1] Anishchik, V.M., Borisenko, V.E., Zhdanok, S.A., Tolochko, N.K., Fedosyuk, V.M. Nanomaterials and Nanotechnologies. - 2008. - Minsk "Publishing Center of BSU". – 375 p.
[2] Ershov, A.P., Dashapilov, G.R., Karpov, D.I. *et al.* Combust. Explos. Shock Waves 57 (2021) 104.

## OP-IB-11

# Disaggregation of Nanodiamonds Prepared by a Shock Wave Compression Method

Tudupova B.B., Shvidchenko A.V.
*Ioffe Institute, St. Petersburg, Russia*
*biligma0201@gmail.com*

Shock wave compressed diamond is the highly promising material for development of electroplated metal/diamond coatings and polishing compositions. However, the main issue for obtaining this application is the high level of impurity concentration in industrial diamond powders and its negative impact on the stability of diamond particles in water and the formation of diamond colloids with particle sizes of less than 1 μm. The study of structural features, physical properties, purification and disaggregation of this diamond will contribute to the expansion of its areas of application.

In this research, the structure of shock wave compressed diamonds was investigated by X-ray and light diffraction methods, UV-Vis spectrophotometry and nitrogen adsorption-desorption analysis. Obtained results show that shock wave compressed diamond particles are low porosity micron sized polycrystals 1 – 10 μm in sizes, consisting of nanodiamond crystallites with a grain size about 20-25 nm and a defective layer with a disturbed diamond crystal lattice (lonsdaleite with layer thickness 5-7 nm).

The applicability of the disaggregation methods developed for the destruction of aggregates of detonation nanodiamonds is considered for the case of shock wave compressed nanodiamonds. Such disaggregation processes consist of three sequential stages: annealing of diamond powder, ultrasonic treatment of annealed diamond in water, and centrifugation of obtained colloids. Several disaggregation processes were carried out with different parameters: 1 - disaggregation without annealing; 2 - annealing in a hydrogen flow at a temperature of 900 °C for 3 hours; 3 - annealing in air at a temperature of 450 °C for 6 hours, 24 hours, and 48 hours. After disaggregation, the high stable aqueous colloid of diamond particles with size of 60 nm was obtained. Thus, the use of the proposed methods of particle disaggregation does not lead to the complete destruction of polycrystalline diamond particles to the state of individual single-crystal diamond particles with a grain size about 20-25 nm. Nevertheless, annealing diamond in air for 24 hours is the most optimal method: the yield of particles < 100 nm reached 8%.

**Acknowledgement:** The work was supported by the State Task № FFUG-2022-0012.

## OP-IB-12

# First Observation of Superheating Phenomenon for Mayenite in Core-Shell Structures C12A7@C by an *In Situ* XRD Technique

Shmakov A.N., Volodin A.M., Vedyagin A.A.
*Boreskov Institute of Catalysis, Novosibirsk, Russia*
*volodin@catalysis.ru*

Calcium aluminate with a mayenite structure ($12CaO \cdot 7Al_2O_3$ abbreviated as C12A7) is the most interesting representative of calcium aluminates and one of the most studied inorganic materials in recent years. Such an interest is stipulated by the ability to vary within a wide range its functional (electrophysical, optical, physicochemical) properties due to a change in the chemical composition of its labile anion sublattice. For the practical use of such materials, an important feature is the preservation of the cationic mayenite framework over very wide ranges of temperatures (up to 1600 °C) and gas phase compositions. The unit cell composition of such a compound can be described by the formula: 1 unit cell = $[Ca_{24}Al_{28}O_{64}]^{4+} \cdot 4X^-$, where either 4 single-charge anions ($OH^-$, $Cl^-$, $F^-$, $H^-$), or 2 double-charge anions $O^{2-}$, or some combinations thereof, can act as $4X^-$. Rather unexpected was the possibility of the formation of the electride state in this system, discovered in the works of Prof. H. Hosono [1]. Such materials, in which electrons $e^-$ act as $X^-$ anions, possess metal conductivity.

The formation of the electride state in mayenite occurs due to the removal of off-lattice ($O^{2-}$) oxygen at high temperatures close to the melting point of this material ($T_{melt}$ ~ 1400 °C). For this reason, it is impossible to form an electride in a dispersed state – mayenite particles are agglomerated and enlarged as a result of their sintering at high temperatures. Previously, we proposed a method for preserving the size of mayenite nanoparticles in the nanometer range when synthesizing C12A7:$e^-$ electride in core-shell structures of C12A7@C type. The carbon coating in such systems prevents direct contact between the oxide core particles, thus allowing one to maintain the initial size of mayenite nanoparticles up to a temperature of 1450 °C [2]. In this work, the evolution of the mayenite phase composition in the C12A7 and C12A7@C systems in a vacuum by an *in situ* XRD method was studied in detail at the temperatures up to 1500 °C. It was demonstrated for the first time that the polycrystalline phase of mayenite in the C12A7@C system can exist even at temperature of 1500 °C, which significantly exceeds the melting point of mayenite.

Fig. 1a shows data on the evolution of the phase composition of mayenite C12A7 with an increase in the temperature of recording XRD patterns in a vacuum. The disappearance of reflections corresponding to the mayenite phase above 1360 °C associated with the melting of the material is clearly seen. At the same time, for the C12A7@C core-shell structure, the polycrystalline phase of mayenite is stable up to 1500 °C, which is the maximum temperature used in experiments (Fig. 1b).

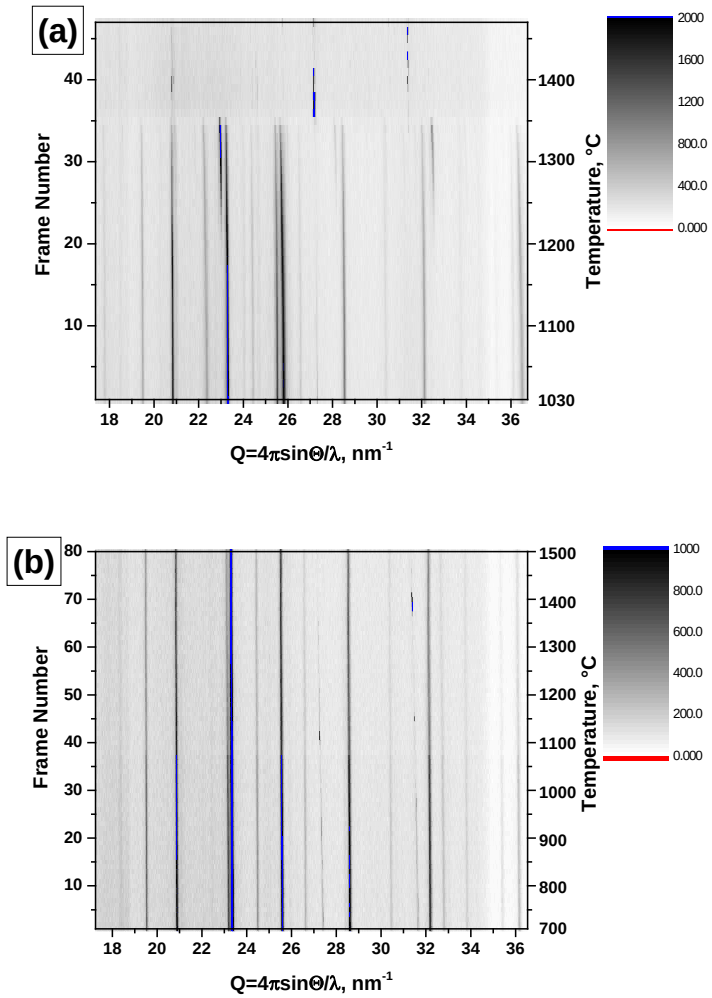


*Fig. 1. High-temperature evolution of the phase composition of mayenite C12A7: (a) pure mayenite; (b) mayenite within the C12A7@C core-shell structure*

It is believed that the overheating phenomenon found in the present work is due to the formation of carbide-like phases on the surface of the oxide core in the C12A7@C structure. Such phases possess a higher melting point. Note that the formation of carbide-like phases was previously observed during the interaction of mayenite with carbon under HPHT (High Pressure, High Temperature) conditions [3].

**Acknowledgement:** This work was supported by the Ministry of Science and Higher Education of the Russian Federation, project No. AAAA-A21-121011390054-1.

**References:**

[1] S. Matsuishi, Y. Toda, M. Miyakawa, K. Hayashi, T. Kamiya, M. Hirano, I. Tanaka, H. Hosono, Science 301 (2003) 626–629.
[2] A.M. Volodin, V.I. Zaikovskii, R.M. Kenzhin, A.F. Bedilo, I.V. Mishakov, A.A. Vedyagin, Mater. Lett. 189 (2017) 210–212.
[3] S.A. Gromilov, A.I. Chepurov, A.M. Volodin, A.A. Vedyagin, Materials 16 (2023) 2083.

## OP-IB-13

# Carbon Quantum Dots Produced through Citric Acid Pyrolysis

Borodina A.M., Kostromin S.V., Bronnikov S.V.
*Institute of Macromolecular Compounds, Russian Academy of Science, St. Petersburg, Russia*
*Anastasia_2998@mail.ru*

Carbon quantum dots (CQDs) were obtained through citric acid (CA) pyrolysis at 200 °C. The obtained CQDs were investigated by UV-vis spectroscopy, FTIR-spectroscopy, Raman-spectroscopy, photoluminescence (PL) spectroscopy, and dynamic light scattering (DLS). The carbonized structure of CQDs was detected and the presence of surface oxygen-containing groups was confirmed. The average CQDs particle size was estimated at about 8 nm. CQDs demonstrate a good PL emission under UV-irradiation with quantum yield (QY) equal to 6.1%. Photoluminescent composite poly(vinyl alcohol)/CQDs films were manufactured.

CQDs are chronologically the last known representatives of carbon nanoparticles. CQDs demonstrate high fluorescence intensity with a high quantum yield, easy surface functionalization, good solubility in water, low toxicity, biocompatibility, chemical stability, low cost, and high photostability [1]. Their distinctive ability is high tunable photoluminescence, which leads to their use primarily as materials in OLED technology. Due to their abilities, they can be used to produce polymer nanocomposites for energy storage applications, in supercapacitors, for environmental applications and for sensing and transfection [2, 3].

The aim of this study was to produce and investigate CQDs through CA pyrolysis. The CA monohydrate was pyrolyzed at 200 °C for 4 h. Since the CA pyrolysis products are known to contain CQDs, molecular fluorophores, intermediates, and by-products, the pyrolysis products were dialyzed in a dialysis bag (1 kDa) for 2 days to separate CQDs from pyrolysis by-products and intermediates.

In the UV-vis spectrum of CQDs the absorbance bands at 340 nm and at 290 nm were recognized. The band at 340 nm corresponds to n–π* electron transitions of the carbonyl groups, whereas the absorbance peak centered at 290 nm relates to π–π* electron transitions of the $sp^2$-hybridized carbon atoms.

Figure 1 shows the PL spectra of purified CQDs as a function of the excitation wavelength. The position of the PL peak weakly depends on the excitation wavelength. This indicates homogeneity of the emission centers. QY of the purified CQDs obtained through the CA pyrolysis was measured as 6.1%.

Using the DLS method, we showed that the purified CQDs demonstrate a narrow size distribution with an average size of about 8 nm.

The carbonized structure of CQDs was determined by Raman-spectroscopy. In the Raman spectra, the presence of defects in the carbonized structure of CQDs and partially disordered

crystals consisting of small $sp^2$-clusters was confirmed. The FTIR spectra confirmed the $sp^2$-carbonated structure and presence of the oxygen-containing groups in CQDs.

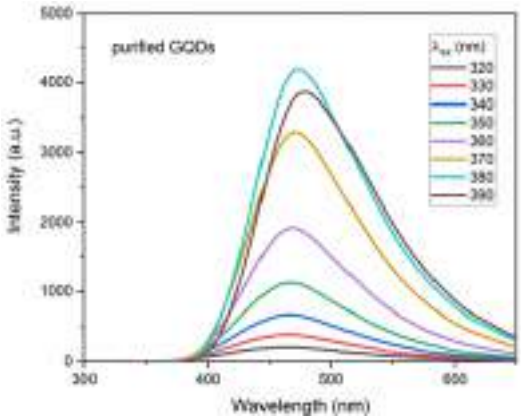


*Fig. 1. PL spectra of the purified CQDs depending on excitation wavelength*

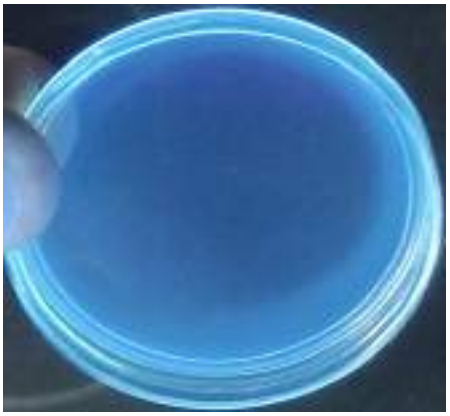

*Fig. 2. PVA/CQDs film under 365 nm UV irradiation*

Poly(vinyl alcohol)mer/CQDs composit films with a CQD content of 1% was obtained. The films demonstrate intensive photoluminescence under UV irradiation at the excitation wavelength of 365 nm (fig. 2). The obtained material can be applied in opto-electronics.

**References:**

[1] N.-A. Tran, N. T. Hien, N. M. Hoang, H.-L. T. Dang, D. Q. Huy, T. V. Quy, N. T. Hanh, N. H. Vu, V.-D. Dao. 548 (2023) 116285.
[2] A. Hebbar, R. Selvaraj, R. Vinayagam, T. Varadavenkatesan, P. S. Kumar, P. A. Duc, G. Rangasam. 313 (2023) 137308.
[3] Z. Feng, K. H. Adolfsson, Y. Xu, H. Fang, M. Hakkarainen, M. Wu. 29 (2021) e00304.

## OP-IB-14

# Synthesis of Multicomponent NiCoFeCoCu Alloys and their Study in Catalytic Pyrolysis of $C_2$ Hydrocarbons

Bauman Y.I.[1], Shtol V.S.[1,2], Popov A.A.[1,3], Pervikov A.V.[1,4], Pustovalov A.V.[1,4], Shubin Y.V.[1,2,3], Volodin A.M.[1], Mishakov I.V.[1,2], Vedyagin A.A.[1]

*1 – Boreskov Institute of Catalysis, Novosibirsk, Russia*

*2 – Novosibirsk State University, Novosibirsk, Russia*

*3 – Nikolaev Institute of Inorganic Chemistry SB RAS, Novosibirsk, Russia*

*4 – Institute of Strength Physics and Materials Science SB PAS, Tomsk, Russia*

*bauman@catalysis.ru*

Carbon nanofibers (CNF) are known as a type of graphite-like carbon nanomaterials which is highly demanded as a modifying additive used to improve the physico-mechanical properties of various composite materials [1]. Nickel-based catalysts are among the most popular catalytic systems used to produce carbon fibers with different structure [2].

The methods to synthesize Ni-containing catalysts are diverse and often involve obtaining nanosized particles of Ni-M alloys stabilized on the surface of various carriers [3]. At the same time, catalysts comprising a nanosized active component have certain disadvantages, including the sintering of metallic particles during high-temperature reductive processing as well as a limited yield of carbon product due to the rapid deactivation of suboptimal-sized particles. Recently, there has been considerable interest to the bulk nickel-based alloys used to create self-organizing catalysts (SOC) characterized by very high activity and productivity for CNFs in catalytic pyrolysis of hydrocarbons. The approach for obtaining SOCs involves utilizing specially synthesized bulk Ni alloys of a given composition that undergo rapid disintegration in the course of a carbon erosion process, resulting in the formation of active sites for nanofiber growth [4]. The study of multicomponent nickel-based alloys and the search for novel ways to create effective SOCs is an area of high scientific interest.

Such multicomponent alloys can be obtained by the method of the electric explosion of wires (EEW). An electric explosion of conductors is caused by the phenomenon of explosive destruction and melting of a metal conductor when a current pulse of very high density passes through it, about 105 A/mm$^2$ [5]. The samples obtained by the EEW method are characterized by the spherical shape of the particles (Fig. 1).

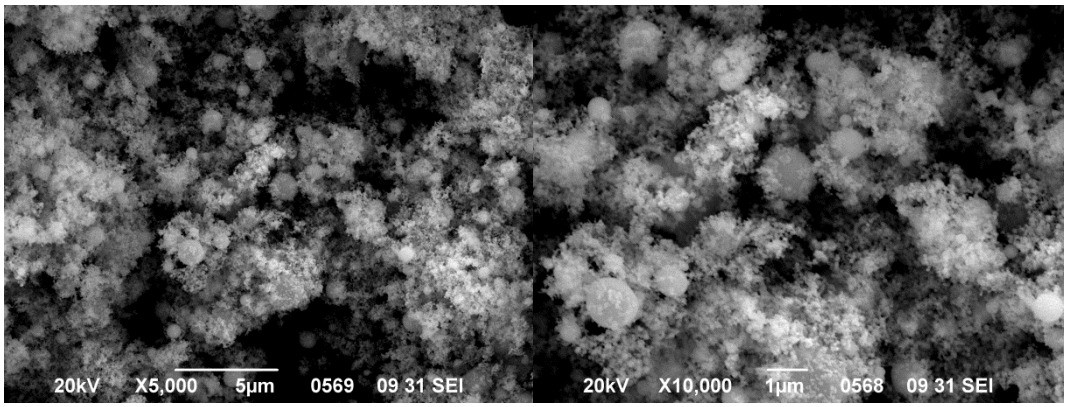


*Fig. 1. Micrographs of the SEM sample of the Ni39Fe35Cr7Co7Cu11 alloy obtained by the EEW method*

## OP-IB-14

In this report we present the results of the catalytic activity study of multicomponent Ni-M1,2,. alloys (where $M_i$ = Fe, Co, Cr, Cu), prepared by the EEW method in the hydrocarbon decomposition reaction for the production of carbon nanomaterials at different temperatures.

The carbon nanomaterial formed on multicomponent alloys is represented by chaotically intertwined filaments with a submicron diameter of ~ 0.25 microns (Fig. 2). The report will discuss the influence of the catalyst's composition and the conditions of $C_2$ hydrocarbons decomposition reaction) on the textural parameters and physico-chemical properties of the resulting carbon nanomaterial.

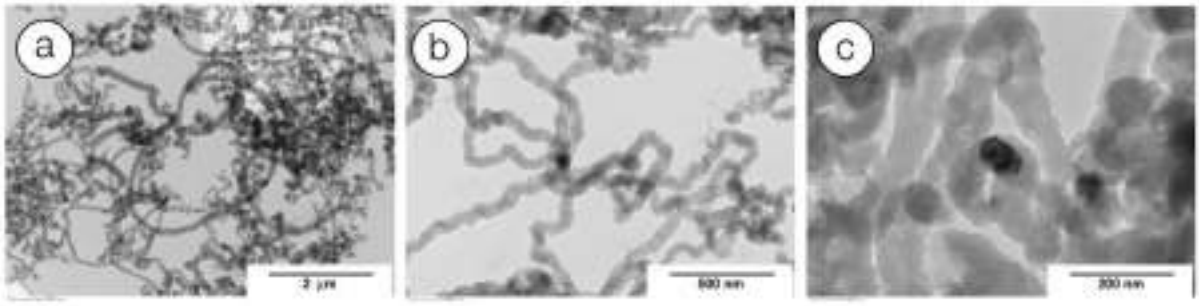


*Figure 2. Morphology of active particles formed as a result of the interaction of ethylene with the sample $Ni_{39}Fe_{35}Cr_8Co_7Cu_{11}$ for 30 min at 550 °C. Pictures of TEM*

**Acknowledgement:** This work was supported by the Russian Science Foundation, grant 22-13-00406.

**References:**

[1] I.V. Mishakov, A.A. Vedyagin, Y.I. Bauman, Y.V. Shubin, R.A. Buyanov. Carbon Nanofibers: Synthesis, Applications and Performance., 2018.
[2] A.A. Aboul-Enein, F.S. Soliman, M.A. Betiha, Int. J. Hydrogen Energy 44 (2019) 31104.
[3] D. Torres, J.L. Pinilla, I. Suelves, Catalysts 8 (2018) 300.
[4] И.В. Мишаков, С.Д. Афонникова, Ю.И. Бауман, и др., Кинетика и катализ 63 (2022) 110.
[5] S.P. Zhuravkov, A.V. Pustovalov, N.A. Yavorovsky, A.V. Korshunov, M.N. Vlasyuk, L.V. Nadeina, KEM, 685 (2016) 596.
[6] A.V. Pervikov, A.V. Pustovalov, S.D. Afonnikova, Y.I. Bauman, I.V. Mishakov, A.A. Vedyagin, Powder Technology. 415 (2023) 118164.

## OP-IB-15

# Functionalized Carbon Dots

Kosolapova K.D.[1], Koroleva A.V.[2], Arefina I.A.[1], Miruschenko M.D.[1], Cherevkov S.A.[1], Spiridonov I.G.[1], Zhizhin E.V.[2], Ushakova E.V.[1], Rogach A.L.[3]
*1 – ITMO University, Saint Petersburg, Russia*
*2 – Saint Petersburg State University, Saint Petersburg, Russia*
*3 – City University of Hong Kong, Hong Kong SAR*
*elena.ushakova@itmo.ru*

Carbon dots attract much attention as an environmentally friendly and cheap luminescent nanomaterial. Functionalization of the carbon dots surface with additives of various nature is a useful way to control their physical and chemical properties. Herein, we demonstrate the changes in chemical composition and optical properties of carbon dots by post synthetic treatment with citric acid, benzoic acid, urea, and o-phenylenediamine. This treatment leads to a formation of carboxyl/imide/carbonyl groups on the surface of carbon dots resulting in an appearance of additional blue (or for CDs treated with o-phenylenediamine blue and green) emission optical centres with preserving the initial optical centres. The increased amount of oxygen along with a decrease in the amount of carbon and nitrogen in treated carbon dots reduces the energy level of their highest occupied molecular orbitals by - 0.9 eV. In addition, the Fermi energy level shifted above the lowest unoccupied molecular orbital energy level for some of the treated carbon dot samples. Thus, the energy structure of carbon dots can be tuned and optimized for further use by functionalizing their surface with organic additives (Fig.1).

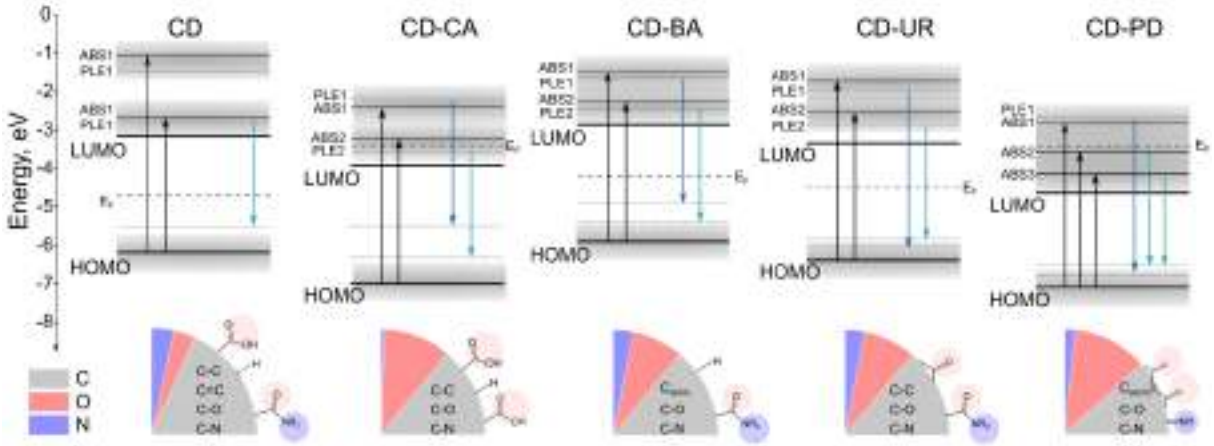


*Fig. 1. Energy level structure (upper panel) and chemical composition (lower panel) of carbon dots*

**Acknowledgement:** This work was supported by the Priority 2030 Federal Academic Leadership Program.

## OP-IB-16

# Study on Carbon Erosion of Ni-Cu Bulk Alloys to Produce an Effective Catalyst of CNF Synthesis

Afonnikova S.D.[1], Veselov G.B.[1], Bauman Y.I.[1], Gerasimov E.Y.[1], Shubin Y.V.[2], Mishakov I.V.[1], Vedyagin A.A.[1]

*1 – Boreskov Institute of Catalysis, Novosibirsk, Russia*

*2 – Nikolaev Institute of Inorganic Chemistry, Novosibirsk, Russia*

*afonnikova@catalysis.ru*

Carbon nanomaterials (CNMs) are currently of great interest because of their unique physical and chemical properties. Thus, CNMs, mostly carbon nanotubes (CNTs) and nanofibers (CNFs), can be used in various fields of science and technology. For example, CNF material is very perspective for creation of various polymer composites. Later works demonstrated that such modification may lead to considerable improvement of their physical and mechanical properties [1]. The catalytic chemical vapor deposition (CCVD) process should be considered as one of promising methods to develop. CCVD is well known to be the most flexible, extremely versatile and economically attractive way to synthesize CNM as well as pure hydrogen free from traces of CO and $CO_2$ gases.

In the present work, the process of catalytic decomposition of light hydrocarbons on self-organizing Ni-M catalysts has been studied. The proposed approach is based on the phenomenon of carbon erosion (CE), during which the disintegration of bulk alloys at high temperature (400-800°C) occurs, driven by the action of hydrocarbon-containing atmosphere [2]. Recent works have shown that such process can be purposefully applied for the synthesis of various carbon nanomaterials [3].

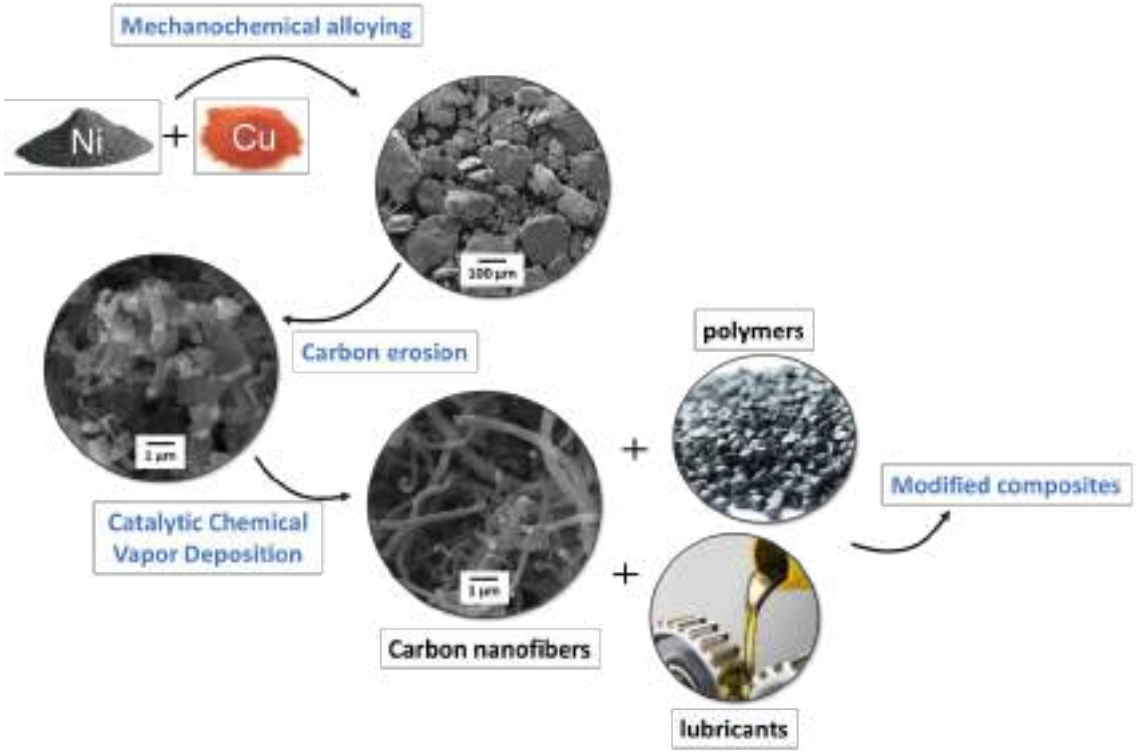


*Fig. 1. Schematic illustration of the experimental design*

Ni-based systems are known to be one of the most active catalysts for CNM synthesis. For instance, the addition of Cu to form an alloy with Ni-based catalyst permits one to stabilize the catalyst's performance in CCVD process [4]. Mechanochemical alloying (MCA) was chosen as the principal method for preparation of Ni-M alloys to be used as the catalyst precursors. This approach is very simple and applicable for alloys preparation. It does not produce by-products, harmful emissions, and wastewater.

The samples of $Ni_{1-x}Cu_x$ alloys (x= 1-15 at.%) were prepared by MCA of metals in a planetary mill. The influence of Cu concentration on the activity of $Ni_{1-x}Cu_x$ alloys in the catalytic pyrolysis of ethylene was studied. It is shown that the introduction of copper in an amount of 11-12 at.% provides an increase in the nickel productivity in the CNF synthesis. The effect of mechanochemical activation time on the phase composition and hydrogen reduction profile (TPR-$H_2$) of $Ni_{0.89}Cu_{0.11}$ samples was studied. The evolution of the phase composition of the pre-activated composite {$Ni_{0.89}Cu_{0.11}$} under heating, reduction and short-term contact with the reaction mixture ($C_2H_4/H_2$/Ar) at 550°C was studied. The initial stage of the CE process was examined by TEM and EDX. It was found that the composition of the active particles coincides with that of the initial alloy.

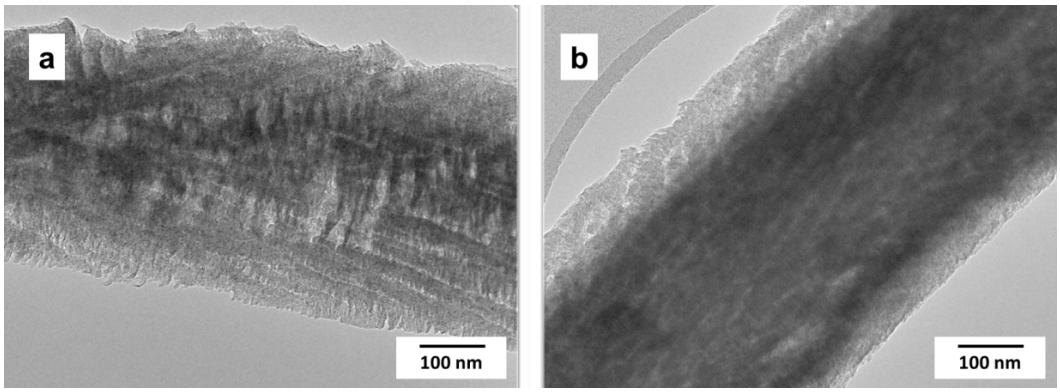


*Fig. 2. TEM images of the CNFs obtained during ethylene decomposition (30 min, T = 550°C): (a) – segmented packaging type, (b) – fishbone type of packaging*

The report will also discuss the morphology, structural features and textural parameters of the obtained carbon nanofibers (Fig. 2). The opportunity to use the obtained CNF material as a modifying additive in polymer composites, as well as an antifriction agent in the composition of lubricants will be also demonstrated.

**Acknowledgement:** This work was supported by the Ministry of Science and Higher Education of the Russian Federation [project No. AAAA-A21-121011390054-1].

**References:**

[1] Sun L.L., Li B., Zhao Y. et al., Nanotechnology 21 (2010) 305702.
[2] Grabke HJ. Mater Corros 54 (2003) 736.
[3] Afonnikova S. D. et al., Materials 15 (2022) 7456.
[4] Reshetenko T. V. et al., Appl Catal A-Gen. 247 (2003) 51.

## OP-IB-17

# Detection of Carbon Dioxide with Pure and Boron Functionalized Carbon Nanotubes

Zaporotskova I.V., Boroznin S.V., Zaporotskov P.A.
*Volgograd State University, Volgograd, Russia*
*boroznin@volsu.ru*

Large concentrations of carbon monoxide in the atmosphere are one of the key causes of global warming. Recently, an increase in the content of carbon dioxide in the atmosphere has been observed, and according to the forecasts of researchers [1], this trend will continue in the coming decades. In this regard, the creation of innovative materials that can significantly reduce the content of $CO_2$ in the atmosphere is an important research task [2, 3]. Filters based on carbon materials are the most promising for solving this problem in the light of the absence in the near future of fundamentally new technologies based on renewable energy sources [4].

In [5], the possibility of modifying carbon nanotubes with a number of materials for using them as highly sensitive sensors for detecting phosgene molecules is considered, but, as shown in [6], in reality, only carbon nanotubes modified with boron are successfully observed, despite the many proposed substances for modifications. Therefore, an interesting research task is to find out which of the concentrations of impurity boron atoms will be the most effective for the adsorption of carbon dioxide on carbon nanotubes.

To clarify this circumstance, we carried out a model experiment to study the interaction of a carbon dioxide molecule and boron-carbon nanotubes containing 15% impurity boron atoms (the so-called BC5 nanotubes) and their functionalization with a carboxyl group. The studies were carried out within the framework of the density functional theory using the B3LYP functional and the 6-31G basis.

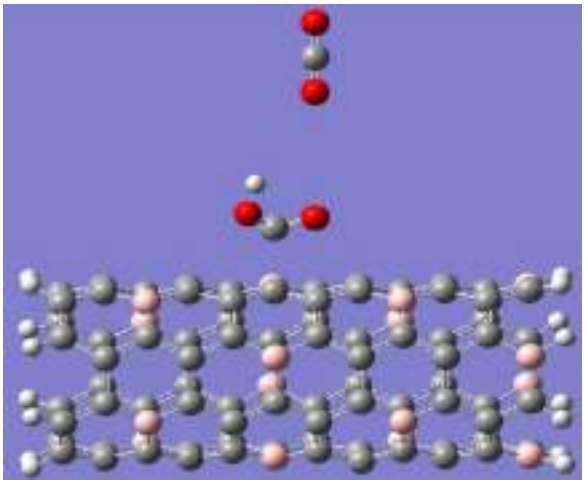

*Fig. 1 Model of attachment of a carbon dioxide molecule to the carbon atom of the carboxyl group that modifies the surface of the $BC_5$ nanotube.*

The results of computer simulation of the processes showed that the interaction of the BC5 boron-carbon nanotube with a carbon dioxide molecule changes the energy of the

system, and the minimum value is achieved when the molecule is located both above the boron atom and above the carbon atom of the surface. This indicates the possibility of adsorption of the molecule in both variants. In addition, it was found that when a molecule is attached to a nanotube that is not functionalized with a carboxyl group, the adsorption energy in both cases is higher than when interacting with a borocarbon nanostructure functionalized with a COOH group.

**Table 1.** The main energy parameters of the attachment of a carbon dioxide molecule to a $BC_5$ nanotube without modification and NT modified with a COOH group

| Sorption center | Adsorption distance, $r_{ad}$, Å | Adsorption energy, eV |
|---|---|---|
| C | 3 | 1.2 |
| B | 2.8 | 1.6 |
| COOH to the surface | 3.3 | 0.9 |
| COOH to the edge | 3.2 | 0.94 |

Thus, there is no need for additional functionalization of the BC5 nanotube surface with a carboxyl group to achieve the desired result of carbon dioxide identification. Such materials can be used to create a new generation of firefighting devices. To use them in such devices, it is sufficient to modify carbon nanotubes with impurity boron atoms without introducing additional functional groups.

**Acknowledgement:** The work was carried out within the framework of the state task of the Ministry of Science and Higher Education of the Russian Federation (topic "FZUU-2023-0001).

**References:**

[1] Sun, Qiao; Wang, Meng; Li, Zhen; Ma, Yingying; and Du, Aijun. CO2 capture and gas separation on boron carbon nanotubes. 1-1 (2013) 758.
[2] He Yabing, Zhou Wei, Krishna Rajamani, Chen, Banglin. Microporous metal-organic frameworks for storage and separation of small hydrocarbons. 48 (2012) 97.
[3] D'Alessandro DM, Smit B, Long JR. Carbon dioxide capture: prospects for new materials. 49(35) (2010) 6058-82.
[4] Haszeldine RS. Carbon capture and storage: how green can black be? 325(5948) (2009) 1647-52.
[5] Katta SS, Yadav S, Pratap Singh A, SanthiBhushan B, Srivastava A. Investigation of pristine and B/N/Pt/Au/Pd doped single-walled carbon nanotube as phosgene gas sensor: A first-principles analysis. 588 (2022) 152989
[6] Sawant SV, Patwardhan AW, Joshi JB, Dasgupta K. Boron doped carbon nanotubes: Synthesis, characterization and emerging applications – A review. 427 (2022) 6348

## OP-IB-18

# Bimetallic Catalysts for Oxygen Electroreduction Based on Carbon Nanotubes and Cobalt, Copper, and Nickel Phthalocyanines

Vinogradov K.Yu., Davydov V.M., Shafigulin R.V., Bulanova A.V.
*Samara University, Samara, Russia*
*winyur@yandex.ru*

Fuel cells (FCs) are promising alternative power sources: they are energy efficient, fault-tolerant, environmentally friendly and silent. But FC also has a significant drawback - a significant cost due to the effect of the platinum catalyst on the electrodes. That is why the search for alternative catalytic materials is an urgent task [1, 2]. In recent years, sources mined with nitrogen and metals have been actively explored. An example of materials for such compounds are catalysts based on carbon nanotubes doped with metal phthalocyanines (Pc). The aim of our work was to study the catalytic properties of carbon nanotubes doped in pairs with copper, nickel, and cobalt phthalocyanines.

The investigated catalysts MWCNT_CoPc_CuPc, MWCNT_CoPc_NiPc, and MWCNT_CuPc_NiPc were obtained by sequential treatment of the calculated CNT mixture and detection of phthalocyanines by ultrasound and high-temperature treatment in an inert nitrogen atmosphere. The resulting catalysts are 5% wt. each of the metals.

The reaction of oxygen reduction on the synthesized catalysts was studied using the potentiometric method. To measure the current-voltage characteristics, a three-electrode electrochemical cell with a rotating disk electrode (RDE) was used. The anode was represented by a platinum electrode; a mercury oxide electrode was used as a reference electrode. A glassy carbon electrode coated with catalysts acted as a cathode. Characterization was carried out in the linear voltammetry mode.

The obtained voltammograms, shown in Figure 1, demonstrate the difference in the properties of the catalysts: the MWCNT_CoPc_NiPc and MWCNT_CuPc_NiPc catalysts showed similar catalytic activity, characterized by a half-wave potential $E_{1/2}$≈0.35 V.

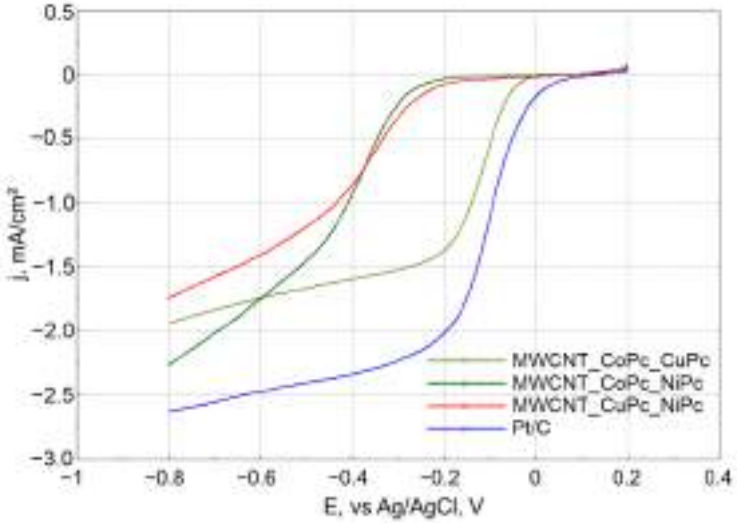


*Fig. 1. Linear voltammograms of the studied catalysts.*

The MWCNT_CoPc_CuPc catalyst showed the best characteristics in the form of a half-wave potential $E_{1/2}$=0, 22 V, which is comparable to the properties of a commercial platinum catalyst ($E_{1/2}$=0.10 V).

According to the graphs of linear voltammetry at different speeds of rotation of the disk electrode (500–2000 rpm), curves were plotted in the Koutetsky–Levich coordinates. Based on the Koutecki-Levich equation and curves in the corresponding coordinates, the numbers of electrons involved in the oxygen reduction reaction were calculated. For the MWCNT_CuPc_NiPc catalyst, n=2.5, which is a rather low value, but for the MWCNT_CoPc_NiPc and MWCNT_CoPc_CuPc catalysts, n≈3.3, which is already a value comparable to the platinum catalyst (n=3.4). Thus, the MWCNT_CoPc_CuPc catalyst is the most promising for further study under real fuel cell conditions.

**References:**

[1] Chen, Siyu, et al. "Nanostructured transition-metal phthalocyanine complexes for catalytic oxygen reduction reaction." Nanotechnology 33.18 (2022): 182001.

[2] Kumar, Yogesh, et al. "Iron and Nickel Phthalocyanine-Modified Nanocarbon Materials as Cathode Catalysts for Anion-Exchange Membrane Fuel Cells and Zinc-Air Batteries." ChemElectroChem 9.20 (2022): e202200717.

## OP-IB-19

# Catalytic Oxygen Reduction Reaction Activity of Lattice Carbons of Metal Doped Nitrogen Codoped Carbons. Theoretical Analysis

Kuzmin A.V., Shainyan B.A.
*A.E. Favorsky Irkutsk Institute of Chemistry of SB RAS, Irkutsk, Russia*
*kuzmin@lin.irk.ru*

Among oxygen reduction reaction (ORR) electrocatalysts a group of non-precious metal-doped nitrogen-codoped graphenes and nanotubes (M–$N_x$–C, where C = Gr, CNT; x = 1 – 4) is unique. M–$N_x$–C catalysts demonstrate high electroconductivity, long-term stability [1] and excellent catalytic activity (M = Co, Fe [2], Cu [3, 4], Sn [5]) for ORR due to low overpotentials close to that of Pt-based catalysts. The activity of M–$N_x$–C catalysts in ORR is attributed to metal centers. In case of M = Fe and Co, the metal is reversibly oxidized by the ORR intermediates, that does not allow to estimate the catalytic activity of other catalytic centers (like carbon atoms adjacent to $MN_x$ fragment) [2]. The addition of catalyst poisons (CO, $Cl^-$, $CN^-$, $SCN^-$, etc.) [4, 6], or possible irreversible adsorption of ORR intermediates [7, 8] can deactivate metal centers. However, only slight decrease of overall ORR activity due to the presence of non-metal centers and, as a result, current-voltage characteristics changes are observed [4, 6]. This is possible only due to the catalytic activity of the carbon atoms of the support.

Our theoretical studies of the ORR mechanism (both associative and dissociative) and thermodynamics on model M–$N_4$–CNTs catalysts includes the early (Ti, V, Zr and Nb) [7, 8] and post transition metals (Cu, Ag and Zn) [9] as well as metalloid Si incorporated in model CNTs, Gr, and fullerene [10-13]. All calculations were performed using PBE/Def2-TZVP//PBE/Def2-SVP (Fig. 1) and $\omega$B97XD/DGDZVP levels of theory and model (6,6)armchair single-walled carbon nanotube $C_{120}H_{24}$ with incorporated $MN_4$ fragment, Fig. 1d. For both metal groups the values of the experimental onset potential were correctly predicted by DFT. We have also shown that the free energy profile on the carbon atoms of the support directly attached to $MN_4$ moiety better corresponds to ORR than that on the metal center.

During the ORR catalytic cycle, the metal center of the M–$N_4$–C catalyst, where M = Ti, V, Zr, Nb and Si, is irreversibly oxidized (poisoned) by the reduced oxygen-containing forms, namely hydroxy HO* (Si) [10-14], dihydroxy 2HO* (Ti, Zr) [7] and oxohydroxy O*HO* (V, Nb) [8], that allowed to assign the catalytic activity to the carbon atoms (C2 active site) of the support, Fig. 1b-e. The free energy profile in Fig. 1e clearly shows possible bifurcation points in the ORR mechanism on the example of model Nb–$N_4$–CNT catalyst. The first point is related to the preference of H* + O*O* $\rightarrow$ O*HO* transformation on metal center over $O_2$ adsorption on C2 active site of dioxo O*O* metal species, $\Delta\Delta G$ = 0.17 eV. The second one is attributed to the change of ORR active center nature from metal to carbon centers not only due to the thermodynamic stability of oxohydroxy O*HO* species on metal center, but also kinetic

preference of ORR to proceed on C2 active site. Indeed, the barrier height for H* + O*HO* → O*H$_2$O* transformation on metal center is 0.88 eV higher than that for the H* + O*O* → O*HO* transformation on C2 active site of oxohydroxy O*HO* metal species. Depending on the metal nature the adsorption of dioxygen molecule on C2 active site is endergonic for some metal poisoned species, while the rate determining step (RDS) is attributed to the final H* + HO* → H$_2$O* transformation. Nevertheless, the free energy profile for ORR on C2 active site of model metal-oxidized Nb(O)(OH)–N$_4$–CNT catalyst at *U* = 1.23 V (the equilibrium potential), Fig. 1c, is close to that of an ideal ORR catalyst.

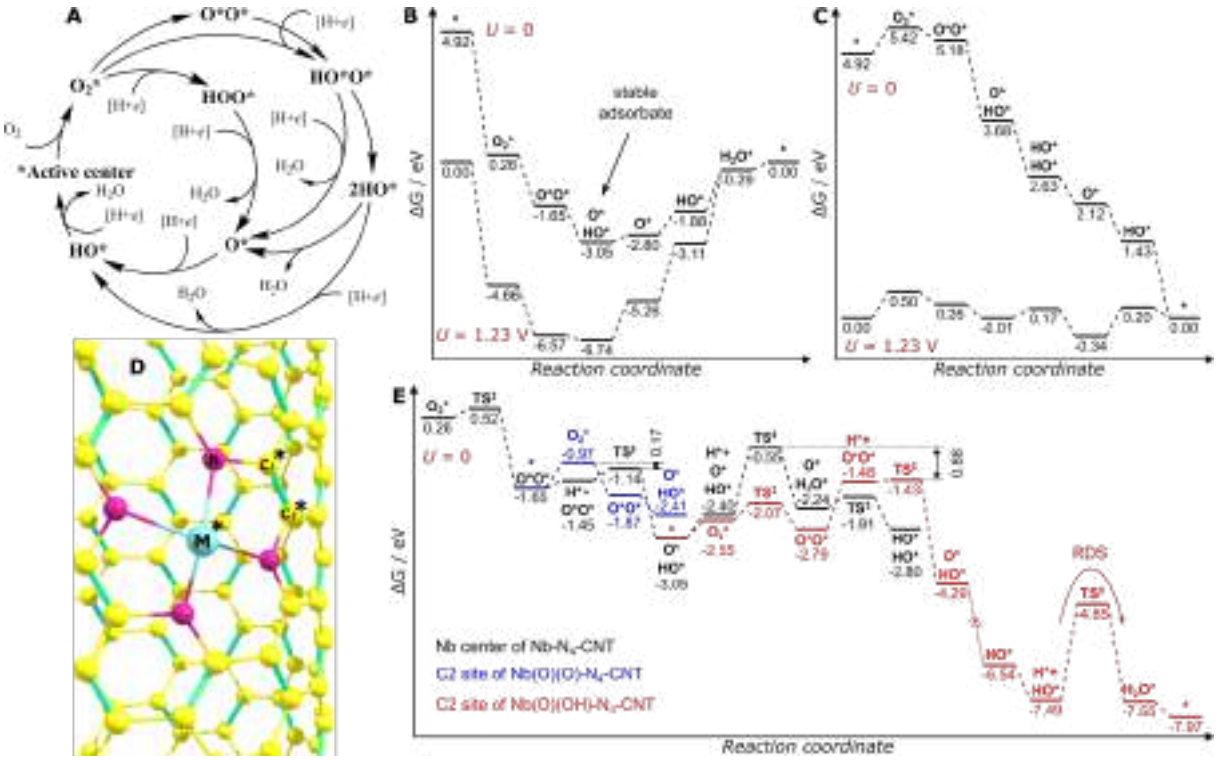


*Fig. 1. (**A**) Associative (inner) and dissociative (outer) catalytic ORR cycles. Free energy profile of ORR on (**B**) niobium metal center of Nb–N$_4$–CNT and (**C**) C2 active site of stable oxohydroxy niobium form, Nb(O)(OH)–N$_4$–CNT. (**D**) Fragment of model M–N$_4$–CNT catalyst. (**E**) A part of free energy profile including transition states and preferable ORR pathways.*

**References:**

[1] L. Osmieri, Chem. Eng. 3 (2019) 16.
[2] K. Liu, S. Kattel, V. Mao, G. Wang, J. Phys. Chem. C 120 (2016) 1586.
[3] D. Wang, C. Ao, X. Liu, *et al.*, ACS Appl. Energy Mater. 2 (2019) 6497.
[4] X. Wen, H. Qi, Y. Cheng, *et al.*, Chin. J. Chem. 38 (2020) 941.
[5] F. Luo, A. Roy, L. Silvioli, *et al.*, Nat. Mater. 19 (2020) 1215.
[6] Q. Zhang, K. Mamtani, D. Jain, *et al.*, J. Phys. Chem. C 120 (2016) 15173.
[7] A. V. Kuzmin, B. A. Shainyan, Int. J. Quantum Chem. 121 (2021) e26809.
[8] A. V. Kuzmin, B. A. Shainyan, Int. J. Quantum Chem. 123 (2023) e27017.
[9] A. V. Kuzmin, B. A. Shainyan, ACS Omega 6 (2021) 374.
[10] A. V. Kuzmin, B. A. Shainyan, Russ. J. Gen. Chem. 92 (2022) 2458.
[11] A. V. Kuzmin, B. A. Shainyan, ACS Omega 5(2020) 15268.
[12] A. V. Vaschenko, A. V. Kuzmin, B. A. Shainyan, Int. J. Quantum Chem. 121 (2021) e26565.
[13] A. V. Vaschenko, A. V. Kuzmin, B. A. Shainyan, Russ. J. Gen. Chem. 90 (2020) 454.

## OP-IB-20

# Heterogeneous Catalysts Based on POM and N-Doped Multiwalled Carbon Nanotubes Impregnated with $Zn^{2+}$ Ions for Synthesis of Acid-Sensitive Epoxides

Lopatkin V.A., Evtushok V.Y.
*Boreskov Institute of Catalysis, Novosibirsk, Russia*
*v.lopatkin@g.nsu.ru*

Development of new catalytic alkene epoxidation systems by green oxidants, primarily hydrogen peroxide, is a challenging goal of modern catalysis, as some epoxides cannot be easily produced by classical methods being sensitive to acid-catalysed ring opening. At the same time, polyoxometalates (POM) – inorganic polynuclear transition metal oxocomplexes – efficiently activate $H_2O_2$ via the heterolytic pathway and, unlike complexes with organic ligands, are thermodynamically resistant to oxidation.

The immobilization of POM on the surface of nitrogen-free multiwalled carbon nanotubes (CNTs) and nitrogen-doped nanotubes (N-CNTs) has been previously found to maintain or increase POM catalytic activity while providing good catalyst reusability [1]. The catalytic activity of POM/(N)-CNTs catalysts and their resistance to leaching of active components are improved if $HClO_4$ acid additives are used in catalyst preparation. On the other hand, the use of $HClO_4$ for POM immobilization generally decrease selectivity for epoxides due to acid-catalysed ring opening.

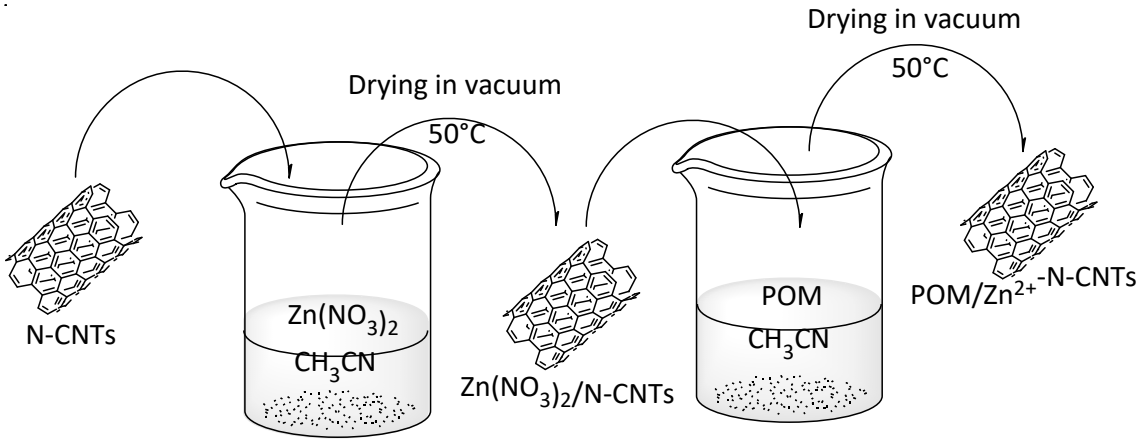


*Fig. 1. POM/$Zn^{2+}$-N-CNTs catalyst preparation*

In this work, we investigated the possibility of avoiding low epoxide selectivity and, at the same time, maintaining robust POM immobilization on CNTs. We chose the Venturello complex $[PO_4\{WO(O_2)_2\}_4]^{3-}$ ($PW_4$) as POM, which do not need protonation for high activity in epoxidation, and to keep it firmly fixed to (N)-CNT, the protons previously originated from $HClO_4$ were replaced by Zn metal ions with small size and high oxophilicity. The catalysts were prepared *(Fig. 1)* by impregnation of (N)-CNTs with $Zn(NO_3)_2$ solution, drying, and then adsorption of $PW_4$ from the solution in $CH_3CN$. The catalysts obtained were characterized by IR, TEM and elemental analysis.

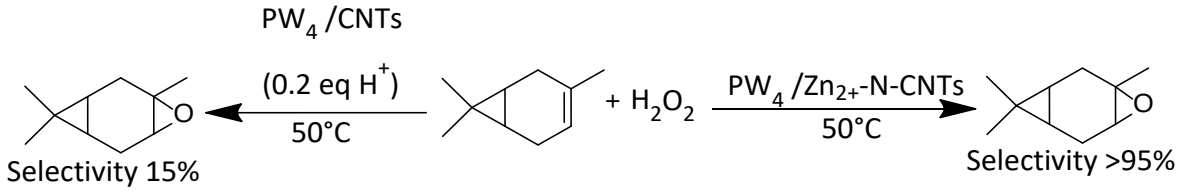


*Fig. 2. 3-carene epoxidation selectivity comparison*

The obtained catalysts $PW_4/Zn^{2+}$-(N)-CNTs showed high acid-sensitive epoxide selectivity (>95%) in 3-carene oxidation *(Fig. 2)*, while oxidation over the most selective $PW_4/H^+$-(N)-CNTs obtained with the addition of minimal amount of acid resulted in the formation of by-products and decreased epoxy selectivity (15%). The new catalysts also showed high activity in the epoxidation of the model substrate - cyclooctene. The main factors influencing the activity and selectivity of these catalysts have been identified. Heterogeneous $POM/Zn^{2+}$-(N)-CNTs catalysts are not susceptible to POM leaching during epoxidation reactions and demonstrated truly heterogeneous catalysis nature.

**Acknowledgement:** This work was supported by the Ministry of Science and Higher Education of the Russian Federation within the governmental order for the Boreskov Institute of Catalysis (project AAAA-A21-121011390008-4).

**References:**

[1] V. Y. Evtushok, V. A. Lopatkin et al., Catalysts 12 (2022) 472.

## OP-IB-21

# $Ni_{1-x}Mo_x$, $Ni_{1-x}W_x$ and $Ni_{1-x-y}Mo_xW_y$ Dispersed Alloy Catalysts: Synthesis, Structure and Transformation in 1,2-Dichloroethane Decomposition Process

Rudneva Y.V.[1], Bauman Y.I.[2], Potylitsyna A.R.[2], Shubin Y.V.[1], Plyusnin P.E.[1], Mishakov I.V.[2], Vedyagin A.A.[2]

*1 – Nikolaev Institute of Inorganic Chemistry, Novosibirsk, Russia*

*2 – Boreskov Institute of Catalysis, Novosibirsk, Russia*

*rudneva@niic.nsc.ru*

In recent decades, the problem of processing highly toxic organochlorine wastes accumulated in industry has become increasingly important. Disposal of such wastes is not an easy task due to the high chemical resistance of most compounds. One of the promising options for solving this problem is the method of thermal decomposition of chlorinated hydrocarbons in the presence of catalysts based on iron triad metals (Ni, Co, Fe) and their alloys. The advantage of the method is the possibility of obtaining fibrous carbon material as one of the main decomposition products of the organic substrate. The resulting carbon material has a high specific surface area, which makes it promising for use in various applications, in particular, in the production of antifriction materials, sorbents, and catalytic supports, as well as in the creation of polymer composite materials with improved functional properties.

Previously, it was shown that nickel-based alloys with the addition of Co, Cu, and Cr show high catalytic activity during the decomposition of chlorinated hydrocarbons [1–3]. In these works, 1,2-dichloroethane (DCE) was used as a model substrate, since it is the main component of vinyl chloride production waste. Within the framework of the present study, methods have been developed for the synthesis of highly dispersed binary and ternary alloys based on nickel with metal additives that increase its catalytic activity (Mo, W). Their physicochemical properties and the transformations of the catalysts during their dispersion during the decomposition of DCE were studied.

$Ni_{1-x}M_x$ (M= Mo, W) and $Ni_{1-x-y}Mo_xW_y$ alloys are the result of annealing in the reductive environment ($H_2$) of specially prepared precursors. Alloy precursors are found as microheterogeneous mixtures containing joint non-equilibrium compounds of nickel compounds and additive metals from an aqueous solution. According to the elemental analysis (ICP AES), the composition of the sample corresponds to the composition set during the synthesis. Obtaining alloys used as a gray powder, consisting of irregularly shaped metal particles. The particles consist of grains connected to each other by bridges to form a porous structure (Fig. 1a). According to XRD data, no impurity phases were found in the obtained alloys. The crystal lattice parameters of the alloys increase with the increasing of the additive metal content, which confirms the formation of substitutional solid solutions. On the diffraction patterns, this phenomenon is clearly expressed as a shift of the position of 331

peaks of alloys in the region of smaller angles, by analogy with a similar peak for pure nickel (Fig. 1b).

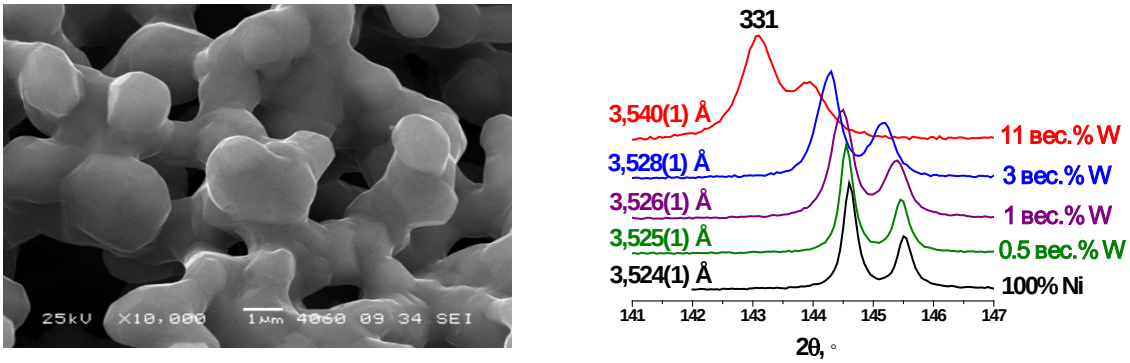


*Fig. 1. SEM micrograph of $Ni_{1-x}W_x$ sample (1.2 wt.% W) (a); a fragment demonstrating the shift of the 331 peaks (b).*

Ex situ XRD showed that the dispersing of the $Ni_{1-x}Mo_x$ alloy proceeds with the decomposition of solid solutions as a result of supersaturation with molybdenum, which occurs when carbon is dissolved in the alloy. The dispersing of $Ni_{1-x}W_x$ and $Ni_{1-x-y}Mo_xW_y$ alloys occurs without changing the initial composition of the catalysts.

**Acknowledgement:** This work was supported by the Russian Science Foundation, grant 21-13-00414.

**References:**

[1] Bauman, Y.I., Mishakov, I.V. et al, Catalysis in Industry 2 (2012)18–24.
[2] Bauman, Y.I., Lysakova, A.S. et al, Nanotechnologies in Russia 9(7–8) (2014) 31–35.
[3] Bauman, Y.I., Mishakov, I.V. et al, Kinetics and Catalysis 52(4) (2011) 1–8.
[4] Chesnokov, V.V., Buyanov, R.A. Uspekhi Khimii 69(7) (2000) 675–692.

## OP-IB-22

# Oxidized Carbon Nanomaterials as Efficient Adsorbents for $Nd^{3+}$ Removal

Navrotskaya A.G., Krivoshapkin P.V., Krivoshapkina E.F.
*ITMO University, St. Petersburg, Russia*
*navrotskaya@scamt-itmo.ru*

The recycle and reuse of rare earth elements (REEs) is currently one of the urgent problems in the world, since they have a great potential in modern technologies and industrial applications. They are essential in high-strength permanent magnets for wind turbines, hard disk drives, speakers, headphones, in alloys for batteries, hybrid vehicles, in phosphors for lighting products, in catalysis, glass production and metallurgy [1].

Among important REEs neodymium (Nd) is considered to be 'critical and shortage material', since it is necessary for use in neodymium-iron-boron (NdFeB) magnets that offer the strongest magnetic field per unit volume. However, Nd natural content in the REE ores is low, meanwhile the processing rates are insignificant, about 1%. Obviously for sustainable market development and sufficiency of these elements in the world, methods of their recovery and reusability are of exceptional interest [2].

Carbon nanotubes (CNTs) and carbon nanofibers (CNFs) are one-dimensional carbon nanomaterials exhibiting a high aspect ratio, easily modified surface, and thermal stability, making them as effective adsorbents for wastewater treatment. Due to strong Van der Waals interactions, initial CNTs and CNFs can easily aggregate, which leads to a decrease in surface area and makes their porous structure inaccessible to adsorbate molecules. The absence of functional groups in their structure causes a slow adsorption rate or low adsorption capacity. Various methods, including strong acid oxidation, activation, and functionalization/combination with other materials, have been used to modify CNTs and CNFs to improve their efficiency in removing contaminants [3].

This study is focused on the adaptation of CNTs and CNFs through acid oxidation functionalization to improve their adsorption properties for neodymium in aqueous solution. Oxidized CNTs (CNT-ox) and CNFs (CNF-ox) were characterized by a set of physicochemical methods. The effect of key parameters such as adsorbent dosage, pH, temperature, $Nd^{3+}$ ion concentration, temperature, and time on $Nd^{3+}$ removal was evaluated.

**Acknowledgement:** This work was supported by state task № FSER-2022-0002 within the framework of the Russian Ministry of Science and Higher Education "Science and Universities" National Project.

**References:**

[1] Ji B., Li Q., Zhang W. Leaching recovery of rare earth elements from the calcination product of a coal coarse refuse using organic acids //Journal of Rare Earths. – 2022. – V. 40. – №. 2. – P. 318-327.
[2] Jyothi R. K. et al. Review of rare earth elements recovery from secondary resources for clean energy technologies: Grand opportunities to create wealth from waste //Journal of Cleaner Production. – 2020. – V. 267. – P. 122048.
[3] Sezer N., Koç M. Oxidative acid treatment of carbon nanotubes //Surfaces and Interfaces. – 2019. – V. 14. – P. 1-8.

## OP-IC-01

# Development of a Model for Predicting Efficient Catalysts for the Process of Urea Electrooxidation

Dmitrieva A.P., Fomkina A.S., Romanenko E.A., Krivoshapkina E.F.
*ITMO University, Saint Petersburg, Russia*
*dmitrieva@scamt-itmo.ru*

Nearly 3 billion people worldwide have limited access to water for drinking, cooking and sanitation purposes. This is partly due to the insufficiently thorough treatment of wastewater, which contains a noticeable concentration of urea (or carbamide). The continuous formation of carbamide due to agricultural and industrial activities leads to its accumulation in significant amounts in the environment, which provokes irreversible processes in water bodies, as well as the production of greenhouse gases [1–3]. Selective electrochemical oxidation of urea helps to reduce the risk of eutrophication of water bodies and allows to simultaneously obtain energy-efficient pure hydrogen and reduce the content of nitrogen oxides – potent greenhouse gases – in the atmosphere. Selective formation of target products of electrochemical reactions can be achieved via the use of an optimal catalyst. A promising solution for this problem is to automate the process of searching for effective reaction conditions by creating a machine learning model that makes it possible to predict the optimal parameters of the electrocatalyst. The aim of this study is to develop a neural network for predicting the morphological features of particles that can be used for selective and efficient urea electro-oxidation.

Taking as input parameters the composition of the catalyst and the reaction conditions, the model would be able to predict the electrocatalytic activity, size and shape of the catalyst particles. By optimizing hyperparameters to improve metrics, training the model, and validating the result experimentally, it would be possible to create a unique tool applicable to optimize any economically and environmentally significant electrochemical process.

To create a training dataset, a database of 1200 catalysts and reaction conditions was initially selected, the use of which is possible for the electrooxidation of urea. After engineering the characteristics describing the catalytic system, the final set of descriptors containing geometric, kinetic, mechanical, thermodynamic, electronic properties, as well as molecular "fingerprints" was chosen, which allows digitizing particles and electrode processes. To create a predictive model, the architecture of a variational autoencoder was developed with the efficiency of predicting the composition and shape of the electrocatalyst with an error of no more than 20% and R2 of no less than 80%. The final optimization of the coding network and decoder parameters was carried out after experimental verification of the predicted data by conducting a validation electrochemical reaction of urea electrooxidation to molecular nitrogen ($N_2$) and hydrogen ($H_2$) with an efficiency of at least 85% and 15% for nitrite and nitrate ions.

## OP-IC-01

In the course of the research work, an optimized algorithm has been developed that will provide a space for possible compositions of catalysts for an electrocatalytic process (including urea electro-oxidation). Such a method would complement rational approaches to directed particle design and fine tuning. In the future, it is planned to create a digital service that will help users choose the appropriate type and morphology of the catalyst for a specific technological task. This approach would reduce the amount of resources required for experimental screening, and ensure efficient upscaling of the process to industrial capacity.

**Acknowledgement:** This research was supported by Priority 2030 Federal Academic Leadership Program.

**References:**

[1] W.T. Mook, M.K. Aroua, G. Issabayeva,. Renewable and Sustainable Energy Reviews, 38 (2014) 36–46.
[2] E. Urbańczyk, M. Sowa, W. Simka, J Appl Electrochem. 46 (2016) 1011–1029.
[3] S.W. Tatarchuk, J.J. Medvedev, F. Li, Y. Tobolovskaya, A. Klinkova, Angewandte Chemie International Edition. 61 (2022).

## OP-IC-02

# Copper Complexes of Sodium Pectate as Oxygen Reduction Catalysts

Lebedeva E.M.[1,2], Nizameeva G.R.[1,2], Nizameev I.R.[1,2], Minzanova S.T.[1,2], Morozov V.I.[1], Mansurov R.N.[2], Gainullin R.R.[1], Kadirov M.K.[1,2]

*1 – Arbuzov Institute of Organic and Physical Chemistry, Kazan, Russia*

*2 – Kazan National Research Technological University , Kazan, Russia*

*elgina.lebed@mail.ru*

This work continues our series on the study of coordination biopolymers, namely, complexes of natural pectin polysaccharides with transition metals as electrocatalysts for the oxygen reduction reaction (ORR). In this work, the transition metal is copper. Synthesis of the complexes (Fig. 1, A and B) was carried out according to the known method [1].

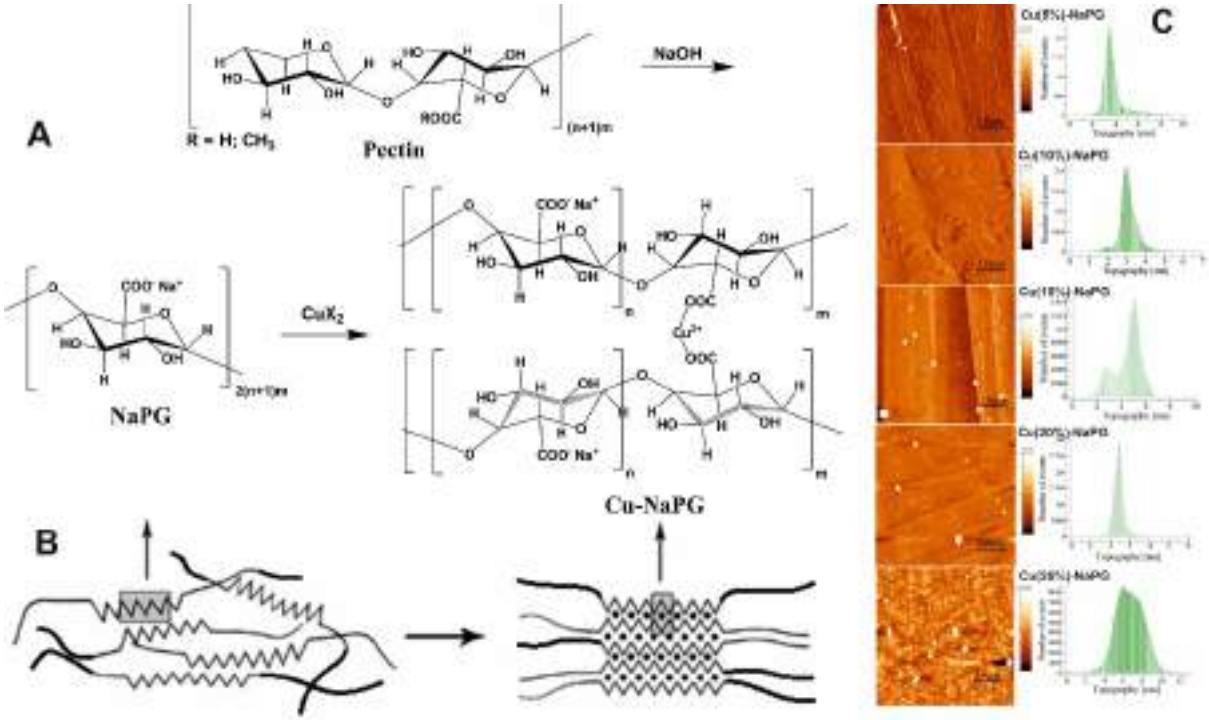


*Fig. 1. Schemes for the synthesis of pectin polysaccharide complexes (n=3-10; m=10-35) with copper (A) and the formation of polymer-complex structures according to the "egg-box" model (B - right), AFM images (left column of C) and particle size distribution (right column of C) for the Cu(n%)-NaPG compounds*

For a number of Cu(n%)-NaPG samples with varying degrees of copper substitution (from 5% to 25%), the film structures formed during their deposition from the liquid phase on the surface of pyrolytic graphite have been studied. Judging by the AFM images (Fig. 1C - left column), for the Cu(15%)-NaPG and Cu(25%)-NaPG samples there are areas of the film not filled with metal. It is possible that because of these breaks in the organic film with jagged edges, the vertical dimensions in AFM images are larger (in the region of 5–6 nm) and have a wider vertical distribution (Fig. 1C – right column). The most optimal substitution values from the point of view of the uniform distribution of metal centers are 5 and 20% samples.

To study the catalytic properties, samples with a denser distribution of copper [Cu(15%)-NaPG, Cu(20%)-NaPG] and [Cu(25%)-NaPG] have been selected. As can be seen (Fig. 2) from the CV curves of the studied coordination biopolymers, all of them exhibit activity of varying degrees with respect to ORR. The Ni(25%)-NaPG compound is approximately 1.05 times more active than Cu(15%)-NaPG and 1.15 times - than Cu(20%)-NaPG. In solutions saturated with argon, there are no reduction peaks.

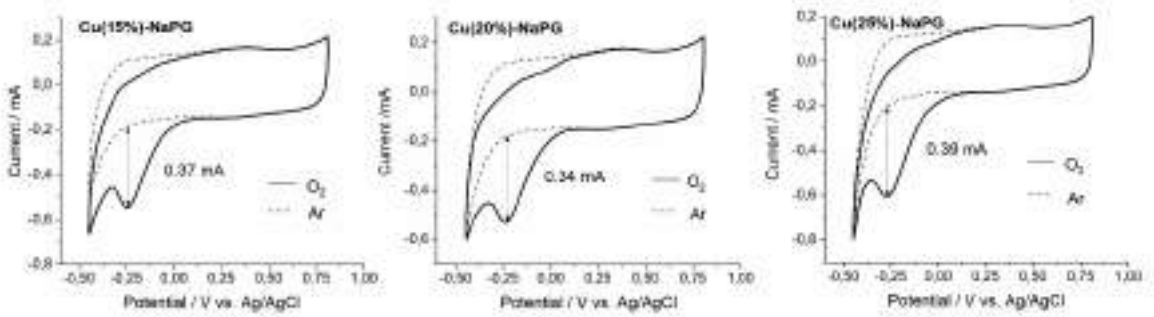


*Fig. 2. CVs with indication of the amplitudes of the cathodic peaks for ORR on GC electrodes modified with coordination biopolymers Cu(15%)-NaPG (left), Cu(20%)-NaPG (center) and Cu(25%)-NaPG (right) in argon-saturated (dashed curves) or oxygen-saturated 0.5 M $H_2SO_4$ (solid curves) at a scan rate of 50 mV $s^{-1}$; GC electrode area: 0.0707 $cm^2$*

Interestingly, as in the case of nickel [1], the optimal number of electrons transferred in one catalytic cycle (hereinafter in parentheses) closest to 4 has a sample with 20% substitution by a transition metal and with the most uniform distribution of copper metal centers [Cu(15 %)-NaPG, 3.11; Cu(20%)-NaPG, 3.95; and Cu(25%)-NaPG, 3.22, respectively].

**References:**

[1] I. Nizameev, D. Kadirov, G. Nizameeva, A. Sabirova, K. Kholin, M. Morozov, L. Mironova, R. Zairov, S. Minzanova, O. Sinyashin, M. Kadirov, IJMS 23 (2022) 14247.

## OP-IC-03

# Design of Ag/Graphene Oxide Catalysts Modified with Transition Metal Oxides for Reduction Reactions

Taratayko A.V., Mamontov G.V.
*Tomsk State University, Tomsk, Russia*
*taratayko1997@mail.ru*

The $CeO_2$ employment in the Ag-containing catalysts contributes to stabilization of silver nanoparticles and cooperation of Ag and $CeO_2$ active sites due to the features of metal–metal oxide interaction, which in turn lead to an increase of catalytic activity in oxidation [1,2] and reduction processes [3,4]. A primary support, for example, graphene oxide, is used to enhance the stability and specific surface area of the Ag–$CeO_2$ system. Nanosized particles of active components are formed on graphene oxide due to its high surface area and abundant oxygen-containing functional groups [5]. A number of papers [5–8] has been devoted to Ag and $CeO_2$ particles deposited on graphene oxide, where the deposition of the active components has been carried out by a precipitation of Ag and $CeO_2$ precursors using basic compounds ($NH_4OH$, NaOH, urea $(NH_2)_2CO$ solutions). However, it is not possible to establish an exceptional effect of a precipitant on Ag and $CeO_2$ nanoparticles formation based on these works due to different ratios of catalyst components, temperature regimes, and other synthesis conditions. This work aims to study the effect of the precipitant nature under other identical synthesis conditions on the physicochemical properties of Ag and $CeO_2$ particles supported on graphene oxide, as well as to study their catalytic activity in the 4-nitrophenol reduction reaction.

Graphene oxide (GO) was synthesized by the oxidative treatment of graphite powder according to the modified Hummers method [9]. Ag- and $CeO_2$-containing catalysts were prepared by the deposition-precipitation method using $AgNO_3$ and $Ce(NO_3)_3$ as the Ag and $CeO_2$ precursors onto graphene oxide. Precipitation was carried out with the solutions of $NH_4OH$ (Ag-$CeO_2$/GO_$NH_3$), NaOH (Ag-$CeO_2$/GO_NaOH), $(NH_2)_2CO$ (Ag-$CeO_2$/GO_carb) or $(NH_2)_2CO$ with preliminary neutralization of the support acidity with a small amount of $NH_4OH$ (Ag-$CeO_2$/GO_carb_neu). The prepared samples were characterized by a set of physicochemical methods: powder X-ray diffraction (XRD), thermogravimetric analysis (TGA), etc. The catalytic activity of the samples was studied in the 4-nitrophenol to 4-aminophenol reduction with sodium borohydride $NaBH_4$ at room temperature and atmospheric pressure in an aqueous medium.

The catalytic reaction of 4-nitrophenol reduction by the Ag-$CeO_2$/GO samples was monitored by recording the UV-vis spectra of the reaction solution (Fig. 1a). Fig. 1b illustrates the kinetic data obtained from the UV-vis spectra at wavelength of 400 nm (4-nitrophenolate ion absorption band). The Ag-$CeO_2$/GO_$NH_3$ catalyst demonstrates the highest activity in the synthesized series (rate constant k = 3.77 $min^{-1}$) due to developed active surface and interaction of Ag and $CeO_2$. Lower catalytic activity of the Ag-$CeO_2$/GO_carb (k = 1.26 $min^{-1}$) and Ag-$CeO_2$/GO_carb_neu (k = 1.73 $min^{-1}$) samples can be associated with lower amount of

the active components because of non-quantitative precipitation of their precursors with urea, which is consistent to the TGA and XRD results. The least activity of the Ag-$CeO_2$/GO_NaOH catalyst (k = 0.89 $min^{-1}$) may be caused by large Ag particles formation (according to the XRD data) with a low active surface that leads to decrease of catalytic activity.

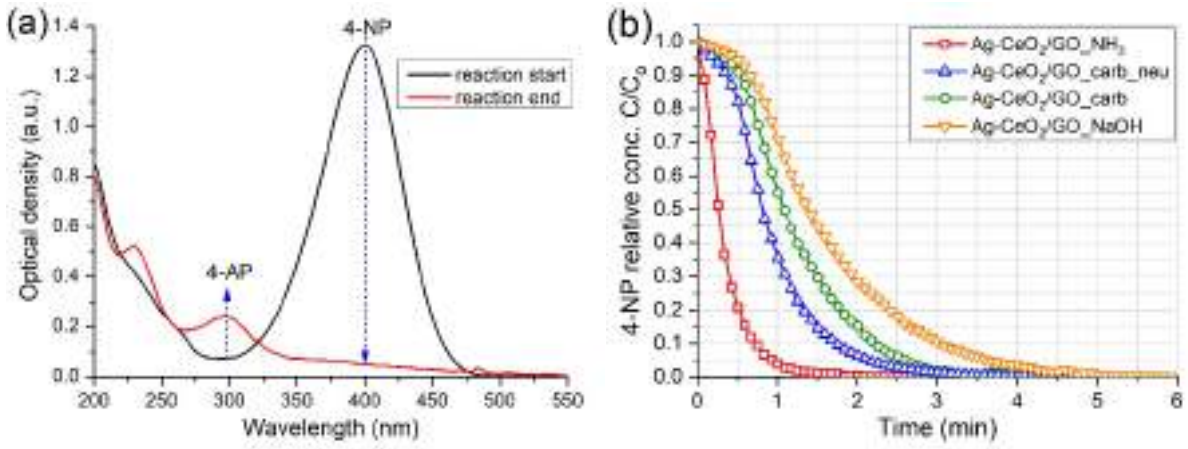


*Fig. 1. UV-vis absorption spectra evolution of the reaction solution (a) and the kinetic curves of 4-nitrophenol reduction with the Ag-$CeO_2$/GO catalysts (b)*

Thus, the effect of the precipitant nature on the Ag-$CeO_2$/GO active surface formation has been revealed. Depending on the precipitant used in the synthesis of the catalysts, rate constant of the catalytic 4 nitrophenol reduction process increased in the series NaOH < $(NH_2)_2CO$ < $NH_4OH$ from 0.89 to 3.77 $min^{-1}$. To obtain the most active catalysts according to the procedure, the precipitant should be basic enough to precipitate the active components' precursors quantitatively and promote their interaction. At the same time, the precipitant should not lead to excessive increase of nanoparticles' size and, as a result, active surface decrease.

**Acknowledgement:** This work was funded by the State assignment of the Ministry of Education and Science of the Russian Federation (project number FSWM-2020-007).

**References:**

[1] M. V. Grabchenko, G. V. Mamontov, V. I. Zaikovskii, V. La Parola, L. F. Liotta, O. V. Vodyankina, Appl. Catal. B 260 (2020) 118148.
[2] N. N. Mikheeva, V. I. Zaikovskii, Y. V. Larichev, G. V. Mamontov, Mater. Today Chem. 21 (2021) 100530.
[3] M. V. Chernykh, N. N. Mikheeva, V. I. Zaikovskii, G. V. Mamontov, Kinet. Catal. 61 (2020) 794.
[4] A. Taratayko, Yu. Larichev, V. Zaikovskii, N. Mikheeva, G. Mamontov, Catal. Today 375 (2021) 576.
[5] A. Taratayko, E. Kolobova, G. Mamontov, Catalysts 12 (2022) 1393.
[6] Y. Wang, C. Lu, Z. Yin, Mater. Lett. 270 (2020) 127723.
[7] Z. Ji, X. Shen, J. Yang, G. Zhu, K. Chen, Appl. Catal. B 144 (2014) 454.
[8] C. Mardani, M. Y. Rizal, R. Saleh, A. Taufik, S. Yin, Appl. Surf. Sci. 530 (2020) 147297.
[9] W. S. Hummers, R. E. Offeman, J. Am. Chem. Soc. 80 (1958) 1339.

## OP-IC-04

# Design of Efficient Supported Bimetallic Palladium Catalysts for Selective Hydrogenation of Acetylene

Yurpalova D.V.[1], Afonasenko T.A.[1], Prosvirin I.P.[2], Bukhtiyarov A.V.[2], Vinokurov Z.S.[2], Khramov E.V.[3], Shlyapin D.A.[1]

*1 – Center of New Chemical Technologies BIC, Boreskov Institute of Catalysis, Omsk, Russia*

*2 – Boreskov Institute of Catalysis, Novosibirsk, Russia*

*3 – National Research Center "Kurchatov Institute", Moscow, Russia*

*omsk-glyzdova@mail.ru*

Supported bimetallic catalysts based on palladium are widely used to accelerate practically important reduction processes, for example, the selective hydrogenation of unsaturated compounds. The hydrogenation reaction of acetylene to ethylene is used both to purify ethylene from the $C_2H_2$ impurity, which is formed during the pyrolysis of petroleum feedstock, and to directly ethylene obtaining from $C_2H_2$, synthesized by pyrolysis of natural gas [1]. It is known that the high selectivity of bimetallic catalysts is achieved due to the formation of bimetallic sites with a specific electronic and geometric configuration. Therefore, it is necessary to use the approaches of catalysts synthesis that improve the efficiency of interaction between palladium and the modifier. At the same time, the modifying effect is also determined by the nature of the second metal and the structure of the bimetallic particles. In this work, Co, Fe, and Mn were used as modifiers because these metals are capable of forming solid solutions and/or intermetallic compounds with palladium. However, there are a small number of works [2-5] on the use of samples based on Pd-Co, Pd-Mn, and Pd-Fe for the hydrogenation of acetylene to ethylene.

Sibunit carbon mesoporous material was used as a catalyst support. Samples were prepared by incipient wetness impregnation with joint aqueous solution of palladium and modifier nitrate. The catalysts were dried at 120°C and reduced in hydrogen at 500 – 700°C. The content of palladium in all samples was 0.5 wt.%. The Pd/M molar ratio was varied from 1/0.5 to 1/4. The state of the active component was studied by XRD, XPS, EXAFS, TEM and EDX. Acetylene hydrogenation was carried out in a model gas mixture (4 vol.% $C_2H_2$ in a hydrogen) in a flow mode at atmospheric pressure at 25 – 95°C.

It was found that Pd and Co supported on Sibunit (C) interact in $H_2$ medium to form bimetallic $Pd_xCo_{(1-x)}$ nanoparticles. The composition of $Pd_xCo_{(1-x)}$ depends on the Pd/Co molar ratio. The content of Co in the Pd-Co nanoparticles increases with an increase in the Pd/Co molar ratio up to 1:2 (to ~41% at. of Co in the bimetallic phase) and then remains at a constant level. A correlation has been established between the content of Co in bimetallic nanoparticles and the maximum ethylene yield in the acetylene hydrogenation reaction. The optimal Pd/Co molar ratio of 1:2÷1:4 was found, which ensures the formation of bimetallic Pd-Co particles containing ~41-43% at. of Co and leads to the ethylene yield of 62-63%. It has been proven that the catalytic properties of the studied Pd-Co/C samples in the process of acetylene

hydrogenation are not related to the influence of the size effect, but, first of all, are due to the influence of the composition of bimetallic sites and the electronic state of palladium. An increase in the reduction temperature of the Pd-Co(1:2)/C catalyst in hydrogen from 500 to 600 and 700°C is accompanied by a further decrease in activity and an increase in the selectivity and yield of the target product (to 66 and 68%, respectively) due to the formation of $Pd_xCo_{(1-x)}$ particles containing ~ 50 and 56% at. of Co, respectively.

The features of the interaction of components in Pd-Mn samples and the catalytic properties of Pd-Mn/C differ from those observed for Pd-Co/C catalysts. According to EXAFS data, Pd and Mn are predominantly present as individual particles after reduction of Pd-Mn/C at 500°C. An increase in the reduction temperature to 600 and 700°C is accompanied by an increase in the number of bimetallic Pd–Mn bonds, indicating the formation of bimetallic sites. An increase in the reduction temperature leads to a decrease in $C_2H_2$ conversion for all series of Pd-Mn samples, which may be due to sintering of the active component and/or the formation of less active Pd-Mn sites. The latter is supported by a significant increase in the ethylene selectivity with an increase in the catalyst treatment temperature from 500 to 700°C. It was found that the highest ethylene selectivity is exhibited by samples with a molar ratio of Pd/Mn = 1/1 regardless of the reduction temperature. The ethylene yield on Pd-Mn(1:1)/C reduced in $H_2$ at 700°C is 75%.

In the series of Pd-Fe/C catalysts, the highest yield of the target product (70%) is typical for samples with a molar ratio of Pd/Fe = 1/2 reduced in $H_2$ at 600-700°C. According to XRD, XPS and EXAFS data, the catalytic properties of this sample is associated with the formation of $Pd_xFe_{(1-x)}$ particles. It can be assumed that the high selectivity is due to the facilitation of ethylene desorption from the surface of $Pd_xFe_{(1-x)}$ solid solution.

Thus, it can be concluded that the catalytic properties of Pd/C can be improved by formation of the mixed Pd-Co, Pd-Mn, and Pd-Fe phases and the maximum yield of the target product increases in the following order: Pd/C (52%) < Pd-Co/C (68%) < Pd-Fe/C (70%) < Pd-Mn/C (75%).

**Acknowledgement:** This work was supported by the Ministry of Science and Higher Education of the Russian Federation within the governmental order for Boreskov Institute of Catalysis (project AAAA-A21-121011390011-4).

**References:**

[1] A. Borodziński, G. Bond, Catalysis Reviews. 48 (2006) 91-144.
[2] R. Ma, T. Yang, J. Sun, Y. He, J. Feng, J. Miller, D. Li, Chemical Engineering Science. 210 (2019) 115216.
[3] W.G. Menezes, L. Altmann, V. Zielasek, K. Thiel, M. Bäumer, Journal of Catalysis 300 (2013) 125–135
[4] V.D. Stytsenko, D.P. Mel'nikov, O.P. Tkachenko, E.V. Savel'eva, A.P. Semenov, L.M. Kustov, Russian Journal of Physical Chemistry A. 5 (2018) 862–869.
[5] F. Melnikov, V. Stytsenko, E. Saveleva, M. Kotelev, V. Lyubimenko, E. Ivanov, A. Glotov, V. Vinokurov, Catalysts. 10 (2020) 624.

## OP-IC-05

# Effect of Magnesium Doping on the Interaction of $Au^{III}$ Precursor Complexes and $Au^0$ Nanoparticles with Alumina Surface in $Au/Mg^{2+}/\gamma–Al_2O_3$ Catalysts

Danilova I.G.[1], Moroz B.L.[2], Bukhtiyarova G.A.[1]
*1 – Boreskov Institute of Catalysis, Novosibirsk, Russia*
*2 – Novosibirsk State University, Novosibirsk, Russia*
*danig@catalysis.ru*

The ability to control the dispersion and morphology, which are the key factors determining the catalytic performance of oxide-supported metal catalysts, is a challenging task of catalyst design and can be enabled by understanding the nature of metal–support interactions. As the metal catalyst support, γ–alumina is the most widely used, because its surface structure is favorable for stabilizing the catalytically active noble metal nanostructures such as gold nanoparticles (GNPs). Doping of alumina with $Mg^{2+}$ ions further enhances the activity of $Au/Al_2O_3$ catalysts in low-temperature CO oxidation, aerobic oxidation of alcohols, selective acetylene hydrogenation *etc* [1, 2]. In this study we examined the effect of magnesium doping on the interaction of $Au^{III}$ hydroxychloride complexes and GNPs formed from them with alumina surface by FTIR and UV-vis diffuse reflectance (DR) spectroscopy in combination with XRD, TEM *etc*., hoping to shed some light on the causes of changes in activity of "gold-on-alumina" catalysts with addition of $Mg^{2+}$ ions.

A series of $Mg^{2+}$-doped aluminas hereinafter denoted as AlMg*x*, where *x* is wt% of Mg (Table 1), was prepared by incipient wetness impregnation of $\gamma$-$Al_2O_3$ (Sasolchemie) with an aqueous $Mg(NO_3)_2$ solution followed by calcination in air at 500°C. The Au/AlMg*x* catalysts were synthesized by deposition-precipitation (DP) technique which involved treating a support with an alkalized $H[AuCl_4]$ solution at 70°C and pH 7, washing a solid sample with water, drying *in vacuo* at 25°C and calcining in air at 300°C.

Table 1. Characteristics of AlMg*x* supports and Au/AlMg*x* catalysts under study.

| Sample | AlMg*x* supports | | | | Au/AlMg*x* catalysts | | |
|---|---|---|---|---|---|---|---|
| | Mg, wt% | $S_{BET}$, $m^2/g$ | LAS | BS | Au, wt% | Mean Au particle diameter (TEM), nm | SPR, nm |
| | | | μ-mol/g | | | | |
| Au/AlMg0 | 0 | 202 | 850 | 578 | 1,95 | 1.9±0.4 | 624 |
| Au/AlMg0.1 | 0.1 | 187 | 897 | 623 | 1.65 | 1.7±0.3 | 571 |
| Au/AlMg0.5 | 0.5 | 190 | 953 | 701 | 1.45 | 1.3±0.3 | 540 |
| Au/AlMg1 | 1.0 | 184 | 1028 | 836 | 1.30 | 1.6±0.3 | 528 |

According to XRD analysis, doping $Al_2O_3$ with Mg leads to the formation of a solid solution with spinel structure containing $Mg^{2+}$ cations in tetrahedral lattice positions. With the increase of Mg addition, the number of surface Lewis acid and base sites (LAS and BS, respectively) increases (Table 1), as determined by FTIRS of adsorbed CO and $CDCl_3$. Simultaneously, there is a decrease in the fraction of the most reactive Al-OH groups with $\nu_{OH}$ at 3775 $cm^{-1}$ (Fig. 1). As a result, after Mg addition, weaker electrostatic interactions prevail between the support

surface and Au(III) complexes; while pristine $Al_2O_3$ mainly links these complexes by ligand exchange reactions with the surface OH groups to form Al-O-$Au^{III}$ bonds. Apparently, for this reason, the amount of Au complexes extracted from the solution during DP process decreases with increasing the Mg loading in $Al_2O_3$. UV-vis DR spectra of uncalcined $Au^{3+}$/AlMg*x* samples (Fig. 2) demonstrate a gradual decrease of the $Cl^- \rightarrow Au^{3+}$ CTT band at 260-270 nm with the growth of Mg content in alumina indicating the appearance of fully hydrolyzed $[Au(OH)_4]^-$ complexes on the support surface instead of $[AuCl(OH)_3]^-$, which should help to reduce the $Cl^-$ content of the samples and favors the formation of smaller $Au^0$ particles during calcination (Table 1).

The FTIR spectra of calcined Au/AlMg*x* catalysts testify that a part of surface OH groups interact with GNPs, forming the Au-O-Al bonds at the particle/support interfaces. In the Mg-doped catalysts, the surface LAS and carbonate species may stabilize finely dispersed $Au^0$ crystallites in addition to the OH groups. Obviously, this can promote the enhanced dispersion of GNPs. In the UV-vis DR spectra, the peak positions of the surface plasmon resonance (SPR) (Table 1) give information about the shape of GNPs in the catalysts under study. The spectra of the Au/AlMg0.5 and Au/AlMg1 catalysts show SPR peaks at 540-528 nm, which are characteristic of spherical GNPs, whereas in the spectrum of the Au/AlMg0 catalyst, the SPR peak shifts to 624 nm that corresponds to oscillation of the free electrons along the long axis of flattened gold particles. This is consistent with the TEM evidences of epitaxial grafting of $Au^0$ crystallites onto the support surface in the AlMg0 catalyst. In addition, FTIR spectra of CO absorbed on the Au/AlMg*x* catalysts will be discussed, revealing the co-existence of Au atoms in various oxidation states on the support surface.

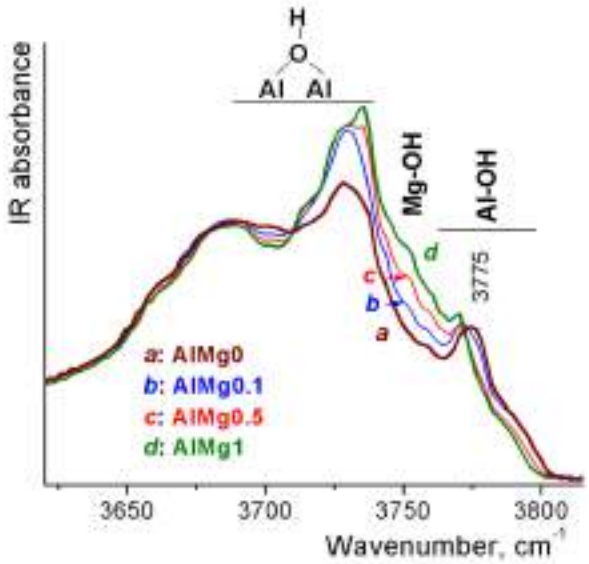


*Fig. 1. FTIR spectra of AlMgx supports.*

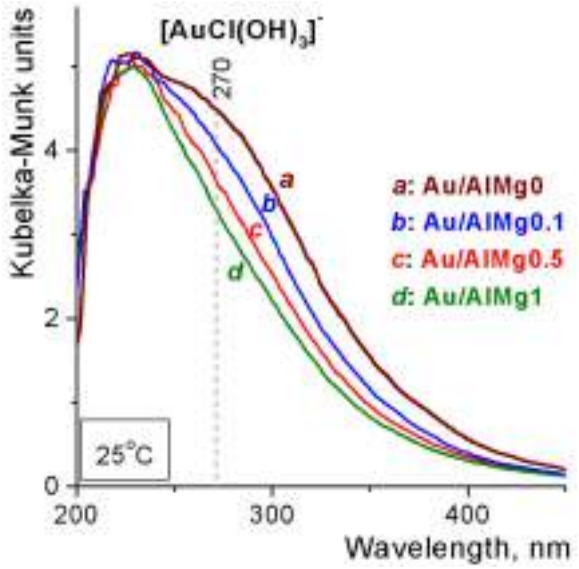


*Fig. 2. UV-Vis DR spectra of $Au^{3+}$/AlMgx catalyst precursor samples.*

**References:**

[1] X. Sun, F. Li, J. Shi, Y. Zhang, H. Su, L. Sun, S. Peng, C. Qi, Appl. Surf. Sci. 487 (2019) 625.
[2] S.A.C. Carabineiro, P.B. Tavares, J.L. Figueiredo, Appl. Nanosci. 2 (2012) 35.

## OP-IC-06

# *In Situ* Synthesized Cu-ZnO Catalysts for the Catalytic Hydrogenolysis of Glycerol

Porukova Iu.I., Samoilov V.O., Ramazanov D.N., Kniazeva M.I., Maximov A.L.
*A.V. Topchiev Institute of Petrochemical Synthesis, Moscow, Russia*
*porukova@ips.ac.ru*

Nowadays, the most part of 1,2-propanediol **(PG)**, an important industrial product, is produced from non-renewable carbonaceous raw materials. To reduce the environmental impact, it is feasible to produce certain industrially important compounds from renewable sources of raw materials. One such production is the synthesis of PG from glycerol **(GL)**, a by-product of biodiesel manufacturing. In 2012, Oleon jointly with BASF launched the bio-PG plant from bio-GL in Ertvelde, Belgium [1]. Nevertheless, research in the area continues, including preparation of heterogeneous catalysts with improved characteristics of the activity, selectivity, stability, and handling safety.

For the processes of hydrogenation and hydrogenolysis, catalysts based on the platinum group of metals, cobalt, nickel, and copper are the most widely used. Copper-containing catalysts have a number of advantages, including low-cost, low toxicity and high selectivity for the hydrogenation of C–O bonds. The main drawback is the low activity compared to the platinum group metals and nickel. However, the promotion of the copper catalysts with other elements (i.e. zinc, nickel, aluminum), as well as an increase in the dispersion of the catalyst allows to level the disadvantage mentioned above.

The authors propose to carry out the process of GL hydrogenolysis to PG using dispersed copper-containing catalysts synthesized *in situ* during the GL hydrogenolysis reaction. Thus, the dispersed catalyst is generated by *in situ* conversion of its precursors, and then catalyzes the GL hydrogenolysis. In order to improve the catalysts synthesized earlier by the authors [2], zinc acetate was added to the initial catalyst precursor, copper acetate (II). During the reaction of GL hydrogenolysis, the main product (PG) was accompanied by three by-products, namely lactic acid **(LA)**, ethelyne glycol **(EG)**, glyceric acid **(GA)**.

The influence of the reaction conditions (alkali dosage, Cu:ZnO ratio, $H_2$ pressure, reaction time) on the products' yield was studied. The addition of alkali was found to play an important role in the formation of the catalytic phase and to co-catalyze the reaction of GL hydrogenlysis. For example, the addition 3 mol % alkali to the feed increased the GL conversion and the PG yield from 1.6 to 21.0 % and from 0.2 to 17.2 %, respectively. The effect of the Zn:Cu ratio (precursor composition) on the GL conversion and the yields of the products was studied (Table 1). The catalyst synthesized *in situ* from zinc acetate was not effective for the PG production (entry 1). However, the addition of zinc acetate to copper acetate in the initial mixture significantly affected the GL conversion and the PG yield (entry 2-5). The highest GL conversion and the PG yield was observed at a Zn:Cu ratio of 3 mol (entry 3). The change of the hydrogen pressure from 1 MPa to 5 MPa led to increase in the GL conversion from 14 to

33% and the PG yield from 9 to 30%. Thus, the rate of PG formation was proportional to the hydrogen concentration in the batch reactor.

Table 1. The influence of the Zn:Cu mol ratio on the GL conversion and the yields of the products. Conditions: T = 220 °C, p($H_2$) = 3 MPa, GL:KOH = 33.3 mol, GL:(Cu+Zn) = 100 mol, τ = 4.0 h, precursor salts = copper acetate(II) and zinc acetate.

| Entry | Zn:Cu, mol | GL conversion, % | EG yield, % | PG yield, % | LA yield, % | GA yield, % |
|---|---|---|---|---|---|---|
| 1 | only Zn | 0.6 | - | - | 0.5 | - |
| 2 | 7 | 10.0 | 0.3 | 7.8 | 1.6 | 0.3 |
| 3 | 3 | 21.0 | 0.5 | 17.3 | 2.7 | 0.5 |
| 4 | 1 | 14.5 | 0.6 | 10.8 | 2.5 | 0.5 |
| 5 | 0.33 | 8.3 | 0.3 | 5.5 | 2.1 | 0.5 |
| 6 | only Cu | 6.0 | 0.2 | 4.2 | 1.3 | 0.3 |

The *in situ* generated catalysts with different ratio of Zn:Cu were investigated by XRD, XPS, SEM and HRTEM methods. According to XRD, the *in situ* formed solid phases consisted of Cu-ZnO composites (entry 2-5). The most promising and finely dispersed catalyst was generated with Zn:Cu ratio of 3 mol. It was represented by copper particles (≤150 nm) surrounded by oblong zinc oxide particles with sizes ranging from a couple of nanometers to 200 nm.

With increasing the reaction time to 48 hours, the GL conversion and the PG yield over the *in situ* generated catalyst with Zn:Cu=3 reached 81 and 77%, respectively, while the catalytic phase did not undergo significant changes in the phase composition and morphology. It has been established, that the activity of *in situ* synthesized copper-zinc oxide catalysts is totally comparable to the industrial copper-chromite hydrogenation catalyst.

**Acknowledgement:** This research was funded by the Russian Science Foundation (RSF), project № 22-13-00252.

**References:**

[1] BASF and Oleon Celebrate Grand Opening of Propylene Glycol Production Plant. Available online: https://www.chemeurope.com/en/news/138616/basf-and-oleon-celebrate-grand-opening-of-propylene-glycol-production-plant.html (accessed on 10 November 2022).
[2] I. Porukova, V. Samoilov, D. Ramazanov, M. Kniazeva, A. Maximov, Molecules. 27 № 24 (2022) 8778.

## OP-IC-07

# One-Step Synthesis of Aromatic Polymeric Supports for Palladium-Containing Catalytic Systems

Bakhvalova E.S.[1], Bykov A.V.[2], Nikoshvili L.Z.[2]
*1 – Tver State University, Tver, Russia*
*2 – Tver State Technical University, Tver, Russia*
*nlinda@science.tver.ru*

The development of new highly porous aromatic polymers is a promising field of catalyst design. The use of porous polymers allows creating various types of catalytically active centers, regulating the access to active centers, and controlling their environment [1]. At the same time, ligandless Pd-containing catalytic systems for the cross-coupling processes belong to the so-called "cocktail" type catalysts, in which the catalyst' morphology continuously changes throughout the reaction [2]. Thus, in order to retain the active metal, it is necessary to ensure its interaction with the aromatic polymeric support. In this regard, the polymers containing heteroaromatic structures as well as containing functional substituent groups are promising.

There is a huge variety of cross-linked polymeric supports for palladium stabilization. However, in many cases polymer synthesis is multistage and includes steps requiring the use of homogeneous palladium complexes as cross-linking catalysts. Tan et al. [3] proposed the one-step method based on the Friedel-Crafts reaction, according to which the condensation of aromatic monomers occurs by rigid methylene bridges in the presence of a catalyst (anhydrous ferric chloride). It was shown that the porous structure and surface area of the resulting polymers are regulated by changing the molar ratio of the cross-linking agent (methylal) to monomers, which ultimately affects the degree of cross-linking.

In the synthesis of hyper-cross-linked aromatic polymers, along with simple organic compounds it is possible to use functionalized monomers and even their combinations [4]. For example, a series of polymers based on benzyl alcohol was synthesized [5]. Using phenol as a monomer, the polymers containing phenolic hydroxyl groups were obtained [3]. Cooper et al. [6] developed microporous polymers by co-polymerization of aniline and benzene [6]. It is noteworthy that at present there are only few publications concerning the use of several different aromatic monomers in the process of one-step synthesis of hyper-cross-linked aromatic polymers. Thus, the one-step synthesis of highly porous functionalized polymers using a combination of several different monomers is a relatively novel area of research, especially aiming the development of heterogeneous catalysts.

In the framework of this work, the one-step synthesis of highly porous polymers (SSA was up to ca. 1000 $m^2/g$) was carried out, followed by the introduction of palladium into the polymeric environment to obtain catalysts for the Suzuki cross-coupling. The synthesis of polymers was based on the use of methylal as a cross-linking agent, and as anhydrous ferric chloride and also aluminium chloride as catalysts. Synthesis was carried out at variation of the

type of monomers (both non-functionalized arenes (benzene, naphthalene, anthracene, phenanthrene) of different structures and substituted aromatic compounds (nitrobenzene, nitronaphthalene, naphthol, benzoic acid, cinnamic acid) were used) and their ratio that allowed controlling the porosity and relative hydrophobicity of the resulting polymeric materials. Moreover, the meso-macroporous sulphated and nitrated derivatives of the polymers were synthesized for the first time.

Using the developed polymers, palladium-containing catalysts were synthesized (1 wt.% Pd) containing either Pd(II) species or Pd(0) nanoparticles and tested in a model reaction of Suzuki cross-coupling between 4-bromanisole and phenylboronic acid. It was shown that under mild reaction conditions (60°C, ethanol-water mixture as a solvent) in air the conversion of 4-bromanisole reached more than 95% for less than 60 minutes of the reaction with high selectivity for the cross-coupling product (4-methoxybiphenyl).

**Acknowledgement:** This work was supported by the Russian Science Foundation, grant 23-29-00604.

**References:**

[1] C. Monterde, R. Navarro, M. Iglesias, F. Sánchez, J. Catal. 377 (2019) 609.
[2] D.B. Eremin, V.P. Ananikov, Coord. Chem. Rev. 346 (2017) 19.
[3] L. Tan, B. Tan, Chem. Soc. Rev. 46 (2017) 3322.
[4] L. Shao, Y. Sang, N. Liu, Q. Wei, F. Wang, P. Zhan Sep. Purif. Technol. 262 (2021) 118352.
[5] Y. Liu, X. Chen, X. Jia, X. Fan, B. Zhang, A. Zhang, Q. Zhang., Ind. Eng. Chem. Res. 57 (2018) 17259.
[6] R. Dawson, T. Ratvijitvech, M. Corker, A. Laybourn, Y.Z. Khimyak, A.I. Cooper, D.J. Adams, Polym. Chem. 3 (2012) 2034.

## OP-IC-08

# Composite Catalysts Based on the $CaO-Fe_2O_3$ System for the Oxidative Conversion of Hydrocarbons

Kirik N.P.[1], Rabchevskii E.V.[1], Shishkina N.N.[1], Kopytov M.A.[2], Solovyov L.A.[1], Anshits A.G.[1,3]
*1 – Institute of Chemistry and Chemical Technology SB RAS, Krasnoyarsk, Russia*
*2 – Institute of Petroleum Chemistry SB RAS, Tomsk, Russia*
*3 – Siberian Federal University, Krasnoyarsk, Russia*
*kiriknp@icct.ru*

Oxide systems based on the calcium ferrites due to their physicochemical properties (high-temperature stability, ability to transport oxygen ions, mixed ion-electron conductivity) are widely studied as catalysts for the CO, hydrocarbons and hydrocarbon's raw materials oxidation and as oxygen carriers for high-temperature cyclic processes of fuels combustion, gasification of coal and biomass, hydrogen generation, etc. [1-5]. An important advantage of calcium ferrite based catalysts over other oxidation catalysts is their high activity at low cost. However, systematic studies of the relationship between the composition, structural characteristics and activity of catalysts have practically not been carried out. In this paper, the influence of the composition of the $CaO-Fe_2O_3$ catalysts with varying $Fe_2O_3$ content in the range of 0-100 wt.% on the activity in the oxidative conversion of methane and in the cracking of atmospheric residues of heavy oils was studied.

The catalysts were obtained by solid state synthesis using $Fe_2O_3$ (h.p.) and CaO (p.) at 900 °C (10 h) and 1000 °C (4 h) in air, followed by cooling at a rate of ~8 °C/min, labeled by the content of $Fe_2O_3$ (wt.%) in the blend $CaO-Fe_2O_3$. The phase composition of the catalysts was determined by XRD. The catalytic tests in the oxidative conversion of methane were performed in a continuous-flow fixed-bed quartz tube reactor at 750 °C using $CH_4:O_2$:He = 82:9:9 (vol.%) feed, at $X_{O2}$=5-10%. The catalytic cracking tests of paraffinic (p=895.2 kg/m$^3$, content (wt.%): 25.50 resins, 0.37 asphaltenes, 15.71 solid paraffines) and asphaltenic (p=976.5 kg/m$^3$, content (wt.%): 37.0 resins, 8.5 asphaltenes) atmospheric residues of heavy crude oils were carried out in a batch reactor at 450 °C and a catalyst content of 10 wt.%.

The composition of the synthesized at 900 and 1000 °C catalysts corresponds to the phase diagram of the $CaO–Fe_2O_3$ system. The intervals 10-58.7, 58.7-74 and 74-95 wt.% of $Fe_2O_3$ correspond to the regions of the phase compositions $CaO–Ca_2Fe_2O_5$, $Ca_2Fe_2O_5–CaFe_2O_4$ and $CaFe_2O_4–\alpha$-$Fe_2O_3$ (Fig. 1a). The results of Fig. 1b show the extreme nature of the dependence of the products formation specific rate in methane conversion on the catalyst composition. The composite catalysts $CaO/Ca_2Fe_2O_5$ (35-55% $Fe_2O_3$) are the most active. An increase of the calcination temperature during the catalysts synthesis does not change the nature of the activity dependence, but leads to a decrease in it, at the points of maximum activity it is lower by more than 5 times. The patterns of changes in the specific activity of the most active catalysts suggest that the active centers are localized at the interface of the phases CaO and

$Ca_2Fe_2O_5$. The greater activity of calcined at 900 °C samples is due to the formation of a more disordered phase of ferrite $Ca_2Fe_2O_5$.

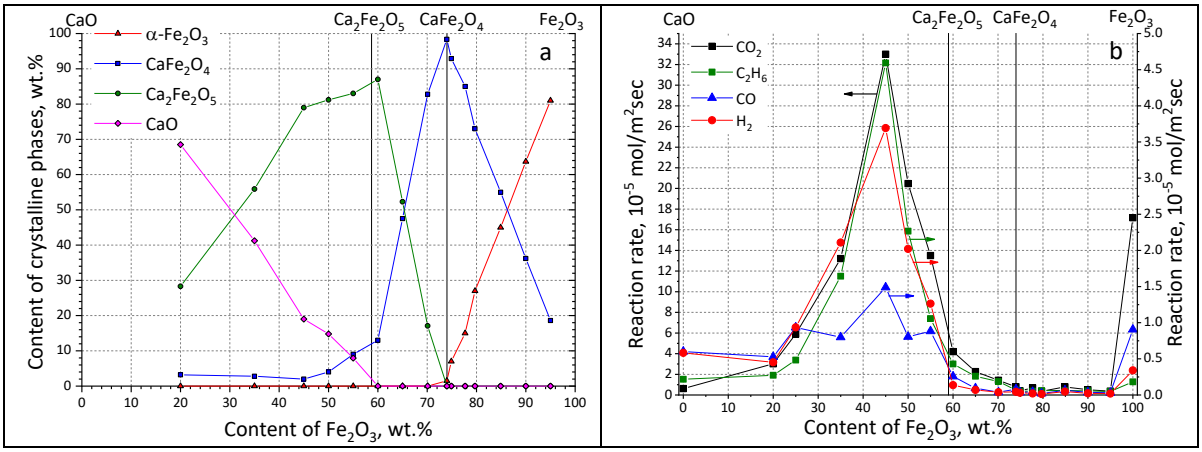


*Fig. 1. The effect of $Fe_2O_3$ content in the CaO–$Fe_2O_3$ system, $T_{cal.}$=900 °C, on the phase composition of catalysts (a), and on the specific rate of CO, $CO_2$, $C_2H_6$, $H_2$ formation in the methane conversion (b)*

The active composite catalyst of 35% $Fe_2O_3$ in methane conversion and single-phase catalyst of 57% $Fe_2O_3$ ($T_{cal.}$=1000 °C) were studied in the cracking of oil residues. The interaction of the residues components with the active oxygen of the catalysts leads to destructive transformations of high-molecular compounds. It was found, the light fractions (ibp - 360°C) yield is 57-73 wt.% in cracking products of paraffinic residue, and 49-65 wt.% in cracking products of asphaltenic residue, and is higher by 11-27 wt.% compared to known oxide catalysts - iron oxides and 30% CuO/$\alpha$-$Al_2O_3$ [6, 7]. It was also found that the percentage of gasoline fractions in light cracking products of paraffinic residue is higher in the presence of a catalyst of 35% $Fe_2O_3$ compared with a catalyst of 57% $Fe_2O_3$, the opposite relationship is observed in light cracking products of asphaltenic residue. Due to the large total yield of gaseous and solid products, 26-31 wt.%, the content of fractions $>$ 360 ° C in liquid cracking products is low.

Thus, it is shown that composite catalysts CaO/$Ca_2Fe_2O_5$ demonstrate high efficiency in oxidative conversion of $CH_4$ and in cracking of atmospheric residues of heavy oils. The active centers are assumed to be localized at the interface of the CaO and $Ca_2Fe_2O_5$ phases.

**Acknowledgement:** This work was conducted within the framework of the budget project FWES–2021–0013 for ICCT SB of the Russian Academy of Sciences.

**References:**

[1]. D. Hirabayashi, D. Hirabayashi**,** T. Yoshikawa**,** et al., Adv. Sci. Technol. 45 (2006) 2169.
[2]. L.A. Isupova, S.V. Tsybulya, G.N. Kryukova, et al., Kinet. Catal. 43 (1) (2002) 122.
[3]. Z. Sun, S. Chena, J. Hua, et al., Appl. Energ. 211 (2018) 431.
[4]. J. Riley, R. Siriwardane, H. Tian, et al., Appl. Energ. 201 (2017) 94.
[5]. M. Ismail, W. Liu, M.S. C. Chan, et al., Energy Fuels 30 (8) (2016) 6220.
[6]. A.G. Anshits, N.P. Kirik, T.G. Sozonova, O.M. Sharonova, RU Patent № 2 442 648 (2012).
[7]. A.K. Golovko, A.G. Anshits, M.A. Kopytov, et al., RU Patent № 2 426 765 (2011).

## OP-IC-09

# Porous Alloys Based on Fe and Co as Catalysts for the Decomposition of Hydrocarbons

Varygin A.D.[1], Popov A.A.[1], Plyusnin P.E.[1], Afonnikova S.D.[2], Maksimova T.A.[2], Shivtsov D.M.[2,3], Shubin Yu.V.[1]

*1 – Nikolaev Institute of Inorganic Chemistry, Novosibirsk, Russia*

*2 – Boreskov Institute of Catalysis, Novosibirsk, Russia*

*3 – Novosibirsk State Technical University, Novosibirsk, Russia*

*a.varygin@g.nsu.ru*

Among the variety of metal-based materials, porous alloys are of particular interest. This interest is due to their higher specific surface area than their bulk metal analogues due to their spongy morphology. Due to their properties, porous alloys are promising objects for heterogeneous catalysis.

Previously, the mechanism of the carbide cycle was described, according to which the iron triad metals (Fe, Co, Ni) are able to catalyze the decomposition of hydrocarbons through intermediate carbide compounds with the formation of carbon nanofibers (CNF) [1]. This catalytic process is a promising way to purify hydrogen-containing gas from hydrocarbon impurities and to utilize chlorine-containing hydrocarbons. It was shown that the use of porous nickel alloys as catalysts for these processes can be promising due to the fact that the developed surface of porous alloys is more easily susceptible to carbon erosion, i.e., the process of alloy self-dispersion with the formation of catalytically active particles [2]. In this case, an important role was played by the choice of an additive metal that provides a higher catalytic activity of the alloy compared to pure metals. It is noteworthy that, for such nickel systems, a maximum of catalytic activity was observed in the range of low contents of the additive metal (1–10 at.%).

Taking into account the results obtained earlier, an urgent task is to search for other alloy systems based on iron triad metals, to develop an approach to the synthesis of porous alloys in the region of low contents of additive metals, and to screen their catalytic activity in the decomposition reactions of various hydrocarbon substrates.

The report presents a technique for the synthesis of porous alloys $Fe_{1-x}M_x$ and $Co_{1-x}M_x$ by reductive thermolysis of specially prepared precursors. The following metals were used as additives: Co, Cu, Fe, Mo, Ni, Pd, Pt, Sn, W. The precursors were microheterogeneous mixtures obtained by co-precipitation of the initial metal compounds under nonequilibrium conditions. Ammonia and oxalate complex salts, nitrates and other compounds were used as initial metal compounds. Co-precipitation was carried out with an excess of chilled acetone (solvent replacement method) or an excess of an alkaline solution. The thermolysis temperature of the precursors was selected using thermal analysis.

The elemental and phase composition of the obtained alloys was determined by AES, AAS, and powder XRD methods. The composition of the phases, which are solid solutions, was

determined on the basis of X-ray data (XRD) on the basis of the calibration dependence of the specific atomic volume of the alloy on the content of the additive metal, built on the basis of literature data.

The dependence of the morphology of porous alloys and their specific surface area on the annealing temperature was studied by TEM, SEM, and low-temperature nitrogen adsorption using the BET method.

Screening of the catalytic activity of a large number of porous alloys with a metal additive content of about 4 at.% in the decomposition of ethylene, a mixture of C3-C4 hydrocarbons, a mixture of C2-C4 hydrocarbons with methane, 1,2-dichloroethane, and others was carried out. The experiments were carried out in a flow reactor with several samples in one experiment. Regularities common for various $Fe_{1-x}M_x$ and $Co_{1-x}M_x$ systems were determined, the results were also compared with the data obtained earlier on nickel alloys.

**Acknowledgement:** This work was supported by the Russian Science Foundation, grant 21-13-00414.

**References:**

[1] R.A. Buyanov, V.V. Chesnokov, Regularities of Catalytic Formation of Carbon Composites for Various Purposes via Decomposition of Hydrocarbons on Iron Subgroup Metals, Eurasian ChemTech J. v.2, 3-4 (2000) 223-230.

[2] A.V. Rudnev, A.S. Lysakova, P.E. Plyusnin, Yu.I. Bauman, Yu.V. Shubin, I.V. Mishakov, A.A. Vedyagin, R.A. Buyanov, Synthesis, Structure and Catalytic Activity in the Decomposition of Chlorine-containing Hydrocarbons, Inorganic Materials v.50, 6 (2014) 1-7.

## OP-IC-10

# Nanostructured Catalysts Based upon Porous Ceramometal Composites

Tikhov S.F., Valeev K.R., Sadykov V.A., Salanov A.N., Dokuchits E.V., Minyukova T.P.
*Boreskov Institute of Catalysis, Novosibirsk, Russia*
*tikhov@catalysis.ru*

Conventional oxide catalysts prepared by extrusion or tableting procedure are highly active as a fine fraction. But, they suffer from poor transport pores, low thermal conductivity and low density as a commercial granules. So, the activity per volume unit is not sufficient. Porous ceramometal catalysts with transition metals oxide active component can fill this gap. Ceramometals are synthesized from a powdered mixtures of $Me_1(+Me_2)$+Al alloyed in a high energy ball milling. Obtained fine powders are then subjected to hydrothermal treatment in special dies, which leads to cementation of the particles into strong monoliths. After heat treatment ceramometal monoliths represent metal particles surrounded by mixed oxide matrix [1]. To increase the activity, oxide powder components were incorporated into ceramometal skeleton. Due to the large number of metallic inclusions, ceramometals have increased thermal conductivity. The developed macroporous structure provides an increased catalytic activity compared to a conventional oxide catalyst. The main feature of cermet catalysts is a hierarchical pore structure with mesopores in the oxide matrix and a developed macropore structure (1-10 μm), which is absent in traditional coated oxide and monolithic honeycomb catalysts (Fig. 1).

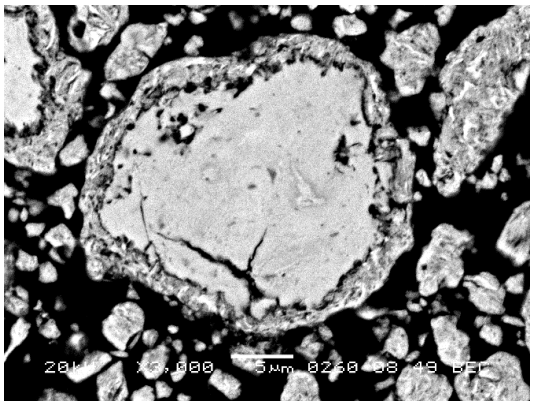

*Fig.1. Typical SEM image of polished section of the ceramometal catalyst [1].*

For the process of fuel combustion at moderate temperatures there was developed honeycomb catalysts $CuO/Al_2O_3$/FeAlO/FeAl of hexahedral and cylindrical (Fig. 2a, b) shape. Laboratory, pilot and stability test were carried out in methane, coal and octane combustion [1-4]. High activity, chemical and attrition stability to fluidized bed conditions have been demonstrated. Combustion with ceramometal catalysts becomes possible to use coal, wood pellets and other different wastes for heat generation.

For the process of low temperature water gas shift (LT-WGS) powdered mixtures of Cu (Fe)+Al were used to prepare porous ceramometal catalyst CuAlO/CuAl [5-8]. To increase thermal conductivity Cu foam was used as reinforcing agent (Fig. 2c) [9]. Obtained ceramometal catalysts were compared with conventional oxide CuZnAl catalyst [5-9]. Ceramometal CuAlO/CuAl catalyst was found to be twofold higher active than oxide one. Reinforcement by Cu foam leads to further increase of activity. So, the hydrogen output in WGS increases about three times. This is the result of higher density of ceramometals (3.5-4.0 g/cm$^3$) comparing to oxides (~2 g/cm$^3$); the developed macropore (0.1-10 μm) structure

which is almost absent in conventional oxide catalyst; more active surface active centers which compensate lower specific surface area of ceramometals. Macropores provide high permeability (permeability coefficient 0.3-1.6·$10^{-14}$ $m^2$). Thermal conductivity of ceramometals is relatively high (about 1.6-4.5 W/mK) while for oxides it is ≤0.5 $W \cdot m^{-1} \cdot K^{-1}$).

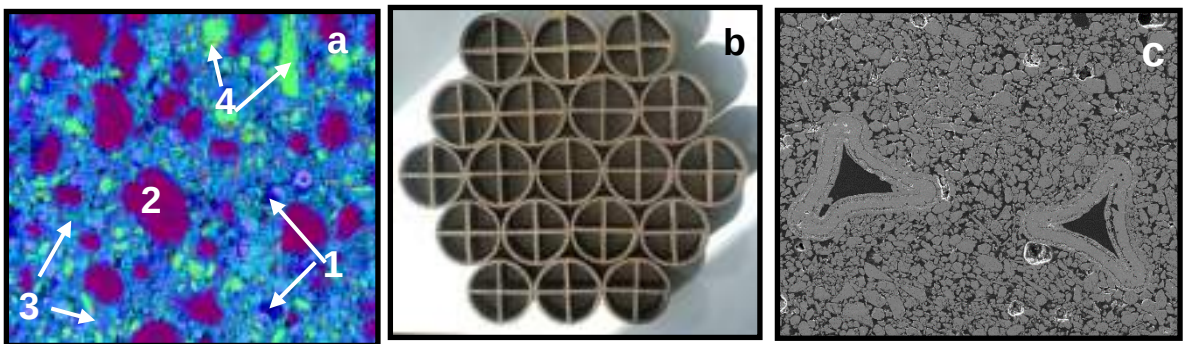


*Fig. 2. Microstructure **(a)**, total view **(b)** of honeycomb catalyst $CuO/Al_2O_3/FeAlO/FeAl$ and **(c)** microstructure of CuAlO/CuAl catalyst with foam. Designations: 1-macropores, 2- $CuO/Al_2O_3$, 3- FeAlO, 4- FeAl.*

For the FTS reaction, the $CoZrO/Al_2O_3/Al$ ceramometal catalyst in the form of a fine fraction showed higher selectivity to $C_{5+}$ and olefins as compared to the CoAl oxide catalyst while having lower to $CH_4$. At the same time, due to the excellent heat-conducting characteristics of the ceramometal catalyst, it was possible to avoid uncontrolled heating of the active layer of the catalyst, which ensured a stable reaction regime at all studied temperatures.

Ceramometal catalysts can be shaped as granules, honeycombs, platelets, thick coatings on metal surfaces. These new materials are very attractive as catalysts for the reactions with high thermal effects. High thermal conductivity allows maintaining an optimal temperature profile in the catalyst's bed. In addition, the control of pore structure is possible on the stage of their preparation. These two features are of great importance for the processes, selectivity of that depends on the pore structure and temperature.

**Acknowledgement:** This work was supported by the Ministry of Science and Higher Education of the Russian Federation within the governmental order for Boreskov Institute of Catalysis (project AAAA-A21-121011390054-1). Special thanks to O.Smorygo for the preparation of foam-based catalysts.

**References:**

[1] Tikhov S.F. et al. Kinet Catal 64 (2023) 94.
[2] Tikhov, S.F. et al. Catal. Sustain. Energy 1 (2012) 82.
[3] Tikhov S.F. et al. Combustion, Explosion, and Shock Waves, 52 (2016) 535.
[4] Parmon V.N. et al. Combustion, Explosion, and Shock Waves 51 (2015) 143.
[5] Tikhov, S.F. et al. RSC Adv. 7 (2017) 42443.
[6] Tikhov S.F et al. Mater Chem Phys 221 (2019) 349.
[7] Tikhov S.F. et al. Chem Eng J 374 (2019) 405.
[8] Tikhov S.F. et al. ACS Omega 5(2020)19928.
[9] S.Tikhov et al. Int J Hydrogen Energy 2023 (doi: 10.1016/j.ijhydene.2022.01.194).

## OP-IC-11

# Influence of BaO Addition on the Thermal Stability of Pd-Rh/$Al_2O_3$-$ZrO_2$ Three-Way Catalysts: Lab-Scale and Pilot-Scale Studies

Alikin E.A.[1], Baksheev E.O.[1,2], Rychkov V.N.[2], Veselov G.B.[3], Kenzhin R.M.[3], Stoyanovskii V.O.[3], Plyusnin P.E.[4], Shubin Yu.V.[4], Vedyagin A.A.[3]

*1 – Ecoalliance LLC, Novouralsk, Russia*

*2 – Ural Federal University, Yekaterinburg, Russia*

*3 – Boreskov Institute of Catalysis, Novosibirsk, Russia*

*4 – Nikolaev Institute of Inorganic Chemistry, Novosibirsk, Russia*

*alikin@eco-nu.ru*

Nowadays, the operation of vehicle internal combustion engines is one of the most common sources of atmosphere pollution. Automobile exhaust gases mainly contain three types of contaminants: carbon monoxide (CO), unburnt hydrocarbons (HC) and nitrogen oxides ($NO_x$). In order to purify the exhaust gases, so-called three-way catalysts (TWC) have been developed. A typical three-way catalytic converter consists of a honeycomb monolithic substrate with supported washcoat containing precious metals (PM). Among PM Pt, Pd, and Rh are usually used as a part of an active component.

Since TWCs should be capable of operating at elevated temperatures, the catalyst should be highly resistant to sintering and phase transformations. Aluminum oxide, one of the most common supports in TWCs, undergoes multiple phase transformation with an increase in temperature. Formation of corundum ($\alpha$-$Al_2O_3$) has the most dramatic effect on catalytic properties and is always accompanied by sintering. A number of additives such as $La_2O_3$ and $ZrO_2$ have been shown to inhibit the alumina phase transformations. Barium oxide is another dopant, which is known to increase thermal stability of alumina. Its interaction with the active PM components, in many cases, leads to a more efficient conversion of nitrogen oxides and hydrocarbons. The aim of the current work was to study the effects of BaO addition on the catalytic properties and thermal stability of the Pd-Rh bimetallic three-way catalysts. Specifically, the possibility of modification of the commercial zirconia-doped support ($Al_2O_3$+3%$ZrO_2$) was of great interest. Commercial nitrate solutions as well as complex salts such as $[Pd(NH_3)_4]_3[Rh(NO_2)_6]_2$ served as precursors for PM. Previous works have demonstrated the prospects of using double complex salts for the preparation of Pd-Rh alloyed particles [1].

The catalytic activity was studied at the lab-scale and pilot-scale levels. At the lab-scale level, the preparation was carried out by an incipient wetness impregnation of the support with the solution of precursors and $Ba(NO_3)_2$ with subsequent calcination. Monometallic Pd- and Rh-containing catalysts demonstrated increased activity in CO oxidation compared to previously reported catalysts without BaO [2]. Surprisingly, in the case of bimetallic catalysts, no such effect was observed. The addition of BaO facilitated the sintering of Pd within the temperature range of 800 – 1000 °C, thus leading to deactivation of the catalyst (Fig. 1). The state of the active components on the surface was monitored using the ethane hydrogenolysis test reaction and diffuse reflectance UV-vis spectroscopy.

At the next stage, the substrate-supported BaO-doped catalysts were prepared. The main characteristics like texture, phase composition, and catalytic activity, were assessed both before and after hydrothermal aging at 1100 °C. The values of specific surface area for the

BaO-doped samples after thermal aging at 1100 °C were higher if compared to the analogous samples without BaO. When $[Pd(NH_3)_4]_3[Rh(NO_2)_6]_2$ was used as a precursor, the most noticeable sintering of the support accompanied by the formation of $\alpha$-$Al_2O_3$ has occurred. However, the addition of BaO inhibited this effect. On the pilot-scale level, the BaO-doped samples demonstrated slightly better performance in terms of the values of $T_{50}$ (temperature of 50% conversion of CO, HC, and $NO_x$) and operation window width (Table 1).

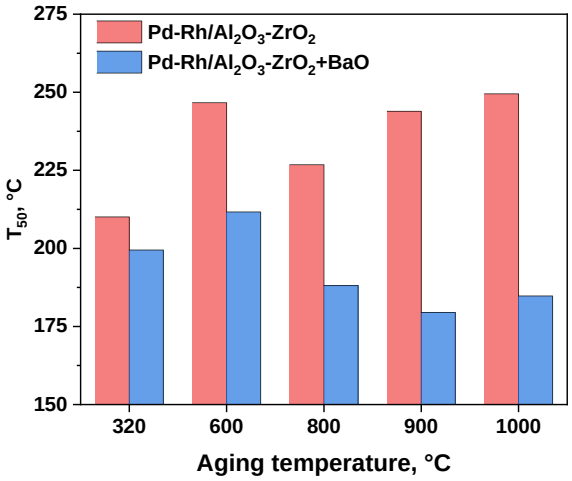


*Fig. 1. Temperatures of 50% conversion of CO in the powder testing (lab-scale level) of the samples under prompt thermal aging conditions. The reactive mixture contained CO, hydrocarbons, NO and an excess of oxygen. The samples were prepared using complex salts.*

In summary, this work demonstrated that the addition BaO affects as positively as negatively the properties of the three-way catalysts containing Pd and Rh. The results obtained allowed us to conclude that the interaction of BaO with alumina changes the metal-support interactions of the latter with rhodium and palladium species.

*Table 1. Catalytic properties of the Pd-Rh samples supported on a substrate (pilot-scale level).*

| Sample | $T_{50}$, °C | | | Conversion at 400 °C, % | | | Operation window width |
|---|---|---|---|---|---|---|---|
| | THC | CO | $NO_x$ | THC | CO | $NO_x$ | |
| **As-prepared** | | | | | | | |
| $Pd-Rh/Al_2O_3-ZrO_2$ | 265 | 242 | 234 | 98 | 97 | 100 | 16.1 |
| $Pd-Rh/Al_2O_3-ZrO_2$+BaO | 259 | 240 | 233 | 98 | 97 | 99 | 20.0 |
| **After hydrothermal aging (1100 °C)** | | | | | | | |
| $Pd-Rh/Al_2O_3-ZrO_2$ | 339 | 321 | 288 | 92 | 93 | 99 | 6.1 |
| $Pd-Rh/Al_2O_3-ZrO_2$+BaO | 333 | 316 | 294 | 92 | 95 | 98 | 7.7 |

**Acknowledgement:** This study was supported by the Ministry of Science and Higher Education of the Russian Federation within the governmental order for Boreskov Institute of Catalysis (project No. AAAA-A21-121011390054-1). Characterization of the samples was performed using the equipment of the Center of Collective Use “National Center of Catalysts Research”.

**References:**

[1] A.A. Vedyagin et al., Top. Catal. 62 (2019) 305-314.
[2] A.A. Vedyagin et al., Emiss. Control Sci. and Technol. 5 (2019) 363-377.

## OP-IC-12

# Acid Impregnation of Raw Kaolin for Synthesis of Automotive Exhaust Catalyst

Ouarab N.[1], Redjdal N.[1], Bouachma S.[1], Sekrane N[2]., Manseri A.[3], Toumert I.[4], Drici N.[3], Benabderazak K.[3], Cheraga H.[3], Menari H.[3]

*1 – Division of Emerging Semiconductor Technologies for Energy (TESE), Semiconductor Technology Research Center for Energetic-(CRTSE), Algiers, Algeria*

*2 – Department of NanoPhysics, Faculty of Science, University of Blida-1, Blida, Algeria*

*3 – Semiconductor Technology Research Center for Energetic-(CRTSE), Algiers, Algeria*

*4 – Division of Nuclear Techniques (DTN), Nuclear Research Centre of Algiers, (CRNA), BP N° 399 Algiers, Algeria*

*n_ouarab@crtse.dz /Ouarab_nourdine@yahoo.fr/o.nouredine@gmail.com*

$CO_{x=1,2}$, $NO_{x=1,2}$, $CH_4$ and $SO_2$ gases are released during the industrial activities, especially the transport sector; they represent serious risks to the environment and public health. Therefore, the development of processes for the reduction of greenhouse gases has become a major concern [1]. Among the different used techniques, the application of catalysts based on ceramic structures of phyllosilicates in honeycomb form has been considered [2]. For such a use, the Algerian kaolin is transformed and enriched, successfully, in white aluminosilicate by a method of acid impregnation of alumina [3] in a specific reactor with mixing and degassing systems. The resulting kaolin is white in color, indicating a stoichiometric equilibrium between alumina (45.983%) and silica (49.609%) after activation, as revealed by WDXRF analysis. The X-ray diffraction spectra of our samples calcined at 800°C exhibit only peaks mainly associated with quartz ($Si_2O_4$) and Meta-kaolinite $Al_2Si_2O_5$-$(OH)_4$ agreeing with reference [4], while the samples undergoing impregnation and calcination treatment at 950°C show more peaks of good quality crystallized kaolinite and other peaks associated with γ-$Al_2O_3$ alumina. However, the implantation iron pyrite nanocrystals embedded in ZrNiSn material on these kaolin substrates reveals surprising physicochemical properties, as to the sulfidation process at different temperature is applied, they acquire other preponderant catalytic and methanation properties in order of activity. The combination of modified kaolin with passivized iron disulfide nanostructures opened a new promising technological way for its use as a catalytic support for the conversion of exhaust gases into fuel [5].

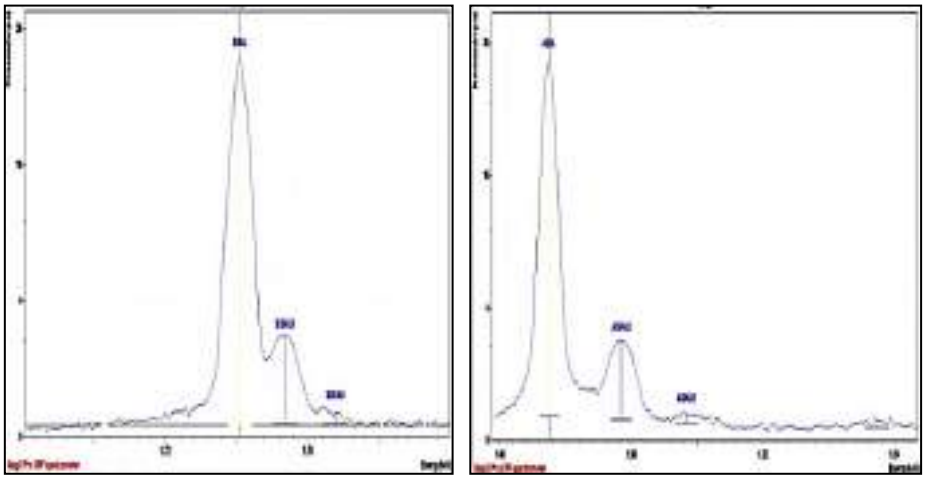

*Figure.1: XRF spectrophotometer spectra of equilibrium between Silicate and alumina amounts in synthesized kaolinite.*

Table.2: Results of chemical analysis by XRD technique revealed the presence of quartz and Mullite phase.

| Ref. Code | Score | Compound Name | Scale Factor | Chemical Formula |
|---|---|---|---|---|
| 00-015-0776 | 70 | Mullite, syn | 0,460 | $Al_6 Si_2 O_{13}$ |
| 01-085-0457 | 65 | Silicon oxide - $-alpha | 1,003 | $Si O_2$ |

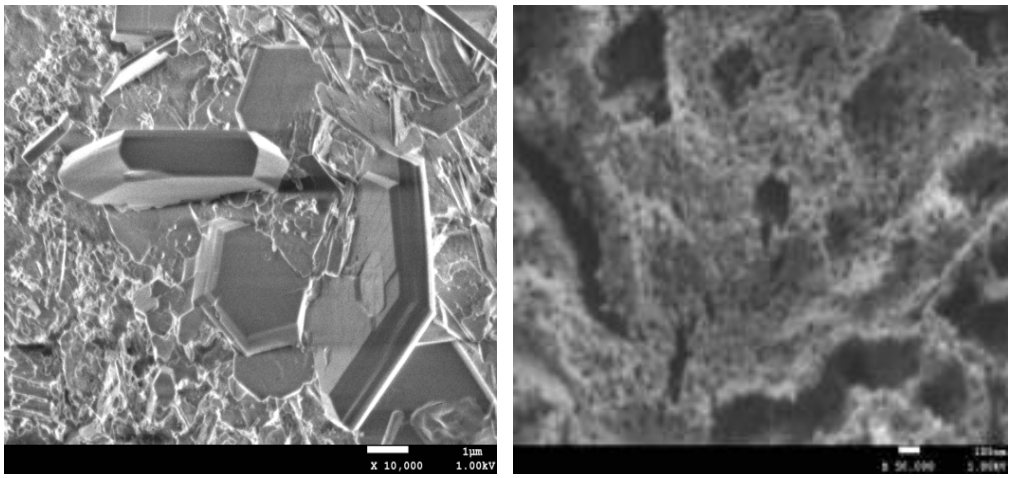


*Figure.2 : SEM micrograph of pyrite nanocrystals implanted in treated kaolinite substrate with mixed matrix catalysts (MMM) based on transition metal disulfide crystals*

**Acknowledgement:** This work was financially supported by the National Research Fund DGRSDT/MESRS (Algeria).

**References:**

[1] H. D. Tan, C. Bing-Hung, L. Duu- Jong, (Bioresource Technology, Netherland, 2013), pp.175– 181.
[2] M.E. Borges and L. Diaz, *A Review* (Renewable and Sustainable Energy Review, 2012) pp. 2839 – 2849.
[3] Y.C. L. Dennis, Xuan Wu, M.K.H. Leung, (Applied Energy, United Kingdom, 2009), pp. 1083–109.
[4] O.S.L. Junior, R.M. Cavalcanti, and T.M. Matos, (Fuel, Netherland, 2013), pp. 604 – 611.
[5] W. Widayat, Ndaru Okvitarini, *and* John Philia, AIP Conf. Proc. 2197, (2020) 030009-1–030009-5.

## OP-II-01

# Development and Research of Composite Corrosion-Resistant and Bioactive Coatings with ZrO2 Particles

Kashin A.D., Sedelnikova M.B.
*Institute of Strength Physics and Materials Science SB RAS, Tomsk, Russia*
*kash@ispms.ru*

Surface treatment of Mg orthopaedic implants is a promising way to make up for their shortcomings, such as their predisposition to corrosion and the tendency to emit large amounts of hydrogen at the site of implantation [1]. We propose modifying the surface of an Mg implant by applying the coating via the method of micro-arc oxidation (also known as plasma electrolytic oxidation) at four different process voltages ranging from 350 to 500 V. Such a coating vastly improves the corrosion resistance, as well as mechanical properties (e.g. adhesion strength, microhardness, etc.) of magnesium implants [2]. Moreover, we can improve physical and mechanical characteristics of these coatings by adding the particles of various refractory oxides to the electrolyte composition. In this work, we have opted for the microparticles of zirconia ($ZrO_2$) due to their excellent mechanical strength and resistance against corrosive media [3]. The resulting coatings were investigated by various research methods. Figure 1 shows the SEM micrograph of the surface morphology of the coating doped with $ZrO_2$ microparticles. We can see that the coating surface has a porous structure with the inclusions of unmelted zirconia particles.

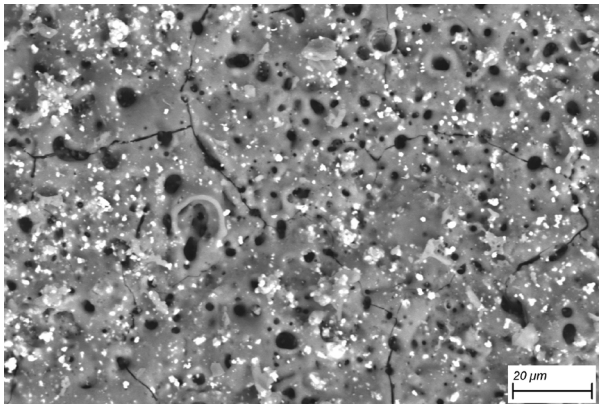


*Fig. 1. SEM image of the coating with $ZrO_2$ particles deposited at the MAO process voltage of 450 V*

It was found via the method of potentiodynamic polarization that the inclusion of $ZrO_2$ improved the corrosion resistance of coated samples by 2 orders of magnitude. The method of scratch-testing has revealed that the adhesive strength of the coatings increased by ≈30%.

**Acknowledgement:** The research was funded by the Russian Science Foundation, grant No. 23-29-00141, https://rscf.ru/en/project/23-29-00141/.

**References:**

[1] Amukarimi, S., Mozafari, M. *MedComm*. 2021; 2: 123– 144.
[2] Li, H., Wen, J., Jin, J., Liu, Y., He, J. *Mater. Corros*. 2022; 73: 414– 426.
[3] Molaei, M., Nouri, M., Babaei, K., Fattah-Alhosseini, A. *Surf. Interfaces*. 2021; 22: 100888.

## OP-II-02

# Novel Electrochemical Studies of the Bioresorbable Magnesium Alloys: Corrosion Phenomena and Hybrid Coating Formation

Gnedenkov A.S., Sinebryukhov S.L., Filonina V.S., Gnedenkov S.V.
*Institute of Chemistry FEB RAS, Vladivostok, Russia*
*asgnedenkov@mail.ru*

A comparative analysis of the corrosion activity of bioresorbable MA8 magnesium alloy (Mg-Mn-Ce system) and Mg-0.8Ca alloy in physiological media (mammalian cell culture medium - MEM and aqueous NaCl solution) was carried out. The influence of the composition, microstructure, and heterogeneity of the biodegradable Mg alloy on its corrosion characteristics at the micro- and mesolevels has been established using local electrochemical methods, gravimetric analysis of the corrosion rate, traditional electrochemical tests, and analysis of the chemical composition of the material surface. Calcium phosphate compounds are the main products formed on the surface of magnesium alloy exposed to MEM. A model of the magnesium alloy corrosion mechanism in MEM is proposed, which includes three stages of surface film development. A diagram was constructed that makes it possible to determine the reactions occurring on the surface of a magnesium alloy in MEM and the thermodynamic probability of the formation of chemical compounds based on local pH values [1–3].

Features of the corrosion process at the microlevel on samples of the Mg alloy with a natural oxide/hydroxide film and with a protective coating formed by plasma electrolytic oxidation (PEO) were established. The mechanism of biodegradation of alloys with hydroxyapatite-containing PEO-coating in the MEM medium was determined. The formation of hydroxyapatite-containing products in the pores and on the surface of the PEO-coating was revealed as a result of ionic synergistic interaction between the magnesium alloy substrate, the protective layer, and the components of the MEM. The modification of the PEO-layer was performed by electrophoretic treatment of the PEO layer using a biopolymer. Composite protective layers limit the access of an aggressive environment to the material, increasing the protective anticorrosion properties of coatings, on the one hand, and, due to their unique composition will accelerate the growth of bone tissue, on the other hand [4–6].

A new method was developed for creating active corrosion protection of magnesium alloys, which prevents the material substrate against degradation even in the case of mechanical damage or degradation of the composite layer in an aggressive environment. Methods for impregnating the porous part of the surface layer of a PEO-coating with nontoxic corrosion inhibitor and following sealing pores with polymeric materials were proposed. The impregnation of the PEO-layer with inhibitor results in the formation of an antibacterial coating on the Mg alloy, which increases the potential for using this material in orthopedics by reducing the frequency infections associated with implants. The obtained results make it possible to consider such formed materials as promising for implant surgery [5,6].

**Acknowledgement:** This work was supported by the Russian Science Foundation, grant 21-73-10148.

**References:**

[1] A.S. Gnedenkov, S.V. Lamaka, S.L. Sinebryukhov, D.V. Mashtalyar, V.S. Egorkin, I.M. Imshinetskiy, A.G. Zavidnaya, M.L. Zheludkevich, S.V. Gnedenkov, Corros. Sci. 168 (2020) 108552.
[2] A.S. Gnedenkov, S.L. Sinebryukhov, V.S. Filonina, V.S. Egorkin, A.Yu. Ustinov, V.I. Sergienko, S.V. Gnedenkov, J. of Magnes. Alloy. 10 (2022) 1326.
[3] A.S. Gnedenkov, D. Mei, S.V. Lamaka, S.L. Sinebryukhov, D.V. Mashtalyar, I.E. Vyaliy, M.L. Zheludkevich, S.V. Gnedenkov, Corros. Sci. 170 (2020) 108689.
[4] A.S. Gnedenkov, S.V. Lamaka, S.L. Sinebryukhov, D.V. Mashtalyar, V.S. Egorkin, I.M. Imshinetskiy, M.L. Zheludkevich, S.V. Gnedenkov, Corros. Sci. 182 (2021) 109254.
[5] A.S. Gnedenkov, S.L. Sinebryukhov, V.S. Filonina, N.G. Plekhova, S.V. Gnedenkov, J. of Magnes. Alloy. 10 (2022) 3589.
[6] A.S. Gnedenkov, S.L. Sinebryukhov, V.S. Filonina, S.V. Gnedenkov, J. of Magnes. Alloy. 2022. In Press.

## OP-II-03

# Development of Biomimetic Organic-Inorganic Coatings for Titanium Implants

Parfenova L.V.[1], Parfenov E.V.[2]

*1 – Institute of Petrochemistry and Catalysis, Ufa Federal Research Center, Russian Academy of Sciences, Ufa, Russia*

*2 – Ufa University of Science and Technology, Ufa, Russia*

*luda_parfenova@ipc-ras.ru*

Modern traumatology and orthopedics require the development of new biocompatible materials, including metal implants, among which titanium devices are the most in demand. To ensure the biocompatibility of implants, methods that change the architecture and composition of the surface layer in order to impart the properties of bone tissue and cell membranes, the so-called biomimetic approach, are widely acquired. Such modeling of surface properties is achieved both by physicochemical methods of coating formation, which approximate the phase composition and three-dimensional structure of the surface layer to the mineral components and morphology of human bone, and by applying an organic matrix containing fragments with various biological functions.

We have developed an approach [1-5], which implies a combination of an inorganic porous oxide sublayer obtained by plasma electrolytic oxidation (PEO) of a metal surface, and biologically active molecules with bisphosphonate anchors affording reliable fixation of the organic layer on a highly developed surface (Fig. 1). The PEO method is an extension of the anodization process to the region of high (up to 600 V) voltages, at which microdischarges remelt the surface and provide a porous oxide layer containing rutile and anatase phases [6]. The morphology of the PEO coating ensures a gradual change in the elastic modulus from the metal implant to the bone, which also increases biomechanical compatibility due to the biomimetic (at the physicochemical level) surface.

High biocompatibility can be achieved through the use of organic materials that must have a high affinity to the metal surface, be non-toxic, prevent the non-specific adsorption of proteins, and also contain various ligands that improve cell adhesion, proliferation and differentiation, exhibit anti-inflammatory and antimicrobial properties. In order to create coatings with such properties, we synthesized a set of amino acid bisphosphonates containing various linkers (BMPS, EMSC, SMCC) modified with integrin-active linear and cyclic RGD peptide [1-3, 5]. The compounds were introduced into the PEO coating on coarse-grained and nanostructured titanium by physicochemical adsorption from solutions. The presence of organic molecules in the coating was confirmed by XPS spectroscopy. *In vitro* studies on models of fibroblasts, mesenchymal stem cells and osteoblast-like cells MG-63 showed the ability of the developed coatings to increase the proliferation and viability of cells on the metal surface. Further, on the basis of a biocompatible polymer matrix, hyaluronic acid, new bisphosphonate derivatives were synthesized [4], which showed the promise of using the

conjugates as coatings that provide antifouling properties of the surface and reduce the adhesion of bacterial cells (*P. aeruginosa*, *S. aureus*, *E. faecium*).

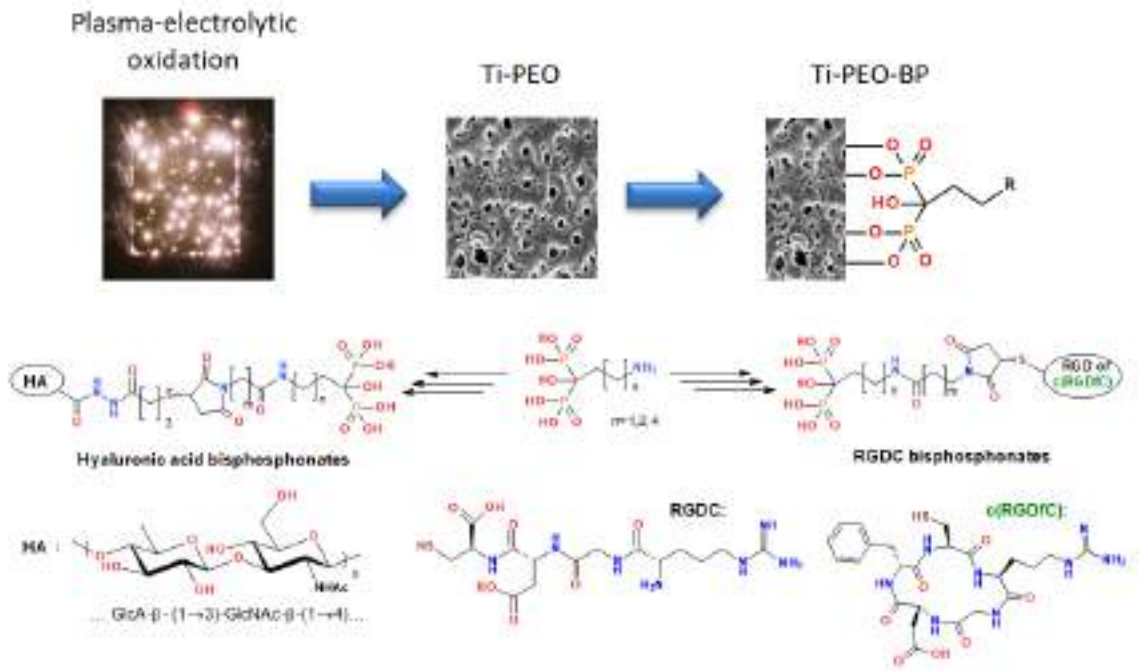


*Fig. 1. Hybrid PEO-bisphosphonate coatings for titanium implants*

**Acknowledgement:** The studies were carried out in accordance with the Federal Program of Ministry of Science and Higher Education of Russian Federation No. FMRS-2022-0081.

**References:**

[1] E.V. Parfenov, L.V. Parfenova, G.S. Dyakonov, K.V. Danilko, V.R. Mukaeva, R.G. Farrakhov, E.S. Lukina, R.Z. Valiev, Surface and Coatings Technology, 357 (2019) 669.
[2] L.V. Parfenova, E.S. Lukina, Z.R. Galimshina, G.U. Gil'fanova, V.R. Mukaeva, R.G. Farrakhov, K.V. Danilko, G.S. Dyakonov, E.V. Parfenov, Molecules, 25(1) (2020), 229.
[3] E.V. Parfenov, L.V. Parfenova, V.R. Mukaeva, R.G. Farrakhov, A. Stotskiy, A. Raab, K.V. Danilko, R. Nagumothu, R.Z. Valiev, Surface and Coatings Technology, 404 (2020) 126486.
[4] L.V. Parfenova, Z.R. Galimshina, G.U. Gil'fanova, E.I. Alibaeva, K.V. Danilko, T.M. Pashkova, O.L. Kartashova, R.G. Farrakhov, V.R. Mukaeva, E.V. Parfenov, R. Nagumothu, R.Z. Valiev, Surfaces and Interfaces, 28 (2022) 101678.
[5] L.V. Parfenova, Z.R. Galimshina, G.U. Gil'fanova, E.I. Alibaeva, K.V. Danilko, V.R. Aubakirova, R.G. Farrakhov, E.V. Parfenov, R.Z. Valiev, Materials, 15 (2022) P. 8120.
[6] Parfenov, E.V., A. Yerokhin, R.R. Nevyantseva, M.V. Gorbatkov, C.J. Liang, and A. Matthews, Surface and Coatings Technology, 269 (2015) 2.

## OP-II-04

# Vancomycin-Loaded Porous Calcium Phosphate Coatings with PLGA Fabricated by Ultrasound-Assisted Micro-Arc Oxidation and Dip-Coating for Drug Delivery

Prosolov K.A.[1], Komarova E.G.[1], Kazantseva E.A.[1,2], Lozhkomoev A.S.[1], Kazantsev S.O.[1], Senkina E.I.[1]

*1 – Institute of Strength Physics and Materials Science, Siberian Branch of Russian Academy of Sciences, Tomsk, Russia*

*2 – National Research Tomsk State University, Tomsk, Russia*

*konstprosolov@gmail.com*

This study investigates the fabrication, structural and mechanical properties, bioactivity, and drug release kinetics of porous calcium phosphate (CaP) coatings on commercially pure titanium, modified with a biodegradable polymer, poly(lactic-co-glycolic acid) (PLGA), for sustained drug delivery. The coatings were deposited using a hybrid ultrasound-assisted micro-arc oxidation (UMAOH) method [1], followed by dip-coating in PLGA (50:50) solution for further modification. The release kinetics of vancomycin (VMN), a widely used antibiotic, from unmodified and PLGA-modified CaP coatings were evaluated in isotonic solution.

The UMAOH method is an innovative approach that combines ultrasonic treatment with micro-arc oxidation to produce porous CaP coatings on titanium substrates. This technique results in the formation of a more uniform porous layer with improved adhesion. The ultrasound treatment contributes to the formation of a homogeneous electrolyte, leading to a more uniform distribution of the coating on the surface of the titanium substrate. The structural parameters of such coating are Ra roughness equal to 3.0–4.0 μm, thickness in the range of 50–55 μm, and a combination of high values of internal and surface porosity, which are equal to 39 and 28%, respectively [2,3]. Moreover, the use of UMAOH result in monetite and β-calcium pyrophosphate phases formation alongside with an amorphous CaP matrix.

The unmodified CaP coatings exhibited a rapid release of VMN, with nearly complete release after 6 hours and a burst release of 75% within the first 10 minutes. In contrast, the PLGA/CaP composite coatings, prepared by dip-coating and impregnated with VMN, demonstrated a steady logarithmic release of the drug over a 7-day period. This controlled release significantly enhanced the therapeutic effect of VMN, ensuring a prolonged antibacterial activity while minimizing potential side effects related to burst release.

The dip-coating process was crucial in extending the VMN release duration, providing an effective and tunable drug delivery system with improved antimicrobial performance. Both unmodified and PLGA-modified CaP coatings displayed strong antimicrobial activity against pathogenic bacteria: methicillin-resistant Staphylococcus aureus (MRSA). Additionally, in vitro cell viability tests confirmed the high biocompatibility of the developed drug delivery system, suggesting its potential for biomedical applications such as antimicrobial coatings and targeted drug delivery in orthopedic and dental implants. The structure and morphology as

well as direct observation of cell spreading across the modified and unmodified by PLGA CaP coatings are described in detail.

In conclusion, this study presents a novel approach to fabricate porous CaP coatings with controlled drug release kinetics by utilizing the hybrid UMAOH method, dip-coating in PLGA, and impregnation with therapeutic agents, such as VMN. The findings demonstrate that the PLGA/CaP drug delivery systems possess promising antimicrobial properties and biocompatibility, warranting further investigation and potential clinical application in various medical fields.

**Acknowledgement:** This research was funded by Russian Science Foundation, grant number 21-7310265.

**References:**

[1] Kazantseva E. A., Komarova E. G., AIP Conf Proc, 020141 (2020), 1-4. [2] Kazantseva E. A., Komarova E. G., J. Phys. Conf.2064 (2021), 012057.
[3] Prosolov K.A., Komarova E.G.; Kazantseva E.A. et al., Materials 15.13 (2022), 4643.

## OP-II-05

# Functionalized Mesoporous Silicas Nanocarrier for Anticancer Chemotherapy

Park S.S.[1], Kong J.[2], Ha C.-S.[2]
*1 – Division of Advanced Materials Engineering, Dong-Eui University, Busan 47340, Republic of Korea*
*2 – Department of Polymer Science and Engineering, Pusan National University, Busan 46241, Republic of Korea*
*pss@deu.ac.kr*

Mesoporous materials are a sort of promising materials with a wide spectrum of applications due to their unique well-defined porous structures that provide high surface area and controllable pore size. Preparation of the organic moiety functionalized mesoporous silicas became a major topic of recent research because it offered a further possibility to tailor the physical and chemical properties of the porous materials. One important way of modifying the physical and chemical properties of mesoporous silicates has been the incorporation of organic components, either on the silicate surface, as part of the silicate walls, or trapped within the channels. The potential use of functionalized mesoporous silicas as efficient drug delivery vehicles is another exciting research field [1-6].

In this work, we studied the controlled release of anticancer drugs controlled by mesoporous silica nanoparticles as nanocarriers. First, we synthesized polyacrylic acid-functionalized MCM-41, which was made to interact with calcium ions, in order to realize enhanced pH-responsive nanocarriers for sustained drug release [7]. MCM-41 was prepared by the sol-gel method. Afterward, a (3-trimethoxysilyl)propyl methacrylate (TMSPM) modified surface was prepared by using the post-grafting method, and then the polymerization of the acrylic acid was performed. After adding a calcium chloride solution, polyacrylic acid-functionalized MSNs with calcium-carboxyl ionic bonds in the polymeric layer, which can prevent the cargo from leaking out of the mesopore, were prepared. The structure and morphology of the modified nanoparticles (PAA-MSNs) were characterized by X-ray diffraction (XRD), Fourier-transform infrared (FT-IR) spectroscopy, transmission electron microscopy (TEM), and $N_2$ adsorption–desorption analysis, etc. The controlled release of guest molecules was studied by using 5-fluorouracil (5-FU). The drug molecule-incorporated nanoparticles showed different releasing rates under different pH conditions. Second, we synthesized alkylammonium-functionalized hollow mesoporous silica (HMS) nanoparticles with sphere morphology by using a surfactant mixture composed of zwitterionic (N-dodecyl-N,N-dimethyl-3-ammonio-1-propane sulfonate, DDAPS) and anionic sodium dodecyl sulfate (SDS) surfactants as structure-directing agents, TEOS and alkylammonium alkoxysilane (TMAPS) as silica sources. The HMS have the particle size of ca. 450 nm with the shell thickness of ca. 60 nm. We studied on the controlled releasing of anticancer drug (fludarabine) using the alkylammonium-functionalized HMS nanoparticles as a support of drug molecules. The drug-loaded HMS nanoparticles showed the cancer cell (MCF-7) viability of 2.5 % after

treatment for 96 h. It is considered that our current materials have the potential as pH-responsive nanocarriers in the field of medical treatment.

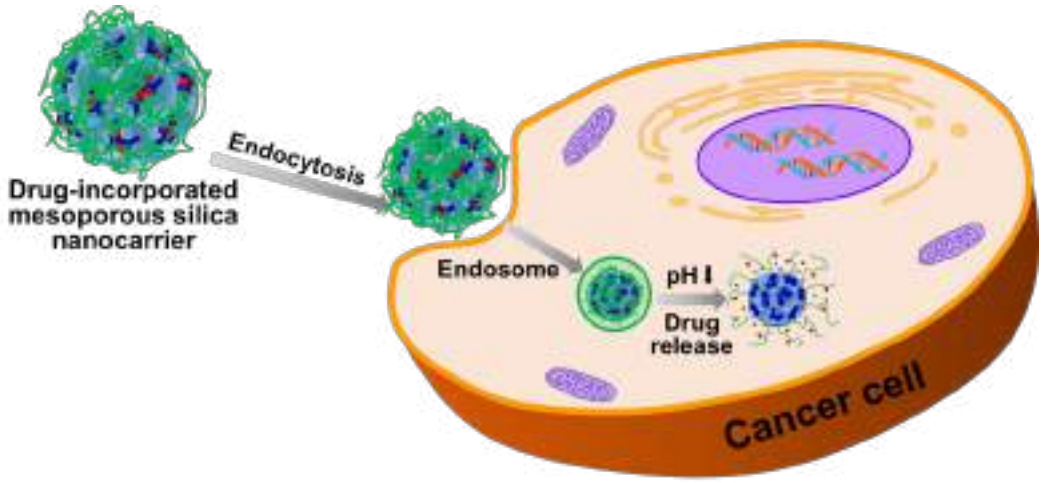


*Fig. 1. Schematic diagram on the release behavior of drug molecules of drug-loaded and functionalized mesoporous silica in the cancer cell.*

**Acknowledgement:** The work was supported by the National Research Foundation of Korea (NRF) Grant funded by the Ministry of Science and ICT, Korea (2021R1I1A3060098, NRF-2021R1I1A3059777 and Brain Korea 21 Plus Program (4199990414196)) and by the Korea Institute for Advancement of Technology funded by the Ministry of Trade, Industry and Energy (P0017531).

**References:**

[1] R. Vathyam, E. Wondimu, S. Das, C. Zhang, S. Hayes, Z.M. Tao, T. Asefa, J. Phys. Chem. C 115 (2011) 13135.
[2] H.-Y. Wu, F.-K. Shieh, H.-M. Kao, Y.-W. Chen, J.R. Deka, S.-H. Liao, C.-W. Wu, Chem. Eur. J. 19 (1985) 6358.
[3] Z. Zhou, M. Hartmann, Chem. Soc. Rev. 42 (2013) 3894.
[4] S.S. Park, M.S. Moorthy, C.-S. Ha, NPG Asia Mater. 6 (2014) e96).
[5] S.S. Park, C.-S. Ha, Adv. Func. Mater. 28 (2018) 1703814.
[6] C.-S. Ha, S. S. Park, Periodic Mesoporous Organosilicas: Preparation, Properties and Applications. Springer Series in Materials Science 281, Springer Nature Singapore Pte Ltd. 2019.
[7] J. Kong, S.S. Park, C.-S. Ha, Materials 15 (2022) 5926.

## OP-II-06

# Cellulose Complex of Arctic Brown Algae as a Basis for the Production of New Materials

Parshina A.E.[1], Bogolitsyn K.G.[1,2], Polomarchuk D.A.[1], Prosankov D.S.[1]
*1 – Northern (Arctic) Federal University, Arkhangelsk, Russia*
*2 – Institute of Ecological Problems of the North, Arkhangelsk, Russia*
*a.parshina@narfu.ru*

Marine brown algae are a valuable source of various types of carbohydrates, such as alginates, fucoidans, and mannitol. At the same time, algal cellulose (AC) is a less studied carbohydrate among the others. AC has a unique set of physical and chemical characteristics that distinguish it from wood celluloses. Additionally, algae are a rapidly reproducible plant source of this natural polymer, and it has great prospects for practical use in obtaining various cellulose materials.

The aim of the study is a comprehensive characterization of the physicochemical properties of the cellulose complex of the Arctic brown algae *Laminaria digitata* and *Saccharina latissima*, and assessment of the possible practical applications. Algae samples were collected in the White Sea. They were ground and subjected to extraction according to the scheme developed by the authors (Fig. 1) [1].

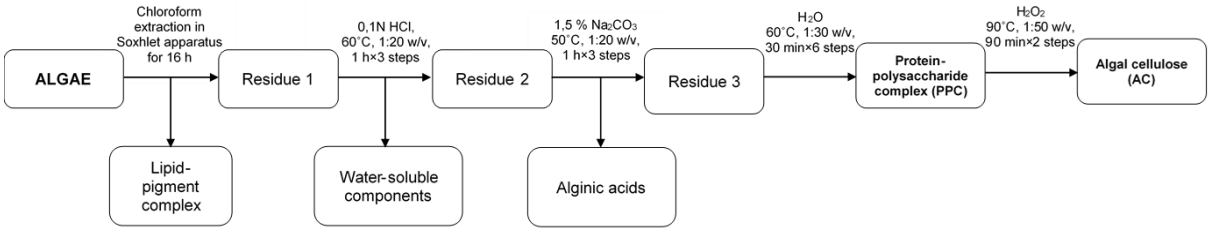


*Fig. 1. Scheme of algal cellulose obtaining*

Freeze-dried samples (Fig. 2) were subjected to further analysis.

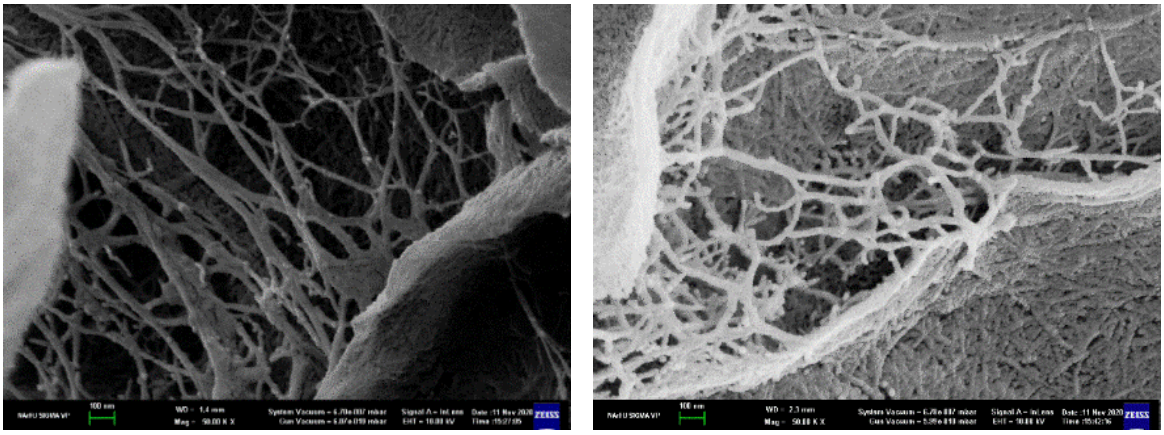

*Fig. 1. SEM images of the cellulose surface L. digitata (left), S. latissima (right)*

Algal cellulose has low degree of polymerization, and crystal structure of the triclinic phase Iα (Table 1). Thus, this polymer is almost entirely made up of reactive cellulose. Up to 54% of AC is accounted for by the amorphous phase. Therefore, it can be assumed that algal

cellulose has developed surface-active properties, including sorption ones. The mesoporous nature of the surface favors volumetric sorption interaction.

*Table 1. Physico-chemical properties of algal cellulose*

| Characteristics | AC *L. digitata* | AC *S. latissima* |
|---|---|---|
| Degree of polymerization, un | 470 | 555 |
| Cellulose Iα, % | 99.6 | 99.3 |
| Degree of crystallinity, % | 61 | 56 |
| Average pore diameter, nm | 11.05 | 9.09 |
| Surface area, $m^2/g$ | 8.48 | 9.72 |
| $pH_{pzc}$ | 4.4 | 4.6 |
| Degree of oxidation, % | 12.3 | 14.3 |

The algae celluloses were further subjected to dissolution in the dimethylacetamide-lithium chloride system (cellulose concentration up to 10%). The resulting cellulose solutions can be used to obtain various materials in the form of films, hydrogels, and fibers [2]. Biodegradability of algal cellulose, biocompatibility and non-toxicity suggests the possibility of using these materials in the biomedical industry as a main component, for example, in production of wound dressings.

**Acknowledgement:** This work was supported by the Ministry of Science and Higher Education State Assignment, project No. FSRU-2023-004.

**References:**

[1] K. Bogolitsyn, A. Parshina, N. Shkaeva, L. Aleshina, A. Prusskii, O. Sidorova, N. Bogdanovich, M. Arkhilin, Russ. J. Phys. Chem. B 15, 8 (2021).
[2] N. Wahlström, U. Edlund, H. Pavia, G. Toth, A. Jaworski, A.J. Pell, F.X. Choong, H. Shirani, K.P.R. Nilsson, A. Richter-Dahlfors, Cellulose from the green macroalgae Ulva lactuca: isolation, characterization, optotracing, and production of cellulose nanofibrils, Cellulose 27, 7 (2020).

## OP-II-07

# Investigation of the RF Magnetron Sputter Deposited Mg- and Sr-Substituted HA Coatings on a Titanium-Niobium Alloy Produced by Additive Manufacturing

Kozadaeva M.[1], Grubova I.Y.[1], Koptyug A.[2], Surmeneva M.A.[1], Surmenev R.A.[1]
*1 – National Research Tomsk Polytechnic University, Tomsk, Russia*
*2 – Mid Sweden University, Östersund, Sweden*
*mariakoz71@gmail.com*

Titanium and its alloys porous structures are widely used in bone replacement surgery due to their low weight, high strength, reduced elastic modulus and good biocompatibility. However, elastic modulus of titanium alloys still much higher than those of bone tissues causing stress-shielding phenomenon which leads to implant loosening [1]. In order to decrease elastic modulus Nb is used as β stabilizing element in titanium alloys [2]. From the point of view of biocompatibility Nb considered to be non-toxic. Additive Manufacturing (AM) techniques allow producing metal implants with the suitable porosity, size, and complex geometry. Metal implants can directly connect to bone, but they do not form chemical bonds with bone tissue. Therefore, various surface modifications are needed to improve the morphological and bioactive bone-bonding ability of Ti-based implant materials [3,4]. An effective strategy to promote osteointegration for enhancing stable long-term fixation by means of full bone ingrowth is the development of coatings made of bioactive materials, such as hydroxyapatites (HA). HA ($Ca_{10}(PO_4)_6(OH)_2$) is widely used in production of osteoconductive ceramic materials for orthopedic and dental applications [5] since it constitutes approximately 70% of the weight of human bone [3].

Calcium ions $Ca^{2+}$ in synthetic HA has the versatility to be substituted by trace amounts of one or more mineral ions present in the natural bone including $Mg^{2+}$ and $Sr^{2+}$. On occasion, it is possible to dope a suitable ion into HA to solve a specific problem, for example $Mg^{2+}$ is substituted for $Ca^{2+}$ to stimulate the bone growth through interacting with osteoblast integrin that serves as a cell-adhesion receptor [6]. A favorable secondary dopant, $Sr^{2+}$, is highly required for enhancing the effect since it can satisfactorily delay the osteoclast activity. Moreover, both elements promote the proliferation and differentiation of osteoblasts [7]. There are many methods of HA coating deposition one of which is radio frequency (RF) magnetron sputtering. This method enables to vary the properties and chemical composition of the coatings effectively, as well as to obtain coatings with a high degree of adhesion [8,9].

The research includes the study of two broad topics: investigation of the Ti-42 wt.% Nb alloy – a novel material for electron beam powder bed fusion process method (AM E-PBF), and RF magnetron sputter deposited coatings of Mg- and Sr-substituted HA, as well as the study of their properties. Up to now there are no articles devoted to the Mg- and Sr-co-substituted HA coatings with the detailed investigations of the influence of the $Mg^{2+}$ and

$Sr^{2+}$ addition and sputtering parameters on the coating properties. There are also no papers investigating such coatings on E-PBF produced samples.

The 10 × 10 × 10 mm cubic specimens were manufactured from Ti-42 wt.% Nb pre-alloyed powders in ARCAM A2 E-PBF machine (ARCAM EBM, GE Additive Company, Mölnycke, Sweden) using different technological regimes. The detailed investigation of the alloy structure and mechanical properties were carried out using OM, SEM, EDX, XRD, EBSD and micromechanical testing. The phase analysis reveals that the alloys consist mainly of β-phase and a small amount of metastable α''-phase. Different types of defects were also revealed in the alloy, depending on the regime. Based on the results of the study, a parameter window was determined for Ti-42 wt.% Nb alloy in this installation. The window includes only two modes with a beam current of 4 mA and a scanning speed of 700 and 800 mm/s.

The initial $Ca_{8.5}Sr_{1.5}(PO_4)_6(OH)_2$ (Sr-HA) and $Ca_{9.5}Mg_{0.5}(PO_4)_6(OH)_2$ (Mg-HA) powders for the sputtering targets were prepared by the mechanochemical method [10]. The content of the substituting ions was chosen by analysis of the literature, based on the values of crystallinity and the results of *in vitro* and *in vivo* biological tests.

The target was pressed and sintered in air at 1100 °C for 1 h. HA films were deposited by RF magnetron sputtering (RF generator − COMDEL, 13.56 MHz) at an RF power of 500 W, the working atmosphere of pure Ar with pressure of 0.4 Pa for different time intervals from 180 to 300 min. The investigations of the structure and composition of the target materials and coatings using the XRD, IR-spectroscopy, and XPS methods showed that the coatings consist only of the HA phase, in contrast to the target materials, which also included the β-TCP phase. The results indicated that the lattice parameters of HA decreased with the addition of Mg and increased with the addition of Sr. This effect can be attributed to the difference in the ionic radius sizes, which decreases in the series Sr, Ca, and Mg (1.12, 0.99 and 0.65 Å) [10]. Based on the results obtained, it can be concluded that the substituting ions are incorporated into the HA lattice, instead of being in other phases.

**Acknowledgement:** This work was supported by the Russian Science Foundation, grant 20-43-04430.

**References:**

[1] P. Heinl, C. Körner, R. F. Singer, Adv. Eng. Mater. 10 (2008) 882.
[2] B. L. Pereira, C. M. Lepienski, Materials Research 23 (2020).
[3] J. M. Yu, H. C. Choe, Appl. Surf. Sci. 432 (2018) 294.
[4] M. Surmeneva, D. Khrapov, M. Kozadayeva, Mater. Chem. Phys. 275 (2021) 125217.
[5] S. Brogini, M. Sartori, G. Giavaresi, J. Mech. Behav. Biomed. Mater. 115 (2021) 104262.
[6] Z. Geng, Z. Cui, Z. Li, J. Mater. Chem. B (2021).
[7] M. S. Safavi, F. C. Walsh, M. A. Surmeneva, Coatings 11 (2021) 1.
[8] R. A. Surmenev, M. A. Surmeneva, I. Y. Grubova, Appl. Surf. Sci. 414 (2017) 335.
[9] S. Oladijo, E. Akinlabi, F. Mwema, IOP Conf. Ser. Mater. Sci. Eng. 1107 (2021) 012068.
[10] N. V. Bulina, O. B. Vinokurova, I. Y. Prosanov, Ceram. Int. 48 (2022) 35217.

## OP-II-08

# Modified Porous Glasses for Medical Applications

Tsyganova T.A.[1,2]
*1 – Institute of Silicate Chemistry RAS, Saint Petersburg, Russia*
*2 – St. Petersburg Scientific Center, Saint Petersburg, Russia*
*Tsyganova2@yandex.ru*

High-silica porous glasses (PGs) have controlled characteristics of the pore space structure (specific surface area, pore size, porosity), excellent adsorption properties associated with a branched inner surface capable of active chemisorption of various substances; thermal, chemical and biological stability and other useful properties [1, 2]. This complex of unique properties determines the possibility of using PGs for medical and biological purposes, for example, as bioactive membranes, carriers for the immobilization of microorganisms [3, 4], encapsulation of agents with disinfectant, algicidal and bactericidal functions for water treatment [5], increasing the thermal stability of the encapsulated substance [6], chemical protection of substances from oxidation in the case of food products [7], etc. In the present work, some results on the synthesis of PG-based materials relevant for medicine are given. For example, the introduction of bioactive silicon-molybdenum heteropolyanion into PG (composition, wt. % $0.2Na_2O{\cdot}4.2B_2O_3{\cdot}95.5SiO_2{\cdot}0.1Al_2O_3$) [8] made it possible to create a filter model for water purification, in which the presence of a bioactive component in PG prevents the reproduction of pathogenic microorganisms on the surface of the filter membrane in the process of water purification. Parameters of the porous structure of the membrane: specific pore volume 0.232 cm3/g; total matrix porosity 34.4%; average pore diameter 7.9 nm. Rigid frame of high-silica glass allows the membrane to be used in pressure filtration (up to 300 kPa) to speed up water filtration processes. In addition, the possibility of filter regeneration followed by multiple reuse of this filter opens up wide opportunities for its use in medical institutions [9-11]. Also, for medical purposes, quartzoid glass containing radioactive cesium can be used as a source of local irradiation of tumors, sterilization of blood and medical materials. Such material can also be used in agriculture for the processing of grain and other products. Quartzoid glass containing non-radioactive cesium (as a model glass) was synthesized by sequential impregnation of PG (composition, wt. % $0.17Na_2O{\cdot}5.96B_2O_3{\cdot}93.75SiO_2{\cdot}0.07P_2O_5{\cdot}0.05F$) [8] with aqueous solutions of $CsNO_3$ followed by sintering until the pores collapsed. During the study, it was found that cesium is fairly evenly distributed over the thickness of the samples and the total content of cesium in the synthesized samples increases (0.79-1.73 wt. %) with an increase in the concentration of the impregnating solution of cesium nitrate for the selected synthesis conditions and an increase in the impregnation time.

**Acknowledgement:** This study was carried out as part of a state task of the ICS RAS with the support of the Ministry of Education and Science of Russia (state registration no.AAAA-A19-119022290087-1 and no. 1021050501068-5-1.4.3 (project FFEM-2022-0004)).

**References:**

[1] O.V. Mazurin, G.P Roskova, V.I. Aver'yanov, and T.V. Antropova, *Dvukhfaznye stekla: Struktura, svoistva,primenenie* (Two Phase Glasses: Structure, Properties,and Applications), Leningrad: Nauka, 1991. 276.
[2] Ming-Hui Sun, Shao-Zhuan Huang, Li-Hua Chen, Yu Li, Xiao-Yu Yang, Zhong-Yong Yuan and Bao-Lian Su, Chem. Soc. Rev. 45(2016) 3479.
[3] D.W. Hutmacher, Biomaterials. 21(2000) 2529.
[4] F. Baino, S. Fiorilli, C. Vitale-Brovarone, Acta Biomaterialia. 42(2016) 18.
[5] Vidya Krishnan, T. Lakshmi, J.of Advanced Pharmaceutical Technology & Research. 4(2013) 78.
[6] J. W. Nicholson, The Chemistry of Medical and Dental Materials: Royal Society of Chemistry: Cambridge. 2002. 242.
[7] A. Tilocca, J. Mater. Chem. 20(2010) 6848.
[8] T.V. Antropova, S.V. Kalinina, T.G. Kostyreva, I.A.Drozdova, I.N.Anfimova, Glass Physics and Chemistry. 41(2015) 25.
[9] T.A. Tsyganova, D.S. Shevchenko, O.S. Magomedova, and O.V. Rakhimova, Glass Physics and Chemistry. 45(2019) 298.
[10] T.A. Tsyganova, O.V. Rakhimova, D.S. Shevchenko, T.V. Antropova, RF Patent 178126, *Byull. Izobret.* 2018. no. 9.
[11] T.A. Tsyganova, O.V. Rakhimova, RF Patent 275652 C1, *Byull. Izobret.* 2021. no. 28.

## OP-II-09

# Phthalocyanine-Graphene Complex for Biomedical Applications

Klimenko I.V.[1], Lobanov A.V.[1,2], Trusova E.A.[3]

*1 – Emanuel Institute of Biochemical Physics of Russian Academy of Sciences, Moscow, Russia*

*2 – Moscow Pedagogical State University, Moscow, Russia*

*3 – Baikov Institute of Metallurgy and Materials Science of Russian Academy of Sciences, Moscow, Russia*

*inna@deom.chph.ras.ru*

Photodynamic therapy (PDT) is now one of the most important conservative treatments for cancer. This method is based on the photosensitizers (Fs, natural or artificially synthesized substances capable of biological tissues photosensitizing) ability to accumulate selectively in tumor or other target tissues and generate singlet oxygen or oxygen-containing free radicals at local exposure of radiation of a certain wavelength corresponding to maximum absorption of Ps.

Among the promising Ps are metal phthalocyanine complexes (MePc). For the effective functioning of MePc as Fs for PDT it is very critical to have MePc molecules in monomeric (isolated) form. But in aqua or aqueous solutions, phthalocyanines, like other tetrapyrrolic compounds, have a strong tendency for self-aggregation with the formation of dimers and other types of aggregates, which reduces photodynamic activity of MePc. Moreover, when developing drugs for biomedical application, it is very important to ensure the stability of complex dispersion in the liquid substances.

In order to reduce hydrophobicity and MePc aggregation in aqua and aqueous solutions new hybrid structures based on oxygen-free graphene and aluminum phthalocyanine chloride (AlClPc, $C_{32}H_{16}AlClN_8$) have been synthesized in liquid media. The sonochemical method was used to obtain a graphene suspension: the ultrasonic exfoliation of the graphene sheets from the surface of synthetic graphite in N,N-dimethylformamide (DMF) or in its mixture with aqua was carried out. [1].

The photophysical properties of these hybrid systems have been studied using optical spectroscopy. The obtained results confirm a successful synthesis.

Comparative analysis of UV-VIS absorption spectroscopy data for the synthesized complex system and the AlClPc reference solution made it possible to determine the effect of graphene on the electronic structure of AlClPc. It has been found that the responses in the region of the *B* and *Q* bands are due to changes in the electronic structure of AlClPc upon its coordination on the surface of the graphene sheet, resulting in charge transfer complex formation.

It has been proved that that the coordination interaction between graphene and AlClPc prevents the aggregation of the latter and stabilizes it in the chemically active monomeric form, which, unlike the phthalocyanine aggregates, has photochemical and luminescent properties

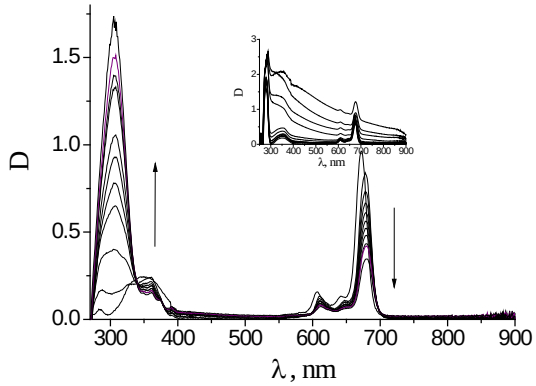


*Fig. 1. UV-Vis spectra of hybrid systems AlClPc-graphene in DMF-aqua mixture and AlClPc-DMF-aqua solutions (inset). The arrows show an increase in the concentration of graphene in the system.*

The results of this study make it possible to predict as well as to control and manage the aggregation behaviour of AlClPc complexes in aqua-organic media. This fact, in turn, provides the AlClPc –graphene complex for using as a platform for vector drag delivery and early diagnosis.

**Acknowledgement:** This work was supported by government funding within the framework of the scientific project "45.9 Theoretical and experimental studies of new materials and hybrid structures, including polyconjugate systems, nanostructures, composite materials and systems of reduced dimension" (FFEG-2019-0001).

**References:**

[1] E. A. Trusova, I. V. Klimenko, A. M. Afzal, A. N. Shchegolikhin, L. V. Jurina, New J. of Chem., 45 (2021), 10448. DOI: 10.1039/d1nj01015h

## OP-II-10

# Supports for Enzyme Immobilization on the Basis of Chitosan and Magnetic Nanoparticles

Matveeva V.G.[1,2], Tikhonov B.B., Lisichkin D.R., Stadolnikova P.Yu., Sulman M.G., Ajay Shivajirao Desai[3], José Cleiton Sousa dos Santos[4]

*1 – Department of Biotechnology, Chemistry and Standardization, Tver State Technical University, Tver, 170026, Russian Federation*

*2 – Regional Technological Centre, Tver State University, Tver, 170100, Russian Federation 3 – Dr. Balasaheb Sawant Konkan Krishi Vidyapeeth, Dapoli, India, College of Fisheries, Ratnagiri, Maharashtra, India*

*4 – University of International Integration of Afro-Brazilian Lusophony, Brazilia*

*matveeva@science.tver.ru*

The immobilization of enzymes makes it possible to significantly increase the efficiency of its use in chemical processes providing its reusability and significantly increasing the enzyme resistance to inhibitory effects. In recent years, biopolymer–based materials including Chitosan, a polysaccharide obtained by deacetylation of chitin, have been widely used as supports for immobilization. Due to the ability to gelation, high sorption capacity, the presence of reactive amino groups, as well as complete biodegradability, chitosane is considered to be one of the most promising materials for the "green chemistry" processes. However, chitosan carriers for enzyme immobilization have insufficiently high mechanical strength and are difficult to separate from the reaction medium due to high swelling and gel structure. In this regard, composite carriers based on chitosan are increasingly being created by modifying chitosan with organic and inorganic components.

Before the synthesis of nanoparticles, chitosan was modified in order to purify it from the impurities. Chitosan was dissolved in a 2 % solution of acetic acid in distilled water and constantly stirred at a rate of 300 $min^{-1}$ for 16 hours. Next, the solution was boiled for 15 minutes for denaturation and precipitation of by-products, after which the mixture was cooled, centrifuged for 10 minutes at 5000 rpm, and filtered through a filter with a pore size of 1 microns. Then the pH of the solution was adjusted to 9 with a 1 M NaOH solution to precipitate chitosan from the aqueous phase and the chitosan precipitate was dried lyophilically.

To obtain magnetically separated chitosan-containing nanoparticles, 15 ml of aqueous solutions of $FeCl_3 \cdot 6H_2O$ (0.4 mol/L) and $FeCl_2 \cdot 4H_2O$ (0.2 mol/L) were mixed in a thermostatically controlled reactor equipped with a reflux, a reagent supply inlet and a mechanical stirrer. The mixture was stirred for 15 minutes at a rate of 400 $min^{-1}$, heated up to 65 °C, after which 10 mL of an aqueous ammonia solution was dropped at a rate of 2 mL/min. Next, 10 mL of purified chitosan solution (0.0625 g in 10 mL of 0.2 M acetic acid) was added to the mixture and kept under constant stirring for 30 minutes. After the synthesis was completed, the particles were separated using a permanent magnet and washed with distilled water to remove non-specifically bound reagents.

The resulting nanoparticles had good magnetic properties, easily and completely separated from the reaction medium using a magnet. The average diameter of the particles (58±2 nm) and their zeta potential (+35.6 mV) were determined by the method of differential light scattering. The particles are stable and retain their magnetic properties and surface characteristics when stored for 1 month at a temperature of +2-+4 °C. Microscopy of the samples showed that most of the particles have a spherical shape with the formation of small agglomerates, easily separated by mechanical action. Figure 1 shows an image of aggregates of synthesized particles obtained using an optical microscope "Biomed-2".

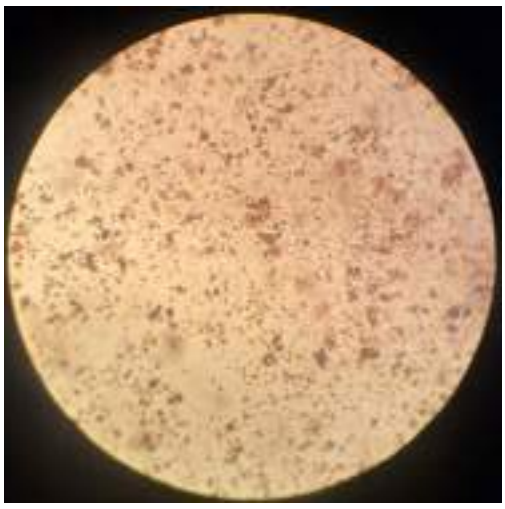

*Fig. 1. Microphotograph of the synthesized particles obtained using "Biomed-2" (1000x)*

IR Fourier spectroscopy of diffusive reflection for samples of synthesized nanoparticles showed the presence of functional groups characteristic for chitosan, which confirms the successful functionalization of magnetite particles by chitosan.

The obtained magnetically separable chitosan nanoparticles can be used as carriers for the immobilization of enzymes and metals in catalytic processes.

**Acknowledgement:** This work was supported by the Ministry of Science and Higher Education, project 075-15-2022-1232.

## OP-II-11

# Immobilization of Cellulase on Nanostructured Supports for Processing Biomass Waste

Sulman A.M.[1], Grebennikova O.V.[1], Sidorov A.I.[1], Matveeva V.G.[1,2]
*1 – Tver State Technical University, Tver, Russia*
*2 – Tver State University, Tver, Russia*
*alexsulman@mail.ru*

Nanobiocatalysts, i.e., enzymes immobilized on nanostructured supports, received considerable attention because they are potential remedies to overcome shortcomings of traditional biocatalysts such as low efficiency of mass transfer, instability during catalytic reactions, and possible deactivation.

Scarcity of conventional fuels due to socioeconomic factors and reluctance of the communities to use them due to environmental aspects of their processing and applications increased the interest of industry in biomass or biomass waste processing to biofuels and value-added chemicals. There are many processing stages to convert lignocellulosic biomass to a direct source of biofuel, but the most important step is the decomposition of cellulose to fermentable (intermediate) sugars which can be a feasible substrate for biofuel [1]. Environmentally favorable avenue for biomass processing is the use of enzymes which decompose cellulose to glucose [2]. However, low thermal and storage stability of enzymes as well as the presence of impurities, enzyme leakage, and a reusability problem are major shortcomings of employing free enzymes. These shortcomings can be minimized or even eliminated by immobilization of enzymes on various supports [3]. The role of support materials is to preserve the enzyme secondary structure as well as to create the favorable interactions with the enzyme [4]. The choice of a suitable carrier is also determined by the enzyme and process types [5].

In the last decade enzymes immobilized on nanostructured supports called nanobiocatalysts received considerable attention. Nanostructured supports are materials containing nanometer size features (normally, between 1 and 100 nm) such as nanoparticles (NPs) of different sizes and shapes including nanorods and nanofibers, materials with pores in a nanometer range, stimuli responsive nano-carriers, etc. [6]. This growing interest is explained by a possibility of nanobiocatalysts to overcome deficiencies of immobilized enzymes on traditional supports. Nanostructured supports minimize diffusion, thus significantly improving mass transfer. Also, these nanomaterials possess a high surface area for the enzyme immobilization, increasing the enzyme loading and improving their positioning on the surface. The latter often results in higher enzymatic activity [7].

In this work we discussed major features of immobilization of cellulase on nanostructured supports. Cellulases are enzymes which degrade cellulose – the most abundant natural polymer which forms plant cell walls. Cellulases are a cocktail of three enzymes: endoglucanases, exoglucanases, and β-glucosidases which are utilized to degrade different

chemical bonds in cellulose [8]. Besides stabilization and possibility of the catalyst reuse, the cellulase immobilization on nanostructured supports may reduce the cellulase surface charge, thus diminishing its non-specific binding to lignin and increasing the interactions with cellulose [9]. Often biomass waste first requires delignification with another enzymatic catalyst before cellulase can efficiently hydrolyze cellulose or co-immobilization of several enzymes on the same support is implemented which is a more prominent trend.

We were focused on a combination of several crucial factors determining the performance of nanobiocatalysts such as methods of cellulase immobilization, types of nanostructured supports, multienzyme nanobiocatalysts, etc. The structure of the study is presented in Scheme 1.

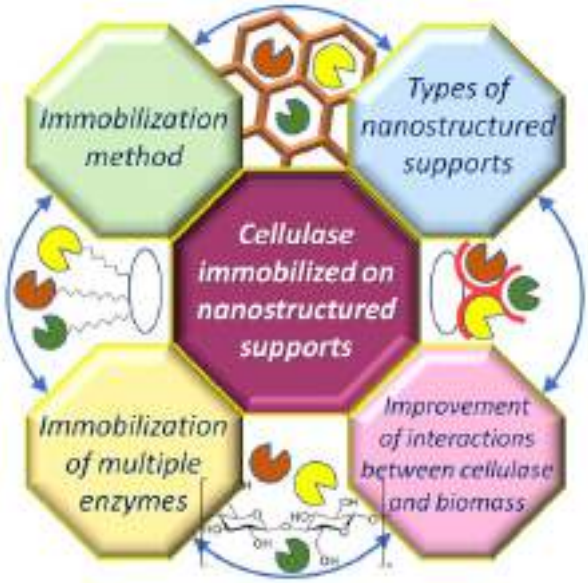


*Fig. 1. Schematic representation of the study structure*

**Acknowledgement:** This work was supported by the Russian Science Foundation, project 22-79-00052.

**References:**

[1] Houfani A.A., Anders N., Spiess A.C., Baldrian P., Benallaoua S. Biomass Bioenergy 134 (2020)105481.
[2] Arumugam A., Malolan V.V., Ponnusami V. Waste Biomass Valorization 12 (2012) 577.
[3] Zanuso E., Gomes D.G., Ruiz H.A., Teixeira J.A., Domingues L. Sustain. Energy Fuels 5 (2021) 4233.
[4] Zdarta J., Meyer A.S., Jesionowski T., Pinelo M. Catalysts 8 (2018) 92.
[5] Muley A.B., Mulchandani K.H., Singhal R.S. Methods Enzymol. 630 (2020) 39.
[6] Medina-Castillo A.L., Ruzic L., Nidetzky B., Bolivar J.M. ACS Appl. Polym. Mater. 4 (2022) 6051.
[7] Cavalcante F.T.T., de A. Falcao I.R., da S. Souza J.E., Rocha T.G., de Sousa I.G., Cavalcante A.L.G., de Oliveira A.L.B., de Sousa M.C.M., dos Santos J.C.S. Electrochem 2 (2021) 149.
[8] Sudhir S.A.P., Singhania R.R., Larroche C., Li Z. Biomass, Biofuels, Biochemicals Advances in Enzyme Catalysis and Technologies. 1st ed.; Elsevier: 2020; p. 472.

## OP-II-12

# Development of Biomedical Fibrous Materials Based on PHB and Hemin

Tyubaeva P.M.[1,2], Olkhov A.A.[1,2], Popov A.A.[1,2]
*1 – Plekhanov Russian University of Economics, Moscow, Russia*
*2 – Emanuel Institute of Biochemical Physics of the Russian Academy of Sciences, Moscow, Russia*
*polina-tyubaeva@yandex.ru*

Today biocompatible polymers of natural origin are widely used for creation of new biomedical materials with unique properties. For instance, poly-3-hydroxybutyrate (PHB) is of great interest among known biopolymers due to its unique properties [1]. The aim of this work was to create new biocompatible fibrous materials based on PHB and Hemin [2] for regenerative medicine (Figure 1).

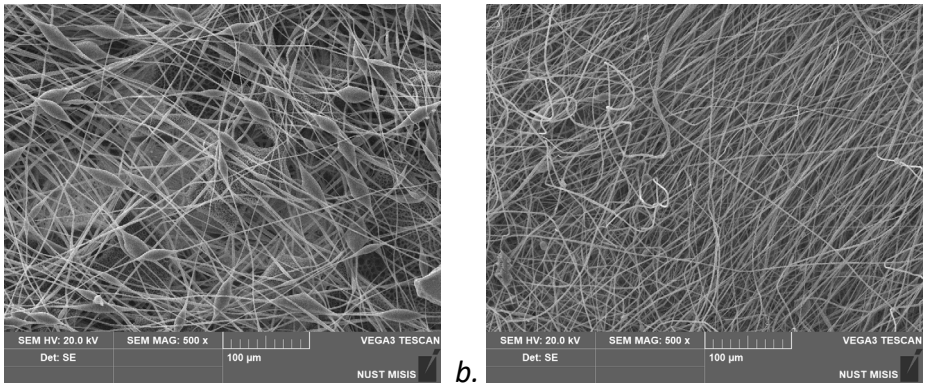


*a.* *b.*

*Fig. 1. Microphotographs of nonwoven fibrous materials based on PHB with different Hemin content: a – 0%; b – 5%.*

Fibrous materials were obtained by double-solution electrospinning process [3]. Thus, the introduction of 5% of Hemin led to a decrease in the average diameter of the fibers from 3.5 to 1.7 microns, the porosity of the material increased by 30%, and the number of defects significantly decreased. Mostly, this effect is due to the improvement of the molding properties of the solution based on PHB, where hemin is an effective modifying additive.

These positive changes in morphology of the fibres affected operational properties of the whole material. The strength of the fibrous layer increased from 1.7 MPa to 5.5 MPa, and the elongation at break increased from 3.6% to 6.1%. The air permeability of the material due to the large number of open pores increased from 0.4 ml to 1.9 ml per unit of time (according to the Gurley method).

Moreover, it was found that Hemin makes a significant contribution to the formation of the crystalline phase of PHB, contributing to a decrease in the proportion of crystalline formations from 65% to 52%, while the longitudinal size of the crystallites increased by 15%.

Of great importance is the high biocompatibility of the obtained materials, which was evaluated by the survival rate of BJ-5ta fibroblasts in comparison with the average survival rate of control cells incubated in the absence of materials. The introduction of Hemin made it

possible to ensure a survival rate of 90-100%, in comparison with pure PHB, where the survival rate was 90%.

The obtained results are a significant reason to recommend these materials for the creation of new biomedical tools for regenerative medicine.

**Acknowledgement:** This work was supported by the Russian Science Foundation, grant 22-73-00038.

**References:**

[1] Kai D., Zhang K., Liow S.S., Loh X.J. New Dual Functional PHB-Grafted Lignin Copolymer: Synthesis, Mechanical Properties, and Biocompatibility Studies // ACS Appl. Bio Mater. 2018. V. 2. P. 127-134.
[2] Dell'Acqua S., Massardi E., Monzani E., et al. Interaction between hemin and prion peptides: binding, oxidative reactivity and aggregation // Int. J. Mol. Sci. 2020. V. 21(20). P. 7553.
[3] Avossa J., Paolesse R., et al. Electrospinning of Polystyrene/Polyhydroxybutyrate Nanofibers Doped with Porphyrin and Graphene for Chemiresistor Gas Sensors // Nanomaterials. 2019. V. 9(2). P. 280.

## OP-II-13

# Conformers of L-Ascorbic Acid in Molecular Structure of Vitamin C and co-Crystals with Nicotinic and Picolinic Acids

Evtushenko D.N., Vodyankina O.V.
*Tomsk State University, Tomsk, Russia*
*vodyankina_o@mail.ru*

L-ascorbic acid (L-Asc) is one of the most well-known and widely used active pharmaceutical ingredients (API), in particular as an apoptosis-inducing agent in cancer cells [1]. However, still there is no complete understanding of the mechanisms of the observed effects.

In our previous work [2], we calculated the total effective charges of L-ascorbic acid molecules in 12 binary co-crystals and in the crystal structure of pristine L-Asc (CSD). The L-Asc molecules in the studied compounds were in different conformational states, which, in addition to geometry, differed in sign of the total effective charge. This work showed that the presence of an effective charge affected the formation of crystalline structures and the system of hydrogen bonds, primarily L-ascorbic acid itself (Fig.1).

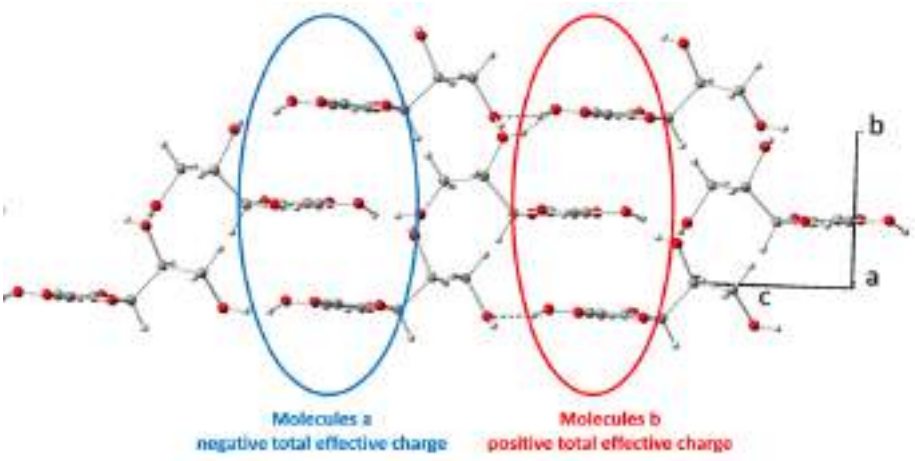


*Fig. 1. A fragment of the crystal structure of the Vitamin C (refcode COFKOA (CSD)) showing ribbons consisting of conformer molecules with negative (molecules a) and positive (molecules b) total effective charge*

In the crystal structure of co-crystals with pyridine-2-carboxylic (picolinic) or pyridine-3-carboxylic (nicotinic) acids, the L-Asc molecules are in only one conformational state with the negative total effective charges. Comparison of the published data on the apoptosis-inducing activity of vitamin C and L-Asc in co-crystals of L-AscPic and L-AscNic shows that the L-Asc in cocrystals possesses the highest ability to induce apoptosis. This may indicate the importance of negatively charged conformers in the apoptosis-inducing activity of L-Asc molecules.

In the report the geometry and features of the electronic structure of these L-Asc conformers, their relative stability, regioselectivity descriptors (Fukui functions), and the distribution of molecular electrostatic potential will be discussed.

**References:**

[1] J. G. Ionescu, B. Poljsak, Int. J. of Cancer Prevention. 3(2010) 1.
[2] D. N. Evtushenko, S. G. Arkhipov, A. V. Fateev, T. I. Izaak, L. A. Egorova, N. A. Skorik, O. V. Vodyankina, E. V. Boldyreva, Acta Cryst. B.76 (2020) 967–978.

## OP-II-14

# Where Well-Known Drugs Meet New Perspectives: Single-Walled Carbon Nanotubes as a Drug Delivery System for Prednisolone and Doxorubicin for Anticancer Therapy

Chetyrkina M.[1], Abalymov A.[1,2], Dozmorov S.[1], Cvjetinovic J.[1], Fedorov F.S.[1], Goldt A.[1], Gorin D.A.[1], Nasibulin A.[1]

*1 – Skolkovo Institute of Science and Technology, 3 Nobel Street, Moscow, 121205, Russia*

*2 – Science Medical Center, Saratov State University, 410012 Saratov, Russia*

*margarita.chetyrkina@skoltech.ru*

According to World Health Organization, cancer is one of the leading causes of deaths worldwide, one patient from six die because of cancer [1]. Enormous variety of approaches for cancer treatment with different origin are utilized by clinicians to fight the disease [2]. However, many patients face complications such as drug-resistance, long recovery after chemotherapy *etc.*, that stimulate search of new drugs and treatment scenarios. At this point, drug-delivery (DD) platforms are staying in the first row, and carbon nanotubes (CNTs) are considered to be promising candidates to construct an efficient drug delivery system. In our study, we, evaluate the stability and toxicity of CNT dispersion containing therapeutic agents, doxorubicin and prednisolone, to be applied as DD system.

We prepared two dispersions of CNTs with therapeutic agents – famous cytostatic drug widely applied for cancer treatment - doxorubicin (DOX) [3], and anti-inflammatory agent prednisolone (PR) usually utilized in chemotherapy to suppress an inflammation response [4]. Secondly, we tested dispersions cytotoxic effects at 5 cell lines: Neuro2A, or N2A, mouse neuroblastoma, L929 connective mouse tissue, A549 human adenocarcinoma, SKOV3 ovarian adenocarcinoma, HEK human embryonic kidney. CNTs produced with CoMoCat (SigmaAldrich, U.S.A.) were dispersed in a regular pharmaceutical prednisolone (Renewal, Russia) with concentration 5 mg/mL of tubes and 10 mg/mL of PR. For preparing the dispersion with DOX, we used CNTs synthesized by HiPco process (Nano Integris, Canada), with concentrations 5 mg/mL of tubes and 10 mg/mL of DOX (Verofarm, Russia). As the reference, we dispersed HiPco tubes in milliQ water. For high-quality dispersions, we used an ultrasonication (Branson 450, Canada) in ice bath during 3 hours and 90 W that have resulted in stable dispersions of CNTs. Zeta potential was measured by ZetaSizer Nano ZS analyzer (Malvern, UK).

Cell culturing was performed in standard T25 (Nest, China) flasks in DMEM (Biolot, Russia) media with additional supplements: 10% of fetal bovine serum (Biolot, Russia), L-glutamine (Biolot, Russia), 100 µg/mL penicillin/streptomycin (Biolot, Russia). Every 2-3 days we replaced media and maintained the cells at incubator (5% $CO_2$ and 37 °C) (Innova, New Brunswick Scientific, U.S.A). At the first step for a standard colorimetric cytotoxic assay, MTT (PanEco, Russia), we reseeded cells at standard 96-well cell culture plates (Eppendorf, Germany) at density $10^4$ cells/well with 200 µL of media. After 24 hours, needed for cells adhesion, we applied 10 µL of the tested substances. As a control group we used cells without addition of

any solution. Incubation with the substances of the interest was performed during the next 72 hours. After, 10 µL of MTT reagent at concentration was applied to each well and incubated for 3 more hours. After incubation, cells media was completely removed and 200 µL of DMSO (Biolot, Russia) reagent was applied. Analysis was performed with a spectrophotometer (Infinite F200, Switzerland) at 555 nm.

We have found that the most sensitive N2A cells demonstrated 70% of alive cells at the highest tested dose of CNTs with PR (7.1 µg/mL) (**Fig.1, A**). Skov3 and L929 show almost the same response to the applied dispersion, near 90% of alive cells at the highest tested dose. HEK and A549 viability is placed in the middle between the culture with a high sensitivity (N2A) and cultures with low response (Skov3, L929). The tested dispersions have some toxicity while only PR suspension have a 100% viability meaning that CNTs insert into cells when compared to the group where we applied just PR without tubes. L929 fibroblasts and N2A neuroblastoma cells were the most sensitive to the incubation with CNTs in DOX (**Fig.1, B**). Skov3 were almost resistant, 80% of cells stayed alive after the incubation with the agent. HEK and A549 are very close in their response to the CNTs diluted in DOX. Still, just DOX itself was more toxic than our dispersion made of CNTs and DOX.

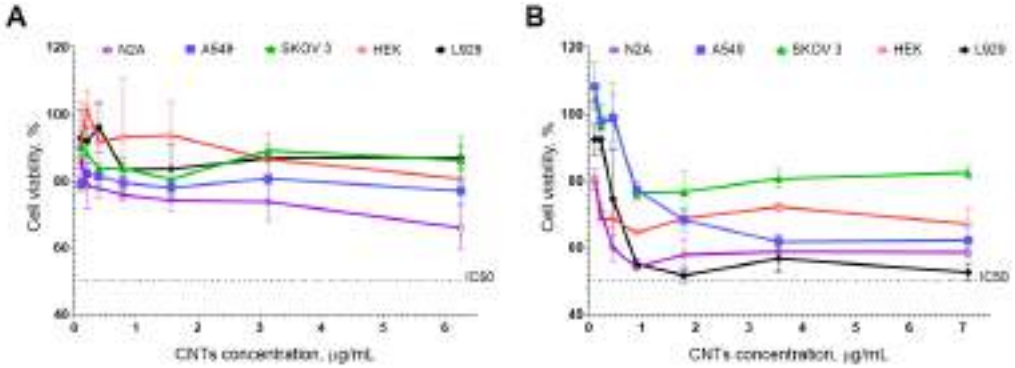


*Fig. 1. Results of the cytotoxic assay for CNTs dispersions with PR (A) and DOX (B).*

Summing up, we prepared and characterized dispersions of CNTs with therapeutic agents – doxorubicin and prednisolone. Extensive cytotoxic studies of the prepared dispersions revealed that toxicity is even less than for DOX, or higher than for PR. Thus, the present work is the first successful demonstration of new possible application of well-known pharmaceuticals in cooperation with CNTs for combinational therapy.

**Acknowledgement:** This study is supported by RSF No. 21-73-10288, *https://rscf.ru/en/project/21-73-10288/.*

**References:**

[1] World Health Organization, Cancer, https://www.who.int/news-room/fact-sheets/detail/cancer
[2] Pucci C, Martinelli C, Ciofani G. Ecancermedicalscience. 2019;13:961. doi:10.3332/ecancer.2019.961.
[3] Thorn CF, Oshiro C, Marsh S, Hernandez-Boussard T, McLeod H, Klein TE, Altman RB. 2011;21(7):440-6. doi: 10.1097/FPC.0b013e32833ffb56.
[4] Mihaela Aldea, Emeline Orillard, Laura Mansi, Aurélien Marabelle, Florian Scotte, Olivier Lambotte, Jean-Marie Michot, , 141,2020, 239-251, doi: 10.1016/j.ejca.2020.09.032.

## OP-II-15

# Autocatalytic Hydrogen Peroxide Production by Bacteria as a New Advantage of Hybrid Living Materials

Lokteva A.
*ITMO University, Saint Petersburg, Russia*
*lokteva@scamt-itmo.ru*

The problem of chronic wounds therapy lies in the multifactorial causes of their occurrence. Often these are disorders of angiogenesis processes and contamination of the wound surface by pathogenic microorganisms. To solve this problem, it is necessary to create a therapeutic agent capable of acting on several causes of chronic wounds. As a system capable of soft regulation of both angiogenesis processes and regulation of the number of pathogenic cultures, it is proposed to use probiotic biosystems operating through the interaction of probiotic bacteria with nanoparticles encapsulated in a hydrogel.

This research work is aimed at creating living hybrid materials for the treatment of infectious diseases. First of all, it is necessary to select probiotic bacterial cultures, nanoparticles that can stimulate the growth of selected probiotic bacteria and activate the synthesis of antimicrobial molecules, prebiotics and a scaffold in the form of hydrogel.

The probiotic bacteria *Lactobacillus acidophilus* ATCC 4356, which are representative of human microbiota, were selected during the study. The selected titanium dioxide nanoparticles had a positive effect on the growth of probiotic cultures at concentrations up to 1mg/ml, stimulated hydrogen peroxide synthesis to 70 µmol/ml after 3 hours of co-incubation and their combination with lactobacilli negatively affected the growth of *Escherichia coli* K12 and *Staphylococcus aureus* MRSA, reducing their numbers from an average of $5.1*10^6$ CFU to $7.4*10^7$ CFU after 3 hours. Nanoparticles and probiotic bacteria had no negative effect on the growth and activity of HPF cell line. The chosen combination of bacteria and $TiO_2$ NPs was embedded in the PNIPAM polymer, which had 10-fold absorption properties and suitable pore size less than 1 µm to prevent bacterial migration and provided active molecules as hydrogen peroxide and milk acid migration. The results of *in vivo* experiments on inflicted wound surfaces in rats show that the obtained live hybrid material has improved wound healing rates by a factor of 4 after 21 days of the experiment.

The results obtained in this study point to the prospect of using live hybrid materials as a new way to combat infectious diseases *in situ*.

## OP-III-01

# Alumina-Based Aerogels for Application in Adsorption and Catalysis

Bedilo A.F.[1], Ilyina E.V.[1], Gerus Y.Y.[1,2], Shivtsov D.M.[1], Shuvarakova E.I.[1], Veselov G.B.[1], Vedyagin A.A.[1]

*1 – Boreskov Institute of Catalysis, Novosibirsk, Russia*

*2 – Novosibirsk State University, Novosibirsk, Russia*

*bedilo@catalysis.ru*

Aerogels are materials obtained by controlled hydrolysis of metal alkoxides with the formation of polymerous gels followed by supercritical drying of the latter. Under supercritical conditions, the liquid-vapor interface that produces the collapse of the initial gel framework during conventional drying is eliminated leaving the gel structure intact. In this report, recent results related to synthesis and application of alumina-based aerogels obtained in our group will be presented.

Calcium aluminate $12CaO\text{-}7Al_2O_3$ (commonly denoted as C12A7), also known as mayenite, recently became an object of particular scientific interest. Its structure features a cationic framework $[Ca_{24}Al_{28}O_{64}]^{4+}$ compensated by the presence of an anionic lattice $4X^-$, where $X^-$ can be $Cl^-$, $OH^-$, $O^{2-}$, $O_2^-$, $H^-$ or even $e^-$.

In this study, aluminum isopropoxide and calcium methoxide were used as precursors for the synthesis of calcium aluminate aerogels. The resulting solution was subjected to hydrolysis with desired amount of deionized water, followed by aging for 16 hours and drying in an autoclave at 265 °C. Specific surface areas of the samples dried in an autoclave increased from 265 to 513 $m^2/g$ when the Ca/Al ratio changed from 3/2 to 1/2 [1]. Depending on the amount of water used at the hydrolysis stage, the specific surface area of the samples with C12A7 stoichiometry varied from 330 to 90 $m^2/g$ after drying in the autoclave. The use of a five-fold excess of water (compared to the stoichiometric amount) led to the formation of crystalline mayenite immediately after autoclave drying [2]. Reasonably high specific surface areas (up to 205 $m^2/g$) were preserved after calcination of the obtained aerogels at 500 °C in the air. The application of the electron paramagnetic resonance using adsorption of spin probes revealed electron-donor, weak electron-acceptor, and radical sites on the surface of all calcium aluminate aerogels calcined at 500 °C [1, 3].

Pd-containing catalysts based on highly dispersed aerogel-derived mayenite samples were prepared using two approaches [4]. Pd@C12A7 was obtained by Pd nitrate addition to a fresh $Ca(OH)_2$-$Al(OH)_3$ gel. Pd/C12A7 was synthesized using incipient wetness impregnation of the mayenite aerogel (Fig. 1, Left). The activity of these samples and reproducibility of their redox behavior were studied in three cycles of temperature-programmed reduction in hydrogen and CO. A prompt thermal aging technique was used to compare the activity of the samples towards CO oxidation. The Pd/C12A7 catalyst demonstrated higher activity in CO oxidation due to higher PdO dispersion [4].

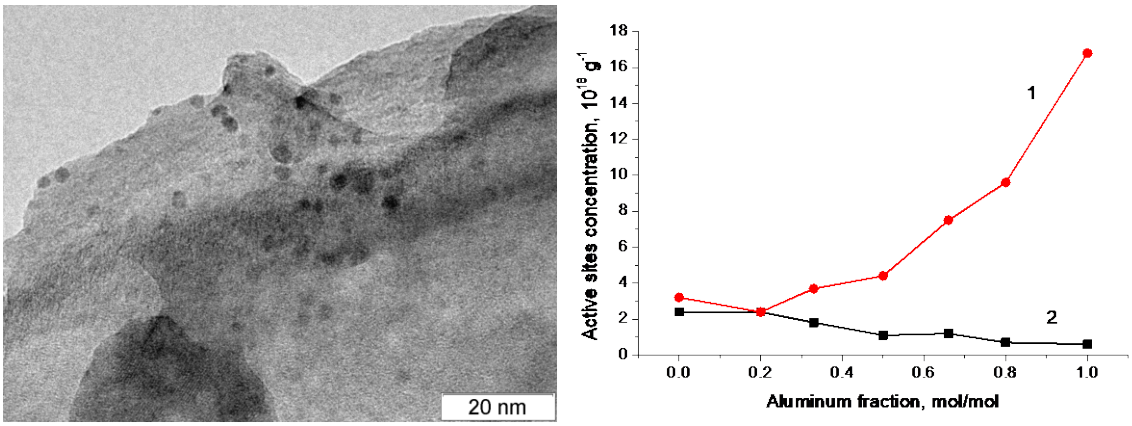


*Fig. 1. Left: HREM image of 1% Pd/C12A7 aerogel. Right: Dependence of the concentrations of electron-acceptor (1) and electron-donor (2) on the composition of $MgO:Al_2O_3$ aerogels.*

Hydrogen production by tetradecahydrophenazine dehydrogenation was studied over catalysts containing Pd supported on a series of magnesium-aluminum oxides prepared by the aerogel method [5]. The synthesized aerogels had high specific surface areas and pore volumes. A surface area as high as 600 $m^2/g$ after calcination at 500 °C was observed for the mixed aerogel with an Mg:Al ratio of 1:4. An increase in the concentration of acidic electron-acceptor sites determined by EPR on the surface of the mixed magnesium-aluminum oxide supports with high surface areas (Fig. 1, Right) was found to result in higher hydrogen production due to the faster dehydrogenation of sterically hindered nitrogen-containing tetradecahydrophenazine heterocycles [5].

Sulfate deposition on the $Al_2O_3$ surface is known to increase its acidity producing superacid catalysts. Sulfated alumina aerogels were synthesized by adding calculated amounts of sulfuric acid to the alumina gel before the autoclave drying. The sulfuric acid introduction was found to result in a noticeable decrease of the pore volume, whereas the high surface area of the $Al_2O_3$ aerogels was preserved. The surface areas of sulfated alumina aerogels after calcination at 550°C usually required to make active acid catalysts was between 450 and 500 $m^2/g$, which is ca. 2 times higher than those of the catalysts prepared by traditional methods.

Overall, alumina-based aerogels synthesized with high-temperature supercritical drying feature high surface areas and are promising materials for various adsorption and catalytic applications.

**References:**

[1] E.V. Ilyina et al., J. Sol-Gel Sci. Technol. 104 (2022) 259.
[2] E.V. Ilyina et al., Mater. Lett. 293 (2021) 129699.
[3] E.I. Shuvarakova et al., Rus. J. Phys. Chem. 16 (2022) 411.
[4] E.V. Ilyina et al., Gels 8 (2022) 809.
[5] D.M. Shivtsov et al., Catalysts 13 (2023) 334.

## OP-III-02

# Proton /Oxygen Ion Conductivity Ratio of Nd Containing $La_{10}W_2O_{21}$/γ-$La_6W_2O_{15}$ Tungstates

Shlyakhtina A.V.[1], Baldin E.D.[1], Vorobieva G.A.[1], Kolbanev I.V.[1], Stolbov D.N.[2], Kasyanova A.V.[3,4], Lyskov N.V.[5,6]

*1 – N.N. Semenov Federal Research Center for Chemical Physics, Russian Academy of Sciences, Moscow, Russia*

*2 – Department of Chemistry, Lomonosov Moscow State University, Leninskie Gory 1-3, Moscow, Russia*

*3 – Institute of High Temperature Electrochemistry, Ural Branch, RAS, Ekaterinburg, Russia*

*4 – Ural Federal University named after the First President of Russia B.N. Yeltsin, Ekaterinburg, Russia*

*5 – Federal Research Center of Problems of Chemical Physics and Medical Chemistry RAS, Moscow region, Chernogolovka, Russia*

*6 – National Research University "Higher School of Economics", Moscow, Russia*

*annashl@inbox.ru; annash@chph.ras.ru*

The search for new materials with pronounced proton or oxygen-ion conductivities is of great importance for the development of solid state ionic and electrochemistry fields. Here, we studied the structure, phase transitions, and ionic (oxygen-ion and proton) conductivity of the pure and Nd containing γ-$La_6W_2O_{15}$-based composites and pseudorhombohedral $La_{14-x}Nd_xW_4O_{33}$ ($x$ = 12, 14) solid solutions. The proton conductor $La_{14}W_4O_{33}$ ($5\times10^{-5}$ S/cm at 600 °C) was found to be a two-phase material consisting of an anion-deficient $La_{10}W_2O_{21}$ fluorite-related phase and the γ-$La_6W_2O_{15}$ orthorhombic phase. The phase content of the pure $La_{10}W_2O_{21}$ cubic phase was ~ 18 wt.% for the γ-$La_6W_2O_{15}$-based composite. A high degree of Nd content in γ-$La_6W_2O_{15}$-based composite leads to formation of solid solutions based on a pseudorhombohedral phase in $La_{14-x}Nd_xW_4O_{33}$ with $x$ = 12 and 14. The Nd -containing γ-$La_6W_2O_{15}$-based composites exhibited proton conductivity, which gradually decreased with increasing Nd content, whereas $La_{14-x}Nd_xW_4O_{33}$ ($x$ = 12, 14) pseudorhombohedral solid solutions were identified as oxygen-ion conductors. $Nd_{14}W_4O_{33}$ has the oxygen -ion conductivity of ~ $4\times10^{-4}$ S/cm at 700 °C ($1.0\times10^{-3}$ S/cm at 900 °C). In contrast to the γ-$La_6W_2O_{15}$ phase, the γ-$La_6W_2O_{15}$-based composite undergoes only a single reversible phase transition at around 910 °C, which can, however, initiate cracks in ceramics.

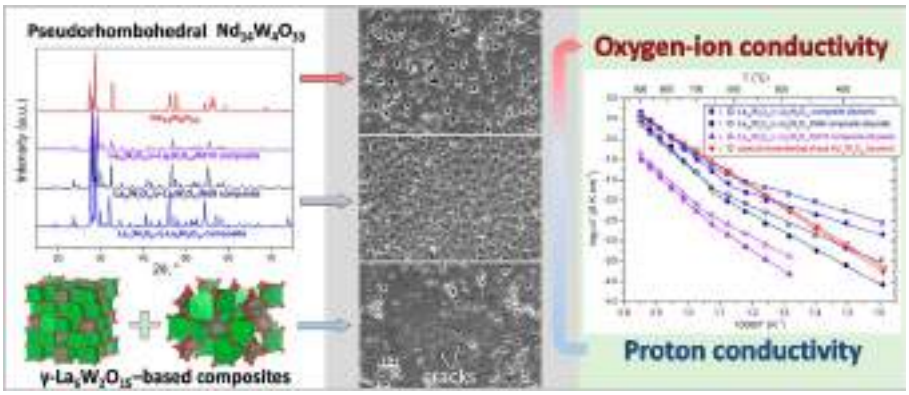


*Fig. 1. The change in structure type, ceramics integrity and conductivity type in the γ-$La_6W_2O_{15}$-based composites with increasing Nd content.*

According to DSC and SEM data, the phase transition near 910 °C can be suppressed by introducing Nd into the γ-$La_6W_2O_{15}$-based composites. The cracking process is enhanced by evaporation of tungsten oxide at T≥1450 °C.

The proton conductivity of γ-$La_6W_2O_{15}$-based composite, consisting of ~ 18 wt.% of $La_{10}W_2O_{21}$, is ~ $6\times10^{-5}$ S/cm at 600 °C. The proton conductivity of $La_{10}W_2O_{21}$-based composite consisting of ~ 81 wt.% of $La_{10}W_2O_{21}$ is ~ $7.5\times10^{-4}$ S/cm at 600 °C, approaching that of the $La_{6-x}WO_{12-\delta}$ fluorite-like proton conductors.

**Acknowledgement:** This work was supported by Russian Foundation for Basic Research grant 20-03-00399. The work was supported partially by the subsidy from the Ministry of Education and Science allocated by the FRC CP RAS for the implementation of the state assignment (No.122040500071-0, No. 122040500068-0) and in accordance with the state task for FRC PCP and MC RAS, state registration No. AAAA-A19-119061890019-5. L.N.V. acknowledges the project of the HSE Scientific and Educational Group (No. 962581).

## OP-III-03

# Aerogels in High Energy Physics, Collaboration of Boreskov Institute of Catalysis and Budker Institute of Nuclear Physics

Shalygin A.S.[1], Predein A.Y.[1], Savelieva M.D.[1], Katcin A.A.[2], Kononov S.A.[2,3], Kravchenko E.A.[3], Barnyakov A.Yu.[2], Danilyuk A.F.[1]

*1 – Boreskov Institute of Catalysis, Novosibirsk, Russia*

*2 – Budker Institute of Nuclear Physics, Novosibirsk, Russia*

*3 - Novosibirsk State University, Novosibirsk, Russia*

*shas@catalysis.ru*

Aerogel is a classic nanomaterial composed of few nanometers particles connected in chains forming a chaotic porous structure with pore sizes from several to hundreds of nanometers. Aerogels have a number of unique properties and characteristics: extremely low thermal conductivity (the best thermal insulation material, resistant to high temperatures), low density and high porosity (the lightest synthetic solid with high specific surface area), outstanding optical properties (low refractive index, transparency), acoustic characteristics (lowest speed of sound), etc.

Due to the unique optical properties, silica aerogels in the form of transparent blocks have found application in high-energy and nuclear physics experiments as a radiators for Cherenkov detectors. $SiO_2$ aerogels occupy an intermediate position in the refractive index scale (1.13–1.007) laying between liquids (water - 1.33) and gases (freon 114–1.0014, $CO_2$ at 10 at m. - 1.0043). This feature of aerogels gives several advantages over liquids and gases to use in Cherenkov detectors: there is no need for high pressures; the blocks are compact, convenient and easy to operate.

Aerogel blocks were synthesized in Boreskov Institute of Catalysis in collaboration with Budker Institute of Nuclear Physics. They were used in the following detectors: SND - n = 1.13 [1] and 1.05 [2], LHCb −1.03 [3] (CERN, Geneva), AMS02–1.05 [4] (for International Space Station mission), CLAS12 RICH -1.05 [5].

This report will provide a description of the unique characteristics and types of silica aerogel blocks: overall sizes, transparency, refractive index [6]. The main parameters and physical tasks of the systems based on aerogel in these experiments are presented.

**Acknowledgement:** This work was supported by the Ministry of Science and Higher Education of the Russian Federation within the governmental order for Boreskov Institute of Catalysis (project AAAA-A21–121011390053-4).

**References:**

[1] A.Y. Barnyakov and al., Nucl. Instruments Methods Phys. Res. Sect. A Accel. Spectrometers, Detect. Assoc. Equip., 598 (2009) 163.

[2] A.Y. Barnyakov and al., Instrum. Exp. Tech., 58 (2015) 30.

[3] T. Bellunato. Nucl. Instruments Methods Phys. Res. Sect. A Accel. Spectrometers, Detect. Assoc. Equip., 598 (2009) 147.

[4] M. Buénerd. Nucl. Instruments Methods Phys. Res. Sect. A Accel. Spectrometers, Detect. Assoc. Equip., 553 (2005) 264.

[5] M. Contalbrigo, E. Cisbani, P. Rossi. Nucl. Instruments Methods Phys. Res. Sect. A Accel. Spectrometers, Detect. Assoc. Equip., 639 (2011), 302.

[6] A.S. Shalygin, A.A. Katcin, A.Y. Barnyakov, A.F. Danilyuk, O.N. Martyanov. Ceram. Int., 47 (2021) 9585.

## OP-III-04

# Application of Nanotubular Titanium Dioxide for the Removal of Cr(VI) from Aqueous Solutions

Sushnikova A.A.[1], Pechishcheva N.V.[1], Zaitseva P.V.[1], Valeeva A.A.[2], Rempel A.A.[1]

*1 – Institute of Metallurgy, Ural Branch of the Russian Academy of Sciences, Yekaterinburg, Russia*

*2 – Institute of Solid State Chemistry, Ural Branch of the Russian Academy of Sciences, Yekaterinburg, Russia*

*sushnikova.ann@gmail.com*

Hexavalent chromium is an ecotoxicant found in wastewater from metallurgical companies. Photosorption (PS) on $TiO_2$ is one of methods to effectively remove chromium from aqueous solutions. $TiO_2$ is known as a photocatalyst capable of reducing Cr(VI) to less toxic Cr(III) under the action of UV irradiation [1]. The purpose of this work is to determine the effect of annealing of nanotubular titanium dioxide on its ability to reduce and adsorb chromium ions from aqueous solutions by visible light.

Nanotubular $TiO_2$ (NT-$TiO_2$) was synthesized by anodizing titanium foil on a Digma setup for 60 min at a voltage of 60 V, then mechanically separated from the substrate. $TiO_2$ nanotubes were annealed in a muffle furnace at a temperature of 350°C for 4 hours. X-ray diffraction (XRD) analysis of NT-$TiO_2$ was performed on an autodiffractometer with high statistics. The specific surface area was measured using a gas (nitrogen) adsorption analyzer. Sorption of chromium from a Cr(VI) solution with a concentration of 4 mg/L was carried out for 3 h (10 mg of sorbent per 7.5 mL of solution); without lighting - in a rotary mixer, under lighting - using a sodium lamp DNaZ-150 W. The total concentration of chromium after sorption was determined on an atomic emission spectrometer with inductively coupled plasma SpectroBlue (Spectro Analytical Instruments), the concentration of Cr(VI) was determined photometrically by the color of the complex with 1,5-diphenylcarbazide.

According to XRD analysis, the synthesized NT-$TiO_2$ has an amorphous structure. After annealing, reflections corresponding to the anatase phase are observed. The specific surface area for the synthesized NT-$TiO_2$ was 16 $m^2/g$, but annealing for 4 hours led to an increase in this value to 50 $m^2/g$.

Without exposure to irradiation, the original sample adsorbed only 6% of the total chromium. When using visible light, this value increased to 36%. Annealing of nanotubular titanium dioxide led to a significant increase in the total sorption of chromium under visible radiation, the sorption was 93%. The percentage of reduction of Cr(VI) to less toxic Cr(III) for the modified samples under the action of visible light was 100%.

**Acknowledgement:** The work was supported by the Russian Science Foundation, grant 21-73-20039.

**References:**

[1] Q. Cheng, Appl. Catal., B, 176 (2015) 740.

## OP-III-05

# Thermoelectric, Magnetic Properties and Electronic Structure of Solid Solutions $CuCr_{1-x}La_xS_2$

Korotaev E.V., Syrokvashin M.M., Filatova I.Yu.
*Nikolaev Institute of Inorganic Chemistry SB RAS, Novosibirsk, Russia*
*korotaev@niic.nsc.ru*

$CuCrS_2$-based solid solutions with a layered structure were considered as a promising functional materials demonstrated a wide range of the functional properties (thermoelectricity [1-4], ionic conductivity, magnetic properties [5], and the metal-dielectric phase transition [1-4]. The cationic substitution of the initial $CuCrS_2$-matrix with transition or lanthanide metal atoms allows one to control the functional properties. This is due to the reconstruction of the electronic structure caused by the additional contribution of the doping atom states. By analyzing the electronic structure features through theoretical and experimental techniques, it is possible to predict and optimize the functional properties of these compounds. The present study comprehensively examines the data obtained from both the experimental effective element selective XPS spectroscopy technique and DFT calculations. The cationic substitution with lanthanide ions is of particular interest, since lanthanide chalcogenides demonstrate promising functional properties, which are primarily determined by the filling and contributions of Ln4*f* levels. It was previously reported, that the cationic substitution of Cr with La ions leads to the electronic structure reconstruction of the initial $CuCrS_2$-matrix and to the greatest increase the Seebeck coefficient value for $CuCr_{0.99}Ln_{0.01}S_2$ (Ln = La ... Lu) solid solutions [1, 3, 4]. Current work involved an analysis of both the experimental and calculated data to study the correlation between the electronic structure features and the functional properties of $CuCr_{1-x}La_xS_2$. The obtained data on the thermoelectric and magnetic properties for $CuCr_{1-x}La_xS_2$ ($x = 0 \div 0.03$) were compared with the results of quantum chemical calculations of the partial density of states of Cu, Cr, La, S atoms and experimental XPS data.

**Acknowledgement:** This study was funded by the Russian Science Foundation (project No. 19-73-10073). The authors acknowledge the Ministry of Science and Higher Education of the Russian Federation.

**References:**

[1] Korotaev E.V, Syrokvashin M.M., Filatova I.Yu. et al., Materials 16 (2023) 2431.
[2] Korotaev E.V., Syrokvashin M.M., Filatova I.Yu. et al., J. Electron. Mater. 47 (2018) 3392.
[3] Korotaev E.V, Syrokvashin M.M., Filatova I.Yu. et al., Sci. Rep. 11 (2021) 18934.
[4] Korotaev E.V., Syrokvashin M.M., Filatova I.Yu. et al., Materials 15 (2022) 8747.
[5] Korotaev E. V, Syrokvashin M.M., Filatova I.Yu., et al. Materials 14 (2021) 5101.

## OP-III-06

# Ultrathin Carbon Layer-Coated Mn-Based Ion Sieve for Lithium Extraction by Electrosorption Method

Xu Xiang
*State Key Laboratory of Chemical Resource Engineering,*
*Beijing University of Chemical Technology, Beijing 100029, China*
*xiangxu@mail.buct.edu.cn*

Around 60% of global lithium resources come from salt-lake brine. Lithium extraction from salt-lake brine is critical to maintain a sustainable supply of lithium and meet its increasing demand for use in electric vehicles and large-scale energy storage devices. Among various methods, the membrane and adsorption are two main methods for lithium extraction. However, it remains a great challenge to separate Li+ ions from coexisting $Na^{+}$, $Mg^{2+}$, and $^{K+}$ ions in the salt-lake brine because of high concentrations of coexisting ions and low concentrations of Li+ ions.[1-2] The electrosorption is a promising method for low-grade lithium extraction because it combines the adsorption with external electric field.[3] Here, we propose a combined strategy of a core−shell structure and hydrophilic modification of a $Li_{1.6}Mn_{1.6}O_4$ electrode to efficiently extract lithium from brine with a high sodium content. The core−shell $Li_{1.6}Mn_{1.6}O_4$@carbon was derived from polydopamine-encapsulated Li1.6Mn1.6O4 via calcination. The carbon shell of ∼2 nm protects Mn from leaching during lithium extraction. Compared with bare $Li_{1.6}Mn_{1.6}O_4$, the lithium extraction capacity of the modified electrode increases from 20 to 39.6 mg/g in a brine with a high Na/Li ratio of 44.78. The coating of polydopamine on the $Li_{1.6}Mn_{1.6}O_4$@carbon electrode reduces the water contact angle from 119 to 86.9°, resulting in a hydrophilic surface. Using an electrochemical adsorption method, the lithium extraction capacity and desorption ratio reach 65.6 mg/g and 86.0%, respectively, which outperforms the present membrane capacitive deionization and electrochemical methods.

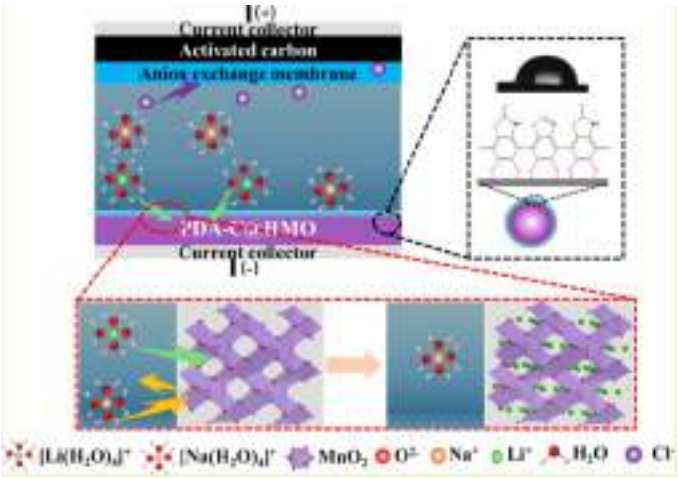


*Fig. 1. Schematic of Lithium Extraction Using the Core@Shell Ion Sieve Membrane via Electrosorption Method*

The modified electrode shows high lithium-ion selectivity and excellent stability due to the reversible redox reactions during lithium extraction/desorption. The strategy proposed here guides the way to the structural design of electrodes for efficient separation of lithium from brine. Future work could focus on the multifunctional modification of the electrode structure to increase both the ion migration and affinity.

**Acknowledgement:** This work was supported by the National Natural Science Foundation of China (grants U20A20138).

**References:**

[1] Song, J. F.; Nghiem, L. D.; Li, X.; He, T., Environ. Sci.: Water Res. Technol. 3 (2017) 593−597.
[2] Sun, Y.; Wang, Q.; Wang, Y.; Yun, R.; Xiang, X., Sep. Purif. Technol. 256 (2021) 117807.
[3] Zhang J., Cheng Z., Qin X., Gao X., Wang M., Xiang, X., Desalination 547 (2023) 116225.

## OP-III-07

# Thermodynamics of Long-Term Adsorption Storage System of Liquefied Natural Gas Vapors Based on Advanced Mesoporous Carbon Xerogel

Menshchikov I.E., Shkolin A.V., Khozina E.V., Grinchenko A.E., Fomkin A.A.
*Frumkin Institute of Physical Chemistry and Electrochemistry, Moscow, Russia*
*i.menshchikov@gmail.com*

Liquefied natural gas is one of the most important and reliable energy carriers; it has such advantages as high energy capacity, eco-friendliness and excellent logistics capabilities [1]. However, its storage in a cryogenic state (at a temperature of ~ 111 K) requires special techniques to protect from boil-off gases (BOG), which emerge due to external heat flow inside a cryogenic vessel or during the refueling process [2]. BOGs are usually released into the atmosphere via protective valves or simply burned in a gasification unit if their rational utilization or recovery is impossible. Such a scenario leads both to gas wastage and greenhouse gas emissions. Therefore, a method of capturing and storing LNG vapors in the adsorbed state is envisioned as an effective way to improve the LNG terminal performance.

A synthetic carbon xerogel (CX) was proposed as a promising adsorbent for methane (one of the main component of BOGs) vapors in the LNG terminal combined with an adsorbed natural gas module (ALNG). The textural properties of CX were investigated by x-ray diffraction, scanning electron microscopy, and low-temperature nitrogen adsorption. Methane adsorption equilibria onto CX were evaluated within a range of absolute pressures from 5 Pa to 10 MPa and at the temperatures varied from 111.7 to 393 K employing semi-automatic bench designed in the laboratory of sorption processes (IPCE RAS) [3, 4]. An approach based on the theories of volume filling of micropores, monolayer capacity on the mesopore surface, and the capillary condensation in the mesopores was applied to the experimental data on methane adsorption to evaluate the adsorption capacity of CX over the sub- and supercritical *P,T*-ranges. A comparison of the adsorption performances of CX and several commercial activated characterized by a wider pore size distribution compared to CX made it possible to identify a difference in the optimal operational conditions of their application for the LNG-ANG technology.

Based on the adsorption data, the thermodynamic functions of the CX/$CH_4$ system, such as differential molar isosteric heat of adsorption $q_{st}$ (kJ·mol$^{-1}$), entropy $S_a$ (kJ·mol$^{-1}$K$^{-1}$) and heat capacity $C_a$ (kJ·kg$^{-1}$K$^{-1}$), were calculated using the Bakaev approach [4], taking into account a non-ideality of the gas phase, thermal and adsorption non-inertness (deformation) of the adsorbent. For this purpose, the adsorption- and thermal-induced deformations of the CX sample were measured experimentally *in-situ* on a laboratory dilatometer of induction type attached to a high-pressure adsorption bench [5] over the temperature range from 213 to 393 K.

Figure 1 shows the experimental and calculated adsorption isotherms of methane on the CX adsorbent for super- (*a*) and subcritical (*b*) conditions. It is evident that the capillary

condensation effect plays a crucial role in selecting temperature regimes for a cyclic performance of the ALNG system.

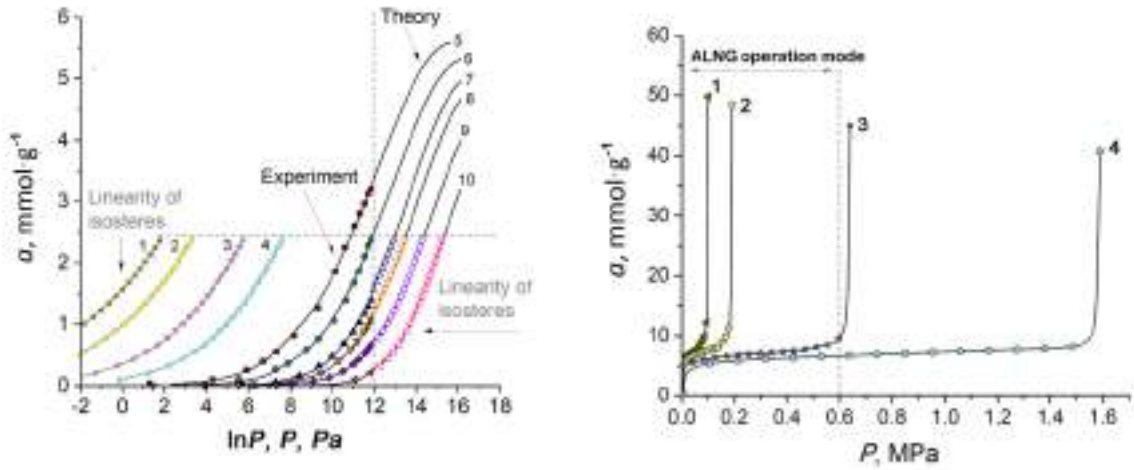


*a* *b*

*Fig. 1. Dependence of methane adsorption onto CX on pressure in semi-logarithmic (a) and a-P (b) coordinates at temperatures, K: 111.7 (1), 120 (2), 140 (3), 160 (4), 213 (5), 243 (6), 273 (7), 293 (8), 333 (9), and 393 (10).*

The calculations using the data on methane adsorption and the porous structure of CX revealed that the adsorbent could be efficient for the capture of LNG vapors in the ALNG combined system at the operational temperatures up to 138.7 K. Under these operational conditions, the methane adsorption proceeds through the mechanisms of volume filling of micropores, formation of monolayers on the surface meso- and macropores, and capillary condensation in mesopores, which accounted for up to 80 % of the total methane uptake. The total adsorption capacity of the ANG system loaded with the CX adsorbent achieves the extraordinary value of 540 $m^3(NTP)\cdot m^{-3}$ at the boiling point of methane because of the capillary condensation in mesopores.

It was found that for the maximum gas discharge from the system loaded with CX; it is enough to raise the temperature of the storage system by a few degrees, up to 140 K. However, if a working temperature in the ALNG tank exceeds 140 K, the adsorbents with a higher fraction of transitional pores with a size ranging from 2 to 3 nm (or supermicropores) and a wide size distribution of mesopores are more efficient compared to the CX adsorbent.

**Acknowledgement:** This work was supported by the Russian Science Foundation, grant 22-73-00184.

**References:**

[1] Global and Russian Energy Outlook 2019. Makarov, A., Mitrova, T., Kulagin, V. (eds); ERI RAS – Moscow School of Management SKOLKOVO, Moscow (2019).
[2] V.M. Markova, V.N. Churashev, Int. J. Econ. Manag., 20 (3), 108–138 (2020).
[3] A.V. Shkolin, A.A. Fomkin, Meas. Tech. 61. 395-401 (2018).
[4] A.V. Shkolin, A.A. Fomkin, I.E. Men'shchikov et al. RF patent No. 2732199, Bul. No. 26 (2020).
[5] A.V. Shkolin, A.A. Fomkin et al. Instrum. Exp. Tech. 51, 150-155 (2008).

## OP-III-08

# Enantioselective Voltammetric Sensors Based on New Chiral Materials

Yarkaeva Y.A., Nazyrov M.I., Maistrenko V.N.
*Ufa University of Science and Technology, Ufa, Russia*
*julijajarkaeva05@gmail.com*

The history of research on the development and application of easy-to-manufacture and cheap enantioselective voltammetric sensors (EVS) for express recognition and determination of optically pure biologically active compounds indicates that progress in the creation of EVS with the required operational and analytical characteristics is associated primarily with using new chiral materials. The use of such materials makes it possible to significantly increase the sensitivity and selectivity of EVS to enantiomers, as well as the reliability of their recognition in real objects [1-2]. In particular, this can be facilitated by the modification of the electrode surface with materials based on homochiral or chiral ligand-modified zeolites, the structure of which contains micro-, meso- and macropores (hierarchical porous structures), as well as their composites with electrically conductive polymers, metal complexes with optically active ligands, etc. Enantioselectivity in such sensors can be due to both the initial chirality of the selector and its modification with chiral or prochiral ligands, as well as the asymmetric arrangement of achiral ligands. In addition, among porous materials that are promising in the creation of EVS, mesoporous carbon and nanostructured carbon black are of interest, which have chemical inertness, high electrical conductivity and high specific surface area, as well as a pore structure ordered at the nanoscale level, which ensures high mass transfer rates [3]. The physical and chemical properties of such materials can be significantly improved by modifying the pores with various components (including chiral ones). The report presents extensive information about materials with micro-, meso- and macroporous structure used in EVS. The results of using such materials (in particular, zeolites, mesoporous graphitized carbon black with chiral selectors immobilized on the surface, etc.) in sensors for recognition and determination of enantiomers of biologically active compounds, manufacturing features, sensor surface morphology, electrochemical and analytical characteristics of sensors are also presented.

**Acknowledgement:** This work was supported by the Russian Science Foundation, grant 21-13-00169.

**References:**

[1] Y. Yarkaeva, V. Maistrenko, L. Zagitova, M. Nazyrov, T. Berestova. Voltammetric sensor system based on Cu(II) and Zn(II) amino acid complexes for recognition and determination of atenolol enantiomers. J. Electroanal. Chem. 2021. Vol. 903. P. 115839.
[2] L. Zagitova, V. Maistrenko, Y. Yarkaeva, V. Zagitov, R. Zilberg, P. Kovyazin, L. Parfenova. Novel chiral voltammetric sensor for tryptophan enantiomers based on 3-neomenthylindene as recognition element. J. Electroanal. Chem. 2021. Vol. 880. P. 114939.
[3] Y. Yarkaeva, M. Nazyrov, Y. Abdullin, P. Kovyazin, V. Maistrenko. Enantioselective voltammetric sensor based on mesoporous graphitized carbon black Carbopack X and fulvene derivative. Chirality. 2023. P. 1–12.

## OP-III-09

# Development of Polymer-Ceramic Li-Conducting Membranes for Li-Metal Hybrid Flow Batteries

Akhmetov N.O.[1], Stevenson K.J.[2]
*1 – Skolkovo Institute of Science and Technology, Moscow, Russia*
*2 – Lomonosov Moscow State University, Moscow, Russia*
*nikita.akhmetov@skoltech.ru*

Lithium-metal hybrid redox flow batteries (Li-HFBs, Fig. 1a), composed of a metallic Li anode and non-aqueous flowing catholyte, are a prospective type of energy storage devices suitable for stationary applications. Accumulating energy from both conventional and renewable sources, the Li-HFBs can either compensate energy drawbacks or mitigate its excess. Beside advantages of conventional redox flow batteries (RFBs) — ease of scaling, independent control of power and capacity — the Li-HFBs possess the simplified architecture (no anolyte tank) and boosted power density due to extremely low electrochemical potential of Li metal. The main challenge impeding the development of the Li-HFBs is a lack of a highly conductive, stable, selective, and affordable membrane that impacts the battery's capacity retention, energy efficiency, and power. One of the prospective membrane classes is the polymer-ceramic composite. In such type, the ceramic filler provides a composite membrane with high ionic conductivity (IC), whereas the polymer matrix protects the filler from environment, improves flexibility, and makes the membrane robust and dense. In this work, we report the advances achieved in the field of developing the composite membrane — $Li_{1.3}Al_{0.3}Ti_{1.7}(PO_4)_3$+poly(vinylidene fluoride) (LATP+PVdF) — for the Li-HFBs.

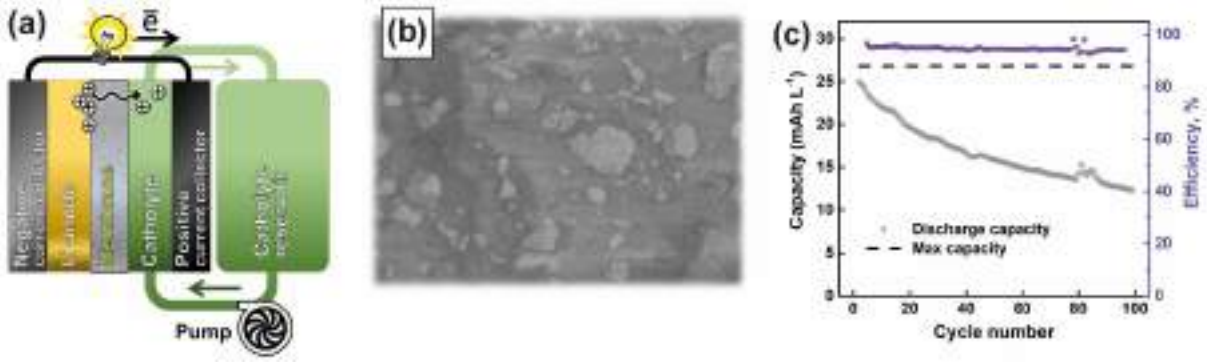


*Fig. 1. (a) Schematic representation of the Li-metal hybrid flow battery. (b) Scanning electron microscopy image of the LATP+PVdF membrane surface. (c) Discharge capacity and coulombic efficiency of the Li-TEMPO cell cycled at 0.5 mA.*

In the last four years, we have come a long way from synthesizing stable NASICON-type LATP ceramic, through optimizing LATP+PVdF's properties, to prototyping the Li-HFB cell equipped with the final composite membrane. In the first part of this report, we describe the optimization of composite membrane's properties varying fabrication parameters: composition, components' pretreatment and mixing procedure, casting solvent, temperature regime, drying conditions, etc. Throughout the work, we assessed the membrane advances

through the prism of its critical properties: IC, selectivity (permeability to catholyte's redox active species), and components stability. The membranes were characterized by the strong set of methods including XRD, FTIR, SEM, EDX, Raman; impedance spectroscopy, cyclic voltammetry, galvanostatic cycling. A specific attention was devoted to the suppression of composite's porosity — the source of the severe membrane's permeability and cell's crossover observed in early stages of the development. The finally optimized LATP+PVdF membranes show mechanical flexibility and robustness (Fig. 1b), promising IC ($1.1\text{-}3.4 \cdot 10^{-4}$ S cm$^{-1}$), low permeability ($0.86 \cdot 10^{-7}$ cm$^2$ min$^{-1}$), and superior stability: electrochemical (>4.7 V), chemical (no phases degradation), and structural (no severe changes in ceramic's cell parameters).

In the second part, we tested the cycling performance of the modified composites in the lithium-(2,2,6,6-tetramethylpiperidin-1-yl)oxyl (Li-TEMPO) hybrid flow cell. Employing a carbonate LiTFSI-based catholyte, after 100 charge/discharge cycles we achieved the decrease of the capacity fade rate from *ca.* 0.79 (initial fabrication route) to 0.35% h$^{-1}$ (modified route). The retention time for 80% of initial cell capacity was drastically prolonged from 8 to 37 h. During the performance test of LATP+PVdF in the Li-TEMPO HFB cell, coulombic efficiency was higher than 94%, whereas no significant changes were observed neither in total cell resistance nor for the membrane's morphology, phase and chemical composition, etc. After 50 cycles, the Li-TEMPO cell retained 70% of initial capacity (Fig. 1c) that is close to the literature data reported for this battery type [1-3].

Finally, we summarize all the advances have been made toward the polymer-ceramic LATP+PVdF development for Li-HFBs. Assuming that the main work on the membrane optimization is almost completed, we emphasize the specific issues associated with the catholyte and cell design to be further overtaken to enhance the performance of Li-HFBs. Overall, the developed class of LATP+PVdF membranes has proved to be quite promising for the Li-HFBs.

**Acknowledgement:** This work was supported by the Skoltech-MIT Next Generation Program "Development of Models for Precise State of Health Determination During Vanadium Flow Battery Operation".

**References:**

[1] B. Ok, W. Na, T.H. Kwon, Y.W. Kwon, S. Cho, S.M. Hong, A.S. Lee, J.H. Lee, C.M. Koo, J. Ind. Eng. Chem. 80 (2019) 545–550.
[2] K. Takechi, Y. Kato, Y. Hase, Adv. Mat. 27 (2015) 2501–2506.
[3] W. Wang, W. Xu, L. Cosimbescu, D. Choi, L. Li, Z. Yang, Chem. Com. 48 (2012) 6669–6671.

## OP-III-10

# Electrochemical Properties of Composite Solid Electrolytes Based on $NaNO_2$ and Aerogel Oxides

Shivtsov D.M.[1], Ilyina E.V.[1], Mateyshina Yu.G.[2], Pochtar A.A.[1], Bedilo A.F.[1]
*1 – Boreskov Institute of Catalysis, Novosibirsk, Russia*
*2 – Institute of Solid State Chemistry and Mechanochemistry, Novosibirsk, Russia*
*danil@catalysis.ru*

To create solid-state electrochemical devices, it is necessary to develop new types of solid electrolytes. Compared to liquid and polymer electrolytes, solid electrolytes are characterized by high mechanical strength. At the same time they are characterized by rather low ionic conductivity [1, 2]. The transition to composite solid electrolytes of the "ionic salt-inert additive" type makes it possible to influence the characteristics of electrolytes by varying the composition of the inert additive and its concentration. The use of alkali metal salts as ionic components of composite solid electrolytes is preferable due to their possible practical application. Currently, the attention of researchers is focused on finding an alternative to lithium electrolytes, such as sodium or potassium electrolytes. For example, $NaNO_2$ is thermally stable up to 271 °C, which makes it possible to consider it as a potential ionic salt in a solid composite electrolyte.

Various nanocrystalline oxides (MgO, $SiO_2$, $Al_2O_3$, etc.) are introduced as inert additives to increase the ionic conductivity of the salt. Oxides must have high specific surface areas, be chemically and thermally stable. The ion transfer in such systems occurs across the phase boundaries [3]. $NaNO_2$-$SiO_2$ nanoscale composite has high electrical conductivity and low activation energy. With an average silicon oxide pore diameter of ≈ 7 nm, the electrical conductivity at T = 455 K reached ≈ $7 \cdot 10^{-4}$ S/cm, compared to $3.6 \cdot 10^{-6}$ S/cm without an inert additive [4].

In this work, it is proposed to investigate the effect of two oxide additives $Al_2O_3$ and MgO on the properties of $NaNO_2$. The oxide materials have been synthesized using the aerogel technology, which makes it possible to obtain nanocrystalline samples characterized by a developed specific surface area and porous structure [5].

At the first stage, freshly prepared magnesium methoxide in toluene solution was used for the synthesis of magnesium oxide, while aluminum isopropoxide dissolved in isopropanol was used for the synthesis of aluminum oxide. The gel was obtained by hydrolysis of these solutions with a stoichiometric amount of water while stirring for 16 hours. The resulting systems were placed in an autoclave heated for 3 hours to 270 °C, the pressure in which reached 80-95 atm. Under these conditions, the surface tension decreases, which allows maintaining a high specific surface area and porosity. The synthesized aerogel samples were calcined in a flow reactor in an argon atmosphere at 500 °C for MgO and 600 °C for $Al_2O_3$.

Table 1 – Structural characteristics of aerogel oxides

| Inert additive | SSA, $m^2/g$ | $V_{pore}$, $cm^3/g$ | $D_{av}$, нм |
|---|---|---|---|
| MgO | 330 | 1.9 | 24 |
| $Al_2O_3$ | 370 | 1.8 | 19 |

For the synthesis of composites (1-x)$NaNO_2$-x$Al_2O_3$ and (1-x)$NaNO_2$-xMgO an inert additive was preactivated at 500°C. Then, $Al_2O_3$ (MgO) and $NaNO_2$ were mixed in a stoichiometric ratio, followed by several iterations of grinding in a mortar and heat treatment at 250 °C for 30 minutes.

The obtained composites were studied by a complex of physicochemical methods (XRD, DSC and impedance spectroscopy). To study the transport properties, tablets made of composites with two silver electrodes were pressed. The electrical conductivity was measured using a two-electrode circuit under vacuum ($5 \cdot 10^{-2}$ mmHg) in the temperature range of 35-225 °C. It was shown that the conductivity of composites is ionic in the entire studied composition range ($0 < x < 1$). By means of heterogeneous doping, it is possible to increase the conductivity value by up to four orders of magnitude compared to the initial salt. The obtained results demonstrate that $Al_2O_3$ and MgO aerogels are promising materials for use as additives to $NaNO_2$ in solid electrolytes.

**Acknowledgement:** This research was funded by the Ministry of Science and Higher Education of the Russian Federation within the governmental order for the Boreskov Institute of Catalysis (project AAAA-A21-121011390054-1).

**References:**

[1] Yu. Mateyshina, N. Uvarov, Solid State Ion. 302 (2017) 77-82.
[2] Yu. Mateyshina, A. Slobodyuk, V. Kavun, N. Uvarov, Solid State Ion. 324 (2018) 196-201.
[3] Yu. Mateyshina, D. Alekseev, V. Khusnutdinov, N. Uvarov, Mater. Today 12 (2019) 13-16.
[4] L. Korotkov, V. Dvornikov, M. Vlasenko, T. Korotkova, A. Naberezhnov, E. Rysiakiewicz-Pasek, Ferroelectr. 444 (2013) 100-106.
[5] E. Ilyina, I. Mishakov, A. Vedyagin, S. Cherepanova, A. Nadeev, A. Bedilo, K. Klabunde, Micropor. Mesopor. Mater. 160 (2012) 32-40.

## OP-III-11

# Single-Phase vs. Two-Phase Intercalation Pathways in Polyanion-Type Cathode Materials for Low-Temperature Sodium-Ion Batteries

Komayko A.I.[1], Shraer S.D.[1], Fedotov S.S.[1], Nikitina V.A.[1,2]
*1 – Skolkovo Institute of Science and Technology, Moscow, Russia*
*2 – Lomonosov Moscow State University, Moscow, Russia*
*alena.komayko@skoltech.ru*

The scarcity of lithium resources has led to the search for alternatives to lithium-ion batteries in the battery market. Sodium-ion batteries (SIBs) have emerged as a viable option due to the abundant supply of sodium in the earth's crust and seawater. Among various SIB cathode materials, $Na_3V_2(PO_4)_2F_3$ has attracted much attention as a promising candidate for high-energy applications [1]. Nevertheless, the presence of a third sodium ion as a "dead weight" limits its specific capacity: this issue was successfully addressed by synthesizing a $KTiOPO_4$-type $NaVPO_4F$, which demonstrated enhanced performance at room temperature in terms of energy density and capacity retention [2].

The two materials, $Na_3V_2(PO_4)_2F_3$ and $NaVPO_4F$, follow different intercalation pathways: biphasic reactions, involving nucleation and growth of new phases are observed for $Na_3V_2(PO_4)_2F_3$, while $NaVPO_4F$ operates via a solid solution mechanism in a wide range of states-of-charge. In this study, we provide a comprehensive kinetic analysis of the main factors, that limit the performance of these materials, and compare the extent, to which they are affected by extreme conditions. By using materials with identical morphologies and particle size distributions we were able to isolate polarization effects characteristic of the two-phase mechanism and quantify contributions of diffusion, charge transfer, nucleation, and phase growth to the performance losses at low temperatures.

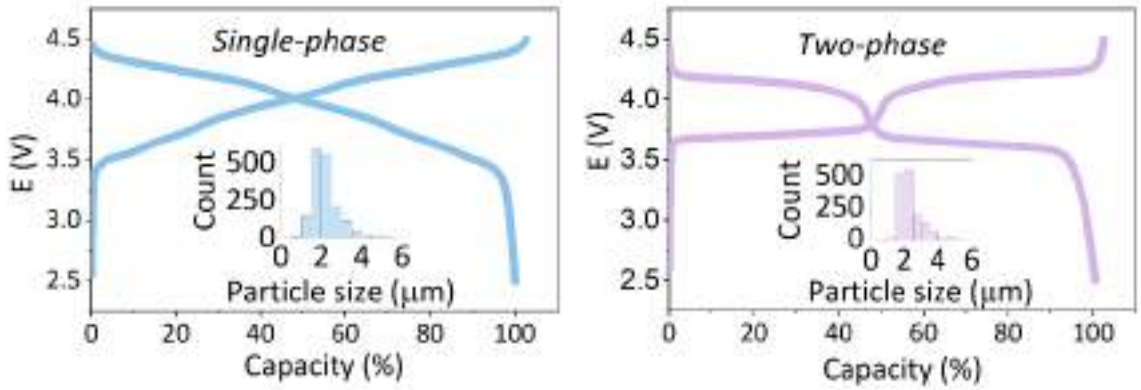


*Fig. 1. Discharge profiles of the materials and size distributions (as insets).*

**Acknowledgement:** This work is supported by Russian Science Foundation (grant 20-73-10248) and by the Center for Energy Science and Technology of Skolkovo Institute of Science and Technology.

**References:**

[1] L. Zhu, H. Wang, D. Sun, Y. Tang, H. Wang J. Mater. Chem. A 8 (2020) 21387.
[2] S.D. Shraer, N.D. Luchinin, I.A. Trussov, et al Nat. Commun. 13 (2022) 4097.

## OP-III-12

# Hydrolytic Oxidation of Cellobiose using Catalysts Containing Noble Metals

Manaenkov O.V.[1], Kislitsa O.V.[1], Sidorov A.I.[1], Demidenko G.N.[1], Nikoshvili L.Zh.[1], Matveeva V.G.[1,2]

*1 – Tver State Technical University, Tver, Russia*

*2 – Tver State University, Tver, Russia*

*ovman@yandex.ru*

The products of glucose oxidation (gluconic and glucaric acids) are in-demand substances. In particular, gluconic acid is widely used in the food, pharmaceutical, metallurgical, and textile industries [1]. The demand for gluconic acid is constantly growing, and it is expected that by 2024, its consumption will reach 120 thousand tons per year [2]. Gluconic acid can be obtained via oxidation of glucose with chemical methods using heterogeneous catalysts, for example, based on gold nanoparticles [3], or with electrochemical methods associated with the use of electrodes made of noble metals [4]. However, the use of these methods in large-scale production is limited due to the harmful impact on the environment due to the high cost of catalysts, the likelihood of their deactivation, and the need for recycling or recovery [4]. More opportunities open up when enzymes are used [4, 5]. However, the most promising is the production of gluconic acid with a biotechnological method, although some researchers also note the disadvantages of this option—a long fermentation process (15–24 h) and high operating costs [5].

The promise of using the possibilities of heterogeneous catalysis for the synthesis of aldonic and aldaric acids from cellobiose is confirmed by the results of some works. For example, Morawa Eblagon et al. [6] used a 1 wt % Au/CX5.6 air citric catalyst for the conversion of cellobiose to gluconic acid with a selectivity of 80 % (T = 418 K, 100 mL of 12 mM/L of cellobiose in water, 75 min, $O_2$ 5 bar). It was shown that among the decisive factors determining the efficiency of the process are the adsorption properties and porosity of the support, which should be taken into account when developing multifunctional catalysts. In the study [7], a series of bimetallic catalysts, Au-M (M = Cu, Co, Ru, and Pd), based on $TiO_2$ were synthesized. The maximum selectivity for gluconic acid (88.5 %) was obtained under the following conditions: cellobiose, 0.6 mmol; catalyst (Cu–Au/$TiO_2$), 0.100 g; $H_2O$, 20 mL; $O_2$, 1 MPa; 145 °C. On the basis of the obtained kinetic data, the authors proposed a reaction route. It was suggested that cellobiose is converted to cellobionic acid; then, gluconic acid is formed due to the cleavage of the β-1,4 glycosidic bond in cellobionic acid.

In this study, for the process of the hydrolytic oxidation of cellobiose to gluconic and glucaric acids, heterogeneous catalytic systems based on support containing noble metals (Pt, Au, Ru, Pd) were proposed.

The study of the synthesized catalysts with the method of hydrogen chemisorption showed that the Pt-containing catalyst was characterized by a significantly larger number of active centers adsorbing hydrogen (Figure 1). As can be seen from the data, the concentration

of active centers on the surface of 3% Pt/HPS MN270 exceeded similar indicators for other catalysts, on average, by six times. This fact can explain the higher activity of the Pt-containing catalyst in the reaction under study compared with catalysts containing other noble metals.

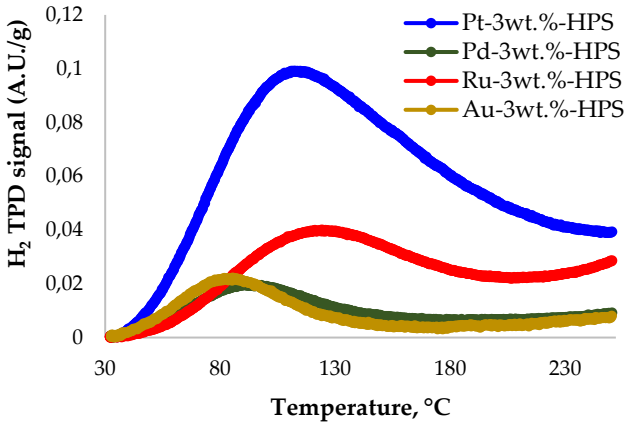


*Fig. 1. Results of TPD analysis of catalysts supported on HPS MN 270*

As a result of the study, an assessment was made of the possibility of using heterogeneous catalysts based on noble metals (Pt, Pd, Au, Ru) in the hydrolytic oxidation of cellobiose to gluconic and glucaric acids. The use of Pt-containing catalytic systems in this reaction was shown to be promising. The optimal process conditions were determined as follows; at a temperature of 145 °C, an $O_2$ pressure of 5 bar, and a substrate/catalyst mass ratio of 4/1, the yields of gluconic and glucaric acids reached 21.6 and 63.4 %, respectively, at 100 % cellobiose conversion. The formal description of the kinetics of cellobiose hydrolytic oxidation was obtained. The mathematic model of cellobiose conversion to gluconic and glucaric acids in the presence of 3% Pt/HPS MN270 was proposed. The kinetic parameter estimation was performed according to the model developed. The results obtained can be further used to create a technology for the catalytic conversion of plant polysaccharides, primarily cellulose, into aldonic and aldaric acids, which are widely used in the chemical, food, pharmaceutical, and other industries.

**Acknowledgement:** This work was supported by the Russian Science Foundation, project 23-79-00009.

**References:**

[1] Sulman A., Matveeva V., Golikova E., Grebennikova O., Lakina N., Doluda V., Karpenkov A.Y., Sulman E. Chem. Eng. Trans. 74 (2019) 487.
[2] Neves L.C.M.D., Vitolo M. World J. Pharm. Pharm. Sci. 9 (2020) 423.
[3] Lim H.Y., Dolzhenko A.V. Sustain. Chem. Pharm. 21 (2021) 100443.
[4] Ma Y., Li B., Zhang X., Wang C., Chen W. Front. Bioeng. Biotechnol. 10 (2022) 864787.
[5] Fernandes S., Belo I., Lopes M. Biochem. Eng. J. 175 (2021) 108133.
[6] Amaniampong P.N., Jia X., Wang B., Mushrif S.H., Borgna A., Yang Y. Catal. Sci. Technol. 5 (2015) 2393.
[7] Armstrong R.D., Hirayama J., Knight D.W., Hutchings G.J. ACS Catal. 9 (2019) 325.

## OP-III-13

# Catalytic Etching and Oxidation of Pt, Pd and Rh in $O_2$ and During $NH_3$ Oxidation at 1133 K

Salanov A.N., Serkova A.N., Zhirnova A.S., Isupova L.A.
*Boreskov Institute of Catalysis, Novosibirsk, Russia*
*salanov@catalysis.ru*

Pt, Pd and Rh are used to obtain alloys that are employed in the production of metal gauze catalysts. Platinum alloy gauzes with the predominant content of platinum are applied in the industrial high-temperature oxidation of ammonia with air oxygen to nitrogen oxide NO, which is used to produce nitric acid [1]. The world's annual production of $HNO_3$ reaches 70–80 million tons. Nearly 80% of the produced acid is consumed to manufacture agricultural fertilizers. We present the results on the oxidation and etching of Pt, Pd and Rh polycrystalline foils (Pt(poly), Pd(poly) and Rh(poly)) after annealing in the $O_2$ atmosphere and $NH_3$ oxidation with air at $P$ ~ 3.6 bar and ca. 1133 K for $t \leq 10$ h. The study was performed using scanning electron microscopy (SEM), energy-dispersive X-ray spectroscopy (EDS) and X-ray diffraction (XRD). The study aimed to obtain new data on the morphology, composition and structure of the etched layers formed upon annealing in $O_2$ and $NH_3$ oxidation on Pt, Pd and Rh. Particular attention was paid to revealing the role of these metals and their oxidation in the nucleation and growth of etching structures during $NH_3$ oxidation. The data obtained made it possible to comprehensively analyze the process of catalytic etching on Pt alloy gauzes initiated by the oxidation of $NH_3$.

After $NH_3$ oxidation on Pt(poly), Pd(poly) and Rh(poly) at 1133 K for 1, 5 and 10 hours, various etched structures, which formed during the catalytic etching, were detected on the surface. Figure 1 displays images of the most typical fragment of etched layers on Pt(poly) (a,b) after $NH_3$ oxidation at 1133 K for 1 h. Images in Figures 1a,b show the etched structure of the metal surface, which forms during the catalytic oxidation of $NH_3$. In Figures 1a,b, one can see regions with hollows (A), which are associated with the segregation of Pt atoms, and pyramidal structures (B), which grow during the catalytic etching. For Pd(poly), images show the etched layer consisting of the metal-oxide fibrous phase, which is formed in the reaction of $NH_3$ molecules with the PdO oxide-oxygen. These images demonstrate fragments of the fibers with a diameter of 25–50 nm and particles with a size of 5–20 nm. For Rh(poly), mages show the nucleation and growth of the fibrous phase in the reaction of $NH_3$ molecules with the oxygen of $Rh_2O_3$ oxide. $Rh_2O_3$ oxide particles with the size of 200–300 nm and nuclei of the growing fibrous phase with the size of ca. 50 nm are detected. Such images demonstrate the etched layers that are formed at the very beginning of the etching process.

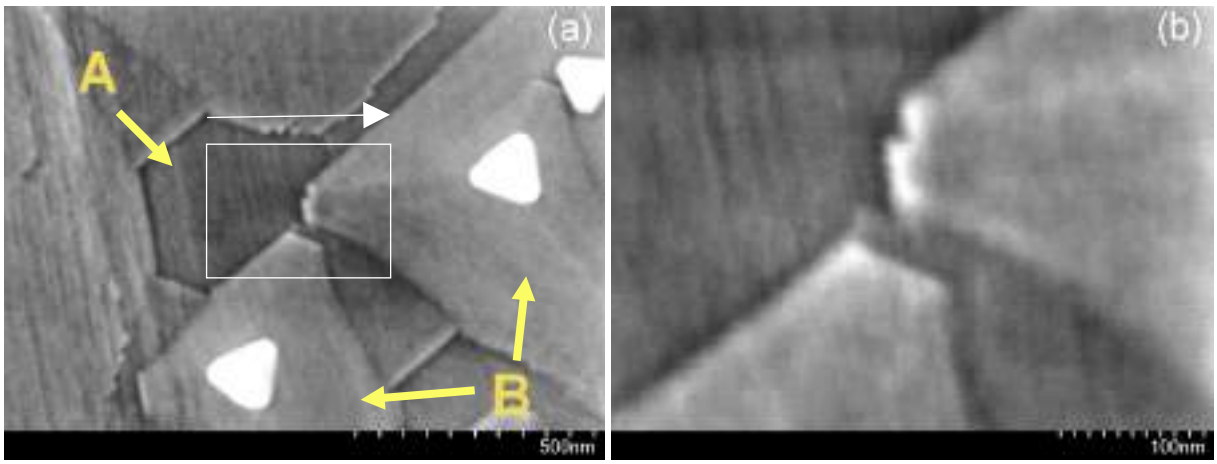


*Fig. 1. SEM images of the Pt(poly) (a,b) surface after $NH_3$ oxidation with air at T = 1133 K for 1 h. Images were obtained in SE mode at $E_0$ = 5 keV and ×100 k (a), ×300 k (b) magnifications using high-resolution SEM (Regulus 8230, Hitachi, Japan).*

According to SEM, EDS and XRD data, during annealing in $O_2$ and $NH_3$ oxidation, platinum was in the metallic state; particles or crystals of $PtO_2$ oxide were not detected. In the course of the reaction between $O_{ab}$ and $N_{ab}$ atoms migrating to the surface, "hotspots" are formed on the defects; as a result, Pt atoms are segregated to the surface. These processes lead to the formation of etch pits and facets; they can be the nuclei of etched structures on Pt. The $Rh_2O_3$ oxide layer is retained on the Rh(poly) surface for the entire period of annealing in $O_2$ and $NH_3$ oxidation. The reaction of $NH_3$ molecules with the oxygen of $Rh_2O_3$ oxide leads to the release of NO molecules into the gas phase and the segregation of $Rh^0$ atoms to the oxide layer surface. The migrating $Rh^0$ atoms can form particles/crystals with the size of 25–50 nm on the $Rh_2O_3$ surface, which can serve as the nuclei of metal-oxide nanofibers, nanocrystals and pyramidal crystals forming the etched structures on Rh. On Pd(poly), a continuous nonuniform oxide layer of PdO particles was detected after annealing in $O_2$, whereas fibrous agglomerates and palladium "cauliflowers" appeared after $NH_3$ oxidation. The revealed surface morphology, chemical composition and structural characteristics indicate that $NH_3$ oxidation proceeds on PdO oxide at the onset of the process ($t$ = 1 h) and then on metallic palladium ($t$ = 5 h).

**Acknowledgement:** This study was financially supported by the Ministry of Sciences and Higher Education of the Russian Federation under the government contract at the Institute of Catalysis, Siberian Branch, Russian Academy of Sciences (project no. AAAA-A21-121011390053-4). The studies were carried out using facilities of the shared research center «National center of investigation of catalysts» at Boreskov Institute of Catalysis.

**References:**

[1] Karavayev, M.M.; Zasorin, A.P.; Kleshchev, N.F. Catalytic Oxidation of Ammonia; Khimia: Moscow, Russia, 1983; pp. 30–122.

## OP-III-14

# Combined $H_2O$ and $CO_2$ Reforming of Methane over Ni Based $CeO_2$-MgO Catalysts: Impacts of Preparation Mode and Pd Addition

Okhlopkova L.B.[1], Prosvirin I.P.[1], Kerzhentsev M.A.[1], Sukhova O.B.[1], Ismagilov Z.R.[1,2]
*1 – Boreskov Institute of Catalysis, Novosibirsk, Russia*
*2 – Federal Research Center of Coal and Coal-Chemistry SB RAS, Kemerovo, Russia*
*mila65@catalysis.ru*

The preferred use of fossil fuels to meet energy demands has created environmental concerns due to significant emissions of environmentally harmful gases ($CO_2$ and $CH_4$). In addition, the depletion of fossil fuel reserves puts humanity in front of the need for the tough energy conservation, the use of new resource-saving technologies [1,2]. Dry methane reforming (DRM) simultaneously converts two harmful gases and the resulting gas mixture of $H_2$ and CO (synthesis gas can be used as a fuel or feedstock in the Fischer-Tropsch process). Combining DMR with steam methane reforming provides two key advantages over single DRM reactions, namely: (i) $H_2O$ increases the O/C ratio in the feed, which promotes soot oxidation; (ii) $H_2O$ provides additional H atoms to form $H_2$, thereby adjusting the $H_2$/CO molar ratio in the product stream. Due to the chemical stability of both $CO_2$ and $CH_4$ $H_2O/CO_2$ reforming of methane (CSMR) is usually performed at 800-1000°C in the presence of catalyst containing platinum group metals or base metal catalyst (Fe, Co or Ni). Low cost and active Ni based catalysts are the best potential for wide industrial use. The Ni dispersion, oxygen vacancy concentration and the interaction between Ni and support affect CSMR performance. The disadvantages of Ni catalysts includes the decrease in activity when used for a long term as a result of the formation of carbon deposits and sintering of the particles of the active component at high reaction temperatures. A mesoporous support based on $CeO_2$-MgO combines the ability to stabilize highly dispersed structures of the active component and generate/transfer reactive species for the oxidation of intermediates formed on Ni catalytic sites. In this article, in order to develop a deactivation-resistant nickel-based CSMR process catalyst, a comparative study of the formation $X_{0.2}Ce_{0.4}Mg_{0.4}O_{1.4}$ (X = Ni, $Ni_{0.97}Pd_{0.03}$) prepared by the sol-gel templated (SGT) method, depending on support precursor and support functionalization method (one-stage synthesis and polyol method) was performed. The samples are marked in accordance with the procedure for their synthesis: the first letter denotes the support precursor - "A" and "C" correspond to acetate and cerium chloride, "S" and "P" correspond to samples obtained by one-stage and polyol methods, respectively. The third letter denotes the activation conditions: "O" and "V" denote activation in air and in vacuum, respectively. For example, Ni-Pd/CeMg-A-S-V, a sample prepared from cerium acetate by a one-stage method based on $Ni_{0.97}Pd_{0.03}$ nanoparticles, and calcined in vacuum at 500°C for 2 hours, then in air at 500°C for 4 h. In some cases, the heat treatment of the catalysts was carried out at two temperatures (700°C or 900°C) in air for 4 h. Characterization techniques, such as BET surface measurement, X-ray diffraction (XRD), X-ray photoelectron

spectroscopy (XPS), and thermogravimetric analysis (TGA) were used to elucidate the effect of preparation conditions on the catalytic properties and establish a correlation with catalytic performance in CSMR.

The use of SGT technology in the preparation of a nickel catalyst based on magnesium-modified cerium oxide $Ce_{0.5}Mg_{0.5}O_{1.5}$ for combined $H_2O/CO_2$ reforming of methane makes it possible to obtain nanocrystalline samples possess narrow pores (5-10 nm) and increased thermal stability due to inhibition of crystallite growth in the support. It has been shown by $N_2$ adsorption at 77K and XRD that the dispersion of the active component is controlled by the pore size of the support, the thermal stability of the mesoporous structure of the support, the method of its functionalization and activation, and increases when cerium acetate is used as a support precursor, at one-stage synthesis, and preliminary activation in vacuum at 300°C. The efficiency of catalysts in CSMR increases with an increase in the dispersion of the active component, an increase in the concentration of defective oxygen (CDO) and when well-dispersed NiPd nanoparticles and clusters of Ni in MgO phase are formed. $Ni_{0.194}Pd_{0.006}Ce_{0.4}Mg_{0.4}O_{1.4}$ catalyst has the highest dispersion and CDO, ensures the resistance of the Ni active component to sintering and stable operation (the yield of the target products is 79% with a conversion of reagents of at least 73% at 750°C) for 15 hours of operation.

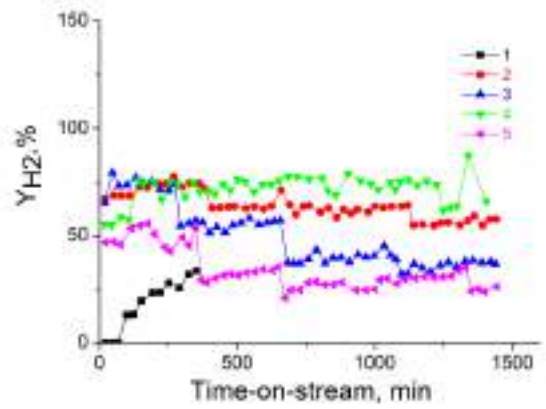


*Fig. 1. Hydrogen yield during CSMR at 750$^0$C. 1- Ni/CeMg-C-S-O; 2- Ni/CeMg-A-S-V; 3- Ni/CeMg-A-S-O; 4- Ni-Pd/CeMg-A-S-V; 5- Ni/CeMg-A-P-O.*

**Acknowledgement:** This work was supported by the Ministry of Science and Higher Education of the Russian Federation within the governmental order for the Boreskov Institute of Catalysis (project AAAA-A21-121011490008-3).

**References:**

[1] S. E. Hosseini, M. A. Wahid, Renew. Sustain. Energy Rev. 57 (2016) 850.
[2] P. Nikolaidis, A. Poullikkas, Renew. Sustain. Energy Rev. 67 (2017) 597.

## OP-III-15

# Glass-Ceramic Matrices Based on Borosilicate Glasses for the Immobilization of Radioactive Wastes

Koroleva O.N., Nevolina L.A., Korobatova N.M.

*South Urals Federal Research Center of Mineralogy and Geoecology of the Urals Branch of the Russian Academy of Sciences, Miass, Russia*

*olgankoroleva@gmail.com*

The problem of radioactive waste recycling has long been relevant due to growing demand for the immobilization and disposal of such hazardous materials. Proceeding from the principle of rationalism in nature management, the harmful effects of such anthropogenic activities should be minimized at the stage of nuclear waste processing. Such consequences are largely mitigated by the correctness of the selected matrix material used for immobilization. Since matrix materials based on borosilicate glasses are the preferred form for the immobilization of highly active waste, such materials are under active development at the Mayak Production Association in Russia, as well as forming the subject of constant research [1, 2]. Glasses and glass-ceramics are widely considered to be among the most reliable materials for the immobilization of radioactive waste. Moreover, there is increased interest in multiphase glass-ceramic materials due to their high chemical resistance, strength, thermal stability and increased capacity for waste. Synthesis and processing conditions play a key role in understanding the degree of their stability depending on external and geochemical conditions at underground waste disposal facilities.

The aim of the present work was to synthesize and investigate the properties of glass-ceramic materials based on borosilicate glasses containing two modifier cations. The synthesis of glass-ceramic materials was carried out by sintering crushed samples at temperatures around *Tg*, followed by crystallization for several hours. Direct annealing from the melt was carried out as an alternative procedure. The influence of various heat treatment modes on the features of glass formation and crystallization processes, as well as on the phase composition and properties of the resulting glass-ceramic matrix materials, was determined. Porous glasses were made from glasses by quenching from a melt. The resulting porous materials were impregnated with aqueous solutions of cesium nitrate, followed by compaction of the glass to form glass-ceramics.

A set of contemporary methods and approaches was used to study the samples. The phase- and chemical compositions, as well as the structure of the materials, were determined using X-ray phase analysis, X-ray spectral microanalysis, and Raman spectroscopy. The thermochemical characteristics of the glasses were determined using the differential scanning calorimetry method. Stability was assessed based on the results of annealing and leaching with parameters corresponding to geochemical environmental conditions. The stability of the obtained materials in aqueous solutions was studied by standard methods.

**Acknowledgement:** This work was supported by the Russian Science Foundation, grant 22-17-20005.

**References:**

[1] G.Sh. Batorshin, I.A. Ivanov, P.V. Kozlov, Yu.G. Mokrov, Quest. Radiat. Safety (in Russian). 71 (2013), 3-11.
[2] S.M. Shaydullin, E.A. Belanova, P.V. Kozlov, M.B. Remizov, E.M. Dvoryanchikova, Chim. Tech. Acta, 8 (2021) 20218105.

## OP-III-16

# Design of Novel Catalysts for Environmental Processes

Kulikova M.V., Maximov A.L.
*A.V.Topchiev Institute of Petrochemical Synthesis, RAS, Moscow, Russia*
*m_kulikova@ips.ac.ru*

The evolution of materials science has led to the formation of such an industry as catalytic design. The design of catalysts with given process efficiency parameters is consistent with the principles of green chemistry. The new trend of using eco-friendly and natural process is also promising for catalytic design. The focus of this work is hydrochar-based catalytic material. Hydrochar can be obtained by directed genesis of any kind of plant biomass via the hydrothermal carbonization (HTC). HTC is a natural process similar to the formation of natural coals through the biomass metamorphism in the earth's crust.

Hydrochar containing catalyst has been tested in environmental-friendly and carbon capture processes: CO hydrogenation (FT synthesis, methanation) and $CO_2$ hydrogenation. Catalysts were prepared in two different ways: incipient wetness impregnation of hydrochar with metal salts and the formation of metal-containing catalyst compositions in situ by hydrothermal synthesis (this approach is also called “fishing process”). Hydrochar-based catalysts have been investigated by a number of physicochemical methods: XRD, TPR, BET, IR-spectroscopy, TEM, SEM.

In all cases, the formation of a polyconjugation system and the presence of oxygen-containing functional groups in hydrochars were established. Such a structure allows effective immobilization of the active ingredient ions on the hydrochar surface. Magnetite is formed with a size of about 7-8 nm in the case of a monometallic system (Fe-containing). In bimetallic systems (Fe, Co-containing), iron-cobalt alloy crystallites 10–20 nm in size are formed.

Hydrochar-based catalysts showed high activity in the hydrogenation of carbon oxides in both cases: conversion of CO close to 100%, $CO_2$ close to 60%. The use of hydrochar as a catalyst component in both carbon monoxide hydrogenation processes results in an atypical product composition. For FT-synthesis on Fe-containing catalyst a lot of isoparaffins (50%) were observed, which is typical for bifunctional catalysts on oxide supports. This effect can be associated with the occurrence of isomerization at weak Lewis centers, which are represented by the magnetite phase. The data on the hydrogenation of $CO_2$ and CO correlate; obviously, on these catalysts, the hydrogenation of $CO_2$ proceeds through the CO stage. The obtained catalytic systems showed activity in the targeted synthesis of isoparaffins.

In contrast to the prevailing trend in petrochemistry to convert $CO_2$ and CO into a variety of hydrocarbons, starting with $C_2$, the authors of this work would like to emphasize the importance of the methanation process to achieve the goals of decarbonization. The catalytic hydrogenation of $CO_2$ and CO to form methane ($CH_4$) has aroused interest among researchers around the world, since it can be used both for storing chemical energy and for direct pumping

into existing gas pipelines. Thus, the process of methane production from carbon oxides perfectly fits to the transition to distributed power generation and zero-emission production.

In this work, for the first time, the fundamental possibility of carrying out the methanation reaction using hydrochar-based catalysts without the pre-activation stage is shown. In this case, the conversion of carbon monoxide was 54% at a temperature of 270°C with a selectivity of methane formation in gaseous products up to 70%. The advantage of these catalytic systems is the possibility of obtaining from any type of plant waste, which makes them affordable and cheap. In terms of green chemistry, they can be considered as bright representatives of new generation eco-friendly materials.

**Acknowledgement:** This work was carried out with financial support from the Russian Science Foundation (RSF Grant no. 17-73-30046P)

## OP-III-17

# Thermal Catalytic Refining of Gases from Fast Pyrolysis of Flax Processing Waste

Lugovoy Yu.V.[1], Chalov K.V.[1], Tarabonko V.E.[2], Kosivtsov Yu.Yu.[1], Sulman M.G.[1]
*1 – Tver State Technical University, Tver, Russia*
*2 – Institute of Chemistry and Chemical Technology SB RAS, Krasnoyarsk, Russia*
*pn-just@yandex.ru*

The technologies of fast pyrolysis are applied to pyrofuel production, however taking into account its low operating ability (high oxygen content and corrosion activity) it is necessary to search for the new technological solutions [1]. To generate electrical energy from plant-based biomass waste the fast pyrolysis technologies focused on the increase of the conversion of the initial raw material to the combustible gases with high heat value and low tars content are more preferable [2]. The disadvantages of most catalysts of gaseous products thermal refining from the tars are their high cost and fast activity loss due to the carbon formed on their surface [3]. So it is necessary to develop cheap and effective catalysts for the thermal refining of pyrolysis gaseous products.

In the north-western region of the Russian Federation there are large constantly replenished stocks of flax shive, which today, for various reasons, is practically not processed.

The flax shive fast pyrolysis process was carried out under inert atmosphere (nitrogen). The feedstock mass loaded into the reactor was 1000 g. The total time of the experiment was 20 min. To estimate the rate of termodestruction of initial source in the presence of the catalysts the rate of gaseous products evolution was controlled during the experiment.

The study of the flax shive fast pyrolysis involving the choice of the most active metal-containing aluminosilicate catalyst of thermal refining of gases from the tars was conducted using the laboratory - scale plant shown in Figure 1.


*Fig.1. Experimental setup for the flax shive fast pyrolysis process*

The gaseous products analysis was performed by the gas chromatography method. The analysis of the fast pyrolysis gaseous products consisted of $C_1$-$C_4$ hydrocarbon, carbon oxides and hydrogen content definition, as well as the express analysis of the lower specific heat

value. The chromatographic analysis of the gaseous products was performed on the base of chromatograph “Kristallux” 4000M and modified chromatograph “Gasochrom 2000”.

The use of metal-containing alumosilicate catalyst in the pyrolysis gas refining from the tars results in the change of the gas volume and heat value. The use of the studied zeolite catalysts containing the iron subgroup metals leads to the change in the concentration of hydrogen, $C_1$-$C_4$ hydrocarbons and carbon oxides.

The concentration of metal on the surface of the alumosilicate catalyst strongly affects the catalyst activity in the thermodestruction process of a pyrolysis gas tars. The gaseous product composition in dependence to the type and concentration of the metal on the catalyst surface. The use of the catalysts also results in the increase in hydrogen concentration; moreover, the growth of hydrogen concentration in a gaseous product increases from Fe to Ni. The increase in alumosilicate catalyst metal content also leads to the increase in hydrogen concentration that is caused by the dehydration reaction of pyrolysis organic products in the presence of iron subgroup metals. The growth of hydrogen concentration in a pyrolysis gas is accompanied by the increase in coke-formation on the catalyst surface, so the use of the catalysts with higher metal content is economically unfavorable. The considerable effect of the studied catalysts on the pyrolysis gas composition can be explained both by the catalyst high activity in the thermodestruction process and thermal decomposition of high-boiling fractions of pyrolysis liquid products.

According to the data received the following conclusions can be made: the optimal temperature for the fast thermolysis treatment of flax shive was about 700 °C; the optimal feedstock size was 1-2 mm at the residence time inside the reactor about 4-5 seconds; 2% Co-ZSM-5 had the highest activity at the catalyst-substrate mass ratio 1:20; the use of zeolite catalysts on the base of iron subgroup metals leaded to the decrease of tars content in the thermolysis gas as well as to the increase $C_1$-$C_4$ hydrocarbons amount, hydrogen and carbon monoxide (II) concentration compared to non-catalytic process.

The use of metal-containing alumosilicate catalyst in the pyrolysis gas refining from the tars results in the change of the gas volume and heat value. Such metal content in the catalyst allows increasing $C_1$-$C_4$ hydrocarbons concentration and removing the tars from the combustible gas of the fast pyrolysis of flax shive.

**Acknowledgement:** The work was carried out with the financial support of the Russian Science Foundation (20-69-47084).

**References:**

[1].W.T. Tsai, M.K. Lee, Y.M. Chang, Bioresour. Technol. 2007 98, 22–28.
[2].Th. Dickerson, J. Soria, Energies. 2013, 6, 514-538.
[3].T.A. Milne and R.J. Evans, DE-AC36-83CH10093 Prepared under Task No. BP811010. 1998, 67.

## OP-III-18

# Propane Transformation on In-Modified BEA Zeolite

Gabrienko A.A., Arzumanov S.S., Stepanov A.G.
*Boreskov Institute of Catalysis, Novosibirsk, Russia*
*gabrienko@catalysis.ru*

Light alkanes are abundant and cheap feedstock to produce different useful chemical products. Conversion to simple aromatic hydrocarbons is one of the options for alkane processing. According to Halász et al. [1], In-modified zeolites demonstrate superior activity and selectivity for light alkane aromatization. However, the properties and performance of In-zeolites have been studied in very few publications [1-7]. To date, the role of indium sites loaded into zeolites and the mechanism of alkane transformation remain unknown. In this report, we present the data obtained by $^{13}C$ MAS NMR method on propane transformation on In/H-BEA zeolite [8]. These results allowed us to shed light on the pathways of propane transformation on In-modified zeolites and the properties of indium species having different composition.

Following the previously tested procedure [9-11], BEA zeolite samples were modified with indium, which formed either $In^+$ or $InO^+$ sites inside zeolite pores, and were characterized by XPS, electron microscopy, and MAS NMR methods.

For propane on $In^+$/H-BEA sample, $^{13}C$ MAS NMR demonstrated that $In^+$ sites exhibit no activity for alkane conversion at 298–723 K. On the contrary, $InO^+$/H-BEA sample performed propane dehydrogenation to propene and oxidation to acetic and propionic acids. Propene formed at $T \leq 423$ K converts to toluene with the assistance of zeolite BAS at $T > 523$ K. Importantly, no propane hydrogenolysis, leading to undesired methane and ethane, was observed to occur at 298–673 K. Thus, two parallel pathways of propane transformation on $InO^+$/H-BEA were revealed: dehydrogenation followed by propene aromatization and oxidation to carboxylic acids.

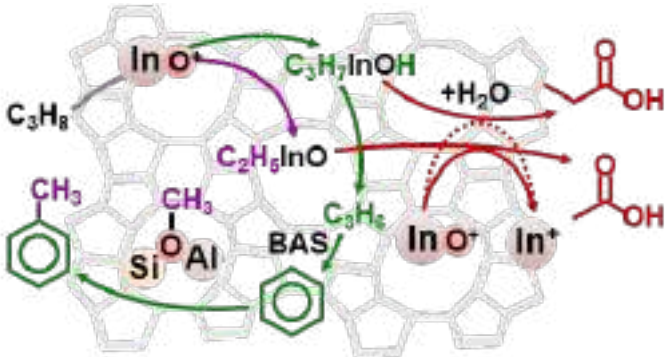


*Fig. 1. Propane transformation pathways on a $InO^+$-modified zeolite. Adapted from ref. [8].*

The mechanism of propane transformation to propene and the carboxylic acids with the assistance of $InO^+$ sites was discussed. It is suggested that propane activation can proceed through either C–H or C–C bond dissociation on $InO^+$ sites. It is inferred that acetic acid may

be formed following the dissociation of the alkane C–C bond, whereas propene and propionic acid are formed after the dissociation of the C–H bond.

**Acknowledgement:** This work was supported by the Russian Science Foundation, grant 22-13-00029.

**References:**

[1] J. Halász, Z. Kónya, Á. Fudala, A. Béres, I. Kiricsi, Catal. Today 31 (1996) 293.
[2] V.I. Hart, M.B. Bryant, L.G. Butler, X. Wu, K.M. Dooley, Catal. Lett. 53 (1998) 111.
[3] G.L. Price, V. Kanazirev, K.M. Dooley, V.I. Hart, J. Catal. 173 (1998) 17.
[4] J. Halász, W. Nyári, E. Meretei, I. Hannus, J.B. Nagy, I. Kiricsi, J. Mol. Struct. 651-653 (2003) 315.
[5] H. Tian, J. Liao, F. Zha, X. Guo, X. Tang, Y. Chang, X. Ma, ChemistrySelect 5 (2020) 3626.
[6] Z. Maeno, X. Wu, S. Yasumura, T. Toyao, Y. Kanda, K.I. Shimizu, Catalysts 10 (2020) 1.
[7] Z. Maeno, S. Yasumura, X. Wu, M. Huang, C. Liu, T. Toyao, K.-i. Shimizu, J. Am. Chem. Soc. 142 (2020) 4820.
[8] A.A. Gabrienko, S.S. Arzumanov, A.V. Toktarev, I.P. Prosvirin, D. Freude, J. Haase, A.G. Stepanov, J. Phys. Chem. C 126 (2022) 16204.
[9] H.K. Beyer, R.M. Mihályi, C. Minchev, Y. Neinska, V. Kanazirev, Microporous Mater. 7 (1996) 333.
[10] R.M. Mihályi, H.K. Beyer, V. Mavrodinova, C. Minchev, Y. Neinska, Microporous Mesoporous Mater. 24 (1998) 143.
[11] Y. Neinska, R.M. Mihalyi, V. Mavrodinova, C. Minchev, H.K. Beyer, Phys. Chem. Chem. Phys. 1 (1999) 5761.

## OP-III-19

# Selective Hydrogenation of 1-Heptene/1-Heptyne Mixture on Mesoporous Silica, Doped with Dy and Modified with Ag

Tokranov A.A., Tokranova E.O., Shafigulin R.V., Bulanova A.V.
*Samara University, Samara, Russia*
*fileona@mail.ru*

Alkenes are an important class of raw materials used in various fields of industrial organic synthesis. In industry, the selective hydrogenation process is mainly used to obtain various compounds, as well as to remove acetylenic compounds, which are undesirable impurities in petroleum fractions, and it is important that their content be reduced to the minimum allowable value [1]. To remove such impurities, fractional distillation is usually used, which requires large energy and material costs. Therefore, the selective hydrogenation of alkynes in the presence of alkenes is currently the most promising method for reducing their content in petroleum fractions.

Promising hydrogenation catalysts are materials based on mesoporous silica gels modified with various metals. Based on the literature data of recent decades, it has been established that one of the ways to improve the characteristics of adsorbents and catalysts based on mesoporous silica gel is doping at the initial stage of template synthesis [2, 3]. It has been established that the introduction of rare earth elements into the structure of the material leads not only to an increase in its activity, but also in its selectivity [4, 5]. Silver is one of the metals that are active in the selective hydrogenation reaction [5–7].

The aim of this work was to synthesize catalysts based on mesoporous silica gel doped with dysprosium, lanthanum, and modified with silver and to study their selectivity in the hydrogenation reaction of a 1-heptyne/1-heptene mixture.

Mesoporous silica gel doped with dysprosium and modified with silver (Dy-Ag/MC) with optimal textural characteristics was obtained by the template method. The physicochemical characteristics of the obtained catalyst were studied by scanning electron microscopy, X-ray fluorescence and X-ray diffraction analysis, inductively coupled plasma mass spectrometry, IR spectrometry, and temperature-programmed reduction.

To study the selectivity of the obtained catalyst in the hydrogenation reaction, a mixture of 1-heptyne/1-heptene was made with a 30% content of 1-heptyne. The reaction was carried out for 10 and 15 minutes at temperatures of 140–160°C. With an increase in temperature, the conversion of heptin-1 and the selectivity for heptene-1 increase (Fig. 1). The optimal time for carrying out the hydrogenation process of a 30% mixture was chosen to be 15 min.

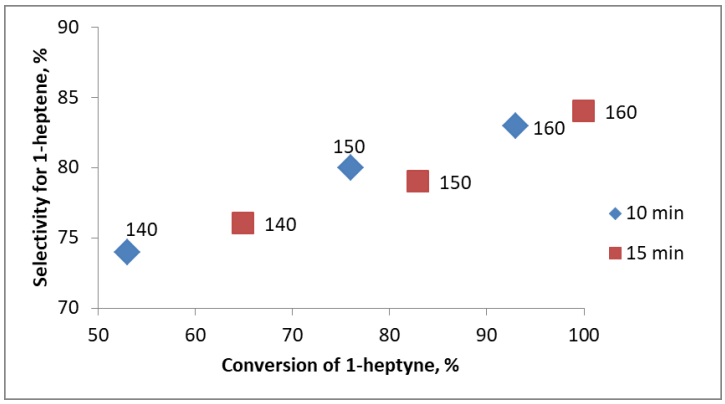


*Fig. 1. The value of 1-heptene selectivity and 1-heptyne conversion at different temperatures on Dy-Ag/MC (3 atm, 10, 15 minutes from the start of the reaction).*

Qualitative analysis of the hydrogenation reaction products of the mixture after 15 min from the start of the reaction on an Agilent 7890 GC gas chromatograph with a mass-selective detector showed that heptane, 1-heptene and its isomers, cis-2-heptene, trans-2, are formed during the hydrogenation of 1-heptyne (Fig. 2).

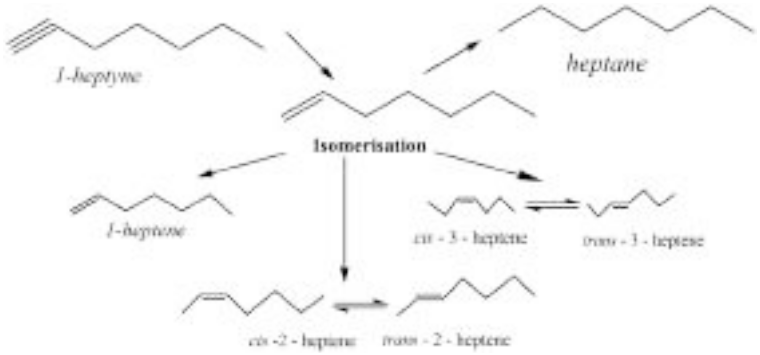


*Fig.2. Hydrogenation reaction products of 1-heptyne on Dy-Ag/MC and La-Ag/MC.*

The most heptane among of the reaction products is formed at a temperature of 150°C on a Dy-Ag/MC catalyst; at 84% of 1-heptyne conversion, the selectivity for alkenes is 79%. At 140 °C, almost the same amount of 1-heptene and heptane is formed, and a decrease in the formation of geometric isomers is observed. At a temperature of 160°C, the conversion of 1-heptyne reaches its maximum, and the selectivity for 1-heptene is 84%.

**References:**

[1] Chanerika, R., Shozi, M. L., Friedrich, H. B. ACS omega. (2022) 7 4026.
[2] Yang, X., Wei, Y., Jiang, Y., Wang, Y., Chen, L., Peng, L., Yan, Y. Ind. Eng. Chem. Res. (2021) 60 5352.
[3] Shafigulin, R. V., Filippova, E. O., Shmelev, A. A., Bulanova, A. V. (2019) Cat. Lett. 149(4) 916.
[4] Zheng, J., Chen, Z., Fang, J., Wang, Z., Zuo, S. J. Rare Earths. (2020) 38 933.
[5] Tokranov, A. A., Tokranova, E. O., Shafigulin, R. V., Pavlova, L. V., Mukhanova, I. M., Platonov, I. A., Bulanova, A. V. React. Kinet. Mech. Catal. (2023) 136 217.
[6] Zhang, Q., Li, J., Liu, X., Zhu, Q. APPL CATAL A-GEN. (2000) 197 221.
[7] Cheng, S., Meng, T., Mao, D., Guo, X., Yu, J., Ma, Z. Nanomaterials. (2022) 12 407.

## OP-III-20

# Zeolitic Imidazolate Frameworks for Acid-Base Catalysis: the Structure-Property-Activity Relationship

Timofeeva M.N.[1], Jhung S.H.[2], Panchenko V.N.[1]
*1 – Boreskov Institute of Catalysis, Novosibirsk, Russia*
*2 – Department of Chemistry and Green-Nano Materials Research Center, Kyungpook National University, Republic of Korea*
*timofeeva@catalysis.ru*

Over the last several decades, metal-organic framework chemistry has received considerable attention from researchers. Among them, zeolitic imidazolate frameworks (ZIFs) represent a new and special subclass of MOFs. Many studies have demonstrated that ZIFs possess unique structural and physicochemical properties that allow them to demonstrate high activity and yield products with high selectivity. Our study also was focused on the extensively examination for their potential in acid-base catalysis. The application of spectroscopic methods as instruments for analyzing the nature of active sites allowed us understanding unusual catalytic behaviour from the perspective of the structure-property-activity relationship. We examined a few reactions that represent the broad range of the potentially promising applications of Zn-ZIFs as heterogeneous catalysts, such as (1) the synthesis of propylene glycol methyl ether from propylene oxide and methanol, (2) synthesis of erythrulose (the monosaccharide) via aldol condensation of formaldehyde and dihydroxyacetone, (3) the synthesis of organic carbonates via the cycloaddition of $CO_2$ to epoxides and transesterification of alcohols with catechol carbonate, and (4) the synthesis of glycidol via transesterification glycerol with dimethyl carbonate [1]. Our study and literature published point to several tentative conclusions:

1. Tuning the affinity for polar molecules (hydrophobic/hydrophilic properties) by varying the chemical composition of the linker may be useful for the application of ZIFs in reactions involving polar reagents (water, alcohols, and aldehydes). The linker can act as an active site for the activation of reagents.

2. The textural properties of ZIFs ($S_{BET}$ and $V_\mu/V_\Sigma$) can be changed in two ways: Replacing $Zn^{2+}$ with $Co^{2+}$ changes and increases the particle size of ZIFs that then lead to an increase in $S_{BET}$ and $V_\mu/V_\Sigma$. The accessibility and number of active sites decrease in this order. These changes may affect reaction rate and selectivity.

3. The number of active sites is fine-tuned on the basis of the chemical composition and particle size of ZIFs. To date, only information on the basicity of ZIFs, which indicates that the strength of basic sites depends on the basicity of linkers and the structure of ZIFs, exists.

4. ZIFs possess a unique combination of acidic sites and basic sites that allow their use in acid–base catalysis. In most reactions, their catalytic behavior is defined by the presence of the "Lewis acid site-basic site" pair. In these cases, the nature of the metal ion and the basicity

of the organic linker should be considered because these parameters are crucial for the activation of reactants and the subsequent rearrangement of intermediates.

5. The effect of particle size has received little attention in the literature. However, the shape and size of particles should be considered because these factors affect textural properties and active site number. Moreover, particle size can provoke problems in the course of cyclic tests and/or the isolation of ZIFs from reaction mixtures.

**Acknowledgement:** This work was supported by the Ministry of Science and Higher Education of the Russian Federation within the governmental order for the Boreskov Institute of Catalysis (AAAA-A21-121011390055-8) and the National Research Foundation of Korea (NRF) grant funded by the Korean government (MSIT) (Grant number: NRF-2020R1A4A1018393)

**References:**

[1] M.N. Timofeeva, V.N. Panchenko, S.H. Jhung, Int. J. Mol. Sci. 24 (2023) 4370

## OP-III-21

# Catalytic Properties of Sodium Pectate Manganese Complexes

Sabirova A.F.[1,2], Morozov V.I.[1], Kadirov D.M.[2], Minzanova S.T.[1,2], Nizameeva G.R.[1,2], Mansurov R.N.[2], Sultanov T.P.[1,2], Gainullin R.R.[1], Kadirov M.K.[1,2]

*1 – Arbuzov Institute of Organic and Physical Chemistry, Kazan, Russia*

*2 – Kazan National Research Technological University, Kazan, Russia*

*aigul84saf@mail.ru*

Manganese complexes of sodium pectate were studied as electrocatalysts for the oxygen reduction reaction (ORR). The synthesis of complexes (Fig. 1A, B)) was carried out by analogy with the known method [1].

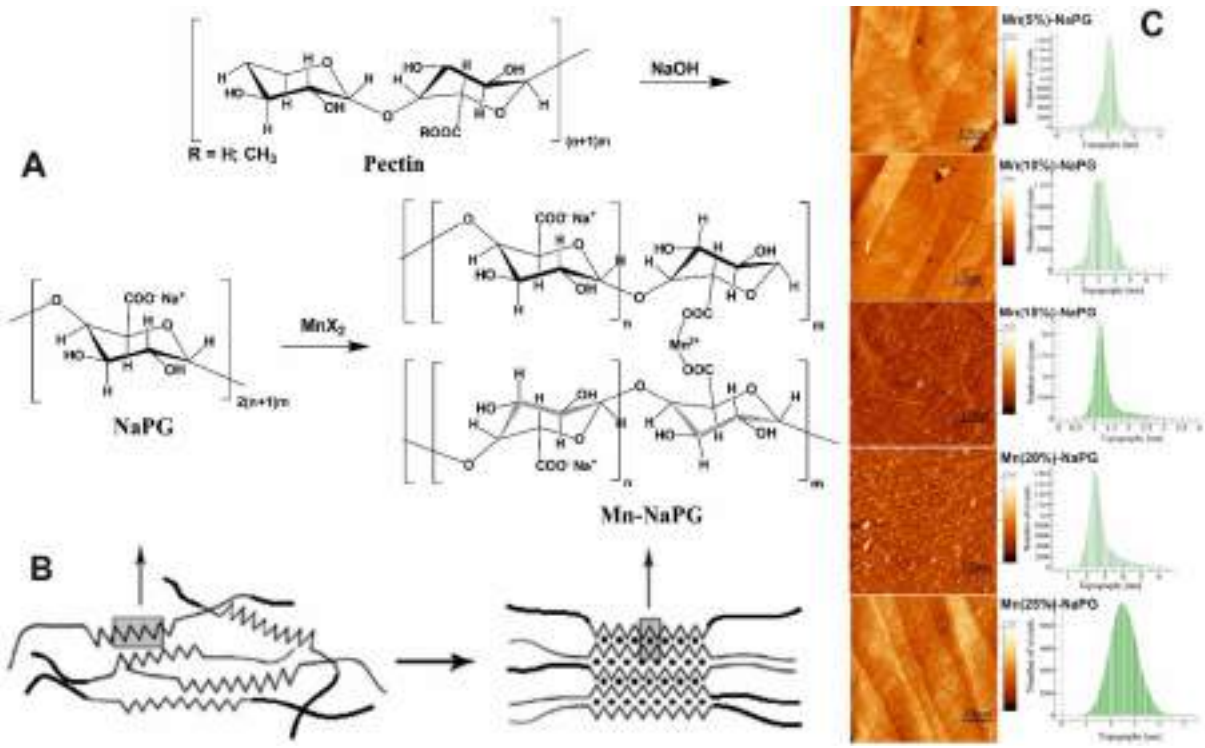


*Fig. 1. Schemes for the synthesis of pectin polysaccharide complexes (n=3-10; m=10-35) with manganese (A) and the formation of polymer-complex structures according to the "egg-box" model (B - right), AFM images (left column of C) and particle size distribution (right column of C) for the Mn(n%)-NaPG compounds*

For a number of samples of Mn(n%)-NaPG with different degrees of manganese substitution (from 5% to 25%), the film structures formed during their deposition from the liquid phase on the surface of pyrolytic graphite were studied. The 20% [Mn(20%)-NaPG] sample appears to be the most optimal substitution value in terms of uniform distribution of metal centers (Fig. 1C).

To study the catalytic properties, samples with the densest manganese distribution - [Mn(15%)-NaPG, Mn(20%)-NaPG] and Mn(25%)-NaPG) have been selected. As can be seen (Fig. 2) from the CV curves of the studied coordination biopolymers, all of them exhibit activity of varying degrees with respect to oxygen reduction. Judging by the amplitude of the oxygen reduction peak, Mn(20%)-NaPG shows the highest activity - 0.45 mA, while for [Mn(15%)-

NaPG, and Mn(25%)-NaPG] - 0.225 and 0.32 mA, respectively. In solutions saturated with argon, there are no reduction peaks.

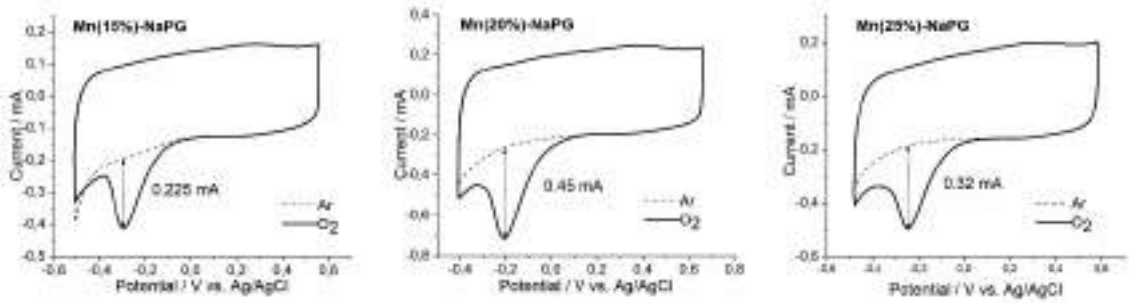


*Fig. 2. CVs with indication of the amplitudes of the cathodic peaks for ORR on GC electrodes modified with coordination biopolymers Mn(15%)-NaPG (left), Mn(20%)-NaPG (center) and Mn(25%)-NaPG (right) in argon-saturated (dashed curves) or oxygen-saturated 0.5 M $H_2SO_4$ (solid curves) at a scan rate of 50 mV $s^{-1}$; GC electrode area: 0.0707 $cm^2$*

**Acknowledgement:** This work was supported by the Russian Science Foundation, grant 22-29-00895.

**References:**

[1] I. Nizameev, D. Kadirov, G. Nizameeva, A. Sabirova, K. Kholin, M. Morozov, L. Mironova, R. Zairov, S. Minzanova, O. Sinyashin, M. Kadirov, IJMS 23 (2022) 14247.

## OP-III-22

# SAPO-Containing Alumina CoMoNi-Catalysts for Hydrotreatment of Heavy Oil: Pore Hierarchy as a Key Parameter for Catalyst Stabilization

Vorobyeva E.E., Shamanaeva I.A., Polukhin A.V., Lysikov A.I., Parkhomchuk E.V.
*Boreskov Institute of Catalysis, Novosibirsk, Russia*
*catherina.vorobieva@gmail.com*

Processing of heavy oil is an important task caused by both the growth in consumption of petroleum products and the possibility of obtaining high-added value products from cheap raw materials [1]. The main problem of the process is the content of polyaromatic molecules – asphaltenes which are the major source of coke. The presence of transport pores with certain size in the support which allow large molecules to be quickly introduced and removed and which have sufficient volume for metal and coke deposits solves problems of fast deactivation. Materials with such a pore system are referred to as hierarchical [2]. The difficulty of hydrotreating heavy oil is also related to the fact that most of the hard-to-recover heteroatoms exist in large refractory molecules. In turn, the coordination of such molecules on the active sites of the catalyst is complicated by steric hindrance [3,4]. Using zeolites as part of the support is one of the ways to solve this problem. Zeolites are able to crack (including C-S bond cleavage) and isomerize molecules removing steric hindrances and improving overall catalyst activity [5]. Zeolite-like silicoaluminophosphates (SAPO) are alternative materials to aluminosilicate zeolites. It is shown that acidity of SAPO is moderate comparing with aluminosilicate zeolites of the same framework structure [6–8]. In addition, some SAPOs are easier and cheaper to produce than zeolites traditionally used due to less expensive molecular templates, but can also perform good stability under severe operating conditions.

Thus, the research was devoted to the study of activity and lifetime of CoMoNi-catalyst containing one-dimensional SAPOs in heavy oil hydrotreatment. A special attention was paid to porous structure of SAPOs and catalyst supports. Porosity of supports was designed by two hard templates. Pore structure containing narrow and wide mesopores and macropores was referred as high-resolved pore hierarchy (HR). In turn, pore structure containing narrow mesopores and macropores was referred as bimodal pore hierarchy (B). Zeolite-like SAPOs also differ in their own pore hierarchy and acidity.

Within the scope of this work, it was firstly demonstrated that zeolite-like crystals influence the formation of the porous structure of the support. Thus, SAPO-5 hexagonal crystals interact with the $Al_2O_3$ precursor weaker comparing with SAPO-11 spherical crystals, creating additional meso- and macroporous space around the SAPO-5 crystals (Fig. 1, *Fig. 2*).

A special pore structure of the $Al_2O_3$-SAPO-n supports effects on CoMoNi active particle formation. The larger pores, the more intense CoMoNi-precursor migration with increasing of final particles. The last one deteriorates catalytic activity in hydrotreating.

Catalytic tests for 100 hours for each catalysts were shown that a special support porosity should be designed depending on pore hierarchy and morphology of zeolite-like material. High-resolved pore hierarchy obtained with acrylic primer performs a number of different functions: effective mass transfer, accessibility of CoMoNi sites, and creating the gradual pore channel expansion. However, such a porous system can adversely affect the size of the active CoMoNi particles, as a result, decreasing the activity in hydrotreating processes.

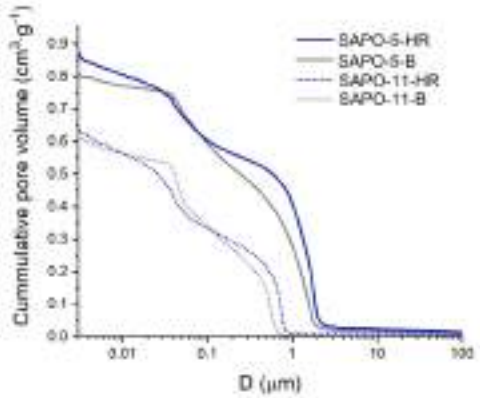


*Fig. 1 Hg-intrusion of catalysts*

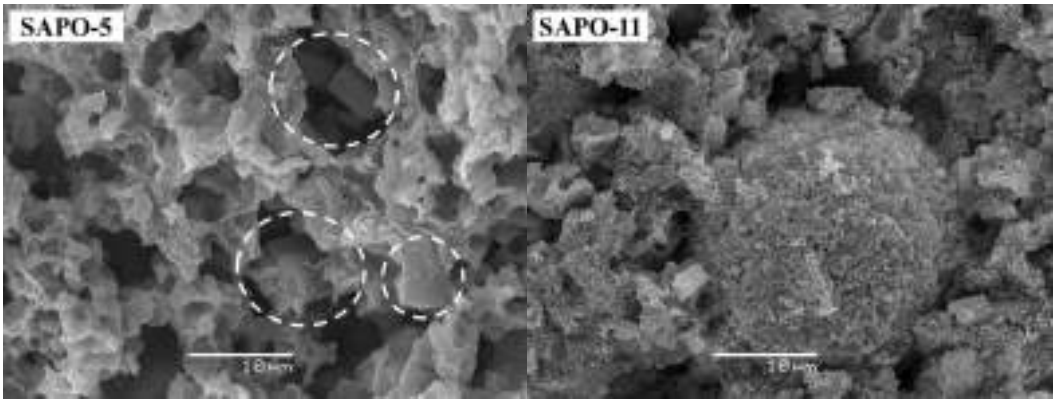


*Fig. 2. SEM images of SAPO-containing supports*

**Acknowledgement:** The study was supported by Ministry of Science and Higher Education of the Russian Federation (project AAAA-A21-121011490008-3).

**References:**

[1] E. V. Parkhomchuk, K. V. Fedotov, A.I. Lysikov, A. V. Polukhin, E.E. Vorob'eva, I.A. Shamanaeva, N.N. San'kova, D.O. Shestakova, Y.O. Chikunova, S.E. Kuznetsov, A. V. Kleimenov, V.N. Parmon, Catal. Ind. 14 (2022) 86–114.
[2] W. Schwieger, A.G. Machoke, T. Weissenberger, A. Inayat, T. Selvam, M. Klumpp, A. Inayat, Chem. Soc. Rev. 45 (2016) 3353–3376.
[3] C. Song, X. Ma, Appl. Catal. B Environ. 41 (2003) 207–238.
[4] M. Bachrach, T.J. Marks, J.M. Notestein, ACS Catal. 6 (2016) 1455–1476.
[5] G. Pérot, Catal. Today. 86 (2003) 111–128.
[6] N. Katada, K. Nouno, J.K. Lee, J. Shin, S.B. Hong, M. Niwa, J. Phys. Chem. C. 115 (2011) 22505–22513.
[7] G. Sastre, D.W. Lewis, J. Chem. Soc. - Faraday Trans. 94 (1998) 3049–3058.
[8] Z. Ma, Z. Liu, H. Song, P. Bai, W. Xing, Z. Yan, L. Zhao, Z. Zhang, X. Gao, Appl. Petrochemical Res. 4 (2014) 351–358.

## OP-III-23

# Methyl Palmitate HDO-Hydroisomerization over SAPO-11-Containing Ni-Phophide Catalysts

Shamanaev I.V., Vlasova E.N., Shamanaeva I.A., Parkhomchuk E.V., Bukhtiyarova G.A.
*Boreskov Institute of Catalysis, Novosibirsk, Russia*
*i.v.shamanaev@catalysis.ru*

Hydrodeoxygenation (HDO) of non-edible vegetable oils, animal fats, and other fatty-acid-based sources results in formation of normal alkanes. These products have high cetane index but poor low-temperature properties [1,2]. Therefore, it is attractive to conduct one-step HDO-hydroisomerization to obtain high quality fuels from renewable sources. Being a member of the class of one-dimensional molecular sieves and having mild acidity SAPO-11 is widely used as isomerization component for n-alkanes transformation [3]. Ni-phosphides are attractive active components for HDO of esters, but there is no information in literature about influence of precursor and preparation conditions on catalytic activity of these systems in one-step HDO-hydroisomerization of fatty acid esters.

The aim of this work is investigation of precursor nature and preparation method influence on physicochemical and catalytic properties of SAPO-11 and $Al_2O_3$-SAPO-11-supported Ni-phosphide catalysts in methyl palmitate (MP – $C_{15}H_{31}COOCH_3$) HDO-hydroisomerization.

Pure SAPO-11 support (S) was synthesized by hydrothermal synthesis in an autoclave at 200 °C for 24 h under stirring. $Al_2O_3$-SAPO-11 composite supports (30 wt.% SAPO-11, AS) were prepared using commercial sources (Disperal 20 from “Sasol” and SAPO-11 from “Zeolyst”) by peptization with $HNO_3$ solution and subsequent extrusion (trefoil-shaped) with a laboratory spritz. Ni-phosphide catalysts were prepared by incipient wetness impregnation of the supports with different precursors: $Ni(CH_3COO)_2$ and $(NH_4)_2HPO_4$ – phosphate precursor (NiP_A), $Ni(OH)_2$ and $H_3PO_3$ – phosphite precursor (NiP_I), $Ni(CH_3COO)_2$ and $H_3PO_2$ – hypophosphite precursor (NiP_H). The precursors were reduced in $H_2$ flow at 600 °C for 1 h. Phosphidation of Ni/S and Ni/AS (in catalytic reactor by 2 wt.% $PPh_3$ in n-dodecane at 250 °C for 2 h or 380 °C for 7 h) was also used to prepare $Ni_2P$/S and $Ni_2P$/AS catalysts (NiP_P samples). The catalysts were characterized by chemical analysis, $N_2$ physisorption, $H_2$-TPR, $NH_3$-TPD, XRD, and TEM. HDO-hydroisomerization was carried out in continuous-flow fixed bed reactor at 340 °C, 2.0 MPa, LHSV=5.3 $h^{-1}$, $H_2$/feed=600 $Nm^3/m^3$.

XRD analysis confirmed formation of $Ni_2P$ phase in reduced and phosphidized samples. Average particle sizes ($D_{TEM}$) in NiP_P/S catalysts increase with increasing of Ni content (from 6.5 nm for 3 wt.% catalyst to 9.9 nm for 12 wt.% catalyst). $H_2$-TPR showed that reduction processes of NiP_A/AS, NiP_I/AS, and NiP_H/AS samples start at different temperatures – lower oxidation state of P precursor results in lower reduction temperatures. $NH_3$-TPD analysis did not show significant differences in acidity between NiP_P/S, NiP_A/AS, and NiP_H/AS

samples (110-145 µmol-$NH_3$/g). NiP_I/AS showed the highest acidity (177 µmol-$NH_3$/g) resulted from the precursor nature.

MP conversion over all catalysts was complete, but product distributions and amounts of iso-alkanes were different (Fig. 1). Activity in isomerization was shown to depend on phosphidation procedure and the amount of Ni in NiP_P/S catalysts. The highest content of iso-alkanes (66% total) was reached over 7 wt.% NiP_P/S after phosphidation at 250 °C for 2 h (Fig. 1) [4]. Metallic Ni/S gave 59% selectivity to iso-alkanes, but high amount of MP converted to cracked products and carbon deposits. Isomerization activity was also shown to depend on precursor nature. NiP_A/AS was shown to give only normal alkanes, NiP_I/AS gave 5% of iso-alkanes, and NiP_H/AS – 21% of iso-alkanes. But in this row the selectivity to cracked products increases.

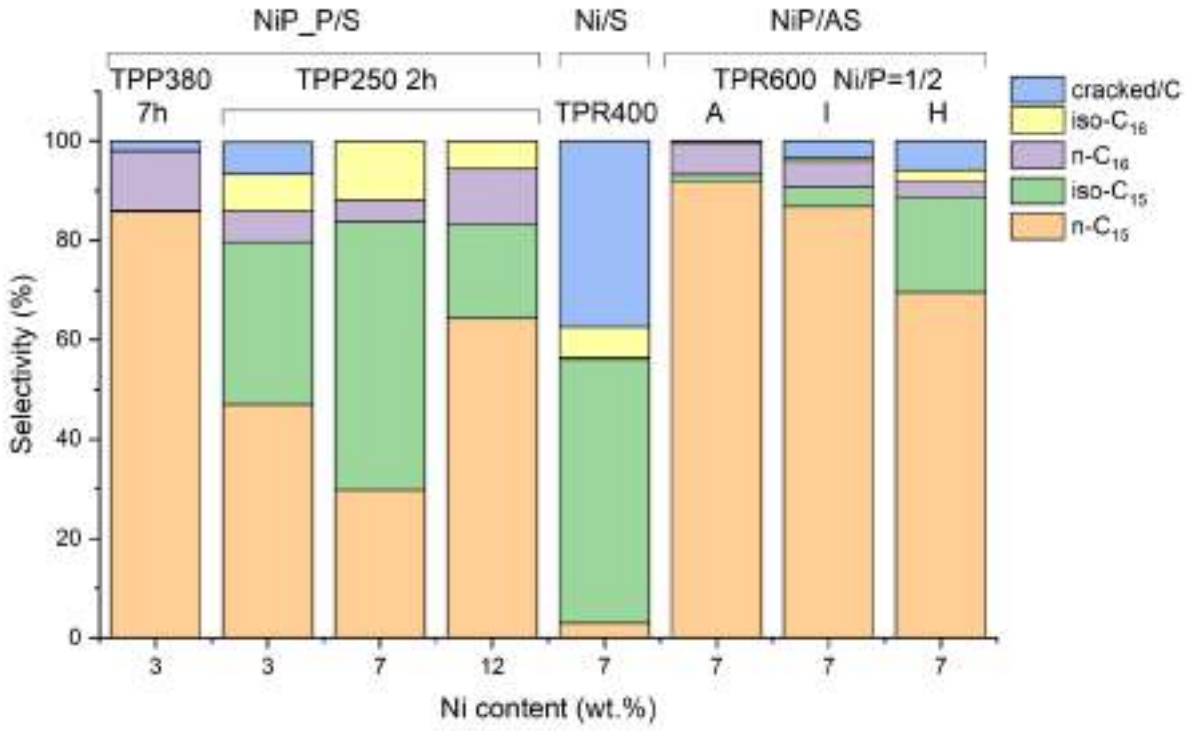


*Fig. 1. Product selectivities over Ni-phosphide and Ni catalysts in MP HDO-hydroisomerization. T=340 °C, 2.0 MPa, LHSV=5.3 $h^{-1}$, $H_2$/feed=600 $Nm^3/m^3$*

**Acknowledgement:** This work was supported by the Russian Science Foundation (grant no. 22-13-00371). The work concerning the preparation of SAPO-11 was supported by the Ministry of Science and Higher Education of the Russian Federation within the governmental order for the Boreskov Institute of Catalysis (project AAAA-A21-121011490008–3).

**References:**

[1] P.M. Yeletsky, R.G. Kukushkin, V.A. Yakovlev, and B. H. Chen, Fuel. 278 (2020): 118255.
[2] R.R.C. Monteiro, I.A. dos Santos, M.R.A. Arcanjo, C.L. Cavalcante Jr., F.M.T. de Luna, R. Fernandez-Lafuente, R.S. Vieira, Catalysts. 12, no. 2 (2022) 237.
[3] I.A. Shamanaeva, E.V. Parkhomchuk, Petroleum Chemistry. 59 (2019) 854.
[4] I.V. Shamanaev, I.A. Shamanaeva, E.V. Parkhomchuk, G.A. Bukhtiyarova, Catalysts. 12, no. 11 (2022) 1486.

## OP-III-24

# Problems of Screen-Printed Carbon Electrodes for Biosensor

Gryaznova M.I., Lugvishchuk D.S., Gryaznov K.O., Filimonenkov I.S., Mitberg E.B., Karaeva A.R., Mordkovich V.Z.
*FSBI Technological Institute for Superhard and Novel Carbon Materials, Troitsk, Moscow, Russia*
*mig@tisnum.ru*

Screen-printing technology development has been a proven choice of a carbon electrode industry for the past three decades. There is a variety of promising nanomaterials for preparation of carbon inks (single and multiwalled nanotubes, graphene and others) described in literature. However the production cost of such new materials is still relatively high to ensure large-scale production of cost-efficient carbon-based biosensors [1].

Complexity of the screen-printing technology is defined not only by the conductive material, but by the combination of many factors and parameters such as polymer binder/solvent composition, solid additives rheological behavior, substrate and its flexibility, screen mesh etc [2]. There is some optimal composition of mass concentration of each component for preparation of carbon-based inks. The world leading commercially available pastes from the companies such as GWENT, Dupont, EMS have composition carbon-based ink with solid phase concentration around 35-40 mass. % [3]. In order to make conductive carbon ink more economically feasible percolation threshold need to be decreased [4].

Nowadays the search for inexpensive and reliable solutions to meet the growing demand for electrochemical biosensors for measuring blood glucose concentration remains relevant. One of the main components of such biosensors is a graphite electrode, which is applied to the substrate using screen printing technology.

This work presents studies of the original graphite paste exfoliated graphite selected as a main electrically conductive component. Optimization of exfoliated graphite/polymer ratio, as well as investigation of solvent/binder compositions were carried out. The results of a comparative analysis of printed electrodes based on it with electrodes made of commercial graphite paste from Gwent Electronic Materials are presented.

The obtained electrodes were characterized by comparable physical and electrochemical parameters (Fig.1). According to the results of scanning electron microscopy of electrodes, graphite paste with exfoliated graphite is suitable for screen printing. The electrical resistivity of the electrodes with thermally expanded graphite was 440 (Ohms×mm$^2$)/m, and the electrodes obtained on the basis of commercial paste — 270 (Ohms×mm$^2$)/m. The biosensor, made on the basis of the original graphite paste, is characterized by a wide range of linearity of response to glucose in the range from 1 to 40 mM, and similar values of currents and sensitivity compared to a commercial analogue.

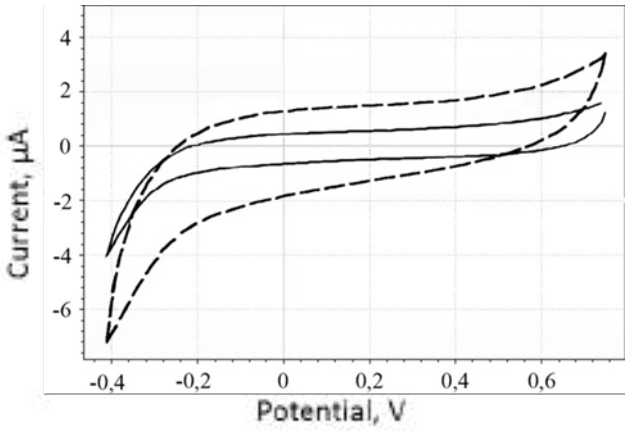


*Fig. 1. Cyclic voltammetry of printed electrodes: «—» – Gwent paste; «– –» – exfoliated graphite paste*

The results of studies of the obtained electrodes have shown that exfoliated graphite is a promising material for use in electrochemical systems, and reducing the concentration of carbon conductive components can significantly reduce the cost of finished graphite paste and increase its commercial potential.

**Acknowledgement:** The authors are grateful to ELTA Company LLC and personally to Yu.F. Glukhov and Z.Y. Nikanorov for supporting the work. The work was carried out using the equipment of the Center for Collective Use of the Federal State Budgetary Institution TISNUM "Research of nanostructured, carbon and superhard materials".

**References:**

[1] Z. Chu, J.Peng, W. Jin, Sens. Actuators B Chem. 243 (2017) 919.
[2] C. Banks, C. Foster, R. Kadara, Screen-Printing Electrochemical Architectures (2016).
[3] S. Fletcher, Electrochemistry of Carbon Electrodes. 16 (2015) 425.
[4] E.P. Mamunya, V.V. Davidenko, E.V. Lebedev, Polym. Compos. 16 (1995) 319.

## OP-III-25

# Graphene-Based Flow Rate Sensor

Andryushchenko V.A.
*Novosibirsk State University, Novosibirsk, Russia*
*vladimir.andryushchenko@gmail.com*

The sensory properties of graphene materials are of great interest due to their unique two-dimensional structure, high conductivity, and large specific surface area. When in contact with liquid media, the properties of the graphene coating can also change. It was shown in [1] that when graphene on a PET/EVA polymer substrate is immersed in distilled water, the electronic structure of graphene changes and its resistance increases. The authors explain this effect by the structuring of water molecules near the graphene layer, which leads to the appearance of electric fields that change the band structure of the graphene layer. Similar structuring is observed near any surfaces immersed in a liquid. The stratification of the density of a liquid essentially depends on the lyophilicity of the surfaces, which is the reason for the dependence of the hydrodynamic parameters of the flow in micro and nanochannels on the wettability of their surface by the working fluid. In addition, according to the data of molecular dynamics modeling, the appearance of flows and a change in their velocity leads to a change in the structuring of liquid molecules near the surface of nanochannels [2, 3]. In this connection, one should also expect a change in the degree of collective influence of liquid molecules on the properties of the graphene surface. The present study is devoted to determining the influence of the shear stress of a liquid near the surface on its interaction with the graphene layer. With the help of molecular dynamics modeling, it was found that a change in the fluid flow rate changes the structuring of molecules in the near-surface zone, and the resistance of graphene. Thus, it has been found that graphene can be used as a flow rate-sensitive sensor.

**Acknowledgement:** This work was supported by the Russian Science Foundation, grant 23-29-00260.

**References:**

[1] V. Andryushchenko, D. Sorokin, M. Morozova, et al. Applied Surface Science 567 (2021) 150843.
[2] P. Alipour, D. Toghraie, A. Karimipour, et al. Journal of Molecular Liquids 275 (2019) 192-203.
[3] T. Yoshioka, R. Kunimori, I. Hisaoka, et al. Separation and Purification Technology 220 (2019) 259-267.

## OP-III-26

# Application of Graphene Nanofluids in Oil Production Industry

Pakharukov Yu.V.[1,2], Shabiev F.K.[1,2], Safargaliev R.F.[1,2], Ezdin B.S.[3], Vasiliev S.A.[3]
*1 – Tyumen State University, 6 Volodarskogo str., Tyumen 625003, Russia*
*2 – Tyumen Industrial University, 38 Volodarskogo str., Tyumen 625000, Russia*
*3 - Novosibirsk State University, 1 Pirogova str., Novosibirsk 630090, Russia*
*faridshab@mail.ru*

The efficiency of oil recovery from oil reservoirs in all producing countries is less than 40%. Low-capacity fields with hard-to-recover reserves are put into production. Some of the fields, usually with the water cut of 80% and more, are removed from the producing stock and transferred to the reserve stock due to the lack of oil recovery technologies. According to experts, the volume of oil in such fields makes up 30% or more of the total volume of the reservoir. Thus, we may conclude that there is a colossal reserve of oil which cannot be recovered with modern technologies. One of the effective methods of enhanced oil recovery is flooding with hot water or steam, micellar, alkaline and polymer solutions, surfactant solutions, sulfuric and hydrochloric acids. These technologies are of low efficiency, as they are not capable of adjusting to the physical and chemical properties of the oil reservoir, and require an individual approach for each field. In addition to low efficiency, most waterflooding technologies are harmful to the environment. As numerous studies show, nanofluids have unique physical and chemical properties [1]. Thus, graphene-like nanofluids have amphiphilicity, which can replace the use of surfactants in the technologies of oil displacement from hard-to-recover fields. This paper presents a study of the impact on the physical and chemical properties of the oil reservoir and oil when exposed to the graphene nanofluids.

One of the main characteristics of the oil-bearing formation is its permeability. Earlier we showed in [2] that the interaction of nanoparticles of graphene (GNP) and oil capillary walls are covered with a corrugated graphene film, which can increase the permeability by several times. Such a mechanism of impact on the permeability of the oil-bearing formation microcapillary requires a detailed consideration. According to the results of permeability studies of various rocks, carried out by the standard technique [3], it was found that with increasing concentration of GNPs initial permeability increases rapidly, then, reaching a maximum, it decreases.

Another important parameter in oil displacement is the viscosity of the displacing and displaced fluids. By controlling the rheology of the oil and the displaced agent, it is also possible to influence the oil recovery factor. A set of rheological studies shows that during the interaction of GNP with hydrocarbon molecules, oil viscosity can both decrease and increase. Figure (1) shows the dependences of the relative viscosity of oil at different temperatures and concentrations of two types of GNPs. For particles of type 1 (GNP1) a decrease in viscosity is observed (Figure 1a). So at concentrations of $5\times10^{-3}$ mass fraction and temperature of 50°C

the decrease in viscosity is 17%. Type 2 particles (GNP2) at ultra-low concentrations ($1.6\times10^{-5}$ wt.%) can increase the viscosity more than 1.5 times (Fig. 1b).

Thus, the controlling parameters of the impact on the walls of the microcapillaries of the oil-bearing rock, and the rheology of the oil is the structure and concentration of graphene nanoparticles. Thus, when creating displacing nanofluids it is necessary to take into account both the structure and concentration of nanoparticles.

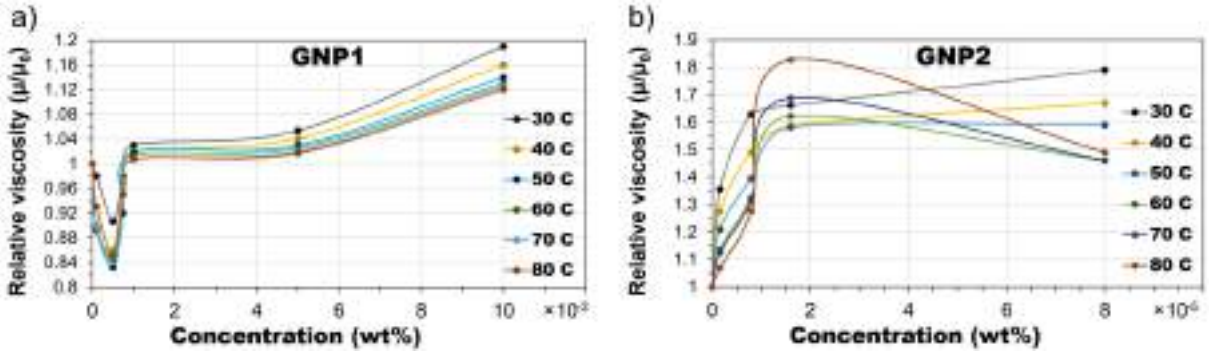


*Fig. 1. Relative viscosity of oil with the addition of graphene nanoparticles at different temperatures and concentrations (a) particles type 1, (b) particles type 2*

Thus, the study of the interaction of GNPs with hydrocarbon molecules reveals a range of new effects and phenomena. One such effect is the self-assembly of GNP at the nanofluid-oil interface. This effect leads to a first order phase transition with the formation of nanocrystallites from hydrocarbon molecules on the GNP surface, as confirmed by our XRD results. Based on the above, it can be argued that the fundamental research of the interaction of hydrocarbons and GNP opens up a new range of applied problems with a view to the practical use of GNP in the energy, oil, chemical and other industries.

**References:**

[1] S. Sikiru, A. Rostami, H. Soleimani, N. Yahya, Y. Afeez, O. Aliu, J. Y. Yusuf, T. L. Oladosu, Graphene: Outlook in the enhance oil recovery (EOR), Journal of Molecular Liquids, 2021, V.321, P.114519

[2] Yu.V. Pakharukov, F.K. Shabiev, R.F. Safargaliev, A.V. Shabieva, Journal of Applied Mechanics and Technical Physics, 2022, V. 63, No. 6, pp. 1005–1009.

[3] OST 39-235-89. Oil. Method for Determining Phase Permeabilities in Joint Stationary Filtration under Laboratory Conditions. Introd. 06.02.1989.

## OP-III-27

# Programmable Mechanochromic Response in 3D Printed Chiral Photonic Elastomers

Choi J.-H.[1], Choi Y.-G.[2], Yoon T.-H.[2], Ahn S.-k.[1]
*1 – School of Chemical Engineering, Pusan National Univ., Busan, Korea*
*2 –Department of Electronics Engineering, Pusan National University, Busan, Korea*
*wisdom1jang@gmail.com*

In this study, we develop a new method to develop cholesteric liquid crystal (CLC) phase-based chiral photonic elastomers via UV-assisted direct ink writing (DIW). Unprecedentedly, the helical axis of the DIW-processed CLC elastomers (CLCEs) was slanted by about 40° along the printing direction, which led to blue- or red-shifting of the reflected structural color of the CLCEs depending on the printing direction and the viewing angle. More interestingly, the mechanochromic behavior of the CLCEs was considerably altered by the printing direction due to the change in the slant angle of the helical axis. By harnessing both the chiroptical and mechanochromic properties of CLCEs, the potential of our CLCE as a novel strain sensor was demonstrated, which could be useful for creating an interesting anti-counterfeiting device.

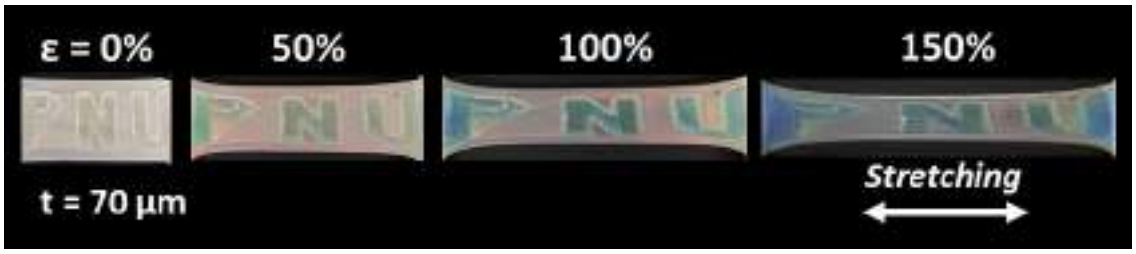


*Fig. 1. Photographic images of CLCE film showing "PNU" letters as it is stretched.*

**Acknowledgement:** This work was supported by Basic Science Research Program and by BK21 four program through the National Research Foundation of Korea (NRF) funded by the Ministry of Education

**References:**

[1] C. P. Ambulo, J. J. Burroughs, J. M. Boothby, H. Kim, M. R. Shankar, T. H. Ware, ACS Appl. Mater. Interfaces, 9, (2017) 37332.
[2] K. M. Lee, M. Rumi, M. S. Mills, V. Reshetnyak, D. R. Evans, T. J. Bunning, M. E. McConney, ACS Appl. Mater. Interfaces, 12, (2020) 37400
[3] J. A. H. P. Sol, H. Sentjens, L. Yang, N. Grossiord, A. P. H. J. Schenning, and M. G. Debije, Adv. Mater., 33, (2021) 2103309

## OP-III-28

# Platinum Ceria-Zirconia Supported Catalysts for the Water Gas Shift Reaction: Structure Diagnostics and Approaches to Boost the Performance

Gorlova A.M.[1], Pakharukova V.P.[1,2], Stonkus O.A.[1,2], Rogozhnikov V.N.[1], Snytnikov P.V.[1], Potemkin D.I.[1,2]

*1 – Boreskov Institute of Catalysis, Novosibirsk, Russia*

*2 – Novosibirsk State University, Novosibirsk, Russia*

*gorlova@catalysis.ru*

Since hydrogen is a perspective alternative to fossil fuels, the catalytic processes of its purification are the objects of intense studies for the last decades. The processes of carbon monoxide removal are of a particular interest because this gas is known to be a catalytic poison. Water gas shift reaction (WGSR) is traditionally used as the first step on the way from synthesis gas (10-30 vol.% CO) to pure hydrogen. Performing this reaction, it is possible to reduce the CO concentration in the hydrogen-rich gas to ≈1 vol.%.

The commercial catalysts for WGSR are already well known: Fe-Cr and Cu-Zn massive oxide catalysts for high- and low-temperature WGSR, respectively. But they turn out to be unsuitable for some applications. For example, they are not the best choice for portative reformers because of the size of the purification unit, since both of the catalysts must be used successively in two reactors to provide for the required CO concentration. In addition, these catalysts require for the long-time activation procedure and are intolerant to oxygen traces in the feed gas. For these reasons, a wide range of alternative catalytic systems is being developed. For example, ceria supported catalysts with transition or/and noble metal as an active component do not have the drawbacks of the commercial ones, but are highly active in WGSR at low temperatures.

In this work, platinum ceria-zirconia supported catalysts were synthesized. They were tested in WGSR in the reformate-simulating mixtures (vol.%: 10 CO, 15 $CO_2$, 30 $H_2O$, 45 $H_2$) and studied by the different physico-chemical methods. By means of pair distribution function (PDF) analysis, HR TEM and CO chemisorption it was shown that using the sorption-hydrolytic deposition technique provides for the highly dispersed (<2 nm) platinum particles on the surface of the oxide support. This leads to the high activity of $Pt/Ce_{0.75}Zr_{0.25}O_2$ systems: the equilibrium CO conversion at WHSV = 30000 $ncm^3 \cdot g_{cat}^{-1} \cdot h^{-1}$ has been reached below 300 °C with 5 wt.% Pt in the catalyst [1]. The structure dynamics of $Pt/Ce_{0.75}Zr_{0.25}O_2$ was studied using XRD and quasi *in situ* XPS techniques. It was shown that total Pt reduction in $H_2$ occurs at 75 °C, and the reduction of the surface of the oxide takes place at higher temperatures due to hydrogen spillover, which leads to oxygen vacancies formation playing an important role in the WGSR.

Pt-Re and Pt-Fe bimetallic ceria-zirconia supported catalysts were also synthesized and tested in WGSR. It was shown that Re addition provides for an increased activity of the catalyst

compared to platinum monometallic one, while doping with Fe allows for the suppression of the side methanation reaction up to 350 °C.

**Acknowledgement:** This work was supported by the Russian Science Foundation, grant 21-73-20075.

**References:**

[1] A.M. Gorlova, M.A. Panafidin, V.A. Shilov, V.P. Pakharukova, P.V. Snytnikov, D.I. Potemkin, Int. J. Hydrogen Energy 48 (2023) 12015.

## OP-III-29

# Photocatalytic Degradation of Dexamethazone and Ceftriaxone by $TiO_2$/Ag Nanoparticles

Chzhou V.R.[1,2], Bakina O.V.[1,2], Suliz K.V.[1]

*1 – Institute of Strength Physics and Materials Science of Siberian Branch Russian Academy of Sciences, Tomsk, Russia*

*2 – Sevastopol State University, Sevastopol, Russia*

*chzhou.vr@ispms.ru*

Persistent organic pollutants are hazardous chemicals that result from rapid and uncontrolled industrialization, urbanization and human activities. Most of these pollutants are toxicity, mutagenicity and carcinogenicity and threaten human health and the planet's ecosystems. Scientists around the world are have long been addressing the global crisis caused by inadequate drinking water quality [1].

Heterogeneous photocatalysis is one of the most promising technologies for water purification. This technology is effective in the degradation of organic pollutants and disinfection of pathogenic microorganisms. There are many antibiotic removal photocatalysts [2]. Among these semiconductor materials, titanium dioxide ($TiO_2$) has been widely used in many photocatalytic applications because of its low toxicity, chemical stability, availability, convenient physical and optical properties, low cost. Nevertheless, the disadvantages of traditional $TiO_2$ photocatalyst are the high recombination rate (within nanoseconds) of photo-generated charge carriers. The spatial separation of electron–hole pairs by local fields may reduce the rate of recombination of photogenerated charge carriers. The noble metal doping of $TiO_2$ is a versatile method for improving its photocatalytic activity [1].

In the present study $TiO_2$/Ag nanoparticles with average particle size 96±2 were synthesized by electric explosion of two twisted wires in oxygen-containing atmosphere. Nanoparticles were characterized by transmission electron microscopy (TEM) and X-Ray diffraction analysis (XRD) using CuKa radiation (XRD-6000, Shimadzu, Japan). TEM image is clearly show the spherical core decorated with silver clusters. XRD data of the $TiO_2$/Ag sample exhibits anatase, rutile and silver phases. Photocatalytic activity were studied in the reaction of degradation of two model dyes – methylene blue (MB) and rhodamine B (RB). The dye decolourization percentages after 60 minutes visible light irradiation were 93% and 43% for MB and RB degradation, respectively. A plausible degradation reaction mechanism was derived from controlled experiments using free radical scavengers. The reusability of $TiO_2$/Ag nanoparticles was performed for five cycles of application for MB degradation. Antibacterial activity of $TiO_2$/Ag nanoparticles was studied using standard suspension method against methicillin resistance *S.aureus*. It was shown that $TiO_2$/Ag nanoparticles 100% inhibit bacterial culture growth. The $TiO_2$/Ag ability of wastewater disinfection under visible light irradiation was shown. We observed water disinfection after 90 minutes irradiation.

Presence steroid hormones and antibiotics in drinking water cause of great concern due to their impact on human and ecosystem. Accordingly the capability of that substances

decomposition in the presence of $TiO_2$/Ag nanoparticles was studied. After 120 minutes of irradiation we obtained 64% and 66% degradation efficiency of dexamethazone (initial concentration 2.5 mg*$l^{-1}$) and ceftriaxone (initial concentration 5 mg*$l^{-1}$) respectively.

**Acknowledgement:** This work was supported by Russian Science Foundation
(Project No. № 21-13-00498)

**References:**

[1] A.M.Sescu, L.Favier, D.Lutic, N.Soto-Donoso, G.Ciobanu, M.Harja. Water.13 (2021) 19
[2] X.Zheng, Z.P. Shen, L.Shi, R.Cheng.Catalysts. 7(2017) 224.

## OP-III-30

# Resistive Tactile Sensor Prototype Based on Biological Nanomaterial

Batrakova I.A.[1], Gorina A.V.[1], Ichkitidze L.P.[1,2]

*1 – Institute for Regenerative Medicine, Sechenov First Moscow State Medical University (Sechenov University), 119991 Moscow, Russia*

*2 – Institute of Biomedical Systems, National Research University of Electronic Technology (MIET), 124498 Zelenograd, Moscow, Russia*

*ichkitidze@bms.zone*

The most sensitive mechanical receptors are located on the tips of the tongue and fingers of a person. Their sensitivity to deformations is in the pressure range $P$ ~ 2-5 mg/mm$^2$ (20-50 Pa). Tactile sensors for robotics with sensitivity up to $P \leq 1$ Pa are already being created, but they have a low degree of biocompatibility, and their use in medical applications is not possible.In this work, we studied a prototype of a resistive tactile sensor based on a thin film containing a matrix of microcrystalline cellulose (MCC, biological material) and a filler of multi-walled carbon nanotubes (MWNTs), i.e. biological nanomaterial MCC/MWNT.

An aqueous dispersion of MCC/MWNTs was deposited on a flexible substrate made of commercial polyethylene (PET, thickness $d_0$~30 µm). The PET substrate had a mass of ~4.5 mg, and the films deposited on it had the following dimensions: 50-200 nm×5 mm×25 mm. The MCC/MWNT film served as a strain-sensing element (TSE). The deformation and measurements of the physical parameters of the TSE were carried out automatically, the data were stored in a computer. The TSE bending angle varied in the range of 0 – 140 °. The TSE with a thickness of $d$ ~ 0.2 µm showed an optical transparency of ~ 80% and a resistance of ~ 0.5 MΩ.

The studied films exhibited the properties of a bipolar strain gauge, i.e. when bending in the form of a concavity, the resistance decreased, and when bending in the form of a convexity, the resistance increased.

Films of biological nanomaterial MCC/MWNT containing ≤0.2% wt. MWCNT, in the load area of 5-30 mg, pressures were recorded in the range of 10-30 Pa. Therefore, the considered prototype of a tactile sensor based on a biological nanomaterial can be the basis for the creation of TSE for medicine (minimally invasive surgery, highly sensitive palpation, endoscopy, etc.).

**Acknowledgement:** This work was funded by Russian Ministry of Science and Higher Education (state assignment №075-03-2023-024 from 13.01.2023). Research at Sechenov University in part of the preparation of magnetic nanoparticles was funded by the Ministry of Science and Higher Education of the Russian Federation under grant agreement No. 075-15-2021-596.

## OP-III-31

# Oxidation of N-(Isopropyl)-N-(Phosphonomethyl)-Glycine with Hydrogen Peroxide in the Presence of Nanostructured Au/Sibunit$^{TM}$ Catalysts

Khlebnikova T.B., Pai Z.P., Yushchenko D.Y., Simonov P.A., Bukhtiyarov V.I.
*Boreskov Institute of Catalysis, Novosibirsk, Russia*
*chleb@catalysis.ru*

Glyphosate, also known as N-(phosphonomethyl)-glycine is the most widely used non-selective herbicide in the world. High demand for glyphosate is also observed in the Russian Federation. According to independent experts, the annual demand of the Russian market for glyphosate based herbicides is 40 thousand tons per year [1]. Despite this, there is no existing production in the Russian Federation. The latter is partly due to the lack of a domestic technology of glyphosate synthesis. Among many methods of the glyphosate synthesis known from the literature the most effective is the method based on the catalytic oxidation of N-(isopropyl)-N-phosphonomethyl glycine with hydrogen peroxide [2]. Oxidation proceeds in the presence of nanostructured Au/Sibunit$^{TM}$ catalysts at high conversion and glyphosate selectivity [3].

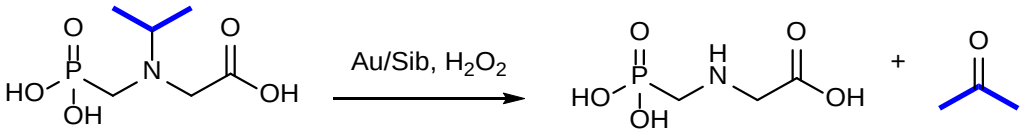


***Scheme. Catalytic oxidation of N-(isopropyl)-glycine.***

As part of the study of nanostructured Au/Sibunit$^{TM}$ catalysts in the reaction of "atom-efficient" synthesis of glyphosate by the catalytic oxidation of N-(isopropyl)-N-(phosphonomethyl)-glycine with hydrogen peroxide, the factors affecting the activity and selectivity of the catalyst were determined. It is shown that: the highest selectivity for glyphosate (up to 93%), observed at almost complete conversion of the substrate, is achieved in the presence of Au/Sibunit$^{TM}$ catalysts with an average particle size of 1.0 to 2.5 nm. The method has been successfully tested in catalytic dealkylation reactions of N-substituted derivatives of N-(phosnomethyl)-glycine. The results obtained can be a fundamental basis for creating a technology for obtaining glyphosate when organizing its production in the Russian Federation.

**Acknowledgement:** This work was supported by the Ministry of Science and Higher Education of the Russian Federation within the governmental order for Boreskov Institute of Catalysis, project AAAA-A21-121011390007-7.

**References:**

[1] https://www.agroinvestor.ru
[2] D.Y. Yushchenko, T.B. Khlebnikova, Z.P. Pai, V.I. Bukhtiyarov, Kinet. Catal. 62 (2021) 331–341.
[3] D.Y. Yushchenko, P.A. Simonov, T.B. Khlebnikova, Z.P. Pai, V.I. Bukhtiyarov, Catal. Commun. 121 (2019) 57–61.

## OP-III-32

# Ring-Expansion from Thiophene to Thiopyran

Gang Zhou
*Lab of Advanced Materials, Fudan University, Shanghai 200438, P. R. China*
*zhougang@fudan.edu.cn*

S-fused polycyclic compounds have been extensively exploited in the fields of medicine, agricultural pharmacology, and organic functional materials. Among the various S-containing heterocycles, five-membered thiophene ring and six-membered thiopyran ring are the most representative building blocks. In comparison to the popular thiophene derivatives which have attracted tremendous attention due to their unique optoelectronic properties, such as intense luminescence, tunable electronic structure, and high charge carrier mobility, fewer reports have focused on the thiopyran analogues, most likely due to the more challenging synthesis and completely different electronic structures.

Recently, we have developed a facile ring-expansion cyclization from five-membered thiophene ring to six-membered thiopyran ring.[1-6] The resulting building block, cyclopenta[*b*]thiopyran, which is isomeric to benzo[*b*]thiophene, has a co-planar structure and may similarly form ideal intermolecular packing. Most importantly, cyclopenta[*b*]thiopyran is isoelectronic to non-alternant hydrocarbon azulene and presents intriguing photophysical and electrochemical properties, such as near-infrared absorption, low oxidation potential, and excellent electrochemical stability. Therefore, cyclopenta[*b*]thiopyran is a promising building block for organic semiconductors towards optoelectronic applications.

**References:**

[1] Y. Lu, Y. Qiao, H. Xue, G. Zhou, *Org. Lett.* **2018**, *20*, 6632−6635.
[2] Y. Qiao, Y. Lu, W. Chen, Y. Chen, M. Baumgarten, G. Zhou, *Chem. Commun.* **2019**, *55*, 5107−5110.
[3] Y. Qiao, L. Yang, J. Zhu, C. Yan, D. Chang, N. Zhang, G. Zhou, Y. Zhao, X. Lu, Y. Liu, *J. Am. Chem. Soc.* **2021**, *143*, 11088–11101.
[4] S. Liu, Z. Zhou, J. Fang, M. Wang, H. Zong, W. Chen, G. Zhou, *Org. Chem. Front.*, **2023**, *10*, 54–61.
[5] W. Chen, S. Liu, Y. Ren, S. Xie, C. Yan, Z. Zhou, G. Zhou, *Chem. Eur. J.*, **2023**, e20220323.
[6] H. Zong, M. Wang, W. Chen, Z.-D. Zhang, J.-W. Cai, C. Shen, L.-X. Li, G. Zhou, S.-D. Wang, *ACS Appl. Mater. Interfaces*, **2023**, doi: 10.1021/acsami.2c10444.

## OP-III-33

# Edible Chitosan/Spider Silk Food Coating for Fruit Preservation

Tracey C.T.[1], Bhatt T.K.[1], Timofeyev M.[2], Dagbaev M.[2], Kurilova O.[2], Krivoshapkin P.V.[1], Krivoshapkina E.F.[1]

*1 – ITMO University, St. Petersburg, Russia*

*2 – Institute of Biology at Irkutsk State University, Irkutsk, Russia*

*traceychantal@gmail.com*

Fruits are highly susceptible to physical, chemical, and microbial spoilage, resulting in massive food waste as approximately one third is discarded after harvesting [1]. Because of this, several preservation techniques designed to slow ripening, softening, oxidation, and dehydration while maintaining nutrition, texture, and flavour profiles have been investigated [2]. Thus far, the use of food coatings has proven very effective. Food coatings exhibit exceptional moisture and gas barrier properties, microbiological stability, good moisture adsorption capacity, and excellent mechanical properties [1]. However, concerns about the compositions of these coatings, which may contain chemicals that adversely react with foods to create hazardous substances, have been raised [3]; therefore, non-toxic, biocompatible, and biodegradable food coatings are preferred. Here, we present an edible food coating made from chitosan obtained from black soldier fly (BSF) exoskeletons and spider silk for fruit preservation.

The coating was obtained by defatting, deproteinizing, decolorizing, then deacetylating chitin found in BSF exoskeletons, and polymerizing the resulting chitosan with silk harvested from spiders and glycerol, which acted as a plasticizer. Several wt.% silk concentrations were explored, and films made from the various coating solutions were casted and characterised. The 0.03 wt% silk/chitosan film was chosen for further experiments since it showed the best mechanical properties. The film had a measured tensile strength and Young's modulus of 21±6 and 15±6 MPa, respectively, which is comparable to that of commercially available high-density polyethylene plastic [4].

The swellabilities of the different films were also tested and, as shown in **Fig. 1a**, the 0.03 wt.% silk exhibited good swelling ability. The film was also found to be hydrophobic (water contact angle = 95.9°), which indicates good barrier properties and resistance to moisture and water vapour (**Fig. 1b**) [5]. The biodegradability of the 0.03 wt.% silk/chitosan film was also explored. Lysozyme and trypsin, which have been shown to degrade chitosan and silk protein, respectively, were used in degradation experiments. As depicted in **Fig. 1c**, appreciable degradation of the film was observed within 6 days. However, trypsin was able to completely degrade the film within the same period (**Fig. 1d**). The antimicrobial properties of the film were also investigated, and it was found to show slight activity against both gram-negative (*Escherichia coli*) and gram-positive bacteria (*Bacillus subtilis*) (**Fig. 1e**).

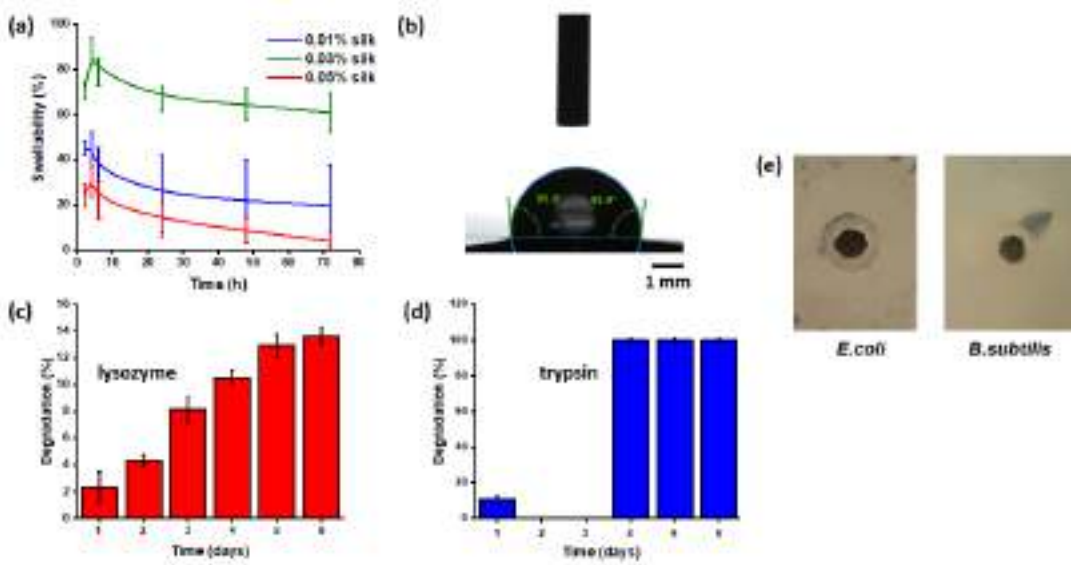


*Fig. 1. (a) Swellability of chitosan/silk films. (b) Water contact angle, (c) lysozyme degradation, (d) trypsin degradation and (e) antimicrobial properties of 0.03 wt.% silk/chitosan film.*

The applicability of the 0.03 wt.% silk/chitosan solution as potential food coating was studied. Ripe strawberries were coated with the 0.03 wt.% silk/chitosan solution and pure chitosan and observed. Uncoated strawberries were used as controls. As shown in **Fig. 2**, after 7 days, strawberries coated in the 0.03 wt.% solution showed no signs of microbial spoilage or discoloration. Therefore, the proposed chitosan/spider silk food coating can be used as food coating.

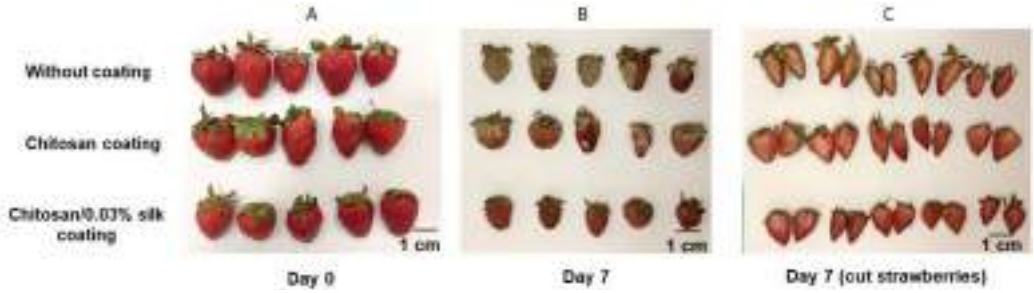


*Fig. 2. Comparison of strawberries coated in 0.03 wt.% silk/chitosan film and pure chitosan with uncoated strawberries.*

**Acknowledgement:** This work was supported by the Ministry of Higher Education of Russia Project No. 075-15-2019-1896.

**References:**

[1] C. T. Tracey, A. V. Kryuchkova, T. K. Bhatt, P. V Krivoshapkin, E. F. Krivoshapkina, *J. Food Eng.* **2023**, *337*, 111231.
[2] M. C. Heller, S. E. M. Selke, G. A. Keoleian, *J. Ind. Ecol.* **2019**, *23*, 480.
[3] M. E. Genovese, J. Zia, D. Fragouli, In *Sustainable Food Packaging Technology*, John Wiley & Sons, Ltd, **2021**, pp. 369–393.
[4] N. Pešić, S. Živanović, R. Garcia, P. Papastergiou, *Constr. Build. Mater.* **2016**, *115*, 362.
[5] M. M. Frota, A. L. A. Mattos, K. W. E. Miranda, H. N. Cheng, A. Biswas, M. do Socorro Rocha Bastos, *Appl. Food Res.* **2022**, *2*, 100213.

## OP-III-34

# Composites of Polyhydroxyalkanoates with Pesticides - a Biodegradable Basis for the Creation of New Generation Preparations for the Protection of Cultivated Plants from Weeds and Phytopathogens

Kiselev E.G.[1,2], Volova T.G.[1,2]
*1 – Institute of Biophysics SB RAS Krasnoyarsk, Russia*
*2 – Siberian Federal University Krasnoyarsk, Russia*
*evgeniygek@gmail.com*

Currently, industrial ecology and "green chemistry" are of great importance in the development of society, the main task of which is the creation of new environmentally friendly materials from renewable sources [1]. One of the topical areas of research is the creation of long-acting pre-emergence pesticide preparations with controlled release of the active substance from a biodegradable polymer matrix. Such preparations have a number of advantages, such as a reduction in the number of crop treatments, prolongation of the action of unstable pesticides, less toxicity, and the ability to solidify liquid pesticides. However, a significant disadvantage is the high cost of biopolymers. One way to reduce the cost of biopolymers is to create composite materials based on them [2-3].

A family of agricultural composite materials designed for the long-term delivery of herbicides and fungicides has been designed for the first time. The resulting composite materials are a polymer frame made of poly-3-hydroxybutyrate (P(3HB)) filled with wood flour (40–45%) and containing up to 10% herbicides (metribuzin, tribenuron-methyl), or fungicides (tebuconazole, azoxystrobin, epoxiconazole).

Using the methods of IR spectroscopy, thermal analysis, X-ray diffraction analysis, scanning electron microscopy, it was found that all interactions of the components in the composition are of a physical nature and do not form chemical bonds with each other.

In the characterized laboratory soil micro ecosystems, the kinetics of the release of active substances into the soil from forms against the background of their biodegradation was studied. For the first time, the isolation and identification of polymer destructors in mixtures with various natural and degradable synthetic materials has been carried out. Using molecular genetic methods, bacteria and fungi were identified as common and specific decomposers of the studied samples, the fragments of the 16S rRNA and 28S rRNA genes of which were deposited in the database.

The factors influencing the destruction of forms in the soil and the release of preparations from the forms have been established. The influence of shape geometry (granules, 3D) and the type of pesticide used on these processes is shown. More rapid destruction of the forms and, accordingly, the yield of preparations are characteristic of granules, which are characterized by low mechanical strength and less stability in the soil, in contrast to denser and stable pressed forms. The yield of preparations largely depended on the solubility of the preparations and was more active for rapidly soluble compounds. An important result was

obtained, indicating the possibility of regulating the rate and duration of the release of active substances from the molds into the soil and, in general, the "lifetime" of the molds by involving various manufacturing methods, as well as preparations with different structures, molecular weights and solubility.

Field tests of the effectiveness of the action of prototypes of long-term herbicidal and fungicidal preparations on crops of grain crops and table beet were carried out on leached chernozems of the Krasnoyarsk forest-steppe.

Fungicidal protection of seeds of grain crops in the form of granules coated with tebucanozol determined the maximum field germination of seeds of spring wheat (92%) and barley (87%).

A persistent prolonging effect of tribenulon-methyl has been established when it is deposited in a biodegradable granule together with tebucanozole. The biological effectiveness of these forms of herbicides on crops of spring wheat reached 85%, barley - 78%.

The biological effectiveness of metribuzin deposited in the granule was comparable to the control drug, a stable prolonging effect on weeds during the growing season was established. Favorably affected the development of beet plants, ensuring the yield of root crops up to 66 t/ha and good marketability of products.

Long-acting fungicide preparations (azoxystrobin, azoxystrobin + mefenoxam and difenoconazole) suppressed the development of phytophthora and alternariosis in the rhizosphere during the entire growing season and reduced the area of plant damage by pathogens by 10-15%, which is 2 times less than in groups of plants treated with commercial drugs. Higher biological activity ensured the maximum number of tubers undamaged by pathogens and a total yield of 22-23 t/ha, which exceeded the yield in groups with industrial fungicides (18.4-20.8 t/ha).

The conducted field tests have confirmed the effectiveness of using polyhydroxyalkanoates as a polymer base for the design of long-acting pesticide preparations.

**Acknowledgement:** This work was financially supported by Project “Agropreparations of the new generation: a strategy of construction and realization” (Agreement No 075-15-2021-626) in accordance with Resolution No. 220 of the Government of the Russian Federation of April 9, 2010, “On measures designed to attract leading scientists to the Russian institutions of higher learning” "Synthesis of polymer samples for film production" - at the expense of the state task of the Ministry of Science and Higher Education of the Russian Federation (project No. 0287-2021-0025)"

**References:**

[1] A.K. Urbanek, W. Rymowicz, A.M. Mirończuk, Appl. Microbiol. Biot. 102 (2018) 7669–7678.
[2] A.B.Tleuova, E. Wielogorska, P. Talluria, J. Control. Rel. 326 (2020) 468-481.
[3] V. Dhananjayan, S. Jayakumar, B. Ravichandran, Eds.; Springer: Cham, Switzerland, (2020), pp. 1-

## OP-III-35

# Absorption of Carbon Dioxide Using Composite Materials Based on Polyethylenimine

Sheshkovas A.Z.[1,2], Veselovskaya J.V.[1], Rogov V.A.[1,2], Kozlov D.V.[1]
*1 – Boreskov Institute of Catalysis, Novosibirsk, Russia*
*2 – Novosibirsk State University, Novosibirsk, Russia*
*sheshkovas@catalysis.ru*

In recent years, research on carbon dioxide capture and reducing the carbon footprint in general has received a lot of attention. Such interest is primarily associated with an increase in the consumption of carbon feedstock, and, as a result, an increase in the concentration of $CO_2$ in the atmosphere, which negatively affects the environment and human health.

Nowadays, there are many absorption systems for capturing $CO_2$, but they all have disadvantages, such as high volatility, high regeneration temperatures, and/or low $CO_2$ absorption capacities. In this paper, we consider a material devoid of these disadvantages, based on the active component (AC) with a polymer structure, in particular, hyperbranched polyethylenimine (PEI). This substance is capable of chemically binding $CO_2$, but in a pure form its use is difficult due to high viscosity, which contributes to a decrease in the rate of $CO_2$ absorption. One of the ways to improve the dynamics of chemisorption is the dispersion of the AC in the pores of supports with a developed porous structure.

As supports for hyperbranched PEI ($M_w$ = 800), we used materials with different surface chemistry and porous structures: silica gels and silicon-zirconium aerogels with different ratios of oxides in the composition. The aim of the work was to study for the obtained composite materials the dependence of their absorption characteristics on the choice of the support and the mass content of the AC.

We synthesized composite sorbents by wet impregnation of the support using an alcoholic solution of PEI with a given concentration. First, the materials were dried in a thermal cabinet at a temperature of 50°C, and then at 100°C in a helium flow. We studied $CO_2$ absorption and thermal characteristics for the obtained composite materials using the methods of thermogravimetric analysis (TGA) and differential scanning calorimetry (DSC). The $CO_2$ absorption capacity of the materials ($a$) was determined at a temperature of 30°C using the gas mixture of $CO_2$ and He, containing 15 vol.% of carbon dioxide.

First of all, a number of experiments were carried out under the same conditions on composite materials with the same PEI content (40 wt%) based on different porous supports (Fig. 1). It was revealed that the most effective supports were silica gel ($SiO_2$-4) and aerogel 10%$ZrO_2$/90%$SiO_2$ (10%Zr/Si). Based on the results obtained, we believe that it is the chemistry of the surface that has the greatest influence on the distribution of the AC over the surface of the support.

Further, the optimal pore filling of the support (silica gel) with the active component was revealed. For PEI, this value is around 50% of the pore volume. At higher values of pore filling, a decrease in the efficiency of $CO_2$ absorption occurs due to hindered gas diffusion.

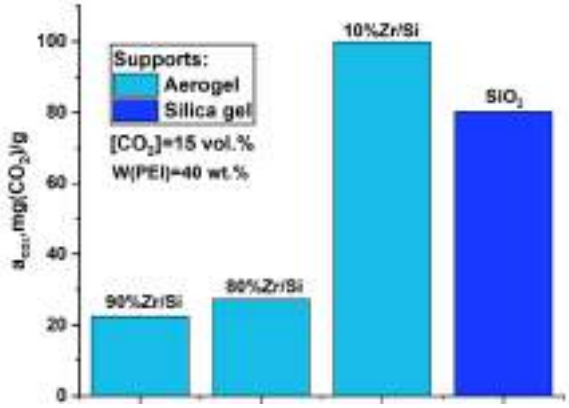


*Fig 1. The dependence of the $CO_2$ absorption capacity of composite materials on the choice of support*

Then the dependence of the sorption characteristics of the materials on the pore size of the support was investigated. To do this, experiments were carried out for a series of silica gels with the same volume content of the AC (50 vol.%). Experiments have shown that for materials impregnated with PEI, an increase in the PEI weight content gives a proportional increase in the value of $CO_2$ absorption per 1 g of the material (Table 1). However, $CO_2$ absorption capacity per 1 g of PEI (*a'*) differs for these materials. The greatest efficiency from dispersion is observed on the support $SiO_2$-2 with an average pore diameter of 6.8 nm (239.6 mg($CO_2$)/g(PEI)), and then there is a decline in the effective values of $CO_2$ absorption for the supports with larger pores. This effect is related to the size of the polymer molecule. On the one hand, the placement of molecules in larger pores leaves more functional amino groups available for reaction with $CO_2$. On the other hand, in pores of too large size, the dispersion effect of PEI may decrease, which we observe in this series of experiments.

Table 1. Porous structure parameters of the supports and $CO_2$ absorption capacities of the corresponding PEI-based composite materials

| **Supports** | **$S_{BET}$ ($\frac{m^2}{g}$)** | **$V_{BET}$ ($\frac{cm^3}{g}$)** | **$d_p$, nm** | **W(PEI), wt%** | **a, $\frac{mg(CO_2)}{g}$** | **a', $\frac{mg(CO_2)}{g(PEI)}$** |
|---|---|---|---|---|---|---|
| **$SiO_2$-1** | 569 | 0.67 | 4.7 | 26.1 | 60.0 | 230.0 |
| **$SiO_2$-2** | 464 | 0.79 | 6.8 | 29.5 | 70.3 | 238.6 |
| **$SiO_2$-3** | 377 | 0.96 | 10.2 | 33.6 | 79.8 | 237.2 |
| **$SiO_2$-4** | 256 | 1.12 | 17.5 | 37.2 | 83.2 | 223.6 |

Thus, the $CO_2$ absorption characteristics of PEI-based composite sorbents strongly depend on both the chemical nature and porous structure of the support. Optimization of these parameters is a key for obtaining the most effective $CO_2$ sorbent.

**Acknowledgement:** The research was supported by the grant of the Russian Science Foundation No. 23-23-10080, https://rscf.ru/en/project/23-23-10080/.

## OP-III-36

# Silica Glass/Mullite Composites Based on Coal Fly Ash Cenospheres as Effective Gas Separation Membranes

Rogovenko E.S.[1], Fomenko E.V.[1], Gareeva A.S.[1,2], Anshits A.G.[1,2]

*1 – Federal Research Center "Krasnoyarsk Science Center of Siberian Branch of the Russian Academy of Sciences", Institute of Chemistry and Chemical Technology, Krasnoyarsk, Russia*

*2 – Siberian Federal University, Krasnoyarsk, Russia*

*rogovenko_elena1989@mail.ru*

Currently, recycling industrial waste to produce high-tech materials with specific properties attracts great attention. Coal fly ashes, the major by-product from pulverized coal combustion, contain hollow spherical particles – cenospheres, which can be useful as gas separation membrane [1, 2]. It was shown that with an increase in the mullite phase in the cenosphere shells in the range from 4 wt % up to 48 wt % helium permeability increases by 2 orders of magnitude [1] and significantly exceeds the analogous values for silicate glasses [2]. These studies concerned morphologically homogeneous narrow fractions of cenospheres with globules of ring structure. Another morphological type of cenospheres is foamy globules with a network structure [3]; their diffusion properties have not yet been considered. The purpose of this work was to obtain a silica glass/mullite composites based on a narrow fractions of cenospheres with different structure and to study its physicochemical characteristics and gas transport properties in relation to He and Ne.

The narrow fractions of cenospheres with a predominant content of globules of a certain structure were used to obtain gas separation membranes (Fig. 1): M −0.063+0.05 mm included 74 % of ring particles with solid shell; R −0.25+0.2 mm contained 57 % of network spheres. From these narrow fractions in an oxidizing atmosphere at 1000 and 1100°C, silica glass/mullite composites containing defective crystal phases (Table 1) were obtained. The formation of these phases led to the extraction of modifier ions from the glass phase and to an increase in the $SiO_2$ content to 91%. It has been established that in the case of ring structure cenospheres, acicular mullite crystallites are formed on the outer and inner surfaces of the globules (Fig. 2 a, b) and for cenospheres with network structure, volumetric crystallization of the shell is observed (Fig. 2 c, d). Acicular mullite crystallites form a singular of crystalline framework, which gives the globule structural stability and the ability to withstand high pressure. The strength characteristics for cenospheres of a network structure are 3-5 times higher compared to cenospheres of a ring structure.

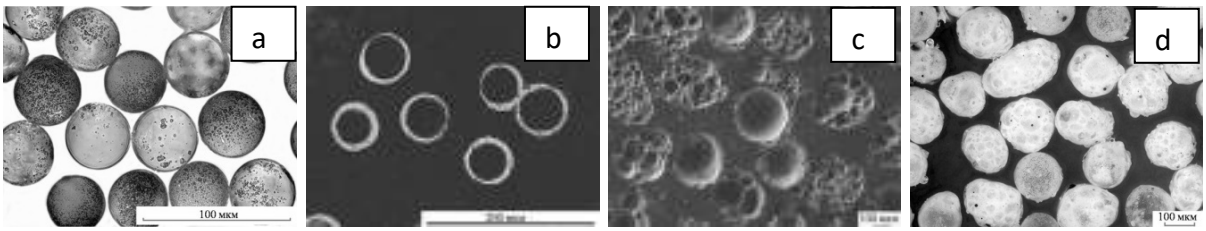


***Fig. 1.*** *SEM images of cenosphere narrow fractions: M −0.063+0.05 (a, b); R −0.25+0.2 (c, d)*

**Table 1.** Chemical and phase composition of silica glass/mullite composites

| Silica glass/mullite composite | Chemical composition (wt. %) | | | | | | | Phase composition (wt. %) | | | | | | |
|---|---|---|---|---|---|---|---|---|---|---|---|---|---|---|
| | $SiO_2$ | $Al_2O_3$ | $Fe_2O_3$ | CaO | MgO | $Na_2O$ | $K_2O$ | Quartz (0) | Quartz (l) | Mullite (0) | Mullite (l) | β-Crystoballite | Anortite | Glass phase |
| M −0.063+0.05 | 62.56 | 32.42 | 1.80 | 0.90 | 1.10 | 0.41 | 0.50 | 0.3 | 1.4 | 9.5 | 20.9 | – | – | 67.9 |
| R −0.25+0.2 | 59.30 | 35.66 | 1.54 | 1.00 | 0.71 | 0.32 | 0.40 | 1.2 | 1.0 | 42.3 | 4.1 | 16.0 | 1.9 | 33.5 |

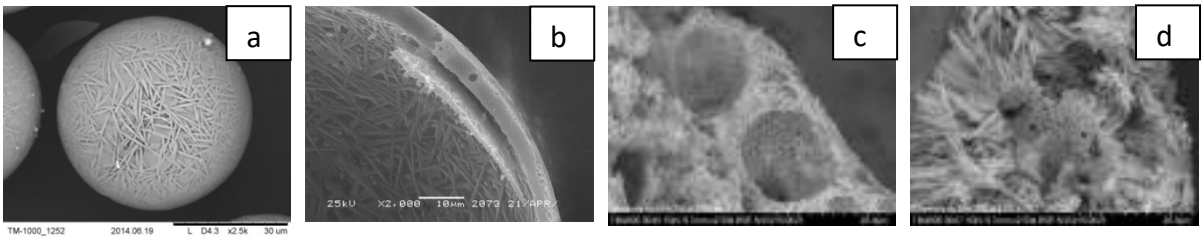


***Fig. 2.*** *SEM images of cenospheres with ring (a, b) and network (c, d) structure*

The investigation of a silica glass/mullite composite gas transport properties in relation to individual gases showed that at a temperature of 280°C $K_{He}$ were $1.7 \cdot 10^{-16}$ and $14.7 \cdot 10^{-16}$; $K_{Ne}$ were $0.01 \cdot 10^{-16}$ and $0.67 \cdot 10^{-16}$ (mol·m)/($m^2$·s·Pa); selectivity αHe/Ne reached 170 and 22 for M −0.063+0.05 and R −0.25+0.2 respectively. Determination of the gas separation properties in relation to He-Ne binary mixture was carried out for a composition of 80 vol. % He and 20 vol. % Ne which corresponds to the helium concentrate obtained in cryogenic technology after low-temperature condensation of all hydrocarbons. At the initial moment, the αHe/Ne selectivity is equal to the ideal selectivity obtained for individual gases and succeeds in enriching the target He component up to 99 vol. %.

Thus, silica glass/mullite composites based on coal ash cenospheres have a high level of permeability and selectivity, and also have high strength characteristics. Along with these, their advantages over known flat, rolled, and hollow fiber membranes are that the efficiency of the gas separation process does not depend on damage to individual globules. All this makes it possible to use the resulting silica glass/mullite composites as effective gas separation membranes.

**Acknowledgement:** This work was conducted within the framework of the budget project FWES 2021– 0013 for Institute of Chemistry and Chemical Technology of the Siberian Branch of the Russian Academy of Sciences.

**References:**

[1] E.V. Fomenko et al., J. RSC Adv. 4 (2014) 9997.
[2] E.V. Fomenko et al., J. Glass Phys. Chem. 45 (2019) 36.
[3] E.V. Fomenko et al., J. Energy & Fuels 29 (2015) 5390.

## OP-III-37

# Design of Polyfunctional Composite Catalysts for Hydrogen Production Reactions

Potemkin D.I., Rogozhnikov V.N., Gorlova A.M., Shilov V.A., Ruban N.V., Sobyanin V.A., Snytnikov P.V.

*Boreskov Institute of Catalysis, Novosibirsk, Russia*

*potema@catalysis.ru*

The processes of hydrogen production from various types of fossil and renewable fuels are energy-intensive multi-route chemical reactions. Selective and high-performance catalysts that combine high activity, thermal conductivity, corrosion and thermal resistance, are required for on-site hydrogen production for fuel cell feeding applications.

In this work a general strategy for the design of catalytic systems for hydrogen production is suggested. It is based on the application of composite catalysts of the "metal nanoparticles/active oxide nanoparticles/structural oxide component/structured metal support" structure. The structured metal support provides efficient heat removal or supply for exo- or endothermic reactions, possesses good hydrodynamic characteristics, and facilitates scale transition. The structural oxide component (aluminum oxide) provides thermal and corrosion resistance and a high specific surface area of the catalytic coating, as well as performing a protective function for the metal support. The active oxide component (mainly cerium–zirconium oxides) increases resistance to carbonization due to oxygen mobility and maintains a high dispersion of the active component due to its strong metal–support interaction. Metal nanoparticles 1–2 nm in size are involved in the activation of substrate molecules.

An approach for catalyst synthesis is illustrated at Fig. 1. FeCrAl alloy wire meshes, formed into cylindrical blocks of specified sizes, to be used as a heat-conducting substrate. By controlled annealing with the formation of a micron α-$Al_2O_3$ layer and subsequent deposition of a η-Al2O3 layer according to the Bayer method (through aluminum hydroxide), a structural layer of η-$Al_2O_3$ with a "breathing" needle-type morphology was deposited onto the FeCrAl alloy surface [1]; then the catalytic active component based on Pt and Rh nanoparticles was deposited onto this layer by sorption-hydrolytic deposition [2].

The efficiency of the proposed strategy is shown for Rh/$Ce_{0.75}Zr_{0.25}O_{2-\delta}$–η-$Al_2O_3$/FeCrAl (Rh/CZ/FCA) catalysts in diesel autothermal reforming (ATR) and liquified petroleum gas partial oxidation. Rh/CZ/FCA exhibited stable operation under commercial diesel ATR conditions (Fig. 2a,b). Pt/$Ce_{0.75}Zr_{0.25}O_{2-\delta}$–η-$Al_2O_3$/FeCrAl catalysts were shown to be highly active in natural gas partial oxidation and autothermal reforming (Fig. 2c). Also Pt/$Ce_{0.75}Zr_{0.25}O_{2-\delta}$–η-$Al_2O_3$/FeCrAl catalysts were shown to be good and selective catalysts in WGS reaction.

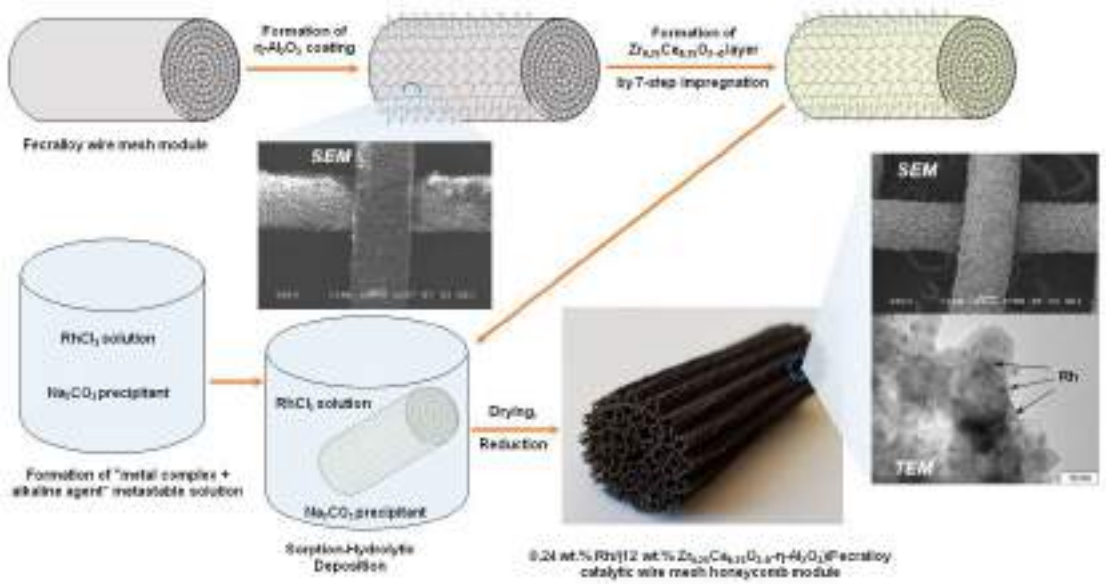


*Fig. 1. General scheme of composite catalysts preparation.*

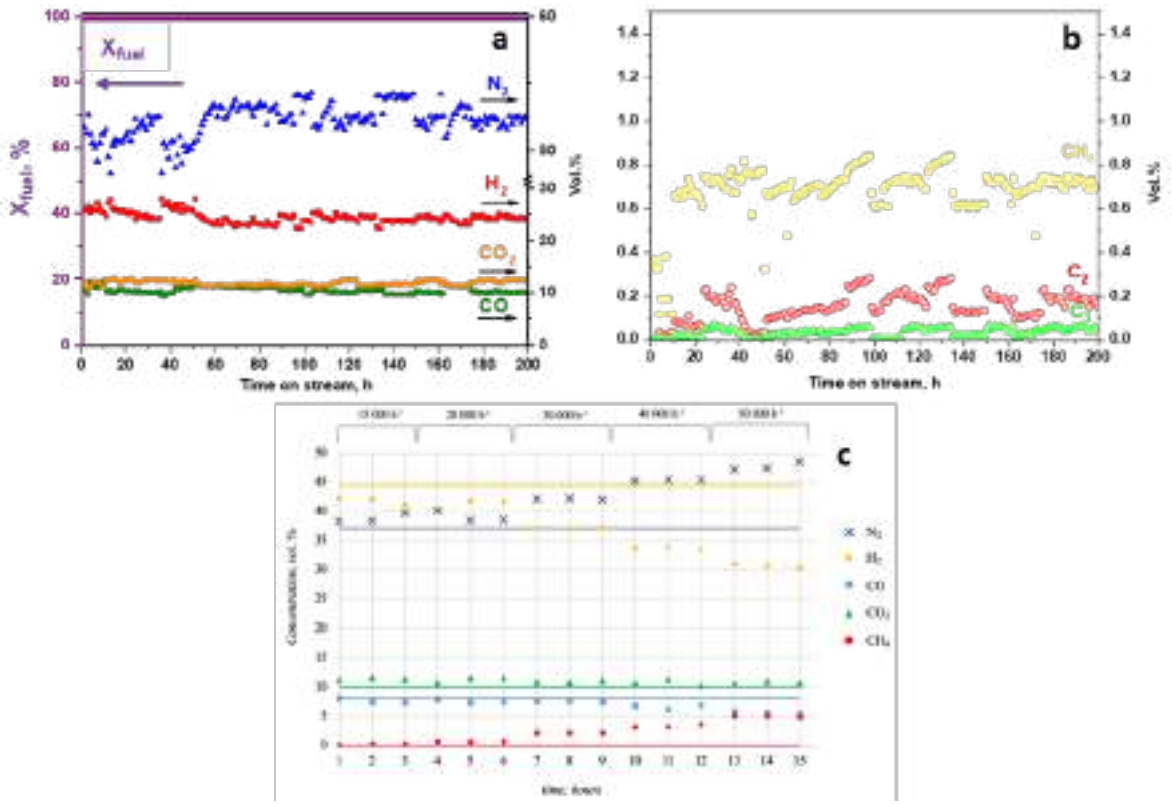


*Fig. 2. Stability tests for diesel ATR over Rh/CZ/FCA catalyst (a, b) and for $CH_4$ ATR over Pt/CZ/FCA (c).*

**Acknowledgement:** This work is supported by the Russian Science Foundation, project 21-79-10377.

**References:**

[1] Shoynkhorova T.B., Snytnikov P.V., Potemkin D.I., et al. // Applied Catalysis B: Environmental 2019. V. 245. P. 40–48.

[2] Shoynkhorova T.B., Simonov P.A., Potemkin D.I., et al. // Applied Catalysis B: Environmental 2018. V. 237. P. 237-244.

# Poster Presentations

## I. Synthesis and Structure of Advanced Materials

**PP-I-1 ÷PP-I-109**

## II. Biomaterials and Bionanocomposites

**PP-II-1 ÷ PP-II-20**

## III. Applications

**PP-III-1 ÷ PP-III-50**

## PP-I-01

# PEGylated Magnetic Nanoparticles for Water Purification from Organic Dyes

Aga-Tagiyeva S.E.[1], Omelyanchik A.S.[1], Magomedov K.E.[1,2], Orudzhev F.F.[1,2], Rodionova V.V.[1]
*1 – Immanuel Kant Baltic Federal University, Kaliningrad, Russia*
*2 – Dagestan State University, Makhachkala, Dagestan, Russia*
*agatagiyewas@gmail.com*

Research on contamination of groundwater and drinking water is of major importance. Therefore, enhancing adsorption of metal oxide nanoparticles has been a subject that has fascinated scientists and engineers for several decades. Wastewater from textile, pharmaceutical and food processing industry have always been a serious environmental problem, which are harmful to aquatic life and even endanger human health. Many dyes as organic contaminants are usually stable and hardly degradated in conventional wastewater treatment techniques including flocculation, coagulation, chemical precipitation and biological oxidation [1]. Developing environment friendly adsorption techniques is thus becoming an important issue to remove organic contaminants in water via simply adsorbing [2]. Methyl blue (MB) is one of the most common dyes which is widely used as the coloring agent and disinfector in pesticides, pharmaceuticals, dyestuffs and varnishes [3], and it is generally adopted as a representative organic pollutant to test the adsorption performance for the removal of organic contaminants from wastewater.

Here, iron oxide magnetic nanoparticles (MNPs) were synthetised by a co-precipitation method and coated with varying concentrations of polyethylene glycol (PEG). PEG is one of the most frequently used synthetic polymers for surface modification of MNPs to achieve high colloidal stability.

An X-ray diffraction (XRD) analysis confirmed the inverse spinel structure of synthesized MNPs (figure 1 (a)). The diffraction peak of 23° for all coated samples is due to the reflex (032) for PEG. As the amount of PEG loading increases, the relative intensity of the reflex that corresponds to it also increases. Figure 1 (b) shows the image obtained by transmission microscopy (TEM) for $Fe_3O_4$+2.0 PEG with an average particle size of $8.0 \pm 1.0$ nm. The average particle size was in good agreement with the XRD results, where the crystallite size of PEG (2.0 g) coated MNPs was approximately 7 nm, respectively.

Fourier transform infrared (FTIR) analysis was carried out to further investigate the adsorption of the PEG on the surface of synthesized MNPs. Figure 1 (c) shows the FTIR spectra of synthesized MNPs coating with different amount of PEG. MNPs showed characteristic bands related to FeO oscillations near 611 $cm^{-1}$. PEG shows characteristic stretching frequencies for –CH and CO at 2907 and 1109 $cm^{-1}$, $–CH_3$ asymmetric and $–CH_3$ symmetric were identified at 1584 and 1297 $cm^{-1}$, respectively. These results confirm modification of the MNPs surface with PEG.

The magnetic properties of samples were investigated using a vibrating sample magnetometer (VSM). Saturation magnetization ($M_S$) of samples coated with PEG decreased from 18 to 12 $Am^2/Kg$ as the amount of PEG loading increased from 0.6 g to 3.0 g (figure 1

(d)). The fact that the volume fraction of magnetite in MNPs coated with PEG is lower than that of MNPs without a coating. The lower volume fraction of magnetite in MNPs coated with PEG compared to those without a coating further confirms the successful PEGylation of MNPs. Despite this, the magnetic properties of the obtained PEGylated MNPs remain relatively high, making them easily separable from the solution using a magnetic field gradient.

Coated nanoparticles exhibit promise as potential candidates for sorption applications due to their water dispersibility, stability in aqueous environments, and significantly strong magnetic properties at room temperature. This is particularly important in water pollution control, where sorption is a critical process. Further research will focus on the use of surface-functionalised magnetic nanoparticles for this purpose.

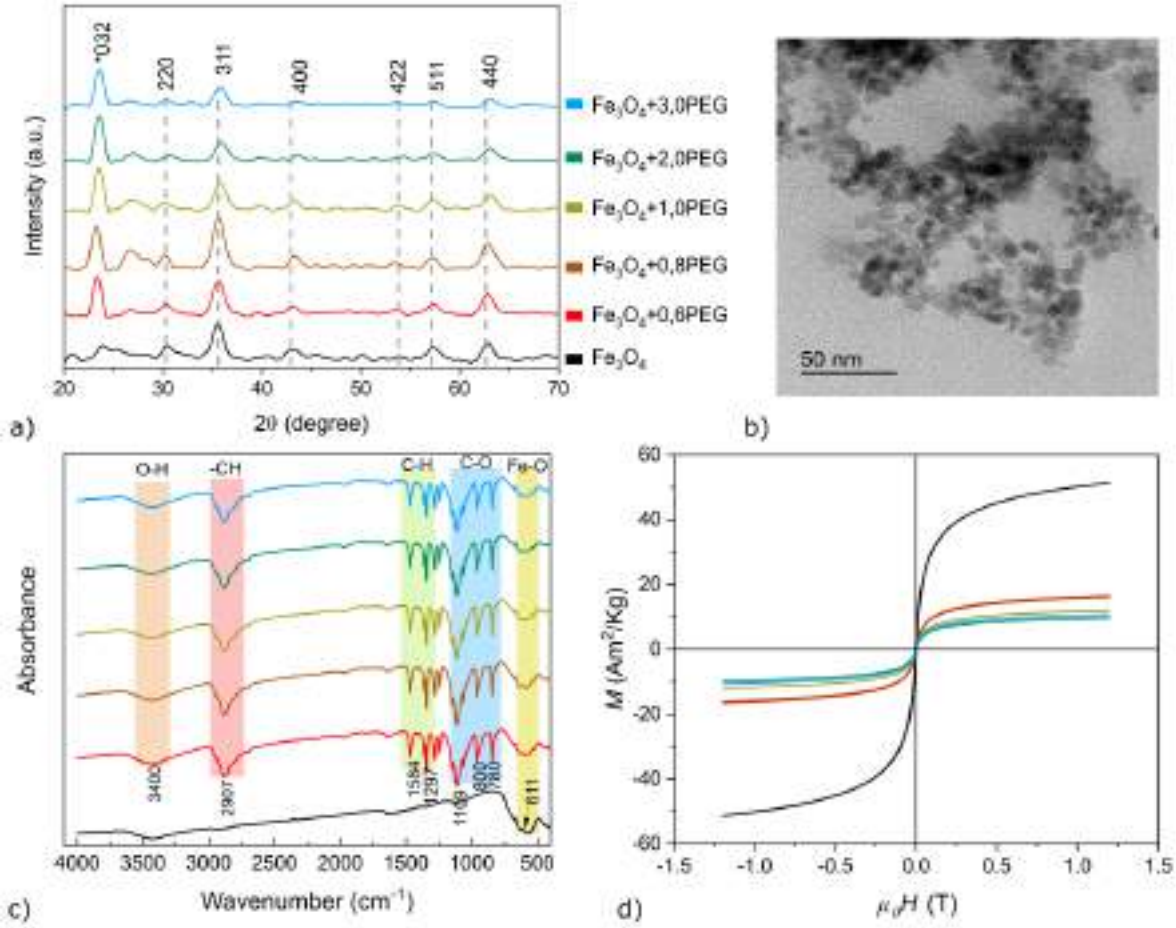


*Fig. 1. a) XRD patterns of MNPs with different loading amount of PEG; b) HRTEM image of Fe3O4+2,0PEG sample; c) FTIR spectra and d) room-temperature M-H loops of all samples.*

This work was supported by the Russian Science Foundation under grant no. 22-22-20124.

**References:**

[1]. Ajji, Z. & Ali, A. M. Adsorption of methyl violet and brilliant blue onto poly(vinylalcohol) membranes grafted with N-vinyl imidazole/acrylic acid. Nucl. Instrum. Methods Phys. Res. Sect. B. 265, 362–365 (2007).
[2]. Ofomaja, A. E. & Ho, Y.-S. Effect of temperatures and pH on methyl violet biosorption by Mansonia wood sawdust. Bioresour Technol. 99, 5411–5417 (2008).
[3]. Meunier, B. Catalytic Degradation of Chlorinated Phenols. Science 296, 270–271 (2002).

## PP-I-02

# Synthesis and Study of the Properties of Catalytic Systems Based on Nanocluster Polyoxometalates

Akimov A.S.[1,2], Akimov Al.S.[1], Petrenko T.V.[1]
*1 – Institute of Petroleum Chemistry SB of the RAS, Tomsk, Russia*
*2 – National Research Tomsk State University, Tomsk Russia*
*Akimov149@yandex.ru*

Nanocluster polyoxometalates, which consist of coordination oxygen polyhedra of molybdenum and tungsten, are a separate class of inorganic iso- and heteropolycompounds, which include more than a hundred atoms of transition metals (molybdenum, tungsten). The study of this class of compounds is relevant from a fundamental point of view, since the properties of polyelectrolytes and colloidal systems are inherent in the above compounds at the same time. In addition, due to the large number of aqualigands on the hydrophilic surface of polyoxometalates and its negative charge, there is the possibility of controlled functionalization of nanoclusters due to different interaction forces (for example, van der Waals and others) [1]. Due to the unique structure of polyoxometalate compounds, there are opportunities for application in various fields (development of membrane-type sensor materials, sorbents and molecular sieves, systems for targeted delivery of drug components and, finally, catalytic systems). The ease of modification of a huge number of compositions (substitution of molybdenum/tungsten or ligands) makes nanocluster polyoxometalates convenient objects for studying the scheme of general composition-structure-property interactions. The composition and structure of polyoxometalates are well studied, but there is not enough information about their physicochemical properties [2]. Thus, of particular interest is the study of the interaction of nanocluster polyoxometalates with nickel (cobalt) salts and carboxylic acids. The above systems can be used as components of catalysts for a number of different processes, including for upgrading/refining hydrocarbon feedstocks.

With the growing demand for clean fuels against the backdrop of an increase in the share of heavy oils with a high content of heteroatomic compounds in the world, in particular in the Russian Federation, the oil refining industry is facing serious economic and technological challenges. In the global market, the demand for middle distillates is constantly increasing, but at the same time, the quality of the available raw materials is falling [3]. Low-quality raw materials need to be processed in order to meet the need for additional fuel that meets the requirements of the Class-5 / EURO-5 regulation. This result is achievable by increasing the share and quality of hydrocatalytic processes. In this regard, the creation of a new generation of catalysts for the deep hydrotreatment of hydrocarbon feedstocks is becoming extremely important.

The aim of this work is the synthesis and study of the properties of nanocluster polyoxometalates (molybdenum and tungsten) and catalytic systems based on them.

**Acknowledgement:** The work was carried out within the framework of the state task of the Institute of Chemical Sciences of the Siberian Branch of the Russian Academy of Sciences, funded by the Ministry of Science and Higher Education of the Russian Federation

**References:**

[1] M. Nikulshina, A. Kokliukhin. Catal Commun. 127 (2019) 51-57;
[2] A. Ostroushko, K. Grzhegorzhevskii Russ. J. Phys. Chem.. 94(4) (2020) 762–771.
[3] S. Bello Energy Fuels. 35 (2021) 10998-11016

## PP-I-03

# Study of the Physico-Chemical Properties of Composite Solid Electrolytes $CsNO_2$-Nanodiamonds

Alekseev D.V.[1,2], Mateyshina Yu.G.[1,2]
*1 – Institute of Solid State Chemistry and Mechanochemistry SB RAS, Novosibirsk, Russia*
*2 – Novosibirsk State University, Novosibirsk, Russia*
*d.alekseev1@list.ru*

Recently, much attention has been paid to the search for new, more energy-efficient, environmentally friendly solutions in the field of energy. The study relates to the field of electrolyte materials with an increased value of ionic conductivity due to the formation of solid-phase composites of the «ionic salt – nanodiamonds» type. Such solid composite electrolytes can be used to create solid-state medium-temperature electrochemical devices.

Early studies have shown that one of the promising classes of solid electrolytes are composite solid electrolytes of the MX – A type, where MX is an ionic salt and A is an inert additive [1]. The physical reason for the formation of composites of this type is the desire of two phases to reduce their surface energy by interacting with the neighboring phase. As a result, new highly conductive amorphous phases, the presence of which is not typical for individual components, may appear in the composite, or high-temperature salt phases may be stabilized. To achieve the maximum effect, it is necessary that the inert additive has a developed specific surface area and is thermally and chemically stable under the conditions of its use. These requirements are met by highly dispersed oxides (MgO, $Al_2O_3$, $SiO_2$, $TiO_2$, $Fe_2O_3$, $ZrO_2$, $CeO_2$, $SnO_2$, etc.) [1], but not all of them are characterized by a relatively high molecular weight. Since most of the characteristics of the final electrochemical device are specific quantities, its development is aimed at minimizing the mass of the device.

Nanodiamonds are a unique carbon material with a high specific surface area ($S_s$ = 300 $m^2/g$), thermally stable up to high temperatures (T ≈ 500 °C), chemically inert with respect to most ionic salts. The introduction of nanodiamonds into the composition of a solid electrolyte will lead to a significant increase in all specific characteristics of the final device, since device characteristics are calculated per unit mass. The uniqueness of the nanodiamond additive also lies in the presence of a polyfunctional shell on its surface and the possibility of its modification in various ways [2]. The presence of a polyfunctional layer on the surface of nanodiamonds makes it possible, by modifying it, to influence the adhesion between the components in the composite.

Cesium nitrite was taken as an ionic salt as a substance with good ionic conductivity ($1.1 \times 10^{-5}$ at 200°C) and stable up to high temperatures ($T_{melt}$ = 398°C).

Thus, the purpose of this study is to develop a solid composite inorganic electrolyte "MX - Nanodiamonds", which has a relatively low weight and an increased value of ionic conductivity in relation to pure salt. In the course of this work, thermal, mechanical, transport,

and electrochemical composites of (1-x)$CsNO_2$ – xC were studied. The results are discussed in the report.

**Acknowledgement:** The work was carried out within the framework of the state task of the ISSCM SB RAS, project No. 121032500065-5.

**References:**

[1] N.F. Uvarov N.F. Composite solid electrolytes. Ed. SB RAS, Novosibirsk. (2008) 258.
[2] Yu. G. Mateyshina, D. V. Alekseev, N.F. Uvarov. Nanomaterials. 11. (2021) 414.

## PP-I-04

# Synthesis and Photocatalytic Properties of Nanocomposites $Fe_2O_3/C_3N_4$ under UV and Visible Light

Bikyashev E.A.
*Southern Federal University, Rostov-on-Don, Russia*
*eabikyashev@yandex.ru*

$Fe_2O_3/C_3N_4$ heterostructures are actively studied as potential photocatalysts for the decomposition of organic impurities and antibiotics, as well as for hydrogen generation or $CO_2$ reduction [1, 2]. In this case, either multiple heat treatments are often used, or homogenization/dispersion of the components is carried out using non-aqueous solutions, ultrasonic baths, and hydrothermal procedures. This usually limits the range of compositions of the studied materials. In addition, there are conflicting data on the effect of pH on their photocatalytic activity [3, 4]. In this work, $Fe(NO_3)_3 \cdot 9H_2O$ and melamine in molar ratios from 1/1000 to 1/25 were used as precursors for the synthesis of the phases of interest and their compositing (hereinafter the symbols Fe/CN_1'1000, Fe /CN_1'250 etc. are used for brevity). The precursors were homogenized on a magnetic stirrer with the addition of a small volume of water. After drying, the mixtures were subjected to a single 4-hour calcination at 550°C in closed crucibles, the furnace heating rate was 5°C/min. For comparison, unmodified $C_3N_4$ was obtained under similar conditions.

According to X-ray diffraction data (Fig. 1), α-$Fe_2O_3$ is reliably detected in most Fe-containing materials (beginning with Fe/CN_1'100), which indicates the formation of macroscopic clusters of this phase.

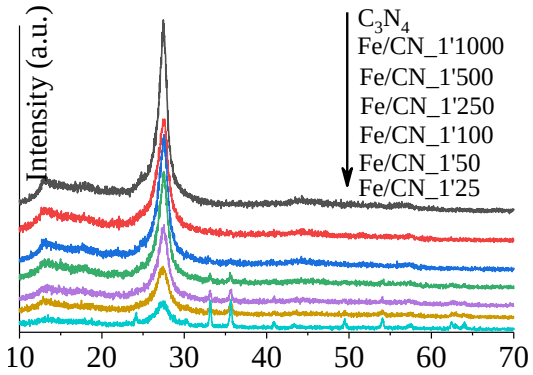


*Fig. 1. XRD patterns of the obtained phases.*

On Fig. 2a shows the diffuse absorption spectra of the powders. It can be seen that, in the process of $C_3N_4$ modification, the edge of its fundamental absorption band is gradually transformed. The processing of the graphs by the Kubelka-Munk method makes it possible to explain this result by the appearance and growing role of indirect interband transitions with a strongly decreasing (up to ~1 eV) band gap. This gives grounds to expect the manifestation of photocatalytic activity in the visible range.

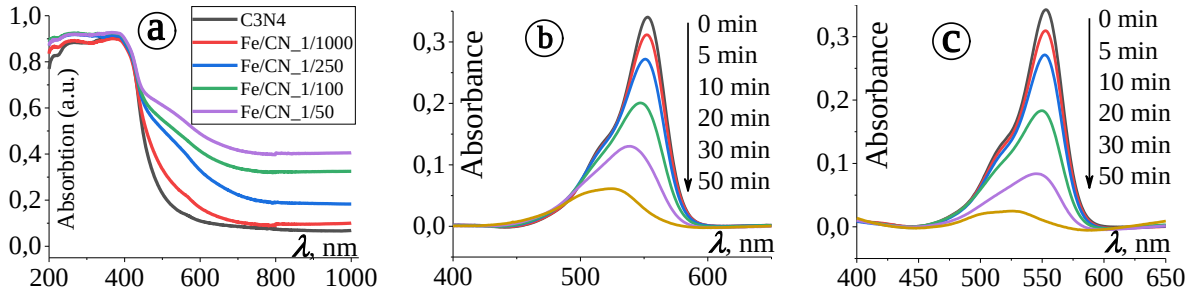


*Fig. 2. Diffuse absorption spectra of some of the investigated phases (a), transformation of the absorption spectral line of RhB in the presence of $C_3N_4$ (b) and Fe/CN_1'1000 (c).*

On Fig. 2 (b, c) shows the absorption spectra of the dye Rhodamine B (RhB) upon irradiation of its solution in the UV range (λ = 250 nm) in the presence of catalytic amounts of $C_3N_4$ and Fe/CN_1'1000. A more efficient degradation of the dye using a composite catalyst can be caused by the redistribution of photoexcited charge carriers between its components. Since the valence band (VB) and conduction band (CB) of α-$Fe_2O_3$ are lower in energy than the corresponding levels of $C_3N_4$, the electrons excited in $C_3N_4$ can either interact with adsorbed oxygen molecules ($O_2 + \bar{e}_{CB} \rightarrow \dot{O}_2^-$), or move to the $Fe_2O_3$ conduction band. Since the VB of the nitride lies above the hole reduction potential, the process $h^+_{VB} + H_2O \rightarrow \dot{O}H + H^+$ is impossible on the $C_3N_4$ surface. However, in the presence of $Fe_2O_3$, it becomes possible to transfer a hole to the α-$Fe_2O_3$ valence band, which hinders the annihilation of the electron-hole pair in the $C_3N_4$ structure. The use of a set of reactive oxygen species scavengers confirmed that the oxidation of RhB is provided by radicals $\dot{O}_2^-$ and triplet oxygen $^1O_2$. With an increase in the content of $Fe_2O_3$ (beginning with Fe/CN_1'250), the catalytic activity noticeably decreases. This can be caused both by the "separation" of the C3N4 and Fe2O3 phases, and by a decrease in the fraction of the irradiated C3N4 surface.

In visible light (λ = 450 nm), $C_3N_4$ and $Fe_2O_3/C_3N_4$ heterostructures exhibited extremely low photocatalytic activity: 2-hour irradiation led to a decrease in the intensity at the maximum of the RhB absorption band by about 10%. At the same time, already after 45 minutes of irradiation in a sulfuric acid medium, the intensity drop is ~40% – ~70% – ~63% when using catalytic amounts of $C_3N_4$, Fe/CN_1'1000 and Fe/CN_1'250, respectively. The role of $H^+$ is apparently associated with the retention of $NH/NH_2$ amino groups in the peripheral regions of graphite-like $C_3N_4$ layers, which is confirmed by the presence of weak absorption in the wavenumber range 2700-3500 $cm^{-1}$ in the IR spectra.

**References:**

[1] Huoli Zhang, Changxin Zhu et. al., Catalysts 8 (2018) 457.
[2] Hui Zhao, Cheng Tian et. al., Environmental Research 195 (2021) 110842.
[3] T.J. Al-Musawi, R. Asgariyan et. al., Magnetochemistry 8 (2022) 137.
[4] J. Singh, S. Basu, Microporous and Mesoporous Materials 303 (2020) 110299.

## PP-I-05

# Effect of Reduction/Nitriding on Structure and Photocatalytic Activity of Tin Dioxide

Bikyashev E.A.
*Southern Federal University, Rostov-on-Don, Russia*
*eabikyashev@yandex.ru*

$SnO_2$ dioxide crystallizes in the rutile structure and is a direct-gap n-type semiconductor with a band gap of ~3.6 eV [1]. In combination with high stability, non-toxicity, and low cost, SnO2 is considered as a promising material for the development of photocatalysts for the degradation of organic pollutants in industrial effluents and closed water bodies [2] mainly under UV irradiation. In this work, we studied the effect of treatment of hydrothermally synthesized tin dioxide in reducing (H2, NH3) and oxidizing ($O_3$) media on its composition, structure, and photocatalytic characteristics with respect to rhodamine B (RhB).

Hydrothermal synthesis was prepared by dissolving tin metal in cooled nitric acid followed by raising the pH to ~6 with an ammonia solution. An equal volume of isopropanol was added to the final aqueous suspension, after which the reaction mixture was placed in a Teflon reactor and thermally stabilized for 16 hours in a steel autoclave at 180°C. After cooling, the solid phase was washed from nitrates and dried at 60°C.

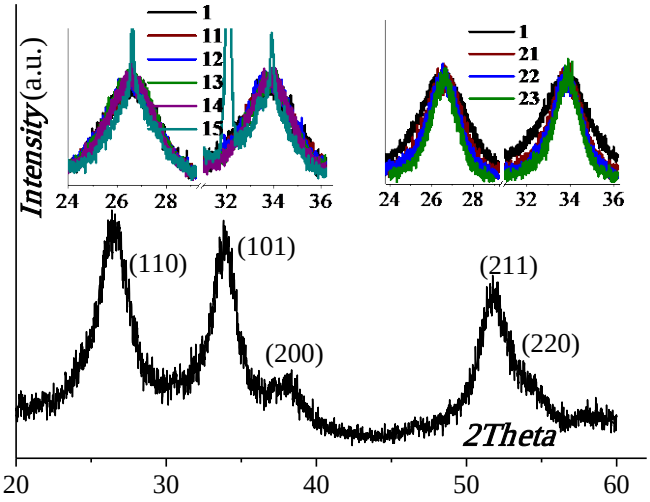


*Fig. 1. Diffraction profile of hydrothermal $SnO_2$. Peaks (110) and (100) of the hydrothermal phase (lines 1) and products of 30-min treatment in $H_2$ flow (lines 11-15) at temperatures 100-150-200-250-300°C u $NH_3$ (21-23): 300-350-400°C.*

The formation of a weakly crystallized rutile-type phase was established by X-ray diffraction (Fig. 1). The average size of coherent scattering regions ($D_{CSR}$) was calculated from the integral width of the reflection (110) using the Scherrer equation. It was ~5 nm. Treatment in $H_2$-flow up to 300°C did not affect $D_{CSR}$. Simultaneously, an impurity of metallic tin appeared (a narrow peak on line 15 at 2theta = 32). SnO oxide was not detected either by diffraction methods or by Mössbauer spectroscopy. In an $NH_3$ flow no signs of $SnO_2$ degradation were found up to 400°C. But the FWHM of the peaks has decreased slightly ($D_{CSR}$ increased to ~10-12 nm).

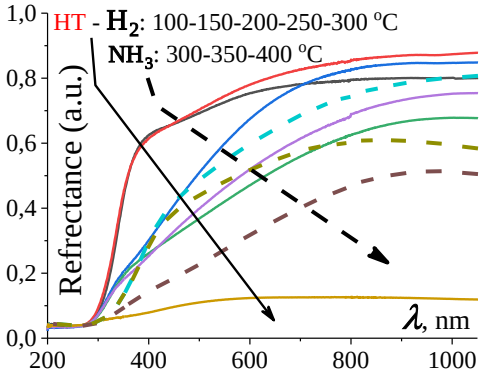


*Fig. 2. Diffuse reflectance spectra of hydrothermal $SnO_2$ and products of its treatment in H2 (solid lines) and $NH_3$ (dashed lines) flow.*

After treatment in an atmosphere of reducing agents, the absorption region shifts to the visible part of the spectrum (Fig. 2). In this case, the edge of the fundamental absorption band of materials loses specific boundaries, and the determination of the value of Eg becomes ambiguous. Apparently, the appearance of a strong oxygen nonstoichiometry gives rise to a large number of local electronic levels in the band gap. It has been found that post-treatment in ozone (200°C, 3 hours) relatively easily eliminates optical absorption in the visible range in hydrogen-reduced materials. Samples treated in $NH_3$ do not discolor, but become light orange, possibly due to partial nitriding. Diffuse reflection plots make it possible to reveal the appearance of indirect-gap transitions with Eg ~ 1.5-2.5 eV.

In the photocatalytic experiments with the RhB dye, a high activity of the hydrothermal phase of SnO2 in the UV range was established (Fig. 3).

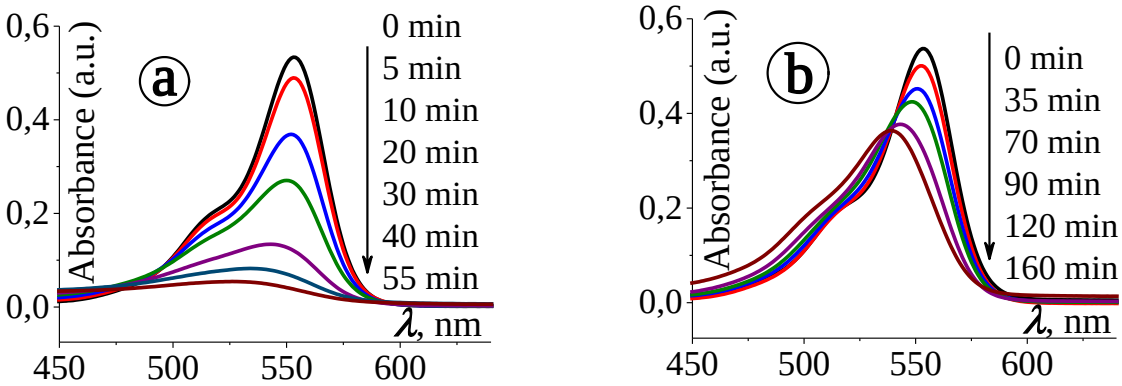


*Fig. 3. Transformation of the absorption spectral line of RhB in the presence of HT $SnO_2$ in the UV range (a) and in the visible* light (b).

The additionally processed phases are inferior to the original hydrothermal form, possibly due to the rapid recombination of electron-hole pairs. In the future, some of the obtained materials are planned to be additionally composited.

**References:**

[1] Jianyuan Yu, Yingeng Wang et. al., Beilstein J. Nanotechnol. 11 (2020) 1321.
[2] S.P. Kim, M.Y. Choi, H.C. Choi, Mater. Res. Bull. 74 (2016) 85.

## PP-I-06

# Room-Temperature Phosphorescence of Nanocomposites Based on Carbon Dots and Polyvinyl Alcohol

Arefina I.A., Kosolapova K.D., Ushakova E.V.
*ITMO University, Saint Petersburg, Russia*
*iaarefina@itmo.ru*

Carbon dots (CDs) are a promising class of luminescent nanomaterials with the size up to 10 nm. CDs can be easily incorporated into various matrices and polymers, thereby obtaining new effects and expanding area of applications. For example, formation of nanocomposites based on carbon dots and polymer leads to suppression vibrational dissipation of charge carriers from the triplet state and allows to the appearance of room temperature phosphorescence (RTP) [1]. Such hybrid materials are of interest for applications in photovoltaics, sensors, data encryption, and they can also be used as solar concentrators to increase the efficiency of charge transfer in solar cells.

In this work, thin-film samples of hybrid nanomaterials based on CDs and polyvinyl alcohol (PVA) as a polymer matrix were studied. CDs were synthesised from citric acid and ethylenediamine by hydrothermal method at 190°C for 8 hours. The resulting solution was dialyzed against deionized water using 3.5 kDa dialysis bag for 24 hours. CDs were then chemically treated to increase O and N amount. For this purpose, citric acid and urea were used as a shell for initial CDs and resulting samples designated as CD-ca and CD-ur, respectively. The modification was carried out by hydrothermal procedure of initial CDs and urea or citric acid at 180°C for 6 hours. Then CD, CD-ca or CD-ur were added to the 10% water solution of PVA and stirred for 40 minutes at 80°C. Thin-film samples were formed by spin-coating of the solutions and then dried under ambient conditions overnight. Also, sample CD-T was made from the film of initial CD and annealed in the oven at 120°C. Thus, 4 thin-film samples were obtained: CD, CD-T, CD-ca and CD-ur.

Absorption spectrum was collected on a spectrophotometer UV-3600 (Shimadzu). Photoluminescence (PL) and RTP spectra and RTP decay were measured on Carry Eclipse (Varian) under 250 and 350 nm excitation wavelengths. RTP decay of all samples was approximated by multi-exponential function.

Aqueous solutions of CD possess absorption peaks at 240 and 350 nm and emission in the region 400-500 nm excited at 240 and 350 nm. All films have absorption peak at 350 nm and demonstrate RTP peak at 500 nm under 250 nm excitation wavelength with FWHM of 110 nm. Samples CD and CD-T show RTP peak at 510 nm with FWHM=120 nm at under 350 nm excitation wavelength. In contrast, treated CD samples (CD-ca and CD-ur) have RTP peak with FWHM equal to 120 nm at 480 nm.

In Table 1 average RTP decay lifetimes of all samples under 250 and 350 nm excitation are summarized. Annealing results in shortening the average RTP lifetime of CD under 250 nm excitation, however lifetime monitored while excited at 350 nm remains unchanged.

Modification via citric acid results in the shortening of RTP lifetime under both excitation wavelengths. The embedding of additional nitrogen atoms through modification with urea does not change RTP decay time exciting under 250 nm but increases it by 25% under 350 nm excitation.

*Table 1. Average RTP decay lifetimes of samples under 250 ($\tau_{250}$) and 350 ($\tau_{350}$) nm excitation wavelength*

| Sample | $\tau_{250}$, ms | $\tau_{350}$, ms |
|---|---|---|
| CD | 200 | 260 |
| CD-T | 136 | 260 |
| CD+ca | 15 | 36 |
| CD+ur | 200 | 350 |

To conclude, 4 thin-film samples based on CDs and polymer were formed. 3 of them except CD+ca demonstrate afterglow visible with naked eye. It was found that annealing of the sample leads to shortening the decay time of the RTP. Additional modification depending on the incorporation of heteroatom (O or N) can lead to both an increase and decrease of RTP decay time. CD+ur sample demonstrates the longest RTP decay time from the set of samples and it is equal to 350 ms at 350 nm excitation and 200 ms at 250 nm excitation.

**Acknowledgement:** This work was financially supported by Priority 2030 Federal Academic Leadership Program

**References:**

[1] W. Zhao, Z. He, B.Z. Tang, Nat. Rev. Mater. 5 (2020) 869.

## PP-I-07

# NIR Emitting Core/Shell PbSe/PbS Nanoplates

Babaev A.A., Skurlov I.D., Cherevkov S.A., Fedorov A.V.
*PhysNano Department, ITMO University, Saint Petersburg 197101, Russia*
*a.a.babaev@itmo.ru*

Colloidal nanocrystals are one of the most exciting materials for the new generation optoelectronic applications due to their size-dependent physical properties. Their 2D form possesses ever more superior properties like extremely narrow emission line widths and suppressed Auger recombination[1]. The development of this field was boosted by the successful synthesis of cadmium chalcogenides nanoplates (NPs) with a monolayer precision and almost ideal thickness uniformity. Unfortunately, the use of NPs of cadmium chalcogenides is limited to the visible region of the spectrum, and direct synthesis to obtain similar NPs for NIR region has not been published. To solve this problem, procedures for the cation exchange of cadmium NPs with mercury and lead were proposed to achieve PL in the near-IR region of the spectrum[2]. However, the stability of such NPs has to be improved, and the cation exchange procedures are poorly studied and optimized.

In this work, we investigated the possibility of obtaining PbSe/PbS core/shell NPs by cation exchange from cadmium chalcogenide NPs. We have found that the reaction temperature and time are the key parameters for preservation of the size and crystallinity of the NPs. Shift in the band gap energy, the PL quantum yield and FWHM of the NPs during the reaction was observed by measuring the spectral properties of the NPs during synthesis. An analysis of the final product using EDX showed that even after day-long reaction significant content of cadmium remains in the NP, which corresponds to similar works[]. Detailed optical measurements using low temperatures showed that the excited state relaxation dynamics in NP did not undergo significant changes in comparison with the core-type NP that we studied earlier.

Finally, the post-processing of NP was studied. The shell growth suppress NP stacking made it possible to use a wider range of methods to create thin NP films using ligand replacement procedures. Using various methods, we obtain continuous layers with a thickness corresponding to several monolayers of face-down NP. These results open up the possibility of using them in various solution processed devices.

**Acknowledgement:** This work was supported by the Russian Science Foundation (19-13-00332П).

**References:**

[1] Diroll B.T., Guzelturk B., Po H., Dabard C., Fu N., Makke L., Lhuillier E., Ithurria S. 2D II-VI Semiconductor Nanoplatelets: From Material Synthesis to Optoelectronic Integration // Chem Rev. 2022.

[2] Galle T., Samadi Khoshkhoo M., Martin-Garcia B., Meerbach C., Sayevich V., Koitzsch A., Lesnyak V., Eychmüller A. Colloidal PbSe Nanoplatelets of Varied Thickness with Tunable Optical Properties //Chemistry of Materials. 2019, 31, 3803−3811.

## PP-I-08

# Mechanism of $Ln_2MoO_6$ (Ln = La, Nd, Sm) Phase Formation from a Mechanically Activated Oxide Mixture

Baldin E.D., Vorobieva G.A., Kolbanev I.V., Shlyakhtina A.V.
*N.N. Semenov Federal Research Center for Chemical Physics, Russian Academy of Sciences, Moscow, Russia*
*baldin.ed16@physics.msu.ru*

The structure and polymorphism of compounds in the 1:1 molar range of the $Ln_2O_3$–$MoO_3$ system, i.e., $Ln_2MoO_6$, have attracted attention since the middle of the last century and it has been shown that oxymolybdates have a layered tetragonal structure in the case of large rare earth cations La, Pr, Nd, and oxymolybdates of heavy REE crystallise in the scheelite structural type [1]. It is well known that solid state synthesis requires long term high temperature annealing with intermediate grinding in the temperature range of 900-1100 °C. At the same time, the volatility of molybdenum oxide and its rather low melting and sublimation temperatures of 801°C and ~600°C, respectively, must be taken into account. These factors can lead to a change in the composition of the samples. For this reason, it is important to study the synthesis of REE oxymolybdates at temperatures lower than 600 °C. Previously, the possibility of obtaining some molybdates $Ln_{10}Mo_2O_{21}$ (Ln = La, Y, Er) with a high content of Ln2O3 at room temperature has been demonstrated [2]. Mechanoactivation of a mixture of initial oxides is known to result in either mechanosynthesis of compounds or formation of nano-sized oxides, affecting the mechanism of compound phase formation during subsequent annealing. The mechanism of phase formation of oxymolybdates Ln2MoO6 (Ln = La, Nd, Sm) from nano-sized precursors with increasing temperature has not been investigated.

This work is devoted to the study of the synthesis of oxymolybdates by the method of mechanical activation of oxides. The starting oxides Ln2O3 (Ln = La, Nd, Sm) and MoO3 were preheated to remove water and carbon dioxide and then ground to a nanoscale state in a SPEX8000 ball mill. The m/a mixture was then studied by differential scanning calorimetry (DSC) to identify thermal effects associated with phase synthesis. Four to six exothermic peaks were observed in all three systems. The structure of the phases before and after exoeffects was determined by X-ray diffraction. It is shown that the synthesis of oxymolybdates La, Nd, Sm proceeds with the intermediate formation of phases rich in molybdenum oxide, namely scheelite-like $Ln_2(MoO_4)_3$ (oxide ratio 1:3, for all REE considered) and $La_2Mo_2O_9$ (1:2, only for lanthanum).

**References:**

[1] Blasse G. Dilanthanide molybdates and tungstates Ln2MO6//Journal of Inorganic and Nuclear Chemistry, 1966, Vol. 28, No. 6-7, P. 1488-1489.
[2] Kolbanev I.V., Shlyakhtina A.V., Degtyarev E.N., Konysheva E.Yu., Lyskov N.V., Stolbov D.N., Streletskii A.N. Room-temperature mechanochemical synthesis of RE molybdates: Impact of structural similarity and basicity of oxides//Journal of the American Ceramic Society, 2021, Vol. 104, No. 11, P. 5698-5710.

## PP-I-09

# Synthesis of Hexagonal Nanophases in the $La_2O_3 – MO_3$ (M = Mo, W) Systems

Baldin E.D.[1], Lyskov N.V.[2,3], Vorobieva G.A.[1], Kolbanev I.V.[1], Karyagina O.K.[4], Stolbov D.N.[5], Voronkova V.I.[6], Shlyakhtina A.V.[1]

*1 – N.N. Semenov Federal Research Center for Chemical Physics, Russian Academy of Sciences, Moscow, Russia*

*2 – Federal Research Center of Problems of Chemical Physics and Medical Chemistry RAS, Moscow region, Chernogolovka, Russia*

*3 – National Research University "Higher School of Economics", Moscow, Russia*

*4 – Emanuel Institute of Biochemical Physics RAS, Moscow, Russian Academy of Sciences, Russia*

*5 – Department of Chemistry, Lomonosov Moscow State University, Moscow, Russia*

*6 – Department of Physics, Lomonosov Moscow State University, Moscow, Russia*

*baldin.ed16@physics.msu.ru*

We present a study of nanophases in the $La_2O_3$-$MO_3$ (M = Mo, W) systems, which are known to contain a variety of good oxygen-ion and proton conductors. Mechanically activated La2O3+MO3 (M = Mo, W) mixtures have been characterized by DSC and XRD with Rietveld refinement, the microstructure of the materials has been examined by SEM, and their conductivity in dry and wet air has been determined using impedance spectroscopy.

In both systems, the formation of hexagonal $La_{18}M_{10}O_{57}$ ($9La_2O_3$:$10MO_3$) (M = Mo, W) nanophases is observed, with exothermic peaks in the DSC curve in the range ~480–520 °C for $La_{18}Mo_{10}O_{57}$ and ~ 685 -760 ºC for $La_{18}W_{10}O_{57}$. The crystallite size of the nanocrystalline tungstates is ~40 nm and that of the nanocrystalline molybdates is ~50 nm.

At higher temperatures (~630–690 and ~1000 °C) we observe irreversible reconstructive phase transitions from hexagonal $La_{18}Mo_{10}O_{57}$ to tetragonal γ- $La_2MoO_6$ and from hexagonal $La_{18}W_{10}O_{57}$ to orthorhombic β-$La_2WO_6$. We compare the temperature dependence of the conductivity of nano- and microcrystalline hexagonal $La_{18}M_{10}O_{57}$ ($9La_2O_3$:$10MO_3$) (M = Mo, W) phases and high temperature phases with different densities. In the coarse-grained $La_{18}W_{10}O_{57}$ ceramic, oxygen ion conduction predominates above 600 °C. Low-density $La_{18}W_{10}O_{57}$ and $La_{18}Mo_{10}O_{57}$ nanoceramics exhibit electron conduction with activation energies of 1.36 and 1.48 eV, respectively, in dry air.

## PP-I-10

# Study of Au-Induced Crystallization Kinetics of *a*-$SiO_x$ Thin Films

Baranov E.A.[1], Zamchiy A.O.[1], Lunev N.A.[1], Konstantinov V.O.[1], Merkulova I.E.[1], Morozova M.A.[1], Vorobyov Y.V.[2]

*1 – Kutateladze Institute of Thermophysics SB RAS, Novosibirsk, Russia*

*2 – Ryazan State Radio Engineering University named after V.F. Utkin, Ryazan, Russia*

*itpbaranov@gmail.com*

The production of high-quality polycrystalline silicon (poly-Si) films on cheap non-intrinsic substrates such as glass can be realized by metal-induced crystallization (MIC) of amorphous silicon-containing materials, including amorphous silicon suboxide (*a*-$SiO_x$, 0<x<2) [1]. MIC has several advantages over other methods (e.g., solid state crystallization) because it does not require high annealing temperatures and is easily scalable, making it very attractive for obtaining poly-Si films for modern photovoltaics. It is possible to vary the structural properties of the final material by controlling the kinetics of nucleation and crystal growth during the MIC process [2]. In this work, we have studied the kinetics of gold-induced crystallization of *a*-$SiO_{0.2}$ thin films.

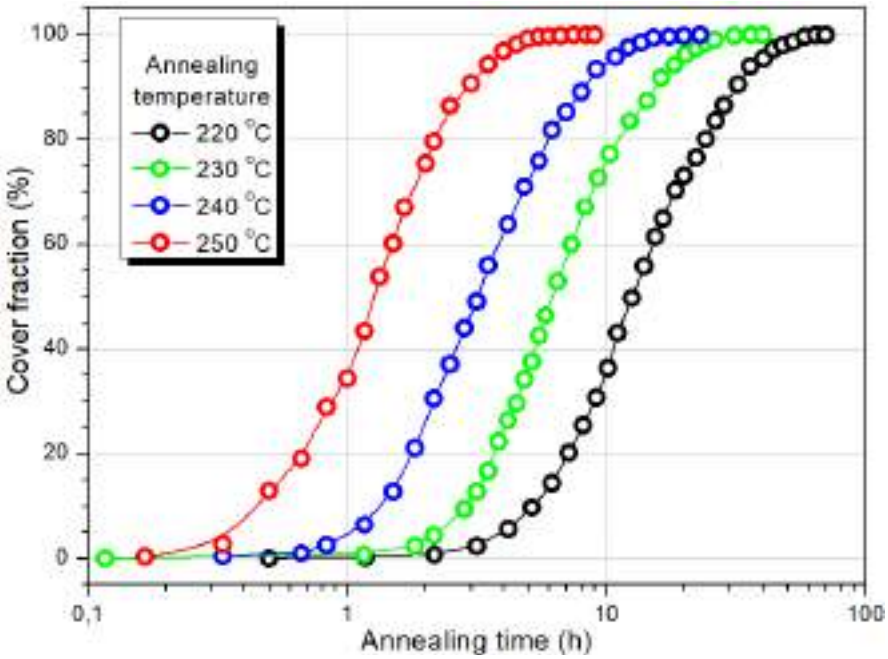


*Fig. 1. Cover fraction versus annealing time for the samples annealed at 220÷250 °C*

The structure of the initial samples was “quartz substrate/Au (30 nm)/*a*-$SiO_{0.2}$ (150 nm)”. Au films were deposited by thermal vacuum deposition method. Suboxide films were obtained by magnetron sputtering method. Annealing of the synthesized samples was carried out in a vacuum chamber equipped with an optical system based on a long-focused optical microscope for in situ monitoring of the crystallization process at temperatures of 220, 230, 240 and

250 °C for 9÷70 hours at a pressure of $5\times10^{-4}$ Pa. Structural and crystalline properties of the resulting poly-Si were studied by Raman spectroscopy and X-ray diffraction method.

Photographs of the top surface of the annealed samples were taken during in situ optical studies and were used to obtain the dependences of the cover fraction (Fig. 1), density of nuclei, and nucleation rate. The result of the curve analysis obtained, carried out in the framework of the Kolmogorov-Johnson-Mela-Avrami theory [3] was the determination of the activation energies of nucleation, crystallite growth and the activation energy of the process as a whole, which were 2.51±0.80, 0.31±0.10 and 1.62±0.15 eV, respectively.

**Acknowledgement:** This work was supported by the Russian Science Foundation, grant 22-79-10079, https://rscf.ru/project/22-79-10079/.

**References:**

[1] Zamchiy A. O. et al. //Vacuum. – 2021. – T. 192. – C. 110462.
[2] Toko K., Suemasu T. //J. of Phys. D: Appl. Phys. – 2020. – T. 53. – №. 37. – C. 373002.
[3] Cohin Y. et al. //Crystal Growth & Design. – 2015. – T. 15. – №. 5. – C. 2102-2109.

## PP-I-11

# Thermal Annealing of Au/$Al_2O_3$/*a*-Ge Thin Film Structure

Baranov E.A.[1], Zamchiy A.O.[1], Lunev N.A.[1], Konstantinov V.O.[1], Merkulova I.E.[1], Morozova M.A.[1], Nepomnyashchikh V.A.[1], Volodin V.A.[2]

*1 – Kutateladze Institute of Thermophysics SB RAS, Novosibirsk, Russia*

*2 – Rzhanov Institute of Semiconductor Physics SB RAS, Novosibirsk, Russia*

*itpbaranov@gmail.com*

Currently, one of the promising methods for obtaining polycrystalline germanium thin films (poly-Ge) is metal-induced crystallization method enabling use the low-temperature substrates such as plastic and glass [1]. In this work, gold was used as a catalyst for the crystallization of amorphous germanium (*a*-Ge) films. The thin $Al_2O_3$ intermediate layer at the Au/*a*-Ge interface was used to reduce the density of nuclei (as a result, increase the size of poly-Ge crystallites).

Au films 80 nm thick were deposited onto quartz glass substrates by thermal evaporation. Then, the $Al_2O_3$ intermediate layer was synthesized using atomic layer deposition. The thicknesses of the intermediate layer were 0.2, 0.4, 0.6, and 0.8 nm. Next, *a*-Ge thin films 140 nm thick were deposited on the sample by magnetron sputtering. The synthesized samples were annealed in a vacuum chamber at temperatures from 220 to 330 °C for several hours at a pressure of $5\times10^{-4}$ Pa.

The use of a thin membrane (0.2 nm) leads to the implementation of the layer exchange mechanism with the formation of poly-Ge. This is clearly seen in the Raman spectra both from the film side and from the substrate side. Increasing the thickness of $Al_2O_3$ to 0.8 nm leads to a significant decrease in the diffusion processes, which completely suppresses the Ge crystallization in the annealing temperature range studied.

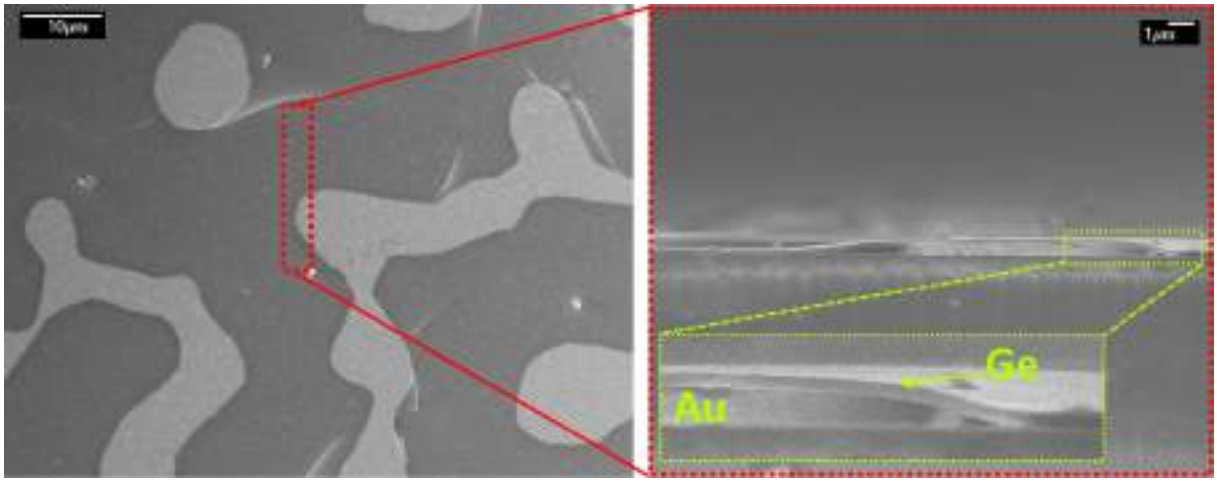


*Fig. 1. SEM images of the surface and cross section of the sample after annealing.*

Figure 1 on the left shows the SEM image of a surface of a sample with a membrane thickness of 0.6 nm after annealing at a temperature of 330 °C. This morphology is typical for $Al_2O_3$ layer thicknesses of 0.4 nm and 0.6 nm. According to the EDS mapping of the elemental composition, the bright areas contain higher content of Au. Figure 1 on the right shows a cross-

sectional image of the sample after annealing. It can be seen that the Au film is absent in the dark regions, while the thickening of the gold film up to ≈500 nm occurred in the light regions. According to Raman studies, the spectra of the bright regions on the side of the film contain features characteristic of *α*-Ge. From the substrate side, there is no signal from Ge in the Raman spectra. At the same time, in the Raman spectra in dark regions, both from the side of the substrate and from the side of the film, there is a signal from amorphous and crystalline germanium.

**Acknowledgement:** This work was supported by the Russian Science Foundation grant No. 22-79-10079, https://rscf.ru/project/22-79-10079.

**References:**

[1] Alexandr O. Zamchiy, and Evgeniy A. Baranov // Coatings. 2022. V.12 (12).

## PP-I-12

# Modeling of Interparticle Forces Modified with Mobile Surfactant Chains

Beloborodov D.[1], Vishnyakov A.[2]
*1 – Skolkovo Institute of Science and Technology, Moscow, Russia*
*2 – Moscow State University, Moscow, Russia*
*Dmitry.Beloborodov@skoltech.ru*

In the present work we quantitatively explore how the interactions between spherical colloid nanoparticles are modified in the presence of mobile surfactants via Monte Carlo simulations. Although nanoparticles with grafted polymer chains have been a popular object of study for some time, only recently the focus has shifted from the particles with fixed binding sites towards the ones with mobile anchors [1]. When two such particles approach each other, the grafted chains can migrate from the near-contact area, redistributing non-uniformly on the particles' surfaces. The interparticle interactions are additionally modified by the non-uniform distribution of the binding sites. The repulsive force between the particles increases with grafting density and chain length due to the entropic cost of chain compression. We also study how the forces between the core particles depend on the core radius and anchor sites distribution and compare our results to the system with fixed anchors. The results are validated by comparing them to the molecular dynamics simulations. The research would be useful in predicting the colloid/polymer mixture behaviour (e.g. self-assembly of patchy particles) and designing coatings [2], rubber and ceramic materials [3].

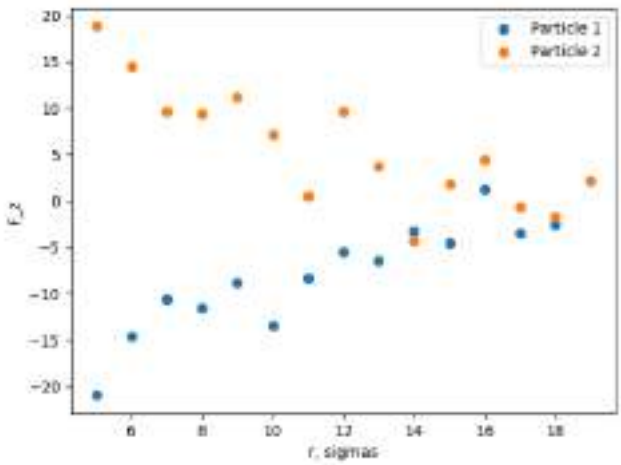


*Fig. 1. Forces along the line of approach for two particles, each with 60 grafted chains of length 30 segments.*

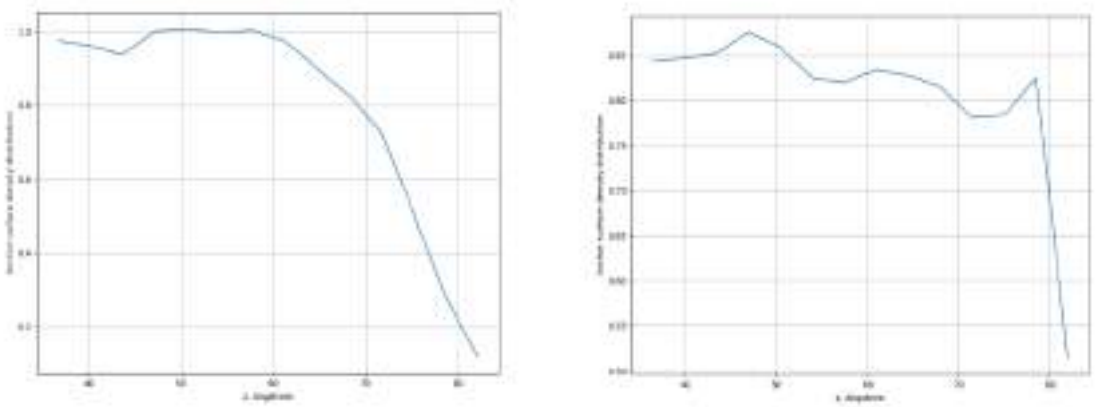

*Fig. 2. Dependence of surface densities of the anchor sites on the coordinate along the line of approach for 2 different particle separation distances, 5 molecular diameters (left plot) and 15 (right plot).*

**References:**

[1] Ł. Baran and S. Sokołowski, "Effective interactions between a pair of particles modified with tethered chains", J. Chem. Phys. 147, 044903 (2017)
[2] Ginzburg, V. V.; Chatterjee, T.; Nakatani, A. I.; Van Dyk, A. K., “Oscillatory and Steady Shear Rheology of Model Hydrophobically Modified Ethoxylated Urethane-Thickened Waterborne Paints.”, Langmuir 2018, 34, 10993−11002.
[3] Chen, H.; Wang, X.; Xue, F.; Huang, Y.; Zhou, K.; Zhang, D., “3D printing of SiC ceramic: direct ink writing with a solution of preceramic polymers”, J. Eur. Ceram. Soc. (2018)

## PP-I-13

# Experimental Study of Organic and Inorganic Compound Adsorption on Biochar Samples

Borodaevskiy M.M., Dubinin Y.V., Yeletsky P.M., Yakovlev V.A.
*Boreskov Institute of Catalysis, Novosibirsk, Russia*
*maxim.borodaevskiy@gmail.com*

The problem of water purification has become especially serious in the modern world. Water pollution may be caused by both organic compounds, as well as inorganic molecules, especially heavy-metal ions, which are known to cause serious health problems. A classic method of water treatment is based on the process of adsorption. Adsorption is the physicochemical process, during which atoms, ions or molecules gather on the contact surface between two phases. Adsorption isn't capable of fully eliminating the presence of polluting objects in liquids, seeing as it can occur only up to a certain equilibrium state, however its cost-effectiveness and ease of use make it an interesting subject of study in the context of water treatment, especially at an early stage of treatment. There exists a wide variety of adsorbents, among which the most widely used are silicon and aluminum oxides, zeolites and activated chars. Biochars in particular attract a lot of attention. Biochars are defined as carbon-containing products of biomass carbonization. A novel and effective method of biochar production has been developed in the Boreskov Institute of Catalysis in Novosibirsk. The method revolves around the carbonization of biological waste in a fluidized catalyst bed [1]. The resulting material is characterized by a developed and large surface area. The further use of these products may also help in solving the problem of biomass utilization.

The following research studies the effectiveness of various types of carbon adsorbents, produced by carbonization in fluidized catalyst bed at different temperatures, in the process of water purification from organic dyes and inorganic heavy-metal ions. Samples of biochars made out of rice husks and wheat bran, as well as peat and activated coal were analyzed. The model organic pollutants were methylene green and bromphenol blue. Copper salts were used as inorganic pollutants. Spectrophotometry was used to define the concentration of polluting compounds in a series of experiments to determine thermodynamic and kinetic characteristics of the process of adsorption. The resulting adsorption isotherms and concentration-time graphs (возможно стоит как-то поменять) were later used to determine the maximum adsorption capacity of the researched samples, the adsorption model, reaction order and activation energy.

**References:**

[1] Yeletsky P.M. et al. Conversion of natural feedstocks to porous carbons via carbonization in fluidized catalyst bed followed by leaching the feedstock mineral template phase: A comparison of biomass and sedimentary raw mапиterials // Fuel Processing Technology. Elsevier B.V., 2022. Vol. 226.

## PP-I-14

# Study of the Sensory Interaction of a Modified Bocarbon BC Nanotube with a Carbon Dioxide Molecule

Boroznina N.P., Zaporotskova I.V., Boroznin S.V., Zaporotskov P.A.
*Volgodrad State University, Volgograd, Russia*
*boroznin@volsu.ru*

This paper examines the possibility of using boron-carbon nanotubes boundary modified with different functional groups, in which the percentage of boron was 50%. The carboxyl group (-COH), the amine group (-NH2) and the nitro group (-NO2) were selected as the modifying groups. nitride nanotubes as sensor elements of devices exhibiting sensitivity to gas-phase carbon compounds. The choice of these functional groups is due to the fact that they are quite strong electron acceptors, since they have negative inductive and mesomeric effects ("tighten" the electron density on themselves), which has a positive effect on the processes of attachment of molecules to the general BC-NO2 system. Also, earlier studies of the interaction of modified boron-carbon nanotubes with alkali metal atoms and ions proved the possibility of creating highly sensitive sensory nanosystems [1-2]

The study consisted of computer modeling of the interaction of a carbon dioxide molecule and edge atoms of functional groups modifying the boron-carbon nanotube (Fig. 1). Further, the dependence of the interaction energy on the position of the molecule relative to the nanosystem was calculated. The simulation was stepwise in addition in 0.1 Å increments. The interaction distance was 1 to 6 Å. Calculations were performed by Density Functional Theory (DFT) using a 6-31G basis.

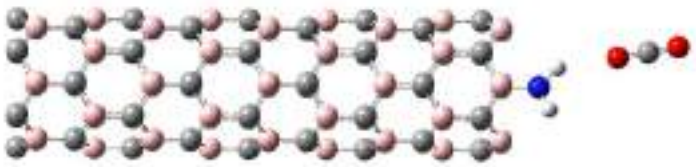

*Fig.1. Model of interaction of a nitro-modified boron-carbon nanotube with a carbon dioxide molecule*

Based on the conducted studies, the presence of sorption and sensory interaction between a modified functional groups boron-carbon nanotube of the BC type and a carbon dioxide molecule was established. The nature of the interaction is a weak Van der Waals interaction. This will allow these sensors to be used many times without destruction and chemical contamination.

These studies can be used to conduct air quality control in residential and industrial premises, as well as in the field of medicine, to determine the composition of air exhaled by a person.

**Acknowledgement:** The work was supported by state task of the Ministry of Science and Higher Education of the Russian Federation (topic "FZUU-2023-0001)

**References:**

[1] S.V. Boroznin. Modern Electronic Materials. 8. 1 (2022) 23.
[2] I.V. Zaporotskova, N.P. Boroznina, S.V. Boroznin. Smart Innovation, Systems and Technologies. 287 (2022) 137

## PP-I-15

# Influence of Support Composition on the HDS/HYD Selectivity of Ni-Zn Sorbents in Reactive Desulfurization of FCC Gasoline

Botin A.A.[1,2], Boldushevskii R.E.[2], Mozhaev A.V.[2], Ghashghaee M.[3], Nikulshin P.A.[1,2]
*1 – National University of Oil and Gas «Gubkin University», Moscow, Russia*
*2 – All-Russia Research Institute of Oil Refining, Moscow, Russia*
*3 – Iran Polymer and Petrochemical Institute, Tehran, Iran*
*botin-andrey@mail.ru*

The removal of sulfur compounds from petroleum products is the most important task of modern oil refining in connection with strict environmental standards. However, for some petroleum products, such as fluid catalytic cracking (FCC) gasoline, hydrotreating is accompanied by an undesirable process of hydrogenation of olefinic hydrocarbons. This effect leads to a decrease in the octane number of gasoline. Therefore, nowadays alternative processes for the desulfurization of hydrocarbon systems, including the process of reactive adsorption of sulfur compounds, are being actively studied. This technology is of interest for the removal of sulfur from the FCC gasoline due to the low pressure of hydrogen and the absence of hydrogen sulfide in the product streams. However, nickel, which is the main active component of sorbents, can exhibit high hydrogenation activity [1, 2]. Therefore, the study of methods for controlling the selectivity of desulfurization reactions with respect to hydrogenation reactions (HDS/HYD selectivity) is an actual task.

In this work, we considered the influence of the composition and characteristics of the support on the HDS/HYD selectivity of adsorptive-catalytic systems. Silicon oxide ($SiO_2$), aluminum oxide ($Al_2O_3$) and mesostructured silicon oxide SBA-15 (SBA), as well as ZnO-$SiO_2$, ZnO-$Al_2O_3$ and ZnO-SBA systems, with a mass fraction of zinc oxide of 25% were used as supports. Sorbents with different surface concentrations of nickel were synthesized by incipient wetness impregnation. The samples were studied by temperature-programmed reduction (TPR), X-ray diffractometry (XRD), X-ray photoelectron spectroscopy (XPS), and transmission electron microscopy (TEM). The desulfurizing activity and the HDS/HYD selective factor were determined on a fixed-bed flow laboratory unit during the desulfurization of model feedstock (1000 ppm S, 20 wt. % olefins) at a temperature of 400°C, a pressure of 0.5 MPa, and a mass flow rate of feedstock of 5.2 h-1. Before research and testing, all sorbents were reduced in a hydrogen flow at a temperature of 400°C and a pressure of 2 MPa.

Table 1 shows the results of studies of adsorptive-catalytic systems with a surface concentration of nickel atoms of 6 at/nm$^2$. Using the XRD, XPS, and TEM methods, it was found that the systems supported by silicon oxide are characterized by a lower degree of interaction between the active phase and the support compared to alumina. This provides a low dispersity of active phase particles and a high mass fraction of metallic nickel on the support surface. In addition, using the TPR and XPS methods, the presence of a strong interaction between zinc oxide and nickel oxide (for ZnO-$SiO_2$ and Ni/ZnO-SBA systems) was established. For ZnO-$Al_2O_3$,

this effect is not observed due to the binding of zinc oxide with aluminum oxide with the formation of mixed spinels.

Table 1. Characteristics and effectiveness of prepared sorbents

| Образец | $Ni^0$ amount on the surface (%) | Active phase particles dispersion (%) | HDS, % | Selectivity factor |
|---|---|---|---|---|
| $Ni/Al_2O_3$ | 5.8 | 16.3 | 96.7 | 1.49 |
| $Ni/ZnO-Al_2O_3$ | 5.3 | 19.8 | 94.2 | 1.05 |
| $Ni/SiO_2$ | 49.5 | 9.2 | 90.4 | 1.66 |
| $Ni/ZnO-SiO_2$ | 35.2 | 14.7 | 93.5 | 3.46 |
| Ni/SBA | 41.1 | 4.7 | 95.8 | 5.07 |
| Ni/ZnO-SBA | 29.3 | 5.1 | 50.9 | 4.37 |

The best results in terms of desulfurization activity and HDS/HYD selectivity were obtained when studying $Ni/ZnO-SiO_2$ and Ni/SBA samples. This effect of reducing the desulfurization activity of the Ni/ZnO-SBA sorbent can be associated with the overlapping of nanotubes with zinc oxide at the support synthesis stage.

As a result of the studies, it was found that the composition of the support and the degree of its interaction with the active phase have a decisive influence on the HDS/HYD selectivity of adsorptive-catalytic systems. The main factors providing high HDS/HYD selectivity of sorbents are high surface concentration of nickel, low dispersion of active phase particles, and strong Ni-Zn interaction.

**Acknowledgement:** The work was funded by RFBR and INSF, project number 20-58-56019.

**References:**

[1] J. Fan, G. Wang, Y. Sun, C. Xu, H. Zhou, G. Zhou, J. Gao Ind. & eng. chem. res. 49 (2010) 8450
[2] K. Zhang, Y. Liu, S. Tian, E. Zhao, J. Zhang, C. Liu Fuel. 104 (2013) 201.

## PP-I-16

# Development of a Method for the Synthesis of Water-Soluble Nanocomposites with Carbon Nanoparticles in a Poly-N-Vinylpyrrolidone Matrix

Chepenko D.S., Usmanov R.T., Emelyanov A.I., Pozdnyakov A.S.
*A.E. Favorsky Irkutsk Institute of Chemistry, Siberian Branch of the Russian Academy of Sciences, Irkutsk, Russian Federation*
*chepenko@irioch.irk.ru*

The development of new technological methods for the synthesis of nanomaterials based on fullerenes has attracted the attention of researchers since the discovery of fullerenes. Polymer nanomaterials based on fullerene $C_{60}$ have wide practical significance in medicine, biology and cosmetology [1].

One of the main requirements for such materials is their water solubility. To date, there are known methods for obtaining water-soluble fullerene $C_{60}$ complexes with poly-N-vinylpyrrolidone, a medical polymer [2-5]. However, the approaches used have a number of significant limitations. Firstly, organic solvents are used, the use of which is highly undesirable in the development of medical and cosmetic preparations. Secondly, the resulting polymer materials usually contain no more than 5 wt.% of fullerene in the final product. In addition, the use of such approaches as ultrasonic exposure and membrane separation significantly complicates the manufacturability of the process.

We have developed a new method for the synthesis of water-soluble nanocomposites with carbon nanoparticles in a poly-N-vinyl pyrrolidone (PVP) matrix based on the use of a single solvent for polymer and fullerene. The use of this approach makes it possible to obtain water-soluble $C_{60}$/PVP complexes with a fullerene content of up to 16 wt.%. Transmission electron microscopy proved that the resulting nanocomposites consist of isolated spherical particles with sizes up to 10 nm, evenly distributed in the volume of the polymer matrix. X-ray diffractograms of nanocomposites clearly differentiate the amorphous halo of the polymer component and the intense reflexes of carbon nanoparticles, which indicates their crystalline state.

On the basis of the Irkutsk Institute of Chemistry SB RAS, the production of fullerene-containing soot is carried out by the method of electric arc evaporation of spectrally pure graphite. The fullerene-containing carbon black produced contains a mixture of various fullerenes: $C_{60}$, $C_{70}$, $C_{76}$, $C_{78}$, $C_{80}$, $C_{82}$, $C_{84}$, $C_{86}$, etc., among which the main ones are $C_{60}$ and $C_{70}$. From the resulting fullerene-containing carbon black, fullerene $C_{60}$ with a purity of more than 99% is extracted by extraction [6,7]. Our own production of fullerenes provides ample opportunities not only for the direct use of $C_{60}$ in research, but also in the future will allow us to switch to low-tonnage production of fullerene-containing polymer materials.

**Acknowledgement:** This research was funded by the Ministry of Science and Higher Education of the Russian Federation, grant number 121021700340-5.

**References:**

[0] C. Sarantes, M. Stoikides, J. Catal. 93 (1985) 417.
[1] H. Kroto, J. Heath, S. O'Brien, R. Curl, R. Smalley, J. Nature., 318 (1985) 162.
[2] Y. Yamakoshi, T. Yagami, K. Fukuhara, S. Sueyoshi, N. Miyata, Chem. Soc., 4 (1994) 517
[3] L. Xiao, H. Takada, X. Gan, N. Miwa, Biomedic. Chem. Let., 16 (2006) 1590
[4] L. Xiao, H. Takada, K. Maeda, M. Haramoto, N. Miwa, J. Biomedic. Pharm., 59 (2005) 351
[5] S. Andreev, D. Purgina, E. Bashkatova, A. Garshev, A. Maerle, J. Carbon, 23 (2015) 792
[6] A. Pozdnyakov, D. Chepenko, A. Emelyanov, RU 212492 U1, 2022.
[7] A. Pozdnyakov, D. Chepenko, A. Emelyanov, Science and Tech. Siberia, 5 (2022) 115

## PP-I-17

# Application of Amphiphilic Carbon Dots for Improvement of Light Harvesting in Optoelectronic Devices

Cherevkov S.A., Vedernikova A.A., Miruschenko M.D., Sandzhieva M.A., Arefina I.A., Stepanidenko E.A., Spiridonov I.G., Ushakova E.V.
*ITMO University, St. Petersburg, Russia*
*s.cherevkov@itmo.ru*

The development of strategies to compensate for losses in light harvesting is important in further improvements in the efficiency of solar cell devices. This can be achieved by development of multilayer active materials, which are composed of layers with efficient absorption in different spectral regions. To date, one of the promising materials for solar energy harvesting is metal-halide perovskites, whose major drawback is the destruction under UV irradiation. To decrease the influence of UV irradiation, it is proposed to use an additional layer, which will efficiently absorb in that spectral region and convert it to lower-energy emission. For that, luminescent carbon nanoparticles as efficient light absorbers in the range of 200-400 nm are attractive. Carbon dots are functional nanostructured composites whose structural parameters and physicochemical properties can be precisely controlled with photophysical characteristics that are not inferior to those of semiconductor nanostructures. The obtained nanostructures have a great potential due to the low toxicity of both precursors and the final product. They are usually synthesized in polar media, and thus are hydrophilic. However, solution-processible optoelectronics demands hydrophobic inks, including conductive polymers; thus, further applications of carbon dots in such devices are highly limited. In this work, the amphiphilic carbon dots are developed and proposed to convert the UV spectral range of sun radiation into visible light via energy down-conversion.

The amphiphilic carbon dots were synthesized by solvothermal method using amines and organic acids as precursors dissolved in acetylacetone. In this case, the solvent not only facilitates the reaction of the precursors as media, but also participates in the formation of carbon dots. The morphology and optical properties of synthesized carbon dots were studied in detail. These nanoparticles can be efficiently redissolved in a set of polar and nonpolar solvents such as tetrachloromethane, chloroform, isopropanol, and water. The energy of optical transitions while changing the solvent is almost the same; moreover, the photoluminescence quantum yield is largest for nonpolar solvents. This observation opens an opportunity to use these carbon dots to fabricate photoactive functional films based on them for the improvement of the working parameters of optoelectronic devices or produce light emitting diodes, which was realized in this work.

**Acknowledgement:** This research was supported by Priority 2030 Federal Academic Leadership Program and the Russian Science Foundation (RSF22-13-00294).

## PP-I-18

# Solvent-Free Solid-State Combustion Synthesis of Nickel Nanoparticles for $CO_2$ Methanation

Dmitruk K.A.[1,2], Mazina O.I.[1], Veselovskaya J.V.[1], Prosvirin I.P.[1], Ishchenko A.V.[1], Rogov V.A.[1], Pochtar A.A.[1], Bulavchenko O.A.[1], Netskina O.V.[1]

*1 – Boreskov Institute of Catalysis, Novosibirsk, Russia*

*2 – Novosibirsk State University, Novosibirsk, Russia*

*k.dmitruk@g.nsu.ru*

The climate change, accelerated by the constant growth of the concentration of greenhouse gases in the atmosphere, is one of the global problems that can be solved with new technologies. One of the possible solutions to this issue involves adsorption of carbon dioxide ($CO_2$) from the atmosphere and its subsequent utilization. Hydrogenation of $CO_2$ to methane, also known as $CO_2$ methanation, is a promising way of recycling carbon dioxide as it yields a product that can be used for energy storage. Moreover, $CO_2$ methanation allows the production of biogas with a higher methane content, and can be used to remove carbon oxides from hydrogen-rich gas mixtures. However, according to the thermodynamic calculations, high selectivity of this reaction is possible only in the temperature range below 400 ˚C, which requires the use of catalysts due to the high energy barrier of the 8-electron reduction of carbon. Platinum group metals, such as Ru, Rh and Pd, demonstrate the highest catalytic activity in $CO_2$ methanation due to their ability to adsorb hydrogen. Nickel exhibits a lesser activity in this reaction, but it is widely used for this purpose due to its low cost [1]. Traditionally, the preparation of nickel catalysts involves an energy-consuming stage of thermal treatment of a precursor. The resulting nickel oxide is then reduced in a stream of hydrogen at a high temperature before being used in the reaction. The stages of nickel oxide formation and its reduction to metal can be combined in the self-propagating high-temperature synthesis method (SHS), using complex compounds of nickel with organic ligands as precursors for the active component. This variant of SHS is often called “solid-state combustion” (SSC) in the literature, because it involves a high-temperature gasification of solid precursors.

It should be noted that most commonly nickel-containing complexes are synthesized using solvents, which have to be disposed of. The environmental impact of complex preparation can be reduced by using solvent-free methods of synthesis, which corresponds to the modern concepts of the development of the chemical industry. Additionally, solvent-free methods considerably simplify the complex preparation process, and yield solid water-free compounds, which can be immediately used in the SSC.

In this work, we propose a new solvent-free method of synthesis of energetic nickel metal-organic compounds by reacting a nickel salt (nitrate or perchlorate) with a liquid ligand, such as ethylenediamine or melted imidazole, which is stable upon melting. The composition

and structure of these complexes have been confirmed by the elemental analysis, FTIR spectroscopy and powder XRD.

The thermal destruction of the acquired complexes has been investigated employing the thermogravimetry with differential scanning calorimetry (TG-DSC) and the dynamic mass spectral thermal analysis (DMSTA) methods at different heating rates. The kinetic parameters of various stages of the nickel complexes decomposition have been estimated using the genetic algorithm with the Coats-Redfern approximation, which led to a better understanding of the thermal destruction mechanism. The acquired data has also been used to calculate the critical temperature of thermal explosion for these complexes in order to assess their thermal stability. It has been shown that all of the synthesized complexes are thermally stable in the temperature range up to ~230 ˚C, and further temperature increase leads to the multi-staged thermal destruction.

The solid products of the gasification of the synthesized compounds have been investigated using FTIR spectroscopy, XRD, XPS and TPR-$H_2$. They were found to consist of nickel oxide mixed with reduced nickel and carbon-containing impurities. It has been shown that, compared with perchlorate-containing complexes, the gasification of the nitrate-containing complexes was carried out to a greater extent, which resulted in significantly less impurities and a more easily reducible nickel-containing product of the SSC. So, the solid products of the gasification of nickel complexes that contain nitrate anions were activated at 250 ˚C in the reaction medium of $CO_2$ hydrogenation and possessed an exceptional catalytic activity in this process.

An $Al_2O_3$-supported catalyst has been prepared using the nickel nitrate complex with imidazole by the SSC method, which was studied using the elemental analysis, XRD, XPS, TPR-$H_2$ and TEM methods. It was shown that the synthesized catalyst contained significantly more of the readily reducible nickel oxide phase than the industrial catalyst NIAP-07-01, demonstrated catalytic activity even at 150 ˚C, and achieved the $CO_2$ conversion rate of 69 % at 350 ˚C, which is nearly 3 times higher than the $CO_2$ conversion rate using NIAP-07-01, which contained 1.5 times more nickel.

As a result of this work, we have proposed a new solvent-free method of synthesis of $CO_2$ methanation catalysts using energetic nickel complexes with organic ligands as precursors of the active phase of the catalyst.

**Acknowledgement:** This work was supported by the Ministry of Science and Higher Education of the Russian Federation within the governmental order for Boreskov Institute of Catalysis, project AAAA-A21-121011390006-0.

**References:**

[1] W. K. Fan, M. Tahir, J. Environ. Chem. Eng. 9 (2021) 105460

## PP-I-19

# Cu-Promoted Ni-$LaCeO_x$/SBA-15 Catalysts for Dry Reforming of Methane and Ethanol Steam Reforming

Dorofeeva N.V.[1], Kharlamova T.S.[1], Grabchenko M.V.[1], Simonov M.N.[2], Larichev Yu.V.[2], Salaev M.A.[1], Vodyankina O.V.[1]

*1 – Tomsk State University, Tomsk, Russia*

*2 – Boreskov Institute of Catalysis, Novosibirsk, Russia*

*nv-dorofeeva@yandex.ru*

The production of hydrogen and synthesis gas using renewable feedstock recycling processes is one of the topical challenges of environmental technologies, which include steam reforming of ethanol and carbon dioxide reforming of methane. The Ni- or Co-based composites as well as their bimetallic formulations are effective catalysts for such processes. Ni-based catalysts have high efficiency in activation of C–C bonds, while suffer from carbon deposition. Traditional or modified supports [1, 2] are used to prevent deactivation due to sintering of nickel particles and reduce carbon deposition. Mesoporous SBA-15 was shown to improve the distribution of nanosized Ni species in its porous structure, and its modification with $CeO_2$ or $La_2O_3$ enhanced the metal-support interaction. Another approach is to add a second metal to reduce carbon deposition or increase hydrogen selectivity [3]. The present work is devoted to study of the structure of the Cu-promoted Ni-$LaCeO_x$ catalysts supported on SBA-15 and their activities in reforming processes, ethanol steam reforming (ESR) and dry reforming of methane (DRM).

The catalysts 12 wt.%Ni-$LaCeO_x$/SBA-15 with La/Ce molar ratios of 1/1 or 9/1 and 3 wt. % Cu were prepared by incipient wetness impregnation and characterized by XRF, $N_2$ adsorption-desorption, SAXS, XRD, $H_2$-TPR, Raman, and STA methods. The ESR reaction was carried out at temperatures of 500–800 °C and initial concentrations of ethanol and water were 2 % and 8 %, respectively. The catalytic properties of the samples in DRM were studied in a feed $CH_4/CO_2$ = 1 at temperatures of 400–800 °C. The stability of catalysts was studied at 650 °C.

It was established that the conditions for the formation of $Ni^0$ particles and the size of the latter depend on the ratio of both oxide modifiers and the presence of copper in the catalysts. An increase in the La/Ce ratio in the modifying additive led to an increase in the dispersion of NiO particles (CSR from 6 to 8 nm) and a stronger support interaction with the precursor of the active component due to the formation of lanthanum nickelate. Vibrational spectroscopy and SAXS data showed that nickel and modifiers were partially incorporated into the SBA-15 structure, which led to the appearance of the Si-O-M bonds (M = Ni, Ce, La). With an increase in the $La_2O_3$ content in the support composition, the temperature of $Ni^{2+}$ reduction increased, and the reducibility of $Ni^0$ decreased. Addition of copper to the catalyst composition led to a reduction of $Ni^{2+}$ at lower temperature and increased the reducibility by 15 %.

The highest ethanol conversion in the temperature range of 500-700 °C was observed on the Ni-$LaCeO_x$/SBA-15 (1:1) catalyst, while at 800 °C, the maximal conversion (100%) was

demonstrated by the Cu-promoted catalyst NiCu-$LaCeO_x$/SBA-15 (1:1). The addition of copper to the composition of the Ni-$LaCeO_x$/SBA-15 (1:1) catalyst resulted in an increase in the hydrogen yield at 800 °C (from 48 to 55 %). In DRM, the maximal conversions of $CH_4$ and $CO_2$ (~64% and 76%, respectively) are observed for catalysts with the modifier ratios La/Ce = 9/1 and 1/1. However, the Ni-$LaCeO_x$/SBA-15 (9:1) system was more stable in the DRM which was associated with the coke oxidation.

**Acknowledgement:** This work was supported by the Russian Science Foundation, grant 19-73-0026.

**References:**

[1] M.A.Salaev, L.F. Liotta, O.V. Vodyankina, Int. J. Hydrog. Energy. 47 (2022) 4489.
[2] A. Haryanto, S. Fernando, N. Murali, S. Adhikari, Energy & Fuels. 19 (2005) 2098.
[3] J.A. Calles, A. Carrero, A.J. Vizcaíno, Microporous Mesoporous Mater. 119 (2009) 200.

## PP-I-20

# Effect of Boron Doping on Sensing Properties of CNTs Functionalized with Nitro Group

Dryuchkov E.S., Zaporotskova I.V., Zaporotskov P.A.
*Volgograd State University, Volgograd, Russia*
*dryuchkov@volsu.ru*

Currently, carbon nanotubes are attracting increasing attention as potential materials for creating sensors of various types. It can be assumed that their sensory properties can be improved by modifying the surface of CNT with impurity replacement boron atoms [1]. Similar nanotubes can be called boron-carbon nanotubes. In this paper, we have examined the effect of impurity boron atoms on the sensory properties of zig-zag type boron-carbon nanotubes (6,0) containing different numbers of boron atoms, namely 50% and 25%. Let's call them BC and $BC_3$ nanotubes. The simulation was carried out using the DFT calculation method, the B3LYP functionality and the basis set of 6-31G [2].

Also, to improve the sensory properties of BC and $BC_3$ nanotubes, their surfaces were functionalized with a nitro group ($NO_2$), the presence of which can lead to an increase in the sensitivity of nanotubes to various atoms and molecules. Nanotubes can be used as sensors to detect various gases, including explosive and toxic substances, due to their high sensitivity to small environmental changes. In addition, carbon nanotubes can serve as the basis for various electronic devices, including transistors, logic elements and microcircuits [3].

The sorption and sensory interaction of nanotubes with lithium, sodium and potassium atoms, which are part of many salts and alkalis, was investigated [4]. The study of the interaction of alkali metal atoms with functionalized carbon nanotubes may be important for the development of nanoelectronics.

Functionalization of the surface of boron-carbon nanotubes was carried out by attaching a nitro group to two possible centers (PC) of the surface of the nanotube: 1 - carbon atom (C) of the surface; 2 - boron (B) of nanotube surface. The functional group was located approximately in the center of the BCNT cluster to eliminate the effect of the influence of edge atoms. At the first stage, the attachment distances of the nitro group to the surface of the nanotube were determined. Further, alkali metal atoms (lithium, sodium, potassium) approached the obtained complexes "BC-$NO_2$," $BC_3$-$NO_2$ "to determine the distances and energy of the sorption interaction. The parameters found are given in Table 1.

*Table 1. Characteristics of sorption interaction between functionalized BCNTs and alkali metal atoms*

| | **BC** | | | | **$BC_3$** | | | |
|---|---|---|---|---|---|---|---|---|
| | **PC: (C) atom** | | **PC: (B) atom** | | **PC: (C) atom** | | **PC: (B) atom** | |
| | **$r_{int}$, Å** | **$E_{int}$, eV** | **$r_{int}$, Å** | **$E_{int}$, eV** | **$r_{int}$, Å** | **$E_{int}$, eV** | **$r_{int}$, Å** | **$E_{int}$, eV** |
| Li | 1,9 | -3,08 | 1,8 | -3,67 | 1,8 | -3,43 | 1,8 | -4,09 |
| Na | 2,1 | -2,60 | 2,1 | -3,14 | 2,1 | -2,93 | 2,1 | -3,52 |
| K | 2,5 | -2,71 | 2,5 | -3,15 | 2,5 | -2,99 | 2,5 | -3,49 |

After the distances at which functionalized BCNTs interact with alkali metal atoms became known, an arbitrary virtual surface on which the presence of these atoms is assumed was scanned to assess the sensory interaction between alkali metal atoms and the complexes "BC-$NO_2$," $BC_3$-$NO_2$. " The data obtained are shown in Table 2. The path along which the surface was scanned and the cluster used in the work are shown in Figure 1

*Table 2. Characteristics of sensory interaction when scanning an arbitrary surface*

| | **BC** | | | | **$BC_3$** | | | |
|---|---|---|---|---|---|---|---|---|
| | **PC: (C) atom** | | **PC: (B) atom** | | **PC: (C) atom** | | **PC: (B) atom** | |
| | **$r_{s\text{-}int}$, Å** | **$E_{s\text{-}int}$, eV** | **$r_{s\text{-}int}$, Å** | **$E_{s\text{-}int}$, eV** | **$r_{s\text{-}int}$, Å** | **$E_{s\text{-}int}$, eV** | **$r_{s\text{-}int}$, Å** | **$E_{s\text{-}int}$, eV** |
| Li | 2,6 | -3,18 | 2,6 | -3,89 | 2,6 | -3,63 | 2,6 | -4,33 |
| Na | 2,6 | -2,78 | 2,6 | -3,35 | 2,6 | -3,12 | 2,6 | -3,76 |
| K | 2,6 | -2,82 | 2,6 | -3,29 | 2,6 | -3,16 | 2,6 | -3,64 |

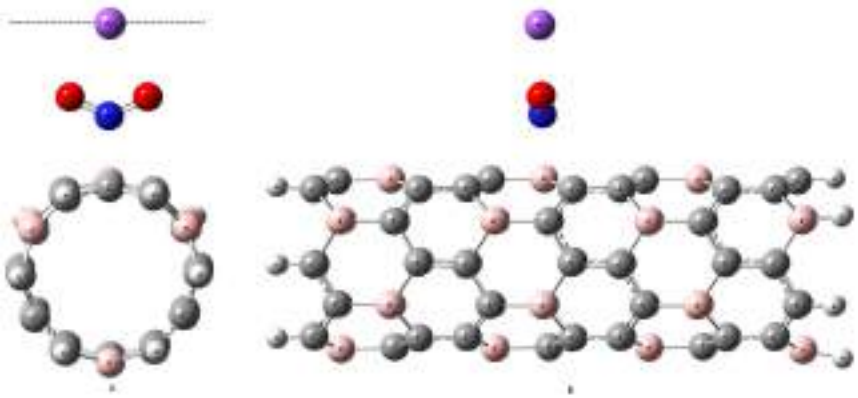

*Fig. 1. A) The path by which the surface was scanned; B) $BC_3$-$NO_2$ complex with alkali metal atom Na*

Summing up, it can be concluded that all functionalized boron-carbon nanotubes studied can be used to detect the presence of alkali metal atoms. Such systems can act as sensing elements of sensor devices. At the same time, an increase in the number of impurity boron atoms in the obtained systems leads to a decrease in the energy of the sensory interaction of the complexes "BC-$NO_2$", $BC_3$-$NO_2$" with alkali metal atoms Li, Na, K.

**Acknowledgement:** The work was carried out within the framework of the state task of the Ministry of Science and Higher Education of the Russian Federation (topic "FZUU-2023-0001).

**References:**

[1] S. Peng, K. Cho, Nano Letters. 3 (2003) 513-517.
[2] F. Nogueira, A. Castro, M.A.L. Marques, Lecture Notes in Physics, 620 (2003).
[3] I.A. Vitale, G. Selvolini, G. Marrazza, Chemosensors. 11 (2023) 77.
[4] L.C.T. Cao, L. Hakim, Characteristics and Applications of Boron. (2022) 40.

## PP-I-21

# Unsaturated Polyketones — a New Type of Functionalized Rubbers

Semikolenov S.V., Kharitonov M.A., Dubkov K.A.
*Boreskov Institute of Catalysis, Novosibirsk, Russia*
*dubkov@catalysis.ru*

Earlier, we have shown that the non-catalytic selective oxidation of C=C bonds in diene rubbers by nitrous oxide, $N_2O$ (the so-called ketonization reaction) opens a synthetic route for obtaining a new type of functionalized polymers and oligomers - unsaturated polyketones (UPKs) [1, 2]. In this work, we have studied the ketonization of butadiene rubbers Buna CB25 and Buna CB35 with different contents of 1,2-units (Tables 1 and 2). The ketonization of rubbers (5 g) by $N_2O$ (0.186 mol) was performed batchwise in a Parr reactor (100 ml) in a benzene solvent (60 ml) at 160–230°C and elevated pressure. A series of UPK samples containing up to 8.1-8.5 wt. % of oxygen in the form of C=O groups was obtained.

**Table 1.** Ketonization of Buna CB25 (99.6 mol. % 1,4-units, 0.4 mol. % 1,2-units) with $N_2O$.

| Sample | $N_2O$ conversion (%) | C=C bonds conversion (%) | Oxygen content (wt. %) | Mn $\cdot 10^{-3}$ | Mw $\cdot 10^{-3}$ | Appearance |
|---|---|---|---|---|---|---|
| CB25-parent | 0 | 0 | 0 | 180 | 370 | rubber |
| CB25-200°C-6 h | 1.9 | 4.2 | 1.2 | 32 | 74 | rubber-like |
| CB25-215°C-6 h | 4.4 | 9.5 | 2.7 | 15 | 38 | rubber-like |
| CB25-230°C-6 h | 8.0 | 17.4 | 4.9 | 6 | 15.8 | fluid polymer |
| CB25-230°C-12 h | 14.1 | 29.6 | 8.1 | 3.3 | 8.5 | liquid |

**Table 2.** Ketonization of Buna CB35 (90.4 mol. % 1,4-units, 9.6 mol. % 1,2-units) with $N_2O$.

| Sample | $N_2O$ conversion (%) | C=C bonds conversion (%) | Oxygen content (wt. %) | Mn $\cdot 10^{-3}$ | Mw $\cdot 10^{-3}$ | Appearance |
|---|---|---|---|---|---|---|
| CB35-parent | 0 | 0 | 0 | 105 | 230 | rubber |
| CB35-200°C-5 h | 2.4 | 4.15 | 1.25 | 8.1 | 20.4 | fluid polymer |
| CB35-200°C-10 h | 4.8 | 8.95 | 2.6 | 3.87 | 9.76 | liquid |
| CB35-230°C-6 h | 10.2 | 19.7 | 5.5 | 1.54 | 3.25 | liquid |
| CB35-230°C-12 h | 17.2 | 31.5 | 8.5 | 0.86 | 1.73 | liquid |

According to NMR data, upon ketonization of both rubbers, mainly ketone groups randomly distributed along the backbone are formed by the reaction of $N_2O$ with internal C=C bonds in 1,4-units (reaction 1, Scheme 1). A certain fraction of reacting internal C=C bonds (~4% for CB25 rubber and ~16.8% for CB35 rubber) is cleaved, leading to the formation of

shorter macromolecules containing aldehyde and end vinyl groups (reaction 2, Scheme 1). As a result, the molecular weight of polymers decreases with increasing conversion of C=C bonds (Fig. 1), and consistency of UPKs varies from a rubber-like form to a viscous liquid (Tables 1 and 2).

**Scheme 1**

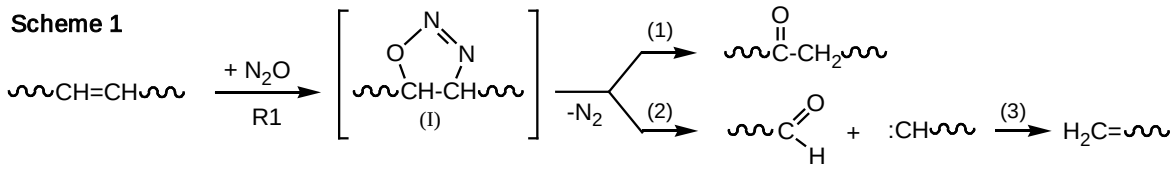


In the case of CB25 rubber, the ketone/aldehyde groups ratio in the obtained UPKs is about 20, and the products of the following structure are obtained:

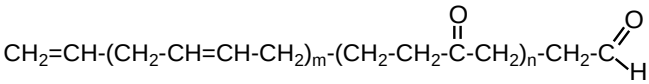


Upon ketonization of CB35 rubber, which contains a significant fraction of 1,2-units (9.6 mol. %), the terminal C=C bonds in such units are additionally oxidized (Scheme 2). As a result, the obtained UPKs contain, along with ketone groups in the backbone, additional aldehyde and ketone side groups. In this case, a fraction of the formed aldehyde groups is higher (the ketone/aldehyde groups ratio is 3.4-5.5).

**Scheme 2**

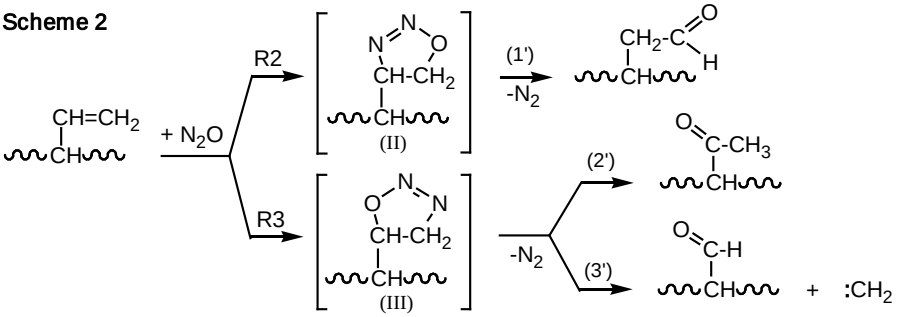


Thus, the ketonization with $N_2O$ is applicable to various types of diene rubbers and allows obtaining UPKs with different structure of monomeric units, controllable molecular weight, and specified concentration of carbonyl groups. The method requires neither catalysts nor expensive reagents. Since $N_2O$ reacts solely with olefinic C=C bonds, the reaction proceeds with high selectivity and does not yield any by-products. Due to their properties, oligomeric UPKs can be considered as promising components of polymeric materials and adhesive compositions [3, 4].

**Acknowledgement:** The study was supported by the Russian Science Foundation (Project No. 23-23-00310, https://rscf.ru/project/23-23-00310/).

**References:**

[1] Dubkov K.A., Semikolenov S.V., D.E. Babushkin, et al., J. Polym. Sci. A, 44(2006) 2510-2520.
[2] Dubkov K.A., Panov G.I., Parmon V.N., Russ. Chem. Rev. 86(2017) 510–529.
[3] Sidorov O.I., Dubkov K.A., Semikolenov S.V., et al., Polym. Sci., Ser. D, 11(2018) 215-224.
[4] Sidorov O.I., Evseev N.E., Dubkov K.A., et al., Polym. Sci., Ser. D, 13(2020) 85-88.

## PP-I-22

# Replacement of $Al_2O_3$ by $Y_2O_3$ in Aluminosilicate Glass Sealants: Effect on Properties and Compatibility with Solid Oxide Fuel Cell Components

Dubovtsev D.I.[1], Vepreva A.I.[1], Saetova N.S.[1,2], Krainova D.A.[1], Kuzmin A.V.[1,2]
*1 – Vyatka State University, Kirov, Russia*
*2 – Institute of Solid-State Chemistry and Mechanochemistry, Novosibirsk, Russia*
*d.dubovtzev@yandex.ru*

Among various alternative power sources, solid oxide fuel cells (SOFCs) are the most promising due to the high efficiency of converting chemical fuel energy into electrical one, flexibility of fuel and low operating costs. Their anode-supported design is widespread because of the ease of manufacturing and rather high specific power values at operating temperatures. The NiO - YSZ composite is a commonly used anode material for SOFC. One of the key drawbacks of the anode-supported SOFC design is unavoidable nickel reduction under the effect of a hydrogen atmosphere. The NiO→Ni transition leads to changes in the value of the coefficient of thermal expansion (CTE). The use of non-crystallising glass sealants could solve this problem.

The previously studied glass sealant of the $59{,}6SiO_2$-$11{,}0Al_2O_3$-$6{,}6ZrO_2$-$3{,}4CaO$-$15{,}4Na_2O$-$4Y_2O_3$ (wt.%) composition is a promising sealant with low tendency to crystalliza-tion [1,2]. However, such sealant could soften at SOFC operating temperature (850 °C), which can lead to the shift of structural elements of the cell, and lead to the loss of sealing of assembling of elements. The use of rare-earth oxides can have a positive effect on the properties of aluminosilicate glass sealants by stabilizing the CTE value and increasing viscosity. In this work the effect of replacement $Al_2O_3$ by $Y_2O_3$ on the physical and chemical properties of the $59{,}6SiO_2$-$(11{,}0\text{-}x)Al_2O_3$-$10{,}6ZrO_2$-$3{,}4CaO$-$15{,}4Na_2O$-$xY_2O_3$ (x = 2; 4; 6; 8; 10 wt.%) glass and its chemical stability in contact with SOFC materials are investigated.

The phase composition of the glass was studied in contact with NiO-YSZ after exposure for 125 and 1000 hours at 850 °C in oxidizing (air) and reducing ($H_2$) atmospheres (Fig. 1). According to the SEM images and maps of element distribution, no interaction products were observed at the glass|NiO-YSZ interface after exposure for 125 h and no ion diffusion occurred. According to the maps of element distribution, the crystal phases found in the glass volume are enriched with Ca. With the growth of the $Y_2O_3$ content, the degree of crystallinity increased. No reaction products were observed at the glass|NiO-YSZ boundary after 1000 h of exposure oxidising and reducing atmospheres.

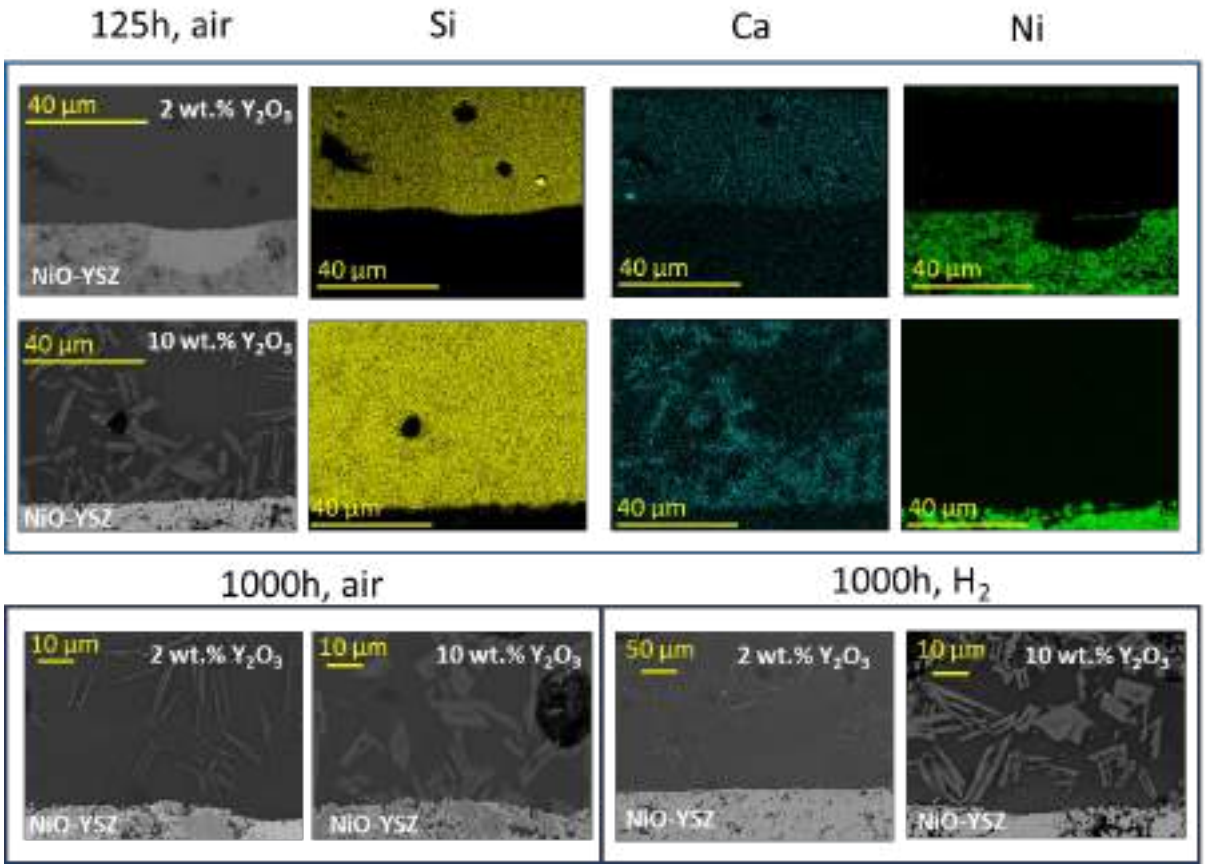


*Fig. 1. SEM images and element distribution maps of glass|NiO-YSZ interface after heat treatment at 850 °C in oxidising (air) and reducing ($H_2$) atmospheres for 125 and 1000 h.*

**Acknowledgement:** This work was supported by the Russian Science Foundation, project no. 21-79-30051

**References:**

[1] D.A. Krainova, N. S. Saetova, et al. 46 (2020) 5193–5200.
[2] D.A. Krainova, N. S. Saetova, et al. 47 (2021) 8973–8979.

## PP-I-23

# The Active Oxygen Intermediates Appearing from UV-Irradiation of Oxygen-Rich $TiO_2$ Photocatalyst

Ershov K.S., Bogomolov A.S., Slepneva I.A., Baklanov A.V.
*Voevodsky Institute of Chemical Kinetics and Combustion, Novosibirsk, Russia*
*KErshov93@gmail.com*

First report on the photocatalyst based on the oxygen-rich $O_2$-$TiO_2$ was presented by Dewkar et al. in paper [1]. These authors showed that this photocatalyst is efficient in photocatalytic oxidation of aromatic primary amines to nitro compounds. Later authors of paper [2] successfully used this catalyst in the photocatalytic reduction of $CO_2$ to high value-added chemical fuels such as methane. These possible applications dictate the interest to the composition of oxygen-rich $TiO_2$ and to the reactive intermediates, which can be generated on its surface by irradiation.

The processes initiated by UV-irradiation of this photocatalyst with the measurements of luminescence in the near IR (NIR) region has been investigated. The experimental setup for IR luminescence registration was similar to the one described earlier [3] and included a laser source of UV radiation, a cuvette with the studied substance suspended in a solvent, an IR-luminescence detector, a monochromator and an oscilloscope. In the spectra of NIR luminescence the signal with the spectrum of adsorbed singlet oxygen, similar to that revealed earlier in paper [3], has been observed. The mechanism of singlet oxygen photogeneration is discussed.

**Acknowledgement:** The authors acknowledge the core funding from the Russian Federal Ministry of Science and Higher Education.

**References:**

[1] G.K. Dewkar, M.D. Nikalje, I.S. Ali, A.S. Paraskar, H.S. Jagtap, A.Sudalai, Angew.Chem. 113 (2001) 419.
[2] L.-L. Tan, W.-J. Ong, S.-P. Chai, A.R.Mohamed, Chem. Comm. 50 (2014) 6923.
[3] A.V. Demyanenko, A.S. Bogomolov, N.V. Dozmorov, A.I. Svyatova, A.P. Pyryaeva, V.G. Goldort, S.A. Kochubei, A.V. Baklanov, J. Phys.Chem. C 123 (2019) 2175.

## PP-I-24

# Pt Modification of Dark $TiO_2$ Prepared by Pulsed Laser Ablation: the Effect of Precursor Nature and Preparation Method on Photocatalytic Properties

Fakhrutdinova E.D., Zinina E.V., Reutova O.A., Svetlichnyi V.A., Vodyankina O.V.
*Tomsk State University, Tomsk, Russia*
*fakhrutdinovaed@gmail.com*

Increasing the efficiency of a material in hedrogen evalution reaction (HER) by loading Pt nanoparticles (NPs) on catalyst surface is one of the common methods for designing photocatalysts [1]. The usage of Pt as co-catalyst can provide an active site for the reduction/oxidation reaction and also facilitate the charge separation through the formation of the Schottky junction between the semiconductor and metal. Previously, we obtained dark $TiO_2$ by the method of pulsed laser ablation, which has an intense absorption due to defective states of the structure [2]. The material showed increased activity in the processes of decomposition of the dye Rhodamine B, phenol, and also has antibacterial properties. In this work, platinum is loaded in order to increase the activity in the HER since dark titanium dioxide exhibits moderate activity. We used several approaches for Pt loading to dark $TiO_2$, as well as various precursors.

The first approach (fig. 1a), the individual colloidal solution of Ti and Pt in water was prepared via pulsed laser ablation (PLA) method using Nd:YAG laser (1064 nm, 7 ns, 20 Hz). Then colloidal solutions were mixed in a certain molar ratio and subjected to ultrasonic treatment, dried in air at 60 °C to up to a powder and annealed at 400 °C. We have used this method previously to modify black titanium dioxide [3]. The second approach (fig. 1b), the colloidal solution of titanium in water was prepared via PLA method in water, then the solution of $(Me_4N)_2[Pt_2(OH)_2(NO_3)_8]$ was added to colloidal solution of titanium and carried out additional laser treatment with a focused beam, then were dried and annealed at 400 °C. Laser treatment by a high power focused beam of the colloid resulted in effective photo- and thermoreduction of platinum from the organic complex similar to work [4]. Powder annealing promoted further embedding and better interaction of platinum with the titanium oxide matrix. Samples obtained by the above methods were compared with the traditional method of loading Pt from $(Me_4N)_2[Pt_2(OH)_2(NO_3)_8]$ by wet impregnation of dark $TiO_2$, followed by annealing at 400 °C. Thus, a series of samples with different platinum content was prepared. The dark $TiO_2$ was prepared using the PLA method.

The samples were studied by X-ray diffraction (XRD), X-ray photoelectron spectroscopy, the Brunauer–Emmett–Teller (BET) to identify the specific surface area, and UV-vis spectroscopy. The photocatalytic activity of the materials was studied in the HER in the presence of glycerol (20 wt. %) as a sacrificial reagent in a flow reactor under LED irradiation (λ=375 and 410 nm). The experiments were carried out with continuous registration of the evolved hydrogen via a gas chromatograph.

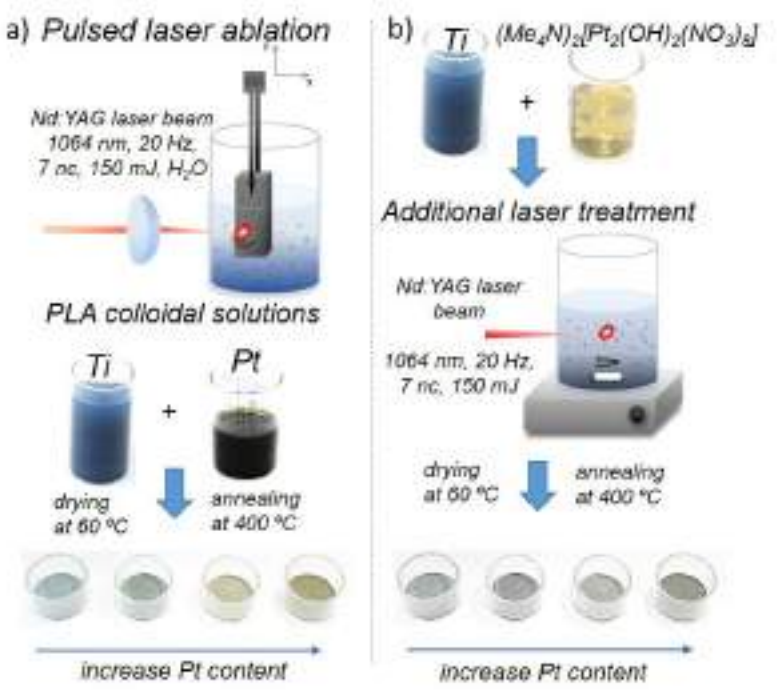


*Fig. 1. The approaches to the synthesis of catalysts*

In all cases, Pt modification increases the activity of dark titanium dioxide. For the best compositions, the efficiency of hydrogen generation increased by more than an order of magnitude. The photocatalytic activity is complexly dependent on the amount of Pt, particle size, states (ionic/metallic), and dispersion of Pt NPs on the surface of dark TiO2. It should be noted that the best results are provided when using a platinum complex. In this case, the small particle size and more homogeneous distribution of platinum in the sample are provided. Thus, using a combination of physical (laser) and chemical synthesis methods, it is possible to significantly increase the efficiency of the photocatalyst for hydrogen generation with minimal platinum loading.

**Acknowledgement:** This work was supported by the Russian Science Foundation, grant 19-73-30026.

**References:**

[1] A.Yu. Kurenkova, A.M. Kremneva, A.A. Saraev, V. Murzin, E.A. Kozlova, V.V. Kaichev, Cat. Let., 151 (2021) 748.
[2] E. Fakhrutdinova, A. Shabalina, M. Gerasimova, A. Nemoykina, O. Vodyankina, V. Svetlichnyi, Mater., 13 (2020) 2054.
[3] E. Fakhrutdinova, O. Reutova, L. Maliy, T. Kharlamova, O. Vodyankina, V. Svetlichnyi, Mater., 15 (2022) 7413.
[4] V.V. Kononenko, K.K. Ashikkalieva, N.R. Arutyunyan, A.M. Romshin, T.V. Kononenko, V.I. Konov, J. Photochem. Photobiol. A, 426 (2022) 113709.

## PP-I-25

# Solvent-Free Synthesis of Birch Wood Xylan Sulfates

Levdansky V.A., Garyntseva N.V., Levdansky A.V.

*Institute of Chemistry and Chemical Technology SB RAS, FRC KSC SB RAS, Krasnoyarsk, Russia*

*garyntseva@icct.ru*

Xylan sulfates have a wide range of biological activities, such as anti-viral, anti-inflammatory, anti-tumor, and anticoagulant activity [1]. The traditional methods for the synthesis of xylan sulfates have some disadvantages such as: a long reaction time (from 2 to 10 h); a high activity of sulfating agents, which leads to partial degradation of the polymer and the use of hazardous solvents such as pyridine or dimethylformamide which may contaminate the products of sulfation, that is unacceptable in the production of medicines [2].

The aim of the present research was the synthesis of xylan sulfates by sulfation of birch wood xylan with the melt of a sulfamic acid-urea mixture without hazardous solvents as pyridine or dimethylformamide.

The initial xylan was obtained by 5% NaOH extraction of birch wood pulp following the peroxide fractionation of birch wood in the “acetic acid – water” medium [3]. The composition of xylan was: 95.13% xylose, 1.52% mannose, 1.48% glucose, 0.97% galactose and 0.89% arabinose. Xylan was sulfated with the melt of a sulfamic acid-urea mixture (Fig.1.). The melt was prepared by heating sulfamic acid and urea together at 110 °C at a molar ratio of 1:1. Sulfation of xilan was performed by mixing dry xylan with the melt of a mixture of sulfamic acid and urea at 110 - 130°C for half an hour.

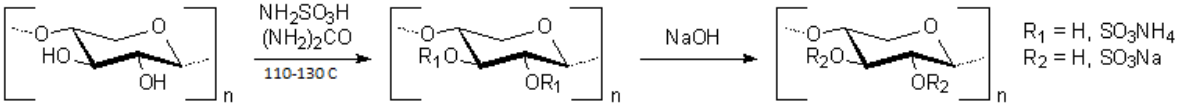


*Fig.1. Scheme of the xylan sulfation with the melt of a sulfamic acid–urea mixture*

The high yield (77.5 wt%) and the high degree of sulfation (1,40) of xylan sulfate was obtained at the temperature 115 °C. The structure of xylan sulfate was confirmed by FTIR and 2D HSQC NMR spectroscopy (Fig.2.).

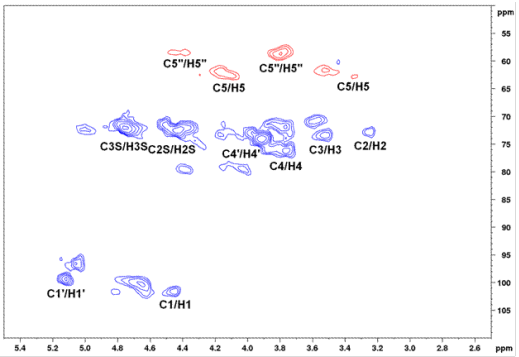


*Fig. 2. HSQC spectrum of xylan sulfate. The assignment of signals is given in Table*

Table. Assignment of $^{1}H$–$^{13}C$ cross signals in the HSQC spectrum of xylan sulfate, obtained by sulfation in the melt of a sulfamic acid–urea mixture.

| Assignment | C1/H1 | C2/H2 | C3/H3 | C4/H4 | C5/H5 |
|---|---|---|---|---|---|
| Chemical shift, ppm | 101.6/4.45 | 72.8/3.25 | 73.4/3.53 | 76.2/3.77 | 62.7/3.35 and 4.12 |
| Assignment | C1'/H1' | C2S/H2S | C3S/H3S | C4'/H4' | C5''/H5'' |
| Chemical shift, ppm | 99.4/5.12 | 72.5/4.44 | 72.0/4.76 | 74.0/3.91 | 58.5/3.80 and 4.39 |

So by the proposed method xylan sulfates with a high DS was obtained using the melt of a sulfamic acid–urea mixture both as reaction media and reagent without any external solvent.

The method allows significantly reducing the duration of the synthesis and eliminating the contamination of xylan sulfates with harmful solvents (pyridine, DMFA).

**Acknowledgement:** This work was supported by the Russian Science Foundation, grant 23-23-00336, https://rscf.ru/project/23-23-00336.

**References:**

[1]. Y. Chen, X. Sun, J. Shan Int. J. Biol. Macrovol. 155 (2020) 1460-1467.
[2]. A. Pfeifer, T. Heinze Carbohydr. Polym. 206 (2019) 65–69.
[3]. V.A. Levdansky, A.A. Kondrasenko, A.V. Levdansky, B.N. Kuznetsov Khimija Rastitel'nogo Syr'ja. 1 (2018) 29-36.

## PP-I-26

# Synthesis and Characterization of Carbon-Coated Calcium Aluminate Aerogels

Gerus Y.Y.[1,2], Bedilo A.F.[1], Ilyina E.V.[1]
*1 – Boreskov Institute of Catalysis, Novosibirsk, Russia*
*2 – Novosibirsk State University, Novosibirsk, Russia*
*ygerus@catalysis.ru*

Calcium aluminate $12CaO•7Al_2O_3$ (commonly denoted as C12A7), also known as mayenite, is an object of particular scientific interest. This material possesses a number of rather peculiar physical and chemical properties, originally described in detail by Hosono et al. [1]. Its structure includes a cationic framework $[Ca_{24}Al_{28}O_{64}]^{4+}$ compensated by the presence of an anionic lattice $4X^-$, where $X^-$ can be $Cl^-$, $OH^-$, $O^{2-}$, $O_2^-$, $H^-$ or even $e^-$.

High specific surface area and developed pore structure are among the key requirements for efficient use of materials as catalyst supports or adsorbents. The aerogel technique involving supercritical drying of a gel is one of effective ways for synthesis of finely dispersed materials. In this study, aluminum isopropoxide and calcium methoxide were used as precursors for the synthesis of calcium aluminate aerogel with mayenite stoichiometry. These alkoxides were dissolved in a mixture of methanol and isopropanol. The resulting solution was subjected to hydrolysis with desired amount of deionized water, followed by aging for 16 hours and drying in an autoclave at 270 °C.

Depending on the amount of water used at the hydrolysis stage, the specific surface area of the samples after the drying procedure varied from 330 to 90 $m^2/g$. The use of a five-fold excess of water (compared to the stoichiometric amount) led to the formation of crystalline mayenite immediately after drying in the autoclave [2]. Reasonably high specific surface areas (up to 205 $m^2/g$) were preserved after calcination of the obtained aerogels at 500 °C in the air [3].

One of significant limitations for application of nanocrystalline metal oxides as catalysts or adsorbents is their tendency to adsorb water, which gradually leads to deactivation. In addition, various phase transformations accompanied by considerable sintering of the material can occur at elevated temperatures. One of the prominent ways to solve these problems is coating of metal oxide particles with porous carbon. Its relatively low hydrophilicity prevents deactivation of the material in a humid environment. In addition, a carbon coating eliminates direct contact between different metal oxide nanoparticles considerably enhancing the thermal stability of the material [4].

In this study, resorcinol added to the reaction mixture before the hydrolysis step was used as an organic precursor for deposition of a carbon coating on the surface of finely dispersed calcium aluminate. The resulting samples were denoted as C12A7@nC, where n stands for molar resorcinol concentration normalized to the sum of calcium and aluminum concentrations in moles. The specific surface area of resorcinol-containing aerogels after drying in an autoclave was as high as 490 $m^2/g$.

A comparison of the specific surface areas of calcium aluminate samples after their high-temperature treatment in an argon flow shows a significant enhancement of the thermal stability with increasing amount of resorcinol (Fig. 1a). Of particular interest is the sample with the highest resorcinol concentration used in this study (C12A7@0.7C). After treatment at 1100 °C in inert atmosphere with subsequent burnout of carbon at 500 °C in an air flow, it retained the surface area as high as 72 $m^2/g$, which exceeds the surface area of pure aerogel-prepared calcium aluminate after the same treatment approximately by a factor of five. On the contrary, direct burnout of organic additives at 1100 °C in an air flow leads to noticeable decrease of the specific surface area for samples with a high content of resorcinol compared to the pure calcium aluminate. The above effects indicate that the formation of a carbon coating during the resorcinol pyrolysis in the inert atmosphere partially prevents sintering of calcium aluminate particles.

Fig. 1(b) shows XRD patterns of C12A7@0.5C and pristine C12A7 aerogel after their treatment at 1100 °C in the argon and air flow. Both samples predominately consist of different calcium aluminate phases, such as $Ca_{12}Al_{14}O_{33}$ and $CaAl_2O_4$ (and $CaAl_4O_7$ for pristine C12A7) with relatively small contribution of $Ca_3Al_2O_6$ and residual CaO. It worth noting that the contribution of $Ca_{12}Al_{14}O_{33}$ is almost two times higher for the C12A7@0.5C sample than for pristine C12A7. So, the carbon coating does not hinder the formation of calcium aluminate phases and such approach can be used to stabilize the size of the calcium aluminate particles after treatment at high temperatures.

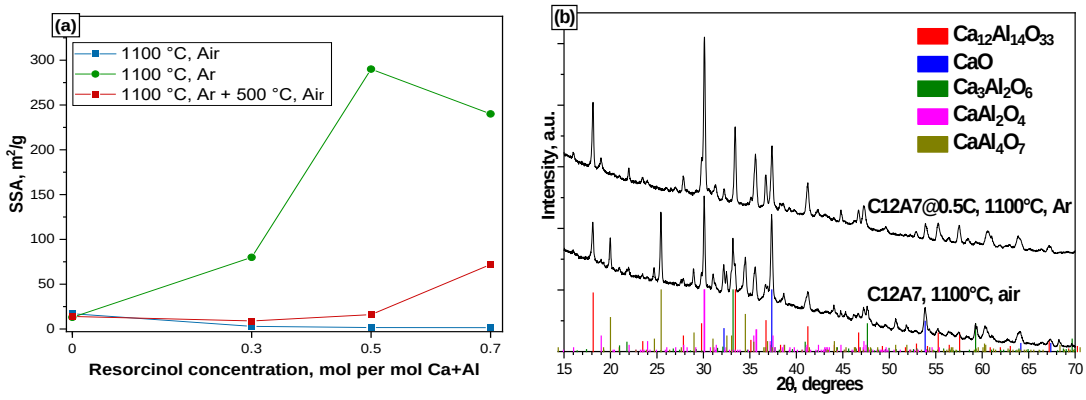


*Fig. 1. (a) Dependence of the specific surface of calcium aluminate samples after heat treatment at 1100 °C under different conditions on the amount of added resorcinol; (b) XRD patterns of C12A7@0.5C and pristine C12A7 aerogel after treatment at 1100 °C*

**Acknowledgement:** This work was supported by the Ministry of Science and Higher Education of the Russian Federation [project No. AAAA-A21-121011390054-1].

**References:**

[1] K. Hayashi et al., Nature. 419 (2002) 462.
[2] E.V. Ilyina et al., Mater. Lett. 293 (2021) 129699.
[3] E.V. Ilyina et al., J. Sol-Gel Sci. Technol. 104 (2022) 259.
[4] A.M.Volodin et al., RSC Adv. 7 (2017) 548524.

## PP-I-27

# Aspects of Solid-State Processing of UHMWPE-Based Electrically Conductive Nanocomposites

Lebedev O.V., Golubev E.K., Kurkin T.S., Shevchenko V.G., Tikunova E.P., Ozerin A.N.
*Enikolopov Institute of Synthetic Polymer Materials Russian Academy of Sciences, Moscow, Russia*
*oleg.lebedev@phystech.edu*

Ultra-high-molecular-weight polyethylene (UHMWPE) is a special high-performance polymer with a unique set of characteristics. Specific types of UHMWPE reactor powders can be processed using the solid-state processing method into high-modulus and high-strength materials [1]. By mixing UHMWPE reactor powders with different types of carbon nanoparticles it is possible to retain the capability of the composites to be processed into a highly oriented state [2]. These composites possess an extremely segregated structure and can be characterized by high levels of functional properties, such as electrical conductivity, at very low filler content values.

The goal of this work is to study different aspects of solid-state processing of composites based on nascent disentangled UHMWPE powders. Particularly, ways to improve nanoparticles distributions in the composites are investigated. Additionally, electrophysical properties of the composites are studied depending on their deformation ratio, nanoparticles type, and temperature.

Several different batches of nascent disentangled UHMWPE reactor powder synthesized were used as the base for the composite materials. As fillers, the following electroconductive carbon nanoparticles of different geometries were used: single-walled carbon nanotubes (SWCNTs); different types of multi-walled carbon nanotubes (MWCNTs), carbon black (CB), and graphene nanoplatelets (GNPs). Also, a special type of double-walled carbon nanotubes (DWCNTs), characterized by exceptional length, was used.

The procedure of the composites preparation consists of preliminary ultrasonication of nanoparticles in hexane, followed by addition of UHMWPE reactor powder in the nanoparticles dispersion. After additional ultrasonication of the mixture, it is dried out and molded at room temperature into plate samples, which later are subjected to rolling with a fixed clearance between two rolls heated up to 120 °C. The clearance between the rolls determines the deformation ratio of the samples. The most even distributions were obtained by optimization of such processing parameters as the time of preliminary ultrasonication of nanoparticles in hexane, time of ultrasonication of UHMWPE/nanoparticles mixtures, and molding time, temperature, and pressure.

Electrophysical characteristics of the obtained composites were investigated depending on the content of the filler in the composites and the deformation ratio of the composites, as well as the temperature. Fig. 1 shows the dependency of logarithm of the relative conductivity (conductivity divided by conductivity of the non-deformed sample) versus the deformation

ratio for the samples of UHMWPE-based composites filled with various nanoparticles. It can be seen that that while conductivity of most of the composites monotonously decreases with the deformation ratio, conductivity of the composites filled with DWCNTs is maintained.

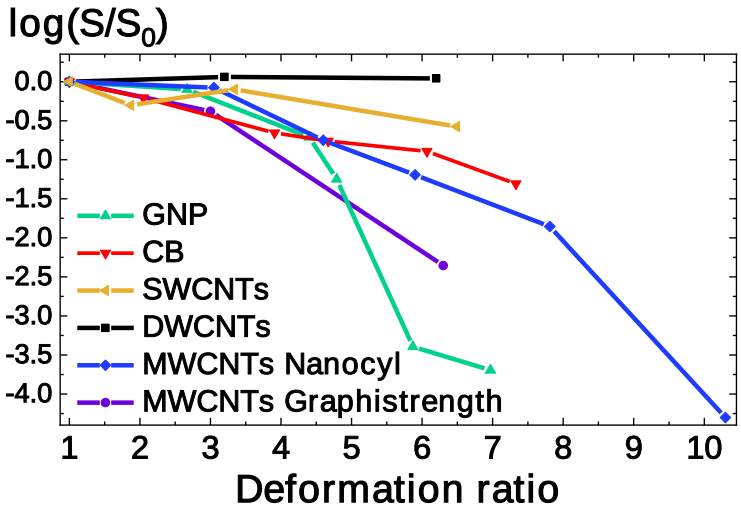


*Fig. 1. Logarithm of the relative conductivity versus the deformation ratio of the UHMWPE-based composite samples filled with: 10 wt.% GNPs, 20 wt.% CB, 1 wt.% SWCNTs, 1 wt.% DWCNTs, 3 wt.% MWCNTs Nanocyl, and 1.5 wt.% MWCNTs Graphistrength.*

The processed oriented composites are also characterized by high EMR shielding properties, as well as interesting temperature dependencies of the electrical conductivity.

The conducted investigation of the influence of solid-state processing parameters allows to formulate a set of recommendations on how to obtain the best distribution of the filler in the composite materials based on nascent disentangled UHMWPE reactor powder. It is demonstrated that by careful consideration of the type of nanoparticles it is possible to obtain a material with relatively high strength and high level of electrophysical characteristics.

**Acknowledgement:** The reported study was funded by RSF according to the research project № 22-13-00359.

**References:**

[1] A. N. Ozerin, E. K. Golubev, S. S. Ivanchev, V. A. Aulov, A. S. Kechek'yan, T. S. Kurkin, E. M. Ivan'kova, N. Y. Adonin, Polym. Sci. Ser. A 64 (2022) 73.
[2] O. V. Lebedev, A. N. Ozerin, A. S. Kechek'yan, V. G. Shevchenko, T. S. Kurkin, E. K. Golubev, E. A. Karpushkin, V. G. Sergeyev, Polym. Compos 40 (2019) E146.

## PP-I-28

# Synthesis of Novel Arylbitetrazole-Based Energetic Materials

Gorbunov Y.K.[1,2], Chaplygin D.A.[1], Fershtat L.L.[1]
*1 – Zelinsky Institute of Organic Chemistry RAS, Moscow, Russia*
*2 – Lomonosov Moscow State University, Chemistry Department, Moscow, Russia*
*yaroslavgor1710@gmail.com*

One of the leading directions in organic chemistry is the synthesis of heterocyclic compounds, study of their reactivity and determination of practically useful properties. Nitrogen-rich systems are of particular interest because of their valuable properties that find application in a number of high-tech industries.

The aim of this work is the synthesis of polynitrogen heterocyclic systems based on formal tandem [3+2] cycloaddition reactions. Aryldiazonium salts **(1)** used as initial substrates undergo [3+2] cycloaddition [1] with diazoacetonitrile **(2)** resulting in a formation of cyanotetrazoles **(3)**, which are introduced into the second [3+2] cycloaddition reaction with sodium azide to form bitetrazoles **(4)** [2].

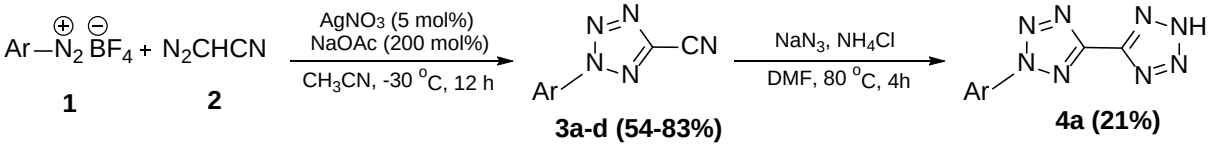


Currently, a set of cyanotetrazoles (**3a-d**) and one target compound (**4a**) bearing p-nitrophenyl moiety were prepared (Fig. 1). Experimental density of the bitetrazole **4a** is 1.58 g $cm^{-3}$.

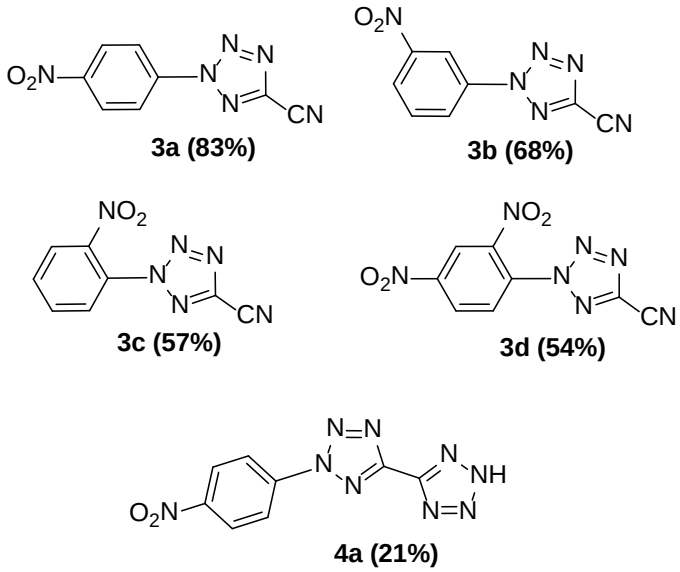


*Fig. 1. Obtained substances*

Attempts to obtain cyanotetrazoles from diamino-1,2,5-oxadiazole and 3-amino-1,2,4-triazole diazonium salts were unsuccessful. In these cases, the preparation of cyanotetrazoles is complicated because of the formation of two cyanotetrazole isomers (Fig. 2) having similar

$R_f$ values, making their separation quite difficult. Optimization of this protocol in regard to heterocyclic-based diazonium salts is currently undertaken in our group.

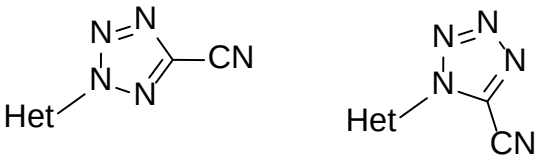


*Fig. 2. Cyano-tetrazole isomers*

**Acknowledgement:** This work was supported by the Russian Science Foundation, grant 21-73-10109.

**References:**

[1] Ming-Yang Xiao, Meng-Meng Zheng, Xing Peng, Xiao-Song Xue, Fa-Guang Zhang, Jun-An Ma. Catalytic direct construction of cyano-tetrazoles, Org. Lett. 2020, 22, 19, 7762–7767.
[2] Haifeng Huang, Prof. Dr. Zhiming Zhou, Lixuan Liang, Jinhong Song, Kai Wang, Dan Cao, Wenwen Sun, Chengming Bian, Dr. Min Xue. Nitrogen-Rich Energetic Monoanionic Salts of 3,4-Bis(1 H-5-tetrazolyl)furoxan, Chem. Asian J. 2012, 7, 707-714.

## PP-I-29

# Synthesis Conditions and Real Structure of $Sr_{n+1}Ti_nO_{3n+1}$ Oxides

Gorkusha A.S.[1,2], Pavlova S.N.[2], Ivanova Y.A.[2], Gerasimov E.Y.[2], Isupova L.A.[2], Tsybulya S.V.[1,2]
*1 – Novosibirsk State University, Novosibirsk, Russia*
*2 – Boreskov Institute of Catalysis, Novosibirsk, Russia*
*Deepforesttt922@gmail.com*

Double perovskite-like oxides of the Ruddlesden-Popper (R-P) series $A_{n+1}B_nO_{3n+1}$ attract attention as materials for various electrochemical devices, as selective oxygen-permeable ceramic membranes and as catalysts for oxidative reactions. For example, these oxides are considered as promising catalysts in the oxidative coupling of methane (OCM). In particular, the catalytic properties of $Sr_2TiO_4$ are superior to perovskite $SrTiO_3$ [1], but strongly depend on the preparation conditions [2], which indicates the importance of studying the real structure of these layered oxides.

In the framework of this work, we synthesized a series of $Sr_{n+1}Ti_nO_{3n+1}$ samples (n = 1–3) obtained from different precursors using the solid-phase synthesis method with the stage of mechanochemical activation in different modes. Single-phase $Sr_2TiO_4$ and $Sr_3Ti_2O_7$ were obtained from $SrCO_3$ and $TiO_2$ at calcination temperatures of 1100°C and higher. The $Sr_4Ti_3O_{10}$ phase could not be obtained under these conditions.

A detailed study of the microstructure of the synthesized oxides using transmission electron microscopy (TEM) and X-ray diffraction showed that these systems often contain planar defects that violate the periodicity in the alternation of layers of the $Sr_{n+1}Ti_nO_{3n+1}$ phases (n = 1–2).

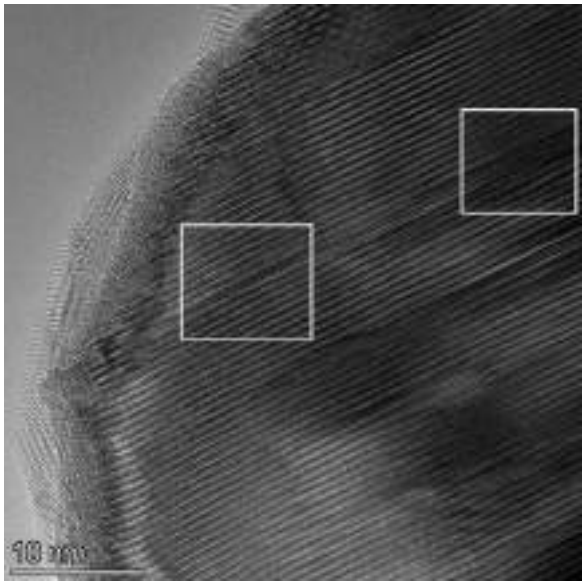

*Fig. 1. TEM image of the real structure of Sr2TiO4.*

The existence of such defects is due to the crystal chemical features of the structural series of $Sr_{n+1}Ti_nO_{3n+1}$ oxides, the members of which are periodic structures consisting of alternating perovskite ($ABO_3$) and rock salt (AO) layers. The sequence of alternation of these

layers is determined for each member of the series, but at the same time, fragments can quite easily appear with a violation of the periodicity of the alternation of these layers, which leads to the formation of structural defects (Fig. 1). Defects of this kind lead to a nonstoichiometry of the crystalline phase in terms of the content of Sr, the “excess” of which is concentrated on the surface in the form of thin layers of SrO and/or $SrCO_3$. Enrichment of the surface with strontium can lead to an increase in the catalytic activity of these systems [3].

We have studied the effect of planar defects on the diffraction patterns of $Sr_2TiO_4$. To simulate diffraction patterns, we used the method of modeling the full profile of diffraction patterns for one-dimensionally disordered structures [4]. Calculations have shown that some reflections are largely shifted with a change in the concentration of defects [5]. Based on this effect, it is possible to estimate the content of planar defects not only in $Sr_2TiO_4$, but also in all other systems with the $A_2BO_4$ structure, since the shift of diffraction maxima does not depend on the chemical composition of the unit cell parameters of a particular object under study.

**Acknowledgement:** Diffraction studies and the development of a method for determining the content of planar defects were carried out with the support of the PRIORITET 2030 program (NSU).

**References:**

[1] W.-M. Yang, Q.-J. Fu, X.-C. Fu, *React. Kin, Mech. and Cat. Lett.* 1995, **54**, 21.
[2] S. Pavlova, Y. Ivanova, S. Tsybulya, S. Chesalov, A. Nartova, E. Suprun, L. Isupova, *Catalysts* 2022, **12**, 929.
[3] D. Ivanov, L. Isupova, E. Gerasimov, L. Dovlitova, T. Glazneva, I. Prosvirin, *Appl. Catal. A Gen.* 2014, **485**, 10.
[4] S. Cherepanova, S. Tsybulya, *Materials Science Forum* 2004, **443**, 87.
[5] A. Gorkusha, S. Tsybulya, S. Cherepanova, E. Gerasimov, S. Pavlova, *Materials* 2022, **15**, 7642.

## PP-I-30

# Correlation between the Activity of Transition Metals Oxides in Ozone Decomposition and $O_3$-Assisted Catalytic Oxidation of n-$C_4H_{10}$

Paramoshin I.V., Bokarev D.A., Kanaev S.A., Stakheev A.Y.
*Zelinsky Institute of Organic Chemistry, Moscow, Russia*
*st@ioc.ac.ru*

Ozone-assisted catalytic oxidation (OZCO) is one of the most promising methods for the neutralization of volatile organic compounds (VOCs). Transition metal oxides deposited on various oxide or zeolite supports are commonly used as catalysts for the OZCO. Their activity in OZCO of VOCs is directly related to their ability to decompose ozone with the formation of highly reactive atomic oxygen O* [1]. Owing to the high oxidative activity of $O_3$, OZCO makes it possible to effectively remove even such low-reactive compounds as alkanes at temperatures of 50–100°C [2]. In this work, we have identified patterns that relate the activity of deposited oxides of transition metals of the 4th period in the ozone decomposition and the reaction of OZCO of n-butane.

Supported oxide catalysts containing 10 wt. % of the metal were prepared by impregnation of γ-$Al_2O_3$ ($S_{BET}$=250 $m^2$/g, UOP). The structure of the catalysts was studied by XRD and $H_2$-TPR. The formation of $V_2O_5$, $Cr_2O_3$, $Mn_2O_3$+$MnO_2$, $Fe_2O_3$, CoO, NiO, CuO, and ZnO was obtained for the corresponding samples.

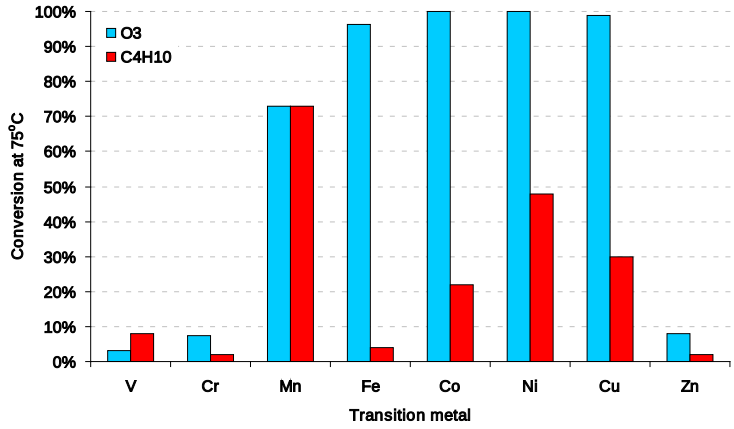


*Fig. 1.Comparison of the activity of transition metals supported on $Al_2O_3$ at 75°C*

The study of the catalyst performances in the OZCO of n-butane (Fig. 1) reveals the nonlinear relationship between the activity in the ozone decomposition and hydrocarbon oxidation.

Since the formation of atomic oxygen O* is a prerequisite for the occurrence of OZCO, the low activity of V, Cr and Zn catalysts in $O_3$ decomposition results in marginal activity in hydrocarbon oxidation at temperatures below 75°C.

On the other hand, the high activity of the Fe, Co, Ni, Cu catalysts favors the OZCO reaction even at temperatures below 50°C. However, the high rate of O* formation is accompanied by its recombination, which competes with OZCO. As a result, the concentration of $O_3$ in the reaction mixture decreases and retards the OZCO process. The optimal activity of $Mn/Al_2O_3$ catalyst in ozone decomposition leads to high efficiency in the OZCO reaction, and the catalyst exhibited the best catalytic performance.

**Acknowledgement:** This work was supported by the Russian Science Foundation (grant no. 23-13-00214).

**References:**

[1] F. Lin, Z. Wang, Z. Zhang, Y. He, Y. Zhu, J. Shao, D. Yuan, G. Chen, K. Cen, Chem. Eng. J., 382 (2020) 123030

[2] A.I. Mytareva, I.S. Mashkovsky, S.A. Kanaev, D.A. Bokarev, G.N. Baeva, A.V. Kazakov , A.Y. Stakheev, Catalysts 11 (2021) 506

## PP-I-31

# Selective Separation of Chlorobenzenes by Halogen Bonding in MOF Deposited on Upcycled PET

Gulyaev R.O., Guselnikova O.A., Postnikov P.S.
*Research School of Chemistry and Applied Biomedical Sciences, Tomsk Polytechnic University, Tomsk, Russia*
*guliaev.g2016@yandex.ru*

Intermolecular interactions play a major role in all processes wherein molecular recognition and self-assembly occur. The halogen bond (HaB) is the attractive interaction wherein a halogen atom acts as the electrophilic site [1]. One of the possible solution to enhance the use of HaB for separation is the hybridization of halogen bonded systems with metal organic frameworks (MOFs) [2]. We thus selected these materials as scaffolds for the adsorption and selective separation of chlorobenzene derivatives (CBs), the pollutants targeted in this study. Here report that iodine functionalized zirconium frameworks (UiO-66-I), prepared by using 2-iodoterephtalic acid (I-TA) as metal ions spacer, have improved sorption performances of CBs than the parent UiO-66 frameworks thanks to the presence on the cavities walls of iodine atoms acting as HaB donor sites. Experimental and theoretical confirmation of the HaB formation between UiO-66-I and CBs was obtained by Raman and X-ray photoelectron spectroscopies as well as by DFT calculations. We found that a 50% presence of I-TA in the UiO-66-I structure optimally balances MOF porosity and HaB donor site ubiquity and leads to unprecedented selectivity in CBs adsorption over non-chlorinated aromatic contaminants. To enhance the added value of the developed materials, waste PET was employed as support for the surface-assisted growth of the frameworks and also as feedstock of the terephtalic acids employed for their construction. The scheme for obtaining the PET@UiO-66-I material and the formation of a halogen bond with chlorobenzene are shown in Figure-1.

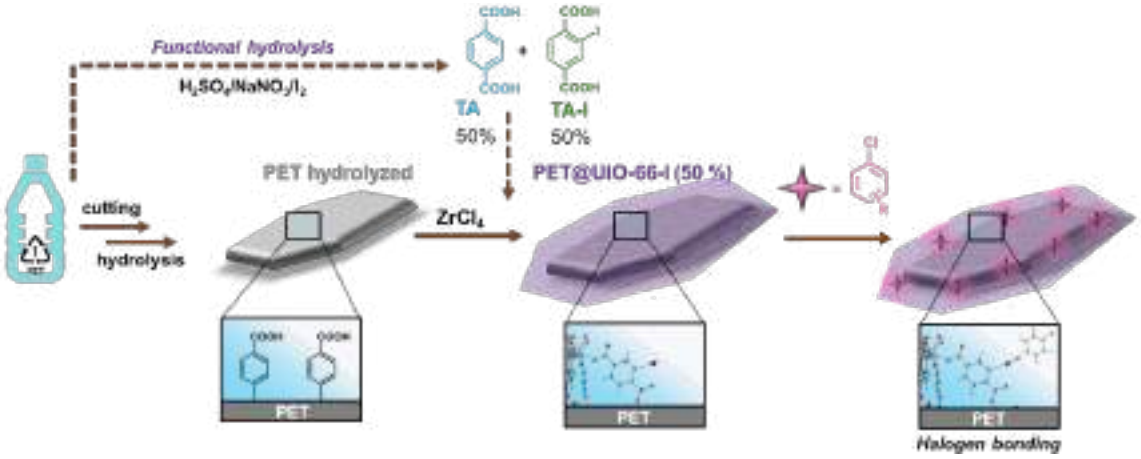


*Fig.5. Preparation of PET@UiO-66-I (50%) from waste PET for the adsorption of CBs.*

n summary, we demonstrated that introduction of halogen bonding (HaB) recognition unit into the structure of MOFs enable to construct functional material for selective separation

and removal of chlorinated benzenes (CBs) contaminants. Firstly, we prepared and characterized a series of UiO-66 with the ranging content of 2-iodoterephtalic acid (I-TA) 0, 33, 50, 67 and 100%. A structure– performance relationship screening demonstrated that the highest adsorption capacity is achieved at 50 % I-TA (UiO-66-I (50%)) by the balancing the number of HaB recognition elements, surface area, and missing ligand defects. The formation of halogen bonding between UiO-66-I (50%) and CB was firstly theoretically shown by DFT calculations and later experimentally verified by UV-Vis, Raman and X-ray spectroscopy.

The HaB has been occasionally used to assemble supramolecular organic frameworks by exploiting the established tendency of nitrogen-based HaB acceptors with iodobenzene derivatives [3] or by resorting to the simultaneous action of HaB and hydrogen bonding (HB). It has also been used to enable and/or increase the functional properties of MOFs. Despite the diversity of previously reported structures, their application for the separation/removal of environmental contaminants is limited.

Here we challenged this limitation by improving the technological appealingness of UiO-66-I (50%) containing HaB element and decreasing the material cost. In the framework of suggested experimental strategy, waste PET was recycled to be a base for surface-assisted growth of UiO-66-I (50%) using released TA/I-TA mixture obtained by Tronov-Novikov method. The prepared PET@UiO-66-I (50%) showed high adsorption capacity for CB described by pseudo-second-order model confirming that the adsorption capacity was related to the number of available HaB sites due to the chemical nature of adsorption. The high adsorption capacity was accompanied by unprecedent selectivity in the separation of CB from non-chlorinated aromatic compounds due to the formation of I···Cl HaB between I in the structure of MOF and CBs. Besides from high separation efficacy, the prepared PET@UiO-66-I (50%) can be recycled for the multiple usage no less than 5 times. The results obtained here suggest that high surface area Zr-MOFs operating in aqueous media and containing HaB donor, or acceptor, sites may be particularly promising for the sequestration of contaminants containing HaB acceptor, or donor, sites, respectively. Moving forward, we anticipate that this work will lay the foundation for the use of halogen bonding for the preparation of functional materials for separation of contaminants.

**Acknowledgement:** Support from the Ministry of Science and Higher Education of the Russian Federation in the framework of the “Mega-grant” project (No. 075-15-2021-585s) and GACR (GACR No. 22-02022S)

**References:**

[1] Legon A. C, Phys. Chem. Chem. Phys. 28 (2010) 7736-7747.
[2] Cavallo, G, Metrangolo, P, Milani, R, Pilati, T, Priimagi, A, Resnati, G, Terraneo, G. Chem. Rev. 116 (2016) 2478-2601.
[3] Olshtrem, A.; Chertopalov, S.; Guselnikova, O.; Valiev, R. R.; Cieslar, M.; Miliutina, E.; Elashnikov, R.; Fitl, P.; Postnikov, P.; Lancok, J.; Svorcik, V.; Lyutakov, O. 2d Mater. 8 (2021) 4.

## PP-I-32

# Plasmon-Enhanced Luminescence of S,N-Doped Carbon Dots

Ibrayev N., Seliverstova E., Amanzholova G.
*Institute of Molecular Nanophotonics, Buketov Karaganda University, Karaganda, Kazakhstan*
*niazibrayev@mail.ru*

Carbon materials have become quite popular in the last decade. It is known that in order to obtain the luminescence of such materials, it is necessary to maintain a clear modulation between their size and surface chemical groups. At present, a large number of carbon-containing nanomaterials with luminescence have been synthesized, among which carbon dots (CDs) can be distinguished. CDs have chemical resistance and photostability, high luminescence efficiency, good biocompatibility and low toxicity. This determines their use in bioimaging, in the creation of protective coatings, LEDs, in solar and photocatalytic cells, sensors [1].

In the present work, the effect of plasmonic nanoparticles (NPs) of Ag on the properties of fast and long-lived luminescence of CDs films with various compositions was studied, which was varied by changing the ratio of citric acid and L-cysteine.

The synthesis of CDs was performed by microwave synthesis method. The molar ratio of citric acid:L-cysteine was equal to 1:0, 1:0.5 and 1:1.

To study the effect of plasmon resonance of silver NPs, CDs solutions were deposited over a top of silver island films (SIF) on quartz substrates. To do this, 5 nm of silver was deposited on solid substrates by magnetron sputtering. Then the films were annealed at 240 °C for 30 minutes. According to the scanning-electron microscopy (SEM) data, silver particles of spherical shape with radius of 50–80 nm were formed in the film after annealing.

Measurements showed that the absorption spectrum (Cary 300, Agilent) of CDs without heteroatoms in the structure (ratio 1:0) exhibits as decreasing curve in the UV range without pronounced maxima. The absorption spectrum of doped CDs a band with a maximum at 360 nm, as well as a shoulder of about 240-250 nm was observed. Synthesized CDs exhibit a fluorescence band (Eclipse, Agilent) in the region of 400-600 nm with a maximum at ~440 nm. Films based on CDs 1:0 have low-intensity fluorescence, the maximum intensity was recorded for CDs 1:0.5 films. In the spectra of long-lived luminescence, a band of luminescence with a maximum at ~560 nm was observed. Gaussian decomposition of the spectra, as well as temperature measurements, showed that the spectrum of long-lived luminescence of synthesized CDs consists of a band of thermally activated delayed fluorescence with a maximum at 440 nm, and phosphorescence with a maximum at 560 nm.

In the presence of SIF, an increase in the intensity of both fast fluorescence and phosphorescence of CDs films was observed (Fig. 2). The greatest increase in the intensity of fluorescence was recorded for the undoped CDs 1:0: if, in the absence of SIF, the fluorescence signal manifests itself at the noise level, then in the presence of plasmonic NPs, it was increased by 32 – 35 times. The lifetime of fluorescence was practically unchanged.

For S,N-doped CDs, the increase in the intensity of fluorescence is equal to 1.3 – 1.6 times, and the reduction in the fluorescence lifetime was 14% and 28% for 1:0.5 and 1:1 CDs, which is associated with an increase in the radiation decay rate of CDs in the near field of silver NPs [2], [3].

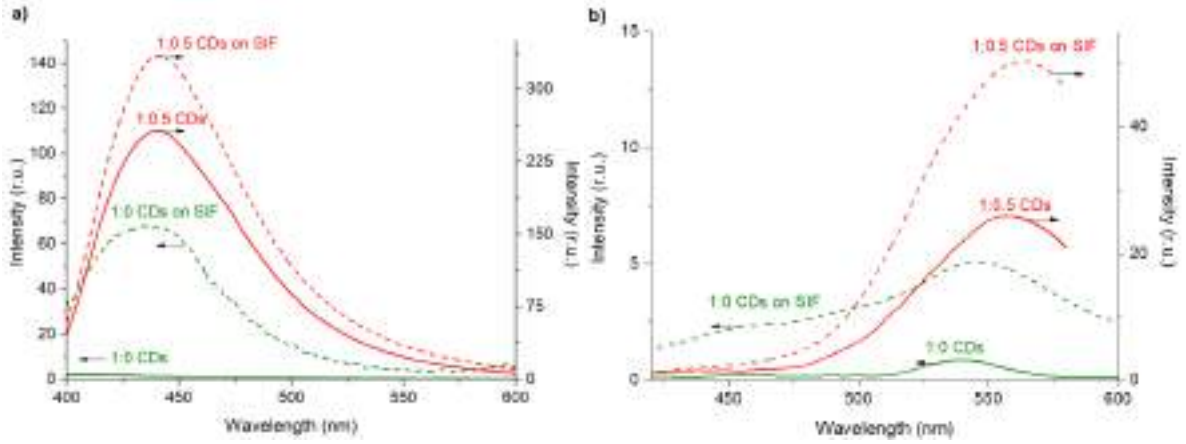


*Fig. 1. Spectra of fluorescence (a) and long-lived luminescence (b) of CDs films with various CA:L-cysteine ratios on the glass and on the SIF surfaces, $\lambda_{exc}$=350 nm*

The phosphorescence of S,N-doped CDs in the presence of plasmonic NPs increases more than the fluorescence (Fig. 1b). As in the case of fluorescence, the highest growth in phosphorescence intensity was registered for 1:0 CDs. The lifetime of long-lived luminescence decreases slightly in this case. The most noticeable changes of luminescence lifetimes were registered for 1:1 CDs. This indicates an increase in the rate of radiative decay $T_1 \rightarrow S_0$ of CDs in the presence of Ag NPs.

**Acknowledgement:** This research is funded by the Science Committee of the Ministry of Education and Science of the Republic of Kazakhstan, grant no. AP09259913.

**References:**

[1] S.H. Song, M.H. Jang, J. Chung, S.H. Jin, B.H. Kim, S.H. Hur, S. Yoo, Y. Cho, S. Jeon, Adv. Opt. Mater. 11 (2014) 1016-1023.
[2] P. Anger, P. Bharadwaj, L. Novotny, Phys. Rev. Lett. 96 (2006) 113002.
[3] E. Seliverstova, N. Ibrayev, G. Omarova, A. Ishchenko, M. Kucherenko, J. Lumin. 235 (2021) 118000.

## PP-I-33

# Acetylene Hydrogenation over Pd/MgO Nanocrystalline system: Effect of the Synthesis Route on Catalytic Performance

Ilyina E.V.[1], Yurpalova D.V.[2], Shlyapin D.A.[2], Veselov G.B.[1],
Shivtsov D.M.[1], Stoyanovskii V.O.[1], Vedyagin A.A.[1]
*1 – Boreskov Institute of Catalysis, Novosibirsk, Russia*
*2 – Center of New Chemical Technologies BIC, Omsk, Russia*
*evi@catalysis.ru*

Ethylene is the most versatile petrochemical feedstock for the production of polyethylene, ethanol, ethylene oxide, ethylene glycol, styrene, dichloroethane, and many other chemical products. The process of hydrogenation of acetylene into ethylene can be used both to purify ethylene from an impurity of alkyne, which is formed at the stage of pyrolysis of crude oil while getting $C_2H_4$ [1], and for direct ethylene production from acetylene [2]. Most often, palladium-based metal systems are used as catalysts for the acetylene hydrogenation reaction due to their high catalytic activity. The efficiency of such catalysts is determined primarily by the dispersity and the electronic state of palladium, which depend on the strength of its interaction with the support and the acid-basic properties of the latter [3, 4].

Previously, we have showed the possibility of applying the sol-gel method including an aerogel approach to synthesize various nanocrystalline systems. Such materials possess both high specific surface area and uniform distribution of the active component, which is important for achieving appropriate performance in catalysis [5, 6]. In this work, a series of Pd/MgO catalysts was synthesized. The samples were identical in palladium content (1 wt.%) but different in the preparation method. Thus, an aerogel method, a sol-gel (SG) method, and an incipient wetness impregnation (IWI) method were used. The preparation procedures were followed by reduction in hydrogen at 500 °C for 3 h. Catalytic tests in the acetylene hydrogenation reaction were performed in a flow regime, in a stream of a gas mixture containing 4 vol.% $C_2H_2$ in hydrogen within the temperature range from 20 to 90 °C.

Using transmission electron microscopy (TEM), it was shown that the palladium particles have a spherical shape and are uniformly distributed over the support. The average size of palladium particles depends on the synthesis method: the most dispersed particles ($D_{av}$ = 2.0 – 2.2 nm) are formed in the case of sol-gel and impregnation methods. The aerogel-prepared samples contain palladium particles of ~ 8.0 nm in size. At the same time, the aerogel-prepared catalysts showed the highest activity: a 50% degree of acetylene conversion was observed already at 35 °C, while in the cases of SG- and IWI-prepared samples, such conversion values were achieved at noticeably higher temperatures of 49 and 65 °C, respectively. It was found that the maximum selectivity toward ethylene at 25 °C of about 60 – 70% is also characteristic of the aerogel-prepared sample (Fig. 1).

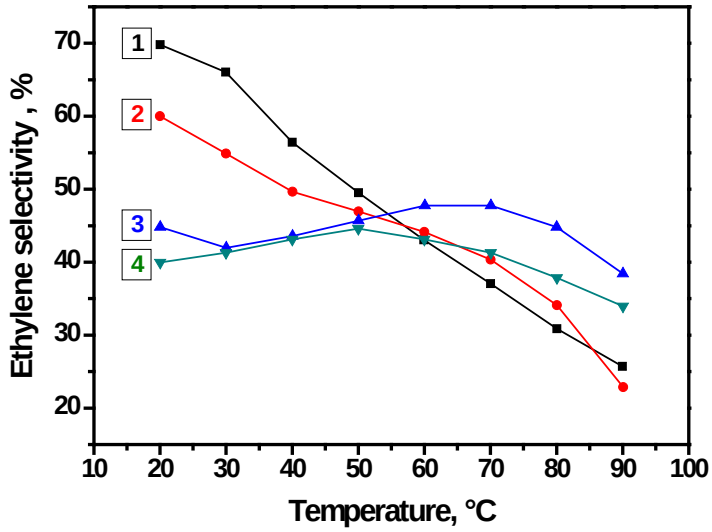


*Fig. 1. Ethylene selectivity in the acetylene hydrogenation reaction over 1% Pd/MgO prepared by different methods: 1 - Aerogel method with $[Pd(NH_3)_4](NO_3)_2$; 2 - Aerogel method using $Pd(NO_3)_2$; 3 - Sol-gel method with $[Pd(NH_3)_4](NO_3)_2$; 4 – Incipient wetness impregnation of aerogel-prepared MgO with $[Pd(NH_3)_4](NO_3)_2$*

As seen, the selectivity toward ethylene for the aerogel-prepared sample decreases by ~ 15% at temperatures above 60 °C, which is apparently caused by the diffusion limitations. Such behavior can be explained by the features of porous structure. Another reason is uniform distribution of the active component over the bulk of the catalyst's granules when just a part of palladium particles is located on the outer surface.

Thus, the aerogel-prepared Pd/MgO catalyst shows high activity in the acetylene hydrogenation reaction and appropriate selectivity toward ethylene at low temperatures.

**Acknowledgement:** This work was supported by the Ministry of Science and Higher Education of the Russian Federation within the governmental order for Boreskov Institute of Catalysis (projects AAAA-A21-121011390054-1 and AAAA-A21-121011390011-4).

**References:**

[1] A. Borodziński, G. Bond, Catal. Rev. Sci. Eng. 48 (2006) 91-144.
[2] D.A. Shlyapin, D.V. Glyzdova, T.N. Afonasenko, V.L. Temerev, P.G. Tsyrul'nikov, Kinet. Catal. 60 (2019) 446-452.
[3] Z. Guan, M. Xue, Z. Li, R. Zhang, B. Wang, Appl. Surf. Sci. 503 (2020) 144142.
[4] Y. He, J. Fan, J. Feng, C. Luo, P. Yang, D. Li, J. Catal. 331 (2015) 118-127.
[5] A.A. Vedyagin, I.V. Mishakov, T.M. Karnaukhov, E.F. Krivoshapkina, E.V. Ilyina, T.A. Maksimova, S.V. Cherepanova, P.V. Krivoshapkin, J. Sol-gel Sci. Technol. 82 (2017) 611-619.
[6] E.V. Ilyina, I.V. Mishakov, A.A. Vedyagin, S.V. Cherepanova, A.N. Nadeev, A.F. Bedilo, K.J. Klabunde, Microporous Mesoporous Mater. 160 (2012) 32-40.

## PP-I-34

# Influence of Preparation Conditions on Activity of Bulk $Co_3O_4$ - Based Catalysts in the $N_2O$ Decomposition

Ivanova Y.A., Isupova L.A.
*Boreskov Institute of Catalysis, Novosibirsk, Russia*
*ivanova@catalysis.ru*

The production of nitric acid is one of the main sources of $NO_X$ and $N_2O$ emissions in the chemical industry. In Russia, in the production of nitric acid, processes of selective catalytic reduction (SCR) of $NO_X$ with ammonia (UKL-7 and AK-72M units) or non-selective reduction with hydrocarbons (AK-72 unit) are used to reduce NOX emissions [1]. In the processes of SCR, $N_2O$ is not removed from the tail gases. It has been established that the $N_2O$ emission per year from one UKL-7 unit is more than 450 tons. Nitrous oxide has a greenhouse effect, which is 310 times higher than that of $CO_2$, and its emissions should also be reduced. The combination of two de-NOX and de-N2O processes in one reactor is very attractive. To date, there are two EnviNOx® technologies from Uhde for the combined removal of $N_2O$ and $NO_X$ from tail gases on a zeolite catalyst [2], both technologies require additional energy consumption for tail gas heating up to 300–600°C. A single-reactor scheme for the abatement of $NO_X$ and $N_2O$ under the conditions of a SCR reactor in Russia at 220-280 °C can be economically advantageous. For such a scheme, it is preferable to use a low-temperature $N_2O$ decomposition catalyst as a second layer catalyst with the geometry of a honeycomb block or cylindrical granules. The catalyst must have necessary activity, mechanical strength, uniformity and must not create hydraulic resistance.

Oxide systems based on cobalt spinel, composition 2 wt.% $Cs/Co_3O_4$, in the form of fractions (0.5–0.25 mm), obtained by precipitation or deposited on a corundum support [3], are capable of effectively decomposing $N_2O$. Massive oxide systems based on cobalt spinel are more active than supported catalysts.

The aim of this work is to study the possibility of making granular and block catalysts based on $Co_3O_4$ for use in a SCR reactor as second-stage catalysts for low-temperature decomposition of nitrous oxide.

From pastes with different water content and organic additives, geometrically structured massive catalysts were obtained by extrusion molding in the form of cylindrical granules (size $4 \times 4$ mm) and a honeycomb block (with a channel parameter: width 2.5 mm, wall thickness 0.5 mm , channel density 22 pcs/ $cm^2$) (fig.1). The rheology of the paste for making the block had to be greatly modified with the addition of molasses. The activity of the sample varied depending on organic additives affecting the rheological properties of pastes and the catalyst geometric form.

The fraction had a high activity, for granules obtained the activity is lower. The reason for the lower activity for simple granules is the incomplete utilization of the granule (it can be improved by optimizing the pore structure). The low activity of the block sample is due to the

problem of obtaining a paste of the required rheology for molding, which led to the loss of the porous structure and a decrease in the specific surface area of the catalyst.

The paper shows the fundamental possibility of using massive cobalt spinel modified with cesium as a second layer catalyst, both in the form of cylindrical granules and in the form of blocks of a honeycomb structure. The technique for preparing blocks of a honeycomb structure requires additional refinement.

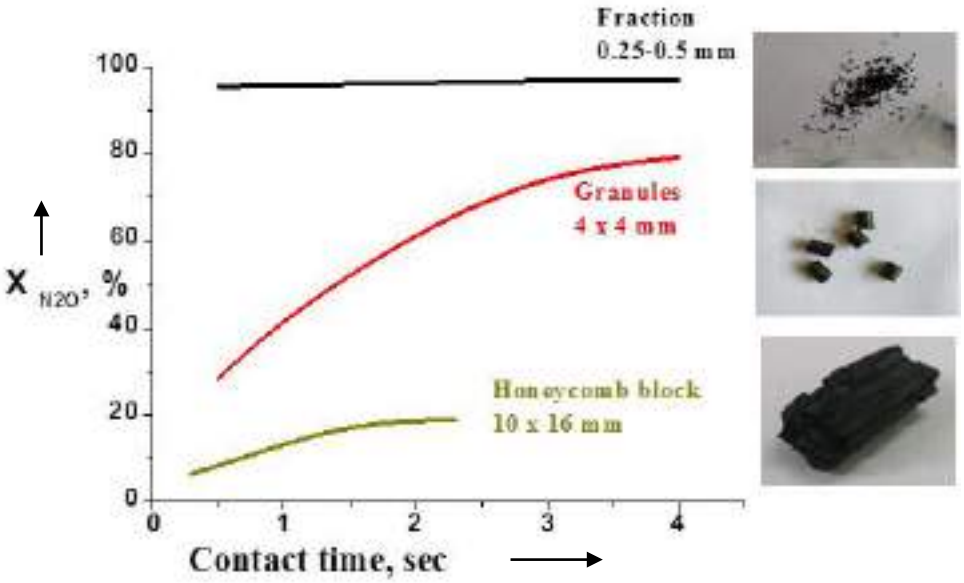


*Fig. 1. Catalytic activity of catalysts based on Co-spinel in the reaction of N2O decomposition (in a mixture of 0.15%$N_2O$+3.6%$O_2$+3%$H_2O$ in He), obtained by extrusion molding of granules, blocks and fraction.*

**Acknowledgement:** This research was funded by the Ministry of Science and Higher Education of the Russian Federation within the governmental order for the Boreskov Institute of Catalysis (projects AAAA-A21-121011490008-3)

**References:**

[1] V.A. Chumachenko, L.A. Isupova, Y.A. Ivanova, E.V. Ovchinnikova, S.I. Reshetnikov, A.S. Noskov, Chem. Sustain. Dev. 28 (2020) 203–212. https://doi.org/10.15372/CSD2020221
[2] M.C.E., Groves, A. Sasonow, J. of Integrative Environmental Sciences 7(S1) (2010) 211-222, https://doi.org/10.1080/19438151003621334
[3] L.A. Isupova, Y.A. Ivanova, Russian Journal of Physical Chemistry 95(3) (2021) 503-511, https://doi.org/10.1134/S0023158419060041

## PP-I-35

# Composite Materials Based on Ni-Cu-PVA Systems as Catalysts for Production of Natural Gas Synthetic Analog

Ivantsov M.I.[1], Bulgakov N.S.[1,2], Sotnikova A.E.[1,3], Krysanova K.O.[1], Kulikova M.V.[1]

*1 – A.V. Topchiev Institute of Petrochemical Synthesis, RAS, Moscow, Russia*

*2 – Mendeleev University of Chemical Technology, Moscow, Russia*

*3 - National University of Oil and Gas «Gubkin University», Moscow, Russia*

*ivantsov@ips.ac.ru*

The increased interest in composite materials is due to their unique properties, since they can not only combine the properties of their constituent parts, exhibiting additivity, but also exhibit synergistic effects. One of the possible applications of composite materials is catalysis, and composites unique characteristics increase the activity and efficiency of catalysts. This is especially true for combating climate change caused by industrial emissions, in particular emissions of carbon oxides, which can be chemically processed into valuable chemical products, including a synthetic analogue of natural gas.

The composite catalyst was prepared by the matrix isolation method, which makes it possible to stabilize the active particles with a polymer or carbon-containing matrix. The formation of the composite was carried out according to a three-stage method. The synthesis temperature was 500°C, since the material obtained under such temperature effects showed the highest activity in the process of hydrogenation of carbon monoxide [1]. The nickel as main metal and copper as an additional component, which acts as an energy promoter, was introduced into the composite system. The main reason of this work is to study the influence of the promoting additive (copper) on the main catalytic and physicochemical properties of the composite material in process of carbon oxides hydrogenation.

IR-Fourier spectroscopy has shown that the introduction of copper promoting amounts does not have a significant effect on the emerging carbon matrix structure. In all cases after heat treatment the formation of polyconjugated structures based on a polymer chain is observed. Whereas by Raman spectroscopy it was established that the obtained materials are characterized by D and G absorption bands, which indicates the formation of a carbon material. And with addition copper to the composite the D/G ratio decreases, which indicates an increase in material graphitization. The formed layered structures has high specific surface area – 214-246 $m^2/g$.

It has been established by XRD that in the process of synthesis a composite material, nickel is reduced to a metallic state, and the absence of reflections of individual phases of copper indicates that copper dissolves in nickel. The TEM method has shown that during the synthesis of the composite material, nanoparticles of the order of 2–6 nm are formed. While the addition of copper leads to the formation of larger nanoparticles with the size of 4–9 nm. It has been established by XPS that, along with oxidized nickel, metallic nickel, which is formed

during the synthesis of the composite, is also present on the surface of the material. The particles are partially coated with carbon material.

Composite materials have shown high activity in the process of carbon monoxide hydrogenation. The nickel phase active in hydrogenation and the protective layer of carbon material formed during the synthesis allows catalytic tests to be carried out without the pre-activation stage, which is used for classical nickel-containing systems based on oxide supports. The composites were tested in an undiluted synthesis gas medium (CO/H2=1/3) at atmospheric pressure and a space velocity of 5000 $h^{-1}$. It has been established that the introduction of 0.1 to 3 wt. % copper in the structure of the catalytic system allows to intensify the methane formation reaction (Kco increases from 29% to 100%, and the maximum conversion temperature is reduced by 60°C). The maximum yield of methane (117 $g/m^3$) was achieved in the presence of a sample with a copper content of 3 wt. %, and exceeds the results obtained in the presence of the unpromoted composite by 4.2 times.

Thus, it has been shown that, on the one hand, the matrix isolation method can effectively introduce promoting components into the composition of the composite material, which contribute to the target process, carbon monoxide hydrogenation. And, on the other hand, the resulting composites exhibit high catalytic activity without the preliminary activation stage.

**Acknowledgement:** This work was carried out within the State Program of TIPS RAS and performed using the equipment of the Shared Research Center “Analytical center of deep oil processing and petrochemistry of TIPS RAS”.

**References:**

[1] Popandopulo, M.V., Ivantsov, M.I., Kulikova, M.V., Zhagfarov, F.G., Chem. Technol. Fuels Oils. J. Catal. 58 (2022) 13.

## PP-I-36

# Features of C12A7 Formation from Amorphous Precursor Obtained by Laser Evaporation

Kapishnikov A.V.[1,2], Mironova M.I.[2], Snytnikov V.N.[1], Geydt P.V.[2], Volodin A.M.[1]
*1 – Boreskov Institute of Catalysis, Novosibirsk, Russia*
*2 – Novosibirsk State University, Novosibirsk, Russia*
*a.kapishnikov@g.nsu.ru*

Calcium aluminate $Ca_{12}Al_{14}O_{33}$ ($12CaO \bullet 7Al_2O_3$ or C12A7) referred as mayenite is the one of the mostly studying inorganic compounds in recent years. The unit cell of this complex oxide consists of the cation framework and anion sublattice containing $4X^-$ or $2X^{2-}$ anions: 1 unit cell = $[Ca_{24}Al_{28}O_{64}]^{4+} \bullet 4X^-$, $X^- = OH^-, Cl^-, F^-$ and etc.. The unique physicochemical properties of C12A7 were discovered and described in details by Hosono's group for last 20 years [1,2]. It was shown that the anion sublattice of C12A7 can contain different anions ($H^-$, $O^{2-}$ and etc.), radicals ($O_2^-$ or $O^-$) and, especially, electrons ($e^-$). In the last case the material can be classified as inorganic electride. The mayenite electride (C12A7:$e^-$) has high electron mobility, low work function (2.9 eV) and resistive switching properties [1,3,4]. Due to these, the C12A7 is of special interest for micro- and nanoelectronic applications, so it is necessary to develop different techniques of fabricating C12A7 thin films for material usage in these fields. Depositing mayenite thin films by different methods often results to the formation of amorphous coatings (a-C12A7) requiring additional heating treatment for crystallization [2] and this is why the knowledge about phase transformations at the heating is important. In this study the amorphous powder material a-C12A7 has been obtained at different conditions by laser evaporation of C12A7 target. After that, the investigation of phase transformations by in situ XRD has been performed at different gas media.

The initial bulk sample of C12A7 was evaporated by $CO_2$-laser irradiation ($\lambda$ = 10.6 μm) into amorphous substance. The procedure was performed at different pressure (3.4 and 91.2 kPa) in chamber. According to SEM data, it results to the different size of the nanoparticles obtained, the smaller size being observed at lower pressure. The a-C12A7 samples, as it is shown by EDX mapping, are partially inhomogeneous, and they have the local regions with different Ca/Al ratio, that may be related to presence of different oxide phases (CaO, $Al_2O_3$, $Ca_{12}Al_{14}O_{33}$ and etc.). The in situ XRD study of recrystallization process of the amorphous mayenite has shown that the process occurs through the crystallization (400-600°C) and decomposition (700°C) of the $CaCO_3$ phase (R-3c space group) which might form in amorphous samples before treatment. The subsequent heating (800-900°C) results to the formation of the well-crystallized mayenite, with some impurities of CaO and amorphous $\gamma$-$Al_2O_3$ phases remaining in the material composition. It can be possible due to keeping constant the total Ca/Al stoichiometry in the samples through the laser evaporation process.

In conclusion, the in situ XRD study has shown the recrystallization of C12A7 from inhomogeneous amorphous substance obtained by laser evaporation. This process may be

performed at acceptable temperature (800-900°C) to avoid undesirable chemical reactions with different substrates during crystallization of a-C12A7 thin films. At the same time, the formation and segregation of impurities detected may promote the film cracking and delamination. The features of a-C12A7 recrystallization process should be accounted developing the fabrication process of C12A7 thin films by different techniques, such as pulsed laser deposition (PLD).

**Acknowledgement:** This research was funded by the Ministry of Education and Science of the Russian Federation, grant No. FSUS-2020-0029.

**References:**

[1] Y. Adachi, S.W. Kim, T. Kamiya, H. Hosono, Mater. Sci. Eng., B 161 (2009) 76.
[2] Y. Toda, M. Miyakawa, K. Hayashi, T. Kamiya, M. Hirano, H. Hosono, Thin Solid Films. 445 (2003) 309.
[3] A. Rybak, I. Yushkov, N. Nikolaev, A. Kapishnikov, A. Volodin, G. Krivyakin, G. Kamaev, P. Geydt, Electronics. 11 (2022) 668.
[4] I. Yushkov, G. Kamaev, V. Volodin, P. Geydt, A. Kapishnikov, A. Volodin, Micromachines. 13 (2022) 1917.

## PP-I-37

# Structural Analysis of $Ru/Ce_{1-x}Zr_xO_2$ Catalysts for the Carbon Dioxide Methanation

Kharchenko N.A.[1,2], Pakharukova V.P.[1,2], Gorlova A.M.[1,2], Stonkus O.A.[1], Saraev A.A.[1], Rogozhnikov V.N.[1], Potemkin D.I.[1]

*1 – Boreskov Institute of Catalysis, Novosibirsk, Russia*

*2 – Novosibirsk State University, Novosibirsk, Russia*

*n.kharchenko@g.nsu.ru*

Scientific studies aimed at reducing the impact of human activities on the environment are of great interest. Reduction of the amount of carbon dioxide emissions into the atmosphere is one of the challenges. The catalytic process of carbon dioxide methanation is of practical importance due to its using for $CO_2$ utilization with simultaneous synthesis of energy carrier, methane.

Ruthenium-based catalysts are known to be highly active in methanation processes at relatively low temperatures (200-250°C) and low loading of an active component (~1-5 wt.% %) [1-3]. It has been reported that the most effective catalysts are based on easily reduced oxide supports, for example, cerium dioxide $Ru/CeO_2$ and mixed cerium-zirconium oxides $Ru/Ce_{1-x}Zr_xO_2$. Despite a large number of studies dealing with the activity of such catalysts, there is little information about their structural organization and structure of ruthenium-containing particles. Complexity of the structural analysis of supported particles lies in their high dispersion. Expanding the understanding the structures of $Ru/CeO_2$, $Ru/Ce_{1-x}Zr_xO_2$ is necessary to establish the relationships between the structural features of catalysts and their catalytic properties. Structural study on such systems requires the use of methods that allow to solve structure at the atomic level and to identify ultra dispersed species. Thus, authors of the study [4] determined the state and local structure of highly dispersed ruthenium compounds in the $Ru/CeO_2$ catalyst by EXAFS (Extended X-ray Absorption Fine Structure) spectroscopy method. Another effective method is the X-ray atomic pair distribution function analysis (PDF analysis). It also allows us to probe the near atomic order.

In this report, the results of structural studies of the supported $Ru/Ce_{1-x}Zr_xO_2$ heterogeneous catalysts will be highlighted. A wide range of structural methods was used: powder X-ray diffraction (XRD) methods, high resolution transmission electron microscopy (HRTEM) and PDF analysis. Some attention will be paid to the study on structural evolution of catalyst upon its activation via reduction with use of *in-situ* XRD and pseudo in situ X-ray photoelectron spectroscopy (XPS).

**Acknowledgement:** This work was supported by the Russian Science Foundation, grant 21–73–20075.

**References:**

[1] Kim A. et al. Mesoporous TiO2 support materials for Ru-based CO2 methanation catalysts //ACS Applied Nano Materials. – 2019. – Т. 2. – №. 5. – С. 3220–3230.

[2] López-Rodríguez S. et al. Effect of Ru loading on Ru/CeO2 catalysts for CO2 methanation //Molecular Catalysis. – 2021. – Т. 515. – С. 111911.
[3] Rynkowski J. M. et al. Characterization of Ru/CeO2-Al2O3 catalysts and their performance in CO2 methanation //Reaction Kinetics and Catalysis Letters. – 2000. – Т. 71. – С. 55-64.
[4] Nakaji Y. et al. Mechanism of formation of highly dispersed metallic ruthenium particles on ceria support by heating and reduction //The Journal of Physical Chemistry C. – 2019. – Т. 123. – №. 34. – С. 20817–20828.

## PP-I-38

# $NH_2$-Modified UiO-66 as Support for Bimetallic PdCu and PdAu Catalysts for 5-Hydroxymethylfurfural Reduction

Timofeev K.L., Morilov D.P., Kharlamova T.S.
*Tomsk State University, Tomsk, Russia*
*kharlamova83@gmail.com*

The development of new functional materials based on metal-organic frameworks (MOFs) for adsorption and catalytic applications is one of the promising trends of modern materials science. The Zr-based MOFs, specifically UiO-66, have attracted an increasing attention due to their unprecedented stability [1]. Modification of the UiO-66 by introducing various functional groups and/or metal centers into its structure ensures additional functionality of the resulting new materials [1]. In particular, the modification of MOFs with $NH_2$ groups makes it possible to change its acid-base properties as well as stabilize metal particles or lay the ground for further modifications [1,2]. However, for tailor-made design of the UiO-66-based bimetallic catalyst, the structural peculiarities and functional properties of the modified UiO-66 and the regularities of the formation of metal particles in the porous space of the MOFs should be well understood.

The present work is devoted to the systematic study of the structural peculiarities, and functional properties of $NH_2$-modified UiO-66 considered supports for PdCu and PdAu catalysts for the conversion of biomass-derived 5-hydroxymethylfurfural (HMF) into valuable products [3,4]. Samples were prepared by solvothermal method. The crystal and pore structures of the materials obtained were confirmed by the X-ray diffraction, IR spectroscopy, low-temperature nitrogen adsorption, and water vapor adsorption. The optical properties of the samples were studied by the UV-visible spectroscopy, and their electrokinetic properties were studied by the electrophoretic light scattering (ELS). Basic properties were investigated by HCl and $CH_3COOH$ adsorption from water solutions. Additionally, the interaction of metal precursors ($Cu(NO_3)_2$, $CuCl_2$, $Pd(NO_3)_2$, $H_2PdCl_4$, $HAuCl_4$) with the MOFs was also considered to reveal the regularities of the formation of metal particles in the porous space of the MOFs.

The effect of $NH_2$-modification on the structural and functional properties of UiO-66 as well as on the composition and dispersion of the metal particles formed in bimetallic PdCu and PdAu catalysts on the basis thereof will be discussed.

**Acknowledgement:** This work was supported by the Russian Science Foundation, grant 23-23-00173.

**References:**

[1] Y. Bai, Y. Dou, L.-H. Xie, W. Rutledge, J.-R. Li, H.-C. Zhou, Chem. Soc. Rev. 45 (2016) 2327.
[2] J. Chen, R. Liu, Y. Guo, L. Chen, H. Gao, ACS Catalysis 5(2) (2014) 722–733.
[3] L. Hua, L. Linc, Z. Wu, S. Zhou, S. Liu, Renewable Sustainable Energy Rev. 74 (2017) 230–257.
[4] C. Xu, E. Paone, D. Rodrıguez-Padron, R. Luque, F. Mauriello, Chem. Soc. Rev. 49 (2020) 4273.

## PP-I-39

# Designing $ZrO_2$-Supported Bimetallic AuPd Catalysts for 5-Hydroxymethylfurfural Oxidation

Kharlamova T.S., Timofeev K.L., Morilov D.P., Vodyankina O.V.
*Tomsk State University, Tomsk, Russia*
*kharlamova83@gmail.com*

Biomass-derived 5-hydroxymethylfurfural (5-HMF) is a multifunctional platform molecule used to synthesize a wide range of valuable compounds [1]. Despite the progress made in the development of catalysts for the 5-HMF transformation [2,3], the further catalyst improvement is required. An approach based on bimetallic compositions can be effective due to the synergistic effect of catalyst components [4]. The present work is devoted to the study of the $ZrO_2$-supported bimetallic AuPd systems for tailor-made design of effective catalysts for the 5-HMF oxidation.

Supported mono- and bimetallic catalysts were prepared by incipient wetness impregnation or deposition-precipitation techniques. Metal NPs were obtained with pulsed laser ablation, and $H_2PdCl_4$, $HAuCl_4$ were used as metal precursors. Supported samples were dried, calcined and/or reduced. The samples were characterized by XRD, UV-vis spectroscopy, XRF spectroscopy, and TEM. The catalytic experiments were carried out in the Parr 5500 HR reactor at 80 °C and under 5 bar $O_2$, with the reaction mixture being analysed by HPLC.

The results obtained indicated that the formation of disperse $Au_yPd_{1-y}$ alloyed NPs can be prerequisite for designing highly effective AuPd/$ZrO_2$ catalyst for the 5-HMF oxidation. Specifically, for AuPd/$ZrO_2$ samples prepared by the consecutive or simultaneous impregnation, the primarily formation of individual coarse Au (>100 nm) and disperse Pd (~10 nm) particles was indicated independently on the impregnation approach used. However, their catalytic performance depended on the preparation approach indicating a different component distribution in the catalysts. The samples prepared via simultaneous introduction of Pd and Au as well as consecutive introduction of firstly Pd and then Au showed low 5-HMF conversion (11-14%) similarly to the Au/$ZrO_2$ sample. The sample prepared via consecutive introduction of firstly Au and then Pd demonstrated notably higher 5-HMF conversion (59%) but it came short to both Pd/$ZrO_2$ and colloidal 100-xAuxPd NPs. The alternative approaches to formation of supported $Au_yPd_{1-y}$ alloyed NPs will be discussed.

**Acknowledgement:** This work was supported by the Russian Science Foundation, grant 19-73-30026.

**References:**

[1] L. Hua, L. Linc, Z. Wu, S. Zhou, S. Liu, Renewable Sustainable Energy Rev. 74 (2017) 230–257.
[2] C. Xu, E. Paone, D. Rodrıguez-Padron, R. Luque, F. Mauriello, Chem. Soc. Rev. 49 (2020) 4273.
[3] K. Timofeev, O. Vodyankina, React. Chem. Eng. 6 (2021) 418-440.
[4] K.L. Timofeev, T.S. Kharlamova, D.M. Ezhov, M.A. Salaev, V.A. Svetlichnyi, O.V. Vodyankina, Appl. Cat. A, 656 (2022) 119121.

## PP-I-40

# Ammonia Evaporation Method for Synthesis of Nickel-Supported Catalysts with High Ni Dispersion

Bukhtiyarova M.V., Shamanaev I.V., Pakharukova V.P., Pochtar A.A., Bukhtiyarova G.A.
*Boreskov Institute of Catalysis, Novosibirsk, Russia*
*mvb@catalysis.ru*

From an economic point of view, Ni-based catalysts with high initial activity are a prospective alternative for the noble metal catalysts for industrial applications such as dry reforming processes and acetone hydrogenation [1]. Nickel-based catalysts are the most frequently used in reforming reactions due to C–C bond rupture capability [2]. However, the use of nickel-based catalysts has been encountering a significant challenge due to active metal sintering and coke deposition, which leads to catalyst deactivation, and consequently poor stability. The strong interaction between the embedded Ni particles and the porous support can yield small Ni particle size and high Ni dispersion, thus reaching the confinement effect and bringing better coke resistance [3]. In addition, previous literature reported on the importance of the high Ni content (usually 10–20 wt.%) on various supports to facilitate the catalytic activity. The aim of the work was to synthesize highly dispersed nickel particles on alumina support. It is postulated that such nickel particles can be obtained by ammonia evaporation method using nickel ammonia complexes as precursor [4].

The aim of this work was obtaining highly dispersed Ni particles supported on γ-alumina by ammonia evaporation method.

In this work we studied several Ni-containing samples differed in preparation method. Supported Ni catalysts (> 8%) were synthesized by the ammonia evaporation technique using different metal precursors. Two metal ammonia complexes were used to prepare catalysts: $[Ni(NH_3)_6]CO_3$ and $[Ni(NH_3)_6](NO_3)_2$. γ-$Al_2O_3$ pellets were added to the metal ammine solution to a round-bottom flask fitted with a reflux condenser in a rotary evaporator. The solution was heated to 95 °C and refluxed to distil off the ammonia for 3 hours. The pellets become green while solution was still blue. The further heating and rotation did not result in changing the color of solution. The samples were dried at room temperature for 12 hours. The obtained pellets had bright green colour.

Another two catalysts were prepared by conventional wet impregnation method of the support pellets with an aqueous solution containing a certain amount of $[Ni(NH_3)_6]CO_3$. The pellets became light-blue. After impregnation, the samples were dried at room temperature for several hours until dryness and then at 150 °C for 45 minutes in a drying oven. The nickel hexamine complex decomposes during this drying stage with the evolution of ammonia to produce “green’ nickel hydroxycarbonate dispersed in the pores of the support. The impregnation and drying was repeated three and four times more. The product was then calcined in air at 280°C for 45 minutes to convert the nickel hydroxycarbonate to nickel oxide.

It is possible to obtain 8.03% and 9.90 wt.% Ni on alumina support with wet impregnation method. Ammonia evaporation method can allow increasing Ni content on the support. X-ray diffraction analysis and chemisorption techniques were used for investigation of particle size and dispersion of nickel particles of the nickel catalysts prepared by different methods.

**References:**

[1] Z. Bao, F. Yu, Adv. Bioenergy. 3 (2018) 43.
[2] J. Llorca, V. Cortés Corberán, N.J. Divins, R. Olivera Fraile, E. Taboada, Renewable Hydrogen Technol. (2013) 135.
[3] Q. Song, R. Ran, X. Wu, Z. Si, D. Weng, J. $CO_2$ Utiliz. 68 (2023) 102387.
[4] C.M. Lok, D. Verzijl, J. van Dijk, US Patent 4490480

## PP-I-41

# Design of Composite with Enhanced Photothermal and Conductive Properties Based on Recycled PET and UiO-66

Kogolev D.A., Metalnikova N.M., Postnikov P.S.
*Tomsk Polytechnic University, Tomsk, Russia*
*kogolev@tpu.ru*

The idea of laser annealing is considered promising for processing polymer-immobilized thin-layer metal organic frameworks (MOFs). In addition, the formation of a thin carbon film on the surface of polymers improves the important characteristics of the obtained materials for the photothermal application due to the thermal insulation properties of the polymer substrate and the absence of heat dissipation [1]. PET can be used as a substrate for flexible electronics, photosensors, pressure sensors and smart clothes due to its flexibility and strength.

A study of the physicochemical properties of PET@LB-UiO-66 showed that laser carbonization led to the formation of a composite from molten PET with an impregnated graphene-like material and ZrC particles [2] (Fig. 1A). Despite the obvious use as a conductive material, we hypothesized that the inclusion of ZrC could provide significant photothermal activity [3]. In addition, the high conductivity of the material should lead to a higher extinction coefficient and, hence, better light absorption.

For this reason, we evaluated the photothermal properties of the prepared material to test its possible applicability in the production of water vapor and desalination, mist dissipation, catalysis, sensorics, bacteria killing, anti-icing and photothermal power generation of smart clothing, microelectronics, and more (Fig. 1C).

Analysis by UV-vis spectroscopy showed a significant increase in the absorbance of PET@LB-UiO-66, especially in the visible range (Fig. 1B), facilitating interaction with light and significantly reducing the band gap compared to PET@UiO-66. To analyze the photothermal response, we measured the temperature after being irradiated with a LED at different wavelengths (455, 530, 660, 780 and 1055 nm;) followed by temperature determination with a thermal infrared camera (Fig. 1C). The temperature of the material was observed to rise rapidly, demonstrating its strong ability to convert visible and infrared radiation into heat.

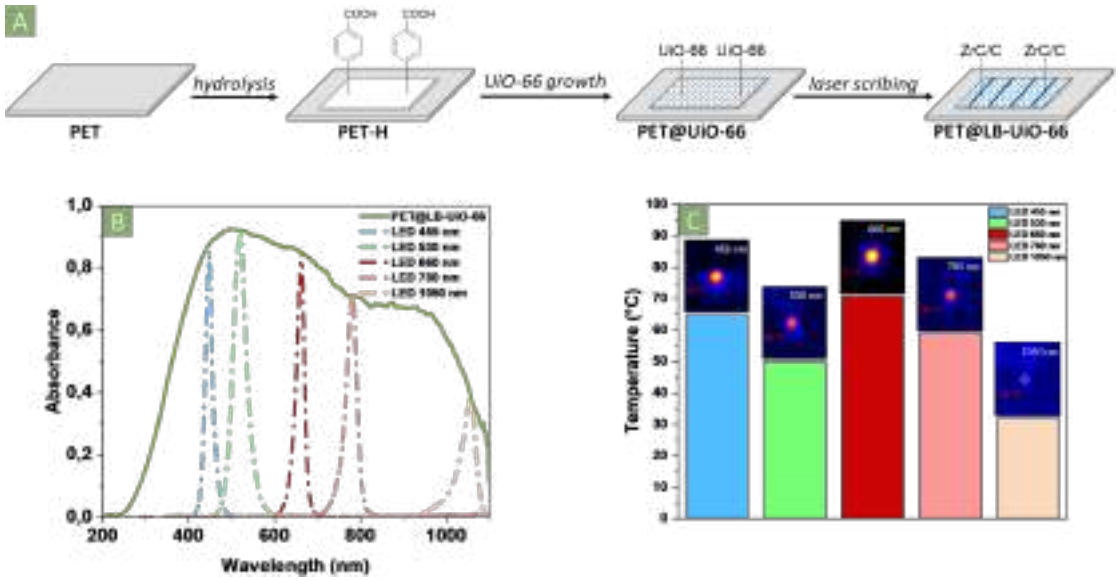


*Fig. 1. (A) Strategy for PET@LB-UiO-66 preparation from recycled PET. (B) UV-vis spectrum of PET@LB-UiO-66 with spectra of LED sources. (C) Photothermal performance of PET@LB-UiO-66 acquired at 5 different wavelengths.*

Thus, given the possibility of using recycled PET as a substrate and used PET bottles as a source of terephthalic acid, functional photothermal materials are competitive with non-waste materials. We expect that further research will focus on the use of PET@LB-UiO-66 for desalination, evaporation, and catalysis [1].

**Acknowledgement:** This work was financially supported by the Ministry of Education and Science of Russia, Agreement № 075-15-2022-244.

**References:**

[1] Q. Y. Wu et al., Adv. Energy Sustain. Res. 2 (2021) 2000056.
[2] D. Kogolev et al., J. Mater. Chem. A. 11 (2023) 1108.
[3] P. Wang et al., ACS Nano. 11 (2017) 3752.

## PP-I-42

# Effect of Micro-Arc Oxidation Voltage and Duration on the Morphology, Phase Structure, Chemical Composition of Calcium Phosphate Coatings

Komarova E.G.[1], Kazantseva E.A.[1,2], Akimova E.B.[3], Khimich M.A.[1,2]
*1 – Institute of Strength Physics and Materials Science SB RAS, Tomsk, Russia*
*2 – Tomsk State University, Tomsk, Russia*
*3 – Tomsk Polytechnic University, Tomsk, Russia*
*katerina@ispms.ru*

The work was focused on the study of the effect of the applied anode voltage (200 V, 350 V) and the duration (1, 2, 4 and 10 min) of the micro-arc oxidation (MAO) process on the morphology, phase structure and chemical composition of calcium phosphate (CaP) coatings on the pure titanium (Ti) substrate.

EDX studies showed that the composition of all MAO CaP coatings was represented by the following elements: calcium, phosphorus, oxygen and titanium. SEM studies showed that during 1 min under the low applied voltage of 200 V, the thin coating with heterogeneous thickness (5.8-15.5 μm) and inhomogeneous morphology was formed. The SEM images illustrated two different surface morphologies, both predominant $TiO_2$ oxide sublayer with numerous crater-like micropores and the local CaP layer with hemispherical structural elements contained internal pores. 2 min of MAO led to the formation of a uniform CaP coating with a typical surface morphology represented by the structural spheroidal elements (spheres) with internal pores. Further increasing the MAO duration up to 10 min was accompanied by a linear increasing the coating's thickness from 28.6 to 55.5 μm [1] and by the following change in its elemental composition. The calcium amount in the coating increased from 3.2 to 5.5 at.%, the titanium amount decreased from 13.6 to 8.9 at.%, the phosphorus and oxygen amounts were unchanged within the ranges of 15.4 – 16.2 at.% and 67.1 – 69.7 at.%, respectively. XRD analysis showed that CaP coatings formed at low voltage of 200 V, regardless of the MAO duration, were in an X-ray amorphous state. It was evidenced by an obvious diffuse scattering region in the 2θ angle range of 20 °– 37 ° on the XRD patterns corresponding to the amorphous CaP phase (Fig. 1). With an increase in the MAO duration from 2 to 10 min, the intensity of the diffuse scattering region did not change. This indicated the uniformity of the phase structure through the thickness of these CaP coatings.

An increase in the anode voltage up to 350 V led to the significant morphological, structural-phase and chemical transformations of the CaP coatings. Under this voltage, regardless of the MAO duration, the thick homogeneous CaP coating with similar surface morphology represented by the spheres, destructed hemispheres, pores inside the spheres, pores between the spheres and plate-like crystals was formed [2]. At the same time, an increase in the MAO process duration from 1 to 10 min led to the linear increase of the thickness from 37.2 to 135.2 μm. That was accompanied by the formation of an inhomogeneous phase structure throughout the thickness of coating. Duration of 1 min

allowed the formation of coating in an X-ray amorphous state, similar to the coatings formed at a low voltage of 200 V. An increase in the MAO duration from 2 to 10 minutes led to the formation of an amorphous-crystalline structure of the coatings. This was evidenced by the increased intensity of reflections at the 2θ angles of 26.3; 26.5 and 30.1° corresponding to the triclinic monetite ($CaHPO_4$) phase, of reflections at the 2θ angles of 26.3; 26.5 and 30.1°, corresponding to the tetragonal β-calcium pyrophosphate (β-$Ca_2P_2O_7$) phase, and a low-intensity diffuse scattering region corresponding to the amorphous CaP phase (Fig. 1). The volume fraction of $CaHPO_4$ phase in the coatings was increased from 51 to 80 % in the amorphous-crystalline coatings. The coating structural-phase transformation from the X-ray amorphous state to the amorphous-crystalline one was attended by the following change in its elemental composition: the calcium amount was increased from 4.0 to 9.7 at.%, the titanium amount was decreased from 12.0 to 6.5 at.%, the phosphorus and oxygen amounts were unchanged in the ranges of 14.6 – 16.1 at.% and 64.6 – 70.4 at.%, respectively.

Thus, this work revealed that the MAO applied voltage and the duration have a significant influence on the formation of a multilevel hierarchical structure, morphology, phase and elemental compositions of the CaP coatings on Ti surface.

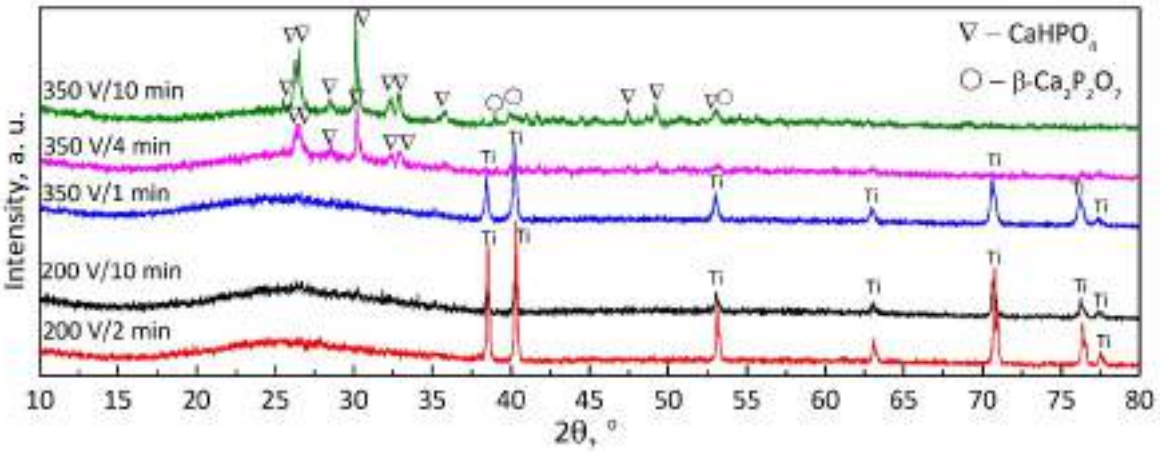


*Fig. 1. XRD patterns of CaP coatings deposited at different voltages with different duration*

**Acknowledgement:** This work was supported by the Government research assignment for ISPMS SB RAS, Project FWRW-2021-0007.

**References:**

[1] E.G. Komarova, Y.P. Sharkeev, M.B. Sedelnikova, I.A. Khlusov, O. Prymak, M. Epple, Materials. 13 (2020) 4116.
[2] E.G. Komarova, M.B. Sedelnikova, E.A. Kazantseva, P.V. Uvarkin, Y.P. Sharkeev, Rus. Phys. J. 63 (2020) 1249

## PP-I-43

# Nickel-Tin Alloy Catalysts for Liquid Organic Hydrogen Carrier Dehydrogenation

Stepanenko S.A., Koskin A.P., Alekseeva (Bykova) M.V., Kaichev V.V., Yakovlev V.A.
*Boreskov Institute of Catalysis, Novosibirsk, Russia*
*koskin@catalysis.ru*

The hydrogen energy development implies the progress in its efficient storage and transportation technologies. Of particular interest is the storage and transportation of $H_2$ as a part of liquid organic hydrogen carriers (LOHCs), which are characterized by high specific hydrogen content and can be reused using hydrogenation/dehydrogenation processes. [1]. A key step in the development of LOHC technologies is the optimization of cycloalkanes dehydrogenation process. This high-temperature (over 300°C) process is traditionally provided over platinum catalysts [1]. The development of catalyst composition without noble metals is a promising alternative to platinum catalysts. In the case of methylcyclohexane (MCH) dehydrogenation, the main disadvantage of $Ni/SiO_2$ is the low selectivity of the process in view of the decomposition of toluene (dehydrogenation product) to benzene and methane. This reduces the amount of using LOHC substrate cycles and leads to hydrogen contamination by methane. Thus, when developing catalytic compositions with nickel content, the main task is to increase the selectivity of the dehydrogenation process.

In our previous works, we have studied the catalytic properties of high-loaded nickel catalysts ($Ni\text{-}SiO_2$, about 60 wt% Ni). In the reduced form, these consists consist of ultrafine Ni particles stabilized by an amorphous silicon dioxide matrix [2]. The effect of Cu- and Zn modification of $Ni\text{-}SiO_2$ on the MCH dehydrogenation selectivity was consistently studied [3,4]. In the presented work, the main attention was paid to the study of the catalytic properties of NiSn catalysts. It has been shown that the use of tin as a modifier makes it possible to achieve the highest selectivity for toluene (close to 100%) while maintaining a high conversion of MCH. The initial $Ni\text{-}SiO_2$ system (Ni100, Fig.1) was synthesized according to [2] and modified with tin according to the method adapted from [3,4]. The catalytic properties of the reduced $Sn/Ni\text{-}SiO_2$ ($Sn_X/Ni_Y$-T, Fig.1) catalysts were studied using a continuous flow reactor described in [3,4]. The MCH conversion ($X_{MCH}$, %) and toluene selectivity ($S_{TOL}$, %) were measured by gas chromatography. As a result of the experiments, the composition of the catalyst (Ni:Sn 80:20 wt%) and the reduction temperature (500 °C) were optimized.

The structure of the initial and reduced $M/Ni\text{-}SiO_2$ (Me: Cu, Zn and Sn) catalytic systems was investigated by a set of physicochemical methods (XRF, XRF in situ, XPS, chemisorption of CO, H2-TPR, TEM, toluene TPD, etc.). Was shown that the high selectivity of the MCH dehydrogenation process is achieved when solid solutions of Ni-Zn or Ni-Sn are formed, which are characterized by a decrease in the adsorption properties of the catalyst in relation to the

reaction product (toluene). In turn, the rapid removal of toluene from the reaction layer reduces the rate of the side process of the LOHC substrate hydrogenolysis.

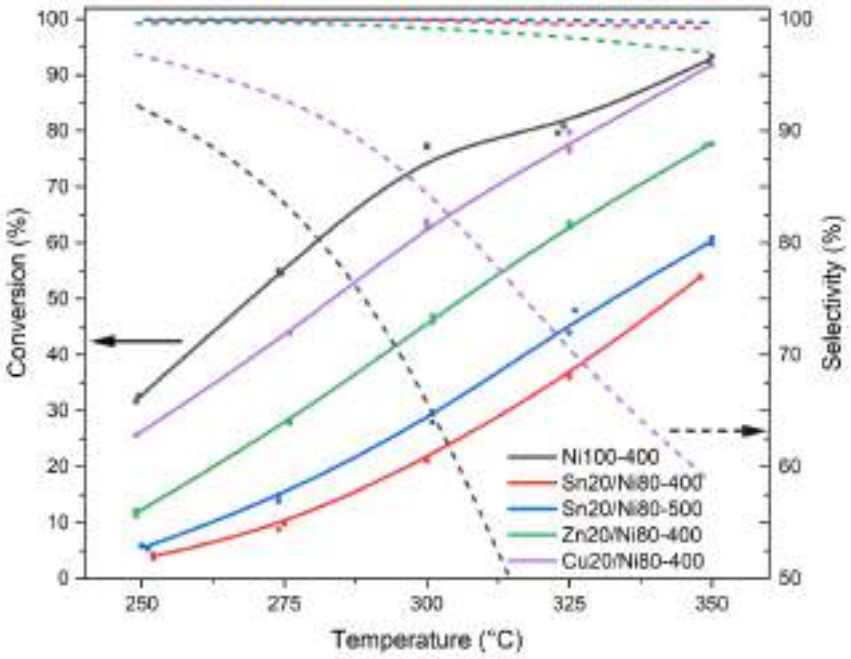


*Fig. 1. Comparison of the catalytic properties of the initial nickel catalyst (Ni100) and modified analogues $M_X/Ni_Y$-T (where, X, Y are the weight fractions of metals; M = Cu, Zn or Sn; T is the reduction temperature ($H_2$, 1 hour, 500 ml/min)). Reaction conditions: continuous flow reaction unit, T 250-350°C, 1 bar, 400 ml/min Ar/$H_2$ (1:1), 0.5 g of the catalyst, WHSV 18.5 $h^{-1}$.*

**Acknowledgement:** This research was funded by the Ministry of Science and Higher Education of the Russian Federation within the governmental order for Boreskov Institute of Catalysis (projects AAAA-A21-121011390007-7).

**References:**

[1] Preuster P., Papp C., Wasserscheid P. // Accounts of Chemical Research. 2017. Vol. 50. P. 74-85.
[2] Ermakova M., Ermakov D. // Applied Catalysis A. 2003. Vol. 245, 277-288.
[3] Gulyaeva Y., Alekseeva (Bykova) M., Bulavchenko O., Kremneva A., Saraev A., Gerasimov E., Selishcheva S., Kaichev V., Yakovlev V. // Nanomaterials. 2021. Vol. 11. P. 1-20.
[4] Alekseeva (Bykova) M., Gulyaeva Y., Bulavchenko O., Saraev A., Kremneva A., Stepanenko S., Koskin A., Kaichev V., Yakovlev V. // Dalton Transactions. 2022. Vol. 51. 6068-6085.

## PP-I-44

# Pathways to Control the Activity and Selectivity of UiO-66-Based Catalysts in Cascade Conversion of Polyols

Kotov A.V., Vodiankina O.V.
*Tomsk State University, Tomsk, Russia*
*vodyankina_o@mail.ru?*

The most well-known method to process the polyhydric alcohols is their cascade oxidative conversion to lactic acid in alkaline media [1]. However, this approach is related to the need for further purification of the products and is also harmful to the environment. It is known from the literature that the key stages in the cascade oxidative conversion of polyols are those related to the formation of pairs of glyceraldehyde/dihydroxyacetone and 2-hydroxypropenal/pyruvaldehyde. These stages can occur at Lewis acid sites [2, 3], which can be $Zr^{4+}$ cations in the composition of the secondary building unit (SBU) of the UiO-66, a metal-organic framework (MOF) with unique properties, including high thermal and chemical stability, large pore volume and high specific surface area [4]. Moreover, of interest are the SBU doped with other cations that exhibit the properties of Lewis acids, e.g., $Sn^{4+}$ and $Ti^{4+}$. Therefore, the study of the effect of transition metal dopants (Sn, Ti) on the properties of active sites on the surface of Zr-UiO-66-L systems (L = -H, -OH, $-NO_2$, $-NH_2$, $-HSO_3$) and on their activity in the processes of keto-enol isomerization of carbonyl compounds in an aqueous medium is decisive in substantiating the mechanisms of the above catalytic processes.

The reaction of the cascade oxidative conversion of glycerol into lactic acid was chosen as a model one (fig. 1). Optimization of the geometry of all structures of isomers was carried out, and their vibrational features were calculated using the ORCA 5.0.3 software package at the B3LYP-D3/6-311G(d,p) level of theory to determine the most probable reaction pathway without the participation of the catalyst in an aqueous solution. The search for transition states (TS) was carried out by the QST1 method, the solvent effect was taken into account using the CPCM model and with the addition of one explicit water molecule to the TS structure.

To detail the proposed mechanism of substrate isomerization with the participation of Lewis acid sites, the optimization and calculation of the vibrational frequencies of the modified clusters with the composition $M_2$-$Zr_4O_4(OH)_4$-L, when M = Zr, Sn, Ti and L = -H, -OH, $-NH_2$, $-NO_2$, $-HSO_3$, was carried out at the B3LYP-D3/ZORA-def2-TZVP level of theory in the gas phase with taking into account relativistic interactions in transition metals. The distribution of electron density (ED) in substituted $M_2$-$Zr_4O_4(OH)_4$-L clusters was determined.

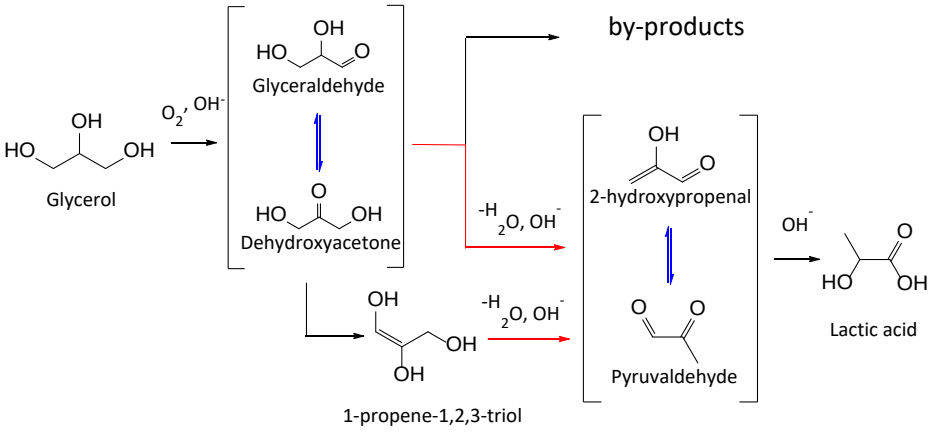


*Fig. 1. Isomerization (blue) and dehydration (red) stages of the oxidative conversion of polyols*

Research has proven that when the solvent is not taken into account, the activation barriers in the isomerization and dehydration stages (Fig. 1) are high ($\Delta G^{\#}$ from 50.0 to 65.0 kcal $mol^{-1}$). When one explicit water molecule is included into the TS structure, $\Delta G^{\#}$ decreases by 10–20 kcal $mol^{-1}$ due to the formation of stable seven-centered rings and the simultaneous transfer of hydrogen atoms.

Changes of the Gibbs energy in the reactions of formation of $M_2$-$Zr_4O_4(OH)_4$ clusters in UiO-66 decreases in a series M = Zr, Sn, Ti, therefore, the $Ti_2$-$Zr_4O_4(OH)_4$ structure is the most stable one. The HOMO visualization showed that the ED of the $Zr_6O_4(OH)_4$ cluster is uniformly distributed over the Zr atoms. The tin-doped clusters $Sn_2$-$Zr_4O_4(OH)_4$ are characterized by the ED concentration on the Zr atoms, while its deficiency is observed on those of Sn. The opposite effect is observed in the $Ti_2$-$Zr_4O_4(OH)_4$ cluster, where the ED is concentrated on titanium atoms. Therefore, the Lewis acidity increases in the series Ti – Zr – Sn, which determines the catalytic properties of these systems.

The report discusses the mechanisms of isomerization of substrates that occur with the participation of substituted and unsubstituted active Lewis sites localized in the structure of $M_2$-$Zr_4O_4(OH)_4$ clusters as well as the possible effect of substituents in the organic linker in the L-UiO-66 structure (L = -H, -OH, $-NH_2$, $-NO_2$, $-HSO_3$).

**Acknowledgement:** This work was supported by the Russian Science Foundation, grant 19-73-30026, https://rscf.ru/en/project/19-73-30026/.

**References:**

[1] Kishida H. et al. Conversion of glycerin into lactic acid by alkaline hydrothermal reaction //Chemistry Letters. – 2005. – Т. 34. – №. 11. – С. 1560-1561.
[2]. Dapsens P. Y., Mondelli C., Pérez-Ramírez J. Highly selective Lewis acid sites in desilicated MFI zeolites for dihydroxyacetone isomerization to lactic acid //ChemSusChem. – 2013. – Т. 6. – №. 5. – С. 831-839
[3] Rahaman M. S. et al. Aluminum-based Metal-Organic Framework as Water-tolerant Lewis Acid Catalyst for Selective Dihydroxyacetone Isomerization to Lactic Acid //ChemCatChem. – 2022 – Т. 14 – №. 4 – С. e202101756.
[4] Cavka J. H. et al. A new zirconium inorganic building brick forming metal organic frameworks with exceptional stability //Journal of the American Chemical Society. – 2008. – Т. 130. – №. 42. – С. 13850-13851.

## PP-I-45

# Design of High-Performance Supported Bimetallic Catalysts for Hydrogen Production

Matus E.V.[1,2], Kovalenko E.N.[1,2], Sukhova O.B.[1], Ismagilov I.Z.[1], Yashnik S.A.[1], Ushakov V.A.[1], Gerasimov E.Y.[1], Kerzhentsev M.A.[1], Ismagilov Z.R.[1,3]

*1 – Boreskov Institute of Catalysis, Novosibirsk, Russia*

*2 – Novosibirsk State Technical University, Novosibirsk, Russia*

*3 – Federal Research Center of Coal and Coal Chemistry, Kemerovo, Russia*

*matus@catalysis.ru*

The effective implementation of synergistic effects between different metals in catalytic reactions is an important topic in catalytic chemistry [1, 2]. The synergistic effect on bimetallic surfaces can be associated with the effects of an ensemble, ligand or deformation caused respectively by chemical composition changes, the interaction between adjacent metal atoms of different elements and modification of surface electronic structure through the variation in orbital overlapping [3]. The introduction of a promoter can increase the Ni catalyst activity and stability against phase transformation, sintering and coking during hydrogen production reactions. So, in our work we study the efficiency and action mode of noble (Pt, Pd) and non-noble (Re, Mo, Sn) metal additives in the composition of Ni supported catalysts for hydrogen production.

The Ni-M catalysts (M = Pt, Pd, Re, Mo, Sn) were prepared with using of $La_2O_3$, $Ce_{0.8}La_{0.2}O_{1.8}$ or $Ce_{0.5}Zr_{0.5}O_2/Al_2O_3$ as supports. The mole ratio of nickel to promoter was in the range of 0.003–0.03. Characterization of fresh and spent Ni-based catalysts by X-ray fluorescence spectroscopy, $N_2$ adsorption, X-ray diffraction, $H_2$ temperature-programmed reduction, high-resolution transmission electron microscopy and X-ray photoelectron spectroscopy were performed. Catalysts were tested in the autothermal reforming (ATR) of methane, steam/$CO_2$ reforming of methane and ATR of ethanol. The composition–characteristics–activity correlation was determined.

Regardless of the composition of the support, the introduction of a promoter does not affect the textural and morphological properties of catalysts but influences their structure, reducibility and performance in catalytic reaction. The $Ni^{2+}$ reduction is intensified in the following order of additives: Mo < Sn < Re < Pt < Pd. In the case of Pt, Pd and Re additives, catalysts obtain the ability to self-activation under the reaction conditions, which allows them to be used without prior reduction. The NiM alloy is formed under reaction conditions improving the stability of the samples against re-oxidation and sintering. Promoted catalysts provide a high yield of hydrogen (70% I n ATR of $CH_4$ and 95% in steam/$CO_2$ reforming of $CH_4$ at 800°C) without deactivation. Rhenium was chosen as the most promising additive, providing a sufficient increase in reducibility and the greatest improvement in sintering resistance among the studied additives.

**Acknowledgement:** This work was supported by the Ministry of Science and Higher Education of the Russian Federation within the governmental order for the Boreskov Institute of Catalysis (project AAAA-A21-121011490008-3).

**References:**

[1] S. De, J. Zhang, R. Luque, N. Yan, Energy Environ. Sci. 9 (2016) 3314.
[2] I.Z. Ismagilov, A.V. Vosmerikov , L.L. Korobitsyna, E.V. Matus, M.A. Kerzhentsev, A.A. Stepanov, E.S. Mihaylova, Z.R. Ismagilov, Eurasian Chem.-Technol. J. 23 (2021) 147.
[3] C. Fan, Y. Zhu, Y. Xu, Y. Zhou, X. Zhou, D. Chen, J. Chem. Phys. 137 (2012) 014703.

## PP-I-46

# The Study of Aqueous Redox-Active Polymer Microgels

Sentyurin V.V.[1], Kozhunova E.Yu.[1,2], Khokhlov A.R.[2], Magdesieva T.V.[1]

*1 – Chemistry Department, Lomonosov Moscow State University, Leninskie Gory 1-3, Moscow 119991, Russia*

*2 – Physics Department, Lomonosov Moscow State University, Leninskie Gory 1-2, Moscow 119991, Russia*

The search for more environmentally friendly batteries has led to increased interest in redox-active materials on the base of organic species, which can be further utilized in composite and fully organic devices. Such species are known for being inexpensive and recyclable, and their cost is not constrained by exhaustion of rare materials. Against this background, redox-active materials which include polymers in their composition are being developed. Polymers can have high charge transport and good storage capacities. Also, incorporation of redox sites into polymer chains improves cycling stability and often solves technical problems.

This study is focused on the creation of a new type of water-soluble polymer containing redox-active pendant groups. The s-tetrazines are among the smallest organic molecules characterized by reversible two-electron reduction in protic media. That makes them good candidates for anolyte solutions. Its other important advantages include high solubility, outstanding chemical stability, and an abundance of chemical properties that allow for further structural modifications. In the present work, two approaches for the obtaining of redox-active polymers were tested: polymerization of tetrazine-containing monomers and incorporation of such fragments into already prepared polymers. Hydrophilic polymeric microgels based on poly-N-isopropylacrylamide [1] were used as carriers of the redox active moieties.

**Acknowledgement:** This work was supported by the Russian Science Foundation, grant 22-13-00115.

**References:**

[1] *J. Phys. Chem. Lett.* 2020, 11, 24, 10561–10565

## PP-I-47

# Atomically Smooth Nanoscale SiO2+TiO2 Film Deposition by Magnetron Sputtering

Andreev A.V., Volpyan O.D., Krasnoborodko S.Yu., Vysokikh Yu.E., Dronskii R.V.
*"Scientific and Technological Center of Unique Instrumentation" of the Russian Academy of Sciences, Moscow, Russia*
*Andreev.alex.vlad@gmail.com*

The main purpose of the study was an attempt to prove the uniformity of a film sprayed by magnetron sputtering from two sources and having a gradient in its composition along the surface of the substrate. Spraying was carried out on a prepared quartz glass substrate using two microwave magnetrons.

The use of two magnetrons simultaneously in one chamber equipped with targets made of titanium (Ti) and silicon (Si) made it possible to achieve a gradient change in the refractive index of the film, from 1.46 for SiO2 to 2.7 for TiO2. The oxidation of the sprayed material was carried out by the injection of oxygen (O) into the magnetron chamber.

The study of the film surface by Contact Topography and Semi-Contact Topography using an atomic force microscope showed excellent results demonstrating the value of the Rms roughness of the film in the range from 0.3 to 0.4nm.

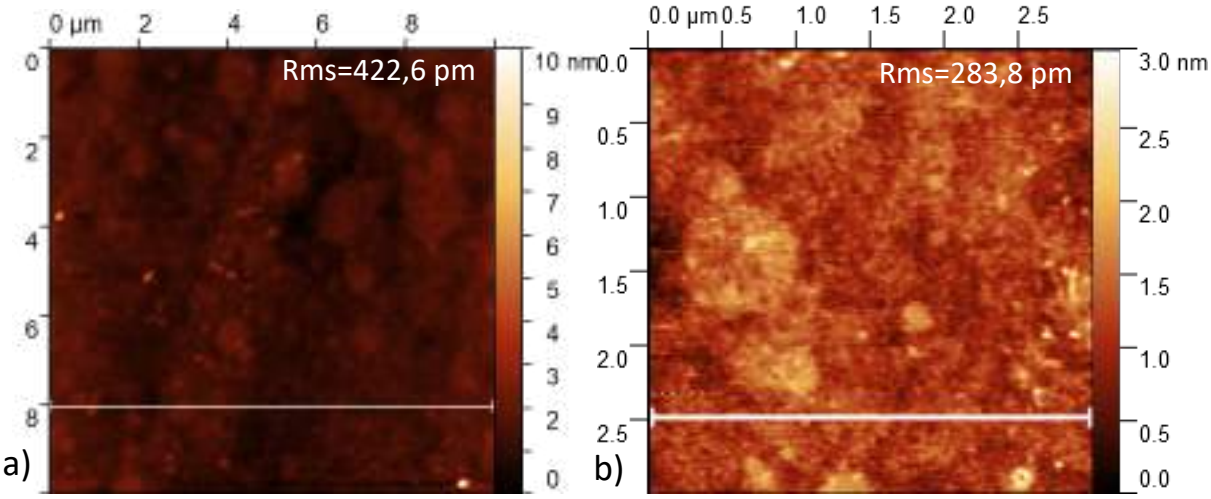


*Fig. 1. Scanned images of the gradient film surface a) 10x10 microns area, b) 3x3 microns area. Each scan corresponds to the Rms value averaged over the entire scan area.*

**References:**

[1] Власов, А.С & Karlina, Ludmila & Комисаренко, Ф.Э & Ankudinov, A.. (2017). Модификация поверхности GaAs и наблюдение эффекта гигантского рамановского рассеяния после диффузии индия. Журнал технической физики. 51. 611. 10.21883/FTP.2017.05.44461.8453.
[2] V.Yu. Fominski , R.I. Romanov, I.S. Vasil'evskii, D.A. Safonov, A.A. Soloviev a, A.A. Ivanov, P.V. Zinin, S.Yu. Krasnoborodko, Yu.E. Vysokikh, V.P. Filonenko . "Pulsed laser modification of layered B-C and mixed BCx films on sapphire substrate" Diamond & Related Materials 114 (2021) 108336.
[3] N.F. Abramov and O.D. Volpyan and Yu.A. Obod and R.V. Dronskii, "Fabrication of nanogradient coatings for laser devices using the method of magnetron sputtering" Quantum Electronics, 43(9) 791, jan 2013 10.1070/QE2013v043n09ABEH015218

PP-I-48

# Development of a Strategy for the Synthesis of [2,2]-Paracyclophanes, Precursors of Poly-Para-Xylylen Coatings, Using High-Performance Catalysts

Kruglyakova O.V., Yushchenko D.Y., Sergeev E.E., Pai Z.P., Khlebnikova T.B.
*Boreskov Institute of Catalysis, Novosibirsk, Russia*
*voroshin@catalysis.ru*

The request to develop the efficient methods for producing [2,2]-paracyclophanes (PCF), the initial dimers for polymer coatings, is caused by the wide range of their applications as protective covers against climatic influences and aggressive environment in medicine, aerospace industry, electronics, light-emitting devices, flat panel displays, etc. Poly-para-xylylene coatings (Parylen D, Parylene N, Parylene C, etc.) are an excellent alternative to standard approaches based, for example, on the use of varnishes to protect electrical components, printed circuit boards from adverse external impacts (dust, humidity, radiation, etc.) [1].

Disadvantages of several known methods of PCF obtaining are: multistage synthesis; small yield of the target product; use of additional reagents in non-stoichiometric quantities. Other methods requires a long reaction time to achieve acceptable yields of PCF (about 70%) or do not imply the reuse of the catalyst at the stage of formation of di-para-xylylene dimer [2].

The quality of the dimeric precursor, PCF, plays the key role in the quality of the final polymer coating. One of the challenging stages of synthesis is the catalytic cyclization of ammonium salt yielding PCF.

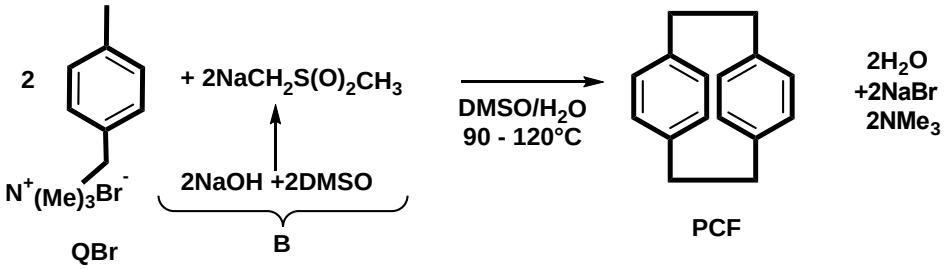


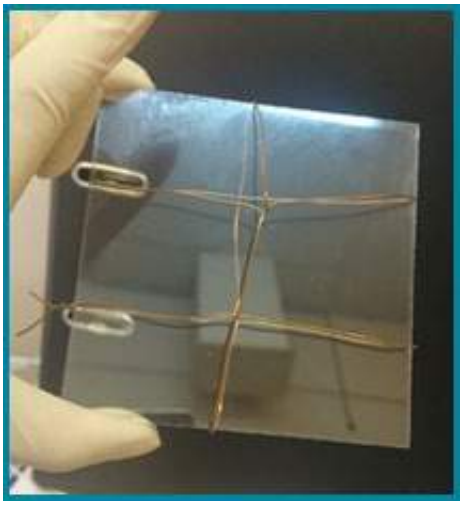

*Fig. 1. Poly-para-xylylene coating based on Parylene C*

In this connection, we studied Hoffmann elimination followed by Vinberg combination using N,N,N-trimethyl-4-methylbenzyl ammonium salts (QBr) as starting compound and previously synthesized demethylate anions (B) as bases initiating the elimination.

As a result, the proposed approach increases the efficiency of the PCF synthesis by performing the cyclization reaction of N,N,N-trimethyl-4-methyl-benzyl ammonium salts in the temperature range of 105 - 120 °C, at atmospheric pressure, in a (DMSO + H2O) medium, affording PCF in high yields

and without formation of the undesirable polymer byproduct. Under the found optimal conditions, the process is simplified significantly, synthesis time is reduced and the base catalyst B can be reused.

**Acknowledgement:** This work was supported by the Ministry of Science and Higher Education of the Russian Federation within the governmental order for Boreskov Institute of Catalysis (project AAA-A21-121011390007-7).

**References:**

[1] Parylene index 2000. Edited by WFBeach, c. 135 www.wfbeach.com.
[2] Gogin L.L. , Yushchenko D.Y. , Konev V.N. , Sergeev E.E. , Zhizhina E.G. , Khlebnikova T.B. , Pai Z.P. Ways of Synthesizing Dichloro-[2,2]-Paracyclophane: A Review Catalysis in Industry. 2019. V.11. N1. P.34-44. DOI: 10.1134/S2070050419010057

## PP-I-49

# Computational and Experimental Investigation of 3D-Printed Polylactide Laminate Composites' Mechanical Properties

Krupnin A.E.[1,2], Zakirov A.R.[2], Krasheninnikov S.V.[1], Sedush N.G.[1], Chvalun S.N.[1]
*1 – National Research Centre "Kurchatov Institute", Moscow, Russia*
*2 – Bauman Moscow State Technical University, Moscow, Russia*
*artkrupnin@gmail.com*

The purpose of this work is to experimentally investigate the applicability of the Tsai-Hill failure criterion for predicting the strength of 3D-printed polylactide (PLA) laminate composites in mechanical tests for uniaxial tension and compression. The mechanical behaviour of the manufactured via fused deposition modelling (FDM) technology parts is described by classical laminate theory. Specimens for uniaxial tension (ISO 527), compression (ASTM D-7264) were manufactured with a Raise3D PRO2 3D-printer. Slicing of the models was carried out via ideaMaker software. Commercial PLA REC (natural color) 1.75 mm filament was used as a material for manufacturing. The temperature of the extruder and the printing bed were 215 °C and 65 °C, respectively; layer height 0.25 mm, printing speed 40 mm / s. Mechanical tests were carried out on the INSTRON 5965 universal testing machine with a constant deformation speed of 1 mm/min. According to the results of tensile and compression tests, the stiffness matrix components of the orthotropic individual lamina and strength were determined. The Poisson's ratio was determined by the digital image correlation (DIC) method.

It was found that the Tsai-Hill criterion is applicable for predicting the tensile strength and yield strength of laminate polymer composite materials manufactured via FDM 3D-printing. The calculated values of the elastic modulus for specimens with various raster angles correlate well with the values obtained experimentally. The error for a laminate with a constant raster angle was 3.3%, for a composite laminate – 4.4% in tensile tests, and 11.9% and 9% in compression tests.

**Acknowledgement:** This work was supported by the State Assignment of the NRC "Kurchatov Institute". Authors also acknowledge support of the Resource Centres "Polymer" additive and virtual technologies for manufacturing and mechanical testing of the specimens.

## PP-I-50

# Composite CO Hydrogenation Catalysts Based on Lignin and Metal Salts

Krysanova K.O.[1,3], Sotnikova A.E.[2], Ivantsov M.I.[1], Grabchak A.A.[1]

*1 – A.V.Topchiev Institute of Petrochemical Synthesis, RAS (TIPS RAS), Moscow, Russia*

*2 – National University of Oil and Gas «Gubkin University», Moscow, Russia*

*3 – Samara State Technical University (Samara Polytech), Samara, Russia*

*k_krysanova@ips.ac.ru*

The hydrothermal carbonization is a process commonly used to upgrade biomass for use as a fuel or feedstock to produce high value added products such as liquid hydrocarbons or adsorbents. The process carried out in the temperature range of 190-250°C, in an anaerobic atmosphere, at autogenous water vapor pressure.

The possibility of obtaining catalytic systems from hydrothermally treated lignin that are active in the process of CO hydrogenation (Fischer-Tropsch synthesis) was studied in this work.

The catalysts were obtained by the incipient wetness impregnation method of hydrothermally treated lignin. Hydrothermal carbonization of lignin was carried out at temperatures of 190-250°C. Next, the dried solid residue of hydrothermal carbonization was impregnated with iron nitrate (Fe(NO3)3·9H2O) dissolved in a water-alcohol solution (1:1 vol.). The resulting mixture was dried in a water bath at a constant temperature of 96°C. After complete drying, the sample was calcined in a fixed bed reactor in an inert atmosphere at 400°C for 1 hour.

Lignin after hydrothermal carbonization was studied by the following methods: TGA, IR-Fourier and Raman spectroscopy, BET, elemental analysis. Lignin-based catalysts were studied by the following methods: FT-IR and Raman spectroscopy, BET, elemental analysis, atomic absorption analysis, XRD.

A deepening of the deoxygenation process was observed with an increase in the temperature of lignin the hydrothermal treatment. The specific surface area of the obtained materials was low and reached 22.6 m3/g upon hydrothermal treatment at 210°C. FT-IR spectroscopy showed a decrease in the number and oxidation of the functional groups of the aromatic rings of lignin. However, the integrity of the aromatic rings was not affected. The presence of oxygen-containing groups in the composition of the material allows the immobilization of iron ions on the surface of the support. With an increase in the treatment temperature, oxygen-containing groups decrease, which leads to a lower iron content in the catalysts. It was shown by Raman spectroscopy that with an increase in the temperature of hydrothermal treatment, a more graphitized structure was formed.

The catalysts were characterized by an iron content of 18 to 24%. The XRD method showed that magnetite (Fe3O4) nanoparticles are formed in the catalytic system.

Catalytic tests of the resulting systems were carried out in the process of CO hydrogenation. It was shown that the catalysts were highly active in above process: the conversion was close to 100%, the yield of C5+ carbons reached 67 g/m$^3$, the selectivity for

the formation of C5+ hydrocarbons varied from 17 to 60%, and the selectivity for the formation of monohydric alcohols did not exceed 7%. It was found that the sample based on hydrothermally carbonized lignin at 250°C has the best catalytic characteristics. The obtained catalyst was characterized by almost 100% CO conversion at 320°C and the yield of C5+ carbons was 67 g/m$^3$.

Thus, the fundamental possibility of forming catalytically active systems based on lignin in the Fischer-Tropsch process is shown. Hydrothermal carbonization of lignin made it possible to obtain a stable carbon material with a functionalized surface, which makes it possible to effectively immobilize ions of the active component.

**Acknowledgement:** The work was carried out within the framework of the Russian Science Foundation project No. 22-23-00900. The studies were carried out using the equipment of the Common Use Center "Analytical Center for Problems of Deep Oil Refining and Petrochemistry" of the Institute of Petrochemical Synthesis of the Russian Academy of Sciences.

## PP-I-51

# Adsorption and Electrooxidation of Dimethyl Ether on Pt/MOx-C Electrocatalysts

Kubanova M.S., Kuriganova A.B., Chernysheva D.V., Smirnova N.V.
*Platov South Russian State Polytechnic University, Novocherkassk, Russia*
*kubanova_mc@mail.ru*

The importance of developing the fuel cells (FC) vehicle industry is emphasized in many countries [1]. Since the cost of FCs largely depends on the cost of Pt-based catalysts, research is primarily focused on development of new highly active materials for fossil fuel oxidation reactions. FCs with direct oxidation of simple organic molecules (such as $CH_3OH$, HCOOH, $CH_3OCH_3$) [2, 3] are of considerable interest due to their relatively simple design. However, the kinetics of organic fuel oxidation still presents certain difficulties that need to be solved.

In this work, we studied the adsorption and electrooxidation of dimethyl ether (DME) on Pt/MOx-C (MOx – $TiO_2$, NiO, $SnO_2$) electrocatalysts obtained by the method of electrochemical oxidation and dispersion of metals [4]. The electrochemical behaviour of DME was studied by cyclic voltammetry and rotating disk electrode techniques.

The results of the study showed that catalysts with a hybrid support based on $SnO_2$ exhibit increased activity in the electrooxidation of DME. It should be noted that the electrochemical oxidation of DME on Pt/$SnO_2$-C starts at a potential of 0.42 V (RHE), which is much lower than for methanol [4], which is very important for practical application in FCs.

The presence of a hybrid support in the composition of the catalyst provides a higher rate of DME oxidation compared to Pt/C, probably due to the presence of surface-active oxides which facilitates the activation of C–H bonds in the methyl groups of the ether [5]. As a result of the conducted studies, Pt/MOx-C catalysts can be recommended as anode materials for fuel cells with direct oxidation of dimethyl ether.

**Acknowledgement:** This study was supported by the Russian Scientific Foundation (grant 20-79-10063).

**References:**

[1] Zhang, Y., J. Wang, and Z. Yao, *Energies.* 2023. **16**(5): p. 2099.
[2] Kumar, V.B., et al.. Materials Today Sustainability, 2022. **17**: p. 100095.
[3] Yaqoob, L., T. Noor, and N. Iqbal, International Journal of Energy Research, 2021. **45**(5): p. 6550-6583.
[4] Kuriganova, A.B., Leontyeva, D.V., Ivanov, S., Bund, A., and Smirnova, N.V. J. Appl. Electrochem., 2016, vol. 46, p. 1245.
[5] Kubanova M.S., Kuriganova A.B., and Smirnova N.V. // Russian J. of Electrochemistry, 2022. 58(10). p. 916–926.

## PP-I-52

# Formation of Nanochannels by Heavy Ions in Graphene Oxide Reinforced Carboxymethylcellulose Membranes for Proton Exchange Membrane Fuel Cells Applications

Kurbanova B.[1], Aimaganbetov K.[2], Karibayev M.[1], Almas N.[1], Ospanov K.[1], Kuanyshbekov T.[3], Akatan K.[3], Kabdrakhmanova S.[4]

*1 – Institute of Hydrogen Energy, International Science Complex Astana, Astana 010000, Kazakhstan*

*2 – Satbayev University, Institute of Physics and Technology, 050032, Almaty, Kazakhstan*

*3 – Sarsen Amanzholov East Kazakhstan University, 18/1 Bitibaeva str., 070002 Ust-Kamenogorsk, Kazakhstan*

*4 – Satbayev University, 050032, Almaty, Kazakhstan*

*kurbanovabaan@gmail.com*

Proton exchange membranes (PEMs) operating at high temperatures above 100 °C with the excellent mechanical, chemical and thermochemical stability have been received much attention, because of their practical application of proton exchange membrane fuel cells (PEMFCs) [1, 2]. Nowadays, a huge number of polymers and polymer-mixed various membranes have been investigated for this application, all of which offer both pros and cons [3, 4]. However, PEMFCs are still lack of ideal membranes with unique properties.

In this work, carboxymethylcellulose (CMC) based membranes with dispersive graphene oxide (GO) sheets were fabricated and investigated for PEMFCs application. These membranes and pristine GO were studied by a combination of XRD, XPS, Raman, Brillouin, FTIR, thermo-mechanical analysis (TGA and Dynamic Mechanical Analysis) and SEM microscopy, while electrophysical characterizations were carried out using electrochemical impedance spectroscopy (EIS) measurements [5]. It was revealed that the addition of CMC to the GO boosts proton conductivity of the whole membrane, while GO provides good mechanical and thermomechanical stability to the membrane. Further, the continuous and ordered nanochannels with well-tailored chemical structures were obtained by irradiation of heavy ions $Kr^{+17}$ with an energy of 1.75 MeV/nucleon on the heavy ion accelerator. The formation of these nanochannels led to the significant increase of proton conductivity at 50% Relative Humidity [6]. Also, FTIR and XPS measurement results show that ion irradiation eliminated the GO's surface oxygen chemical bonds (C=O, C-O), and led to the formation of C = C, C – C bonds, whereas these changes connected with an increase in conductivity [7].

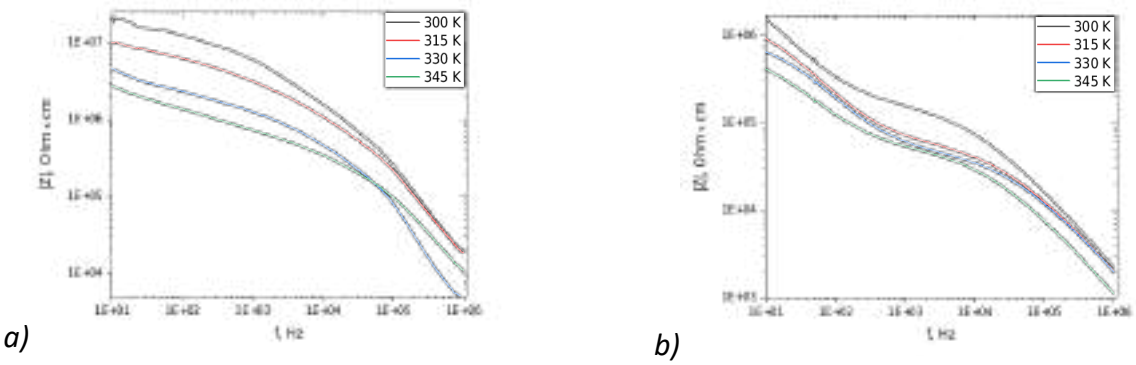


*a)* *b)*

*Figure 1. Frequency dependence of the impedance with a change in temperature, a) GO, b) GO + CMC*

**References:**

[1] Selyanchyn, O.; Selyanchyn, R.; Lyth, M.S. A Review of Proton Conductivity in Cellulosic Materials. Front. Energy Res. 8:596164. doi: 10.3389/fenrg.2020.596164

[2] Madih, K.; El-Shazly, A.H.; Elkady, M.F.; Aziz, A.N.; Youssef, M.E.; Khalifa, R.E. A facile synthesis of cellulose acetate reinforced graphene oxide nanosheets as proton exchange membranes for fuel cell applications. Journal of Saudi Chemical Society (2022) 26, 101435.

[3] Sharma, P.P.; Tinh, V.D.C.; Kim, D. Improved Oxidative Stability by Embedded Cerium into Graphene Oxide Nanosheets for Proton Exchange Membrane Fuel Cell Application. Membranes 2021, 11, 238. https://doi.org/10.3390/ membranes11040238

[4] Cai, Y.; Yue, Z.; Xu, S. A novel polybenzimidazole composite modified by sulfonated graphene oxide for high temperature proton exchange membrane fuel cells in anhydrous atmosphere. J. Appl. Polym. Sci. 2017, DOI: 10.1002/APP.44986

[5] K. P. Aimaganbetov, A. U. Aldiyarov, S. R. Zhantuarov, N. Zh. Almasov, E. I. Terukov, and N. S. Tokmoldin; A Low Temperature Cell for High Frequency Electrophysical Measurements of Semiconductor Devices, Instruments and Experimental Techniques, 2021, Vol. 64, No. 6, pp. 886–890. DOI: 10.1134/S0020441221050146

[6] He, G.; Chang, C.; Xu, M.; Hu, S.; Li, K.; Zhao, J.; Li, Z.; Li, Z.; Yin, Y.; Gang, M.; Wu, H.; Yang, X.; Guiver, M.D.; Jiang, Z. Tunable Nanochannels along Graphene Oxide/Polymer Core–Shell Nanosheets to Enhance Proton Conductivity. Adv. Funct. Mater. 2015, 25, 7502–7511.

[7] Malinsky, P.; Mackova, A.; Miksova, R.; Kovacikova, H.; Cutroneo, M.; Luxa, J.; Bousa, D.; Strochova, B.; Sofer, Z. Graphene oxide layers modified by light energetic ions. Phys. Chem. Chem. Phys., 2017, 19, 10282.

## PP-I-53

# Selective Oxidation of Glycerol to Lactic Acid on Hybrid Pd-Bi@UiO-66-$HSO_3$ Catalyst

Kurmanova M.D., Kurmanbaeva K.A., Torbina V.V., Svetlichnyi V.A., Vodyankina O.V.
*Tomsk State University, Tomsk, Russia*
*vodyankina_o@mail.ru*

Currently, conventional methods of production of lactic acid, a valuable product for bio-renewable polymers, possess a number of disadvantages, including high cost of catalysts and the process duration [1]. The catalytic oxidation of glycerol is a promising method to produce lactic acid, which is a by-product in the manufacturing of biofuels. Usually, this reaction is realized at the excess of alkali in the reaction mixture [2]. However, from both an economic and environmental points of view, it is important to choose a catalyst for direct production of lactic acid from glycerol in a neutral aqueous medium.

It was found that the oxidative conversion of this polyol into lactic acid occurs via several stages, including oxidation with subsequent dehydration, and isomerization of the corresponding intermediates. Accordingly, the catalyst must possesses noble metal-based active sites that are able to catalyse the first stage of glycerol oxidation as well as Lewis and Brønsted acid sites participating in the consecutive stages of dehydration/isomerization of the intermediates. In the present work, a hybrid metal-organic framework (MOF) based on Zr-UiO-66 structure with $HSO_3$-substituted linkers is used as a support for bimetallic Pd-Bi particles.

The MOF was synthesized by mixing of zirconyl nitrate and terephthalic acid in DMFA with HCl addition as a moderator [3]. Then the UiO-66 sample was modified by $HSO_3$ groups using chlorosulfonic acid [4]. Metal particles were immobilized on the MOF by impregnation from two solvents [5] to prepare the Pd-Bi@UiO-66-$HSO_3$ hybrid catalyst with Pd /Bi ratio of 9/1 (2.5 wt% bimetals in the catalyst). For comparison, the pristine bimetallic Pd-Bi particles were obtained by pulsed laser ablation method with the same ratio of metals as in the hybrid sample.

The catalysts were tested under static conditions in a batch reactor at 100 °C at an oxygen pressure of 10 bar for 7 h. The used catalyst mass was 41 mg per 30 ml of 0.3 M glycerol solution. The composition of the products and glycerol in the reaction mixture was determined using the HPLC method.

The catalytic properties of the Pd-Bi nanoparticles prepared by PLA method, a mechanical mixture of Pd-Bi NPs and MOF as well as the hybrid Pd-Bi@UiO-66-$HSO_3$ catalyst were investigated. It was shown that the Pd-Bi@UiO-66-$HSO_3$ catalyst was characterized by the highest activity and selectivity due to porosity, effective spatial arrangement of active species on the surface, their structure and smaller size in comparison with Pd-Bi PLA dispersion. It was noticed that high conversion of glycerol observed for mechanical mixture of Pd-Bi NPs and

UiO-66-$HSO_3$ may be explained by the glycerol adsorption on the MOF surface as well as by non-selective glycerol transformation.

To study the reaction ability of Lewis and Brønsted acid sites at the dehydration/rearrangement stages, the dihydroxyacetone conversion was tested over the modified and unmodified MOF samples, i.e., UiO-66-$HSO_3$ and UiO-66. An increase in the UiO-66-$HSO_3$ catalyst loading increased the dihydroxyacetone conversion and the selectivity towards lactic acid. Taking into account that these reactions were rather slow under neutral conditions, the use of UiO-66 as a catalyst led to an increase in the dihydroxyacetone conversion and selectivity towards lactic acid. After modifying the MOF by $HSO_3$ groups, the selectivity towards lactic acid increased, while dihydroxyacetone conversion decreased due to a partial blockage of the active sites by $HSO_3$ groups. It was shown that dihydroxyacetone conversion and selectivity towards lactic acid increased at the temperature interval of 100-130 °C.

The reuse experiments over the UiO-66-$HSO_3$ catalyst showed that the dihydroxyacetone conversion and selectivity towards lactic acid decreased, which is connected with a decrease in the availability of the active acid sites of the modified MOF due to the adsorption of the reaction by-products during the first cycle. This assumption was confirmed by the IR spectroscopy data. According to the results of ICP AES, XRD, and low-temperature nitrogen adsorption, it was found that the crystal structure of the sample was preserved, and no new phases were observed after catalysis. Specific surface area of the catalyst decreased slightly after the first cycle.

Thus, the synthesized hybrid Pd-Bi@UiO-66-$HSO_3$ catalyst possesses a unique structure and nature of active sites for the oxidative conversion of glycerol into lactic acid in a neutral medium. Its catalytic properties depend on the sizes and location of the bimetallic Pd-Bi NPs on the surface relative to each other as well as to Lewis and Brønsted acid sites of UiO-66-$HSO_3$, which is confirmed by experiments with PLA Pd-Bi NPs with and without UiO-66 mixture. In addition, the catalyst retains its structure after catalysis and can be reused. The mechanism of the conversion of glycerol and intermediates will be discussed.

**Acknowledgement:** This work was supported by the Russian Science Foundation, grant 19-73-30026.

**References:**

[1] F. A. C. Martinez, E. M. Balciunas, J. M. Salgado, J. M. D. González, A. Converti, R. P. de Souza Oliveira, Trends in food science & technology 30 (2013) 70.
[2] L. S. Sharninghausen, J. Campos, M. G. Manas, R. H. Crabtree, Nature Communications 5 (2014) 1.
[3] V.V. Torbina at al. Catalysis Today 333 (2019) 47–53.
[4] C. G. Piscopo, Microporous and Mesoporous Materials 208 (2015) 30.
[5] S. Ten at al. Materials 13 (2020) 5471.

## PP-I-54

# Laser-Assisted Carbonization of Surface-Grown Ni-BDC towards Waste-Based Smart Materials

Kurtsevich E.A., Kogolev D.A., Postnikov P.S.
*Tomsk Polytechnic University, Tomsk, Russia*
*Katyacha95@mail.ru*

Polymer upcycling is a modern direction for the creation of smart materials. Nowadays polyethylene terephthalate (PET) is actively used for the production of different materials and goods due to technological properties (transparency, high strength, plasticity, high barrier properties). Unfortunately, widespread its broad application provides increasing stress on the environment.

PET consists of terephthalic acid (TA) as a main structural motif. TA serves as an organic linker in the one of the most common classes of metal-organic frameworks (MOFs), such as Ni-BDC. Ni-BDC-based MOFs may be used as electrode materials. Carbonization is a necessary process for such applications. It converts semiconductive Ni-BDC to conductive Ni@C [1 – 3].

Here, we developed the laser-assisted method of Ni-BDC carbonization on the surface of PET with formation of conductive material.

The general scheme of Ni-BDC carbonization is shown in Fig. 1. The Nelder-Mead method was used for the optimization of Ni-BDC carbonization. We varied the parameters of laser power and movement speed until the lowest value of sample resistivity was obtained. After surface carbonization, the resistivity of samples was measured using the four-point probe technique. The best surface resistance of Ni@C was equal 12,2±2,5 Ω/sq. Optical image, SEM images and Nelder-Mead`s scheme are presented in Fig. 2.

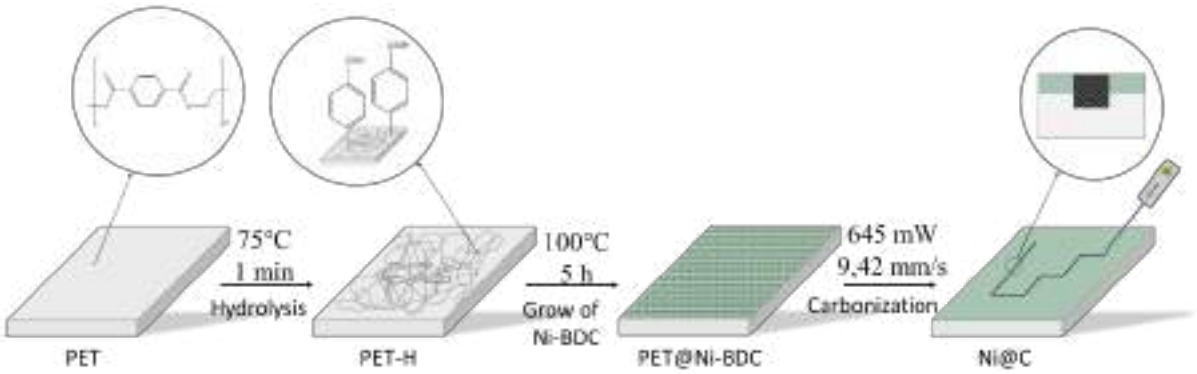


*Fig. 1. The principal scheme of Ni-BDC carbonization on PET surface*

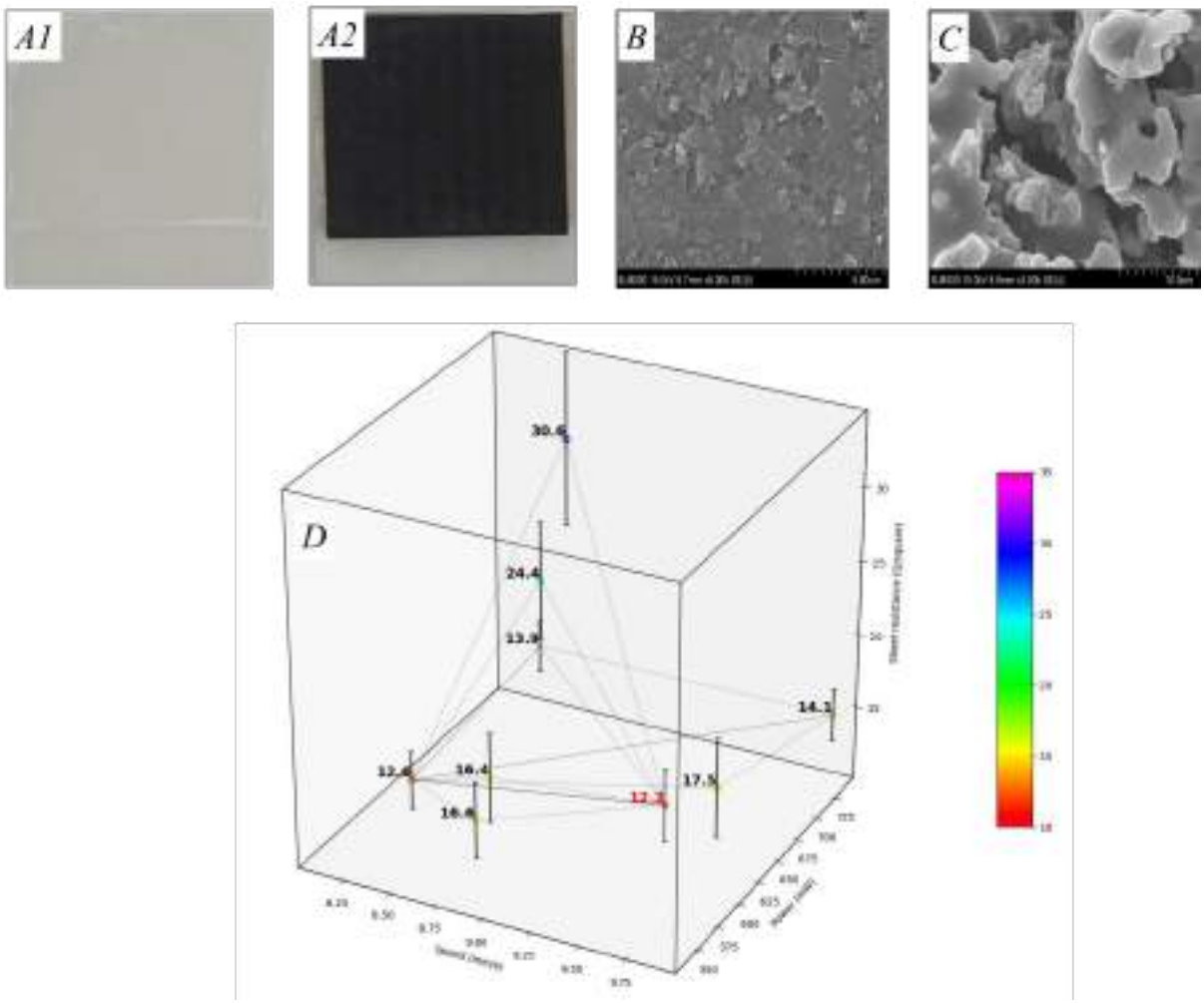


*Fig. 2. Images of material as before (A1) and after (A2) laser treatment, SEM images of PET@Ni-BDC (B) and Ni@C (C), the scheme of Nelder-Mead`s optimization (D)*

Thus, the developed method allows obtaining prospective electrode materials with high conductivity based on PET waste.

**Acknowledgement:** This work was supported by the Ministry of Education and Science of Russia, Agreement № 075-15-2022-244.

**References:**

[1] Z. Chen et al., J. Mater. Chem. A. 7 (2019) 14971.
[2] G. Zhao et al., Anal. Chem. 94 (2022) 10557.
[3] D. Kogolev et al., J. Mater. Chem. A. 11 (2023) 1108.

## PP-I-55

# Synthesis, Growth and Luminescence Properties of Rare Earth Borates $KSrY(BO_3)_2:R^{3+}$ (R=Ce, Tb, Er)

Kuznetsov A.B.[1], Zholdas Y.A.[2], Kokh K.A.[1], Gorelova L.A.[3], Sofich D.O.[4], Kokh A.E.[1]

*1 – Sobolev Institute of Geology and Mineralogy SB RAS, Novosibirsk, Russia*

*2 – Al-Farabi Kazakh National University, Almaty, Kazakhstan*

*3 – Saint Petersburg State University, Saint Petersburg, Russia*

*4 – Vinogradov Institute of Geochemistry SB RAS, Irkutsk, Russia*

*ku.artemy@igm.nsc.ru*

Today an attention of scientific community is directed towards quadruple borate systems $R_2O_3$–MeO-$M_2O$–$B_2O_3$ (where M=alkali metal, N=alkaline earth metal, R=rare-earth element). This is due to the large number of compounds promising as nonlinear optical crystals, phosphors etc. Among the recently opened compounds there are $K_7MR_2(B_5O_{10})_3$, $MNR(BO_3)_2$, $MNRB_6O_{12}$, $Li_3Ba_4Sc_3B_8O_{22}$, $LiNR_2(BO_3)_3$, $LiCaR_5(BO_3)_6$ and other. Despite the wide range of crystal structures, most of the compounds have a centrosymmetric layered structure. Therefore, that may be of interested as phosphors for the range from IR to near UV. Layered structure contributes to the improvement of the borate compounds optical properties.

$NaBaR(BO_3)_2$ was one of the first compound in new $MNR(BO_3)_2$ family. This compound crystallizes in the space group $R\bar{3}c$ and has polymorphic transformation of the order-disorder type at 775 °C (Sc) and 375 °C (Y). A similar behavior was shown for the NaSrR(BO3)2 family of compounds, which has a transition from low-temperature C2/c to high-temperature $R\bar{3}$ in the temperature range from 457.7 °C (Y) to 548.4°C (Lu). It should be noted that in low-temperature modifications rare-earth elements have distorted octahedral positions, whereas in high-temperature modifications polyhedra have the shape of a regular octahedron. However, for three cationic compounds with potassium $KNR(BO_3)_2$ and lithium $LiNR_2(BO_3)_3$ no such transitions were noted

In this work the structural features, thermal and optical properties of $KSrY(BO_3)_2:R^{3+}$ (R=Ce, Tb, Er) solid solutions were considered. The choice of the $R^{3+}$ atom ($R^{3+}$ =Ce, Tb, Er) as a doping element is due to the fact that such compounds have a high luminescence intensity in different light spectrum region. Thus, it is possible to obtain a phosphor in the UV ($Ce^{3+}$), visible ($Tb^{3+}$), or IR ($Er^{3+}$) spectral region. However, due to an electronic structure, one of the main problems of compounds with terbium and cerium is a tendency to oxidation 4+ state. As a rule, compounds containing 4+ are not luminophores and those with $Tb^{4+}$ are not transparent in the visible region. A main result of this work consists in the elaboration of synthesis techniques providing +3 oxidation state for all dopants under study.

**Acknowledgement:** This work was supported by state assignment of IGM SB RAS.

## PP-I-56

# Effect of Annealing on the Characteristics of Polymer Nanocomposites

Lebedev O.V.[1], Golubev E.K.[1], Kurkin T.S.[1], Piskarev M.S.[1], Goncharuk G.P.[1], Nepomnyashchikh V.V.[1], Yablokov M.Yu.[1], Shchegolikhin A.N.[2], Ozerin A.N.[1]

*1 – Enikolopov Institute of Synthetic Polymer Materials Russian Academy of Sciences, Moscow, Russia*

*2 – N. M. Emanuel Institute of Biochemical Physics Russian Academy of Sciences, Moscow, Russia*

*oleg.lebedev@phystech.edu*

The effect of change of morphology of multicomponent polymer composites with time is well known and was a subject of thorough investigations in the past years [1]. Especially of interest can be composites modified with functional nanoparticles, such as carbon nanoparticles, since migration of such nanoparticles to the interface between different polymer phases in the composites can significantly change functional characteristics of the material, e.g., electrical conductivity. As it was demonstrated earlier, electrical conductivity of polymer nanocomposites based on different types of thermoplastics and filled with different types of electrically conductive fillers steadily increases if to measure it in real time while annealing the composites in a closed mold at temperature above the melting point of the chosen polymer matrix [1]. It was attributed to the migration of the nanosized filler to the boundaries of the composite melts.

In this work, characteristics of different polymer composites based on such commonly used thermoplastics as polypropylene (PP) and polyethylene (PE) filled with such fillers as carbon black (CB) and nanodiamond soot (NDS) were investigated. NDS is a filler of a special interest since depending on its synthesis parameters its properties can be varied due to the changes of the structure and composition of the filler [2].

The time dependencies of characteristics of polymer composites were obtained by measuring the characteristics after different periods of annealing of the polymer materials at 200°C in a closed mold. The investigated characteristics were the following: electrical conductivity; tribological properties (friction coefficient, contact temperature, wear); mechanical characteristics in isopropanol/water mixture medium for different , adhesion characteristics (peel resistance, surface energy), microhardness, FTIR spectroscopy, viscometry, and scanning electron microscopy.

It can be seen in Fig.1 that such characteristics as yield stress (Fig.1a), measured for samples submerged into isopropanol, and peel resistance (Fig.1b) depend on time of annealing even if to consider the changes attributed to changes in the polymer matrix itself. The character of changes depends on both filler type and its content in the polymer matrix. For example, it can be seen that CB and NDS have an opposite effect on the characteristics depending on the annealing time.

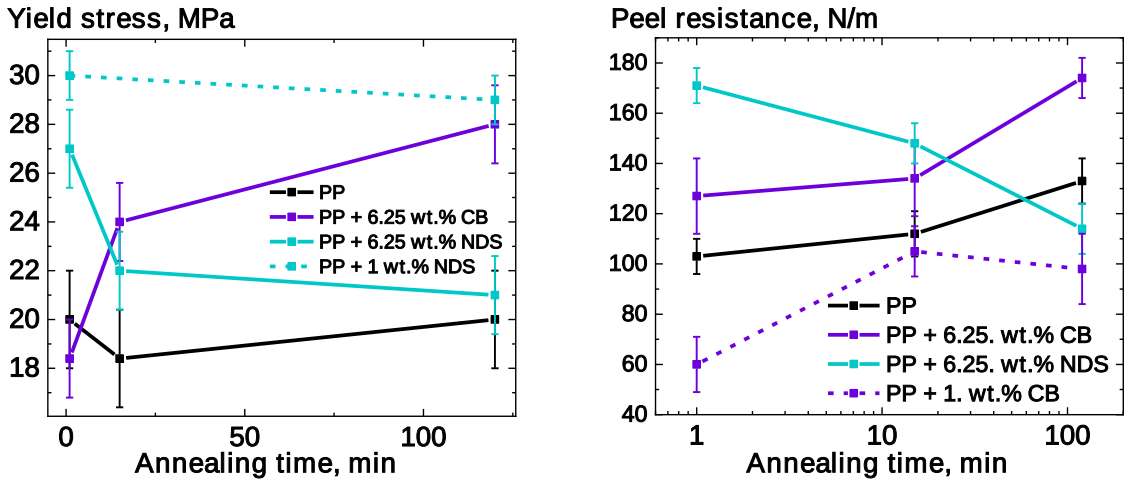


*Fig. 1. (a) Yield strength and (b) peel resistance of composites based on PP filled with different weight fractions of CB and NDS versus time of annealing at 200°C in a closed mold.*

Overall, it was noted that the changes in characteristics of the polymer composites with annealing time do agree with the assumption of enrichment with nanoparticles of the surface layers of the composites melts due to the nanoparticles migration process as it was discussed in [1] independent of the type of polymer matrix (PP or PE) or filler (CB or NDS) used. The obtained results correspond to the data obtained using more direct approaches for investigation of the distribution of the nanosized carbon filler in the surface layer. Such methods included electron microscopy, Raman scattering, and time-of-flight mass spectrometry for secondary ions. Special approaches based on Raman scattering and mass spectrometry were developed to be able to directly observe the filler concentration profile in a composite surface layer, demonstrating its enrichment [3].

The results of the work demonstrate that by careful consideration of the type of a polymer matrix, filler type and its content in a polymer composite, and parameters of mixing and postprocessing of the mixtures it is possible to predict the trajectory of further changes of different characteristics of the polymer composite material with time. Especially it can be of importance if the composite material are subjected to an additional treatment at elevated temperatures.

**Acknowledgement:** The reported study was funded by RSF according to the research project № 22-13-00359.

**References:**

[1] O.V. Lebedev, G.P. Goncharuk, and A.N. Ozerin, Polymers 13 7 (2021) 1030.
[2] O.V. Lebedev, T.S. Kurkin, E.K. Golubev, A.L. Vasiliev, A.K. Gatin, G.P. Goncharuk, and A.N. Ozerin, C 8 4 (2022) 69.
[3] M.Yu. Yablokov, A.N. Shchegolikhin, O.V. Lebedev, G.P. Goncharuk, and A.N. Ozerin, Russ. Chem. Bull. 70 9 (2021) 1816–1821.

## PP-I-57

# Synthesis and Characterization of Stretchable Polyurethane through Movable Polyrotaxane-Based Sliding Effect

Chaijun Lee[1], Md Hasan Turabee[1], Jinwoong Jung[2], Ildoo Chung[1]
*1 – Department of Polymer Science and Engineering, Pusan National University, Busan 46241, Korea*
*2 – Dongah Chemical Co., ltd, Yangsan, Korea*
*idchung@pusan.ac.kr*

Mechanically strong polymer has gained popularity in recent years because of their potential applications. However, synthesis of such polymer is still a challenge because of low fatigue resistance. In this study, highly stretchable low covered movable slide-ring polymer gel was synthesized by crosslinking with diisocyanate and end-capped beta cyclodextrin (CD) polyrotaxane. $^{1}$HNMR and FTIR spectroscopies were used to characterize the polyrotaxane. The formation of polyurea polypropylene glycol (PPG) was also confirmed by GPC. The slide ring movement of crosslinked CD on PPG polyurea urethane backbone allow to stretch without deformation. The tensile strength of the polymer gel was increased significantly with compared to non-crosslinked polyrotaxane. These unique properties of the resulting gels potentially act as flexible materials and create new opportunities for biomedical applications.

*(a)* *(b)*

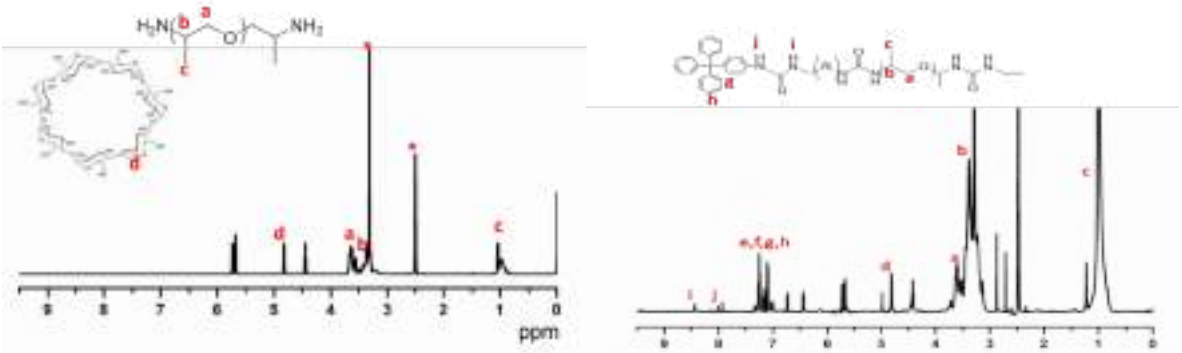


*Fig. 1. 1HNMR spectrum of (a) PPG-ϐCD, (b) PPG-ϐCD-PU-MDI-END.*

*(a)* *(b)*

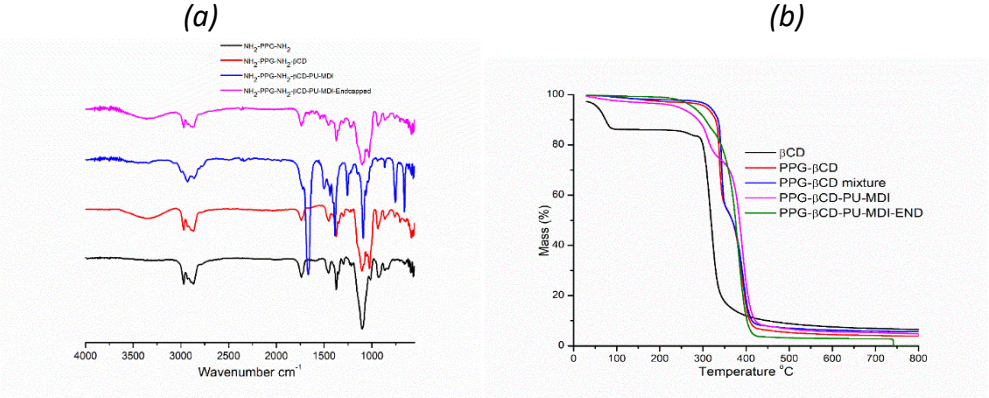


*Fig. 2. (a) FTIR Spectra of polymer and polyrotaxane., (b) TGA curve of beta cyclodextrin, PPG-ϐCD, PPG and ϐCD mixture, PPG-ϐCD polyurea urethane and End capped polyrotaxane.*

**Acknowledgement:** This work was supported by Technology Innovation Program (20011422) funded by the Ministry of Trade Industry & Energy (MOTIE, Korea)

**References:**

[1] Akira Harada, Jun Li & Mikiharu Kamachi, “The molecular necklace: a rotaxane containing many threaded a-cyclodextrins” , NATURE, 1992, VOL 356, 325-327.
[2] Lan Jiang, Chang Liu, Koichi Mayumi, Kazuaki Kato, Hideaki Yokoyama, and Kohzo Ito, “Highly Stretchable and Instantly Recoverable Slide-Ring Gels Consisting of Enzymatically Synthesized Polyrotaxane with Low Host Coverage”, Chem. Mater. 2018, 30, 5013−5019.

## PP-I-58

# Synthesis and Characterization of Polyrotaxane based on Mono-6-Tosyl-β -Cyclodextrin

Chaijun Lee[1], Jihyun Lee[1], Jinwoong Jung[2], Ildoo Chung[1]
*1 – Department of Polymer Science and Engineering, Pusan National University, Busan 46241, Korea*
*2 – Dongah Chemical Co., ltd, Yangsan, Korea*
*Leecj0928@pusan.ac.kr*

β-Cyclodextrin(β-CD) is a type of cyclic oligosaccharide used in various fields such as drug delivery, gene therapy, catalyst, chemical sensor, and liquid crystal. Mono-6-deoxy-6-(p-tolylsulfonyl)-β-cyclodextrin (TsO-β-CD) was synthesized by replacing one hydroxyl group among 21 hydroxyl groups in β-CD under various pH conditions using p-toluenesulfonyl chloride(p-TsCl),and used to synthesize polyrotaxane by threading TsO-β-CD on PPG-diamine with a molecular weight of 2000, followed by end capping using Trt-Gly-OH, N-Hydroxysuccinimide (NHS), ethylene dichloride (EDC). The synthesized CD derivatives and polyrotaxane were characterized by $^{1}$HNMR and FTIR spectroscopies.

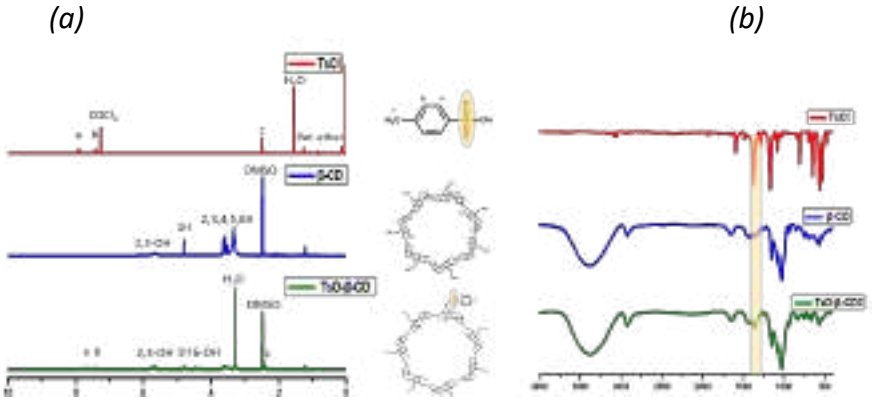


*Fig. 1. (A)1H NMR and (B)FT-IR spectra of p-TsCl, β-CD and TsO-β-CD.*

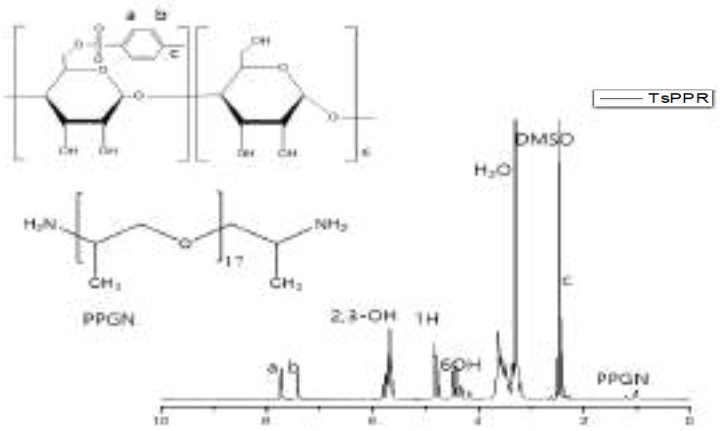


*Fig. 2. $^{1}$H-NMR spectroscopies of Polyrotaxane.*

**Acknowledgement:** This work was supported by Technology Innovation Program (20011422) funded by the Ministry of Trade Industry & Energy (MOTIE, Korea)

**References:**

[1] Liu, H., Qi, C., Feng, Z. et al. Adsorption of trace thorium(IV) from aqueous solution by mono-modified β-cyclodextrin polyrotaxane using response surface methodology (RSM). J Radioanal Nucl Chem 314, 1607–1618 (2017).
[2] Xu, L.; Xing, C.-Y.; Ke, D.; Chen, L.; Qiu, Z.-J.; Zeng, S.-L.; Li, B.-J.; Zhang, S. Amino-Functionalized β-Cyclodextrin to Construct Green Metal−Organic Framework Materials for CO2 Capture. ACS Appl.Mater. Interfaces 2020, 12, 3032−3041.

## PP-I-59

# Synthesis and Characterization of Flexible and Strong Polyurethane using PPG-βCD-Polyrotaxane as a Chain Extender

JiHyun Lee[1], SuMin Kwak[1], KyungMan Choi[2], Ildoo Chung[1]
*1 – Pusan National University, Busan, Korea*
*2 – Korea Institute of Footwear and Leather Technology, Busan, Korea*
*jh11369@pusan.ac.kr*

Highly stretchable polymer have getting much attention because of their unique properties. In this study, a highly stretchable polymer was synthesized by crosslinking polyurethane with pre-synthesized polyrotaxane from polypropylene glycol (PPG) with low covered cyclodextrin (CD) which acts as both chain extender and crosslinker. Polyrotaxane was used to synthesized by threading beta cyclodextrin (β-CD) along the axis of PPG-diamine polymer backbone followed end capped with 2,4,6-trinitrobenzene sulfonic acid (TNBSA). The synthesized polyurethane and polyrotaxane were characterized by $^{1}$HNMR and FTIR spectroscopies. Coverage of polyrotaxane was adjusted by mole ratio of PPG and β-CD. DSC and TGA were used to characterize thermal properties of polyrotaxane and polyurethane.
Polyrotaxane (PR) which has multiple rings threaded onto a molecular axle can move freely[1]. So, it has stretch property[2]. The number of β-CD in polyrotaxane decreased with decreasing the mol ratio of β-CD and PPG diamine. The PPG-βCD-PR was characterized by NMR and FT-IR spectroscopies. Especially, PPG-βCD-PR was characterized by UV-Vis for terminal group analysis of the peak of nitro group at 255 nm. PU also characterized by FT-IR spectroscopies. The isocyanate peak at 2269 $cm^{-1}$ was disappeared. Through this, it can be seen that the polymers are well synthesized. Also, as the ratio of polyrotaxane increased, both tensile strength and elongation were increased.

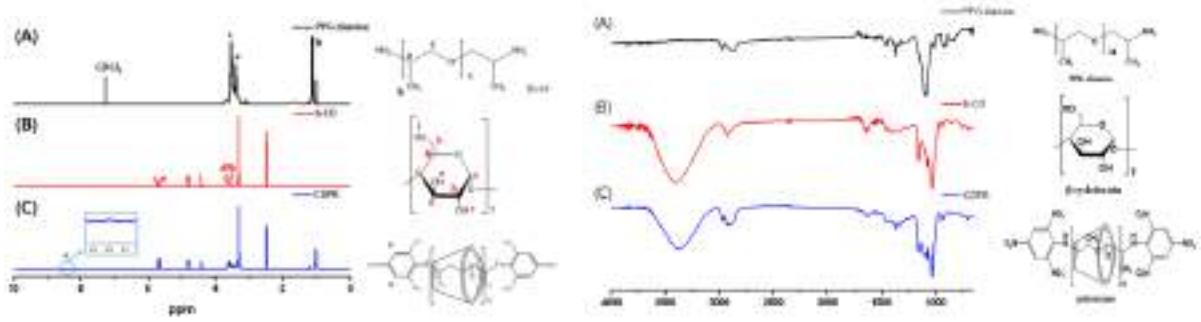


*{A}* *(B)*

*Fig. 1. A)1H NMR and (B)FT-IR spectra of (A) PPG diamine, (B) β-CD, and (C) polyrotaxane.*

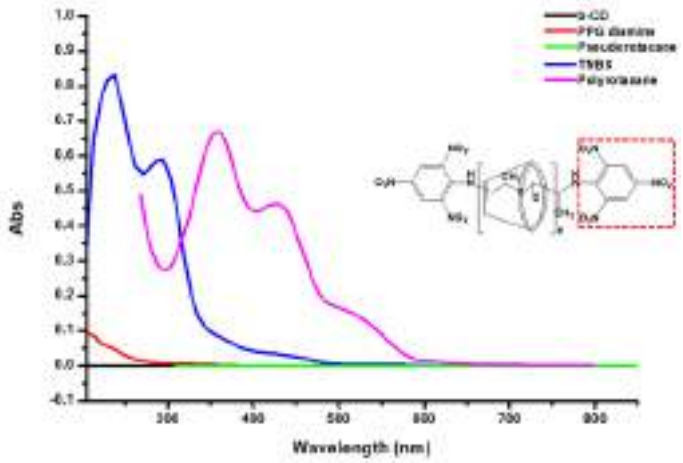


*Figure 2. FT-IR spectra of Prepolymer and Polyurethane.*

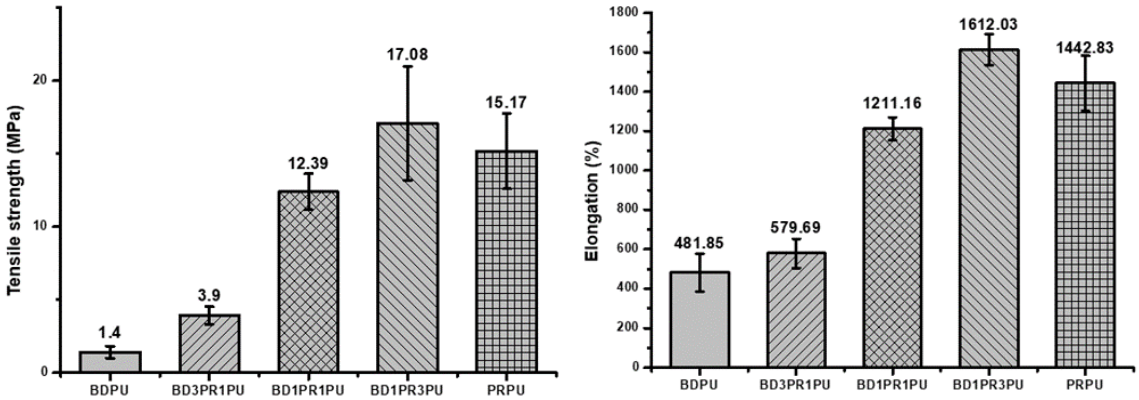


*(A)* *(B)*

*Figure 3. (A)Tensile strength and (B)Elongation of Polyurethane.*

**Acknowledgement:** This work was supported by the Technology Innovation Program (20011422) funded by Ministry of Trade, Industry & Energy (MOTIE, Korea).

**References:**

[1] Hakariya, M.; Arisaka, Y.; Masuda, H.; Yoda, T.; Tamura, A.; Iwata, T.; Yui, N. Tissue Adhesion-Anisotropic Polyrotaxane Hydrogels Bilayered with Collagen. Gels 2021, 7, 168. https://doi.org/10.3390/gels7040168

[2] Noda, Y., Hayashi, Y. and Ito, K. (2014), From topological gels to slide-ring materials. J. Appl. Polym. Sci., 131, 40509, doi: 10.1002/app.40509

## PP-I-60

# Synthesis and Characterization of Highly Stretchable Polyurethane Based on Polyrotaxane Composed of Movable Non-Covalent Bonds

JiHyun Lee[1], SuMin Kwak[1], JinWoog Chung[2], Ildoo Chung[1]
*1 – Pusan National University, Busan, Korea*
*2 – Dongah Chemical Co., ltd, Yangsan, Korea*
*jh11369@pusan.ac.kr*

The study of physically strong and stretchable polymers is still a challenge. In this study, highly stretchable low covered movable slide-ring polymer was synthesized by crosslinking with diisocyanate and poly(propylene glycol)-dimethyl-β-cyclodextrin polyrotaxane. The slide ring movement of crosslinked DM-β-CD on polyurethane backbone allows to stretch without deformation. These unique properties of the resulting gels potentially act as flexible materials and create new opportunities for biomedical applications[1, 2]. The low covered polyrotaxane and polyurethane were characterized by FT-IR, $^{1}$H-NMR and UV-vis spectroscopies. In addition, and the elongation of polyurethane according to the content of polyrotaxane was shown through tensile strength measurement.

The polyrotaxane was synthesized by poly(propylene glycol) and DM-β-CD(dimethyl-β-cyclodextrin)[3]. The polylotaxane was introduced into polyurethane as a chain extender and a crosslinking agent to synthesize polyurethane with excellent flexibility. In 1H-NMR data, the peak of DM-β-CD and the peak of PPG were shown in pseudo polyrotaxane, and the TNBS peak of polyrotaxane was also shown. Also, in FT-IR data, successful synthesis was confirmed through the presence of the O-H peak of pseudo polyrotaxane and the N-O peak of polyrotaxane. It was confirmed through an optical microscope that phase transition by LCST appeared in pseudo polyrotaxane[4]. The thermal characteristics of DM-β-CD and complex were confirmed through DSC. Tm of DM-β-CD appears at 75°C, but Tm increases to 100°C as complex is formed, and in the case of physical mixture, Tm is lower than complex. In DSC datas of pseudo polyrotaxane and polyrotaxane, Tc and Tm of PPG were shown, and the crystal peak of PPG was not shown in mixture. In the case of PU, a Tg peak appeared at -25°C, and in the case of PRPU incorporating polyrotaxane, it was confirmed that Tc and Tm peaks appeared due to polyrotaxane.

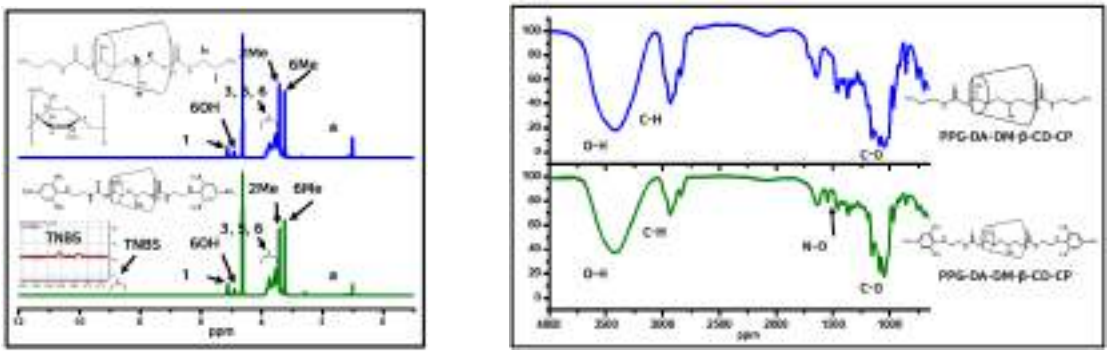


*(A)* *(B)*

*Fig. 1. (A)1H NMR and (B)FT-IR spectra of polyrotaxane.*

*Fig. 2. Temperature-dependent phase shifts of polyrotaxane.*

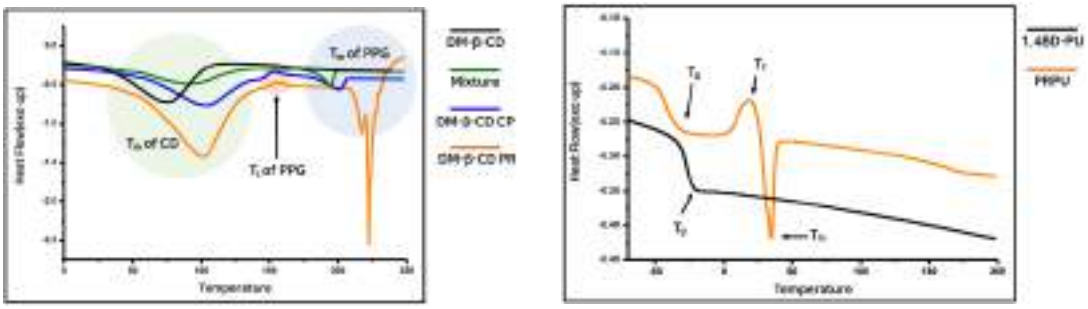

*(A)* *(B)*

*Fig. 3. DSC curves of (A)polyrotaxane (B)polyurethane.*

**Acknowledgement:** This work was supported by the Technology Innovation Program (20011422) funded by Ministry of Trade, Industry & Energy (MOTIE, Korea).

**References:**

[1] Ma, Xing and Zhao, Yanli. Biomedical Applications of Supramolecular Systems Based on Host–Guest Interactions. Chemical Reviews. 2015, 115 (15), 7794-7839

[2] Kohei Koyanagi, Yoshinori Takashima, Hiroyasu Yamaguchi, Akira Harada. Movable Cross-Linked Polymeric Materials from Bulk Polymerization of Reactive Polyrotaxane Cross-Linker with Acrylate Monomers. Macromolecules. 2017, 50 (15), 5695-5700

[3] Taishi Higashi, Jun Li, Xia Song, Jingling Zhu, Masatoshi Taniyoshi, Fumitoshi Hirayama, Daisuke Iohara, Keiichi Motoyama, and Hidetoshi Arima. Thermoresponsive Formation of Dimethyl Cyclodextrin Polypseudorotaxanes and Subsequent One-Pot Synthesis of Polyrotaxanes, ACS Macro Letters. 2016, 5 (2), 158-162

[4] Tamura, A.; Nishida, K.; Yui, N. Tailoring the Temperature-Induced Phase Transition and Coacervate Formation of Methylated β-Cyclodextrins-Threaded Polyrotaxanes in Aqueous Solution, Macromolecules. 2016, 49, 16, 6021–6030

## PP-I-61

# SILD Synthesis of $Mn_3[Fe(CN)_6]_2 \cdot nH_2O$ Nanosheets as Novel 2D Analogue of Prussian Blue for High-Performance Metal-Ion Batteries

Kaneva M.V., Tenevich M.I., Lobinsky A.A.
*Ioffe Institute, Saint Petersburg, Russia*
*lobinski.a@mail.ru*

The Prussian blue analogues (PBAs) is a prospective candidates as electrode materials for metal-ion batteries due to its facile synthesis, open framework structures, high specific surface areas, tuneable composition, designable topologies and rich redox couples [1;2]. However, its poor electrical conductivity and mechanical properties are the main factors limiting its use.

The solution to this problem may consist in obtaining 2D nanocrystals of PBAs with a morphology of the so-called "nanosheets", which is due to a set of their unique physical and chemical properties. The flat 2D structure of such materials provides a sufficient number of active adsorption centres. Another key characteristic of 2D materials is their ultra-small thickness, on the order of a few nanometres, so charge carriers can travel extremely short distances from the volume to the surface, while significantly improving electronic conductivity [3].

The present study 2D nanosheets of $Mn_3[Fe(CN)_6]_2 \cdot nH_2O$ synthesized on nickel foam substrate (Fig. 1), exhibited high capacity performance. We described a simple and direct technique for producing 2D $Mn_3[Fe(CN)_6]_2 \cdot nH_2O$ nanosheets using successive ionic layer deposition (SILD) from aqueous solutions of $MnSO_4$ and $K_3[Fe(CN)_6]$ and investigated of its electrochemical performance.

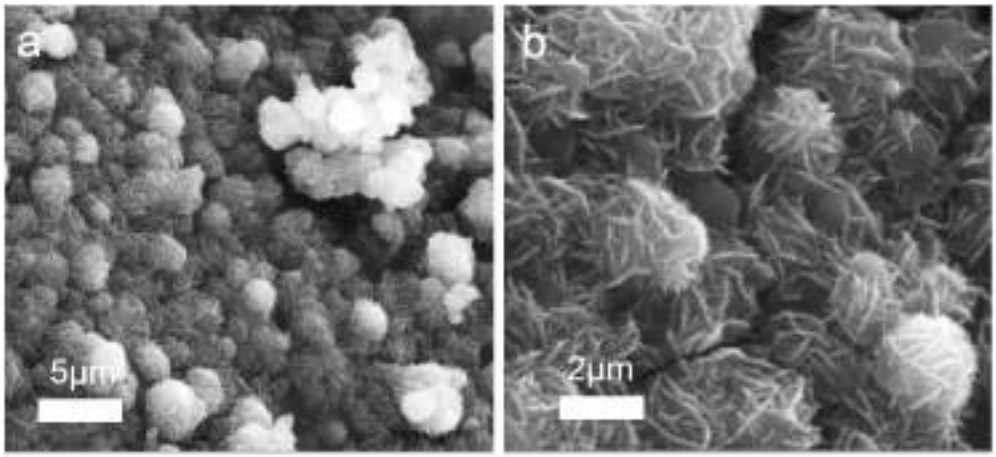


*Fig. 1. SEM images of $Mn_3[Fe(CN)_6]_2 \cdot nH_2O$ with different magnification*

The SILD method allows regulating a wide range of synthesis conditions (the number of processing cycles, the processing sequence, the processing time in reagent solutions, the concentration, anionic composition and pH of reagent solutions, the heating of the obtained samples, etc.) to influence the morphology, composition and structure of the synthesized compounds, as well as to obtain various 1D, 2D and 3D nanomaterials, which is important for creating of high-effective electroactive materials [4].

## PP-I-61

Obtain $Mn_3[Fe(CN)_6]_2 \cdot nH_2O$ nanosheets are examined as cathode materials for metal-ion batteries and supercapacitors. As a result, $Mn_3[Fe(CN)_6]_2 \cdot nH_2O$/nickel foam showed excellent performance when utilized as an cathode of supercapacitors, and its specific capacities were 1032 and 327.5 F/g at 1 A/g and 230 F/g at 0.1 A/g in 1M NaOH, 1M $Na_2SO_4$ and 1M $ZnSO_4$ aqueous electrolytes, respectively.

**Acknowledgement:** This work was supported by the Russian Science Foundation, grant 22-23-20138.

**References:**

[1] K. Hurlbutt, S. Wheeler, I. Capone, M. Pasta, Joule 2 (2018) 1950–1960.
[2] X. Wu, Y. Ru, Y. Bai, G. Zhang, Y. Shi, H. Pang, Coord. Chem. Rev. 451 (2022) 214260.
[3] A. Lobinsky, V. Popkov, Electrochem. Mater. Technol. 1 (2022) 20221008.
[4] V.P. Tolstoy, Russ. Chem. Rev. 75 (2006) 161.

## PP-I-62

# Mechanochemical Synthesis of Magnesium Substituted Hydroxyapatite

Makarova S.V., Bulina N.V. Vinokurova O.B.
*Institute of Solid State Chemistry and Mechanochemistry SB RAS, Novosibirsk, Russia*
*makarova@solid.nsc.ru*

Hydroxyapatite (HA) belongs to a class of important bioactive materials due to its chemical similarity to human bone tissue and teeth. HA is an inorganic material with the chemical composition $Ca_{10}(PO_4)_6(OH)_2$ and has a hexagonal structure with the symmetry space group $P6_3/m$ [1]. HA is widely used in various fields of medicine such as dentistry and maxillofacial surgery. The introduction of various ions into the HA structure improves the physicochemical properties of the material [2]. It is known that magnesium plays an important role in bone metabolism [3]. Magnesium deficiency can lead to decreased bone mass, slower bone growth, and osteoporosis. Magnesium-substituted apatite is mainly obtained by the precipitation method, which is a multi-stage process and requires subsequent product purification [4-5].

The purpose of this study was to explore the possibility of mechanochemical synthesis of magnesium-substituted HA with the participation of several sources of magnesium.

The process of mechanochemical synthesis of magnesium-substituted HA has been studied. A series of samples with different concentrations of magnesium ions was obtained. The synthesis was carried out in the AGO-2 planetary ball mill for 30 minutes. The initial reagents were taken in a stoichiometric ratio based on the reactions 1-2. The magnesium oxide (reaction 1) and magnesium dihydrogen phosphate (reaction 2) were considered as a magnesium source.

(1) $6CaHPO_4 + (4-x)CaO + xMgO \rightarrow Ca_{10-x}Mg_x(PO_4)_6(OH)_2 + 2H_2O$

(2) $(6-2x)CaHPO_4 + (10-x)CaO + x(Mg(H_2PO_4)_2 \cdot 4H_2O) \rightarrow Ca_{10-x}Mg_x(PO_4)_6(OH)_2 + nH_2O$,

where x = 0.0 – 1.5

Table 1. Concentrations of HA and impurity phases of the as-synthesized powders

| Source of Mg | Degree of substitution x(Mg) | HA, % | $CaHPO_4$, % | MgO, % |
|---|---|---|---|---|
| – | 0 | 100 | – | – |
| MgO | 0.25 | 100 | – | – |
| | 0.5 | 99 | – | 1 |
| | 1.0 | 98 | – | 2 |
| | 1.5 | 86 | 10 | 4 |
| $Mg(H_2PO_4)_2 \cdot 4H_2O$ | 0.25 | 100 | – | – |
| | 0.5 | 100 | – | – |
| | 1.0 | 100 | – | – |
| | 1.5 | 100 | – | – |

Using X-ray phase analysis, it was found that, starting from a concentration x = 0.25, in the samples synthesized with the introduction of magnesium oxide (see reaction 1) there is a

phase of the unreacted reagent MgO (see Table 1). However, the lattice parameters of the HA phase in these samples decrease with increasing in the concentration of introduced magnesium. This is due to the fact that the ion size of the introduced magnesium cation ($r(Mg^{2+})$ = 0.89 Å) is smaller than the calcium cation ($r(Ca^{2+})$ = 1.00 Å). It should be noted that at x = 1.5, the tricalcium phosphate phase is formed, which is a product of HA decomposition [6]. This indicates the instability of the formed HA structure.

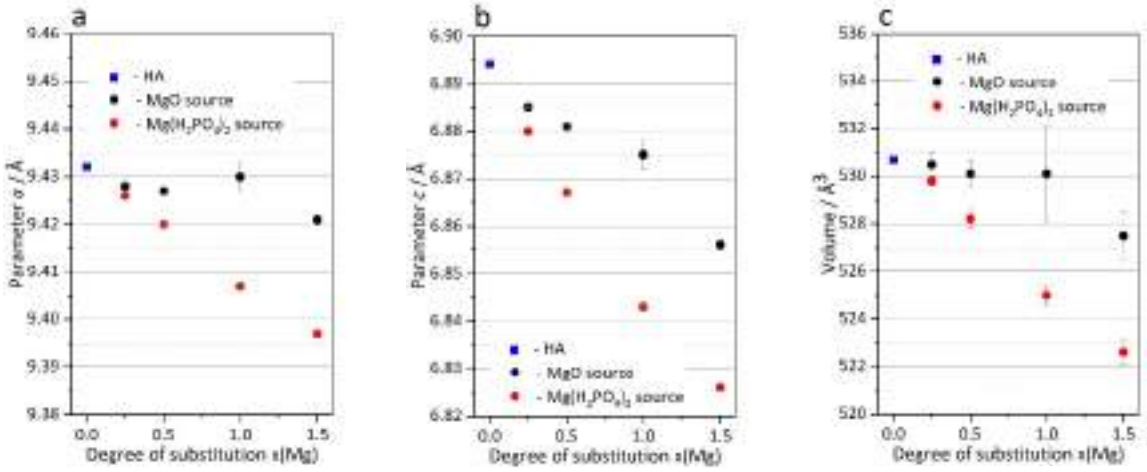


*Fig. 1. Evolution of structural parameters of the as-synthesized powders*

In the case of using magnesium hydrogen phosphate (see reaction 2) as the initial reagent, single-phase synthesis products were obtained, where the only phase is the HA phase. Moreover, the lattice parameters of this sample deviate significantly from the values of the unsubstituted HA.

It can be concluded that the local environment of the substituent cation in the initial reagent plays an important role in the formation of a strong structure of substituted HA. Therefore, the synthesis of magnesium-substituted HA proceeds better from magnesium phosphate than from its oxide. What is associated with the phosphate environment of the cation in the HA lattice.

**Acknowledgement:** The study was supported by a grant from the Russian Science Foundation (RSF), no. 21-12-00251.

**References:**

[1] R.S. Lee, M.V. Kayser, S.Y. Ali, J. Anat. 208 (2006) 13-19.
[2] M. Šupová, Ceram. Int. 41 (2015) 9203-9231.
[3] Si L. Han, W.J. Zhang, X.Q. Jiang, Chin. J. Dent. Res. 22 (2019) 93-104.
[4] L. Stipniece, K. Salma-Ancane, N. Borodajenko, M. Sokolova, D. Jakovlevs, L. Berzina-Cimdina, Ceram. Int, 40 (2014) 3261-3267.
[5] X. Yuan, B. Zhu, G. Tong, Y. Su, X. Zhu, J. Mater. Chem. B, 1 (2013) 6551-6559.
[6] M.V. Chaikina, N.V. Bulina, O.B. Vinokurova, K.B. Gerasimov, I.Y. Prosanov, N.B. Kompankov, O.B. Lapina, E.S. Papulovskiy, A.V. Ishchenko, S.V. Makarova, Ceram. 5 (2022) 404-422.

## PP-I-63

# Microdispersed $Ni_{1-x}Sn_x$ Alloys as Catalysts for Synthesis of Carbon Nanofibers

Maksimova T.A.[1,2], Popov A.A.[2], Varygin A.D.[2,3], Shivtsov D.M.[1,4], Bauman Y.I.[1], Mishakov I.V.[1,3], Shubin Y.V.[2,3], Vedyagin A.A.[1]

*1 – Boreskov Institute of Catalysis, Novosibirsk, Russia*

*2 – Nikolaev Institute of Inorganic Chemistry, Novosibirsk, Russia*

*3 –Novosibirsk State University, Novosibirsk, Russia*

*4 –Novosibirsk State Technical University, Novosibirsk, Russia*

*maksimova@catalysis.ru*

Nowadays, nanosized materials attract a great interest of investigators owing to a wide range of their practical application. Carbon nanomaterials (CNMs), in particular carbon nanofibers (CNFs) and carbon nanotubes (CNTs), take a special place among the diversity of carbon nanostructures. The conventional way to synthesize CNMs is based on catalytic pyrolysis of light hydrocarbons over nickel or nickel alloys (Ni-M) used as a catalyst. By varying the nature and concentration of the modifying metal (M), it is possible to improve significantly the activity and productivity of catalyst, as well as to "tune" the structural properties of produced carbon nanomaterial. Thus, both the development of new effective catalysts for CNM synthesis and search for an optimal way for CNMs production appear to be an actual problem to solve.

The authors have previously suggested the approach based on carbon erosion (CE) of bulk Ni-M alloys used as catalyst precursors for decomposition of hydrocarbon to produce CNF [1]. CE is known as a process of gradual and irreversible destruction of bulk metals and alloys, affected with prolonged exposure to a carburizing reaction medium at temperatures above 400°C [2]. CE process proceeds via several stages: 1) dissolution of atomic carbon in alloy volume, 2) graphite phase nucleation in the grain boundaries area, and 3) subsequent growth of the filamentous carbon. Carbon erosion ultimately results in complete disintegration (fragmentation) of the polycrystalline structure of a bulk alloy with the formation of large number of highly dispersed metallic particles, serving as CNF growth centres. It is important to note that catalytic systems resulting from CE process possess a higher productivity in relation to CNF synthesis compared to supported catalysts [3]. The presence of an alloy component M in the composition of Ni-catalyst can significantly promote its activity and slow down deactivation. In particular, the addition of 10-15 at. % copper to a nickel leads to an increase in activity and stability of Ni-catalyst in the ethylene pyrolysis reaction with the CNF production [4].

This work is focused on effect of tin addition on the activity of a nickel catalyst in the pyrolysis of light $C_2$-$C_4$ hydrocarbons to produce CNF material. A series of $Ni_{1-x}Sn_x$ ($0.0025 \div 0.25$) catalyst samples was synthesized by the thermolysis of multicomponent precursors, which makes it possible to obtain alloys in the form of microdispersed powders (see Fig. 1). The synthesized catalysts were tested in catalytic pyrolysis of ethylene ($C_2H_4/H_2$/Ar

mixture) and $C_2$-$C_4$/$H_2$ mixture using a quartz reactor equipped with a McBain balance at temperatures of 550-650°C.

It was shown that the addition of tin in a low concentration allows one to increase the activity of nickel catalyst in the process of catalytic pyrolysis of $C_2$-$C_4$ hydrocarbons: the most active samples appeared to be alloys with the Sn addition less than 1 at. % (see Fig. 1).

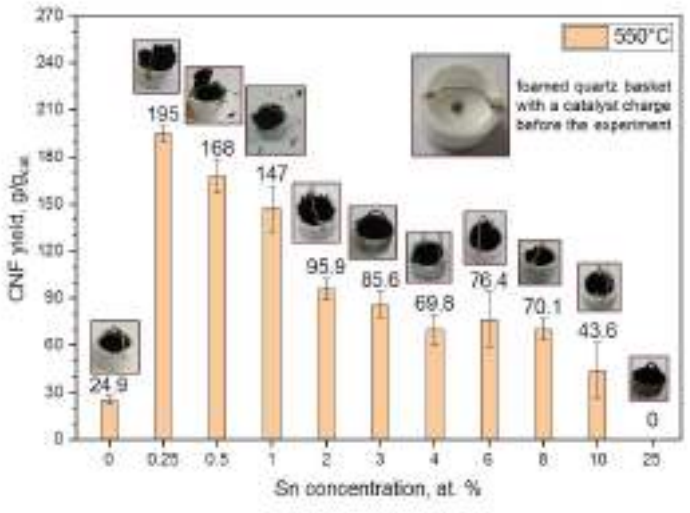


*Fig. 1. Effect of tin concentration in the $Ni_{1-x}Sn_x$ alloy on the CNF yield during the pyrolysis of ethylene ($C_2H_4/H_2/Ar$) at 550°C.*

According to TEM data (see Fig. 2), the morphology of the carbon material is represented by long submicron filaments (up to 150 nm) and nanofibers (d = 25-80 nm).

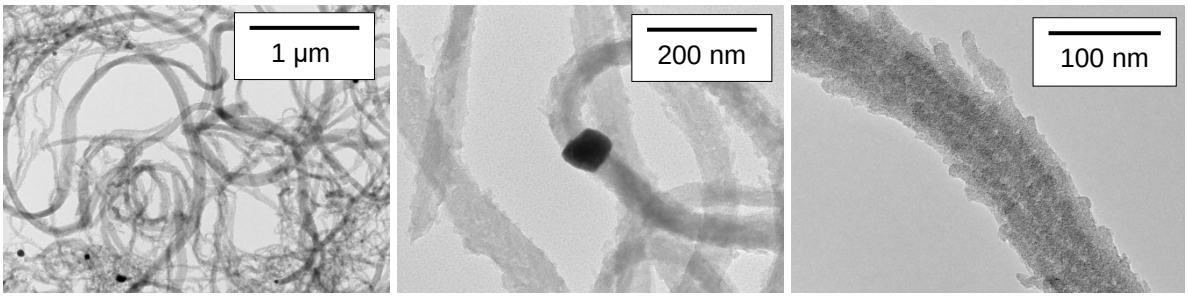


*Fig. 2. TEM images of the carbon material produced via ethylene pyrolysis at 600°C.*

The report will consider the structural and textural characteristics of the resulting carbon nanomaterial, as well as the kinetic regularities of the processes of its formation on designed $Ni_{1-x}Sn_x$ alloy catalysts.

**Acknowledgement:** This work was supported by the Russian Science Foundation, project № 21-13-00414.

**References:**

[1] I.V. Mishakov, A.A. Vedyagin, Y.I. Bauman, Y.V. Shubin, R.A. Buyanov, Carbon Nanofibers: Synthesis, Applications and Performance / Ed. C.-H. Lee. Nova Science Publishers: NY (2018) 77.
[2] H.J. Grabke, Materials and Corrosion 54 (2003) 736.
[3] Y.I. Bauman, I.V. Mishakov, D.V. Korneev, Y.V. Shubin, A.A. Vedyagin, R.A. Buyanov, Cat. Today 301 (2018) 147.
[4] S.D. Afonnikova, I.V. Mishakov, Y.I. Bauman, M.V. Trenikhin, Y.V. Shubin, A.N. Serkova, A.A. Vedyagin, Top. Catal. 2022 (in progress) https://doi.org/10.1007/s11244-022-01739-7

## PP-I-64

# Effect of the Modifying Ruthenium Additive on the Structure and Activity of Iron-Containing Catalysts

Markova M.E., Stepacheva A.A., Matveeva V.G., Sulman M.G.
*Tver State Technical University, Tver, Russia*
*mashulikmarkva@gmail.com*

The synthesis of hydrocarbons from carbon and hydrogen oxides is one of the most studied processes at present. The Fischer-Tropsch process makes it possible to obtain a wide range of gaseous, liquid and solid products. Modern research is mainly aimed at obtaining liquid gasoline-type hydrocarbons.

Fischer-Tropsch synthesis is a structure sensitive process [1], i.e. the molecular mass distribution of the reaction products strongly depends on the structure of the active sites of the catalyst, as well as on the particle size of the catalytically active phase. The study of the structure of the active sites of iron-containing catalysts has shown that iron in the catalyst is presented by a combination of various compounds, such as metallic iron, iron oxides and iron carbide. The most common tendency is that either $Fe_3O_4$ or the carbide phase exhibit catalytic activity in iron catalysts [2-4].

Iron-containing particles are prone to agglomeration during synthesis and drying. To prevent this process, various modification methods consisting in the addition of structural promoters (e.g. group VIII metals) are used. Ruthenium added to transition metals, in addition to catalytic behaviour, can be considered as a structural promoter.

In this paper, the synthesis of catalytic systems based on hyper-crosslinked polystyrene (HPS) by deposition under subcritical conditions is proposed. The effect of the addition of ruthenium compounds on the structural characteristics of an iron-containing catalyst has also been studied. The method of deposition under subcritical conditions makes it possible to obtain oxide forms of the metal-containing phase.

In the case of monometallic catalytic systems, a wide distribution of iron-containing particles by size was noted. This is associated with the formation of agglomerates of the metal-containing phase with an average diameter of 10-40 nm (Fig.1a). The addition of 1% by weight of ruthenium compounds to the system leads to a significant decrease in particle sizes to 4-5 nm (Fig.1b).

According to the data of elemental mapping, the joint deposition of iron and ruthenium salts leads to the formation of uniformly distributed metal compounds on the surface of hyper-crosslinked polystyrene (Fig. 2).

The catalytic properties of the synthesized samples were investigated in the liquid-phase Fischer-Tropsch synthesis. The addition of Ru to the Fe-containing catalyst was found to lead to an increase in the CO conversion, as well as the selectivity towards $C_5$-$C_{11}$ hydrocarbons. Being the structural promoter, Ru affects both the catalyst activity and selectivity of the process.

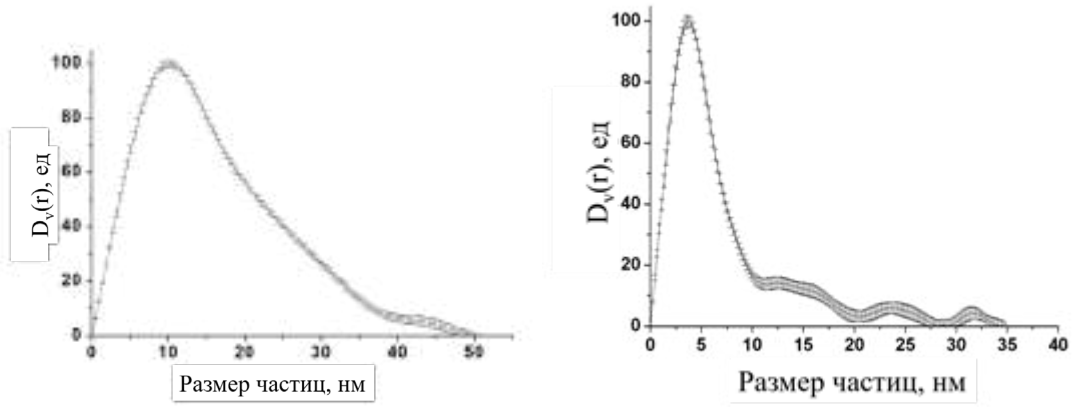


*Fig. 1. SAXS curves for the monometallic catalyst 2%Fe-HPS (a) and for the ruthenium-modified catalyst 2%Fe-1%Ru-HPS (b)*

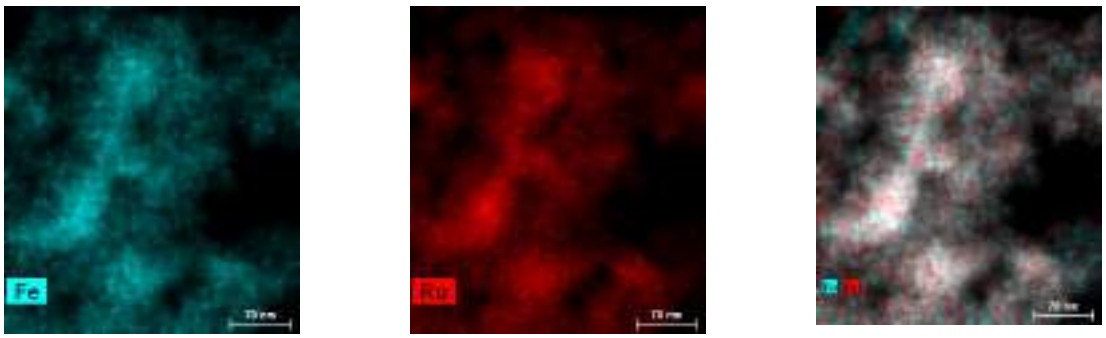


*Fig. 2 - Element mapping of the sample 2%Fe-1%Ru-HPS*

**Acknowledgement:** This work was supported by the Russian Science Foundation, grant 23-23-00653.

**References:**

[[1] J.-X. Liu, P. Wang, W. Xu, E.J.M. Hensen, Engineering. 3 (2017) 467.
[2] J. J. C. Geerlings, J. H. Wilson, G. J. Kramer, H. P. C.E. Kuipers, A. Hoek, H. M. Huisman, Appl. Catal. A. 186 (1999) 27.
[3] A. A. Adesina, R. R. Hudgins, P. L. Silveston, Catal. Today. 25 (1995) 127.
[4] D.V. Peron, A.J. Barrios, A. Taschin, I. Dugulan, C. Marini, G. Gorni, S. Moldovan, S. Koneti, R. Wojcieszak, J.W. Thybaut, M. Virginie, A.Y. Khodakov Appl. Catal. B. 292 (2021) 120141

## PP-I-65

# Novel Polyethylene Composite Materials, Obtained via *In-Situ* Ethylene Polymerization over the Titanium-Magnesium Catalyst Supported on Nano-Oxides and Carbon Nano-Materials

Matsko M.A.[1], Panchenko V.N.[1], Shundrina I.K.[2], Zakharov V.A.[1]
*1 – Boreskov Institute of Catalysis, Novosibirsk, Russia*
*2 – N.N. Vorozhtsov Novosibirsk Institute of Organic Chemistry, Novosibirsk, Russia*
*Matsko@catalysis.ru*

Polyethylene (PE) composite materials were synthesized by *in-situ* ethylene polymerization in the presence of titanium-magnesium catalyst (TMC) anchored on the surface of pre-dehydroxylated nanooxides ($ZrO_2$, $SiO_2$, $TiO_2$, globule and nano-fibers (Nafen™ (NF)) of $Al_2O_3$) or carbon nanotubes. These catalysts have been prepared by sequential treatment of nano-materials with an organomagnesium compound ($MgBu_2$) and $TiCl_4$ with formation of TMC on the surface of nano-filler [1-3].

Scanning electron microscopy was used to investigate the PE formation on the surface of nano-fillers, see as an example the PE/ $TiO_2$ composite particles on fig 1. In all cases PE has a globular structure and coats nano-filler particles. During *in-situ* polymerization partial destruction of agglomerates of nano-fillers is observed leading to more uniform distribution of filler. Morphology of composites depends on the type of nano-filler.

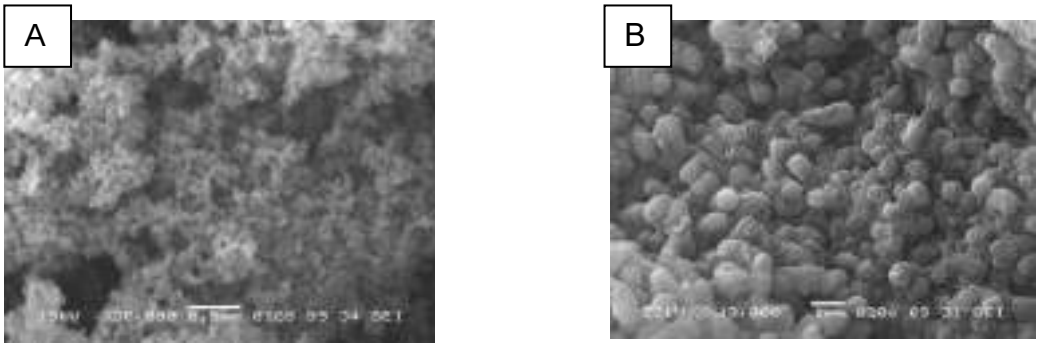


*Fig. 1. SEM data on the Initial nano-$TiO_2$ (A) and composite 210 gPE/g $TiO_2$ (B)*

Thermo-physical properties of composites were studied by DSC and DMA. Introduction of nano-fillers (0.1-0.6 weight %) results in increase of melting temperature and reinforcing of PE (increase of storage modulus of composites).

Examples of practical application of obtained nanocomposites are given.

**Acknowledgement:** This work was supported by Ministry of Science and Higher Education of the Russian Federation (project AAAA21-121011490008-3)

**References:**

[1] Panchenko V.N., Zakharov V.A., Matsko M.A. Polymer Science Series B. 64 (2022) 791.
[2] Kostyukov A.I., Panchenko V.N., Rakhmanova M.I., Nashivochnikov A.A., Matsko M.A., Suprun E.A. Materials Chemistry and Physics. 273 (2021) 125140:1.
[3] Zdanovich A.A., Semikolenova N.V., Kuznetsov V.L., Matsko M.A., Moseenkov S.I., Zakharov V.A. Journal of Applied Polymer Science. 136 (2019) 48212:1.

## PP-I-66

# Finely Controlled Nanocatalysts for Coal Mine Methane Conversion

Matus E.V., Kerzhentsev M.A., Ismagilov I.Z., Nikitin A.P., Sozinov S.A., Ismagilov Z.R.
*Federal Research Center of Coal and Coal Chemistry, Kemerovo, Russia*
*matus_e@mail.ru*

Supported metal nanoparticles and nanoclusters are effective catalytic systems that are used in various catalysis processes [1, 2]. Reducing the size of particles to the nanometer level leads to a change in their melting temperature, heat capacity, thermal conductivity, and the appearance of unique electronic, optical and magnetic properties. Due to specific physicochemical properties and a high concentration of coordinatively unsaturated centres, nanocatalysts have unique functional properties, combining high activity and selectivity. The development of new compositions and methods for the controlled synthesis of nanocatalysts with desired functional properties is an urgent task.

In this work, different chemical synthesis approaches (impregnation, sol-gel method, polymerizable complex method, exsolution approach) were considered to obtain supported Ni nanoparticles with controllable compositions and sizes. The genesis and properties of the catalysts were established using X-ray fluorescence analysis, thermal analysis, $N_2$ adsorption, ex situ and in situ X-ray diffraction, Raman spectroscopy, electron microscopy, EDX analysis and temperature-programed hydrogen reduction. The composition-structure-properties correlation was established and stable against deactivation Ni catalysts for coal mine methane reforming processes were developed.

As example, for the citrate sol-gel (SG) method, it was found that with an increase in the citric acid/metals molar ratio from 0 to 1, the textural characteristics (specific surface area: 76→100 $m^2/g$) of $Ce_{0.2}Ni_{0.8}O_{1.2}/Al_2O_3$ catalysts, dispersion (average particle size: 10→5 nm) and reducibility (temperature of maximum $H_2$ consumption: 580→530°C) of the Ni-containing species improve. For calcined in air at 500°C catalysts, it was shown that $Ni^{2+}$ cations were stabilized in the NiO or in the $CeO_2$-based solid solution. The proportion of the latter was maximum at citric acid/metal molar ratio equal to 0.25, which was chosen as the optimal value. After reductive activation at 800°C of $Ce_{0.2}Ni_{0.8}O_{1.2}/Al_2O_3$ samples, the catalytically active metal $Ni^o$ nanoparticles of ~7 nm in size were formed for effective reforming of coal methane to synthesis gas. At 850°C, the 20 wt. % $Ce_{0.2}Ni_{0.8}O_{1.8}/Al_2O_3$-SG catalyst provides 100% hydrogen yield at full $CH_4$ conversion and 85% $CO_2$ utilization.

**Acknowledgement:** The investigation was carried out with support from the Russian Science Foundation under Project No. 22-13-20040, https://rscf.ru/project/22-13-20040/» and from the Region – the Kemerovo Region – Kuzbass.

**References:**

[1] L. Liu, A. Corma, Chem. Rev. 118 (2018) 4981.
[2] E.V. Matus, L.B. Okhlopkova, O.B. Sukhova, I.Z. Ismagilov, M.A. Kerzhentsev, Z.R. Ismagilov, J. Nanopart. Res. 21 (2019) 11.

## PP-I-67

# Laser Synthesis and Study of the Optical Properties of $ZrO_2:Eu^{3+}$ Depending on the Particle Size

Nashivochnikov A.A., Kostyukov A.I., Snytnikov V.N.
*Boreskov Institute of Catalysis, Novosibirsk, Russia*
*mataiassaiatam17@gmail.com*

Zirconia-based materials are widely employed in various fields of science and technology due to such properties of $ZrO_2$ as thermal and chemical stability, mechanical strength and biocompatibility. In addition, such optical properties as high refractive index, large band gap, and low phonon energy are responsible for the significant interest in $ZrO_2$-based luminescent materials. For example, over the past decade, great prospects have been demonstrated for the use of europium-doped $ZrO_2$ materials ($ZrO_2:Eu^{3+}$) as temperature sensors [1], biomarkers [2], for anti-counterfeiting applications [3]. For all the above applications, the use of nanosized $ZrO_2:Eu^{3+}$ is assumed. However, the effect of particle size on their optical properties has not yet been studied.

This work is devoted to the study of the structural and optical properties of $ZrO_2$ depending on the particle size. For this purpose, a $ZrO_2:Eu^{3+}$ series with an $Eu^{3+}$ concentration of 4 wt. % and particle sizes of 3.0, 3.6, 6.9, 10.6, and 12.0 nm was synthesized by laser vaporization. It was shown by XRD that the phase composition of the obtained nanopowders is represented mainly by the tetragonal $ZrO_2$ phase (90 %) with a small amount of monoclinic phase (10 %) and does not depend on the particle size. It was found by HRTEM that the synthesized nanoparticles are characterized by a close to spherical shape, a narrow size distribution, and weak agglomeration (fig. 1), and EDX mapping showed that Eu is uniformly distributed in the $ZrO_2$ structure.

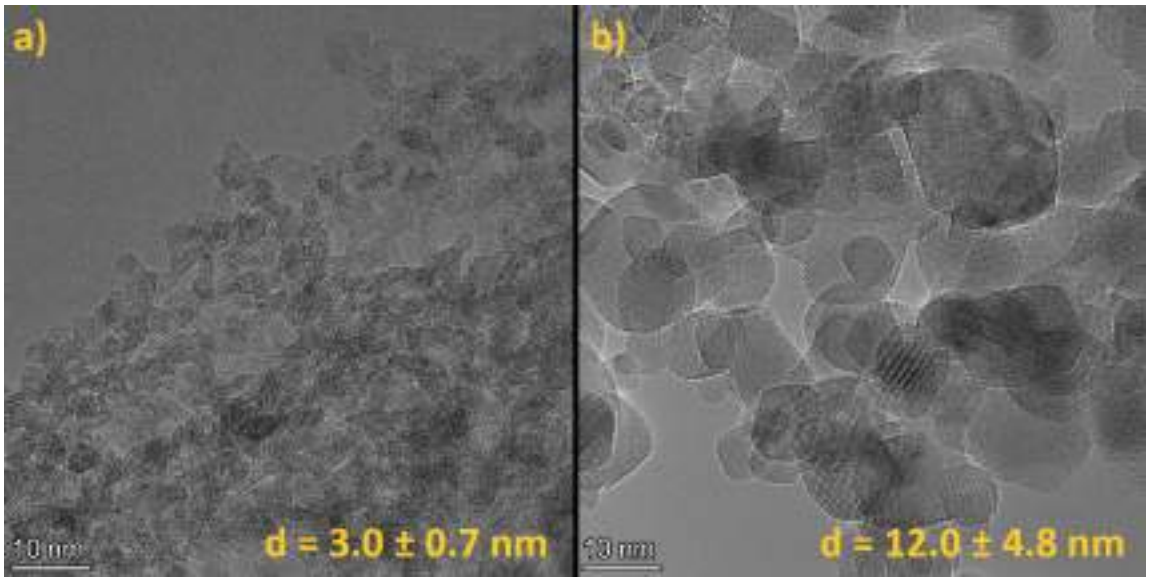


*Fig. 1. TEM images of $ZrO_2:Eu^{3+}$ samples with the smallest (a) and largest (b) particle sizes*

Thermal analysis revealed that a decrease in the particle size of $ZrO_2:Eu^{3+}$ is accompanied by a considerable growth in the number of adsorbed OH and $CO_x$ groups. IR spectroscopy made it possible to identify the main types of these adsorbed molecules. The UV-vis DRS study showed that the optical band gap decreases with decreasing particle size from 5.7 eV to 5.0 eV, while the width of the subband associated with the levels of oxygen vacancies, on the

contrary, increases. This indicates that the number of vacancies decreases with decreasing particle size, which is also confirmed by the color of the synthesized samples, which changes from dark gray to white.

The photoluminescence spectrum of the obtained nanosized $ZrO_2:Eu^{3+}$ consists of broad bands in the region of 410–570 nm caused by the emission of OH groups and oxygen vacancies, and several series of narrow bands associated with intraconfigurational transitions in the $Eu^{3+}$ ion (Fig. 2). A decrease in the particle size is accompanied by a significant increase in the intensity of the band with a maximum at 438 nm, which was attributed to the luminescence of OH groups, and a decrease in the $Eu^{3+}$ luminescence intensity. At the same time, the appearance and growth of a band near 615 nm is observed, which becomes the most intense band in the red region of the spectrum for samples with a particle size of 3.0 and 3.6 nm. It was shown that this band belongs to surface $Eu^{3+}$.

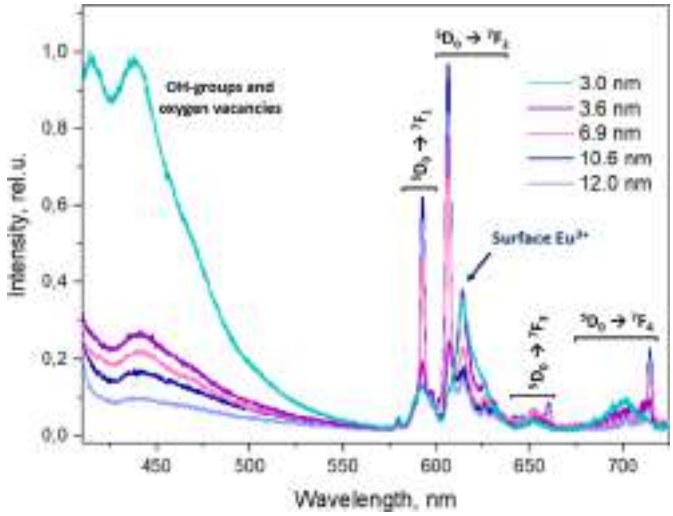


*Fig. 2. PL spectra of $ZrO_2:Eu^{3+}$ in dependence on the particle size at $\lambda_{ex}$ = 395 nm*

The absolute quantum yield of photoluminescence, measured for the entire region of the spectrum, decreases with particle size from 7 to 3.5 %, which is associated primarily with a decrease in the number of oxygen vacancies. At the same time, it was shown that the quantum yield measured only for the $Eu^{3+}$ emission region does not depend on the particle size. It was revealed that the color coordinates of the $ZrO_2:Eu^{3+}$ emission shift from pink-red to blue with decreasing particle size.

Thus, it was shown that the key factor affecting the optical properties of $ZrO_2:Eu^{3+}$ with decreasing particle size is the decrease in the number of oxygen vacancies, the increase in the number of OH groups, and the fraction of surface europium. It is expected that the results obtained will open up possibilities for optimizing luminescence of nanophosphors based on $ZrO_2:Eu^{3+}$ for various applications.

**Acknowledgement:** This work was supported by BIC project (project No. AAAA-A21-121011390009-1)

**References:**

[1] J. Zhou, R. Lei, H. Wang, Y. Hua, D. Li, Q. Yang, D. Deng, S. Xu, Nanophotonics 12 (2019) 1.
[2] A. Bugrov, R. Smyslov, A. Zavialova, D. Kirilenko, D. Pankin, Nanosyst.-Phys. Chem. Math. 9 (2018) 378.
[3] A. King, R. Singh, B. Nayak, Colloids Surf. A: Physicochem. Eng. Asp. 631 (2021) 127715.

## PP-I-68

# Tin-Modified Zr-UiO-66 Metal-Organic Framework as a Catalyst for Cascade Conversion of Dihydroxyacetone to Lactic Acid

Nikulaichev S.N., Kurmanbayeva K., Torbina V.V., Vodyankina O.V.
*Tomsk State University, Tomsk, Russia*
*lenenskiwedonot@mail.ru*

Lactic acid (LA) production is one of the most attractive ways for glycerol valorization. However, this process is a cascade reaction that proceeds through multistep oxidative and non-oxidative pathways [1]. The first step is the oxidation of primary or secondary hydroxyl group with the formation of glyceraldehyde or dihydroxyacetone (DHA), respectively. In the presence of Lewis acid catalyst, glyceraldehyde is rapidly converted into a thermodynamically more stable DHA. Lewis acid sites of the support also promote the dehydration and rearrangement reactions of the intermediates to produce lactic acid efficiently. Thus, the appropriate sites on the support surface play a key role in selective transformation of glycerol to LA. In our group it was shown that the immobilization of Pd-Bi nanoparticles in the Zr-based metal-organic framework UiO-66 led to the LA formation from glycerol in the absence of a base. The aim of the present work is to increase the Lewis acid strength of corresponding sites by partial substituting of Zr atoms in the UiO-66 structure.

The Sn-Zr-UiO-66 was synthesized under solvothermal conditions in a Teflon-lined stainless steel autoclave according to the procedure similar to the one described in Ref. [2] with a replacement of required amount of $Zr(NO_3)_2{\cdot}2H_2O$ by $SnCl_2{\cdot}2H_2O$. The materials obtained were characterized by XRD, low-temperature $N_2$ adsorption, Raman, FT-IR and DR-UV-vis, SEM techniques. Catalytic experiments were carried out in the thermostatted Parr reactor. 30 mL of DHA aqueous solution (0.3 M) and 200 mg of the catalyst were kept at 100 °C under vigorous stirring for 4 h. Reaction mixture after catalyst separation was analyzed by HPLC.

According to the results of SEM and EDAX analysis, in all samples the Zr/Sn molar ratio is close to the theoretical one, and the metals are distributed homogeneously in most particles. However, the formation of extraframework $SnO_2$ was confirmed by both XRD and low-temperature $N_2$ adsorption measurements. A decreasing of the surface area and pore volume with the increasing of the Sn/Zr molar ratio was observed. At the same time, the insertion of Sn into Zr-UiO-66 led to a significant increase in selectivity towards lactic acid (Table 1).

*Table 1. Catalytic activity of Sn-Zr-UiO-66 with different Zr/Sn molar ratios*

| Zr/Sn molar ratio | DHA conversion, % | Selectivity, % | | |
|---|---|---|---|---|
| | | LA | pyruvaldehyde | formic acid |
| 1/0 | 51 | 43 | 12 | 10 |
| 2/1 | 48 | 54 | 35 | 10 |
| 1/1 | 48 | 65 | 4 | 4 |

Further investigations in order to clarify whether the Sn species exchanging the Zr atoms in the UiO-66 structure or Sn formed in the oxide phase are responsible for observed catalytic activity are in a progress.

**Acknowledgement:** This work was supported by the Russian Science Foundation, grant 19-73-30026-П.

**References:**

[1] N. Razali, A. Z. Abdullah, Applied Calatysis A, General. 543 (2017) 234.
[2] V.V. Torbina et al., Catal. Today. 333 (2019) 47.

## PP-I-69

# Tailored Mechanical Property of Liquid Crystal Elasmtomer Fiber Actuator

Seung-Joon Oh, Suk-kyun Ahn
*School of Chemical Engineering, Pusan National University, Busan, Republic of Korea*

Liquid Crystal Elastomer (LCE), which can respond to various external stimuli with large and reversible contractions, has long been recognized as potential candidate for artificial muscles. . Unlike 2D or 3D structures, fiber can deform quickly and demonstrate many actions by design pattern. However, the recent reports of LCE fibers demonstrated exciting opportunities to create intelligent textiles as well as micro-actuators with fast response.[1-3] We make LCE Fiber continuously using 3D printer set-up, and fiber contracts repeatably well. However, the low mechanical property makes LCE fiber hard to apply to weaving. Herein, we make LCE fiber stronger using a liquid crystal solution. In our experiments, we make LC Elastomer fiber stronger using a double network strategy with almost no reduction in strain compared to pristine. We also decrease the stickiness of LCE fiber which is unfavorable to clothing system, and we make a weaving sample with long LCE fiber well.

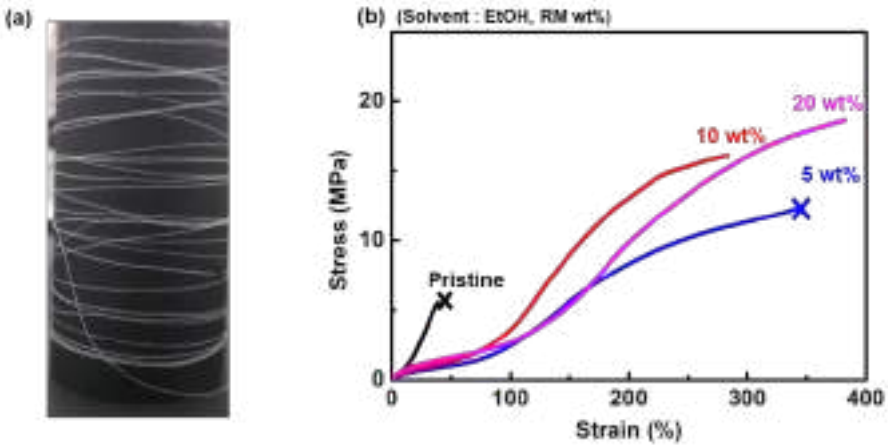


*Fig. 1. (a) Photograph of continuous single strand of LCE fiber. (b) Mechanical properties of monodomain LCE fiber with double-network strategy*

**Acknowledgement:** This work was supported by Basic Science Research Program and by BK21 four program through the National Research Foundation of Korea (NRF) funded by the Ministry of Education

**References:**

[1] Mohand O. Saed, Soft Matter, 17, 5436(2021).
[2] Eugene M. Terentjev, Macromolecules, 55, 810(2022)
[3] Eugene M. Terentjev, Adv. Mater., 2210689(2023)

## PP-I-70

# Microhardness Evolution of Laser-Deposited Equiatomic FeNiCr Coatings In Situ Alloyed with $B_4C$

Okulov A.V.[1], Korobov Yu.S.[1], Stepchenkov A.K.[1], Makarov A.V.[1], Iusupova O.S.[1], Kuznetsova T.V.[1], Korkh Yu.V.[1], Kharanzhevskiy E.V.[2]

*1 – Institute of Metal Physics, Ural Branch of the Russian Academy of Sciences, 620077 Ekaterinburg, Russia*

*2 – Udmurt State University, 426034 Izhevsk, Russia*

*okulovartem@imp.uran.ru*

The authors present mechano-structural characterization of laser-deposited equiatomic medium-entropy alloy (MEA) FeNiCr coatings additionally in-situ alloyed with 3 and 5 wt.% $B_4C$. The FeNiCr-$B_4C$ coatings were deposited on AISI 1040 steel substrate by short-pulsed laser cladding. In particular, the microhardness evolution of the coatings reinforced with $B_4C$ is demonstrated here. The XRD analysis confirmed the presence of the single face-centered cubic (FCC) γ-phase (space group Fm-3m) in the above alloys, independently of the $B_4C$ content. However, highly-sensitive Raman spectroscopy made it possible to identify the $B_4C$ phases and define the Raman spectra evolution depending on the concentrations of the latter. Based on the SEM microstructural analysis, it was established that the cross-sections of all synthesized specimens are characterized by average coating thickness of 350 ± 20 μm and sufficiently narrow (100 ± 20 μm) "coating-substrate" transition zone. All synthesized coatings were found to have a small number of pores and cracks. Mechanical characterization of the FeNiCr-$B_4C$ coatings showed that in-situ alloying with 5 and 7 wt.% $B_4C$ is resulted in noticeable increase in microhardness by 86 and 157 %, respectively, compared to previously reported $B_4C$-free FeNiCr coating. Therefore, the combination of in-situ alloying process with increasing the $B_4C$ content can be considered as promising method for synthesis of strength engineering MEA FeNiCr coatings.

**Acknowledgement:** The research was carried out within the state assignment of Ministry of Science and Higher Education of the Russian Federation (themes "Additivity" No. 121102900049-1 and "Structure" No. 122021000033-2) by means of the equipment of the Collaborative Access Center "Testing Center of Nanotechnology and Advanced Materials" of the IMP UB RAS.

**References:**

[1] S. Dadbakhsh, R. Mertens, L. Hao, et al., Adv. Eng. Mater. 21 (2019) 1801244.
[2] N.V. Gokhfeld, A.V. Okulov, M.A. Filippov, et al., Phys. Solid State 64 (2022) 356–361.
[3] P.H. Mayrhofer, C. Mitterer, J. Musil, Surf. Coat. Technol. 174 (2003) 725–731.
[4] K.Y. Xie, V. Domnich, L. Farbaniec, et al., Acta Mater. 136 (2017) 202–214.
[5] L. Zhu, P. Xue, Q. Lan, et al., Opt. Laser Technol. 138 (2021) 106915.
[6] M. Schneider, G. Laplanche, Acta Mater. 204 (2021) 116470.
[7[ A. Fu, B. Liu, W. Lu, et al., Scr. Mater. 186 (2020) 381–386.

## PP-I-71

# Graphitization as a Way to Stabilize Textural Characteristics of Alumina under Hydrothermal Conditions

Parfenov M.V.[1,2], Kazakova M.A.[1,2], Selyutin A.G.[2,3], Ishchenko A.V.[1,2], Kazakov M.O.[1,2]
*1– Boreskov Institute of Catalysis, Novosibirsk, Russia*
*2 – Novosibirsk State University, Novosibirsk, Russia*
*3 – Synchrotron Radiation Facility SKIF, Boreskov Institute of Catalysis, Kol'tsovo, Russia*
*parfenov@catalysis.ru*

Gamma alumina is a widely used support for catalysts of various processes. Nevertheless, γ-$Al_2O_3$ has a significant drawback, which relates to its instability in hydrothermal conditions, and might be essential for biomass refining processes. In the case of aqueous-phase processes, hydrothermal conditions result in transformation of γ-$Al_2O_3$ to boehmite, which is accompanied by degradation of the porous structure and leads to rapid catalyst deactivation.

In this work a simple one-stage approach is proposed to protect γ-$Al_2O_3$ porous structure from collapse under hydrothermal conditions [1]. This approach is based on modifying the surface of γ-$Al_2O_3$ with graphitic carbon by gas-phase chemical deposition of ethylene on the alumina surface at a temperature of 680 °C. The degree of alumina surface coverage was adjusted by varying the treatment time (5–240 min). The obtained samples were denoted as C@$Al_2O_3$-x, where x is the time of treatment. Hydrothermal treatment (HTT) of C@$Al_2O_3$-(5-240) samples was carried out in an autoclave with a Teflon liner at 200 °C for 5 h without stirring. Materials characterization before and after HTT was performed by CHNS analysis, X-ray diffraction, transmission electron microscopy, nitrogen physisorption, and Raman spectroscopy.

The C@$Al_2O_3$ samples contained from 1.4 to 25.5 wt. % of carbon, which corresponded to the number of graphene layers from 0.09 to 1.57. It was estimated that treatment in ethylene flow at 680 °C for 120 min and more leads to the formation of a monolayer carbon coating on the alumina surface. HRTEM data shows that the morphology of γ-$Al_2O_3$ sample is represented by a mixture of polycrystalline lamellar particles up to 5 nm in size and needle-shaped particles with a length of 20 nm or more and does not change during graphitization. It has been established that carbon in C@$Al_2O_3$ samples, regardless of the graphitization time, is present in the form of nanocrystalline graphite with a graphene fragment size of less than 5 nm.

However, increase in graphitization time from 5 to 240 min leads to slight decrease of BET surface area of C@$Al_2O_3$ samples from 217 to 167 $m^2/g$ (Fig. 1). It has been shown by XRD that the initial γ-$Al_2O_3$ transforms into boehmite during hydrothermal treatment (Fig 2a), which leads to a decrease in the surface area by 80% (Fig. 1). Whereas, a monolayer graphite coating of alumina under hydrothermal conditions contributes to the formation of a mesoporous C@boehmite composite (Fig. 2b) with a high specific surface area and a pore volume similar to the initial material (Fig. 1). The structure of the carbon deposit after the hydrothermal treatment of the samples is completely preserved. At the same time, hydrothermal treatment

promotes an increase in the graphitization degree of carbon deposits due to the partial removal of disordered and defective carbon fragments from the surface of $C@Al_2O_3$ samples.

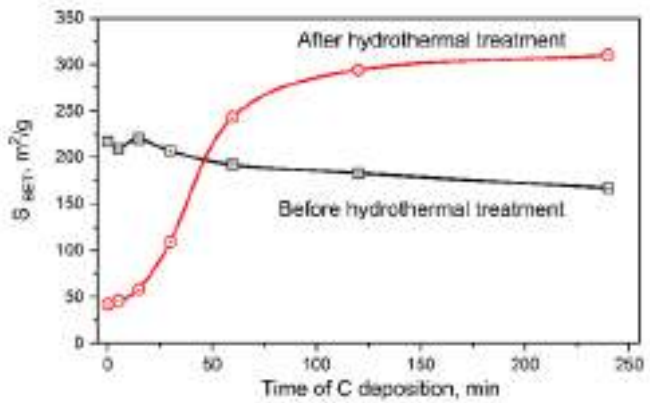


*Fig. 1. BET surface area of γ-$Al_2O_3$ and C@$Al_2O_3$-(5–240) samples before and after hydrothermal treatment.*

It should be noted that an increase in the duration of hydrothermal treatment from 5 to 72 h does not lead to additional structural and textural changes, which indicates the stability of the formed C@boehmite composite. Thus, the graphite coating makes it possible to adapt γ-$Al_2O_3$ to hydrothermal conditions, which will allow using $C@Al_2O_3$ composites as a support for catalysts of various aqueous-phase reactions.

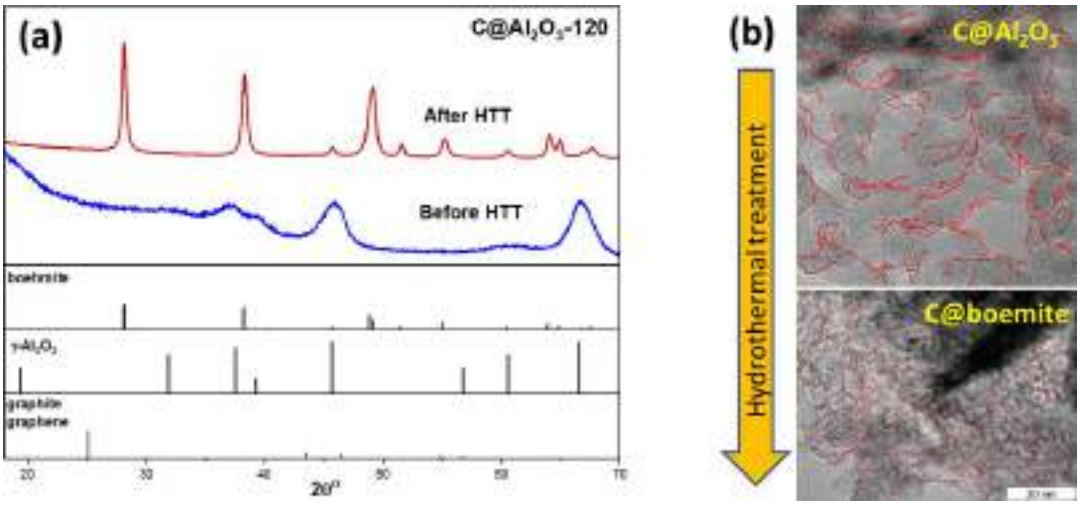


*Fig. 2. C@Al2O3-120 sample before and after HTT (5 h, T=200 °C): a) XRD data, b) HRTEM images.*

**Acknowledgement:** The study was funded by Russian Science Foundation according to the research project № 21-73-10039, https://rscf.ru/project/21-73-10039/

**References:**

[1] M.A. Kazakova, A.G. Selyutin, M.V. Parfenov, A.V. Ishchenko, M.O. Kazakov, Graphitization of alumina as a way to stabilize its textural characteristics under hydrothermal conditions, Micropor. Mesopor. Mat, 341 (2022) 112038.

## PP-I-72

# Ln/Fe-Doped $Sr_2TiO_4$ Layered Perovskites: Effect of Synthesis Method and Composition on Physical-Chemical and Catalytic Properties in Oxidative Coupling of Methane

Pavlova S.N.[1], Gorkusha A.S.[2], Tsybulya S.V.[1,2], Nartova A.V.[1], Rogov V.A.[1], Isupova L.A.[1]
*1 – Boreskov Institute of Catalysis, Novosibirsk, Russia*
*2 – Novosibirsk State University, Novosibirsk, Russia*
*pavlova@catalysis.ru*

Layered Ruddlesden-Popper $A_{n+1}B_nO_{3n+1}$ perovskites have a wide range of applications including their use as promising heterogeneous catalysts. Among them, $Sr_2TiO_4$ is considered as the active catalyst for oxidative coupling of methane (OCM) – a potential direct route to produce $C_2$ hydrocarbons, in particular, ethylene [1]. It is known, that substitution of perovskite A or/and B positions with cations of different nature and charge enables tailoring concentration and type of surface defects, active oxygen species and basic sites defining perovskite OCM activity [2]. Furthermore, their peculiarities and catalytic activity are strongly influenced by a preparation method and synthesis parameters [3].

In this work, the impact of the nature of cations partially replacing Sr (La, Nd, Pr) or Ti (Fe) and the method of their introduction in $Sr_2TiO_4$ on the morphological, structural, redox properties and OCM catalytic activity was studied.

$Sr_{2-x}Ln_xTi_{1-y}Fe_yO_4$ (Ln= La, Pr, Nd, x=0, 0,1; y =0-0.3) were prepared by sol-gel method using polymeric precursors. To obtain 5% Ln/$Sr_2TiO_4$, parent $Sr_2TiO_4$ was impregnated with water solutions of La, Pr, or Nd nitrates, correspondingly. All “as prepared” samples were calcined in air at 900-1100°C. The samples were characterized by BET, FE-SEM, XRD, XPS, $H_2$-TPR. The OCM catalytic activity was studied in a fixed-bed reactor at 750–900 °C and 75 000 $h^{-1}$ GHSV, the reaction mixture was $CH_4$:$O_2$:$N_2$ = 46:11.5:42.5% vol., $CH_4$:$O_2$ = 4.

According to XRD data the parent $Sr_2TiO_4$ is a single phase sample. The phase composition of $Sr_{1.9}Ln_{0.1}TiO_4$ samples prepared via sol-gel method depends on the nature of the doping Ln cation and annealing temperature. The samples annealed at 900°C along with layered strontium titanates contain $SrTiO_3$ (excluding Pr) and Ln-oxides of high dispersion. Some decrease in the lattice parameters of titanates doped with $La^{3+}$ and $Nd^{3+}$relative to the pure ones indicates their partial embedding in $Sr^{2+}$ position of the perovskite. The annealing of the samples at 1100°C results in formation of layered perovskites only and lowering Ln-oxides dispersion. For 5% Ln/$Sr_2TiO_4$ samples prepared using impregnation, the unchanged structure of parent $Sr_2TiO_4$ and the presence of the pronounced Ln-oxides reflections show that all Ln-cations are not embedded in the perovskite. And in so doing, the dispersion of oxides in all impregnated samples are smaller as compared with one for the sol-gel samples. FE-SEM micrographs of La-doped samples confirmed this: only highly dispersed $La_2O_3$ particles less than 200 nm are observed for the sol-gel sample while there are large agglomerates The up to 1 μm in the impregnated one. For $Sr_2Fe_xTi_{1-x}O_4$ (x=0.1-0.3) annealed at 900 and 1100°C,

the main phase is the layered perovskite with the changed lattice parameters that shows the insertion of Fe cations in $Ti^{4+}$ sites of the perovskite. Analysis of $H_2$-TPR data has enabled to distinguish chemisorbed oxygen species facilitating formation of $CO_x$ and surface lattice oxygen species involved in the $C_2$ selective formation being reduced in low temperature and medium or high temperature region, correspondingly (Fig.1). The results show the marked increase in the amount of chemisorbed oxygen in the case of Pr and Fe doped perovskites while for La and Nd doped samples there are more surface lattice oxygen reduced at medium temperature. The highest concentration of chemisorbed oxygen in the case of $Sr_{1.9}Pr_{0.1}TiO_4$ is also confirmed by XPS data.

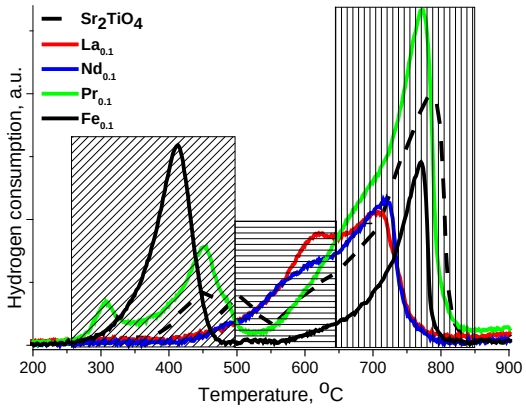


*Fig. 1. $H_2$-TPR spectra for Ln/Fe doped samples.*

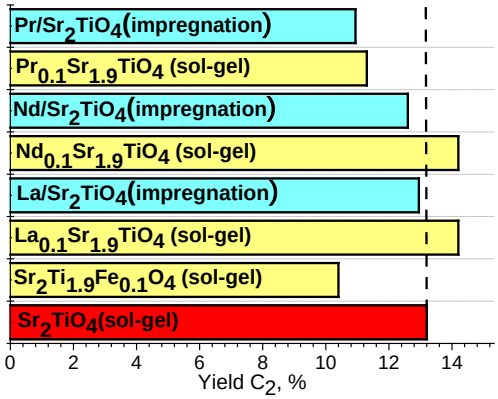


*Fig.2. $C_2$ yield for the catalysts in OCM at 900 °C*

The impregnation of the parent $Sr_2TiO_4$ by the correspond nitrates decreases the OCM activity of all 5% Ln/$Sr_2TiO_4$ samples especially in the case of Pr. Such activity drop of impregnated La and Nd-doped samples could be due to low dispersion of Ln oxides in them. The testing of "sol-gel" $Sr_{1.9}Ln_{0.1}TiO_4$ and $Sr_2Fe_yTi_{1-y}O_4$ in OCM have shown that La and Nd increase the $C_2$ yield while Pr and Fe are markedly lowering it as compared with parent $Sr_2TiO_4$ (Fig. 2). The results obtained suggest that the high $C_2$ yield over "sol-gel" La and Nd doped samples stems from the absence of chemisorbed oxygen leading to the $CO_x$ formation and the appearance of surface lattice oxygen reduced at medium temperature (Fig. 1). The activity drop in the case of sol-gel Pr and Fe doped samples is conditioned by the presence of a large amount of chemisorbed oxygen facilitating $CO_x$ formation and decreasing $C_2$ selectivity.

**Acknowledgement:** This work was supported by the budjet project AAAA-A21-121011490008-3 for Boreskov Institute of Catalysis.

**References:**

[1] W.M. Yang, Q.J. Yan, X.C. Fu, React. Kinet. Catal. Lett. 54 (1995) 21–27.
[2] Y. Sim, D. Kwon, S. An, J.-M. Ha, T.-S. Oh, J.C. Jung, Mol. Catal., 489(2020)110925.
[3] Y.A. Ivanova, E.F. Sutormina, N.A. Rudina, A.V. Nartova, L.A. Isupova, Catalysis Com., 117 (2018) 43–48.

## PP-I-73

# Coal-Firing Waste to Nanocomposites for 3D Printing

Petropavlovskii K.S., Petropavlovskaya V.B., Novicpenkova T.B., Zavadko M.Y., Sulman M.G.
*Tver State Technical University, Tver, Russia*
*victoriapetrop@gmail.com*

3D printing technologies are developing extremely rapidly and have recently been actively used in various areas of production [1]. One of the most used methods is printing by layer-by-layer extrusion using organo-mineral raw material mixtures. The essence of this method is to extrude a quick-hardening mixture. An important role is given to the composition of the ink - the raw mixture. The introduction of organomineral complexes into the compositions of gypsum compositions makes it possible to regulate not only their structural-mechanical, but also technological properties [2, 3].

To substantiate the possibility of using a nanocomposite based on a gypsum mixture, the authors conducted experiments using mixtures of various compositions. The dispersity of the applied nanofillers, as well as the type of viscosity modifiers, differed significantly in the experiments.

Based on the results of the studies, the effectiveness of the use of a nanomodifier based on an aluminum-containing filler of nanosized dispersion, metakaolin and a polycarboxylate plasticizer was established. The introduction of a nanomodifier into the composition made it possible to increase not only the structural and mechanical properties of the gypsum nanocomposite, but also the manufacturability of the raw mixture. Amorphous aluminosilicate was a man-made filler. The intergranular voids of gypsum stone were filled with particles of an active mineral additive - metakaolin. The active additive entered into chemical interaction with calcium hydroxide, as well as other impurity alkaline oxides. As a result, a dense structure of the gypsum composite was formed.

The introduction of a nanomodifier into the composition made it possible to increase not only the structural and mechanical properties of the gypsum nanocomposite, but also the manufacturability of the raw mixture. Amorphous aluminosilicate was a technogenicfiller. The intergranular voids of gypsum stone were filled with particles of an active mineral additive - metakaolin. The active additive entered into chemical interaction with calcium hydroxide, as well as other impurity alkaline oxides. As a result, a dense structure of the gypsum composite was formed. The synthesized structure is represented by calcium sulfate dihydrate crystals and an amorphous phase of aluminosilicate filler (Fig. 1).

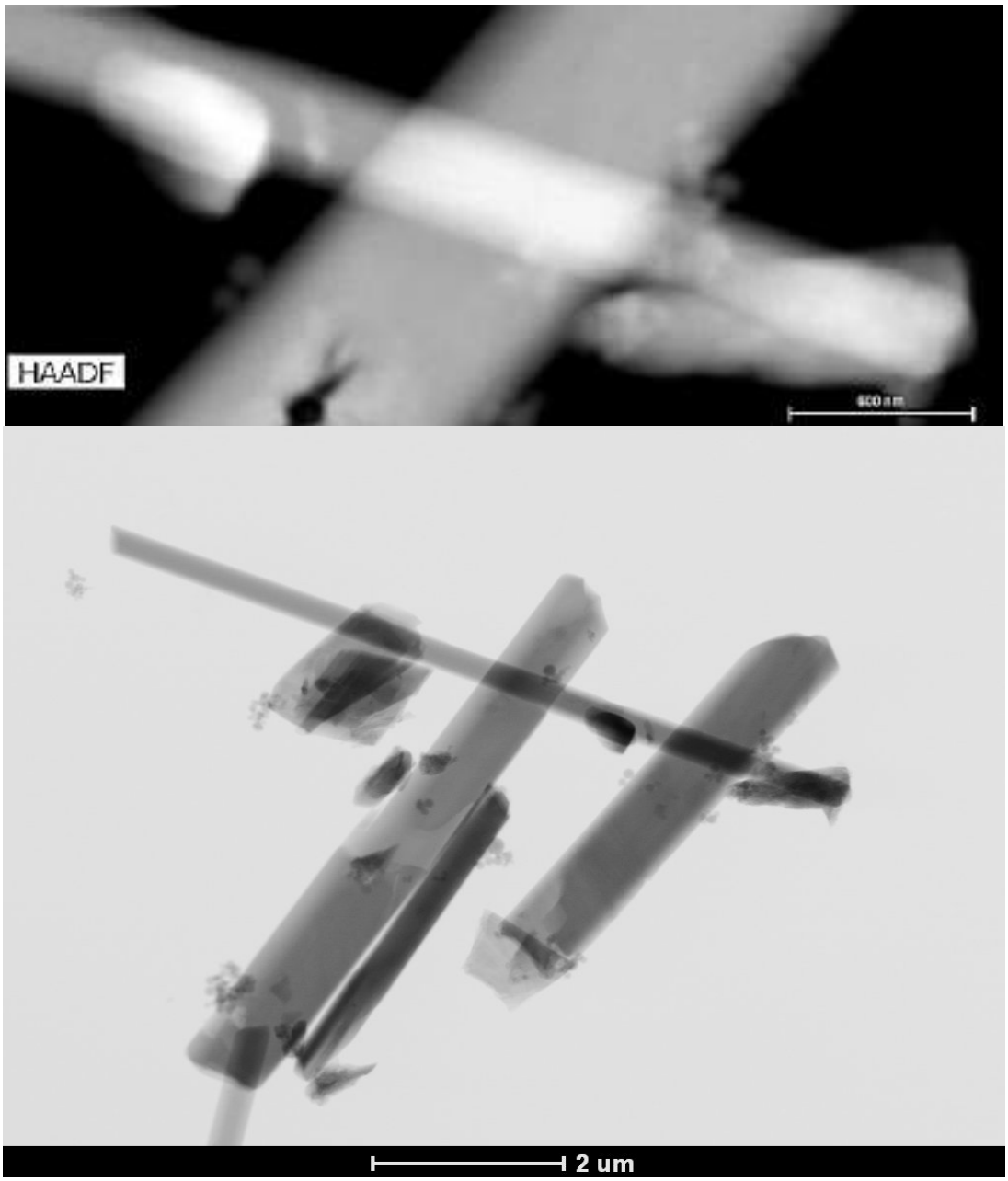


*Fig. 1. PEM- Images of the nanocomposite structure*

**Acknowledgement:** This work was supported by the Russian Science Foundation, grant №21-79-30004.

**References:**

[1] R.H. Mukhametrakhimov, I.M. Vakhitov, Izvestiya KGASU 4(42) (2017) 350–359.
[2] N.I. Alfimova, E.E. Shadsky, N.A. Nikiforova, Izvestiyavuzov. Investments. Construction. Real estate. 2(17) (2016) 120–128.
[3] Y. Chen, S. Chaves Figueiredo, Z. Li, Z. Chang, K. Jansen, O. Çopuroğlu, E. Schlangen, Cem. Concr. Res. Elsevier Ltd. 132 (2020) 106040.

## PP-I-74

# Effect of Bismuth Ferrite Concentration on Magnetic and Structural Properties of PVDF-Based Composites

Petrukhin D.A., Salnikov V.D., Omelyanchik A.S., Ershov P.A., Rodionova V.V.
*Immanuel Kant Baltic Federal University, Kaliningrad, Russia*
*denisrussia2000@gmail.com*

Multiferroic materials exhibit both ferroelectric and ferromagnetic properties. These materials have great potential for various applications such as data storage, sensors, energy harvesting, catalysis and even biomedicine [1]. There are just few natural materials that possess multiferroic properties, among them the most frequently studied is bismuth ferrite ($BiFeO_3$) with perovskite crystal structure. $BiFeO_3$ possess weak ferromagnetic properties with saturation magnetization less than ~1 emu/g and one of the important tasks is to increase it by varying magnetic structure of bismuth ferrite itself or by creating composite materials. On the other hand, polymer-based multiferroics have some advantages over their inorganic counterparts, such as low density, flexibility, and ease of processing [2]. However, the challenge with polymer-based multiferroics is to achieve strong coupling between the magnetic and electric properties.

In this work, we focused on studying the effect of bismuth ferrite ($BiFeO_3$) concentration on the magnetic and structural properties of polyvinylidene fluoride (PVDF) based composites. PVDF is a well-known piezoelectric polymer and can be used as a matrix for multiferroic composites. PVDF can exist in several crystalline phases, amount them the β-phase and γ-phase is the most piezoelectrically active and thus it is more favourable to produce multiferroic composites. One of the strategies to increase formation of β-phase and γ-phase is adding of $BiFeO_3$ nanoparticles which act as nucleating agent inside the polymer matrix [3]. Moreover, $BiFeO_3$ nanoparticles have their own piezoelectric response and can enhance dielectric properties of composites.

To synthesize $BiFeO_3$ nanoparticles $Fe(NO_3)_3{\times}6H_2O$ and $Bi(NO_3)_3{\times}6H_2O$ were dissolved in glycine at 80°C. The resulting solution was stirred for 15 minutes at the same temperature, followed by the addition of $HNO_3$ (65%) to the mixture. Resulting solution was placed at a magnetic stirrer and heated at 150°C until evaporation, which led to the direct conversion of gel into the nanocrystalline powder. Obtained powder was ground mortar and placed in an oven for 2 hours at 450°C in ambient atmosphere. The finished $BiFeO_3$ powder was washed with MeCOOH and water to remove any leftover impurities. To produce $BiFeO_3$/PVDF composite, the polymer and the particles were dissolved in N,N-dimethylformamide were dispersed in ultrasound for 2 hours. Then composite films with different concentrations of nanoparticles were fabricated by solution casting assisted by doctor blade technique. The composite material (consisting of PVDF and $BiFeO_3$) was characterized using Scanning Electron Microscopy (SEM) for microstructural features, X-ray Diffraction (XRD) to investigate its

structural properties, and Vibrating Sample Magnetometry (VSM) to evaluate its magnetic properties.

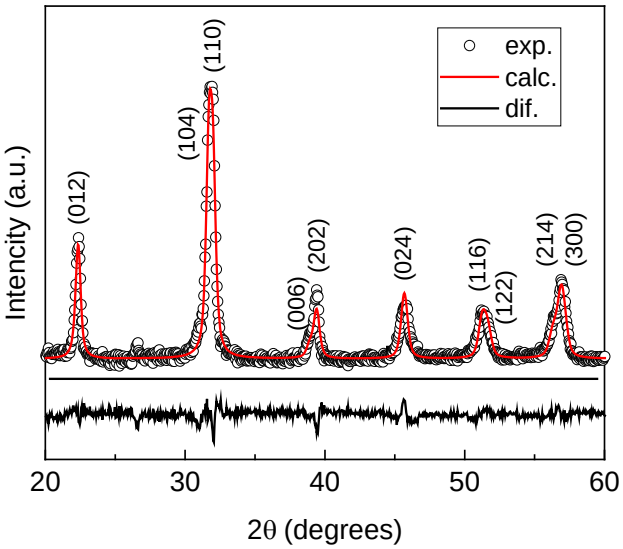


*Fig. 1. XRD patterns of obtained $BiFeO_3$ nanoparticles.*

At the next stage of research, it is planned to conduct chemical alloying of the pure phase of BFO to study the effect of impurity atoms and ion injection on magnetic properties. The literature data on the doping of the perovskite structure suggest that an increase in the magnetic and, therefore, multiferroic properties of $BiFeO_3$ is expected, which makes it useful in such areas as spintronics, magnetic memory, photocatalysis, etc.

**Acknowledgement:** This work was supported by the Russian Science Foundation, grant 21-72-30032. We acknowledge the Centre for development of gifted children (Kaliningrad) for provision of XRD measurements.

**References:**

[1] Kopyl S, Surmenev R, Surmeneva M, Fetisov Y and Kholkin A 2021 Magnetoelectric effect: principles and applications in biology and medicine– a review *Mater. Today Bio* **12** 100149
[2] Martins P and Lanceros-Méndez S 2013 Polymer-based magnetoelectric materials *Adv. Funct. Mater.* **23** 3371–85
[3] Tripathy A, Maria Joseph Raj N P, Saravanakumar B, Kim S J and Ramadoss A 2023 Tuning of highly piezoelectric bismuth ferrite/PVDF-copolymer flexible films for efficient energy harvesting performance *J. Alloys Compd.* **932** 167569

## PP-I-75

# Effect of Ruthenium Addition to Palladium-Rhodium Nanoalloys on Their Catalytic Activity in CO Oxidation

Plyusnin P.E.[1], Shubin Yu.V.[1], Asanov I.P.[1], Kenzhin R.M.[2], Stoyanovskii V.O.[2], Vedyagin A.A.[2]
*1 – Nikolaev Institute of Inorganic Chemistry SB RAS, Novosibirsk, Russia*
*2 – Boreskov Institute of Catalysis, Novosibirsk, Russia*
*plus@niic.nsc.ru*

In the last decades, various nanoalloys have attracted an increased interest from researchers. The use of nanoalloys in catalysis can be especially distinguished [1-4]. As a rule, catalysts containing nanoalloys in their composition demonstrate improved performance characteristics, in particular, higher catalytic activity and thermal stability.

Three-way catalysts used for the purification of automotive exhaust gases from CO, unburnt hydrocarbons, and nitrogen oxides contain platinum group metals (Pt, Pd, and Rh) as active components. Thermal decomposition of the double complex salts (DCS) deposited on the support allows these metals to be obtained in an alloy (solid solution) state. Recently, we have reported the advantages of this approach for the stabilization of Pd-Rh catalysts deposited on a number of supports [5-7]. The partial replacement of rhodium with the third metal additionally enhances the properties and reduces the cost of the catalytic composition [8,9].

In the present work, alumina-supported trimetallic catalysts containing Rh, Ru and Pd in their composition were synthesized and studied in comparison with bimetallic Pd-Rh/$Al_2O_3$ reference sample. The starting compounds were solid solutions of double complex salts of corresponding metals synthesized by known procedures. The single phase of the synthesized complexes was confirmed by X-ray diffraction analysis. The synchronous thermal analysis method was applied to investigate the process of thermolysis of synthesized DCS in both reducing and oxidizing atmospheres. The influence of the conditions of the thermolysis processes (heating rate, final thermolysis temperature) on the phase composition and the size of the trimetallic particles of the final products was established. It has been found that in the process of thermal decomposition, it is possible to obtain alloy nanoscale trimetallic (Rh-Ru-Pd) particles of a given composition anchored on the surface of an oxide support.

The activity and stability of the catalyst compositions obtained were examined in CO oxidation reaction carried out under prompt thermal aging conditions. In Figure 1, catalytic performance of the prepared Pd-Rh-Ru/$Al_2O_3$ catalyst is compared with that for Pd-Rh/$Al_2O_3$ reference sample. As seen, the addition of ruthenium only slightly improves the initial activity of the catalytic system but significantly increases its thermal stability. The state of each metal was characterized by diffuse reflectance UV-vis spectroscopy and X-ray photoelectron spectroscopy.

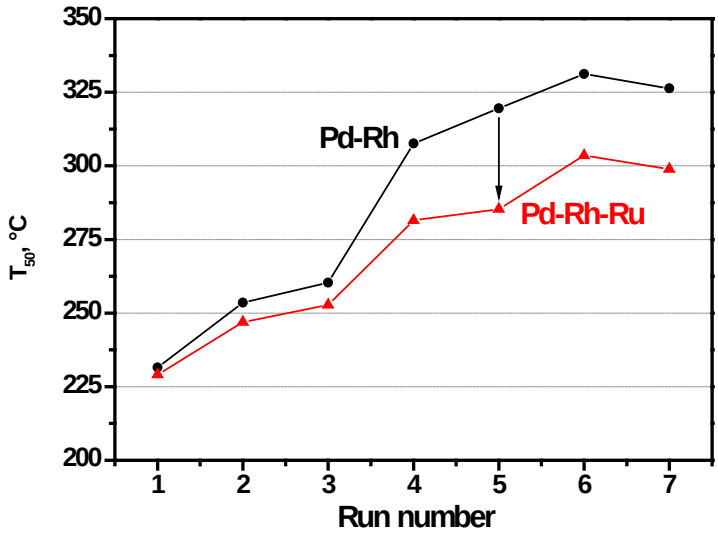


*Fig. 1. Catalytic performance of bimetallic Pd-Rh/$Al_2O_3$ and trimetallic Pd-Rh-Ru/$Al_2O_3$ samples in consecutive runs under PTA conditions*

**Acknowledgement:** This work was supported by the Ministry of Science and Higher Education of the Russian Federation, projects N121031700315-2 and AAAA-A21-121011390054-1.

**References:**

[1] W. Yang, J. Guo, J. Ma, N. Wu, J. Xiao, M. Wu, J. Alloys Compnd. 926 (2022) 166937.
[2] Y. Li, H. Deng, Z. Zhou, P. Yang, J. Fei, Y. Xie, Appl. Surf. Sci. 608 (2023) 155131.
[3] G.H. Lee, J. Kim, Solid State Sci. 135 (2023) 107063.
[4] G. Lv, Z. Zhang, S. Liu, F. Tao, J. Wang, Y. Meng, Y. Yang, Chem. Eng. J. 453 (2023) 139816.
[5] A.A. Vedyagin, E.A. Alikin, R.M. Kenzhin, M.Y. Tashlanov, V.O. Stoyanovskii, P.E. Plyusnin, Y.V. Shubin, I.V. Mishakov, Reac. Kinet. Mech. Catal. 129 (2020) 117-133.
[6] A.A. Vedyagin, R.M. Kenzhin, M.Y. Tashlanov, V.O. Stoyanovskii, P.E. Plyusnin, Y.V. Shubin, I.V. Mishakov, A.V. Kalinkin, M.Y. Smirnov, V.I. Bukhtiyarov, Emiss. Control Sci. Technol. 5 (2019) 363-377.
[7] A.A. Vedyagin, Y.V. Shubin, R.M. Kenzhin, P.E. Plyusnin, V.O. Stoyanovskii, A.M. Volodin, Top. Catal. 62 (2019) 305-314.
[8] A.A. Vedyagin, Y.V. Shubin, R.M. Kenzhin, P.E. Plyusnin, V.O. Stoyanovskii, Processes. 8 (2020) 928.
[9] A.A. Vedyagin, V.O. Stoyanovskii, R.M. Kenzhin, P.E. Plyusnin, Y.V. Shubin, Doklady Phys. Chem. 506 (2022) 131-137.

## PP-I-76

# Synthesis of Functionalized Carbon Nanomaterials from Organochlorine Compounds over Ni-Catalysts and Their Possible Application

Potylitsyna A.R.[1], Bauman Y.I.[1], Ozerova A.M.[1], Tayban E.S.[1], Lipatnikova I.L.[1], Netskina O.V.[1], Vedyagin A.A.[1], Shubin Y.V.[2], Mishakov I.V.[1]

*1 – Boreskov Institute of Catalysis, Novosibirsk, Russia*

*2 – Nikolaev Institute of Inorganic Chemistry, Novosibirsk, Russia*

*potylicy@catalysis.ru*

Currently, carbon nanomaterials (CNM), as well as functionalized carbon nanomaterials (F-CNM), are highly demanded objects of scientific researches. Most of the articles demonstrate their high strength, large specific surface area and porosity, and good electrical and thermal conductivity [1]. To date, composite materials (lubricants, concrete products, polymers, etc.), sorbents, catalysts, and carriers have already been developed on the basis of CNM [2].

Most commonly the surface of CNM is modified with atoms of nitrogen, oxygen, boron, phosphorus, or chlorine. F-CNM have a number of advantages over carbon materials that do not contain heteroatoms on their surface. The use of such materials as carriers increases the dispersion of the deposited catalysts due to strong electronic interaction and increased adhesion. As a consequence, the activity, productivity, and selectivity of the deposited systems increase. Therefore, F-CNM appear to be a promising substitute for traditional catalyst carriers in processes such as hydrodechlorination. Another promising direction is the use of functionalized carbon nanomaterials as adsorbents of toxic wastes from aqueous media. The special porous structure and large specific surface area allow small pollutant molecules to be firmly adsorbed in carbon materials [3]. Thus, adsorption of organochlorine and subsequent hydrodechlorination will allow the purification of wastewater from chlorine-containing wastes.

In this work, functionalized carbon nanomaterials were obtained by the joint catalytic decomposition of aliphatic chlorinated hydrocarbon ($C_2HCl_3$) and a nitrogen-containing substrate ($CH_3CN$) on self-organized Ni-M alloys. Nitrogen-free CNM were synthesized by decomposition of trichloroethylene ($C_2HCl_3$) only. The presence of chlorine in the substrate determines not only the elemental composition of the resulting product, but also its unique segmented structure. The periodic process of chlorination/dechlorination of the catalyst surface determines the pulsed growth mode of carbon filaments with a pronounced segmented structure (Fig. 1). Due to the loose graphite packing, the obtained carbon nanofibers are characterized by high textural parameters ($S_{BET}$ up to 400 $m^2/g$ and $V_{pore}$ up to 1 $cm^3/g$).

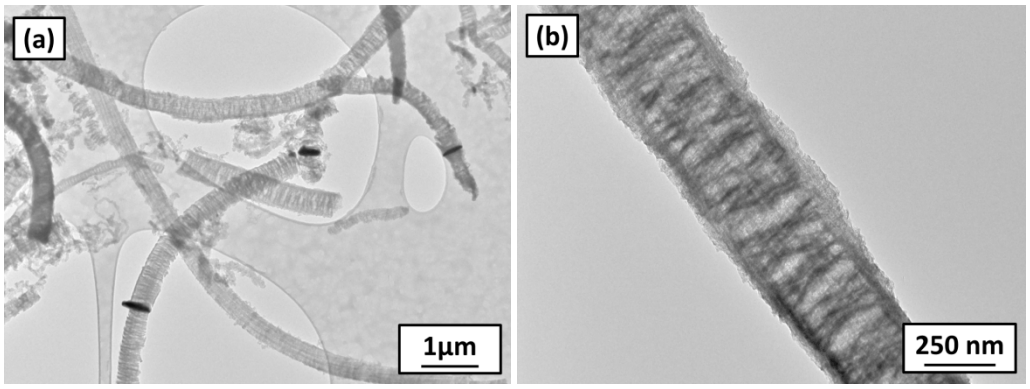


*Fig. 1. Transmission electron microscopy images of segmented carbon nanofibers obtained by the decomposition of trichloroethylene over a Ni96-Mo4 catalyst at 550 °C*

It is worth noting that the presence of nitrogen in the reaction medium, also affects the textural characteristics of the product. There is an increase in the specific surface area due to a greater defectiveness of the structure with the introduction of nitrogen.

This work discusses an application prospects of the obtained modified samples as adsorbents of 1,2-dichlorobenzene (DCB) from aqueous medium. Due to the difference in specific surface area, the adsorption capacity of CNM and N-CNM differs (0.0037 mol·$g^{-1}$ for CNM and 0.0051 mol·$g^{-1}$ for N-CNM). Also in this study, Pd nanoparticles (1.5 wt%) were deposited on the CNF's surface to produce hydrodechlorination catalysts. The results showed that the process is completed with 100% yield in 1 hour for all carbon samples.

In this work, the physicochemical and textural characteristics of the carbon product will be presented. The results of using CNM and F-CNM as carriers of palladium catalysts for DCB hydrodechlorination will also be presented.

**Acknowledgement:** This work was supported by the Russian Science Foundation, grant 22-13-00406.

**References:**

[1] L. Feng, N. Xie, J. Zhong, Materials. 7 (2014) 3919.
[2] D. Yadav, F. Amini, A. Ehrmann, Eur. Polym. J. 138 (2020)109963.
[3] A.M. Ozerova, A.R. Potylitsyna, Y.I. Bauman et al. Materials. 15 (2022) 8414.

## PP-I-77

# Exotermic Reactions in Mechanoactivated Ti-Fe Powder Mixes

Pribytkov G.A., Baranovskiy A.V. Korthova V.V., Firsina I.A., Krivopalov V.P.
*Institute of Strength Physics and Materials Sciences, Tomsk, Russia*
*gapribyt@mail.ru*

Intermetallic compounds $Fe_2Ti$ and FeTi find practical application as hydrogen accumulators (FeTi) or as magnetic materials ($Fe_2Ti$). Because of features of the Ti-Fe equilibrium diagram production of the intermetallic compounds by conventional metallurgy presents problems. Therefore powder metallurgy methods in a combination with preliminary mechanoactivation of the powder mixes [1,2] are widely used. A possibility to produce single-phase $Fe_2Ti$ and FeTi compounds from Fe and Ti powder mixes is investigated in our work. Powder mixes of 2F+Ti and Fe+Ti compositions were treated for 20 minutes in Activator 2S planetary ball mill at 40g intensity. The balls to powder ratio was equal 20. The mechanoactivated mixes were heated up in argon media with average rate of 100 degrees per minute. At 500 °C a sharp temperature rise (thermal explosion) appeared on the thermograms (fig 1) as a result of exothermal reaction in a mixtures. The rise rate in 2Fe+Ti mixture turned out much more, than that in Fe+Ti mixture. According to XRD analysis $Fe_2Ti$ compound is a major phase in the reaction products independently of the mixture composition. The reason is, on our opinion, the greater $Fe_2Ti$ negative enthalpy as compared to that of FeTi (-87.45 and-40.58 kcal/mol., accordingly). Next following high-temperature annealing failed to get single-phase mode of the thermal explosion products. On the basis of the received results a conclusion is drawn, that the thermodynamic factor (negative enthalpy of the interemitallics) is critically important for phase composition of the reaction products in the Ti and Fe powder mixtures.


*a)* *b)*

*Fig.1. Heating thermograms of mechanoactivated powder mixtures: 2Fe+Ti (a) u Fe+Ti (b). 1 – sample temperature; 2 – reactor wall temperature.*

**Acknowledgement:** This work was supported by the Russian Science Foundation, grant 23-29-00106.

**References:**

[1] Tetsuji Saito. Journal of Alloys and Compounds **364** (2004) 113–116.
[2] V.Yu. Zadorozhnyy , S.N. Klyamkin, M.Yu. Zadorozhnyy, D.V. Strugova, G.S. Milovzorov, D.V. Louzguine-Luzgin , S.D. Kaloshkin. Journal of Alloys and Compounds **707** (2017) 214-219.

## PP-I-78

# Synthesis of Nanoporous Materials by Magnesium-Thermal Reduction of Oxide Compounds of Tantalum and Niobium

Orlov V.M., Prokhorova T.Yu., Kryzhanov M.V.
*Tananaev Institute of Chemistry - Subdivision of the Federal Research Centre «Kola Science Centre of the Russian Academy of Sciences», Apatity, Russia*
*t.prokhorova@ksc.ru*

One of the ways to obtain powders with a large specific surface area is the reduction of tantalum and niobium pentoxides with magnesium vapor [1]. Due to the peculiarities of the reduction mechanism of these compounds with magnesium vapor, metal powders are obtained, the particles of which are characterized by a mesoporous structure [2].

Complex oxide compounds of tantalum and niobium, for example, $Mg_4Ta_2O_9$, $Mg_4Nb_2O_9$, can also be used as reduction precursors. The resulting metal powders also have a mesoporous structure, but with a smaller thickness of metal particles and magnesium oxide particles separating them. Essentially, the reduction product is a nanoscale composite: metal-magnesium oxide. After leaching of magnesium oxide, the metal particle is a spongy structure, the specific surface of which is determined by the number and size of pores. The parameters of the porous structure are determined not only by the reduction conditions, but also by the morphological features of the precursor itself. For example, the reduction of tantalum pentoxide of various genesis under the same conditions yielded powders with a specific surface area of 4 to 20 $m^2/g$ (Fig. 1).

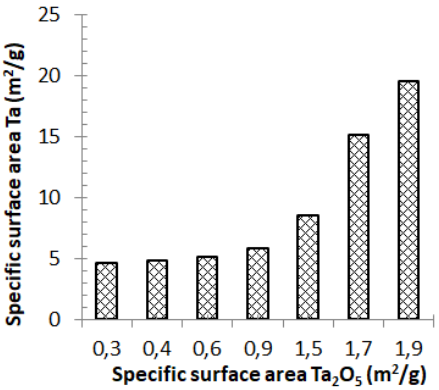


*Fig. 1. Dependence of the specific surface of Ta on the specific surface of $Ta_2O_5$*

Considering this factor, using $Mg_4Ta_2O_9$ and $Mg_4Nb_2O_9$ as precursors, we obtained tantalum powders with a specific surface area of up to 80 $m^2/g$ and niobium powders with a specific surface area of up to 170 $m^2/g$, in which 2/3 of the surface area falls on pores with a diameter of less than 5 nm [3, 4].

**References:**

[1] H. Haas, C. Schnitter, N. Sato [et al.] // CARTS Europe 2008 Proceedings. (2008) 157.
[2] R. Müller, M. Bobeth, H. Brumm, [et al.] // Int. J. of Materials Research. 98 (2007) 1138.
[3] V.N. Orlov, M.V. Kryzhanov, A.I. Knyazeva // Prot. Met. Phys. Chem. Surf. 52 (2016) 814.
[4] V.N. Orlov, M.V. Kryzhanov // Russian Metallurgy (Metally). 7 (2016) 596.

## PP-I-79

# The Effect of Polyethylene with Grafted Maleic Anhydride on the Properties of Secondary Polypropylene with the Inclusion of Aluminosilicate Microspheres

Psyanchin A.A., Zakharova E.M., Zakharov V.P.
*Ufa University of Science and Technology, Ufa, Russia*
*artps96@yandex.ru*

Aluminosilicate (ASM) and hollow glass microspheres (HGM) are promising fillers for recycled polypropylene (PP) due to their high chemical resistance, cheapness and low true density, due to which it is possible to obtain lightweight and durable plastic products with the possibility of their recycling. Due to the incompatibility of polypropylene and aluminosilicate microspheres in the preparation of polymer composites, the tensile strength of the samples decreases, and therefore the purpose of this work was to study the effect of polyethylene with grafted maleic anhydride (PE MA) on the properties of secondary polypropylene containing aluminosilicate and hollow glass microspheres.

The inclusion of 1 to 5% polyethylene with maleic anhydride practically does not change the melt flow rate of polymer composites and at the same time an increase in the tensile strength of polymer composites is observed using the AGS-X Shimadzu testing machine (Fig. 1).

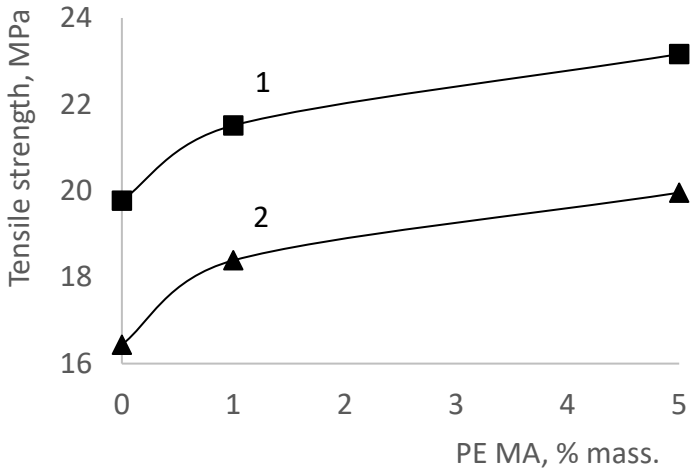


*Fig. 1. The change in the tensile strength of PP ASM (1) and HGM (2) polymer composites with the addition of a joint agent.*

According to the exo- and endothermic curves obtained by differential scanning calorimetry, it was also found that the addition of PE MA leads to an increase in the melting and glass transition temperatures of polymer composites.

**Acknowledgement:** This research was funded by the Ministry of Science and Higher Education of the Russian Federation (scientific code FZWU-2023-0002).

## PP-I-80

# The Effect of Partial Lead Substitution on the Stability of Hybrid Perovskites under Powerful Electron Fluxes

Rasmetyeva A.V.[1], Ustinova M.I.[2], Kukharenko A.I.[1], Sarychev M.N.[1], Troshin P.A.[2], Zhidkov I.S.[1]
*1 – Ural Federal University, Ekaterinburg, Russia*
*2 – FRC PCP and MC RAS, Chernogolovka, Russia*
*a.v.rasmetieva@urfu.ru*

Metal halide perovskite solar elements demonstrate the greatest potential for photovoltaics due to their low cost, suitable band gap and high solar energy conversion efficiency (PCE) [1]. However, the toxicity of Pb and point defects in polycrystalline films are an urgent problem, which may be solved by partial substitution of lead [2]. Recently, there has been a growing interest in the research of perovskite solar cells for space applications. The most important factor in space conditions may be the impact of cosmic particle radiation. In this work we study the effect of partial lead substitution on the stability of hybrid perovskites under powerful electron fluxes.

To study perovskite systems $CsFAM_xPb_{1-x}I_3$ with partial lead substitution, 32 systems were selected: reference $CsFAPbI_3$ and systems containing 31 different cations in the amount of 1 mole percentage relative to the lead content, i.e. $CsFAM_{0.01}Pb_{0.99}I_3$ compositions, where M = $Bi^{3+}$, $Eu^{2+}$, $Zn^{2+}$, $Fe^{2+}$, $Sn^{2+}$, $Ba^{2+}$, $Cd^{2+}$, $Sn4^{+}$, $Hg^{2+}$, $Pt^{2+}$, $Co^{2+}$, $Ce^{3+}$, $Ag^{+}$, $Ca^{2+}$, $Nd^{3+}$, $Ni^{2+}$, $La^{3+}$, $Sr^{2+}$, $Mn^{2+}$, $Ge^{2+}$, $Dy^{2+}$, $Er^{3+}$, $Cu^{+}$, $Lu^{3+}$, $Mg^{2+}$, $Sb^{3+}$, $Tb^{3+}$, $Y^{3+}$, $In^{3+}$, $Gd^{3+}$ и $Yb^{2+}$. Samples received 5 different doses of electrons ($1\cdot10^{14}$, $3\cdot10^{14}$, $1\cdot10^{15}$, $3\cdot10^{15}$ and 1 $10^{16}$ e/cm2) and then were investigated for changes in optoelectric characteristics.

We analysed data on the intensity and position and position of the photoluminescence maxima and identified 15 the most stable materials, where M = $Eu^{2+}$, $Sr^{2+}$, $Ge^{2+}$, $Cu^{+}$, $La^{3+}$, $Ce^{3+}$, $Tb^{3+}$, $Yb^{2+}$, $Dy^{2+}$, $Y^{3+}$, $Er^{3+}$, $Lu^{3+}$, $Gd^{3+}$, $Ni^{2+}$ and $Ag^{+}$. All these materials show only minor changes in the PL spectra relative to the reference values.

Another degradation process that can occur in Cs0.12FA0.88PbI3 films and related materials is its segregation into α-FAPbI3 and CsPbI3. XRD of films before and after irradiation with 1·1016 el/cm2 fluence showed the presence of an initial degree of segregation for most films, regardless of changes in their photoluminescent properties.

Electron fluxes causes the formation of small grains on the surface, the outlines of which correspond to increased content of $FA^{+}$ cation in them, which indicates phase segregation with the formation of individual $FAPbI_3$ crystallites.

Images of films obtained using SEM showed a decrease in the crystallinity of the material and the appearance of new small grains in the films. The material near the crack boundaries with a width of 0.5 microns has low conductivity, probably due to decomposition into yellow phases δ-CsPbI3 and δ-FAPbI3.

The greatest resistance of the morphology of films to electron irradiation was demonstrated by the compositions $Cs_{0.12}FA_{0.88}Pb_{0.99}La_{0.01}I_{\sim3}$, $Cs_{0.12}FA_{0.88}Pb_{0.99}Lu_{0.01}I_{\sim3}$,

$Cs_{0.12}FA_{0.88}Pb_{0.99}Ag_{0.01}I_{\sim 3}$, $Cs0_{.12}FA_{0.88}Pb_{0.99}Dy_{0.01}I_{\sim 3}$: their films practically do not contain cracks and newly formed grains on the surface. In other cases, the nature of formed cracks and their regularity indicate that their appearance may be due to the peculiarity of focusing the electron beam on the irradiation unit.

**Acknowledgement:** This work was supported by the Russian Science Foundation, grant 22-61-00047.

**References:**

[1] W. Nie et al., Science 10, 522 (2015).
[2] J.W. Wang et al., Energy Environ. Sci. 9, 2892 (2016).

## PP-I-81

# Advantages of Laser Electrodispersion for the Synthesis of CO Oxidation Catalysts with Low Loading of Precious Metals

Rostovshchikova T.N.[1], Shilina M.I.[1], Maslakov K.I.[1], Gurevich S.A.[2], Yavsin D.A.[2], Veselov G.B.[3], Stoyanovskii V.O.[3], Vedyagin A.A.[3]

*1 – Lomonosov Moscow State University, Moscow, Russia*

*2 – Ioffe Institute, RAS, St. Petersburg, Russia*

*3 – Boreskov Institute of Catalysis, Novosibirsk, Russia*

*rtn@kinet.chem.msu.ru*

The laser electrodispersion (LED) technique was used to design high-performance Pd and Pt catalysts based on alumina and zeolites for the processes of total (TOX) and preferential (PROX) CO oxidation. The selective deposition of finely dispersed nanoparticles produced in the laser torch plasma leads to the formation of crust-type catalysts [1]. Figure 1 shows the principle of the LED technique and the exterior view of the setup. Their high activity originates from the fact that a dense coating of individual nanoparticles is formed on the outer support surface even at a low metal loading ($10^{-2}$ wt.%) [2]. Based on TEM, XPS, FTIR studies, the relationship between structure and catalytic performance was established.

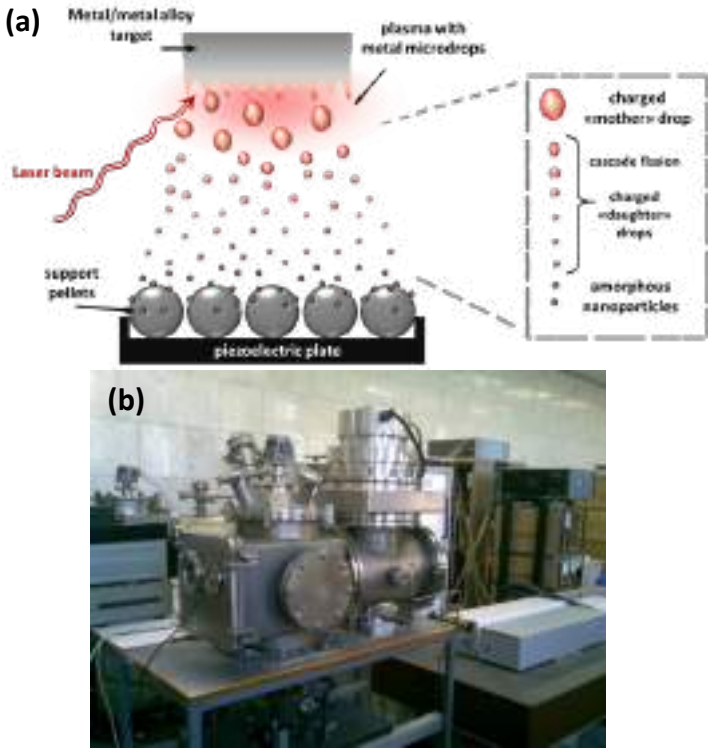


*Fig. 1. Principle scheme of the LED technique (a) and exterior view of the LED setup (b).*

Both Pd and Pt catalysts on HZSM-5 were more active in TOX if compared with alumina-based ones. Thus, the $T_{50}$ parameter (temperature of the 50% CO conversion) for the 0.01%Pd/ZSM-5 catalyst was 20 °C lower than that for the chemically prepared 0.55%Pd/$Al_2O_3$ sample [3].

The synthesized Pd samples were also tested in CO oxidation under prompt thermal aging conditions. When the model reaction mixture containing CO, $O_2$, NO and hydrocarbons (HC) was used, the 0.03%Pd/$Al_2O_3$ catalyst demonstrated the best thermal stability during heat treatment up to 1000 °C (Fig. 2) [4]. In the case of zeolite-based system, an effect of HC trapping is well seen. This effect is connected with adsorption of HC inside zeolite pores on the Pd-modified sites and their subsequent partial oxidation to CO.

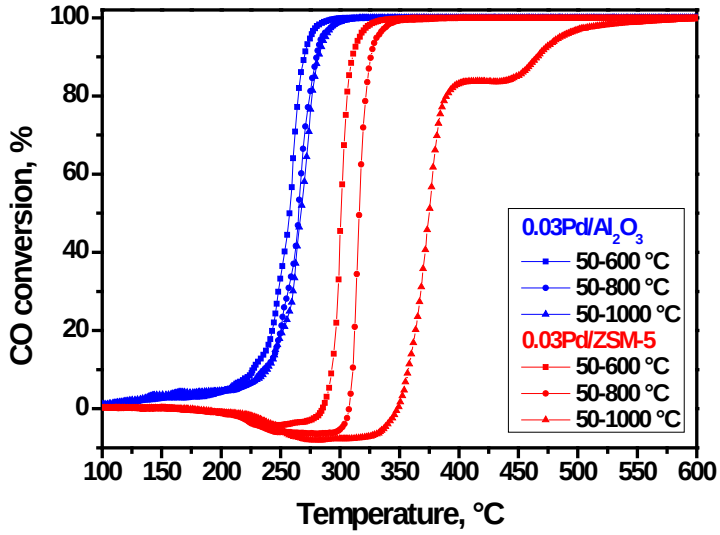


*Fig. 2. Light-off curves in CO oxidation under prompt thermal aging conditions for the 0.03Pd/$Al_2O_3$ and 0.03Pd/ZSM-5 samples.*

The Pt/ZSM-5 catalysts were more active and selective in the CO-PROX process in a $H_2$-rich mixture. The improved activity and stability was found when 0.05% Pt was deposited via LED on the ZSM-5 support pre-modified with Co [5]. The synergistic catalytic action of Pt and Co provides the hydrogen purification (<10 ppm) from CO in a wide temperature range from 50 to 150 °C, that even overlaps the operating window of 60–80 °C of proton exchange membrane fuel cells (PEMFC). In terms of their activity, stability, and selectivity, LED-prepared composites exhibit significantly superior properties with regard to supported catalysts obtained via conventional chemical methods.

**Acknowledgement:** This work was performed using the equipment purchased within the framework of the Lomonosov MSU Development Program. The Center of Collective Use “National Center of Catalysts Research” is acknowledged as well.

**References:**

[1] T.N. Rostovshchikova, E.S. Lokteva, M.I.Shilina et al., Russ. J. Phys. Chem. A, 95 (2021) 451.
[2] E.V. Golubina, T.N. Rostovshchikova, E.S. Lokteva et al., Appl. Surf. Sci. 536 (2021) 147656.
[3]T.N. Rostovshchikova, S.A. Nikolaev, I.N. Krotova et al., Russ. Chem. Bull. 71 (2022) 1179.
[4] T.N. Rostovshchikova, M.I. Shilina, S.A. Gurevich et al., Dokl. Phys. Chem. 506 (2022) 123.
[5] M. Shilina, I. Krotova, S. Nikolaev et al., Hydrogen, 4 (2023) 154.

## PP-I-82

# Magnetic Resonance and Magnetism of Carbonized Sodium Pectate Nickel Complex

Sabirova A.F.[1,2], Kadirov D.M.[2], Minzanova S.T.[1,2], Morozov V.I.[1], Nizameev I.R.[1,2], Drobyshev S.V.[2], Batulin R.G.[3], Karakhanov A.T.[3], Gafurov M.R.[3], Kadirov M.K.[1,2]

*1 – Arbuzov Institute of Organic and Physical Chemistry, Kazan, Russia*

*2 – Kazan National Research Technological University, Kazan, Russia*

*3 – Kazan Federal University, Kazan, Russia*

*aigul84saf@mail.ru*

Carbonization of nickel complexes of sodium pectate Ni-NaPG in an inert atmosphere to high temperatures according to certain protocols leads to the formation of nickel nanoparticles with interesting magnetic properties. The samples were synthesized by the carbonization of sodium polygalacturonate, 20% of which was replaced by nickel [Ni(20%)-NaPG], in an inert atmosphere at various temperatures.

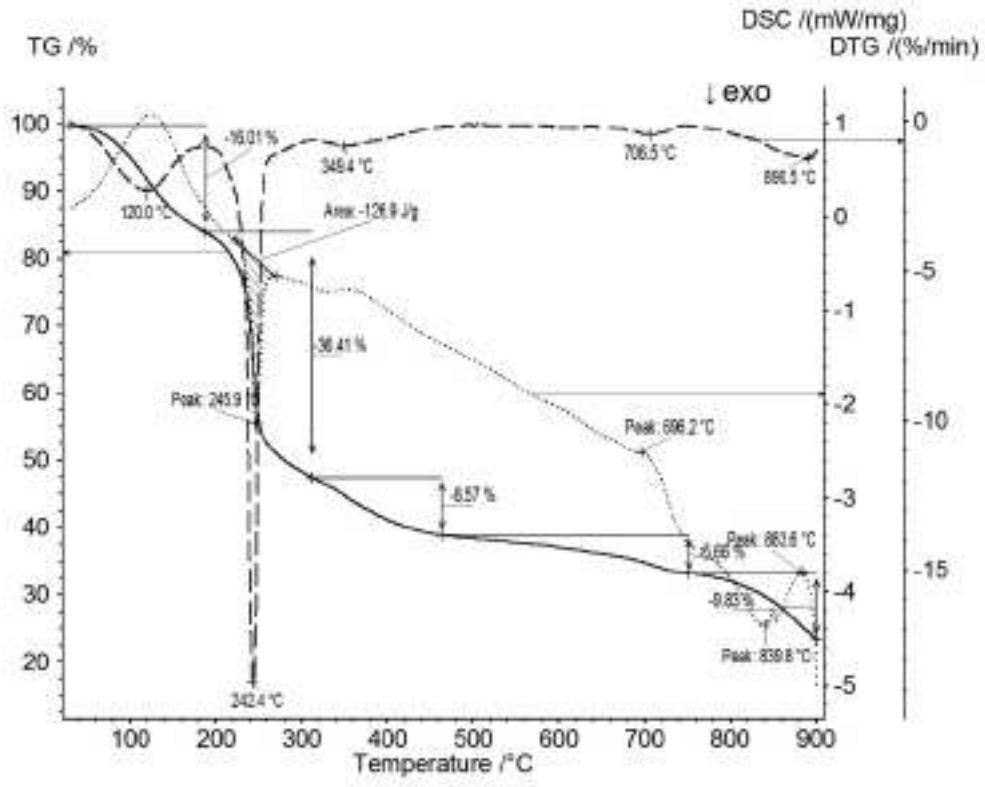


*Rice. Fig. 1. TG/DSC curves of Ni(20%)-NaPG in an argon atmosphere: TG—solid line, DTG—dotted line, DSC—dashed line.*

The TG/DSC curve of Ni(20%)-NaPG shown in Fig. 1 indicates that the thermogram has 5 noticeable weight loss stages: at 120.0°C, 242.4°C, 349.4°C, 706.5°C, and 890.5°C. Fourier IR spectra show that the main gaseous product at the first stage of weight loss is water, at the second stage decarboxylation and decomposition occur. After the second, third, and fourth mass losses, temperatures of 280°C, 550°C, and 800°C were chosen, up to which carbonization was carried out according to special protocols. The magnetic properties of samples in polycrystalline form (powders) of Ni(20%)-NaPG were measured after carbonization to

temperatures of 280, 550 and 800°C. Figure 2 shows the dependences of the specific magnetization on the magnitude of the magnetic field at a temperature of 5 K. After carbonization up to 280 °C, the magnetization of the sample linearly depends on the field, which is typical for paramagnets (Fig. 2, left). At the same time, the magnetization does not reach saturation up to 90 kOe. During carbonization up to T=550 °C and 800 °C, the magnetization value increases and a hysteresis loop and behavior characteristic of samples with ferromagnetic interactions appear (Fig. 2, on the right).

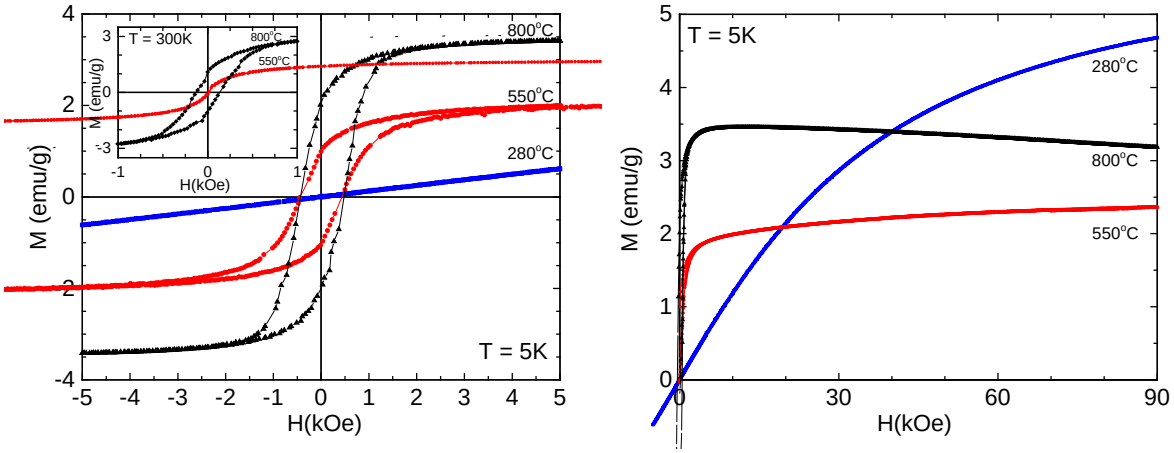


*Fig.2. Dependence of the specific magnetization on the magnitude of the magnetic field at temperatures of 5K and 300K (inset). Samples Ni-NaPG$_{280\,C}$, Ni-NaPG$_{550\,C}$, Ni-NaPG$_{800\,C}$. Signatures correspond to the synthesis temperature. Left – field range B<5 kOe, right - field range 0-90 kOe*

The electron magnetic resonance spectra (Fig. 3) independently confirm the magnetic measurements.

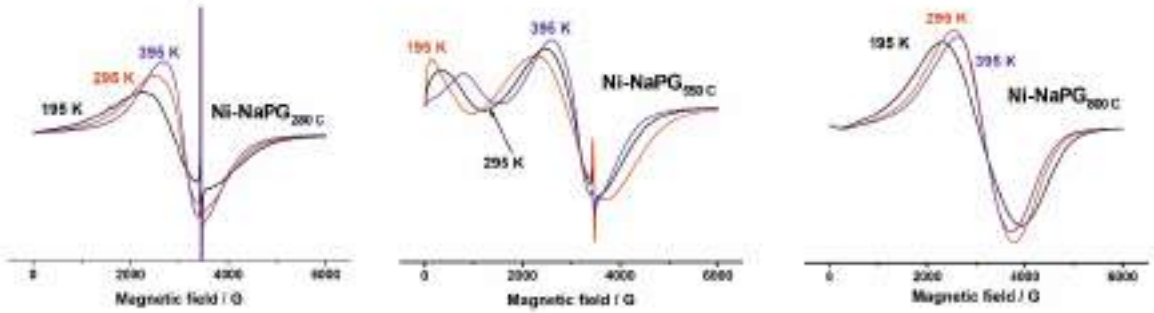


*Fig. 3. Спектры EMR Ni-NaPG$_{280\,C}$, Ni-NaPG$_{550\,C}$, Ni-NaPG$_{800\,C}$.*

**Acknowledgement:** This work was supported by the Russian Science Foundation, grant 22-29-00895.

## PP-I-83

# Radiation Thermal Sintering of Oxide and Composite Materials for Hydrogen Energy

Sadykov V.A.[1], Sadovskaya E.M.[1], Bespalko Yu.N.[1], Eremeev N.F.[1], Mikhailenko M.A.[2], Bryazgin A.A.[3], Korobeynikov M.V.[3]

*1 – Boreskov Institute of Catalysis, Novosibirsk, Russia*

*2 – Institute of Solid State Chemistry and Mechanochemistry, Novosibirsk, Russia*

*3 – Budker Institute of Nuclear Physics, Novosibirsk, Russia*

*sadykov@catalysis.ru*

Modern technologies of material processing for obtaining functional materials with unique characteristics are being intensively developed. Advanced sintering techniques such as microwave sintering, laser sintering, hot pressing, etc. are utilized for obtaining durable gas-tight functional ceramics for energy applications, since conventional sintering in a furnace does not always allow to achieve required tightness.

Radiation thermal sintering (RTS) by electron beams is based on bombardment of ceramic samples and functional layers by high-energy electron beams. The main features are dissipation of radiation energy in heterogeneous structure, thermal-diffusional stimulation of mass transfer due to forming point defects as well as amplification of thermally induced lattice vibrations and solid state reactions during synthesis, which allows to reduce sintering temperature and processing time. RTS technique can be applied for a wide range of materials including SOFC electrolytes, cathodes and anodes as well as permselective layers of membranes, catalysts, etc. Processing by e-beams can be applied for direct sintering of layered metal composites, zirconia, zirconia-corundum composites, Ln ferrites, Pr nickelate-cobaltites and their nanocomposites with doped ceria, etc.

The efficiency of the RTS was demonstrated for Ni-Zn and Mn-Zn ferrites synthesis via achieving the maximal transformation of the initial oxide mixtures into the ferrites [1]. Perovskites (such as Pr nickelates-cobaltites) and perovskite – fluorite nanocomposites after RTS maintain their transport properties such as a high oxygen mobility (Fig. 1) [2]. Advances were achieved in radiation thermal sintering of hydrogen separation materials such as Ln tungstates/molybdates and their nanocomposites with NiCu (Fig. 2), however, further optimization of sintering conditions is required [3]. RTS was demonstrated to be efficient technique for obtaining functional layers of solid oxide fuel cells and permselective membranes with required performance [2,4].

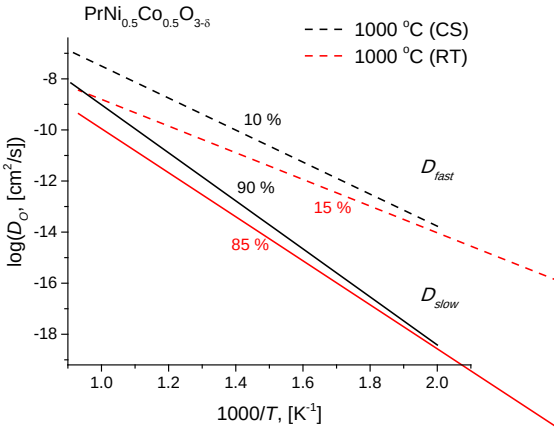


*Fig. 1. Arrhenius plots for oxygen tracer diffusion coefficient for $PrNi_{0.5}Co_{0.5}O_3$ sintered by conventional (CS) and radiation-thermal (RT) sintering at 1000 °C [2].*

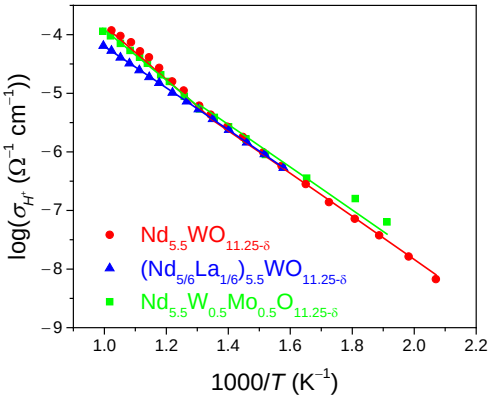


*Fig. 2. Protonic conductivity of Nd tungstates sintered using electron beams at 1100 °C [3].*

**Acknowledgement:** Different parts of this work were supported by the Russian Science Foundation, grant 23-73-00045, Ministry of Science and Higher Education of the Russian Federation within the governmental order for Boreskov Institute of Catalysis (project AAAA-A21-121011390009-1), Institute of Solid State Chemistry and Mechanochemistry SB RAS (project FWUS-2022-0001) and Budker Institute of Nuclear Physics SB RAS (project 4.0.02.0123).

**References:**

[1] A.A. Bryazgin, M.V. Korobeynikov, S.A. Kondratiev, V.I. Rostovtsev, Long-range effects in the interaction of an electron beam with crystalline substances, International Conference "Radiation Solid State Physics", 2019, pp. 55-64

[2] V.A. Sadykov, N.V. Mezentseva, L.N. Bobrova, O.L. Smorygo, N.F. Eremeev, Y.E. Fedorova, Y.N. Bespalko, P.I. Skriabin, A.V. Krasnov, A.I. Lukashevich, T.A. Krieger, E.M. Sadovskaya, V.D. Belyaev, A.N. Shmakov, Z.S. Vinokurov, V.A. Bolotov, Y.Y. Tanashev, M.V. Korobeynikov, M.A. Mikhailenko, Advanced Materials for Solid Oxide Fuel Cells and Membrane Catalytic Reactors, in: Advanced Nanomaterials for Catalysis and Energy. Synthesis, Characterization and Applications.– Elsevier.,2019.– pp.435-514

[3] V. Sadykov, Y. Bespalko, E. Sadovskaya, T. Krieger, V. Belyaev, N. Eremeev, M. Mikhailenko, A. Bryazgin, M. Korobeynikov, A. Ulihin, N. Uvarov, Nanomaterials 12(19) (2022) 3282.

## PP-I-84

# Development of a Thermoplastic Ceramic Feedstock for FGF 3D-Printing

Sagun A.I.[1], Toropkov N.E.[1], Lerner M.I.[1], Tkachev D.A.[2]
*1 – Institute of Strength Physics and Materials Science SB RAS, Tomsk, Russia*
*2 – Tomsk State University, Tomsk, Russia*
*ais43@yandex.ru*

**Introduction**. Additive manufacturing technologies have gained significant relevance in the production of ceramic products, owing to the growing needs of the industry. The ability to manufacture complex-shaped products that cannot be obtained through conventional molding methods has been a key driver in the increasing interest in 3D printing technology. Among the various 3D printing methods, Fused Granulate Fabrication (FGF) stands out as one of the cheapest and easiest to implement for ceramic product manufacturing.

Ceramic FGF printing involves the use of thermoplastic materials (feedstocks) consisting of a solid component and a polymer binder. The printed product undergoes a debinding process to remove the polymer component. This can be achieved either by thermal heating or dissolution in an organic solvent, with a combination of both methods often utilized. During debinding, a portion of the polymer binder is removed through dissolution, while the remaining portion determines the green strength of the product. The final firing process removes the remaining binder, making debinding a critical stage in the manufacturing process. Inadequate removal of the binder or incorrect debinding techniques can result in product distortions, cracks, and voids [1]. Therefore, studying the debinding process is crucial to ensure high-quality ceramic products are obtained.

**Work objective**. Producing feedstock using a polyol polymer-based binder and investigating the impact of debinding methods on the state of the green products.

**Methodology.** Starting materials consisting of $ZrO_2$ (ZT-3Y-E) and a binder based on polyol polymers were mixed using a single-screw extruder at 170 °C. To increase the homogeneity of the feedstocks, the material underwent four additional extrusions at 150 °C. Formulations containing $ZrO_2$ - 52, 53, 54, 56 and 58% vol. were prepared. The melt flow index (MFI) was measured for the feedstocks using Zwick/Roell Cflow plastometer.

The printed samples were subjected to solvent debinding, which involved placing pre-weighed samples in a container filled with acetone for 2, 3 or 4 days at room temperature. After debinding, the samples were dried either at 100 °C or 40 °C. The mass loss during debinding (MLD) was determined by weighing the dried samples on analytical scales.

**Results**. The findings of the MFI determination have been presented in Figure 1, with the turning point on the graph being attributed to the emergence of thixotropic properties in the melt. Two compositions, containing 52 and 53% vol. of the solid component, were selected to investigate the influence of debinding conditions.

Table 1 illustrates the outcomes of the solvent debinding process, expressed as the percentage of polymer removed from its initial quantity. The MLD was observed to increase

with debinding time, and was not influenced by the drying method employed. However, drying the samples at a temperature of 100 °C resulted in the formation of cracks, owing to the rapid evaporation of acetone and the difference in the TCLE of the sample regions with and without a binder. On the other hand, no cracks were detected in the samples that were allowed to age in acetone for 4 days, since a greater quantity of binder had been removed. Additionally, no cracks were found in the samples dried at 40 °C.

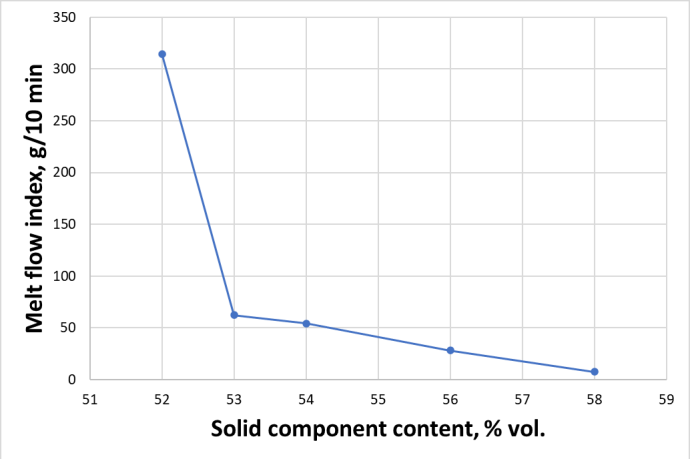


*Fig. 1. Change of MFI with an increase in the amount of the solid component*

*Tab. 1. Mass losses during debinding with different drying regimes*

| Debinding duration, days | Percentage of the removed binder from the initial polymer amount, % mass | | | |
|---|---|---|---|---|
| | Drying at 100 °C | | Drying at 40 °C | |
| | ZM52 | ZM53 | ZM52 | ZM53 |
| 2 | 44.77 | 44.86 | 45.11 | 43.49 |
| 3 | 49.87 | 49.98 | 48.88 | 49.13 |
| 4 | 52.51 | 52.32 | 52.32 | 51.46 |

Thus, feedstock containing zirconium dioxide was synthesized. The compositions, containing 52 and 53% vol. of the solid component, were selected based on MFI values. The impact of the drying regime following solvent debinding was investigated, with observations made regarding the condition of the samples.

It was observed that insufficient debinding time resulted in cracking of the samples subjected to extreme drying conditions. Hence, it is recommended to either extend the debinding duration or reduce the drying temperature to maintain the integrity of the samples.

**Acknowledgement:** The work was performed according to the Government research assignment for ISPMS SB RAS, project No. FWRW-2022-0002.

**References:**

[1] R. Enneti, S. Park, R. German, S. Atre. 27 (2012) 103.

## PP-I-85

# Synthesis of Porous Materials Based on Poly(styrene-co-divinylbenzene) from High Internal Phase Emulsions

Sankova N.N.[1], Shestakova D.O.[1,2], Parkhomchuk E.V.[1,2]
*1 – Boreskov Institute of Catalysis, Novosibirsk, Russia*
*2 – Novosibirsk State University, Novosibisk, Russia*
*natalya@catalysis.ru*

To date, polymerization of concentrated emulsions highly contributes to the development of hierarchically porous structures. The creation of macroporous catalysts, electrochemical sensors and materials for cell and tissue cultivation can be mentioned as promising applications of polymerised internal phase emulsions (PolyHIPEs). Incorporation of functional monomers and/or various types of nanoparticles can further improve substrate-material interaction and expand the scope of application of such materials [1],[2].

Emulsions that have at least 74% internal phase volume are usually defined as High Internal Phase Emulsions (HIPEs). Using emulsion templating method we prepared PolyHIPEs that contain $TiO_2$ or magnetic nanoparticles in the walls (Fig.1). By using functional co-monomer – 10-undecenoic acid carboxylated PolyHIPEs samples were also prepared. The obtained materials have wide pore size distribution in the region of 100 nm-100 microns (Fig.2). If the concentrated emulsions were stable, we were able to obtain the materials with the porosity of more than 80%, including the emulsions stabilized with inorganic nanoparticles.

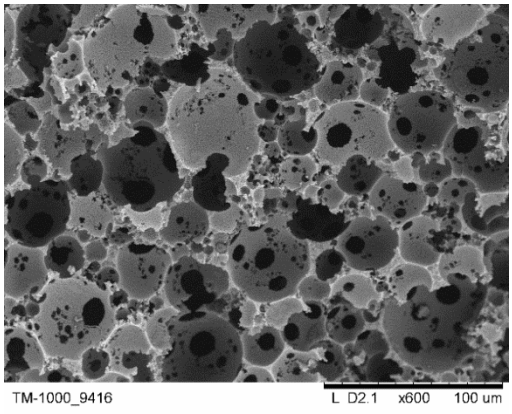


*Fig. 1. Macroporous material based on poly(styrene-co-divinylbenzene) with $TiO_2$ nanoparticles*

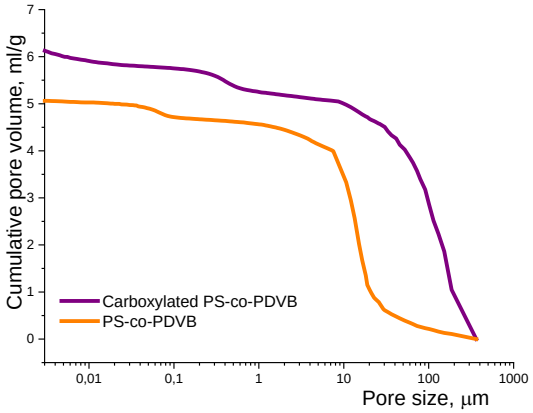


*Fig. 2. Hg-intrusion curves of macroporous poly(styrene-co-divinylbenzene) samples*

**Acknowledgement:** Our work was supported by the Ministry of Science and Higher Education of the Russian Federation within the governmental order for Boreskov Institute of Catalysis (project AAAA-A21-121011490008-3).

**References:**

[1] B. Aldemir Dikici, F. Claeyssens, Front. Bioeng. Biotechnol. 8 (2020).
[2] N.R. Cameron, Polymer (Guildf). 46 (2005) 1439–1449.

## PP-I-86

# Influence of the Solvent on the Dynamics of Excited Electrons in Plasmonic Nanoparticles of Silver

Ibrayev N., Seliverstova E., Kanapina A.

*Institute of Molecular Nanophotonics, Buketov Karaganda University, Karaganda, Kazakhstan*

*genia_sv@mail.ru*

The phenomenon of localized plasmon resonance is an attractive topic of research in the last few decades due to the possibilities of its practical application. Plasmonic nanoparticles of noble metals increase the efficiency of various optical and optoelectronic phenomena, including Raman scattering and photo catalysis [1-5], and also improve the characteristics of organic LEDs and photovoltaic devices.

Flash photolysis methods are used to study the dynamics of electronic excitation in plasmon nanoparticles (NP) of metals. This is due to the fact that this method is very highly sensitive, allows detecting single LF and investigating the dynamics of fast-flowing processes [6].

In this paper, the effect of the solvent on the dynamics of excited electrons in the Ag NP is investigated.

Silver NPs were synthesized by laser ablation of a silver target in ethanol using an Nd:YAG laser with $\lambda_{gen}$ = 532 nm, pulse duration$t_{pulse}$ = 8 ns and pulse energy equal to 73 MJ. The ablation time is 15 minutes. The concentration of NP silver in the resulting solution was $3.73 \cdot 10^{-10}$mol/L. The average diameter of the NPs (ZetasizerS90, Malvern) was equal to 19.3±4.1 nm. Next, solutions were prepared with a constant concentration of NP Ag, but with a different ratio of ethanol and water, which was equal to 1:0, 1:1 and 0:1.

The absorption spectra of the samples were measured using a Cary-300 spectrophotometer (Agilent). The spectra and kinetics of the transient absorption were studied by pulsed photolysis using an LP-980K spectrometer (Edinburgh Instr.) when excited by Nd:YAG laser radiation (LQ215, SolarLS) with $\lambda_{exc}$ = 355 nm with pulse energy E =15.6 MJ and pulse duration $t_{pulse}$ = 7 ns.

Measurements have shown that the spectrum of stationary absorption of plasmonic NP Ag in ethanol, water and water-ethanol solutions practically does not change. The maximum of the steady–state absorption spectrum of NP Ag shifts to the red region with an increase in the proportion of water in the solution - from 396 to 402 nm. At the same time, there is also an increase in optical density from 0.064 to 0.09 (Table).

In contrast to transient absorption, the solvent composition has a strong influence on the kinetics of transient absorption of plasmonic NPs (Fig. 1, Table). The maximum optical density of the transient absorption ΔOD is observed for a solution of NP silver in ethanol. When water is added, it drops 2.5 – 5 times. The duration of the transient absorption of NP Ag is also

reduced – the long-term component almost completely disappears already at the ethanol ratio:water is 1:1.

*Table – Data on the optical density parameters of stationary (D) and transient (ΔOD) absorption of NP Ag in solutions with different ratios of ethanol and water, $\lambda_{exc}$= 355 nm, $\lambda_{reg}$= 380 nm.*

| Ethanol:$H_2O$ ratio | $\lambda_{max}$, нм | D | ΔOD | $\tau_1$, нс | $\tau_2$, μс |
|---|---|---|---|---|---|
| 1:0 | 396 | 0,064 | 0,077 | 26,6 | 107 |
| 1:1 | 400 | 0,073 | 0,030 | 24,5 | – |
| 0:1 | 400 | 0,090 | 0,014 | 20,2 | – |

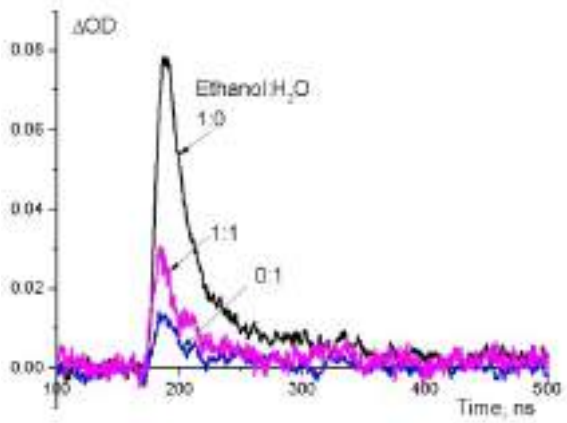


*Fig. 1. Kinetics of the transient absorption of Ag NPs (19.3±4.1 nm) in solutions with different ratios of ethanol and water*

Thus, an increase in the number of water molecules around the Ag NP leads to a decrease in both the intensity and duration of the transient absorption of Ag NP obtained by laser ablation.

The long-lived transient absorption of NP Ag can be explained on the basis of the concept of interfacial micro-convective heat exchange between the surface of the NP metal and the molecules of the medium [6]..

**Acknowledgement:** This research is funded by the Science Committee of the Ministry of Education and Science of the Republic of Kazakhstan, grant no. AP14870117.

**References:**

[1] Dzhanabekova R.; Ibrayev N., Bull. Univ. Karaganda-Phys. 1 (2020) 18.
[2] Ibrayev N.K., Zhumabekov A.Z., Seliverstova E.V., Eurasian J. Phys. Funct. Mater. 3 (2020) 261.
[3] Ibrayev N., Afanasyev D., Omarova G. Eurasian Phys. Tech. J. 2(2021) 29.
[4] Siavash Moakhar R., Gholipour S., Masudy-Panah S. et al., Recent Adv. Sci. 7 (2020) 1902448.
[5] Seliverstova E., Ibrayev N., Omarova G. et al., J. Lumin. 235 (2021) 118000.
[6] Ibrayev N., Seliverstova E., Kucherenko M., J. Lumin. 245 (2022) 118760.

## PP-I-87

# Triple Alloys of the Pt-Mo-W System as the Thermal Decomposition Products of Complex Salts

Serebrennikova P.S.[1,2], Lagunova V.I.[2], Zadesenets A.V.[2], Gromilov S.A.[1,2]
*1 – Novosibirsk State University, Novosibirsk, Russia*
*2 – Nikolaev Institute of Inorganic Chemistry, Novosibirsk, Russia*
*ps.serebrennikova@yandex.ru*

Multimetallic complex salts (CS) have attracted great deal of attention in recently as precursors for the synthesis of a wide class of nanomaterials, in particular, multicomponent alloys of refractory metals. Previously, researchers considered bimetallic complex salts mainly, that were easily synthesized and stable in composition. This approach significantly limited the composition of the obtained alloys to two kinds of metal atoms and the stoichiometry of the precursors. Nowadays, when the attention of materials scientists is focused on studying the properties of multicomponent high-entropy systems with different ratios of metals, it becomes interesting to adapt the existing technology of complex salts thermolysis to obtain them. Theoretically, this can be done by the thermolysis of the isostructural double CS co-crystallization products. However, in this case, the main issue in finding the "method of preparation/phase composition/properties" regularity for thermolysis products is the question of phase-uniformity and homogeneity of the precursor solid solution. In present work, an attempt to obtain triple alloys of the Pt-Mo-W system, interesting due to their possible catalytic properties [1], by the thermolysis of the $[Pt(NH_3)_4]MoO_4$ and $[Pt(NH_3)_4]WO_4$ co-crystallization product is made.

For the synthesis of $[Pt(NH_3)_4](WO_4)_{0.5}(MoO_4)_{0.5}$, 0.0238 g of $Na_2WO_4{\cdot}2H_2O$ and 0.0176 g of $Na_2MoO_4{\cdot}2H_2O$ (molar ratio Mo:W = 1:1) were dissolved separately in a minimum volume of water. The resulting salt solutions were mixed, and then a solution of 0.0559 g $[Pt(NH_3)_4](NO_3)_2$ was added to the resulting mixture. The sedimentation of a white crystalline product was observed in a short time.

A comprehensive X-ray study of both a series of individual single crystals (Bruker D8 Venture, equipped with the Incoatec IμS 3.0 tube, three-circle goniometer, the PHOTON III CPAD detector with a resolution of 768x1024 and a pixel size of 135x135 microns, Mo$K_\alpha$-radiation) and the entire polycrystalline sample (Bruker D8 Advance, Bragg-Brentano scheme, Cu$K_\alpha$-radiation, LYNXEYE XE-T detector) were performed. In the last case, the 5% weight impurity of $Na(NO)_3$ was detected. While studying individual single crystals, it was found that the resulting product is homogeneous and is the solid solution $[Pt(NH_3)_4](WO_4)_x(MoO_4)_{1-x}$ with $x \approx 0.5$. The composition of the obtained crystals was further refined using Zen law and the original method of the unit cell parameters refining [2].

Thermal decomposition of several samples (polycrystalline one and individual single crystals) was carried out in the $H_2$ atmosphere, at the temperature of 1000 ° C for 8 hours. In all cases, the formation of a single-phase metal product based on a hexagonal close packed

cell was demonstrated. The formation of a homogeneous alloy of the Pt-Mo-W system was confirmed by scanning electron microscopy on the JSM 6700F CM device equipped with an EDX analyzer.

**Acknowledgement:** The research was supported by the Ministry of Science and Higher Education of the Russian Federation, N 121031700313-8 and Priority 2030; the research was carried out at the expense of the grant of the Russian Science Foundation No. 22-23-00672, https://rscf.ru/project/22-23-00672/.

**References:**

[1] V. Lagunova, et al, Int. J. Hydrog. Energy. In press (2022). DOI: 10.1016/j.ijhydene.2022.09.086
[2] P.S. Serebrennikova, S.A. Gromilov, J. Struct. Chem. 63 (2022) 1820. DOI:10.1134/S0022476622110129

## PP-I-88

# Atomistic Perspective on the Lithium Self-Diffusion and Crystallite Growth Using Machine Learning Interatomic Potential

Sergeev A.V.[1,2], Kondratyeva Y.[1]

*1 – Semenov Federal Research Center for Chemical Physics, Moscow, 119991, Russia*

*2 – Faculty of Physics, Lomonosov Moscow State University, Moscow, 119991, Russia*

*a.sergeev@chph.ras.ru*

Application of Li-metal negative electrodes free of any extra weight associated with the host materials such as graphite or silicon is one of the promising ways of enhancing modern lithium batteries. Unfortunately, the morphological instability of lithium during its electrodeposition upon charge cycle makes this approach unfeasible in practical applications. The growth of fibrous crystals knowns as 'whiskers' or 'dendrites' leads to rapid capacity fading due to the formation of 'dead lithium' and short-circuiting of lithium-metal batteries. The mechanism of lithium whisker growth is a subject of debate. Several models of the process are proposed, however, most of the experimental observations corroborate the one suggesting the insertion of atoms into the base of a growing whisker by analogy with tin whiskers growth. Thus, mass-transfer of the freshly deposited lithium toward the root of the whisker should has a major impact on the growth regime. Therefore, we employed molecular dynamic (MD) simulations to investigate the contribution of defects, such as grain boundaries (GB), vacancies and interstitial atoms, to lithium self-diffusion rate.

A novel Machine Learning Interatomic Potential for Li, which was trained basing on the DFT calculation results [1], was employed to ensure the high accuracy of the simulations. Our results predict amorphous structure of the twist grain boundaries at room temperature [2]. The lithium flux along such GBs exhibits square root dependence on the amplitude of the applied external force, i.e. it can be accurately described by a viscous liquid flow model. A simulation procedure that includes continuous insertion of extra atoms into the GB region enabled explicit modeling of lithium crystallite growth via absorption of newly deposited atoms at the grain boundary and their subsequent building into the crystal lattice (see Fig. 1). Simulation of self-interstitial defect diffusion predicts it that such defects predominantly propagate along <111> axes resulting in highly correlated motion and its non-Arrhenius behaviour [3]. At room temperature diffusion coefficient of self-interstitial defect is calculated to be about 6 times higher than that of a vacancy. The obtained results enable further quantitative modeling of the mass transfer process in polycrystalline lithium feeding the whisker growth.

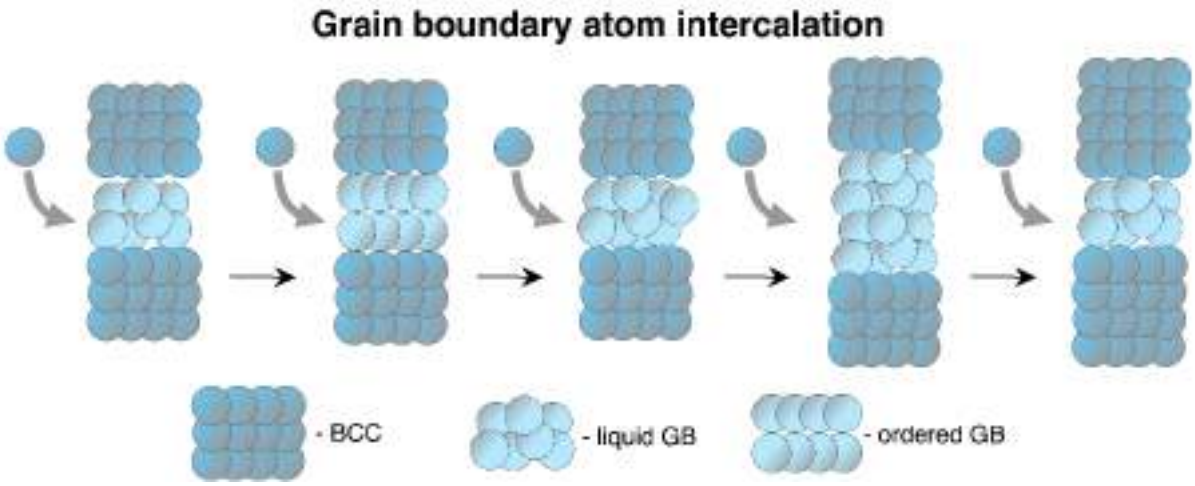


*Fig. 1. Grain boundary evolution upon lithium deposition*

**Acknowledgement:** This work was supported by the Russian Federation President grant № МК 3049.2022.1.3 (075-15-2022-369).

**References:**

[1] I.S. Novikov, K. Gubaev, E.V Podryabinkin, A.V Shapeev, Mach. Learn. Sci. Technol. 2 (2021) 025002
[2] Sergeev A. V. et al., Acta Mater. 233 (2022) 117988
[3] Sergeev A. V. et al., Materialia 28 (2023) 101718

## PP-I-89

# Synergistic Nanostructured Catalysts of CO Oxidation Based on Co/Ce and Cu/Ce Modified Zeolites ZSM-5

Shilina M.I.[1], Ivanin I.A.[1], Krotova I.N.[1], Udalova O.V.[2]
*1 – Lomonosov Moscow State University, Moscow, Russia*
*2 – Semenov Federal Research Center for Chemical Physics, RAS, Moscow, Russia*
*mish@kinet.chem.msu.ru*

CO oxidation is one of the most studied reactions both in terms of analyzing the key stages of heterogeneous catalytic processes and for the purpose of application for the removal of hazardous environmental pollutants. The implementation of this process, especially at moderate and low temperatures, is of interest for the purification of industrial and automobile exhaust gases. Oxide systems $Co_3O_4/CeO_2$ and $CuO/CeO_2$ are promising catalysts for CO oxidation. The use of zeolites modified with transition metals makes it possible to create new types of active sites that are not typical for oxide systems. This is due to the fact that the aluminosilicate framework of the zeolite stabilizes isolated metal cations $M^{n+}$ and oxocations $[M_xO_y]^{m+}$ (Fig.1) [1–3]. Modified zeolites containing two different metals may differ from mixed oxides in the mechanism of the synergistic effect in catalysis.

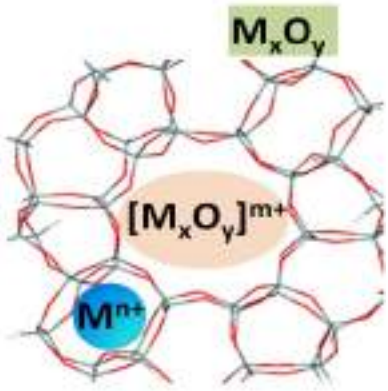


*Fig. 1. States of extra framework metal species in zeolite*

Series of catalysts based on Co/Ce and Cu/Ce-modified zeolites ZSM-5 (Si/Al=15, 27.5 and 40) have been synthesized by sequential incipient wetness impregnation with 1.7 – 4 wt. % Co, 2.6 - 4 wt. % Cu and 0 – 6 wt. % Ce. The total concentration of introduced metals was chosen in order to minimize the formation of oxides on the surface. The catalytic oxidation of carbon monoxide is carried out on modified Co/Ce/ZSM-5 and Cu/Ce/ZSM-5 zeolites at the temperatures of 50–200 °C. Based on TEM, XPS, UV-vis-DRS, DRIFTS and in situ CO-reduction studies the nature of active sites was revealed and the relationship between structure and catalytic performance was established. In the systems under study a pronounced synergistic effect of catalytic action of cobalt (or copper) and cerium is observed, associated with the various redox interaction between the metals.

The ratio of the components is of greatest importance for the catalyst activity. The dependence of the temperature for reaching 50% CO conversion on the catalyst composition

of Co/Ce/ZSM-5 displays minimum corresponding to the most active catalyst 2.5Co/2Ce/Z (Fig.2) [2,3]. It means that there is an optimal cobalt:cerium atomic ratio close to 3:1. It was shown that $Co^{III}$- $Ce^{III}$-containing catalytically active species with Co-O-Ce bridges can be formed in the zeolite channels. Most likely, these species are mixed Co-Ce oxo-cations $[Co_xCeO_y]^{n+}$. In the DRIFT spectra of adsorbed CO, the appearance of a new band of 2179 $cm^{-1}$ was found [2].

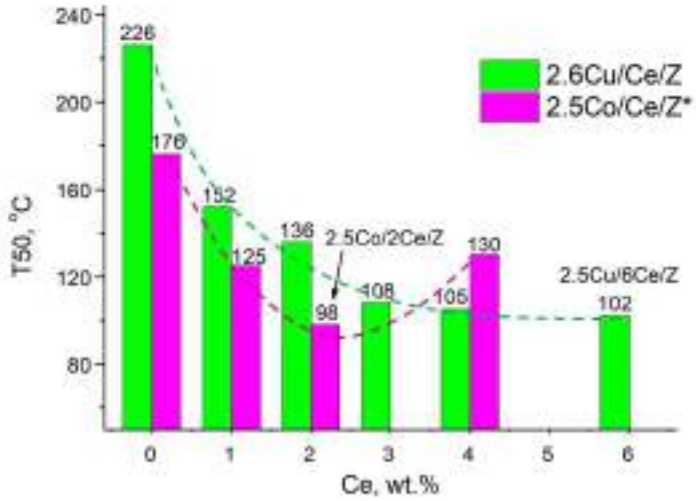


*Fig. 2. Temperatures of 50% CO Conversion (T50) on 2.6Cu/Ce/Z-55 and similar cobalt-containing 2.5Co/Ce/Z-55 catalysts*

In bimetallic Cu/Ce/ZSM-5 systems a pronounced synergism of the catalytic action of metals is observed with the introduction of even small additions of cerium (Cu:Ce=6). With an increase in the cerium content to Cu:Ce=1, the temperature of achieving 50% CO conversion (T50) decreases and tends to a limiting value close to 100°C. The observed dependence of Cu/Ce/ZSM-5 activity on catalyst composition distinguishes from the extreme dependence of T50 in the Co/Ce/ZSM-5 systems (Fig.2).

An increase in the Si/Al ratio of the zeolite from 15 to 40 contributes to a higher catalytic activity of the Cu/Ce system, in contrast to the Co/Ce/ZSM-5 catalysts, for which the activity in CO oxidation rises with increasing the aluminum content in the zeolite framework [2,3]. Different patterns of catalytic activity depending on the composition of the catalysts are explained by the different nature of the active sites in the Cu/Ce/ZSM-5 and Co/Ce/ZSM-5 systems.

**Acknowledgement:** This work was performed using the equipment purchased within the framework of the Lomonosov MSU Development Program.

**References:**

[1] Shilina M.I., Rostovshchikova T.N., Nikolaev S.A. et al., *Mat. Chem. Phys.* 223 (2019) 287.
[2] M.I Shilina., O.V. Udalova., I.N., Krotova et al., ChemCatChem 12 (2020) 2556.
[3] I.A. Ivanin, I.N. Krotova, O.V. Udalova et al., Kinetics and Catalysis, 62 (2021), 799

## PP-I-90

# Development of Ti3C2Tx+Fe3O4 Nanocomposite Materials for Water Remediation

Shilov N.R., Sobolev K.V., Omelyanchik A.S., Magomedov K.E., Rodionova V.V.
*1 – Immanuel Kant Baltic Federal University, Kaliningrad, Russia*
*nikolayshilov2002@gmail.com*

MXenes are a new class of two-dimensional nanomaterials with the general formula $M_{n+1}X_nT_x$, where M is an early transition metal, X is either C or N and $T_x$ is a surface functional group, typically -OH, -O or -F; n is an integer index that usually takes values from 1 to 3.[1] MXenes have found wide application in various fields, such as energy, medicine, sensors, environmental remediation and others.[2] In environmental protection technology, MXenes are comprehensively studied due to their huge adsorption capacity and the demonstrated ability to absorb heavy metals ions and radionuclides, as well as dyes from the aqueous medium.[3]-[5] However, the problem with removing MXene particles from treated water is still unsolved.

Composite materials containing MXenes, decorated with various nanoparticles, can enhance the functional properties of MXenes and provide the opportunity of their fine-tuning. Nanoparticles of different chemical compositions, shapes and sizes have now been grown on MXenes.[6]-[8] Creation of a composite with magnetic nanoparticles (MNPs) can solve the problem of removing MXenes from the purified water by means of the external magnetic field.

In this work we consider the decoration of Ti3C2Tx MXene sheets with Fe3O4 MNPs using ultrasound-assisted co-precipitation synthesis technique. First, Ti3C2Tx+Fe3O4 composite material was created and characterized by means of XRD, SEM-EDX and TEM. It was found that the growth of magnetite promoted additional delamination of the multilayer MXenes, leading to the formation of single or few-layer flakes, fully covered with MNPs. This fact lets us assume that the new, cheap and eco-friendly approach to produce magnetic MXene-based composites was successfully developed. This synthesis method can be extended to various other compositions, such as CoFe2O4 (CFO). In addition, it was observed that increasing the concentration of MXenes during the co-precipitation process leads to an increase in the size of Fe3O4 from 14 nm to 52 nm. Magnetic properties of the obtained composites were studied using VSM and SQUID. It has been shown that the saturation magnetization of composites varies from 16 A $m^2$ $kg^{-1}$ to 38 A $m^2$ $kg^{-1}$ in proportion to the mass content of magnetic particles in the composite. Then, the absorption properties of the composites towards Cu(II) ions from aqueous media were studied. It was proved that MXene sheets still possess high adsorption capacity, being enriched at the same time by ferrimagnetic properties which allowed complete removal of the adsorbent from water.

**Acknowledgement:** This work was supported by the Russian Science Foundation, grant 22-12-20036.

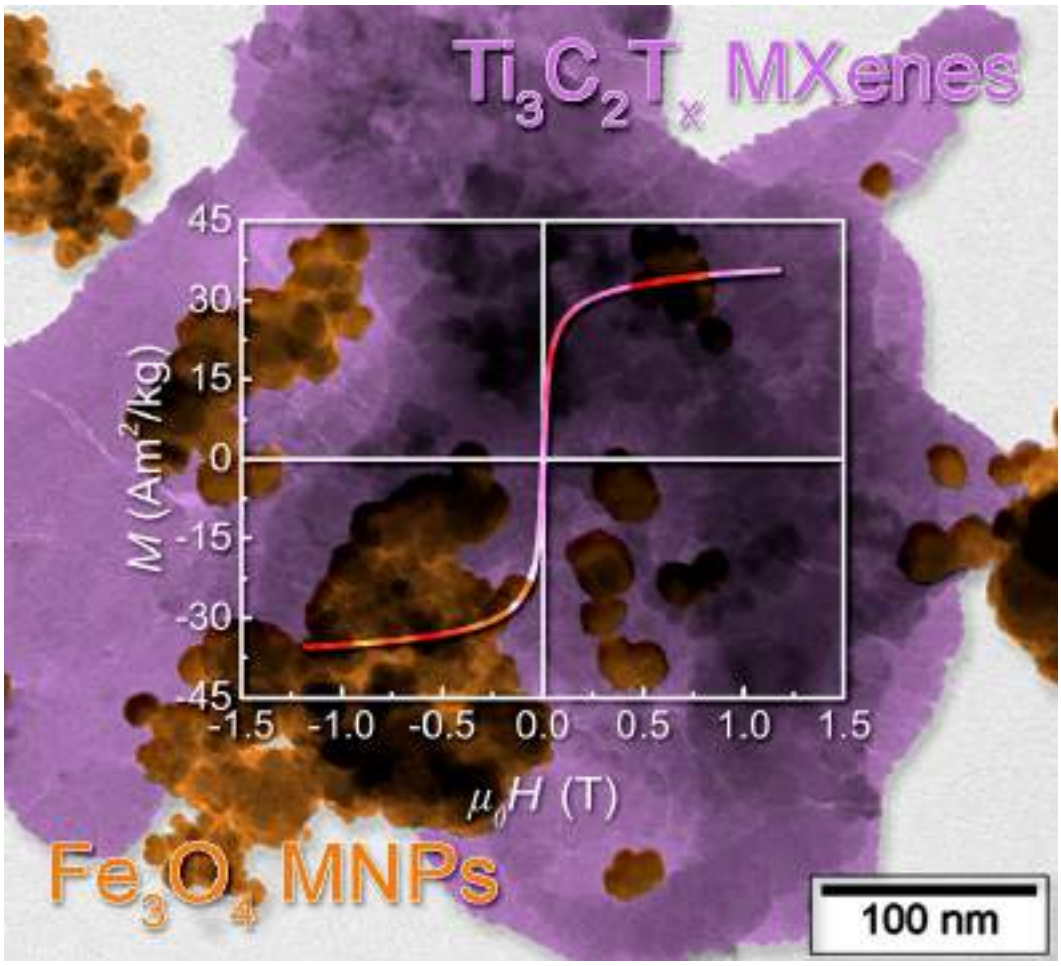


*Figure 1. TEM image of Ti3C2Tx+Fe3O4 (1:2 mass ratio between two components) composite material and M vs H loop, demonstrating its superparamagnetic behavior.*

**References:**

[1] M. Naguib, V.N. Mochalin, M.W. Barsoum, Y. Gogotsi, Adv. Mater. 2014, 26, 992.
[2] M. Khazaei, A. Mishra, N.S. Venkataramanan, A.K. Singh, S. Yunoki, Curr. Opin. Solid State Mater. Sci. 2019, 23, 164.
[3] X. Hu, C. Chen, D. Zhang, Y. Xue, Chemosphere 2021, 278, 130206.
[4] L. Wang, H. Song, L. Yuan, Z. Li, Y. Zhang, J.K. Gibson, L. Zheng, Z. Chai, W. Shi, Environ. Sci. Technol. 2018, 52, 10748.
[5] V. Thirumal, R. Yuvakkumar, P.S. Kumar, S.P. Keerthana, G. Ravi, D. Velauthapillai, B. Saravanakumar, Chemosphere 2021, 281, 130984.
[6] M. Rethinasabapathy, G. Bhaskaran, B. Park, J.-Y. Shin, W.-S. Kim, J. Ryu, Y.S. Huh, Chemosphere 2022, 286, 131679.
[7] F. Qiu, Z. Wang, M. Liu, Z. Wang, S. Ding, Ceram. Int. 2021, 47, 24713.
[8] J. Su, X. Zhao, W. Zhou, C. Wang, P. Zhang, J. Mater. Sci. Mater. Electron. 2021, 32, 25919.

## PP-I-91

# Ionic Conductivity, Dielectric Properties and Spectroscopic Characterization of "Stuffed" $Tm_2(Ti_{2-x}Tm_x)O_{7-x/2}$ (x = 0, 0.1, 0.18, 0.28, 0.74) Pyrochlores

Gorshkov N.V.[1,2], Baldin E.D.[1], Rassulov V.A.[3], Karyagina O.K.[4], Stolbov D.N.[5], Shlyakhtina A.V.[1]

*1 – N.N. Semenov Federal Research Center for Chemical Physics, Russian Academy of Sciences, Moscow, Russia*

*2 – Yu.A. Gagarin Saratov State Technical University, Saratov, Russia*

*3 – N.M. Fedorovsky All-Russian Scientific Research Institute of Mineral Raw Materials, Moscow, Russia*

*4 – Emanuel Institute of Biochemical Physics RAS, Moscow, Russia*

*5 – Department of Chemistry, Lomonosov Moscow State University, Moscow, Russia*

*annashl@inbox.ru; annash@chph.ras.ru*

$Tm_2(Ti_{2-x}Tm_x)O_{7-x/2}$ ($x$ = 0, 0.1, 0.18, 0.28, 0.74) solid electrolytes were investigated as the base element of the SOFC stack (SOFC batteries) with potential of operating in the medium temperature range (600-700 °C), using methane as fuel. The design of new oxygen-conducting materials is of important point for their possible utilization in the solid oxide fuel cells.

The oxygen ion conductivity of $Tm_2(Ti_{2-x}Tm_x)O_{7-x/2}$ ($x$ = 0, 0.1, 0.18, 0.28, 0.74) "stuffed" pyrochlores ceramics was investigated by electrochemical impedance spectroscopy (two-probe AC) in dry and wet air. It is shown that the synthesis of precursors using the co-precipitation method and the choice of temperature for the decomposition of the precipitate plays an important role in obtaining dense and high conductive ceramics. The maximum total conductivity of $Tm_2(Ti_{2-x}Tm_x)O_{7-x/2}$ ($x$ = 0.18) was found to be ~ $2.96\times10^{-3}$ S/cm at a temperature of ~ 770ºC. The conductivity of the fluorite-like solid solution $Tm_2(Ti_{2-x}Tm_x)O_{7-x/2}$ ($x$ = 0.74) is an order of magnitude lower. However, for the first time in the $Ln_2O_3$-$TiO_2$ ($Ln$ = Er-Lu) systems, a proton contribution of ~ $5\times10^{-5}$ S/cm at 600 ºC was found for $Tm_2(Ti_{2-x}Tm_x)O_{7-x/2}$ ($x$ = 0.74). X-ray diffraction with Rietveld refinement optical spectroscopy and temperature dependence of dielectric permittivity followed the structural disorder in a series of solid solutions with increasing thulium oxide content. It is shown that the use of fast and slow cooling rates of thulium series solid solutions has different effects on the properties of the ceramics. Slow cooling initiates the growth of fluorite nanodomains in the pyrochlore matrix, and the creation of such nanostructured and high-density composites is a promising direction for the synthesis of highly conductive solid electrolytes for SOFCs. It has been suggested that high-temperature annealing of nano-sized precursors with a nominally stoichiometric composition of $Tm_2Ti_2O_7$ promotes the formation of lightly doped "stuffed" pyrochlore, which exhibits the high oxygen-ion conductivity.

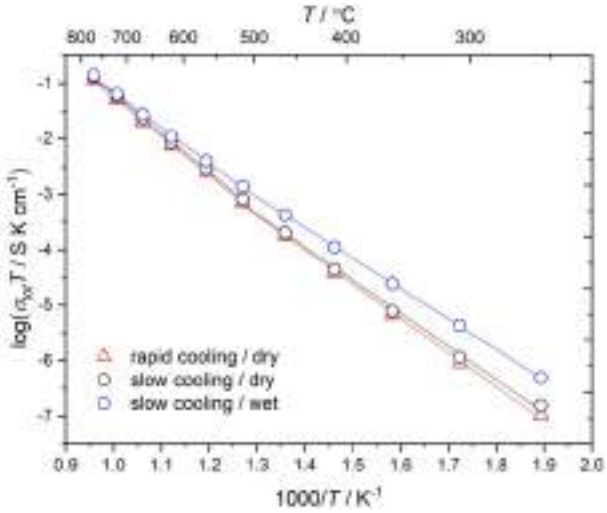


*Fig. 1. Arrhenius dependence of total conductivity for rapidly cooled (in dry air (red triangles)) and slowly cooled (in dry (black circles) and wet air (blue circles)) fluorite $Tm_2(Ti_{2-x}Tm_x)O_{7-x/2}$ (x = 0.74).*

**Acknowledgement:** The work was supported partially by the subsidy from the Ministry of Education and Science allocated by the FRC CP RAS for the implementation of the state assignment (No.122040500071-0).

## PP-I-92

# Synthesis and Characterisation of Alumina and Calcium Aluminate with Deposited Sulfates

Shuvarakova E.I., Bedilo A.F.
*Boreskov Institute of Catalysis, Novosibirsk, Russia*
*Katerina.shuv@gmail.com*

Deposition of sulfates on the γ-$Al_2O_3$ surface is known to lead to a substantial increase of its acidity and catalytic activity in acid-catalyzed reactions. It was even claimed that sulfated alumina might have superacid sites. The catalytic properties of sulfated alumina generally resemble those of sulfated zirconia, which is more widely known due to its higher acidity and catalytic activity. However, low cost, high surface area, wide availability, and reasonable thermal stability make sulfated alumina an attractive catalyst for acid catalyzed processes that do not require very high acid strength [1].

Calcium aluminates of different stoichiometry have been studied for a long time. They are used as components of cement mixtures and as catalyst supports. Calcium aluminate of the stoichiometric composition $12CaO{\cdot}7Al_2O_3$ (commonly referred to as C12A7) with a mayenite crystal structure is of particular interest. The attention paid to this class of materials is due to the discovery of theirunique electrophysical and chemical properties, which were studied in detail in the studies by the Hosono group [2].

C12A7 samples were synthesized according to the procedure described previously [3]. CaO obtained by decomposing the $CaCO_3$ at 700 °C was quickly poured under vigorous stirring into a suspension containing the calculated amount of aluminum hydroxide in water. The resulting mixed hydroxide was dried and calcined in air. This technique makes it possible to significantly reduce the synthesis temperature and to obtain highly dispersed nanocrystalline materials with mayenite crystalline structure and a specific surface area of about 80 $m^2/g$ after calcination at 500 °C.

Sulfates were deposited on the surface of mayenite and commercial alumina by impregnation method using ammonium sulfate solutions with calculated concentrations. After impregnation all the samples were dried at 100 °C and calcined in air at 500 °C.

Samples of sulfated aluminium oxide were also prepared using the aerogel method. The term aerogel refers to gel materials where the liquid phase is replaced by gas. Under supercritical conditions, the liquid-vapor interface causing the collapse of the gel framework during conventional drying is eliminated preserving the gel structure after drying. Aerogels have found their application in catalysis mainly because of their high specific surface area, which makes it possible to have a greater number of active sites per unit mass [4].

To prepare alumina aerogels, aluminum isopropoxide solution in isopropanol was subjected to hydrolysis with stoichimetric amount of deionized water, followed by aging for 16 hours and drying in an autoclave at 265 °C. The obtained aerogels were amorphous to X-rays. Their surface area was close to 600 $m^2/g$ after the supercritical drying and 400 $m^2/g$ after

calcination in air at 550 °C. The sulfuric acid introduction led to the pore volume decrease, whereas the high surface area of the $Al_2O_3$ aerogels was preserved. The surface areas of sulfated alumina aerogels after calcination at 550°C usually required to make active acid catalysts was between 450 and 500 $m^2/g$, which is ca. 2 times higher than those of the catalysts prepared by traditional methods.

Active sites on the surface of obtained material were investigated by EPR using suitable spin probes. This method is based on using specific molecules which selectively interact with the surface sites yielding surface paramagnetic species. The concentration of the sites was determined by integration of the EPR spectra registered immediately after activation at 500 °C and the spin probe adsorption and after additional heating at 80°C for 18 h.

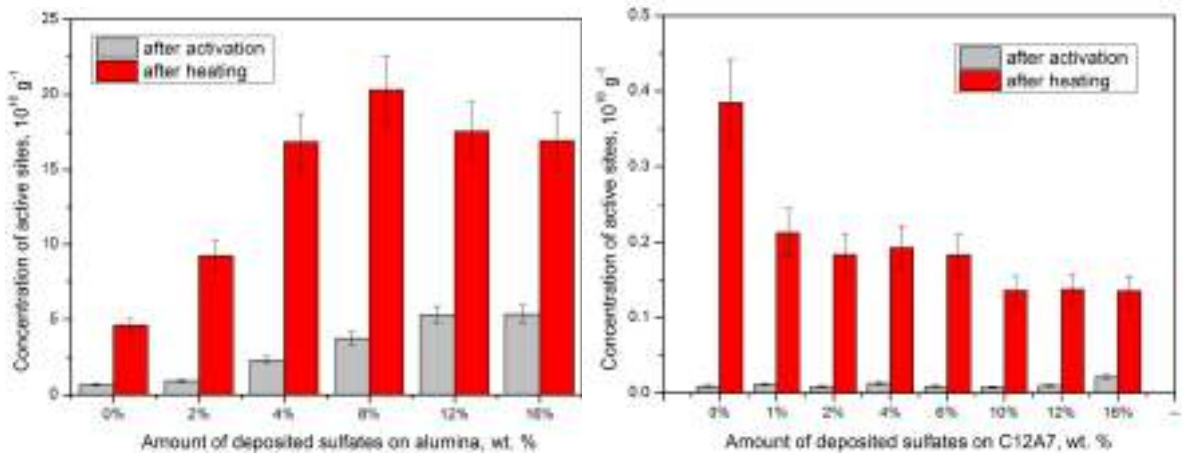


*Fig. 1. Concentrations of active sites tested with perylene on the surface of sulfated alumina (left) and sulfated mayenite (right)*

The concentration of the strongest active sites tested with perylene ($C_{20}H_{12}$) after activation significantly increases with the increase of sulfates concentration on the surface of alumina to 16 wt.%. The concentration of weaker cites obtained after heating at 80°C increases to 8 wt.% (Fig 1, left). On the aerogel materials, the amount of such active sites is almost two times higher due to larger specific surface area and also increases with the increase of sulfates concentration. An opposite situation is observed after perylene adsorbtion on sulfated mayenite (Fig 1, right). The deposition of sulfates practically does not influence the concentration of the strongest sites and leads to decreasing of weaker sites concentration.

**References:**

[1] A.F. Bedilo, E.I. Shuvarakova, A.A. Rybinskaya, D.A. Medvedev, *J. Phys. Chem. C* 118 (2014) 15779.
[2] K. Hayashi, S. Matsuishi, T. Kamiya, M. Hirano, and H. Hosono, *Nature (London, U.K.)* 419, 462 (2002).
[3] Kapishnikov A.V. , Kenzhin R.M. , Koskin A.P. , Volodin A.M. , Geydt P.V., *Materials*, (2022), 15, 778:1-11
[4] Ilyina E.V. , Bedilo A.F. , Cherepanova S.V. , Gerus Y.Y. , Shuvarakova E.I. , Vedyagin A.A., *J. Sol-gel Sci Technol (*2022) 104, 259

## PP-I-93

# Frost-Resistant Polymeric Material Based on Unsaturated Polyketone and Chlorine-Containing Epoxy Oligomers

Sidorov O.I.[1], Belyakov D.A.[1], Dubkov K.A.[2], Semikolenov S.V.[2]

*1 – Soyuz Federal Center for Dual-Use Technologies, Dzerzhinskyi, Moscow oblast, Russia*

*2 – Boreskov Institute of Catalysis, Novosibirsk, Russia*

*soyuz@fcdt.ru*

Modern technology requires the development of elastic polymeric materials with high frost and oil resistance. In this regard, it is promising to use a new type of reactive oligomers, namely, unsaturated polyketones (UPK) [1-3]:

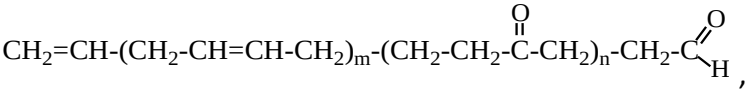

as a basis for creation of such polymeric compositions with enhanced properties.

In this work, a new polymeric material was formulated using UPK containing 7.8 wt. % oxygen in the form of C=O groups and the following additional components:

- chlorine-containing epoxy oligomer containing 28 wt. % of epoxy groups:

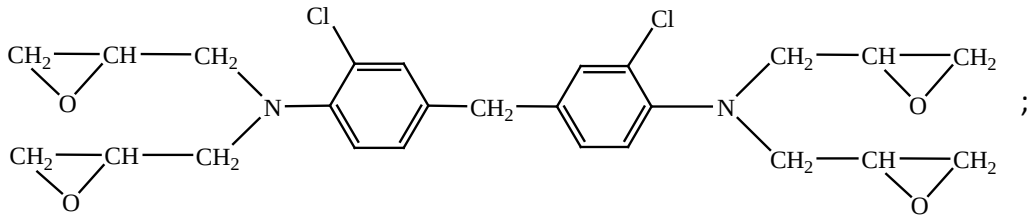

- chlorine-containing epoxy oligomer containing 25 wt. % of epoxy groups:

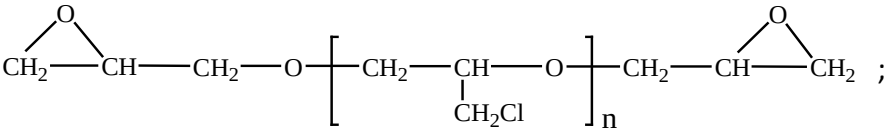

- quinol ether as a cross-linking agent for UPK:

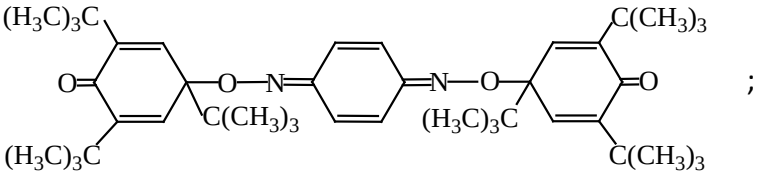

- isomethyl tetrahydrophthalic anhydride as a cross-linking agent for epoxy oligomers:

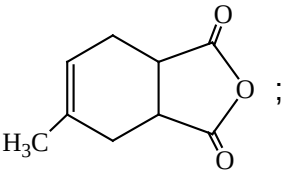

- ionic liquid as a catalyst for curing epoxy oligomers:

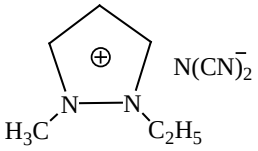

It has been established that the developed frost-resistant polymeric material exhibits elastic properties in a wide temperature range and is characterized by an increase in deformation with a decrease in temperature from +50°C to –50°C (Table 1), as well as by a low swelling capacity (no more than 5.5% at 70°C) in mineral oil.

**Table 1.** Mechanical properties of the UPK-based polymeric material.

| Characteristic | Temperature, °C | | |
|---|---|---|---|
| | +50 | +20 | -50 |
| Tensile strength, σ, kgf/cm$^2$ | 5.1 | 5.6 | 34.8 |
| Deformation at break, ε, % | 16.6 | 15.1 | 40.6 |
| Tensile modulus, $E_{10\%}$, kgf/cm$^2$ | 32.7 | 44.0 | 174.0 |

Thus, a frost and oil resistant elastic material has been created on the base of unsaturated polyketone – a new type of reactive oligomers, and chlorine-containing epoxy oligomers. This material with enhanced properties is promising for application at low temperatures in various fields of technology.

**Acknowledgement:** The study was supported by the Russian Science Foundation (Project No. 23-23-00310, https://rscf.ru/project/23-23-00310/).

**References:**

[1] Dubkov K.A., Semikolenov S.V., D.E. Babushkin, et al., J. Polym. Sci. A, 44(2006) 2510-2520.
[2] Sidorov O.I., Dubkov K.A., Semikolenov S.V., et al., Polym. Sci., Ser. D, 11(2018) 215-224.
[3] Sidorov O.I., Evseev N.E., Dubkov K.A., et al., Polym. Sci., Ser. D, 13(2020) 85-88.

## PP-I-94

# Support Properties in Applied to the Formation of Sulfur Dioxide Oxidation Catalysts

Kovalenko O.N., Simentsova I.I., Paukshtis E.A.
*Boreskov Institute of Catalysis, Novosibirsk, Russia*
*oven@catalysis.ru*

In modern catalysts for the oxidation of sulfur dioxide, the active component is a mixture of alkali metal oxosulfatovanadates salts on a carrier — silica gel of natural or synthetic origin. A characteristic feature of sulfuric acid catalysts is that at temperatures above 250-300°C their active component represents a melt, which due to capillary forces and adhesion with the support, wets $SiO_2$ particles and fills the pores of the support. Thus, the adhesive properties of the carrier are one of the factors determining the uniformity of the distribution of the active component on the surface of the carrier. In turn, it is known, that the carrier surface charge (in particular, its acid-base properties) is one of the main factors determining the degree of surface wetting by polar liquids, such as a melt of alkali metal oxosulfatovanadates.

The aim of this work was investigated the influence of the conditions of support treatment, which preceded the catalyst synthesis, on the acid–base properties of a support. Natural a diatomite were used as a support. The properties of the support were changed by modify it with vanadium pentoxide using the method of impregnation by moisture capacity using a solution of vanadyl sulfate, 5.35–16.12 g/l. The surface acidity of samples of the original and modification diatomite were determined by the method of the weight titration Zërensena-de Bryuina by the point of zero charge. The number and strength of acidic and basic sites in the samples were studied by IR spectroscopy using carbon monoxide and deuterochloroform as probe molecules, respectively. The activity of the catalysts on the original and modified diatomite were tested* at a temperature of 420°C, GHSV=4000 $h^{-1}$ of the mixture 10% vol. $SO_2$ in the air, on a fraction of the catalyst of 0.1-0.25 mm.

It has been shown that on modifying of diatomite proceeds in specific adsorption of $V_2O_5$ on the basic sites of impurity oxides of Al, Ti, and Fe. As a result, the diatomite surface is positively charged: a) according to IR spectroscopy, the basic sites disappear, and the strength of the acid sites increases; b) the point of zero charge decreases (7.85 $\rightarrow$ 3.97). The activity of the catalyst on the modified diatomite by 15% exceeds the activity of the catalyst on the original diatomite. Thus, it can be assumed that modification with vanadium contributes to the uniform distribution of the melt of the active component on the support and leads to a decrease in the ignition temperature of the catalyst.

*tested catalytic activity of the samples was carried out by the employees of the SWG on research and testing of new materials in catalysis

## PP-I-95

# Thermocatalytic Decomposition of Methane on Ni/PVA Composites Promoted with MgO

Sotnikova A.E., Ivantsov M.I., Krysanova K.O.
*A.V. Topchiev Institute of Petrochemical Synthesis, RAS (TIPS RAS), Moscow, Rusia*
*sotnikova.anast@ips.ac.ru*

Hydrogen is a promising zero emission fuel primarily used for power/electricity generation in fuel cells. The catalytic decomposition of methane is a promising process for producing hydrogen. As a result, in addition to the target product, valuable carbon nanomaterials are formed, without $CO_x$ emissions [1].

The most common catalysts for methane decomposition are carbon materials [2]. To increase the activity of carbon-containing catalysts, a method for introducing a certain amount of metals into the system is being studied. In most studies, Ni is assessed as one of the most active and available metals for methane pyrolysis [3]. The introduction of MgO into the composition of catalysts contributes to a higher dispersion of the base metal [4].

Polymers are attractive materials for obtaining various carbon materials. Their advantages are inexpensive and versatile materials that can be given any shape. Polyvinyl alcohol (PVA) differs from most polymers in its simple structure and tendency to form structures with a high carbon content [5].

In this work, catalysts based on PVA were obtained. The polymer was dissolved with heating and stirring in distilled water. Next, the combined aqueous solution of $Ni(NO_3)_2 \cdot 6H_2O$ and $Mg(NO_3)_2 \cdot 6H_2O$ was added to the resulting solution. Distilled water was removed from the resulting joint solution by drying to constant weight. Heat treatment of the catalyst precursor was carried out in $N_2$ flow at 500℃ for 1 hour. According to the results of microscopy, it was determined that the synthesized composite materials are layers with evenly distributed metal-containing particles in a carbon matrix. The composites differed in the active phase particle size of 2–10 nm. The XRD showed that composite materials mainly contain nickel metal particles. A distinctive feature is the absence of a preliminary activation stage, since the decomposition of PVA results in a highly dispersed catalytic system with partial reduction of NiO.

The catalysts showed high activity in the range of 700-800℃. In the reaction of methane decomposition (99.9 vol.%) on the synthesized catalysts, the maximum conversion was 40%. The introduction of the MgO promoter contributed to the stabilization of NiO particles. As a result, the reduction temperature shifted towards higher. The introduction of the MgO promoter made it possible to increase the yield of hydrogen per mass of pure Ni from 1.2 to 2.6 mol/$g_{Ni}$.

During the decomposition of methane, in addition to hydrogen, carbon nanotubes (CNT) were formed on Ni-based catalysts. The resulting CNT were characterized by a high length-to-diameter ratio. The CNT length varied 1-6 μm, the outer diameter was 40-60 nm, and the inner

diameter was 10- 20 nm. The number of layers in the obtained CNT depends on the size of the encapsulated Ni and averaged from 30 to 90.

**Acknowledgement:** This work was carried out within the State Program of TIPS RAS. The work was carried out using the equipment from the Center for Collective Use “Analytical Center for Problems of Deep Oil Refining and Petrochemistry” TIPS RAS (A.V.Topchiev Institute of Petrochemical Synthesis, Russian Academy of Sciences).

**References:**

[1] Pudukudy M, Yaakob Z, Jia Q, Sobri Takriff M., New J Chem 42 (2018) 14843–14856.
[2] Muradov N., Catal Commun 2 (2001) 89–94.
[3] Chen J, He M, Wang G, Li Y, Zhu ZJ., Int J Hydrogen Energy 34 (2009) 9730–9736.
[4] Sharma SK, Khan TS, Singha RK, Paul B, Poddar MK, Sasaki T, et al., Appl Catal A Gen 623 (2021) 118239.
[5] Faupel F, Zaporojtchenko V, Strunskus T, Elbahri M., Adv Eng Mater 12 (2010) 1177–1190.

## PP-I-96

# Gd-Doped Carbon Nanodots as a Promising Contrast Agent for MRI

Ondar S.O.[1,2], Vedernikova A.A.[1], Miruschenko M.D.[1], Badrieva Z.F.[1], Brui E.A.[1], Stepanidenko E.A.[1]

*1 – ITMO University, Saint Petersburg, Russia*

*2 – Saint-Petersburg State Institute of Technology, Saint Petersburg, Russia*

*stepanidenko.e@mail.ru*

Carbon nanodots (CDs) are a new nanomaterial with a surface rich in different functional groups and photoluminescence (PL) band in a range from UV-vis up to red and near infrared (NIR) emission, tuned by synthesis conditions. The long-wavelength spectral range is important for bio-applications since is regarded as biological window. Therefor due to the low-toxicity and NIR PL CDs are widely investigated as nanoprobe for bioimaging and may allow decrease the autofluorescence during the analysis. Besides, the state-of-the-art investigation are headed to formation of multi-functional nanoprobe based on CDs. For instance, the doping of emissive CDs by metal ions is promising for fabrication of contrast agents (CAs) for magnetic resonance imaging (MRI) and computed tomography (CT). Therefore, this study is aimed to formation of dual-modal nanoprobe by the one-pot synthesis of CDs from commonly used organic precursors (citric acid / o-phenylenediamine) and the sources of Gd-ion.

Here we present the water-soluble CDs with long-wavelength PL band. We investigated the relaxation times (T1 and T2) of protons in water during MRI in the presence of Gd-doped CDs and registered the changes in these times. The relaxivities (r1 and r2) were calculated. It was observed that synthesized Gd-doped CDs have properties of positive CA. To summarize, the suggested CDs are promising as multifunctional nanoprobe for bioimaging since demonstrate both long-wavelength emission and a capability of influencing relaxation time during MRI.

**Acknowledgement:** The study was supported by the Russian Science Foundation (RSF) grant No. 22-73-00090, https://rscf.ru/project/22-73-00090/. Part of the work devoted to MR experiments was supported by a grant for scientific school НШ-2359.2022.4.

## PP-I-97

# The Use of Ash and Slag Waste as Components of Building Materials

Chalov K.V., Kosivtsov Yu.Yu., Lugovoy Yu.V., Sulman M.G.
*Tver State Technical University, Tver, Russia*
*sulmanmikhail@yandex.ru*

Ash and slag waste (ASW) is a finely dispersed mineral material remaining as a result of burning brown and hard coal at power plants. The use of this type of waste in industry is one of the ways to solve the issue of energy and resource conservation. The share of ASW involvement in economic cycle in Russia does not exceed 10%. The use of waste in industrial production will also provide a solution to the environmental problem of the pollution by industrial waste.

Alumosilicate hollow microspheres can be extracted from ash and slag waste, which can be used in the design of multiphase binding systems [1]. The introduction of ash can also affect the quality of the building material, improving its grain composition and reducing the stratification of the raw mixture, thereby increasing the uniformity of the resulting material [2].

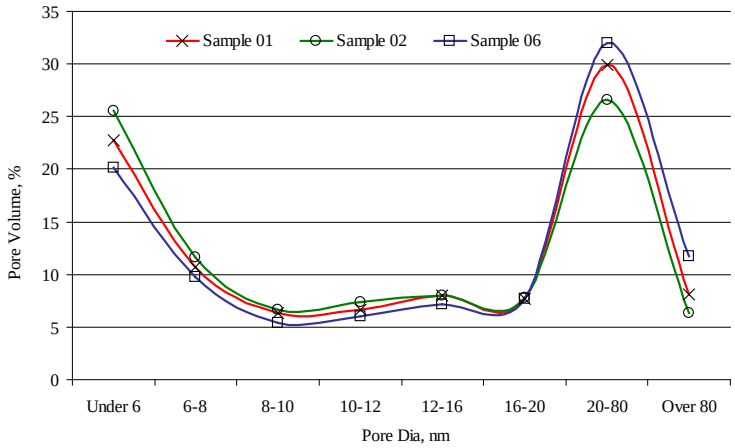


*Fig. 1. Pore diameter distribution for mineral binder formations*

In this paper, the influence of aluminosilicate concentrate on the strength characteristics of mineral binder compositions based on gypsum is investigated. A thermogravimetric study of gypsum-based samples was carried out. The strength characteristics for compression and fracture are investigated. The structure and pore size distribution of mineral binders were also investigated by low-temperature nitrogen absorption.

**Acknowledgement:** This work was supported by the Russian Science Foundation, grant 21-79-30004.

**References:**

[1] K. Celik, C. Meral, A. P. Gursel, P. K. Mehta, A. Horvath, P. J.M. MonteiroБ, Cement & Concrete Composites. 56 (2015) 59–72.
[2] M.C.G. Juenger, R. Siddique, Cement and Concrete Research. 78 (2015) 71–80.

## PP-I-98

# Thermoelectric Properties and Valence Band Electronic Structure of $Ln_xMn_{1-x}S$ Solid Solutions

Syrokvashin M.M.
*Nikolaev Institute of Inorganic Chemistry SB RAS, Novosibirsk, Russia*
*syrokvashin@niic.nsc.ru*

The development of the highly efficient thermoelectric materials (TEMs) is considered as one of the main trends of the modern material science. Usually, TEMs are used for fabrication of the thermoelectric generator (TEG) devices. TEGs based on the high-efficient thermoelectric materials is considered as alternative for the traditional power generation sources. The direct conversion of the waste-heat into electricity using TEGs, are expected to be a promising procedure to solve the global electricity demand growth problem. TEMs could be used as a power sources in various electronic devices such as solid state temperature sensors or as part of the power sources in the autonomous devices. For instance, in the TEG-based wearable smart devices which could use the body heat as a power source, or in the hybrid electric vehicles engines. The cation-substituted solid solutions based on the lanthanide or transition metal chalcogenides are considered to be a promising thermoelectric materials. The functional properties of these compounds could be modified by the variation of both type and concentration of the doping atoms. The lanthanide-doped solid solutions $Ln_xMn_{1-x}S$ based on MnS-matrix are considered as promising functional materials with the thermoelectric and magnetic properties. However, the electrophysical properties, including the Seebeck coefficient, of the semiconductor compounds largely depend on the electronic structure (the DOS distribution in the Fermi-level region). Thus, the electronic structure study is one of the key aspects in the prediction and optimization of the thermoelectric properties. For instance, the thermoelectric properties of the *p*-type semiconductors are determined by the DOS distribution in the valence band, for *n*-type semiconductors – the distribution in the conduction band. Thus, the current work involved the study of the electronic structure features of $Ln_xMn_{1-x}S$ (Ln = Dy, Tm, Yb; x = 0.01; 0.05). The data on the valence band structure was obtained using X-ray photoelectron spectroscopy (XPS). The obtained experimental results were compared with the results of quantum-chemical calculations of the partial DOS contributions in the valence band. The obtained data were compared with the temperature dependences of the Seebeck coefficient for $Ln_xMn_{1-x}S$. It was found that cationic substitution leads to the Seebeck coefficient increase compared to the initial MnS-matrix. The contributions of Ln *f*- and Mn *d*-states prevails over the sulfur *s*-states of. It was shown that the Seebeck coefficient temperature dependences character is significantly affected by the lanthanide atom type and concentration due to the presence of the additional Ln *f*-states in the Fermi-level region. An increase of the lanthanide concentration to x = 0.05 leads to the

significant Seebeck coefficient decrease due to the concentration metalto-dielectric transition.

**Acknowledgement:** The authors acknowledge the Ministry of Science and Higher Education of the Russian Federation (project No. 121031700313-8).

## PP-I-99

# Synthesis and Investigation of Optical Properties of Chiral $CsPb(Cl,Br)_3$ Perovskite Nanocrystals

Timkina Yu.A.[1], Batueva E.A.[1], Skurlov I.D.[1], Litvin A.P.[2], Ushakova E.V.[1]
*1 – International Research and Education Centre for Physics of Nanostructures, ITMO University, Saint Petersburg, 197101 Russia*
*2 – Key Laboratory of Automobile Materials MOE, School of Material Science & Engineering, Jilin University, Changchun 130012, China*
*yu.a.timkina@itmo.ru*

Nanocrystals with perovskite-type symmetry are unique, actively studied materials with easily tunable optical properties. They have already been implemented everywhere in many areas [1]. At the moment, an urgent scientific task is to expand the functionality of perovskite nanocrystals to give them additional properties. One of these properties is an optical activity. The creation of chiral metal halide perovskite nanocrystals and study of their properties has not only fundamental but applied significance. These nanomaterials are extremely promising for optoelectronics, sensors, and the selective biotags creation [2]. However, is currently a difficult task to create chiral perovskite nanocrystals with ligand-induced optical activity.

In this work, nanocrystals of chiral perovskite with the chemical composition $CsPb(Cl,Br)_3$ were obtained. First, achiral CsPbCl3 nanocrystals were synthesized by hot injection. Then, chiral properties were imparted by introducing the chiral ligands R-(+)-α-methylbenzylamine and (S)-(-)-α-methylbenzylamine (R-/S-MBA) in the form of R-/S-MBA:Br salt into the nanocrystal solutions. The presence of R-/S-MBA in the composition of the ligand shell was registered using Fourier transform infrared (FTIR) spectroscopy. The crystal structure of both the obtained chiral nanocrystals was determined using X-ray diffraction (XRD). The chiral properties of $CsPb(Cl,Br)_3$ perovskites were evaluated by circular dichromium spectroscopy. The position of the peak in the circular dichroism spectra of chiral $CsPb(Cl,Br)_3$ nanocrystals falls at a wavelength of 380 nm, which corresponds to a high-energy optical transition. The absorption dissymmetry coefficient (gabs) for both types of nanocrystals reached $\pm 4.5 \cdot 10^{-5}$. The mechanism of optical activity induction during the treatment of perovskite nanocrystals with chiral salts is under further study.

**Acknowledgement:** This work was supported by the Russian Science Foundation (21-73-10131).

**References:**

[1] Cao Z. et al. Optical studies of semiconductor perovskite nanocrystals for classical optoelectronic applications and quantum information technologies: A review // Adv. Photonics. 2020. Vol. 2, № 5. P. 8–10.
[2] Xiao L. et al. Novel properties and applications of chiral inorganic nanostructures // Nano Today. 2020. Vol. 30.

## PP-I-100

# Fabrication, Characterization and Biodegradability of Oil–in–Water Pickering Emulsions Stabilized by Cellulose Nanocrystals

Udoratina E.V., Sitnikov P.A., Legki Ph.V., Druz Yu.I., Ushakov N.V., Torlopov M.A.
*Institute of Chemistry of Komi Science Centre of the Ural Branch of the Russian Academy of Sciences, Syktyvkar, Russia*
*udoratina-ev@chemi.komisc.ru*

In the last decade, with the development of nanotechnology, there has been a steady increase in research on Pickering emulsions as an alternative to traditional surfactant compounds. Pickering emulsions are widely used in the food, cosmetic, medical, and oil refining industries. In the oil industry, which is prone to frequent oil spills, the use of Pickering emulsions is relevant for dispersing crude oil during a spill response. However, when using such systems, there is a problem with the stabilization of microemulsions with solid nanoparticles. To solve this problem, it is necessary to study the influence of the structure, interface structure, and morphology of the solid emulsifier on colloid emulsion formation.

This paper presents the results of studies on the effect of cellulose nanocrystals (CNC) on the formation and stability of Pickering emulsions in a crude oil–water system depending on the ratio of components, ionic strength, and pH of the medium. In addition, this paper presents the results on the biodegradation of emulsions by natural microorganisms.

Rod-like particles with native ($CNC_H$) and partially acetylated ($CNC_{Ac}$) surfaces, with average geometric dimensions of approximately 200 nm (length) and 8 nm (width, thickness), that were characterized by a highly ordered structure (crystallinity index of 0.88) were obtained by cellulose solvolysis. The obtained cellulose nanocrystals were characterized by electron microscopy, XRD, and FTIR spectroscopy (Fig. 1). The obtained CNCs were used as solid-phase emulsifiers and stabilizers of water–oil mixtures.

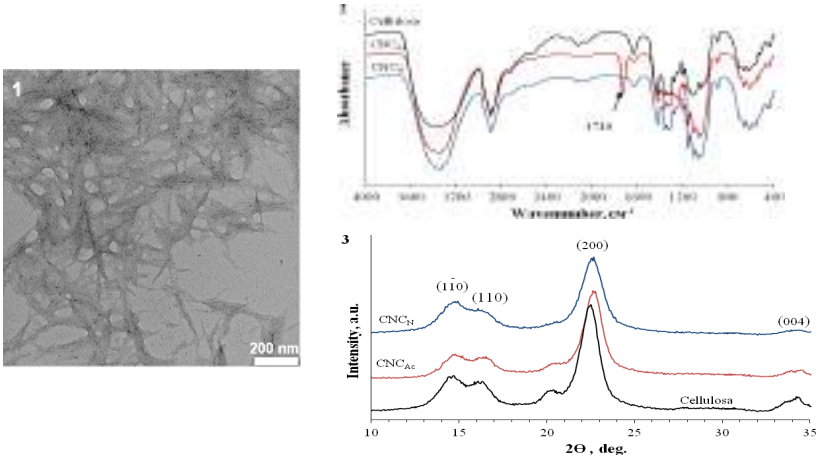


*Fig.1. Photomicrographs (TEM, 1), FTIR spectra (2) and diffraction patterns (XRD, 3) of CNC*

By varying the mass concentrations of CNCs and concentrations of supporting electrolytes (NaCl), optimal compositions for obtaining stable Pickering emulsions in the oil–water system were determined. It has been established that "oil-in-water"- type emulsions have been

obtained in the system with 3.5 mg/cm$^3$ $CNC_N$. The average size of dispersed phase drops is 6.9 ± 2.0 µm, which decreases to 3.1 ± 1.0 µm at 7.0 mg/cm$^3$ $CNC_N$. The system with $CNC_{Ac}$ contents of 7.0 and 14.0 mg/cm$^3$ produces stable oil-in-water emulsions with average drop sizes of 3.1 ± 0.8 and 1.5 ± 0.4 µm, respectively (Fig. 2).

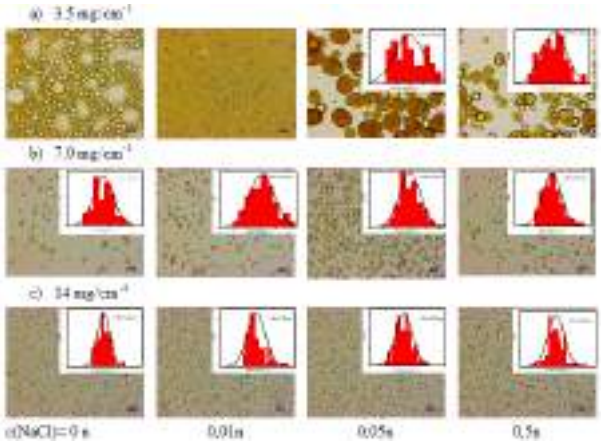

*Fig.2. Dependence of emulsion droplet sizes in the system crude oil–water on CNC content and molar concentration of supporting electrolyte*

The rheological properties of oil emulsions stabilized with CNC were studied. These systems were found to be non-Newtonian pseudoplastic fluids.

Biodegradation of the emulsions by autochthonous microorganisms was evaluated. The formation of oil emulsions in water stabilized with acetylated nanocellulose contributes to more effective oxidation of oil by *Rhodococcus egvi* bacteria under aerobic conditions. Chromatographic analysis showed that the residual content of hydrocarbons in the emulsion was 20–25% after incubation with microbial inoculums for 30 days (Table).

**Table** Analysis of hydrocarbon content in samples after incubation for 30 days

| Scheme of experiment | Residual hydrocarbon content, % |
|---|---|
| Oil without dispersing | 82±5 |
| Inoculums + oil without dispersing | 64±5 |
| Oil emulsion with $CNC_{Ac}$ 3.5 mg/cm$^3$ | 26±5 |
| Inoculums + oil emulsion with $CNC_{Ac}$ 3.5 mg/cm$^3$ | 20±5 |
| Oil emulsion with $CNC_{Ac}$ 7 mg/cm$^3$ | 25±5 |
| Inoculums + oil emulsion with $CNC_{Ac}$ 7 mg/cm$^3$ | 19±5 |
| Oil emulsion with $CNC_{Ac}$ mg/cm$^3$ | 23±5 |
| Inoculums + oil emulsion with $CNC_{Ac}$ 14 mg/cm$^3$ | 20±5 |

**Acknowledgement:** This work was supported the Russian Science Foundation, grant 22-23-00271, https://rscf.ru/en/project/22-23-00271/.
The authors would like to thank Falcon Scientific Editing (https://falconediting.com) for proofreading the English language in this paper.

## PP-I-101

# Functional Polysilsesquioxanes Containing Imidazole/Triazole Side-Chain Groups

Bolgova Yu.I., Usmanov R.T., Chepenko D.S., Trofimova O.M., Pozdnyakov A.S.
*A.E. Favorsky Irkutsk Institute of Chemistry, Siberian Branch of the Russian Academy of Sciences, Irkutsk, Russian Federation*
*usmanov@irioch.irk.ru*

Heterochain organosilicon polymers (polyorganosiloxanes), due to a combination of unique and practically important properties, such as high chemical, thermal and mechanical stability, low dielectric constant, hydrophobicity, biocompatibility, are increasingly being used in various fields of science, engineering and technology. In recent years, the requirements of advanced technologies have created as need for new high performance polysiloxanes, for example as precursors for coatings, binders, additives, and ceramics. Alkoxy(alkyl)silanes $RSi(OAlk)_n$ are a unique class of organosilicon compounds that have hydrolytically active functional groups at the silicon atom. These groups can undergo a hydrolytic polycondensation reaction that results in the formation of high molecular weight compounds [1,2].

Poly(propylimidazolylsilsesquioxane) and poly(propyltriazolylsilsesquioxane) have been synthesized using sequential two-step reactions. At the first stage, the monomers 1-[3-(trimethoxysilyl)propyl]-1*H*-imidazole and 1-[3-(trimethoxysilyl)propyl]-1*H*-1,2,4-triazole were synthesized by nucleophilic substitution reaction of the chlorine atom of (3-chloropropyl)trimethoxysilane by the 1*H*-imidazolyl or 1*H*-1,2,4-triazolyl group (Scheme 1).

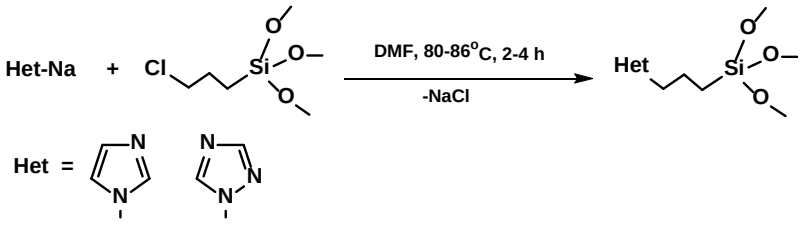


*Scheme 1. Synthesis route towards monomers*

The obtained compounds were isolated as a colorless liquids and characterized by elemental analysis, FT-IR, $^{1}H$, $^{13}C$ and $^{29}Si$ NMR and mass spectrometry.

The second stage, direct hydrolysis of (trimethoxysilyl)propyl derivatives of 1*H*-imidazole and 1*H*-1,2,4-triazole in deionized water without the use of an acidic or basic catalyst, followed by polycondensation to give poly(propylazolylsilsesquioxane) (Scheme 2). Products are white solids soluble in many organic solvents. The weight average molecular weight ($M_w$) of siloxanes 9000–12500 Da with a unimodal molecular weight distribution, was determined by gel permeation chromatography.

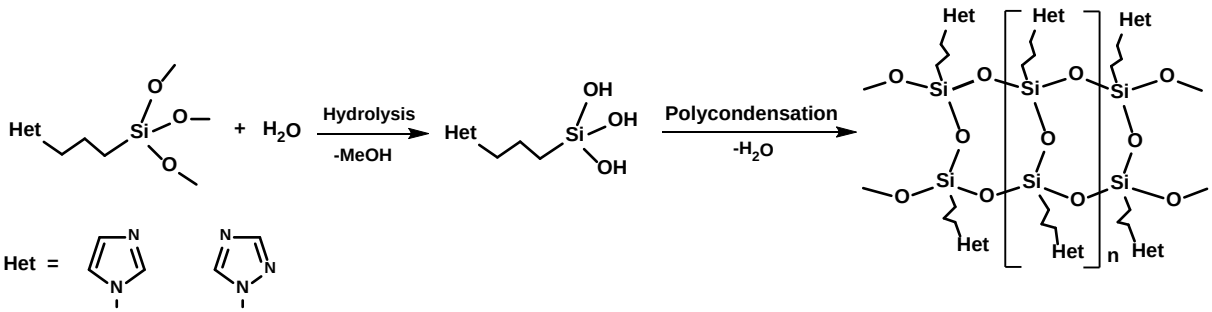


*Scheme 2. Synthetic pathway of ladder poly(propylazolylsilsesquioxane)*

The structure of the synthesized polysilsesquioxanes was confirmed by elemental analysis, FT-IR and $^{1}H$, $^{13}C$, $^{29}Si$ NMR spectroscopy. The $^{29}Si$ NMR spectra of silsesquioxane showed a one signal at δ -67.09 and -68.93 ppm, respectively. These signals corresponding to the Het$(CH_2)_3$-$SiO_{3/2}$ unit with a very narrow peak width at half-height, $w_{1/2}$, of 0.15 ppm (for poly(propylimidazolylsilsesquioxane)) and 0.65 (for poly(propyltriazolylsilsesquioxane)) ppm. This indicates a high degree regularity of polymers **3** and **4** structure [3]. FT-IR analysis also confirmed that polysilsesquioxanes have a ladder structure according to the literature date [2,4]. In the IR spectra, two absorption bands are observed at 1110 and 1029 $cm^{-1}$, due to stretching vibrations of the Si–O–Si siloxane bond. There are no absorption bands due to the Si–OH bonds vibrations. The thermal behavior of siloxanes was characterized by thermogravimetric analysis. Polysilsesquioxanes are characterized by heat resistance up to 340 and 320 °C, respectively.

Thus, highly regulated ladder-structured polysilsesquioxanes containing Imidazole/triazole side-chain groups soluble in solvents were synthesized. These compounds can be the precursors for silicon-based materials for a wide variety of industrial.

**Acknowledgement:** This work was supported by the Russian Science Foundation, grant 23-23-00518.

**References:**

[1] Y. Kaneko, Polymer 144 (2018) 205.
[2] M. Unno, A. Suto, E. Matsumoto, Russ. Chem. Rev., 82 (2013) 289.
[3] Z.-X. Zhang, J. Hao, P. Xie, X. Zhang, C.C. Han, R. Zhang, Chem. Mater., 20, (2008) 1322.
[4] H. Seki, T. Kajiwara, Y. Abe, T. Gunji, J. Organomet. Chem., 695 (2010) 1363.

## PP-I-102

# Light Bullets in a Disordered System of Carbon Nanotubes

Verevkina K.Yu., Verevkin I.Yu., Belonenko M.B.
*Federal State Autonomous Educational Institution of Higher Education "Volgograd State University", Volgograd, Russia*
*verevkina@volsu.ru*

As is known, solitons are eigenmodes of problems arising in dispersive nonlinear media [1]. Examples of such problems can be Bose-Einstein condensates, optical waveguides and a system of carbon nanotubes [2-4]. Note that the latter system was considered in the approximation when carbon nanotubes are evenly distributed over the sample volume. In addition, an equation was obtained for carbon nanotube systems, which is a generalization of the nonlinear Schrodinger equation [5].

Nonlinear Schrodinger equations (NUS), with focusing or defocusing nonlinearity, are universal models that make it possible to consider solitons of all personal types. Varieties of solitons can be radically supplemented in spatially inhomogeneous conditions [6]. Usually nonlinear lattices are used, i.e. periodically spatially modulated changes in the nonlinearity coefficient.

An extension of the nonlinear Schrodinger equations was introduced by Laskin in [7], in the form of a fractional equation:

$$\varepsilon_s(p) = \pm\gamma_0\sqrt{1+4\cos(ap)\cos\left(\frac{\pi s}{m}\right)+4\cos^2\left(\frac{\pi s}{m}\right)}$$

where $s = 1,\ 2\ \ldots\ m$, the nanotube has the type $(m,0)$ $\gamma_0 \approx 2.7$ eV, $a = 3b/2\hbar$, $b = 0.142$ nm the distance between neighboring carbon atoms. In this case, the effective equation obtained in [5] is:

$$i\frac{\partial B}{\partial z}+\frac{D}{2}\frac{\partial^2 B}{\partial \tau^2}-\frac{\omega_0^2}{c^2}B\sum_q\sum_l b_q\frac{(-1)^l q^{2l+1}|B|^{2l}}{l!\,(l+1)!\,2^{2l}}=0,$$

where here $\omega_0$ - is the characteristic frequency, τ - is the time in the accompanying coordinate system, D - is the dispersion of group velocities, R - is the nonlinearity coefficient. Note that the electromagnetic pulse field has the form:

$$A(z,t) = Re\{B(z,t)\cdot exp[i(kz-\omega t)]\}.$$

where A is the vector potential of the electromagnetic pulse: A=(0, A(z,t),0,0).
In the resulting effective equation , the replacement was performed:

$$\frac{\partial^2 B}{\partial^2 \tau^2} \to \frac{d^\alpha B}{d\tau^\alpha}$$

here α is the order of the fractional derivative 1<α<2.
The main result obtained is shown in the figure below:

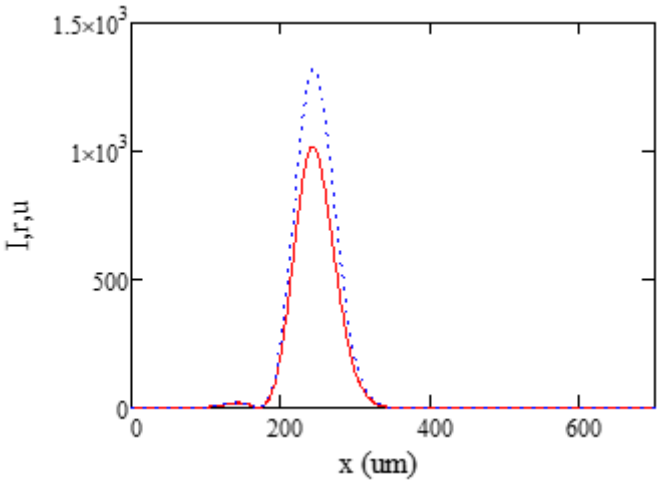


*Fig. 1. the solid curve α=1.6, the dashed curve α=1.7. I – intensity is expressed in relative units.*

Thus, it can be concluded that the order of the fractional derivative, i.e. the degree of disorder of the medium significantly affects the momentum dynamics.

**Acknowledgement:** The work was carried out within the framework of the state task of the Ministry of Science and Higher Education of the Russian Federation (topic "FZUU-2023-0001").

**References:**

[1] Zakharov, V.E., Manakov, S.V., Novikov, S.P., Pitaevskii, L.P.: Theory of Solitons: Inverse Scattering Transform. Nauka publishers, Moscow (1980) [English translation: Consultants Bureau, New York (1984)].
[2] Strecker, K.E., Partridge, G.B., Truscott, A.G., Hulet, R.G.: Bright matter wave solitons in Bose-Einstein condensates. New J. Phys. 5, 73.1-73.8 (2003).
[3] Abdullaev, F.Kh., Gammal, A.G., Kamchatnov, A.M., Tomio, L.: Dynamics of bright matter wave solitons in a Bose-Einstein condensate. Int. J. Mod. Phys. B 19, 3415-3473 (2005).
[4] Bagnato, V.S., Frantzeskakis, D.J., Kevrekidis, P.G., Malomed, B.A., Mihalache, D.: Bose-Einstein conden- 9 sation: Twenty years after. Rom. Rep. Phys. 67, 5-50 (2015).
[5] A. V. Zhukov, R. Bouffanais, M. B. Belonenko, and E. G. Fedorov, Modern Physics Letters B 27, 1350045 (2013).
[6] Kartashov, Y.V., Astrakharchik, G.E., Malomed, B.A., Torner, L.: Frontiers in multidimensional self-trapping of nonlinear fields and matter. Nat. Rev. Phys. 1, 185- 197 (2019).
[7] Kartashov, Y.V., Astrakharchik, G.E., Malomed, B.A., Torner, L.: Frontiers in multidimensional self-trapping of nonlinear fields and matter. Nat. Rev. Phys. 1, 185- 197 (2019).

## PP-I-103

# Highly Dispersed Pd/MgO Catalysts Based on Nanocrystalline MgO Prepared via Sol-Gel Method

Veselov G.B.[1], Ilyina E.V.[1], Shivtsov D.M.[1,2], Stoyanovskii V.O.[1], Vedyagin A.A.[1]
*1 – Boreskov Institute of Catalysis, Novosibirsk, Russia*
*2 – Novosibirsk State Technical University, Novosibirsk, Russia*
*g.veselov@catalysis.ru*

Materials based on nanocrystalline magnesium oxide attract great attention of researchers. The main property of MgO is its pronounced basic properties. MgO is known as a highly reactive destructive sorbent for various hazardous organic compounds such as freons [1]. MgO nanoparticles find use in organic synthesis as heterogeneous basic catalysts of reactions such as aldol reaction, amide synthesis, Michael reaction and etc. [2]. Another important application of MgO-based materials is $CO_2$ capture where MgO due to high surface basicity possesses rather high $CO_2$ adsorption capacity [3]. The advantage of such materials is the thermal instability of their surface carbonates at high temperatures, which allows for regenerating the sorbents via thermal treatment. In heterogeneous catalysis, nanocrystalline MgO is considered as a support [4,5].

However, MgO-based catalysts are not widely applied in industry. One of the reasons is the absence of large-scale manufacturing of such materials with high specific surface area (SSA). On the lab-scale level, one of the most prospective approaches is alkoxide sol-gel synthesis of $Mg(OH)_2$ gels followed by supercritical drying. This method produces MgO with SSA as high as 350 $m^2/g$ after calcination at 500 °C. The preparation of two-component systems based on MgO also poses significant difficulties. The commonly used impregnation method does not allow obtaining uniform distribution of the active component, and the porous structure of MgO undergoes significant shrinkage during the drying stage.

In our previous works, the alkoxide sol-gel method was modified to obtain two- and three-component oxide systems [6,7]. The method is characterized by rather wide scope and allows for introducing the second component of different nature ($VO_x$, $MoO_3$, $WO_3$, NiO, CuO, $CoO_x$, $FeO_x$ and etc.) into the MgO matrix. In this work, such approach is applied to the preparation of Pd/MgO catalysts. 1 wt.% Pd/MgO catalysts were prepared using supercritical drying (aerogel-prepared, AP) as well as ambient conditions drying (xerogel-prepared, XP). In addition, both the incipient wetness impregnation (Pd/MgO-IWI) and EDTA-assisted impregnation methods (Pd/MgO-EDTA) were used to deposit Pd on the surface of pure aerogel-prepared MgO.

According to the data presented in Fig. 1a, samples can be ranked by their initial activity as follows: Pd/MgO-EDTA ≈ Pd/MgO-IWI > Pd/MgO-XP > Pd/MgO-AP. This is attributed to the differences in particle size of Pd as well as its localization and oxidation state, as is determined by transmission electron microscopy and UV-Vis spectroscopy. It is important to note that the initial activity of the best sample within the Pd/MgO series is noticeably higher if compared to

the activity of Pd/γ-$Al_2O_3$ catalyst based on commercial alumina support (Fig. 1b). It can be concluded that the Pd/MgO catalysts prepared via the optimized procedure can be applied in the oxidation processes, which do not require elevated temperatures.

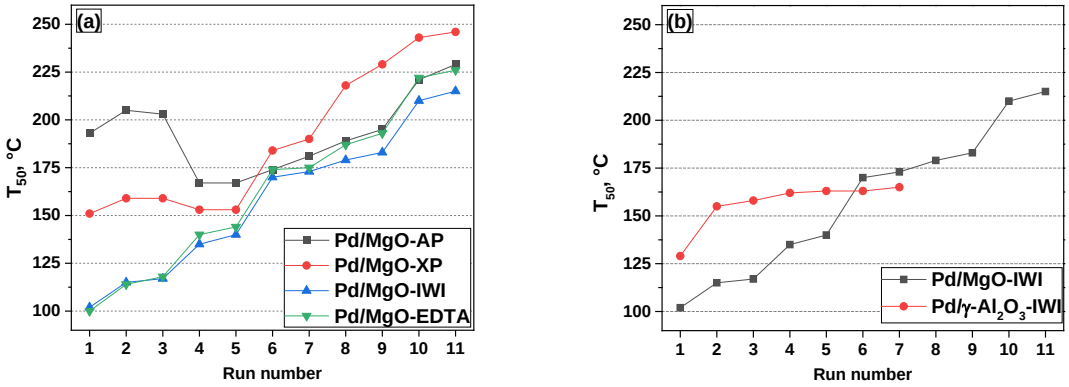


*Fig. 1. 50%-conversion temperatures ($T_{50}$) in 11 runs of temperature-programmed heating with the increase in final temperature according to the following procedure (runs 1 and 2 – 320 °C; runs 3 and 4 – 600 °C; runs 5 and 6 – 800 °C; runs 7, 8 – 900 °C; runs 9, 10 – 1000 °C; run 11 – 500 °C): (a) – comparison of Pd/MgO catalysts prepared by various approaches; (b) – comparison of Pd/MgO u Pd/γ-$Al_2O_3$ prepared by the incipient wetness impregnation method.*

**Acknowledgment:** This work was supported by the Ministry of Science and Higher Education of the Russian Federation [project No. AAAA-A21-121011390054-1]. Characterization of the samples was performed using the equipment of the Center of Collective Use "National Center of Catalysts Research".

**References:**

[1] A.F. Bedilo at al., J. Phys. Chem. C 118 (2014) 13715-13725.
[2] H. Dabhane et al., Eur. J. Chem. 12 (2021) 86-108.
[3] I.A. Iugai et al., Surf. Coat. Technol. 400 (2020) 126208.
[4] E.V. Ilyina et al., J. Sol-gel Sci. Technol. 68 (2013) 423-428.
[5] G.B. Veselov et al., Reac. Kinet. Mech. Catal. 136 (2023) 233–250.
[6] G.B. Veselov et al., Materials 13 (2020) 4404.
[7] A.A. Vedyagin et al., J. Sol-gel Sci. Technol. 82 (2017) 611-619.

## PP-I-104

# $SiO_2$ Aerogels Modified by Organic Chelating Groups

Vlasenko N.E., Lermontov S.A., Sipyagina N.A., Malkova A.N.
*IPAC RAS, Chernogolovka, Russia*
*gmxten@yandex.ru*

Aerogels are unique mesoporous materials with extremely low density, large specific surface area, as well as high porosity, which provides low thermal conductivity. Aerogels containing amino groups are used as extragents of noble metals and catalysts that combine the properties of both heterogeneous and homogeneous catalysts. At the moment, various types of aerogels have been well studied, but the aminosilans *N*-(2-aminoethyl)-3-aminopropiltrimetoxysilan (AEAPTMS) and 3-aminopropiltrimetoxyisilan (APTMS) have a great scientific and practice interest due to their high reactivity and donor ability. This work is devoted to the modification of the surface and the study of the texture characteristics of materials based on the AEAPTMS and APTMS aerogels, as well as the development of methods for obtaining new highly effective catalysts based on aminomodified aerogels, which, due to the presence of a high specific surface area and optical activity, can find use as stereoselective catalysts.

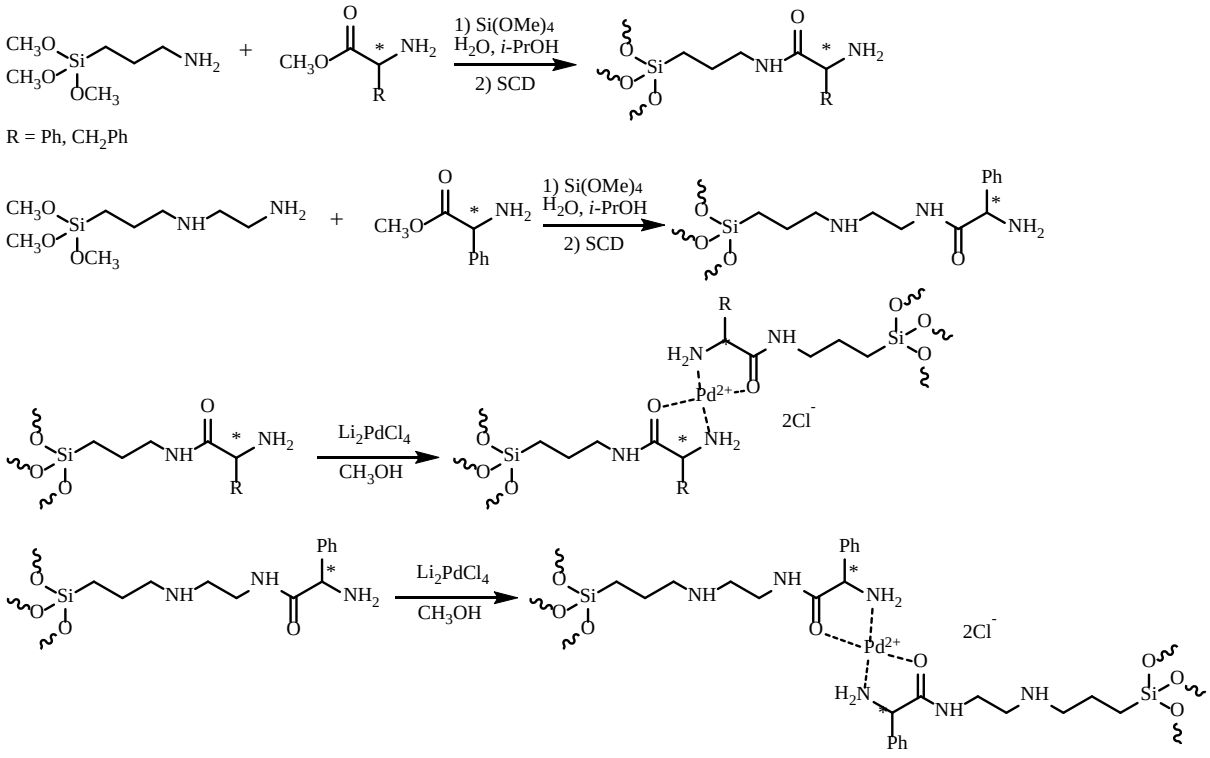


**Acknowledgement:** A financial support from the Russian Science Foundation (Grant №23-73-00028) is greatly acknowledged.

## PP-I-105

# Local Structure of $LiGe_2(PO_4)_3$ Glasses and Glass-Ceramics

Vlasov M.I.[1], Tsymbarenko D.M.[2], Pershina S.V.[1]
*1 – Institute of High-Temperature Electrochemistry UB RAS, Yekaterinburg, Russia*
*2 – Lomonosov Moscow State University, Moscow, Russia*
*m_vlasov@ihte.uran.ru*

Research on all-solid-state lithium batteries which use solid electrolytes is one of the most actively developing fields in energy related science. However, use of solid electrolyte leads to a number of new challenges hindering fabrication of stable and effective batteries possible to be commercialized. To overcome these challenges a comprehensive study of the properties of electrolyte materials is required. Analysis of the available in the literature data concerning this filed indicated that for solid electrolytes such properties like lithium-ion conductivity, long-range order structure and their inter-relations are well studied, but the features of the short-range order are not considered [1]. Thus, in current work it was proposed to evaluate the sort-range order structure of glasses and glass-ceramics based on $LiGe_2(PO_4)_3$ which is one of the most promising materials for Li-conducting solid electrolytes.

The local structure of the materials was studied by measuring total X-ray scattering with following Pair Distribution Function (PDF) analysis. Influence of partial substitution of Ge to Al and of degree of glass crystallization on the local structure was considered. It was revealed that both glass and glass-ceramic samples show local structure described by GeO6 octahedrons surrounded by PO4 tetrahedrons. For glass samples local order correlations are limited by the second coordination sphere of Ge atoms.

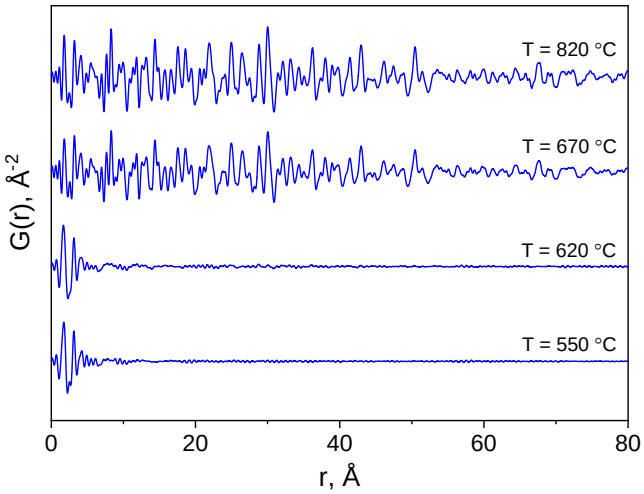


*Fig. 1. PDF functions for $Li_{1.5}Ge_{1.5}Al_{0.5}(PO_4)_3$ of various crystallization degrees achieved by annealing at different temperatures T*

**Acknowledgement:** This work was supported by the Russian Science Foundation, grant 22-73-00261.

**References:**

[1] C. Li, et. al., Sust.Mater.Technol. 29 (2021) e00297.

## PP-I-106

# Preparation of Silver Nanocomposites by Thermolysis of Metal-Containing Monomers of Unsaturated Acids

Zarubina A.O., Zhinzhilo V.A., Uflyand I.E.
*Department of Chemistry, Southern Federal University, Rostov-on-Don, Russia*
*karginova@sfedu.ru*

In recent years, metal-containing monomers (MCM) have been widely studied, which have unsaturated bonds or functional groups in molecules that can enter homo-, copolymerization or polycondensation reactions. One of the advantages of MSM is the possibility of single-stage production of polymer complexes of metals in which each coordination fragment contains a metal ion in each spatial configuration. MSM has been most widely studied on the example of unsaturated metal carboxylates, the simplest representatives of which are metal acrylates. In addition, carboxylate complexes have an interesting structure, due to various ways of coordination of metal ions by carboxylate groups. Metal salts based on unsaturated dicarboxylic acids represent a large group of MSM that are actively studied by specialists in the field of coordination and polymer chemistry [1].

Silver nanoparticles stand out favorably among various metal nanoparticles due to the manifestation of a wide range of properties: plasmonic, antibacterial and catalytic activity, chemical stability, and good thermal and electrical conductivity. Silver (I) salts based on carboxylic acids have recently become the object of increased attention of researchers in the field of supramolecular chemistry, crystal engineering and coordination polymer chemistry [2].

The aim of this work was the synthesis of new silver-containing monomers based on unsaturated carboxylic acids. Silver itaconate was obtained by direct reaction of silver nitrate with itaconic acid in water in an alkaline medium. Figure 1 shows the IR spectrum of silver itaconate. An intense but rather narrow peak in the region of 3418 $cm^{-1}$ corresponds to the vibrations of the hydroxo group in the composition of the water of crystallization. The sharp peak at 1561 $cm^{-1}$ is attributed to the asymmetric stretch vibration of C=O, whilst the peak at 1385 $cm^{-1}$ is from the symmetric stretch vibration of C=O. Δν is equal to 176 $cm^{-1}$, which may indicate the bidentate mode of coordination of the metal–carboxyl group bond ($C_{2v}$ symmetry). A weak absorption signal in the region of 644 $cm^{-1}$ corresponds to the metal–oxygen bond.

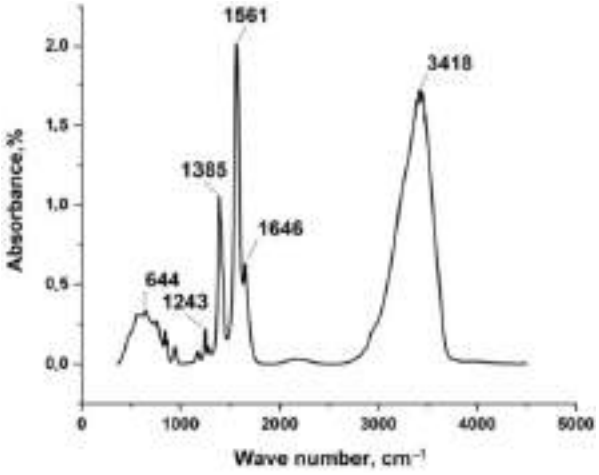


***Figure 1.*** *IR spectrum of silver itaconate.*

Analysis of the SEM image of silver itaconate thermolysis products makes it possible to establish a morphological feature associated with the fact that spherical formations with sizes from 6.8 to 72 nm are visualized on the surface against the background of hollow carbon nanotubes with a diameter of 10 to 42 nm (Figure 2).

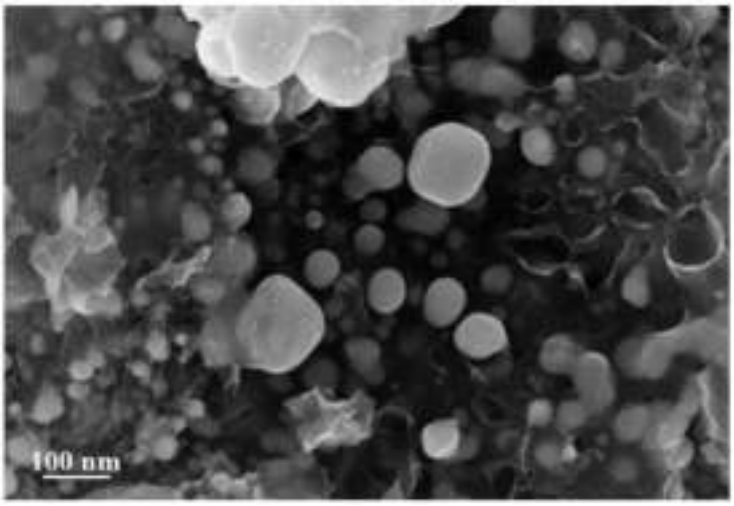


***Figure 2.*** *SEM image of silver itaconate thermolysis product.*

Thus, conjugated thermolysis of silver itaconate in an inert atmosphere leads to the formation of metal–carbon nanocomposites containing metal nanoparticles evenly distributed in a stabilizing carbon matrix. The obtained nanomaterials are stable; during their long-term storage, there are no changes in the chemical composition, size, and shape of nanoparticles. The proposed method for producing nanoparticles is simple and inexpensive, which makes it suitable for large-scale production.

**Acknowledgement:** This work was financially supported by the Russian Science Foundation (ProjectNo. 22-13-00260).

**References:**

[1] G.I. Dzhardimalieva, I.E. Uflyand, J. Coord. Chem. 70 (2017), 1468–1527.
[2] S.A. Semenov, V.Y. Musatova, D.V. Drobot, Russ. J. Inorg. Chem. 64 (2019), 786–797.

## PP-I-107

# The Effect of A-Cation Substitution on the Stability of Hybrid Perovskites under Powerful Electron Fluxes

Zhidkov I.S.[1,2], Rasmetyeva A.V.[1], Ozerova V.V.[3], Sarychev M.N.[1], Troshin P.A.[3], Kurmaev E.Z.[1,2]
*1 – Ural Federal University, Yekaterinburg, Russia*
*2 – Institute of Metal Physics UB RAS, Yekaterinburg, Russia*
*3 – FRC PCP and MC RAS, Chernogolovka, Russia*
*i.s.zhidkov@urf.ru*

In recent years much attention has been paid to organo-inorganic hybrid halide perovskites as promising materials for photovoltaics due to their high efficiency, low cost, and exceptional optical characteristics [1]. However, the active layers mainly consist of monocationic components with poor stability, such as $MAPbI_3$ and $FAPbI_3$ (MA – $CH_3NH_3$, FA – $CH_2(NH_2)_2$). Substitution of the A-cation can improve the optical absorption of perovskite films, decrease the trap state density in the films, and increase the internal structural and thermal stability of materials [2]. The use of perovskite solar cells has great potential in space technology. In this case, the most important factor in space conditions may be the effect of radiation from cosmic particles. In this work, we consider the effect of partial substitution of the A-cation on the stability of hybrid perovskites to powerful electron fluxes. XRD, XPS, PL, SEM, and AFM methods were used to study samples after irradiation with electron fluences from $10^{14}$ to $10^{16}$ e/cm$^2$.

The photoluminescence of the $FAPbI_3$ and $(CsFA)PbI_3$ films is rapidly quenched with an increase in the electron dose, which indicates the appearance of deep traps as a result of radiation damage to the material. In the cases of $MAPbI_3$ and $(CsMAFA)PbI_3$, a slower decrease in the photoluminescence intensity is observed, which is associated with the presence of methylammonium cations in their structure, which promote the healing of defects.

According to XPS spectra materials containing $MA^+$ cations are the least resistant to accelerated electron beams. Systems containing monovalent $FA^+$ and/or $Cs^+$ cations are the most promising for further studies. For all films irradiated with high-energy electrons there is no decrease in the I:Pb ratio with the increasing of irradiation dose, which excludes the formation of $PbI_2$ as a product of photochemical decomposition. Also, there is no systematic decrease in the N:Pb ratio, which does not indicate the release of metallic lead.

Analysis of the XPS N 1s spectra shows that irradiation of $MAPbI_3$ and $(CsMAFA)PbI_3$ perovskites with high-energy electron beams leads to their partial decomposition, which is accompanied by the appearance of additional structural elements, the contribution of which increases with the irradiation dose. This effect is much less pronounced in the case of $CsFAPbI_3$ and $FAPbI_3$.

Thus, the study of the resistance of $APbI_3$ perovskites to irradiation with high-power fluxes of electrons with an energy of 8.5 MeV showed that photochemical degradation is observed

for $MAPbI_3$ and $(CsMAFA)PbI_3$ perovskites, while $MAPbI_3$ and $(CsMAFA)PbI_3$ demonstrated remarkable stability up to fluences of the order of $10^{16}$ $cm^{-2}$.

**Acknowledgement:** This work was supported by the Russian Science Foundation, grant 22-61-00047.

**References:**

[1] J. Berry et al., Adv. Mater. 27 (2015) 5102.
[2] J. Gong et al., Energy Chem.27 (2018) 1017.

## PP-I-108

# Synthesis and Properties of Bicomponent Complex Systems Based on Organic Acid and Polyoxometalate Compound

Zhirov N.[1], Akimov A.S.[1,2], Zhuravkov S.P.[3]
*1 – Institute of Petroleum Chemistry, Tomsk, Russia*
*2 – Tomsk State University, Tomsk, Russia*
*3 – Tomsk Polytechnic University, Tomsk, Russia*
*krigsnu@gmail.com*

Every year the need for catalysts for the processing of heavy raw materials increases. In particular, these include systems based on transition metals (Mo, W, Co, Ni...). Catalysts based on them increase the depth of processing and make it possible to involve heavier raw materials in the process. Thus, the development of new catalytic systems is an urgent task of our time. One of the approaches is to obtain new active components. One of the promising reagents is molybdenum blue - a mixture of non-stoichiometric oxides in the oxidation state +5-+6. However, a small number of studies on this topic attract the attention of scientific groups. The purpose of this work was to obtain deposited Mo-containing aluminum oxide systems and study their properties using a set of modern physicochemical methods.

A feature of our systems is the original method of obtaining molybdenum blue with the involvement of mechanochemical synthesis [1]. This approach does not require a large amount of specialized equipment and reagents, and the synthesis itself takes place in 2 stages - mechanoactivation of the precursor and the addition of a reducing medium. Industrial powder γ-$Al_2O_3$ was chosen as a support for catalytic systems, since it is widely distributed, available, and has an optimal set of physical and chemical properties. Citric acid was also introduced into the systems as a chelating agent to prevent side reactions of interaction between the active component and the carrier. The catalytic systems were prepared by one of the traditional impregnation methods in excess of the impregnating solution. The impregnating solution is an alcoholic solution of molybdenum blue, in which a sample of citric acid was previously dissolved. The synthesis procedure is described in more detail in [2]. The excess impregnating solution was decanted, and the resulting catalyst system was subjected to heat treatment at various temperatures for 4 hours. The names of the obtained samples are presented in Table 1.

*Table 1. Conventional names of synthesized systems*

| Sample | K-1 | K-2 | K-3 | K-4 |
|---|---|---|---|---|
| Treatment temperature, °C | 25 | 100 | 300 | 400 |

Figure 1 shows the results of IR spectroscopy of the resulting systems. It can be seen from the figure that thermal treatment does not significantly affect the overall profile of the spectra. Broad absorption bands (absorption bands) in the range of 500-900 $cm^{-1}$ refer to

structural fragments of Al-O-Al and Al-O. In this region, there is a high chance of overlap with the corresponding oxide molybdenum structures in the regions of 560-580 and 720-790 $cm^{-1}$. The band of medium intensity in the region of 1140 $cm^{-1}$ characterizes the vibrations of the citrate skeleton, and in the region of 1640 $cm^{-1}$, apparently, it refers to physically sorbed water.

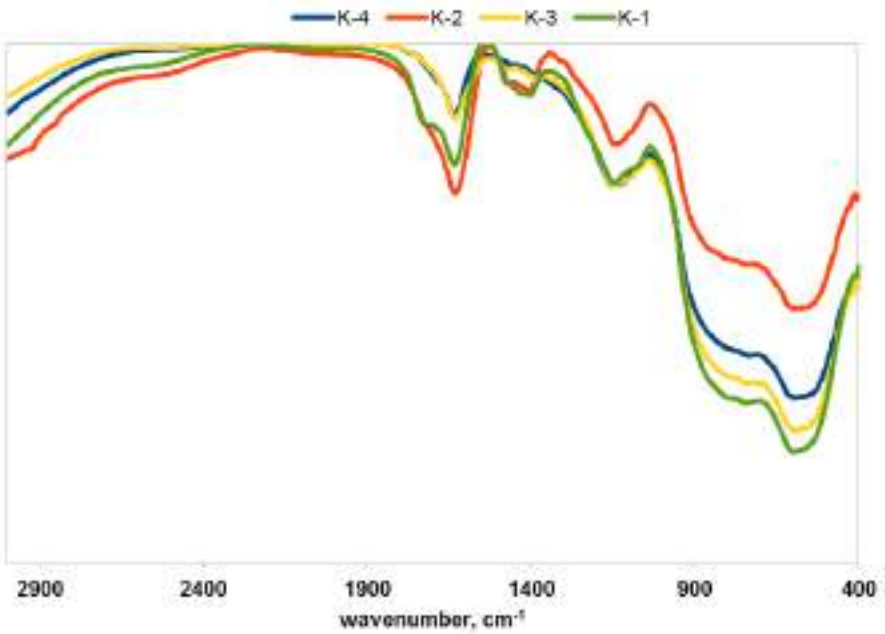


*Fig. 1. Results of IR-spectroscopy*

**Acknowledgement:** The work was carried out within the framework of the state task of the Institute of Chemical Sciences of the Siberian Branch of the Russian Academy of Sciences, funded by the Ministry of Science and Higher Education of the Russian Federation

**References:**

[1] A. Akimov, N. Sviridenko , M. Morozov, T. Petrenko, S. Zhuravkov, S. Kazantsev, S. Panin. IOP Conf. Series: Materials Science and Engineering. 597 (2019) 012015.
[2] O. Klimov, A. Pashigreva, G. Bukhtiyarova, S. Budukva, M. Fedotov, D. Kochubey, Y. Chesalov, V. Zaikovskii, A. Noskov Catal. Today. 150 (2010) 196-206.

## PP-I-109

# The Structural-Mechanical Properties of the Molding Pastes and the Granular Magnesium Aluminates Depending on the Preparation Conditions

Kruglyakov V.Yu., Zhuzhgov A.V., Protsenko R.S., Isupova L.A.
*Boreskov Institute of Catalysis, Novosibirsk, Russia*
*krugl@catalysis.ru*

The use of magnesium aluminate as a carrier of catalysts in different catalytic processes is of significant practical interest due to neutral acid-base characteristics of the surface and its high thermal stability. Traditional methods of obtaining of alkali-earth metals aluminates are a ceramic (with high-temperature sintering) and a sol-gel. We previously published the results of obtaining of alkali-earth metals aluminates using a hydrothermal treatment of a suspension of the product of thermal activation of Gibbsite in salts solutions with the production of powder material after mild calcining of formed gels [1-3], while granular supports and catalysts are used in catalytic processes.

The purpose of the work is to obtain granules of the carrier based on the magnesium aluminate with the spinel structure with high values of the specific surface area, mechanical strength and volume of pores. The granules were obtained by extrusion forming of pastes through a draw plate with a diameter of 4 mm:

- based on gels formed during hydrothermal treatment of suspensions;
- based on powders obtained after drying of gels at $200^0$ C;
- based on powders obtained after heat treatment of dried gels at $550^0$ C.

After molding, all granules were calcined at 550 $^O$C for 4 hours. The conditions of hydrothermal treatment and used raw materials are described in [1].

The properties of the molding pastes were determined using the Anton Paar viscosimeter with the RH7 rotor and the conical plastometer of P.A. Rebinder's design. Texture characteristics and a mechanical strength were determined for calcined at 550 $^o$C granules.

The gel obtained when magnesium nitrate was used as a row material for hydrothermal treatment is not suitable for extrusion molding, it has a moisture content of more than 60% and is characterized by viscosity value V = 1.17 KP. The gel obtained when magnesium oxide was used is suitable for extrusion molding, has a moisture content of 38.5%. The mass belongs to the 0 structural-mechanical type with a significant predominance of elastic deformations (more than 60%), it has values of plastic strength Pm = 2.87 KPa and viscosity v = 3.12 KP. The properties of dried gels are given in table 1.

Table 1- Properties of dried gels

| № | Source of Mg | $S_{sp}$, BET/ BJH , $м^2/g$ | $V_{pores}$, $см^3/g$ | $D_{pores}$, нм |
|---|---|---|---|---|
| 1 | Nitrate | 93.968/71.981 | 0.220 | 4.303 |
| 2 | Oxide | 198.366/137.464 | 0.507 | 3.138 |

The molding masses obtained from dried gels differ in structural-mechanical properties and belong to different structural-mechanical types (0-for “nitrate” mass and 2- for “oxide” mass.) In the molding “nitrate” pastes, elastic deformations prevail, and in the “oxide” mass - elastic. These masses have values of plastic strength PM = 4.5KPa for “oxide” sample and 6.2 KPa for “nitrate” sample; viscosity values V = 3.52 KP for “oxide” sample and 3.65 KP for “nitrate” sample. Properties of the granules obtained after calcination of the extrudates are given in table 2.

Table 2- Properties of granules after calcination

| № | Source of Mg, Temperature of Gel treatment | $S_{sp}$ BET, $м^2/g$ | Strength, MPa | $V_{pores}$, $см^3/g$ | $D_{pores}$, нм |
|---|---|---|---|---|---|
| 1 | Oxide, without h/t | 200.0 | 1.5 | 0.52 | 3.80 |
| 2 | Nitrate, 200 $^{O}C$ | 150.0 | 5.0 | 0.23 | 3.80 |
| 3 | Oxide, 200 $^{O}C$ | 200.0 | 3.0 | 0.52 | 3.80 |
| 4 | Nitrate, 550 $^{O}C$ | 102.2 | 3.5 | 0.22 | 4.85 |
| 5 | Oxide, 550 $^{O}C$ | 108.2 | 2.1 | 0.45 | 3.10 |

Pastes prepared from calcined gels have properties that are close to ceramic pastes: both samples belong to the 2-nd structural-mechanical type, have the elasticity values $\lambda = 0.70$ in an “oxide” sample and 0.69 in “nitrate” sample; the periods of relaxation $\theta = 2285$s in an “oxide” sample and 2230 s in “nitrate” sample. Values of plastic strength PM = 14.4 KPA in an “oxide” sample and 15.3 KPA in “nitrate” sample and viscosity values V = 5.08 KP in an “oxide” sample and 5.30 KP in “nitrate” sample. The properties of granules obtained from these molding pastes are given in the table 2, samples 4-5.

All molding pastes obtained from dried or calcined gels had close values of optimal molding moisture of 20-22%. The molding pastes prepared using “nitrate” samples compared to “oxide” samples (from dried or calcined gels) have higher values of viscosity and plastic strength, and calcined granules have higher mechanical strength. The use of magnesium oxide allows to obtain carriers with sufficient strength and higher values of the specific surface area and the volume of pores.

**Acknowledgement:** This work was supported by the budget project AAAA-A21-121011490008-3 for the Boreskov Institute of Catalysis.

**References:**

[1] Zhuzhgov A.V., Kruglyakov V.Y., Suprun E.A., Protsenko R.S., Isupova L.A.//Russian Journal of Applied Chemistry. 2021. T. 94. № 2. C. 152-161.
[2] Patent RU 2735668 S1, 05.11.2020.
[3] Zhuzhgov A.V., Kruglyakov V.Y., Glazneva T.S., Suprun E.A., Isupova L.A. Wasteless Synthesis and Properties of Highly Dispersed MgAl2O4 Based on Product of Thermal Activation of Gibbsite // Chemistry. 2022. V. 4. N. 2. P. 316-328. https://doi.org/10.3390/chemistry4020024.

## PP-II-01

# Laser Processing for Biodegradable Composites Based on Reduced Graphene Oxide and Polymer

Abyzova E.G., Dogadina E.M., Petrov I.S., Bolbasov E.N., Vorobev A.O., Plotnikov E.V., Sheremet E.S., Rodriguez R.D.
*Tomsk Polytechnic University, Tomsk, Russia*
*abyzovaeg@gmail.com*

In recent years, significant attention has been devoted to research on medical implants with active electronics. These implantable devices offer effective solutions to critical clinical problems [1]. However, the use of standard materials presents a disadvantage for doctors and patients as it requires removal or re-operation and can cause chronic inflammatory reactions [2]. To overcome these challenges, the development of biodegradable composites has become increasingly important due to growing concerns over environmental sustainability. Biodegradable implants have emerged as a promising solution, as they offer attractive propositions for future biomedical technologies and mitigate some environmental problems.

Reduced graphene oxide (rGO) is a material that has gained widespread interest in recent years. This derivative of graphene oxide is obtained through a photonic, chemical, or thermal reduction process of graphene oxide and exhibits remarkable properties, such as high surface area and good electrical conductivity [3]. One promising application of rGO is its integration into composites with other materials, which could lead to the development of sustainable and high-performance materials. To solve the problem of monitoring important indicators of the human body, it is proposed to use reduced graphene oxide (rGO) with a biodegradable polymer to develop electronic components embedded into implants for wireless monitoring. The graphene oxide laser reduction process is used to create electronic devices of the arbitrary shapes. This technology can improve patient care while minimizing adverse environmental impacts. However, the development of suitable materials that meet both functional and safety requirements remains an important challenge.

To enhance the successful integration of reduced graphene oxide, we opted for a biodegradable polymer substrate, namely polylactic acid (PLA). The process involved depositing a graphene oxide solution onto 3D-printed PLA polymer films, which were then reduced using a 405 nm laser. It was experimentally shown that the layer of reduced graphene oxide remained stable after mechanical action and being in environments from acidic to alkaline. The resulting rGO/PLA composite displayed remarkable chemical and mechanical stability.

To assess the toxicity and biocompatibility of rGO/PLA samples, they were sterilized and placed in buffer solution and culture medium for varying durations, ranging from 1 to 120 days. Remarkably, the test results revealed that cells grew on the surface of all samples, while maintaining their viability. Furthermore, there was no release of toxic substances from the films, and no bacterial growth was observed. These findings indicate that the newly-developed

biodegradable electronic components hold immense potential as implantable electronics with impact in healthcare.

**Acknowledgement:** The work was supported by Russian Science Foundation grant № 22-12-20027, https://rscf.ru/project/22-12-20027/ and the funding from Tomsk region administration.

**References:**

[1] Cha, G. D., Kang, D., Lee, J., & Kim, D.-H. Bioresorbable Electronic Implants: History, Materials, Fabrication, Devices, and Clinical Applications. Advanced Healthcare Materials, (2019), 8(11), e1801660.
[2] Hosseini, E. S., Dervin, S., Ganguly, P., & Dahiya, R. Biodegradable Materials for Sustainable Health Monitoring Devices. ACS Applied Bio Materials, (2021), 4(1), 163–194.
[3] Tarcan, R., Todor-Boer, O., Petrovai, I., Leordean, C., Astilean, S., & Botiz, I. Reduced graphene oxide today. Journal of Materials Chemistry. C, Materials for Optical and Electronic Devices, (2020), 8(4), 1198–1224.

## PP-II-02

# Design and Structural Self-Organization of Water-Soluble Nanobiocomposites of Ferrite and Bismuth Oxide with a Polysaccharide Matrix

Aleksandrova G.P.[1], Sapozhnikov A.N.[2]
*1 – Irkutsk Institute of Chemistry, Irkutsk, Russia*
*2 – Irkutsk Institute of Geochemistry, Irkutsk, Russia*
*alexa@irioch.irk.ru*

Recently, the development of metal oxide nanoparticles NP for the application in biomedical studies and clinical practice for drug delivery, enhancement of the MRI contrast, , targeted hyperthermia, and creation of biomarkers has received significant attention. This can be achieved via the creation of nanostructured drugs based on biocompatible matrices for targeted delivery of pharmacophore oxides. Iron and bismuth are among the most important and promising bioactive elements.

We obtained nanocomposites, the key fragments of which are nanosized bismuth ferrite [1], bismuth and iron oxide [2] nanoparticles via a safe “green” route. The general features of self-assembly of iron and bismuth oxides were shown; it was revealed that the arabinogalactan matrix [3] acts as strong stabilizer of those oxides particles which became hydrophilic and watersoluble. The metal oxide nature of the nanoparticles and biphasic structure of the nanocomposites was demonstrated by means of X-ray diffraction analysis. The morphology of new self-organizing nanobiocomposites, which were dispersed in water, was studied, and the sizes of bismuth ferrite, bismuth and iron oxide nanoparticles were determined. There are established mechanisms of the matrices interaction with the metal oxide nanoparticles in the context of metal-polymer nanocomposites synthesis [4]. The specificity of the synthesis and the use of a natural polysaccharide as a stabilizing matrix for the forming NPs provides tunable sizes and a narrow distribution of the dispersion of the resulting particles, determines their long-term aggregative stability, and makes it possible to obtain biocompatible NCs.

**References:**

[1] G.P. Aleksandrova, A.C. Bogomyakov, A.N. Sapozhnikov, V.I. Ovcharenko. Russ.Chem.Bull. 7 (2022) 1453.
[2] G.P. Aleksandrova, B.G. Sukhov, B.A. Trofimov, A.N. Sapozhnikov, A.S Boymirzaev. Russ. J. Gen. Chem. 4 (2020) 672.
[3] V.I. Dubrovina, S.A. Vityazeva, Zh.A. Konovalova, O.V. Yur´eva, T.P. Starovoitova, V.V. Voitkova, G.P. Aleksandrova, V.S. Polovinkina. Immunomodulatory Effect of Metal-containing Nanocomposites. Megaprint, Irkutsk. 2017. 77 p.
[4] G.P. Aleksandrova, A.S. Boymirzaev, I.V. Klimenkov, B.G. Sukhov, B.A. Trofimov. Nanotechnologies in Russia. 14 (2019) 41.

## PP-II-03

# Synthesis and Characterization of L-lysine Polyurethane (LPU) Nanoparticles for Drug Delivery System

Soojeong Choi, Seoeun Oh, Ildoo Chung
*Department of Polymer Science and Engineering, Pusan National University, Busan, Korea*
*soojeong9901@pusan.ac.kr*

To obtain biodegradable biomaterial for matrix of drug delivery, L-lysine polyurethane(LPU) was designed using poly(ethylene glycol) (PEG) as a soft segment, 1,6-hexamethylene diisocyanate(HMDI) as a hard segment and L-lysine ethyl ester(LEE) as a chain extender. LEE was synthesized by esterification of L-lysine with ethanol using thionyl chloride. PEG has biocompatibility so it is suitable for biomaterial polyurethane. LPU nanoparticles were fabricated by using water-in-oil-in-water double emulsion technique for encapsulating anticancer drugs. The structure and composition of the resulting polyurethane was confirmed by $^{1}$H-NMR, $^{13}$C-NMR, FT-IR spectroscopies, and the molecular weight of polyurethane was characterized by GPC analysis. The morphology of nanoparticles was confirmed by DLS, FE-SEM and TEM.

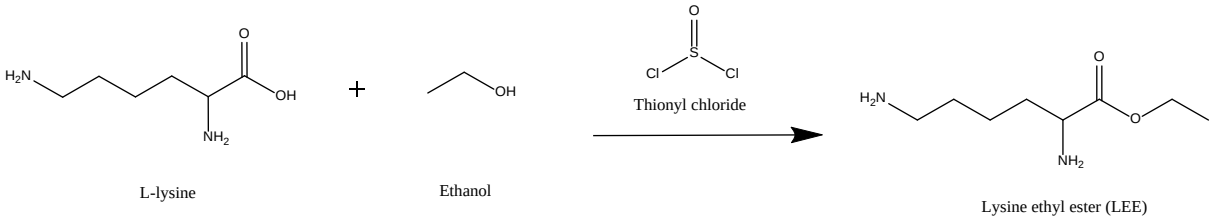


*Fig. 1. Scheme for the synthesis of LEE.*

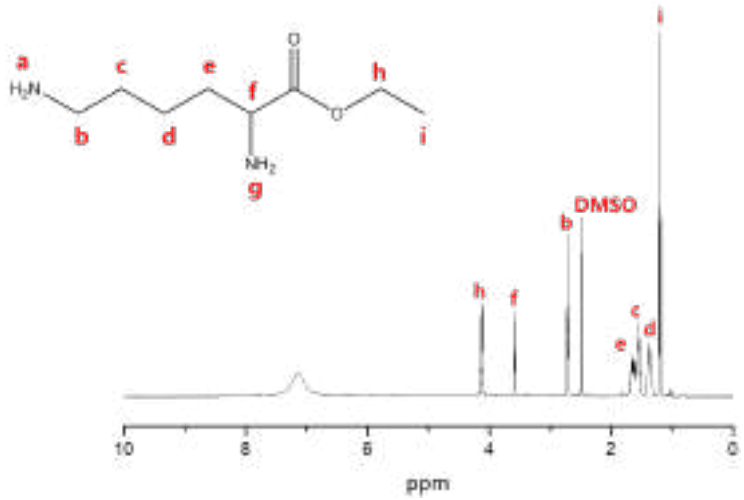


*Fig. 2. $^{1}$H-NMR spectrum of LEE.*

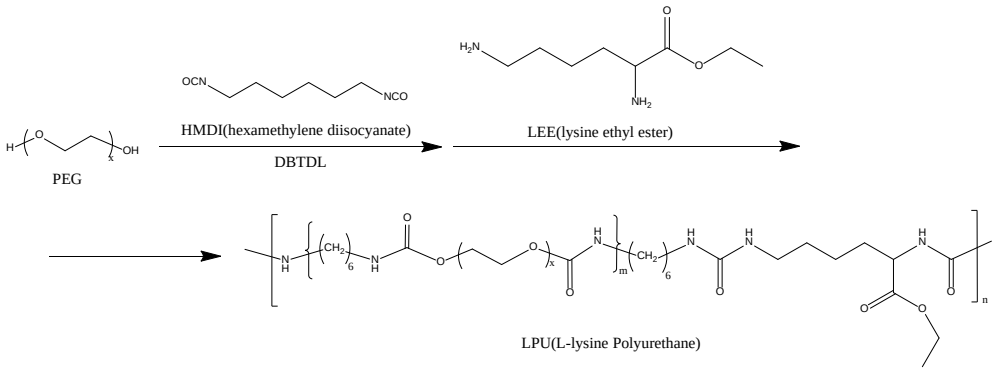


*Fig. 3. Scheme for the synthesis of LPU.*

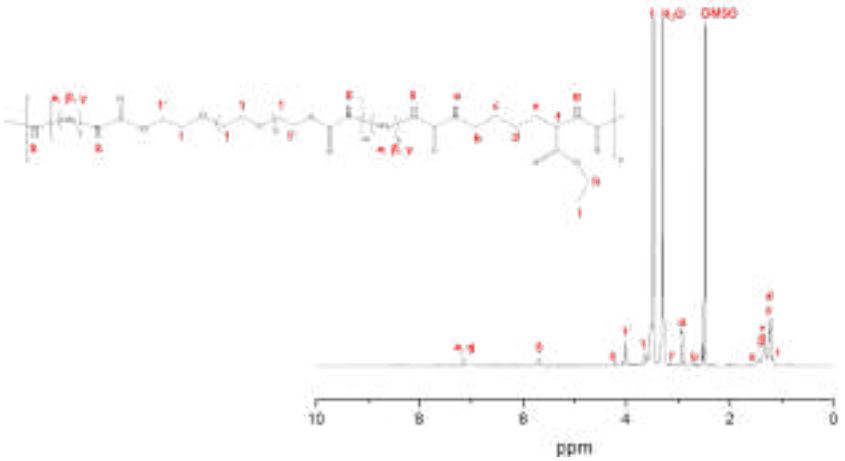


*Fig 4. $^{1}$H-NMR spectrum of LPU.*

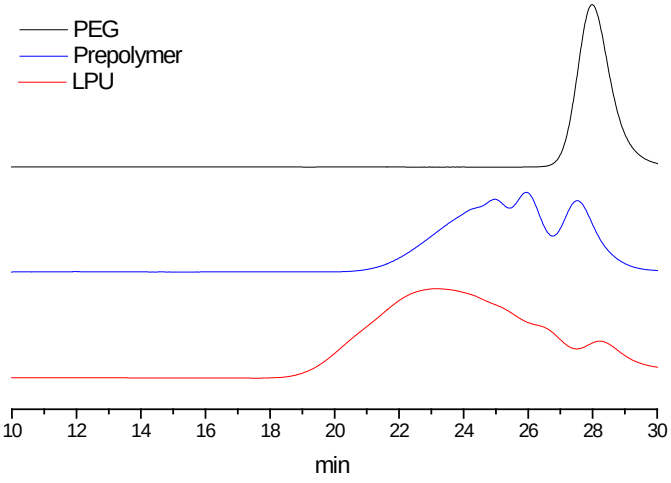


*Fig. 5. GPC analysis of LPU.*

**Acknowledgement:** This research was supported by Basic Science Research Program through the National Research Foundation of Korea (NRF) funded by the Ministry of Education (2022R1I1A3053556116218206530010 1)

**References:**

[1] Soo-Yong Park, Yang H. Yun, Bum-Joon Park, Hyung-Il Seo, Ildoo Chung, Fabrication and Biological Activities of Plasmid DNA Gene Carrier Nanoparticles Based on Biodegradable L-Tyrosine Polyurethane, Pharmaceuticals, 2022, vol 15, 17-33

[2] Soo-Yong Park, Jiin Kang, Ji-Young Yoon, Ildoo Chung, Synthesis and Characterization of Polyfumarateurethane Nanoparticles for Sustained Release of Bupivacaine, Pharmaceutics, 2020, vol 12, 281-293

## PP-II-04

# Synthesis and Characterization of L-Threonine Polyurethane (LTHU) Nanoparticles for Drug Delivery System

Soojeong Choi, Seoeun Oh, Ildoo Chung
*Department of Polymer Science and Engineering, Pusan National University, Busan, Korea*
*soojeong9901@pusan.ac.kr*

The L-threonine polyurethane (LTHU) for matrix of drug delivery vehicle was synthesized using desaminotyrosyl L-threonine hexyl ester (DLTHE), poly(lactic acid)-poly(ethylene glycol)-poly(lactic acid) (PLA-PEG-PLA) and 1,6-hexamethylene diisocyanate (HMDI). The DLTHE was prepared based on the L-threonine hexyl ester (LTHE), which was pre-synthesized by esterification with hexanol, and used as a chain extender in LTHU polymerization. Furthermore, LTHU was designed to be degradable through the hydrolysis and enzymatic degradation of ester and amide linkages in its polymer backbone. Using water-in-oil-in-water double emulsion techniques, LTHU nanoparticles were fabricated for encapsulating anticancer drugs such as carboplatin. All the synthetic processes were confirmed by $^{1}$H-NMR, $^{13}$C-NMR and FT-IR spectroscopies, and molecular weights of PLA-PEG-PLA and LTHU were confirmed by GPC analysis. The morphologies of nanoparticles were characterized by DLS, FE-SEM and TEM and drug encapsulation was confirmed by confocal laser scanning microscope and fluorescence microspe. Drug loading efficiency and encapsulation efficiency were also confirmed by UV/Vis spectroscopy.

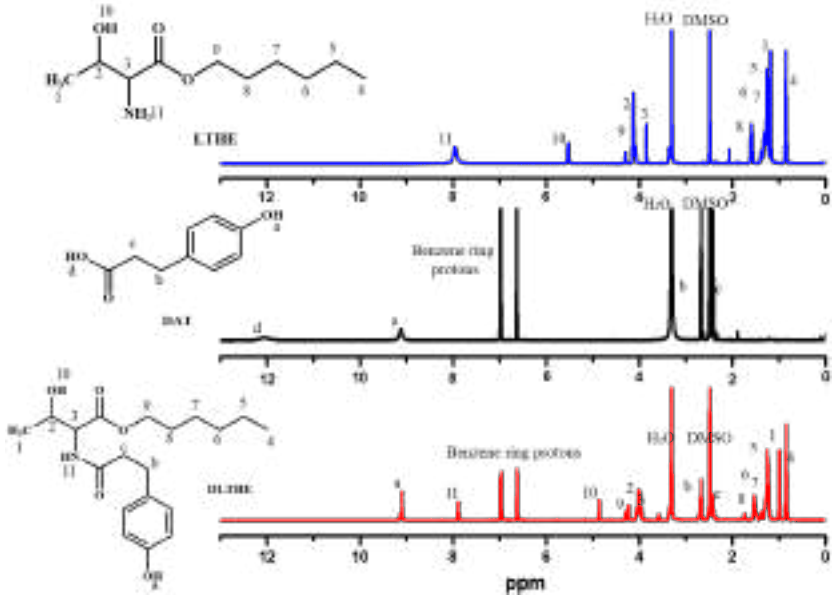


*Fig. 1. $^{1}$H-NMR spectra of LTHE, DAT, DLTHE.*

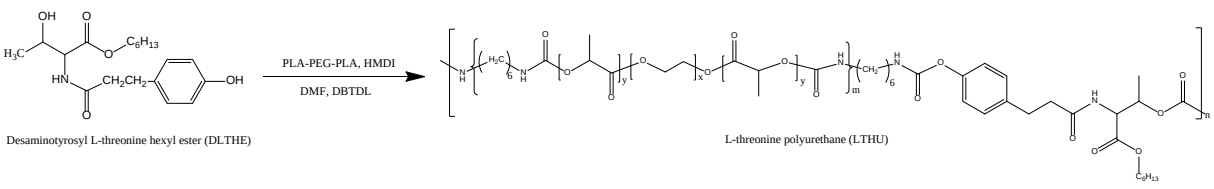


*Fig. 2. Scheme for the synthesis of LTHU.*

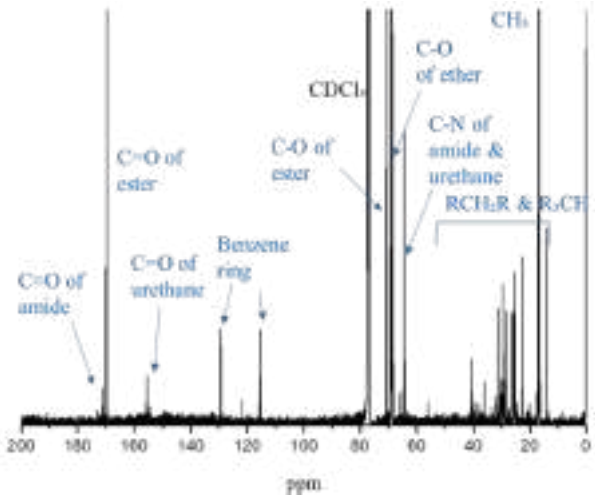


*Fig. 3. $^{13}$C-NMR of LTHU.*

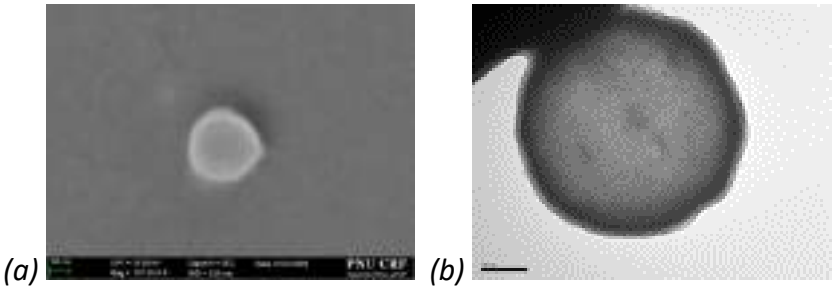


*Fig. 4. (a) SEM image and (b) Tem image of LTHU Nanoparticles.*

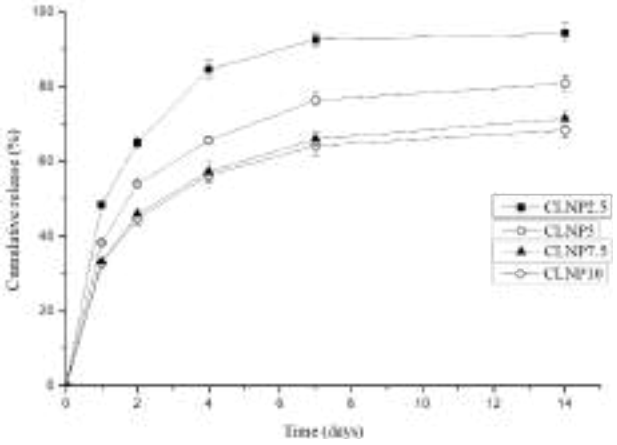


*Fig. 5. In vitro cumulative release of nanoparticles in PBS.*

**Acknowledgement:** This research was supported by Basic Science Research Program through the National Research Foundation of Korea (NRF) funded by the Ministry of Education (2022R1I1A3053556116218206530010 1)

**References:**

[1] Soo-Yong Park, Yang H. Yun, Bum-Joon Park, Hyung-Il Seo, Ildoo Chung, Fabrication and Biological Activities of Plasmid DNA Gene Carrier Nanoparticles Based on Biodegradable L-Tyrosine Polyurethane, Pharmaceuticals, 2022, vol 15, 17-33

[2] Soo-Yong Park, Jiin Kang, Ji-Young Yoon, Ildoo Chung, Synthesis and Characterization of Polyfumarateurethane Nanoparticles for Sustained Release of Bupivacaine, Pharmaceutics, 2020, vol 12, 281-293

## PP-II-05

# Comparison of Mechanical Properties of Modern Polymer Composites Used for Bone Tissue Regeneration

Gerasimova D.S., Moskalyuk O.A.
*Laboratory of Polymer and Composite Materials «SmartTextiles», IRC–X-ray Coherent Optics, Immanuel Kant Baltic Federal University, 14, A. Nevsky Str., Kaliningrad 236041, Russia*
*dst-678677g@mail.ru*

The bone frame is a three-dimensional temporary mechanical structure that mimics the extracellular matrix (ECM) of bone tissue and creates favorable conditions for the processes of bone remodeling and regeneration. The ideal three-dimensional scaffold consists of a biocompatible, biodegradable material with mechanical properties similar to the tissue in which it will be implanted. In native bone hydroxyapatite crystals form a structure and provide the compression resistance, collagen creates tensile strength and bending resistance. The reconstruction of the physical structures and functions of protein, mineral and cellular components of bone is the goal for developers creating materials for bone tissue engineering.

In this paper, an analysis of chronic polymeric composite materials prescribed today for the purpose of bone tissue is carried out (fig. 1). The mechanical strength of the frame is necessary to hold the structure in the place of implantation. Based on the analysis of the data, samples of composites were identified with mechanical characteristics approaching those of natural bone tissue. The prospect of developing biopolymer composites with a given level of mechanical properties is shown.

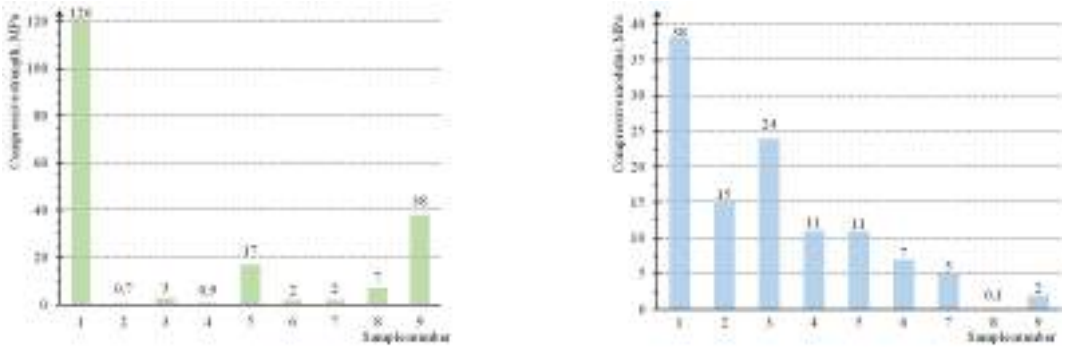

*a)* *b)*

*Figure 2. Comparison of the mechanical properties of the existing scaffolds: a - compressive strength; b - compressive modulus [1-6]*

**Acknowledgement:** This research was supported from the Russian Federal Academic Leadership Program Priority 2030 at the Immanuel Kant Baltic Federal University.

**References:**

[1] A. Bharadwaz; A. C. Jayasuriya, Mater. Sci. Eng. 110 (2020) 110698.
[2] Q. U. Ain et al., Mater. Sci. Eng. C 75 (2017) 807–815.
[3] A. R. Farmani et al., J. Polym. Environ. 31 (2023) 870–885.
[4] K. Deng et al., Front. Mater. 9 (2022).
[5] R. Ziadlou et al., Mater. Sci. Eng. C 120 (2021) 111701.
[6] A. N. Dehkordi et al., J. Drug Deliv. Sci. Technol. 76 (2022) 103827.

## PP-II-06

# The Role of Amino Acids in the Formation of Modifications of Calcium Carbonate Obtained from Bile Solution

Golovanova O.A.
*Department of Inorganic Chemistry of Dostoevsky Omsk State University, Omsk, Russia*
*golovanoa2000@mail.ru*

The processes of calcium carbonate precipitation in biological fluids (in particular in the bile system) are complicated, so a solution of the problem of stone genesis in bile-containing media is not only of medical significance but also holds scientific interest from the viewpoint of determination of the physicochemical properties of these compounds.

The reasons for selective crystallization of a polymorphous modification of calcium carbonate in the process of pathogenic mineralization are of complicated nature and are to a high extent determined by the specificity of physicochemical and kinetic factors governing the formation of stones. In turn, the formation of calcium carbonate crystals as nucleation centres in bile saturated with cholesterol may promote cholesterol crystallization and the formation of gallstones. Therefore, experimental modeling of these conditions is an urgent and practically significant task.

Of the gallstones formed in the human body, it is the metastable calcium carbonate polymorph that is formed to a greater extent, namely, vaterite (it is unstable when in a pure form; a monotropic phase transition to calcite occurs over time as the deposit ages in solution or under heating), because of its crystallization conditions. This feature of the phase composition of the inorganic component of choleliths is of interest, since its study can elucidate the true causes of gallstone formation and help in the development of new drugs and ways to prevent this disease.

To study the physicochemical conditions of crystallization and the phase composition of calcium car bonate polymorphs formed in the real settings of the human body, it currently seems possible to use thermodynamic modeling methods, as well as synthesis and characterization of the synthesized samples. To approximate the model being created to the real settings and to simulate its various states in this study, we use the concentrations of the substances in question such that are the norm for a healthy average person. The variations of these concentrations may correspond to various pathological changes in the state of human bile.

This work is targeted at the thermodynamic and experimental modeling of calcium carbonate crystallization from a bile solution by varying the solution composition (precipitating ions, amino acids, albumen) and experimental parameters (concentrations of substances introduced into the system).

As a result of the thermodynamic modeling of the formation of calcium carbonate in a model solution of bile (inorganic composition), it was found that during the functioning of the human body, crystallization of calcium carbonate normally does not occur (Fig.1). The

occurrence of local high supersaturations of precipitate-forming ions in bile can lead to the formation of $CaCO_3$ solid phase nuclei and further crystallization of gallstones.

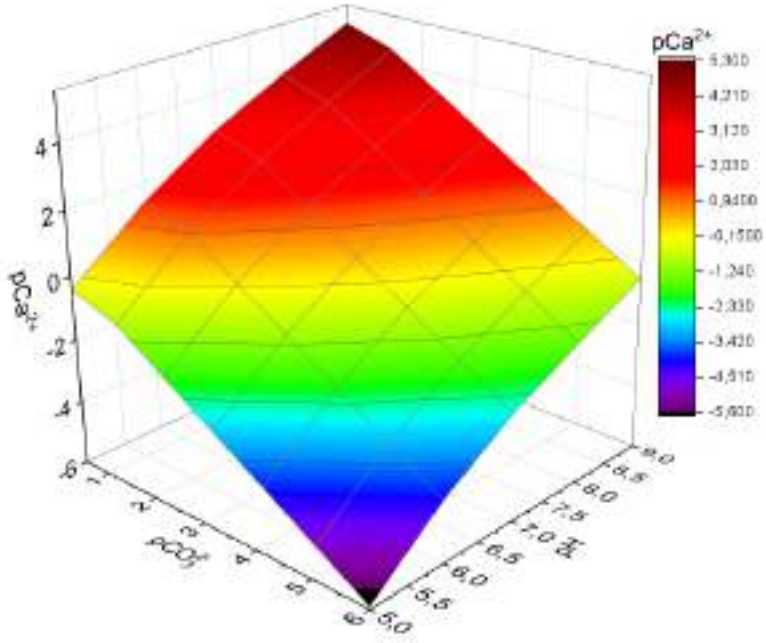


*Fig.1. Stability field of $CaCO_3$ in a model solution at pH from 5 to 9.*

Calcium carbonate was synthesized from bile-containing solutions. It was determined that the samples synthesized in the absence of bile and with its concentration 1 mass % contain calcite. An increase in bile content in the initial solution from 5 to 100 mass % promotes vaterite crystallization. Studies of the effect of bile on the mass of the solid phase showed that the mass of the precipitate increases in proportion with an increase in bile concentration in the initial solution. Investigation of the dissolution of synthesized samples in NaCl (0.9 mass %) and EDTA (0.05 mol/L) solutions revealed that the presence of bile components in the solid samples causes a decrease in the rate of their dissolution.

Having performed experimental modeling of calcium carbonate crystallization in a human bile model solution, we found that essential amino acids virtually have no effect on the formation of low-soluble compound (CaCO3), but they yet change the qualitative phase composition of the resulting powders. When present in average physiological concentrations, glycine, glutamic acid, and albumen separately do not modify the composition of the synthesized samples relative to the calcium carbonate obtained in a purely bile model solution. However, when their concentrations increase to the highest values permissible for their joint presence, they enhance the formation of vaterite, the metastable calcium carbonate polymorph, as the major phase.

**Acknowledgements:** The research was carried out within the state assignment of ministry of science and higher education of the Russian Federation, theme no. 075-03-2023-149.

## PP-II-07

# Fabrication and Properties of 3D Printable Dental Composite Containing Catechol Polymer

Chaeyoung Jeon, Ildoo Chung
*Department of Polymer Science and Engineering, Pusan National University, Busan, Korea*
*pnu83285@pusan.ac.kr*

Catechol-containing polymers, which have excellent adhesion function derived from mussels, have recently attracted much attention. Strong interaction between interfaces due to the catechol group with the hydrogen bond allows to apply to various field. Dopamine, 3,4-dihydroxyphenylalanine (DOPA) with catechol moieties, were selected as a starting material to synthesize polymerizable monomer by reacting with methacrylic anhydride. The synthesized dopamine methacrylamide (DMA) was characterized through FT-IR, $^{1}$H-NMR and $^{13}$C-NMR spectroscopies and mixed with ethoxylated bis-GMA (EBPDMA) with various compositions to 3D print by DLP technique. Catechol-functionalized polymers are synthesized by free radical polymerization of dopamine methacrylamide (DMA) and methyl methacrylate (MMA) in DMF. The polymer with the crosslinked structure was characterized through GPC, FT-IR and $^{1}$H-NMR spectroscopies. The mechanical properties of fabricated specimens such as compressive and flexural strengths were evaluated by UTM.

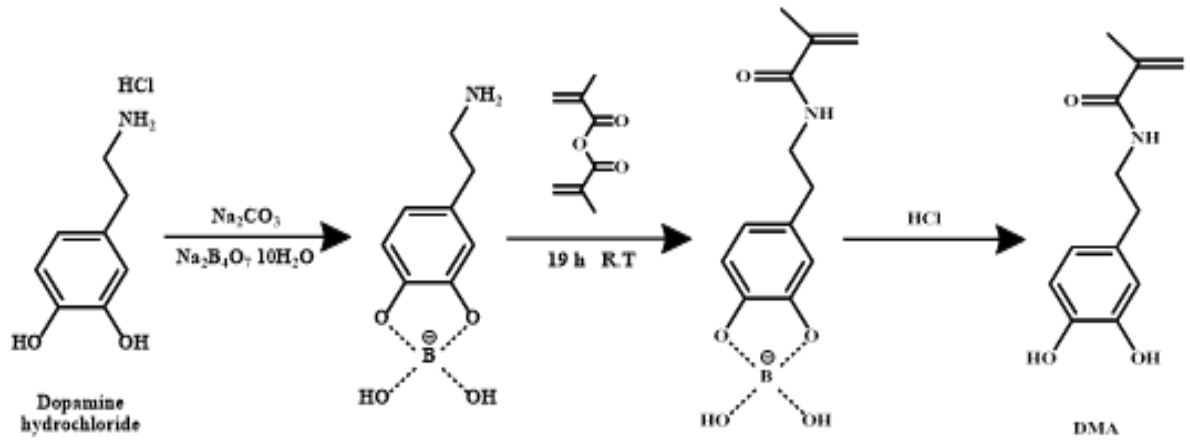


*Fig. 1. Synthesis scheme of Dopamine methacrylamide(DMA).*

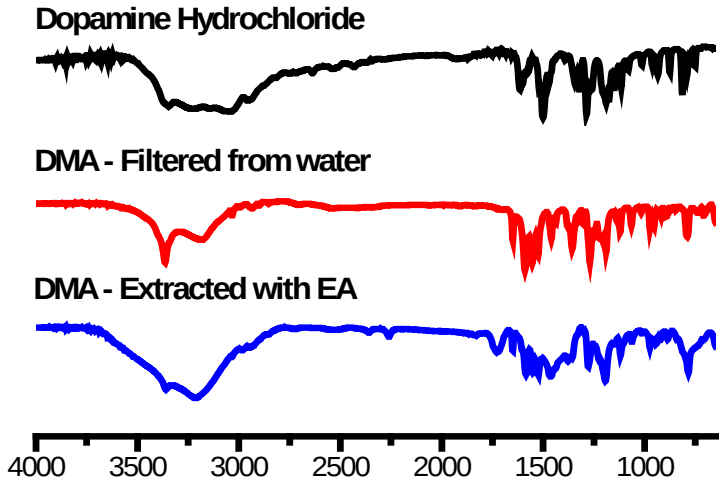


*Fig. 2. FT-IR spectra of Dopamine methacrylamide(DMA).*

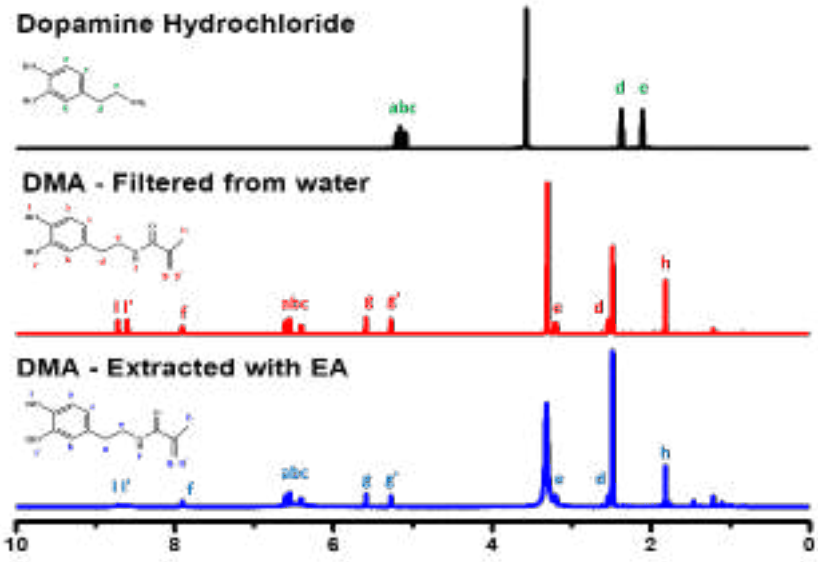


*Fig. 3. $^{1}$H-NMR spectra of Dopamine methacrylamide(DMA).*

**Acknowledgement:** This research was supported by Basic Science Research Program through the National Research Foundation of Korea (NRF) funded by the Ministry of Education (2022R1I1A3053556116218206530010 1)

**References:**

[1] Zhiwen Zeng, “Synthesis and characterization of incorporating mussel mimetic moieties into photoactive hydrogel adhesive”, Colloids and Surface B: Biointerfaces, 2018, vol. 161, pp. 94-102
[2] Kang Li, “The application of mussel-inspired molecule in dentin bonding”, Journal of Dentistry, 2012, vol. 99, 48, 6238-6240

## PP-II-08

# Fabrication and Properties of PEKK-Based Hybrid 3D Printable Dental Composite Resin

Chaeyoung Jeon[1], Sujin Kim[2], Ildoo Chung
*Department of Polymer Science and Engineering, Pusan National University, Busan, Korea*
*pnu83285@pusan.ac.kr*

Poly aryl ether ketones (PAEKs) has now gradually become the leading polymer material in the fields of biomedical polymer, due to its good biocompatibility and high thermal, mechanical properties. Among PAEKs, PEKK has advantages such as higher thermal stability, better mechanical properties, versatile chemistry due to two ketone bonds compared to other PAEKs. We focused on poly(ether ketone ketone) based oligomer to improve the mechanical properties of dental resin. In this study, HEMA-terminated poly(ether ketone ketone) oligomer (CAEKK-HEMA) was synthesized using carboxylic acid-terminated poly(ether ketone ketone) oligomer (CA-EKK) and 2-hydroxyethyl methacrylate (HEMA) and characterized by FT-IR, $^1$H-NMR, and GPC. The mixture of CAEKK-HEMA and ethoxylated bis-GMA (EBPDMA) with various ratios were photopolymerized by DLP 3D printing technique and their mechanical properties such as compressive and flexural strength were investigated.

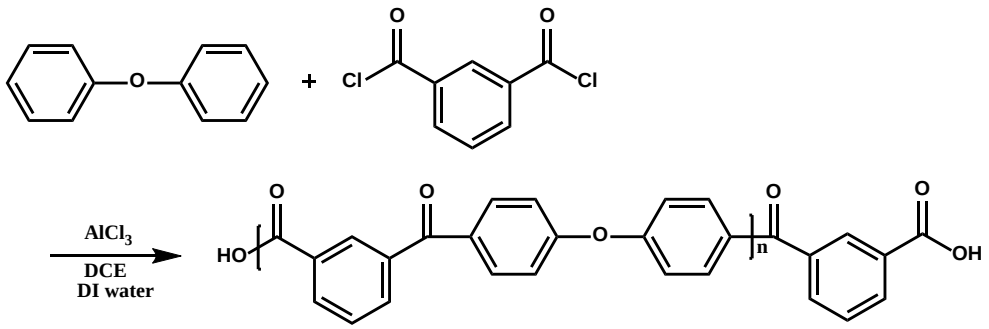


*Figure 1. Reaction scheme of CAEKK.*

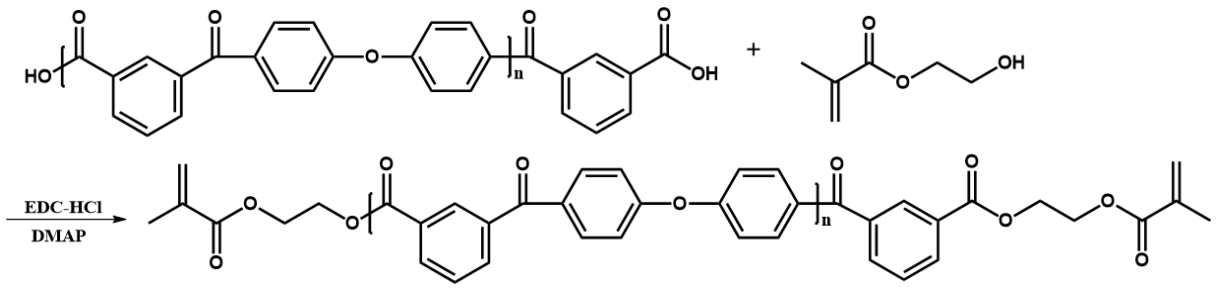


*Figure 2. Reaction scheme of EMAEKK.*

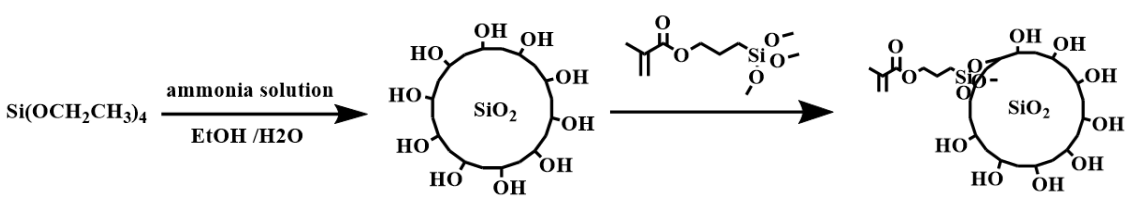


*Figure 3. Reaction scheme of Silica Nanoparticle.*

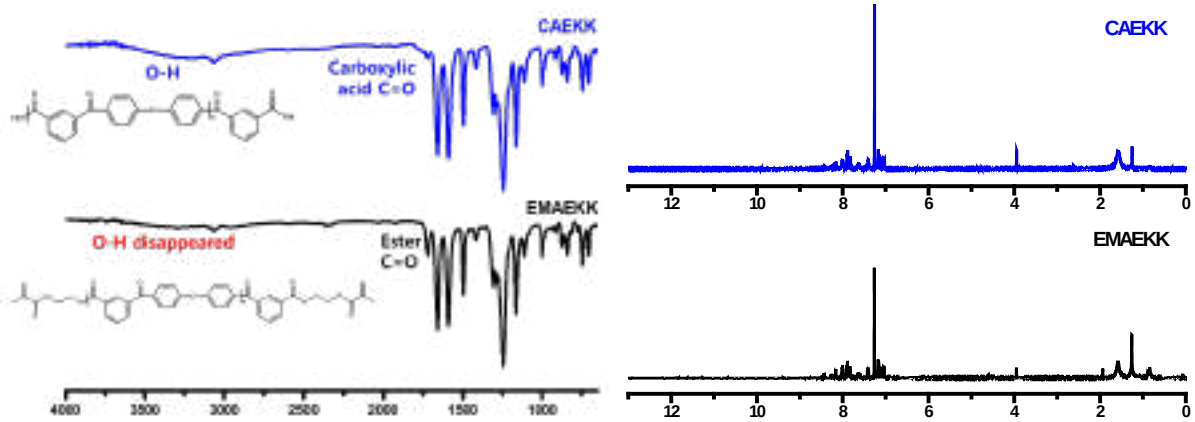


*Figure 4. FT-IR and H-NMR spectra of CAEKK and EMAEKK.*

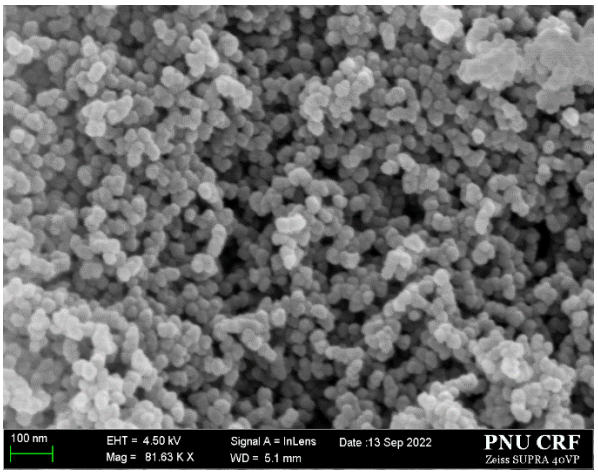


*Figure 5. SEM image of Silica Nanoparticle.*

**Acknowledgement:** This research was supported by Basic Science Research Program through the National Research Foundation of Korea (NRF) funded by the Ministry of Education (2022R1I1A3053556116218206530010 1)

**References:**

[1] Sakaguchi, Yoshimitsu, Masaya Tokai, and Yasuo Kato. "Synthesis of poly (ether ketone) by Friedel—Crafts acylation: effects of reaction conditions." Polymer 34.7 (1993): 1512-1515.
[2] Sakaguchi, Yoshimitsu, et al. "Polymerization Behavior of Poly (ether ketone) via Friedel–Crafts Acylation Studied by End-Group Analysis with 1 H NMR." Polymer journal 34.3 (2002): 219-224.

## PP-II-09

# Aluminum Phthalocyanine Chloride Aggregation in Aqueous and Aqueous-Organic Media

Klimenko I.V.[1], Astakhova T.Yu.[1], Timokhina E.N.[1], Lobanov A.V.[1,2]
*1 – Emanuel Institute of Biochemical Physics of Russian Academy of Sciences, Moscow, Russia*
*2 – Moscow Pedagogical State University, Moscow, Russia*
*inna@deom.chph.ras.ru*

In recent decade, photodynamic therapy (PDT) has become one of the most important treatment for cancer and various neoplasms, as far as in therapy of purulent wounds and trophic ulcers. Tetrapyrrole compounds nowadays are usually used as photosensitizer (Ps), a substance capable of biological tissues photosensitizing. The aromatic macroheterocyclic compound of aluminum phthalocyanine chloride (AlClPc, $C_{32}H_{16}AlClN_8$) is a Ps of a second generation which is characterized by high hydrophobicity, photoactivity and photostability, high absorbance coefficient in the region of 650–680 nm (so-called therapeutic window), high quantum yield of singlet oxygen ($\Phi_\Delta$ = 9.1) and rather high selective penetration into tumour tissue[1]. But in aqua or aqueous solutions AlClPc, like other tetrapyrrolic compounds, has a strong tendency for stacking (self-aggregation) with the formation of dimers and other types of aggregates, which reduces its photodynamic activity. The understanding of the mechanisms of interchromoform interaction in aqua and aqueous solutions can help in solving the problem of reducing aggregation in aqueous and physiological solutions.

In this work the process of AlClPc complex aggregation in N,N-dimethylformamide (DMF) and DMF-aqua solution with different concentration of aqua was studied by quantum mechanical theoretical calculations and experimental methods of optical absorption and fluorescence spectroscopy. The experimental results obtained for aqueous-organic medium indicate the existence of a critical concentration of aqua (~ 7.8 %), in which the ratio of monomers and dimers (J-aggregates) of AlClPc changes dramatically. Quantum chemical methods were used to evaluate all possible AlClPc structures. The adsorption and fluorescence spectra of these structures were calculated in time-dependent electron Density Functional Theory (DFT) approximation.

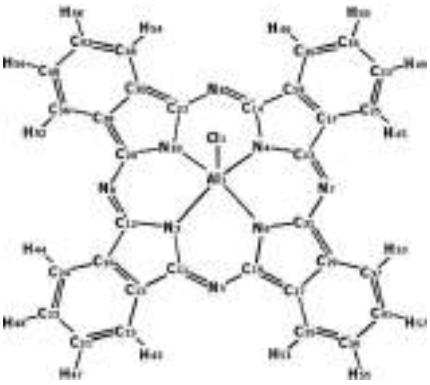

*Fig. 1. Optimized structure of AlClPc monomer with atomic numbers*

All the results demonstrate depending AlClPc photophysical parameters on its monomer/dimer ratios in solution, which is determined by concentration of the dye and aqua in the system and make it possible to predict the aggregation behavior of AlClPc complexes in aqua-organic media, as well as to control and manage their aggregation behaviour.

**Acknowledgement:** This work was supported by government funding within the framework of the scientific project "45.9 Theoretical and experimental studies of new materials and hybrid structures, including polyconjugate systems, nanostructures, composite materials and systems of reduced dimension" (FFEG-2019-0001). The calculations were carried out mainly by the supercomputers in Joint Supercomputer Center of RAS (JSCC RAS)

**References:**

[1] I.V. Klimenko, E.A. Trusova, A.N. Shchegolikhin, A.V. Lobanov, L.V. Jurina, Fullerenes, Nanotubes and Carbon Nanostructures, 30 (2022) 133. DOI:10.1080/1536383X.2021.1976754.

## PP-II-10

# Structural Features and Crystallization of $Na_2O$-$Cs_2O$-$B_2O_3$-$SiO_2$ Glasses for Immobilization

Nevolina L.A., Koroleva O.N.

*South Urals Federal Research Center of Mineralogy and Geoecology of the Urals Branch of the Russian Academy of Sciences, Miass, Russia*

*nevolina@mineralogy.ru*

Borosilicate glasses have long been the preferred form for the immobilization of high-level radioactive wastes due to their ability to dissolve a wide range of waste components and ease of modification to optimize their properties. However, a significant drawback of glass-matrices is the low rate of loading with radionuclides. One approach to solving this problem envisages a multiphase system using glass with crystalline inclusions [1]. The formation of certain ordered phases additionally contributes to an increase in the resistance of the matrix to physical impacts [2]. In recent years, interest in glass-ceramics based on glasses has significantly increased [3-5].

The present work set out to study model borosilicate glasses and glass-ceramics containing Cesium atoms as a radionuclide simulator. The aim of the work to evaluate the crystallization ability of glasses depending on the composition and method of crystallization. For this purpose, glass samples of the $Na_2O$-$Cs_2O$-$B_2O_3$-$SiO_2$ system were synthesized. The ratio of oxides corresponds to those used for immobilization glasses. Synthesis of glass-ceramics was carried out in two ways: directed crystallization and pressing followed by annealing.

The structure of the initial borosilicate glasses and glass-ceramic samples obtained on their basis was studied by Raman spectroscopy (Fig. 1). X-ray diffraction analysis was applied for identification of crystalline phases. The content of crystalline phases was calculated by the Rietveld method. The distribution of the radionuclide simulant element was evaluated using scanning electron microscopy.

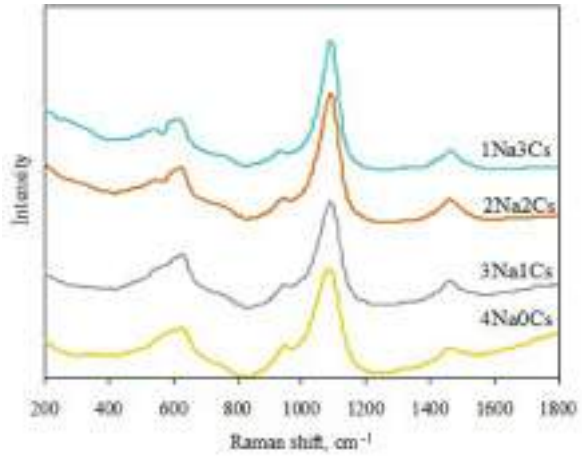


*Fig. 1. Raman spectra of the $Na_2O$-$Cs_2O$-$B_2O_3$-$SiO_2$ glasses.*

The results demonstrated that the structure and properties of the resulting glass-ceramic material are determined by the composition of the original glasses. Due to the ratio of modifier cations in glasses with a constant boron-to-silicon ratio, the determined crystalline phases in glass-ceramics are significantly affected by the anionic structure. In addition, the formation and growth of crystals depends on the technological scheme of synthesis.

**Acknowledgement:** This work was supported by the Russian Science Foundation, grant 22-17-20005.

**References:**

[1] M. Ojovan, V. Petrov, S. Yudintsev, Sustainability. 13 (2021), 4117.
[2] C. Jantzen, M. Ojovan, Russ. J. Org. Chem. 64 (2019), 1611-1624.
[3] I. Bardez-Giboire, A. Kidari, M. Magnin, J.-L. Dussossoy, S. Peuget, R. Caraballo, M. Tribet, F. Doreau, Ch. Jegou, J. Nucl. Mater. 492 (2017), 231-238.
[4] J.J. Neeway, R.M. Asmussen, E.M. McElroy, J.A. Peterson, B.J. Riley, J.V. Crum, J. Nucl. Mater. 515 (2019), 227-237.
[5] H. Zhu, F. Wang, Q. Liao, Y. Zhu, J. Nucl. Mater. 532 (2020), 152026.

## PP-II-11

# Development of New Approaches to Assessing the Safety of Nanocomposites

Novikov M.A.
*FSBSI East-Siberian Institute of Medical and Ecological Researh, Angarsk, Russia*
*novik-imt@mail.ru*

**Introduction:** For quite a long time, the study of the toxicity of nanoparticles and nanomaterials has occupied the minds of scientists from all over the world, but a unified research protocol has not yet been adopted. In the Russian Federation, a regulatory and methodological toolkit has been developed that surpasses foreign analogues in some parameters (a higher volume of necessary toxicological and biomedical studies, as well as the number of parameters used to assess safety), however, based on the principles of classical toxicology. Based on them, the TAC values for silver nanoparticles in the water of reservoirs (0.05 mg/l) have been established to date, however, the indicator for silver in the macroform is a similar value [1]. MPC in the air of the working area for titanium oxide nanoparticles differs by only an order of magnitude (0.1 and 10 mg/m$^3$)[2]. This is a paradox, since nanoparticles have unique properties compared to materials in the macroform: high surface activity, stability of biomolecular absorption, small size comparable to biomolecules, pronounced magnetic properties and biocompatibility, which, on the one hand, open up wide opportunities for their application, and, on the other hand, are possible reasons for adverse effects. The data accumulated in domestic and foreign studies indicate the involvement of intracellular processes in the formation mechanism toxicity of nanoparticles and nanomaterials, in connection with which we believe that, along with classical methods, new methodological approaches should be used that take into account cellular and intracellular effects of action.

**Materials and methods:** A classical study of the average lethal dose and toxic properties of nanocomposites consisting of nanoparticles of silver, bismuth, gadolinium with the same diameter of 2-8 nm, the same round shape, encapsulated in a natural matrix of arabinogalactan, obtained from Siberian larch wood, was carried out. Solutions of nanometals were administered orally for 9 days at a dose of 500 µg per 1 kg of body weight of outbred laboratory rats. Methods for studying toxicity included morphological, morphometric, immunohistochemical, electron microscopic methods for subacute oral administration.

**Results and discussion:** According to the results of the study, all metal-containing nanobiocomposites were assigned to hazard class 4, having DL50 when administered intragastrically more than 5000 mg/kg of animal weight.

In a morphological study of the nervous tissue of the test animals with the introduction of silver arabinogalactan, expansion of perivascular spaces, thickening of the walls of vascular arteries, swelling of myocytes and endothelial cells, in addition to neuronophagia and the presence of dark neurons, were observed. The impact of bismuth also had an impact on the morphological structure of the nervous tissue in the form of perivascular edema of the vessels, loosening of the myocytes of the vascular wall was observed. When exposed to gadolinium, neuronophagia was observed, and a large number of degeneratively altered neurons were also noted.

Electron microscopic examination of neurons revealed changes (multiple deformations of the nuclei, an increase in the area of mitochondria) only when exposed to silver nanoparticles.

The effectiveness of arabinogalactan as a container for the delivery of nanoparticles to the brain has been proven. Thus, in the study of brain tissues using an electron microscope with a field emitter and an energy-dispersive detector for elemental analysis after exposure

to silver arabanogalactan, silver nanoparticles were detected in the structure of the nervous tissue, which proves the fact of their penetration through the blood-brain barrier.

An increased level of DNA damage was found in the brain cells of animals of the silver arabinogalactan group, which indicates that it has a genotoxic effect. With the introduction of other nanometals, the cell damage index did not differ from the control values in the study by "DNA comets"method.

Evaluation of the immunohistochemical results of the study of the expression of the proapoptotic protein caspase-3 in neurons of white rats revealed an increase in the expression of immunopositive cells and dark (dead neurons) under the influence of silver arabinogalactan. Under the influence of nanogadolinium, multidirectional changes in the number of immunopositive and immunonegative cells were observed. Changes in the number of cells in the nanobismuth group were not significant. Thus, activation of the proapoptotic protein caspase-3 was observed only when exposed to silver arabinogalactan.

In the study of the expression of the anti-apoptotic protein bcl-2 with the introduction of silver arabinogalactan, as well as in the study of caspase, an increase in the percentage of dark and immunopositive neurons is observed, however, it is less pronounced. These results indicate an insufficient degree of activity of this anti-apoptotic protein, which cannot suppress the activity of caspase. In the case of nanobismuth, there is an increase in dark neurons and a slight decrease in immunopositive neurons. Together with studies of caspase, we believe that exposure to nanobismuth does not lead to the development of the apoptotic process. The study of bcl-2 under the influence of gadolinium showed a significant increase in the number of dark and a sharp decrease in the number of immunopositive neurons. In this case, we can talk about the selective action of this nanocomposite.

According to the results of an immunohistochemical study of the activity of proteins-markers of apoptosis cacpase-3 and bcl-2, only when exposed to silver nanocomposite, a pronounced apoptotic process is observed, which is irreversible.

Based on the results obtained, we have identified the following facts and patterns:

1) To assess the neurotoxicity of nanocomposites, along with the methods of classical toxicology, it is necessary to apply methods of intracellular assessment of the action of substances: morphometric, immunohistochemical.

2) The development of an apoptotic process can serve as a key criterion for the nanohazard of compounds.

3) Molecular diagnostics of the expression of intracellular proteins additionally provides a higher degree of reliability of the apoptotic process with different methods of exposure to nanocomposites.

**References:**

[1] Zagainova A.V., Artemova T.Z., Dmitrieva R.A., Gipp E.K., et al. On the effect of metal nanoparticles present in the aquatic environment on bacteria and continuous Hep-2 cell cultures and BGM // Hygiene and Sanitation, No. 1, 2013, p. 76-80.

[2] Abdullin, I. Sh., Kanarskaya, Z. A., Khubathuzin, A. A., Kalashnikov, D. I. et al. Nanodispersed materials based on titanium oxide in the microbiological, medical and food industries. Bulletin of the Kazan Technological University, No. 15 (10), 2012, 158-165.

## PP-II-12

# Evaluation of Biocomposites' Defectiveness, the Effect of Defectiveness on Water Absorption

Pantyukhov P.V.[1,2], Shelenkov P.G.[1], Khaidarov B.B.[2,3], Popov A.A.[1,2]
*1 – Emanuel Institute of Biochemical Physics of Russian Academy of Sciences, Moscow, Russia*
*2 – Plekhanov Russian University of Economics, Moscow, Russia*
*3 – National University of Science and Technology "MISiS", Moscow, Russia*
*pantyukhov@mail.ru*

The production of biocomposite polymer materials increase every year. Manufacturers of packaging materials intend to be environmentally responsible because of their own ESG strategies and as a respond to the consumers' request. Biocomposites consist of synthetic polymer matrix and natural (vegetable or animal origin) fillers [1]. Different raw materials may be used as a filler. In most part of the works the cellulose or starch are being used. But these polysaccharides are very valuable and expensive. Plant waste are cheaper, and their application in biocomposites also solves the problem of their disposal. Wood flour (WF) is widespread and cheap material; however, the particles of WF have irregular shape. It may cause the defects in the structure of biocomposite, made of polymer matrix and WF. Earlier it was shown that complex fraction of the filler even after filtering through the sieve with 200 μm mesh have large aggregates and form defects in biocomposite [2]. For this study WF particles were filtered though 100 μm mesh. Microcrystalline cellulose (MCC) was chosen as a referent filler, it has more smooth particles. MCC was also filtered through 100 μm mesh. Photomicrographs of the fillers, prepared by scanning electron microscopy, are presented in Fig. 1.

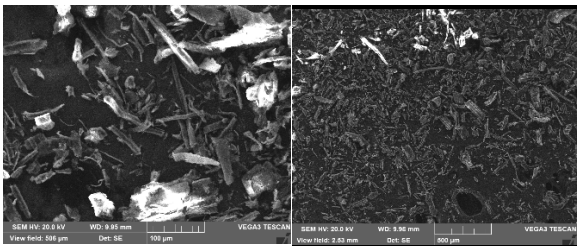

*Figure 1a. Photomicrographs of wood flour (WF)*

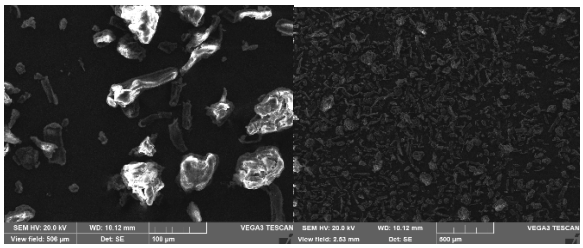

*Figure 1b. Photomicrographs of microcrystalline cellulose (MCC)*

According to the previous works, ethylene vinyl acetate (EVA) matrix was chosen as the most appropriate polymer matrix [3], [4]. In this study EVA grade with 15% of vinylacetate and MFI = 6 g/10 min was chosen as a matrix. Biocomposites were mixed in melt condition by heated rolls at a temperature of 130-150 °C. After they were crushed and molded by hydraulic press with plates heated to 140 °C. As a result, white flat sheets were obtained from biocomposites with MCC, and brown ones from biocomposites with WF. Different content of the fillers was added to EVA: 50, 60, 70 wt.%. Visually it was obvious that the composite with 70 wt.% of WF had a lot of voids and defects. In contrast, the same composite with 70wt. %

of MCC was homogenous with well dispersed filler's particles. For evaluation of the defectiveness of biocomposites the defect ratio was calculated as the difference between theoretical density of biocomposite and its real density. Theoretical density was calculated as a sum of densities of matrix and filler. Real density was measured by hydrostatic weighting in liquid media. The obtained results on the defect ratio are presented in Table 1. It can be seen that there is a large defect rate gap between 60 and 70% of WF. It means that WF_70 composite is very defective and cannot be used for the manufacture of products as it is.

Table 1. Defect ratio, calculated as the difference between theoretical and real densities of biocomposites

| Filler \ Filler content | 50 wt.% | 60 wt.% | 70 wt.% |
|---|---|---|---|
| Microcrystalline cellulose (MCC) | 5 | 6 | 6 |
| Wood flour (WF) | 3 | 4 | **9** |

The defectiveness of composites effect on the water absorption index (Table 2). With an increase in the concentration of the filler, water absorption increased. It was expected since only polar cellulose-containing filler can absorb water. The difference in water absorption between MCC_60 and MCC_70 was just 4.2%. At the same time, the difference between WF_60 and WF_70 was 10.0%. Probably, water penetrates into the defective areas of the biocomposite and remains there even after removing the sample from the water. The water absorption index quite accurately characterizes the defectiveness of biocomposites. The difference between two fillers is also obvious – 70% composites with WF had twice higher water absorption that the same ones with MCC. It can be explained by irregular shape and wide size distribution of WF particles that can be seen from photomicrographs in Figure 1.

Table 2. Water absorption of biocomposites

| Filler \ Filler content | 50 wt.% | 60 wt.% | 70 wt.% |
|---|---|---|---|
| Microcrystalline cellulose (MCC) | 11.6 | 13.5 | 17.7 |
| Wood flour (WF) | 14.1 | 20.1 | **30.1** |

**Acknowledgement:** This work was supported by Plekhanov Russian University of Economics.

**References:**

[1] M. Brebu, Polymers 12 (2020) 166
[2] A.K. Zykova, P.V. Pantyukhov, N.N. Kolesnikova, et al., J Polym Environ 26 (2018) 1343–1354
[3] P.G. Shelenkov, P.V. Pantyukhov, A.A. Popov, IOP Conf. Ser.: Mat. Sci.Eng., 369-1 (2018) 012043
[4] P.G. Shelenkov, P.V. Pantyukhov, A.A. Popov, Mat. Sci. Forum, 992 (2020) 306–310

## PP-II-13

# Antibacterial Calcium Phosphate Coatings Prepared by RF Magnetron Sputtering from Sintered Powders: Structure and Properties

Prosolov K.A.[1], Luginin N.A.[1,2], Khimich M.A.[1], Lastovka V.V.[1], Glukhov I.A.[1], Sharkeev Y.P.[1,2]
*1 – Institute of Strength Physics and Materials Science, Siberian Branch of Russian Academy of Sciences, Tomsk, Russia*
*2 – National Research Tomsk Polytechnic University, Tomsk, Russia*
*konstprosolov@gmail.com*

Deposition of biocoatings using radio frequency (RF) magnetron sputtering of Cu, Sr, and Zn substituted hydroxyapatite (HA) onto various substrates for biomedical applications, with a focus on orthopedic and dental implants is a new and developing direction of medical materials science. In the present work a detailed examination of the RF magnetron sputtering technique, process parameters, and the resulting characteristics of the substituted HA coatings, including their crystal structure, morphology, chemical composition, and *in vitro* biocompatibility are discussed. As substrates commercially available titanium alloy and biodegradable Mg-Ca alloy were used.

RF magnetron sputtering was employed to deposit substituted HA coatings at a sputtering power ranging from 100 to 300 W, with Ar flow rates of 20 sccm at various deposition durations. The resulting substituted HA coatings exhibited a nanocrystalline structure, with average crystallite sizes ranging from 20 to 50 nm. The substitution levels of Cu and Zn in the structure of targets for deposition were found to be 0.2 at% and 0.5 at%, respectively.

It has been established that amorphous calcium phosphate (ACP) coatings were deposited on Mg-Ca or Ti allos substrates using RF magnetron sputtering when the substrate temperature and working distance was below 150 °C and 70 mm and more, respectively. When working distance was reduced to 60-50 mm and grounded shielding was applied. This resulted in increase of substrate temperature and provided energy impact to the growing coating. As a result a poorly crystalline HA coating with a growth direction of $[002]_{HA}$ was deposited. The as-deposited ACP coatings were then annealed at 400 °C for three hours in an Ar atmosphere to crystallize a coating up to 1 μm in thickness, resulting in close to stoichiometric hydroxyapatite (HA).

Corrosion current was estimated for mentioned above compositions and it was found that it is the highest (4100 nA) for the as-deposited ACP coating, 910 nA for the crystalline HA coating after annealing, and 411 nA for the crystalline HA coating with a post-deposition of an additional ACP layer. Moreover, the study revealed that the corrosion resistance of a metastable ACP coating is time-dependent if samples are stored at ambient conditions. Additionally, the corrosion resistance of Mg-Ca alloy could be significantly decreased if the ACP coating is doped with Cu, starting at 0.2 at.%.

In vitro biocompatibility assessment using human osteoblast-like cells (MG-63) revealed that the deposited substituted HA coatings promoted enhanced cell adhesion and

proliferation compared to pure HA coatings. After 72 hours of culture, cell proliferation on the substituted HA coatings was roughly 1.4 times higher than on the ACP coatings. Notable antibacterial effect was also evident for deposited Zn or Cu containing CaP coatings [1].

The other major advantage of an RF magnetron sputtering is lay in the fact that this method allows to tailor the surface morphology of CaP coatings and construct highly oriented structures with the direction dictated by the atomic shadowing effect when the substrate is deposited at an oblique angle [2]. ACP thin films were deposited using RF magnetron sputtering in two different geometries: at an oblique angle (80° relative to the sample holder surface) and at a normal flux incidence (NFI) angle on Si and Ti substrates. The surface features transitioned from globular-like to elongated, elliptical, and fine-grained structures oriented towards the deposition flux (in the oblique angle case).

Heat treatment in an Ar atmosphere at 700 °C for 3 hours led to the crystallization of the previously amorphous obliquely deposited thin films, accompanied by a rapid change in surface morphology. X-ray diffraction (XRD) analysis of annealed samples showed a singlephase HA structure with a (300) preferential orientation for both oblique angle and NFI samples on Si. However, for oblique angle samples, redistribution of peak intensity was observed, with noticeable growth in the (002) plane for both Si and Ti substrates. Furthermore, oblique deposition of ACP on Ti resulted in the formation of a structure closely resembling the HA lattice of the sputtering target. It is noteworthy that these samples exhibited the lowest value of compression strain. It is also worth noting that the surface nanoroughness was significantly altered by oblique deposition, changing the roughness from 307 ± 210 pm to 943 ± 160 pm and even higher, up to 9 ± 0.9 nm for the annealed HA coating. Overall, oblique angle deposition is a promising and powerful technique for controlling not only surface nanoroughness but also morphology type. Additionally, it enables the fabrication of hierarchically structured surfaces by combining various deposition methods.

In conclusion, this study demonstrates the potential of RF magnetron sputtering as an effective method for the deposition of substituted HA biocoatings with enhanced osteoconductivity and biocompatibility. Further research is needed to explain the stability of amorphous calcium phosphate coatings and their future applications in clinical practice, paving the way for the successful development of advanced orthopedic and dental implants.

**Acknowledgement:** The work was performed according to the Government research assignment for ISPMS SB RAS, project FWRW-2021-0007.

**References:**

[1] Prosolov K.A., Mitrichenko D.V., Prosolov A.B. et al., Coatings, 11 (2021), 809.
[2] Prosolov K.A., Khimich, M. A., Rau, J. V. et al. Surf. Coat. Technol., 394 (2020), 125883.

## PP-II-14

# Synthesis of Magnetic Polymer Microspheres for Bio-Medical Applications

Shestakova D.O.[1,2], Sankova N.N.[1], Parkhomchuk E.V.[1,2]
*1 – Boreskov Institute of Catalysis, Novosibirsk, Russia*
*2 – Novosibirsk State University, Novosibirsk, Russia*
*shestakova@catalysis.ru*

Express diagnostic methods based on the use of polymer microspheres as carriers are the routine in the diagnosis of infectious diseases, diabetes, cardiovascular diseases, inflammations of various nature, cancer, etc. [1–3]. The surface of polymer particles in such systems is modified with antibodies, antigens, DNA and RNA fragments, which allows obtaining polymer materials with specific respond to certain proteins, microorganisms, nucleic acid sequences.

Generally, polymer particles have to meet several requirements to be used as carriers. They have to be spherical with coefficient of variation less than 10%. The size range is determined by the diagnostic methods and can vary from tens of nanometers to several micrometers. In some cases there is a need in magnetic properties for more convenient cleaning process or planar diagnostic methods (particle are immobilized on the surface in the presence of magnetic field) [3].

There are several well-known techniques for the introduction of magnetic phase in polymer particles either at the stage of polymer particle synthesis or after their formation [3,4]. The later approach is more promising since wider range of polymer microspheres can be obtained in the first step. One of the most popular ways of introducing magnetic phase is co-precipitation method based on the simultaneous precipitation of ferric and ferrous iron salts [5,6]. However, this method demands high density of functional groups on the particle surface and, thus, cannot be widely used. To resolve this problem the dynamic swelling method was proposed, which involves swelling of a polymer particle in a good solvent in the presence of a modifying component (e.g. magnetic phase [7]). The only requirement is the stability of microspheres in a good solvent, e.g. crosslinked particles.

In the present work our main focus was the synthesis of carboxylated crosslinked particles in the size range of 3-6 μm with their subsequent modification by magnetic nanoparticles of 20 nm in size. Different types of polymerization (dispersion, precipitation, activated swelling) were used to obtain monodisperse particle. The activated swelling technique proposed by Ugelstad [8] have shown the most reproducible and scalable results. The particles obtained were spherical and smooth, 5 μm in size with coefficient of variation less than 10% (Fig. 1). To obtain such particles kinetic of swelling, influence of size and amount of seed particles, influence of amount of swelling agent (dibutyl phthalate) and monomers (styrene, divinylbenzole, styrene), type of initiator (azobisobutyronitrile, benzoylperoxide) were investigated. The following modification of polymer particles with magnetic phase by dynamic swelling resulted in precipitation of magnetic nanoparticles on the microspheres' surface and

not their introduction inside as was expected. Thus, magnetic properties of the particles obtained were unstable due to desorption and decreased in several months after the synthesis. Nevertheless, after 5 months magnetic polymer particles can still be immobilized by the influence of magnetic field (permanent magnet of 8.62 kg) (Fig. 2). Though further modification of such particles is needed the results obtained can be used for further development of the production of Russian test-systems based on the magnetic polymer microspheres.

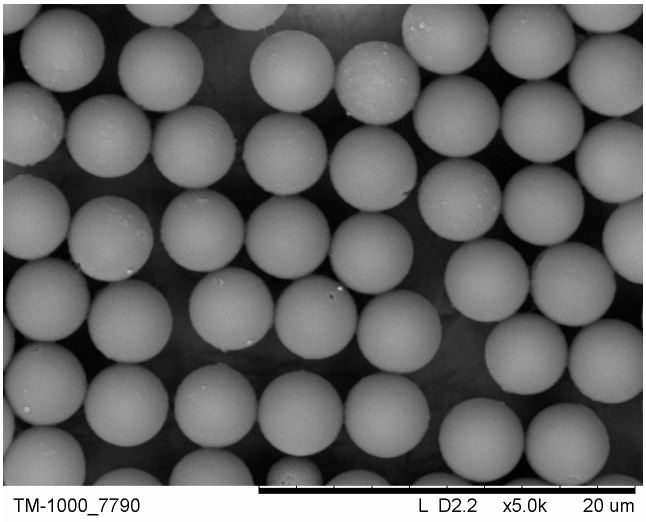


*Fig. 1. Carboxylated crosslinked polymer particles obtained by dynamic swelling technique*

*Fig. 2. Immobilisation of magnetic polymer microspheres by the influence of permanent magnet of 8.62 kg*

**Acknowledgement:** Our work was supported by the Ministry of Science and Higher Education of the Russian Federation within the governmental order for Boreskov Institute of Catalysis (project AAAA-A21-121011490008-3)

**References:**

[1] J. Chou, J. Wong, N. Christodoulides, P.N. Floriano, X. Sanchez, J. McDevitt. 12 (2012) 15467–15499.
[2] J. V. Jokerst, Z. Chen, L. Xu, R. Nolley, E. Chang, B. Mitchell, J.D. Brooks, S.S. Gambhir, C. Kumar-Sinha. 10 (2015).
[3] N. Sankova, P. Shalaev, V. Semeykina, S. Dolgushin, E. Odintsova, E. Parkhomchuk. 138 (2021) 49890.
[4] А.Ю. Гервальд, И.А. Грицкова, Н.И. Прокопов. 79 (2010) 249–260.
[5] J. Ugelstad, T. Ellingsen, A. Berge, O. Helgee. 1988.
[6] J. Zhang, S. Xu, E. Kumacheva. 126 (2004) 7908–7914.
[7] C. Yang, Q. Shao, J. He, B. Jiang. 26 (2010) 5179–5183.
[8] J. Ugelstad, P.C. Mórk, K.H. Kaggerud, T. Ellingsen, A. Berge. 13 (1980) 101–140.

## PP-II-15

# Investigation of Changes in the Physicochemical Properties of Multin-Tonnage Packaging Polymer Compositions on the Example of Low Density Polyethylene in the Process of Biodegradation

Varyan I.A.[1,2], Zinovyev S.V.[3], Kolesnikova N.N.[1,2], Popov A.A.[1,2]
*1 – Plekhanov Russian University of Economics, Moscow, Russia*
*2 – Emanuel Institute of Biochemical Physics of the Russian Academy of Sciences, Moscow, Russia*
*3 - Lomonosov Moscow State University, Moscow, Russia*
*ivetta.varyan@yandex.ru*

Recently, a significant portion of municipal solid waste has been non-biodegradable plastic packaging. Among the waste, polyethylene (PE) is especially common. PE is a petroleum-based polymer that, due to its low cost and excellent performance, is very often used in the production of plastic packaging [1]. Since the recycling rate of plastic waste is much lower than the release rate, this leads to the accumulation of plastic in the environment and, as a result, to the emergence of a number of related environmental problems. If nothing is done, in the near future this situation can lead to disastrous consequences. To solve this problem, much attention has been paid to the development of biodegradable polymers from renewable sources [2,3]. Once in waste, such polymers are able to undergo a biodegradation process, which is the process of changing the chemical structure of the polymer from a more complex to a simpler one under the influence of various biological factors, such as soil bacteria, mold fungi and various atmospheric microorganisms. The end products of a biodegradation process typically include CO2, CH4, water, biomass and other natural substances that have a positive effect on environmental balancing [3].

In this study, a technology for the production of biodegradable materials is proposed based on low-density polyethylene with the addition of natural rubber (NR). It is shown that, with good biodegradability, such materials also have satisfactory operational physical and mechanical properties. This suggests that materials based on PE/NR composites can be used to create a wide range of products for the needs of agriculture and other industries.

Biodegradation tests were carried out by composting PE/NR polymer film samples in synthetic soil, prepared in accordance with GOST 9.060-75. The soil moisture content was maintained at 60% throughout the testing period. This value was chosen based on the fact that it is optimal for the biological activity of microorganisms used in our tests. Biodegradation of polymer films was characterized by assessing changes in the appearance and weight of the samples after exposure to soil over time up to 18 months (Figure 1).

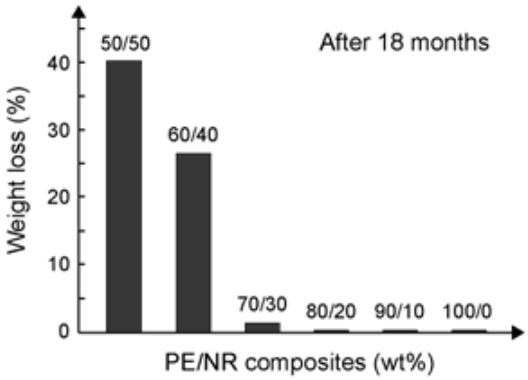


*Fig. 1. Weight loss of composite PE/NR samples with natural rubber content in the range of 0-50% as a result of biodegradation after 18 months in synthetic soil.*

As shown in Figure 1, after 18 months of exposure of the PE/NR composite samples to the soil. So, for samples with a polyethylene to rubber ratio of PE/NR = 50/50 and 60/40, the weight loss increased significantly and amounted to 40 and 26%, respectively. In addition, the value of weight loss increased slightly for the sample with 30% NR content. Note that all these composites are characterized by the highest water absorption, which probably contributes to the growth and development of microorganisms.

**References:**

[1] Gisha E. Luckachan, G.E., Pillai C.K.S. (2011). Biodegradable polymers-a review on recent trends and emerging perspectives. Journal of Polymers and the Environment 19, 637–676
[2] Zhong, Y., Godwin, P., Jin, Y., Xiao, H. (2020). Biodegradable polymers and green-based antimicrobial packaging materials: A mini-review. Advanced Industrial and Engineering Polymer Research 3, 27-35
[3] Mangaraj, S., Yadav, A., Bal, L.M., Dash, S.K., Mahanti, N.K. (2019). Application of biodegradable polymers in food packaging industry: A comprehensive review. Journal of Packaging Technology and Research 3, 77–96

## PP-II-16

# Fibrous Biomedical Materials Based on Polyoxybutyrate with Additives

Tyubaeva P.M.[1,2], Varyan I.A.[1,2], Olkhov A.A.[1,2], Popov A.A.[1,2]
*1 – Plekhanov Russian University of Economics, Moscow, Russia*
*2 – Emanuel Institute of Biochemical Physics of the Russian Academy of Sciences, Moscow, Russia*
*Ivetta.varyan@yandex.ru*

The development of biomedical nanocomposite fibrous materials with valuable polystructural properties based on biodegradable semicrystalline polymers and modifying agents is an urgent problem of modern materials science and environmental safety. In this work, composite fibrous materials based on semicrystalline biodegradable poly-3-hydroxybutyrate (PHB), PHB and porphyrins of natural origin (FeClTPP, MnClTPP, ZnTPP) and approximation (hemin) - methods of electrospinning and double solution molding (for materials with hemin) [1].

The purpose of this study is to study the structure resulting from changes in the type and concentration of the additive introduced, on the properties (including antimicrobial activity against the action of pathogenic and conditionally pathogenic microorganisms and the degradation process under environmental conditions) of nonwoven materials based on modified PHB.

Aging experiments were carried out in accordance with ASTM G7/G7M-21 (“Standard Practice for Natural Aging of Materials”). Samples were exposed to outside air in accordance with standard protocol D1435-13 ("Standard Practice for Outdoor Weathering of Plastics"). According to the protocol, wooden weathering posts were inclined at an angle of 90° with respect to the horizontal line.

The dimensions of the samples were 40 mm × 40 mm × 0.3 mm (length, width, thickness, respectively). Similar samples were placed as a blank in a dark and dry place. The samples are fastened with white cotton threads; one side of the samples was fastened with adhesive tape. The duration of each weathering experiment was 3 months (June-August, average temperature 21°C, average humidity 75.7%, geographic location: 55°45'N, 37°37'E).

The stability of biodegradable PHB/hemin materials containing 5% hemin under the influence of environmental factors was studied. Microscopic images of the test samples before and after degradation are shown in Figure 14.

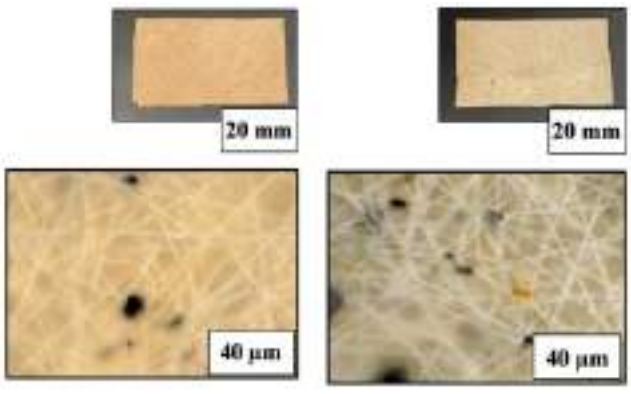


*a* *b*

*Fig. 1. Sample images before (A) and after (B) environmental degradation.*

## PP-II-16

PHB nonwoven materials containing porphyrins with metal ions, upon completion of degradation within 60-90 days, PHB/hemin materials remain practically undamaged: the material has retained its integrity and shape.

**Acknowledgement:** This work was supported by the Russian Science Foundation, grant 22-73-00038.

**References:**

[1] Avossa J., Paolesse R., et al. Electrospinning of Polystyrene/Polyhydroxybutyrate Nanofibers Doped with Porphyrin and Graphene for Chemiresistor Gas Sensors // Nanomaterials. 2019. V. 9(2). P. 280.

## PP-II-17

# Development of Starch/Cellulose Nano-Fibre Composites

Zerun Zhan[1], Huifang Xie[2], Litao Ma[2], Long Yu[1,2]
*1 – Centre for Polymers from Renewable Resources, SFSE, SCUT, Guangzhou, China*
*2 – Institute of Chemistry, Henan Academy of Sciences, Zhengzhou, China*
*felyu@scut.edu.cn*

Application of cellulose nano-fibre (CNFs) to reinforce starch-based materials is an ideal composite system because they are almost perfect compatible since both two substances basically contain same chemical unite glucose [1-3]. Actually this kind of composite can be classified as self-reinforce composites, in which both matrix and reinforce agents contain the substances with same chemical structure [4]. Cellulose fibre, particularly at nanoscale, have attracted huge attention to develop starch-based biodegradable composites recently due to various advantages including higher compatibility, reinforce efficiency, light transparency, and easier processing as well as edible etc.

Starch is the most promising natural polymer because of its inherent biodegradability, overwhelming abundance and annual renewability. Starch-based polymers offer a very attractive low cost base for new biodegradable polymers due to their low material cost and ability to be processed with conventional plastic processing equipment. Starch films have been widely used in both food as well as non-food applications. Improvement of mechanical properties of starch-based materials is an ongoing challenge due to its poor mechanical performance, particularly tensile strength. To improve these mechanical properties, various blending and compositing techniques have been developed [5-8], such as blending with different biodegradable polyesters or reinforcing with mineral or natural fillers including various cellulous CNFs.

Generally, there are two sources of raw materials used to prepare CNFs: wood and non-wood. Woods are normally used to prepare cellulose nano-crystalline (CNCs), while non-woods are commonly used to prepare cellulose nano-fibre (CNFs). In this presentation, we will report our work about starch/CNF composites based on brief review of previous achievements and introduce some applications. Two kinds of CNFs were used in this work: one is commercially available CNC (solid content 2%) purchased from Northern Century; and other one CNF (solid content 0.5%) is from Okara prepared in our laboratory. The results showed that CNC increased more rigidity while CNF increased some toughness.

**Acknowledgement:** Authors would like to acknowledge the financial fund from National Natural Science Foundation of China (CN) (22178124, 32272340), Thanks Prof. Yong Huang (China Academy of Sciences) for kindly providing nano-cellulous sample used in this work.

**References:**

[1] L. Yu, K. Dean, L. Li, Prog Polym Sci 2006, 31, 576.
[2] L. Meng; H. Liu,; H. Yu; Q. Duan; et al., Ind Crops and Products 2019, 134, 43.
[3] A. Ali, Y. Chen, H. Liu, L. Yu, et al., Inter. J. Bio. Macrom., 2019, 129, 1120.
[4] C. Gao, L. Yu, Liu H, Chen L. Prog Polym Sci 2012;37:767.
[5] Liu H, Xie F, Yu L, Chen L, Li L. Prog Polym Sci 2009, 34,1348.
[6] Q.Duan, L. Meng, H. Liu, L. Yu, K. Lu, S. Khalid, L. Chen, J. Polym. Envi., 2018, 27(1), 158.
[7] Q. Duan, Z.i Zhu, Y. Chen, et al., ACS Sust. Chem. & Eng., 2022. online.
[8] M. Alee, Q. Duan, Y. Chen, H. Liu, Jet al., ACS Sust. Chem. & Eng., 2021, 11960.

## PP-II-18

# Study of the Possibility of Creating a Drug Coating for Biliary Stents Based on the Copolymer "Polylactic Acid-Polycaprolactone" Modified with Carbon Nanotubes and Doxorubicin

Zaporotskova I.V., Zvonareva D.A., Chesheva M.F.
*Volgograd State University, Volgograd, Russia*
*zvonareva@volsu.ru*

Mechanical jaundice usually refers to a symptom complex that occurs when the outflow of bile through the bile ducts of the liver is disturbed. This disease is an indication for stenting. Unfortunately, over time, physicians noted a number of disadvantages of endobiliary stenting, the main of which was restenosis [1]. Also, within the first few hours after the completion of stenting procedure, there may be a risk of serious complications such as thrombosis and restenosis. To reduce the risks of such complications, as well as to improve the future results of the operation, the use of stents with special drug-coated (DC) to provide local transportation, quality application of the drug substance on the surface of the biliary stent and prolonged drug release, a polymeric carrier complex is required.

The study proposed an ultrafine drug coating consisting of two polymers (polycaprolactone (PCL) and polylactic acid (PMC)), carbon nanotubes (CNT) affecting the stability and preservation of LP on the stent surface due to its unique sorption properties, and the drug doxorubicin (DOX), which has pronounced anti-tumor activity [2,3,4].

Quantum-chemical calculations of the interaction of its main components, performed by the DFT method, were performed to prove the feasibility and effectiveness of the new ultrathin drug coating [5]. The model of the complex "PCL+PMC+UNT+doxorubicin" is shown in Figure 1.

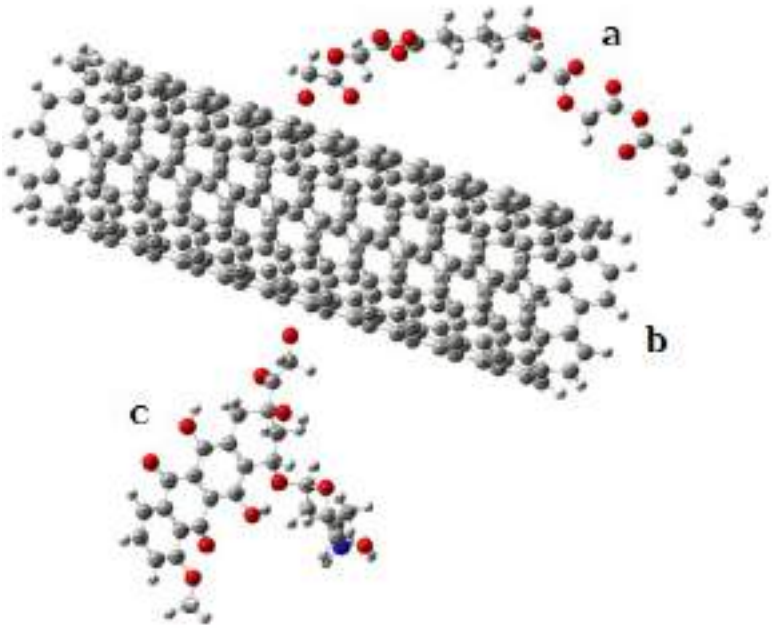


*Fig. 1. Model of the complex "copolymer (PCL+PMK) (a) + CNT (b) + doxorubicin (c)"*

Based on the analysis of the results of calculations of doxorubicin attachment to the "copolymer + CNT" complex, we plotted the dependence of the potential interaction energy of the coating components (Figure 2).

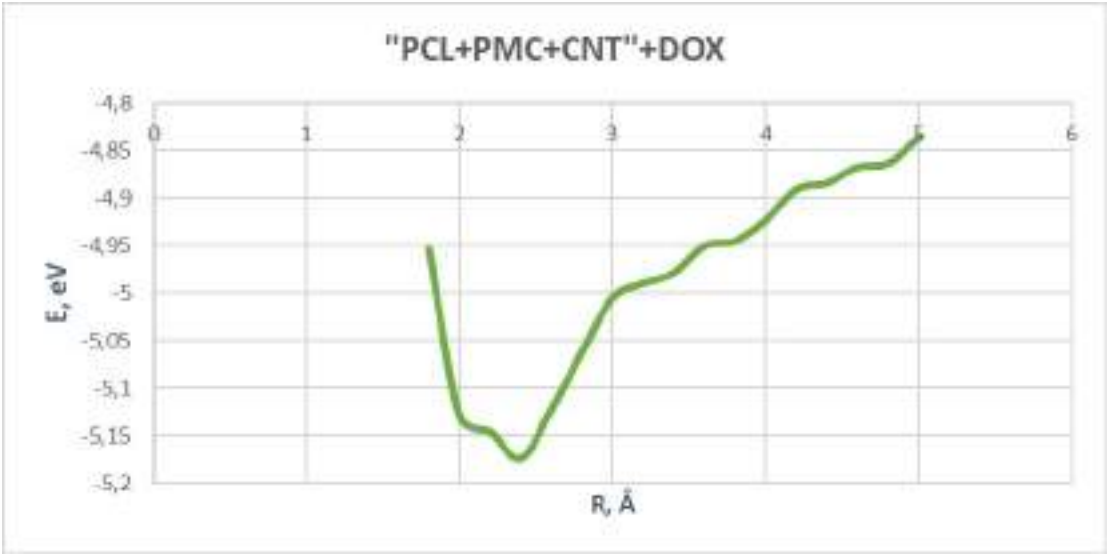


*Fig. 2. Energy curve of adsorption energy (eV) versus distance (Å) of the complex structural complex "PCL+PMC+UNT" + DOX*

The presence of the curve minimum at a distance of 2.4 Å, corresponding to the energy $E_{ads}$ = -5.17 eV and the distance of physical interaction between doxorubicin and the center of the complex consisting of copolymer and CNT, proves the possibility of a fairly easy desorption of the drug from the carrier polymer and its gradual entry into the body.

**Acknowledgement:** The work was carried out within the framework of the state task of the Ministry of Science and Higher Education of the Russian Federation (topic "FZUU-2023-0001).

**References:**

[1] A. V. Andreev, V. M. Durleshter, A. I. Leveshko [et al]. Antegrade biliary stenting in the treatment of mechanical jaundice. 24 (2019) 25-35.
[2] M. I. Stilman, A. V. Podkorytova, S. V. Nemtsev [et al]. Technology of polymers for medical and biological purposes. Polymers of natural origin. (2015) 328.
[3] Baimova, Y. A. Graphene, nanotubes and other carbon nanostructures. (2018) 212.
[4] O. Tacar, P. Sriamornsak, C.R. Dass. Doxorubicin: an update on anticancer molecular action, toxicity and novel drug delivery systems. 65 (2013) 157-170.
[5] J. P. Perdew, Y. Yang. Functional approaches to non-locality and correlation in density functional theory. (2020) 152-153.

## PP-II-19

# New Carbon Mineral Sorbents for Medicine

Rachkovskaya L.N.[1], Volodin A.M.[2], Rachkovsky E.E.[1], Kruglyakov V.Yu.[2], Yastrebova E.S.[3], Smagin A.A.[2], Nimaev V.V.[1]

*1 – Research Institute of Clinical and Experimental Lymphology – Branch of the Institute of Cytology and Genetics, Siberian Branch of the RAS, Novosibirsk, Russia*

*2 – Boreskov Institute of Catalysis, Novosibirsk, Russia*

*3 – Voevodsky Institute of Chemical Kinetics and Combustion, Siberian Branch of the RAS, Novosibirsk, Russia*

*reed@academ.org*

Currently, the close attention of specialists in the field of medicine to the problem of cleansing the intercellular space is justified. It is shown that through the impact on the lymphatic system, directly or indirectly, it is possible to achieve a greater effect from treatment. One of the effective ways of exposure is sorbents, which are synergists of the lymphatic system. The successful use of sorbents, including carbon mineral ones, has formed a new direction – sorption medicine with certain requirements for the properties of sorbents (safety, strength, porosity, sorption activity) [1]. Under modern conditions, it is necessary to search for new opportunities in the creation of domestic sorption carbon mineral materials using various sources of the carbon component of sorbents.

**The purpose of this work** is to study the possibility of obtaining new carbon mineral sorbents with an assessment of their safety and prospects.

**Materials and methods**. Sorbents based on porous gamma aluminum oxide with a particle size of 0.2-0.8 mm with a specific surface area of 201.3 $m^2/g$ (JSC "Catalyst", Novosibirsk) were studied. As a carbon source – propane-butane gas in the sorbent $Al_2O_3$@C–800, polysaccharides from renewable resources of plant origin in the sorbent $Al_2O_3$@C–600, single-walled carbon nanotubes OUNT (Tuball-99TM, manufacturer: OCSiAl, Novosibirsk, Russia) in the sorbent $Al_2O_3$@PDMS-OUNT. Polydimethylsiloxane binder (PDMS), an organosilicon polymer (LLC "Penta", Novosibirsk), was used to obtain a sorbent with nanotubes. The porous structure of the samples was estimated by the specific surface area (S) determined by the standard method. The adsorption activity of the samples was determined by sorption of methylene blue dye and vitamin $B_{12}$ spectrophotometrically (ApelPD-303UV). The safety of sorbents (as hemosorbents) was assessed by their effect on red blood cells under model conditions of blood perfusion through glass columns (3 $cm^3$) with sorbents (2 $cm^3$). During perfusion, the patient's blood was used before and after hip replacement surgery in accordance with the protocol of the clinical trial (approval of the LEK NIIKEL, Protocol No. 115 of 12/24/2015.). To study the character-ristics of red blood cells in the work, a scanning flow cytometer was used (SPC, LLC "Cytonova", Russia Novosibirsk).

**Results and discussion**. The obtained samples of sorbents of black color $Al_2O_3$@C–800, $Al_2O_3$@C–600 and silver color sample with nanotubes $Al_2O_3$@PDMS-OUNT (production temperature up to $150^0$C) with carbon dioxide content, respectively: 10.2%, 7.3%, 0.02% had surface values of 175.0; 162.8; 198.0 $m_2/g$; sorption activity against the marker of low–molecular compounds - methylene blue dye 17.3%, 19.3%, 7.1%, respectively, and for the marker of high-molecular compounds - vitamin B12: 70%,

86.5% and 26.2%, respectively. It should be noted that for a sorbent without carbon $Al_2O_3$@PDMS ($S_{ud}$. 200.0), the adsorption value of $B_{12}$ is 0.6%. In the blood analysis, parameter values for populations of 6000 red blood cells in each sample were expressed as an average value ± standard error (Origin 2017 software). The following morphological parameters of erythrocytes were determined: diameter, maximum and minimum cell thickness, cell volume and surface area, cell sphericity index, spontaneous curvature of the membrane, dimensionless spontaneous curvature of the membrane, hemoglobin content in one erythrocyte and hemoglobin concentration. The morphological parameters of erythrocytes were minimally affected by the sorbents $Al_2O_3$@C– 800, $Al_2O_3$@C– 600. The morphological parameters of erythrocytes were minimally affected by the sorbents $Al_2O_3$@C– 800, $Al_2O_3$@C– 600. Sorbent $Al_2O_3$@PDMS - OUNT caused the most obvious morphological changes, including a decrease in hemoglobin concentration, but not exceeding the ranges measured on 20 donors. An important functional parameter is the number of active anion exchangers (band 3 proteins). The band 3 protein participates in the transfer of anions through the phospholipid bilayer of cell membranes. Perfusion of blood samples through a column with the sorbent $Al_2O_3$@C-800 (in comparison with perfusion of blood through an empty glass column) caused a moderate change - the number of band 3 proteins decreased 2.3 times; in the case of a sorbent with nanotubes, the decrease was 3 times. The number of band 3 proteins in the case of the sorbent $Al_2O_3$@C-600 decreased only 1.6 times.

**Conclusion.** The results of the work showed that, in general, the carbonmineral sorbents studied, obtained using different sources for the carbon component, have a moderate effect on the morphofunctional parameters of red blood cells during its perfusion through columns with sorbents. The marked more pronounced decrease in erythrocyte hemoglobin and the number of anion exchangers in the case of a sorbent with nanotubes does not go beyond the ranges measured on 20 donors. It can be noted that the carbon content in the sorbent with carbon nanotubes ($Al_2O_3$PDMS@OUNT) is 500 times less compared to the sorbent $Al_2O_3$@C-800 obtained by standard technology, and the sorption activity for the dye MG and vitamin $B_{12}$ is only 2.4-2.6 times lower, respectively. The parameters of the porous structure for the sorbent with nanotubes ($Al_2O_3$@PDMS-OUNT) are close to the parameters of the sorbent γ- $Al_2O_3$@PDMS without carbon. The sorption of vitamin $B_{12}$ by a sorbent with nanotubes is 40 times higher than the activity of a sorbent without carbon (γ- $Al_2O_3$@PDMS), which indicates a significant contribution of single-walled carbon nanotubes to the sorption activity of the sorbent surface. Changes in the parameters of red blood cells in contact with hard surfaces of sorbents allows us to predict the preference of certain technological solutions, depending on the tasks.

**References:**

Borodin Yu.I., Konenkov V.I., Parmon V.N., Lyubarsky M.S., Rachkovskaya L.N., Bgatova N.P., Letyagin A.Yu. Biological properties of sorbents and prospects of their application // Successes of modern biology. – 2014. – Vol. 134, N 3. – p. 236-248.

## PP-II-20

# Synthesis and Characterization of $Ti_3C_2T_x$ MXenes for Photothermal Therapy

Motorzhina A.V., Shilov N.R., Davkina A.V., Anikin A.A., Murzin D.V., Levada K.V., Sobolev K.V.
*Immanuel Kant Baltic Federal University, Kaliningrad, Russia*
*AMotorzhina1@kantiana.ru*

$Ti_3C_2T_x$ MXene is a novel 2D material showing good photothermal effect and biocompatibility [1]. Therefore, the possibilities of $Ti_3C_2T_x$ MXenes for multimodal tumor therapy need to be developed urgently. In this work, we synthesize 2D $Ti_3C_2T_x$ MXenes by etching the $Ti_3AlC_2$ MAX phase with LiF and HCl for 24 h at 35 °C. The synthesized samples were dried and characterized by XRD and SEM-EDX. The analysis showed the presence of the $Ti_3C_2$ phase in the samples.

$Ti_3C_2T_x$ MXenes powder was diluted in sterile distilled water at concentrations of 500 and 100 µg/ml and then dispersed using ultrasound. Obtained MXenes suspensions were examined by visible light spectroscopy in the wavelength range from 400 to 1000 nm. The results show an absorption peak at a wavelength of 810 nm (Fig. 1), which is typical for MXenes of $Ti_3C_2T_x$ composition [1]. The absorption peak at a wavelength of 810 nm corresponds to the second tissue transparency window [2]. Hence, $Ti_3C_2T_x$ MXenes is suitable material for photothermal therapy.

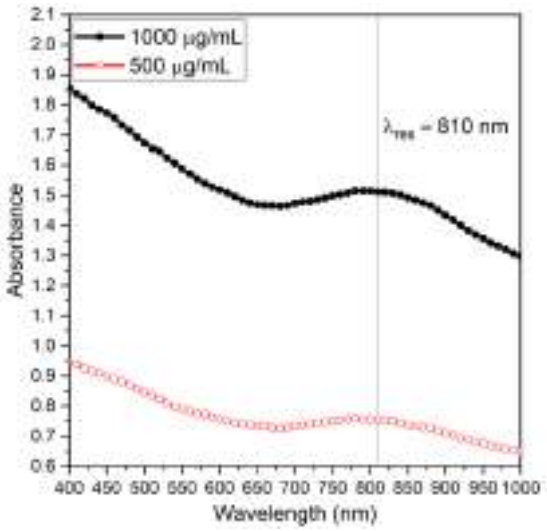


*Fig. 1. Experimental absorption spectra for $Ti_3C_2T_x$ MXenes with different concentrations*

Biocompatibility analysis of Ti3C2Tx MXenes was obtained using the WST-1 viability test. Well-established and high proliferative SK-MEL-28 and HuH7 adherent cell cultures were used for experiments. Cell cultures were incubated due to standard protocols (at 37 °C in humidified 5% CO2 atmosphere) in DMEM nutrient medium. Ti3C2Tx MXenes were added to the nutrient medium to obtain 10, 50, 100, and 500 µg/ml treatment solutions. After 24 h cultivation cells were stained using WST-1 (Roche Diagnostics GmbH) and the absorbance was measured using a microplate reader Multiskan FC (Thermo Scientific).

**Acknowledgement:** This work was supported by the Russian Science Foundation, grant 22-12-20036.

**References:**

[1] G. Liu, J. Zou, Q. Tang, X. Yang, Y. Zhang, Q. Zhang, W. Huang, P. Chen, J. Shao, X. Dong, ACS Appl. Mater. Interfaces 9 (2017) 40077
[2] Zh. Zhou, Y. Li, M. Peng J. Chem. Eng. 399(2020) 125688

## PP-III-01

# High Lanthanum Oxide Content Glasses for Optical Applications

Alekseev R.O., Savinkov V.I., Sigaev V.N.
*Mendeleev University of Chemical Technology, Moscow, Russia*
*alexeev-roma@mail.ru*

Today the development of high refractive index glasses is one of the most demanded tasks in the entire sector of optical instrumentation. The high refractive power of glass can be used not only to minimize spherical and chromatic aberration, but also to reduce the size of lens systems and the number of used components.

Lanthanum oxide containing glasses are widely used in optical materials science, since high values of the refractive index and dispersion are combined well with both their manufacturability and the opportunity to produce optically homogeneous blanks. The high content of lanthanum oxide (>25 mol.%) makes it possible to achieve higher optical parameters ($n_d$ > 1.9). However, commercial optical glasses generally contain no more than 20 mol% $La_2O_3$. This is due to the high tendency of the melt to crystallize, which reduces the manufacturability of the glass. In order to develop technological glasses with a high refractive index, search for optimal compositions with a high content of lanthanum oxide is topical.

In this study, the stable glass formation areas in the systems $La_2O_3$–$Al_2O_3$–$B_2O_3$–$SiO_2$ (LABS) and $La_2O_3$–$Nb_2O_5$–$B_2O_3$ (LNB) with a high content of lanthanum oxide were specified. Also, we found that the introduction of significant amounts of $La_2O_3$ into glasses of the magnesium aluminosilicate system of certain compositions makes it possible to vary the refractive index of the residual glass phase in glass-ceramics without significantly affecting the crystallization behavior of the original glasses. Promising matrix compositions for adding of modifying oxides $Nb_2O_5$, BaO, $Ga_2O_3$, $TiO_2$, $ZrO_2$, $Ta_2O_5$, CaO, ZnO in amounts allowing preparation of optically homogeneous glasses with a high refractive index ($n_d$ ≥ 1.95) were prepared using a laboratory technology for melting, manufacturing and annealing of multicomponent glasses.

**Acknowledgement:** This work was supported by the Russian Science Foundation, grant № 19-19-00613-П.

## PP-III-02

# Metal Cluster and Nanoparticle Mobility in Aromatic Polymer Network of Styrene-Divinylbenzene

Bykov A.V., Demidenko G.N., Nikoshvili L.Zh., Pinyukova A.O.
*Tver State Technical University, Tver, Russia*
*BykovAV@yandex.ru*

The work is aimed at studying the mobility of clusters and small metal nanoparticles in styrene-divinylbenzene copolymers. The study of the effect of the reducing time of a metal-containing catalytic system stabilized in styrene-divinylbenzene on the mobility and its activity in the reaction of liquid-phase hydrogenation of arenes.

The effect of the reducing time of metal/MN100 systems by molecular hydrogen at elevated temperatures on its activity and selectivity in the process of liquid-phase hydrogenation of benzene and naphthalene was studied. Based on the density functional theory, quantum chemical modeling of M19 clusters was carried out in the UKS/ZORA/BP/def2-TZVP approximation. The adsorption on optimized benzene ring clusters was studied. Based on the obtained data, the mobility of M4, M9, and M19 clusters in the pores and on the surface of a styrene-divinylbenzene copolymer containing 11 mole percent divinylbenzene was studied by molecular dynamics methods at 300 °C.

The study shows that the resulting polymer has a developed network of micro- and mesopores. The adsorption energy of clusters on the polymer mesh was found to be significant. The conformational movements of the styrene-divinylbenzene polymer during gas-phase reduction make a significant contribution to the diffusion of clusters in the polymer medium and limit the growth rate of particles.

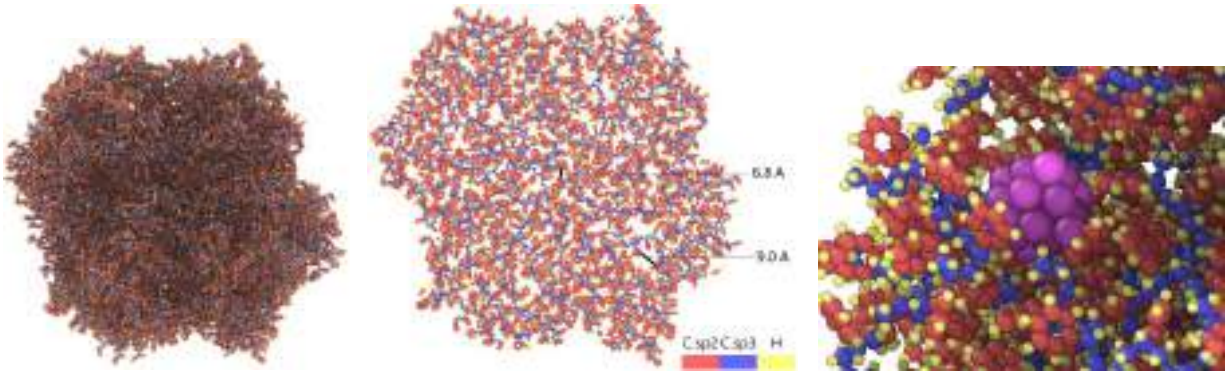


*Fig. 1. Optimized structure of styrene-divinylbenzene particle (74070 atoms, 11% mol divinylbenzene), 20 Å thick section and metal particle in the polymer*

**Acknowledgement:** This work was supported by the Russian Science Foundation, project 23-23-00090.

## PP-III-03

# Synthesis and Characterization of Polyaniline Doped with Copper Ions as Sensor Material for Non-Enzymatic Determination of Carbohydrates in Liquids

Davletkildeev N.A.[1], Lobov I.A.[1], Mosur E.Yu.[1], Fayazov R.A.[2]
*1 – Omsk Scientific Center SB RAS, Omsk, Russia*
*2 – Dostoevsky Omsk State University, Omsk, Russia*
*dna_mail@mail.ru*

Polyaniline (PANI) attracts considerable interest due to the combination of unique properties that allow it to be used as a material for various practical applications. Thus, PANI doped with copper ions exhibits selective catalytic properties with respect to the oxidation of carbohydrates, which can be used in the creation of non-enzymatic glucose sensors [1].

In this report, PANI doped with copper ions ($Cu^{2+}$) was synthesized by chemical oxidative polymerization of aniline in two different ways: PANI formed by post-synthesis introduction of copper ions (ex-situ $Cu^{2+}$-PANI) and PANI obtained by introduction of copper ions during synthesis (in-situ $Cu^{2+}$-PANI). The morphology and elemental composition of PANI (scanning electron microscopy, atomic force microscopy, energy-dispersive X-ray spectroscopy), its molecular structure (IR spectroscopy), electronic structure and catalytic activity in the glucose oxidation reaction (UV-Vis spectroscopy) were characterized.

The $Cu^{2+}$-PANI materials obtained by two methods have a molecular structure characteristic of PANI and differ significantly in morphology, packing density of the polymer chain in molecular tangles, copper content and the degree of interaction of copper ions with the polymer. It is shown that ex-situ $Cu^{2+}$-PANI is a sparse grid of intertwined fibril-like structures consisting of globular particles with a diameter of 50-150 nm and is characterized by a high packing density of the polymer chain, high copper content (up to 8 at. %) and a low degree of interaction of copper ions with the polymer. In-situ $Cu^{2+}$-PANI is formed by randomly distributed globular particles with a diameter of 100-350 nm and is characterized by looseness of the molecular tangle, lower copper content (up to 2 at. %) and a high degree of interaction of copper ions with the polymer.

The study of the catalytic activity of both ex-situ $Cu^{2+}$-PANI and in-situ $Cu^{2+}$-PANI materials in the reaction of glucose oxidation showed that glucose samples treated with $Cu^{2+}$ doped PANI contained a significant concentration of glucose oxidation products (hydrogen peroxide), while in the control glucose sample treated with HCl doped PANI, glucose oxidation products were absent.

**Acknowledgement:** The study was performed in the framework of State Assignment for the Omsk Scientific Center SB RAS (project № 121021600004-7).

**References:**

[1] S.K. Shukla, M.M. Demir, P.P. Govender, A. Tiwari, S.K. Shukla, Sens. Actuators B Chem. 242 (2017) 522.

## PP-III-04

# The Role of Basic Sites in $H_2O_2$-Based Oxidations over UiO-66

Evtushok V.Yu., Larionov K.P., Lopatkin V.A., Stonkus O.A., Kholdeeva O.A.
*Boreskov Institute of Catalysis, Novosibirsk, Russia*
*evtvas@catalysis.ru*

Among the family of metal-organic frameworks (MOFs), Zr-based MOFs have been extensively studied as catalysts for selective oxidation due to their high activity in $H_2O_2$ activation and their ability to retain the structure under conditions when often other MOFs would be degraded [1]. The unusual properties of Zr-MOFs in peroxide activation are clearly manifested in the oxidation of thioesters, when an unusually high selectivity (>99%) for sulfone is observed already at low conversions and at oxidant deficiency conditions [2]. Previously, this was observed mainly in catalytic oxidations involving nucleophilic activation of $H_2O_2$, which usually requires basic conditions.

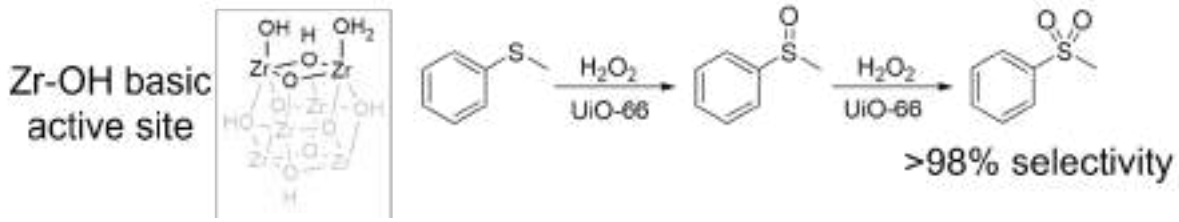


In this work, the main factors governing the activity of Zr-MOF in the oxidation of thioethers with aqueous $H_2O_2$ were studied using typical 12-coordinated Zr-MOF UiO-66 with terephthalate linkers and methyl phenyl sulfide (MPS) as a model substrate. Two series of UiO-66 samples differing in the particle size, defectiveness, and composition have been synthesized and characterized by $N_2$ adsorption, PXRD, TGA, FTIR, HRTEM, SEM, $^1$H NMR, and ICP-OES. The basic sites in UiO-66 samples were quantified by liquid-phase adsorption of isobutyric acid. The number of basic sites depends on the defectiveness and amount of modulator capping defects of UiO-66 and can be controlled by dehydration/hydration process. The number of basic sites was found to be close to the number of terminal Zr-$OH_2$/OH groups in the MOF defects determined by combinations of $^1$H NMR/TGA and $^1$H NMR/ICP-OES, suggesting that the basic sites are represented by Zr-OH groups at open Zr sites. The catalytic activity of UiO-66 in MPS oxidation correlates with the number of basic sites if nanosized UiO-66 samples (20-30 nm) are used to avoid diffusion limitations. Acid additives retard both thioether oxidation and $H_2O_2$ dismutation, indicating the key role of the basic Zr-OH groups in selective oxidations with $H_2O_2$ over Zr-MOFs.

**Acknowledgement:** The work was supported by RSCF grant № 21-73-00239

**References:**

[1] O.A. Kholdeeva, N.V. Maksimchuk, Catalysts 11 (2021) 283.
[2] O.V. Zalomaeva, V.Y. Evtushok, I.D. Ivanchikova, T.S. Glazneva, Y.A. Chesalov, K.P. Larionov, I.Y. Skobelev, O.A. Kholdeeva, Inorg. Chem. 59 (2020) 10634-10649.

## PP-III-05

# Monitoring the Remediation of Oil-Contaminated Permafrost Soils on the Territory of the Tank Farm

Glyaznetsova Yu.S., Zueva I.N., Chalaya O.N., Lifshits S.H.
*Institute of Oil and Gas Problems, Siberian Branch of the RAS, Yakutsk, Russia*
*glyaz1408@mail.ru*

Rational nature management is one of the priorities of the State Energy Policy of the Russian Federation [1]. According to the Ministry of Ecology of the Republic of Sakha (Yakutia), over the past 12 years, the number of oil and OP spills has amounted to more than 316 cases, including the Arctic zone. The problem of remediation of disturbed lands in permafrost conditions is difficult, since the soils are characterized by a low potential for self-recovery. In extreme climatic conditions, a thin organogenic soil horizon is formed, the content of the main biogenic elements in which is extremely low, and microbiological processes are slowed down. The presence of permafrost also complicates the transformation of oil hydrocarbons (HC).

In the central part of Yakutia, on the territory of the oil depot the experiment was carried out on the biological remediation of soils polluted with diesel fuel. For this, experimental sites were laid. The bioremediation technology consisted of the treatment the soils with the biological product based on hydrocarbon oxidizing microorganisms (HCOM) isolated from permafrost soils of Yakutia [2].

The initial content of oil products (OP) in the soils ranged from 24533 mg/kg to 67528 mg/kg. 2.5 months after the biological treatment, the residual content of OP in the soils decreased by 18 times. According the data of FT-IR spectroscopy decrease in the concentration of OP was accompanied by a change in the structure-group composition of soil extracts. The configuration of the IR-spectra of the initial samples is determined exclusively by the HC components: the predominance of methylene, methyl groups and aromatic cycles - a number of intense absorption bands (a.b.) in the range of 650 – 1000 $cm^{-1}$, 1380, 1460 and 1600 $cm^{-1}$, which is typical for soils contaminated with OP, in this case, diesel fuel (fig. 1 a).

2.5 months after biological treatment, the type of the IR-spectra changed. In the spectrum intense a.b. appeared at 1700 – 1740 $cm^{-1}$ and 1170 $cm^{-1}$, which indicate a high content of carbonyl groups and ether bonds, relatively. According chemical composition, this sample is close to the background and by the IR spectrum it does not contain any noticeable signs of oil pollution (fig. 1 a).

The biodegradation of oil pollution is indicated an increase in the values of the relative absorption coefficients of carbonyl groups ($D^{I}_{1700}$) and ether bonds ($D^{I}_{1170}$), which were calculated from the ratio of optical densities of a.b. 1700 $cm^{-1}$ and 1170 $cm^{-1}$ to optical density a.b. methyl and methylene groups 1460 $cm^{-1}$ (Fig. 1 a). These coefficients increased by 2 times for carbonyl groups and 4 times for ether bonds.

According to GC/MS data, the composition of individual saturated HC changed in the process of oil pollution degradation. In the soil extracts of initial samples, relatively low

molecular homologues with maxim of n-alkanes on n-$C_{15,16,17}$ dominated in the n-alkanes composition (Fig. 1 b). The values of the ratio (i-$C_{19}$ +i-$C_{20}$)/(n-$C_{17}$+n-$C_{18}$) and the CPI coefficient are close to unity. 2.5 months after biological treatment the appearance of second maximum of n-alkanes in the high-molecular region on n-$C_{31}$ was noted. In the composition of saturated HC, the quantity of relatively low-molecular homologues of n-alkanes decreased. At the same time the content of isoprenoids increased, as the values of the CPI coefficient.

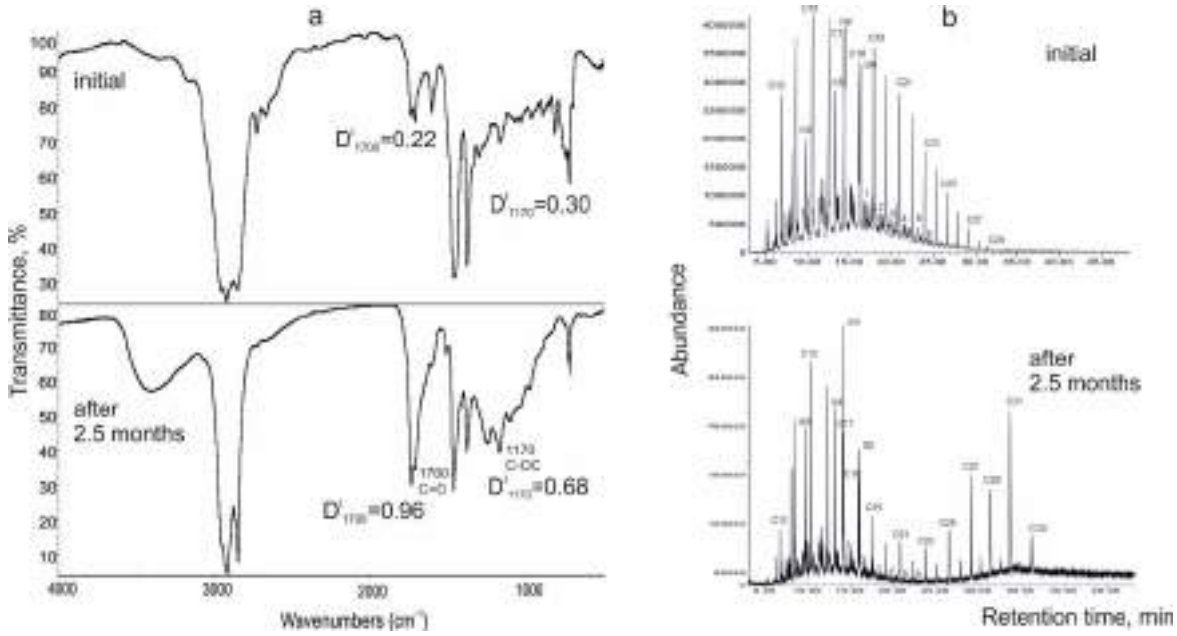


*Fig. 1. Geochemical characteristics of the soils: a - IR-spectra of soil extracts samples before and 2.5 months after biological treatment; b - Mass chromatograms saturated HC*

The detected directional changes in the composition of saturated HC, redistribution of HC both within homologous series and between different rows of homologues, as well as changes in chemical structure of the soil extracts simultaneously with the decrease in the residual content of OP indicate the processes of biodegradation of oil pollution had took place.

The results of the experiment showed the effectiveness of the treatment performed on the bioremediation of polluted permafrost soils using the developed biological product based on aboriginal HCOM.

**Acknowledgement:** This work was supported by the governmental orders (project 122011200369-1) using the scientific equipment of the Center for Collective Use of the FRC YSC SB RAS within the framework of grant no. 13.TsKP.21.0016.

**References:**

[1] Government of the Russian Federation. Order on approval of the Energy Strategy of the Russian Federation for the period up to 2035 (June 9, 2020 No 1523-r). 2020. Moscow, Russia.

[2] Shihranov, O. G., Glyaznetsova, Yu. S., Erofeevskaya, L. A., Nikolaeva, A. V. Bioremediation methods of oil-contaminated soil for the climatic conditions of the far north and the assessment of their effectiveness. Science and Technologies: Oil and Oil Products Pipeline Transportation. 2015. 17(1), pp. 90-97.

## PP-III-06

# Flexible Mn-Rich Cathode for High Energy Density Lithium Metal Batteries

Young-Kuk Hong, Seung-Hyeok Kim, Sang-Young Lee
*Yonsei University, Seoul, Republic of Korea*
*youngkuk95@yonsei.ac.kr*

In contrast to enormous progresses in electrode active materials, little attention has been paid to electrode sheets despite their crucial influence on practical battery performances [1,2]. Here, as a facile strategy to address this issue, we demonstrate dual heteronanomat skeletons-based Mn-rich electrodes for high energy density lithium metal batteries. Among various electrode materials, overlithiated layered oxide (OLO) materials are chosen to explore feasibility of this new electrode architecture and achieve unprecedented cell capacity. Heteronanmat skeletons composed of Polymeric nanofiber/CNT that play a crucial role in constructing 3D-bicontinuous ion/electron transport pathways and allow for removal of metallic foil current collectors.

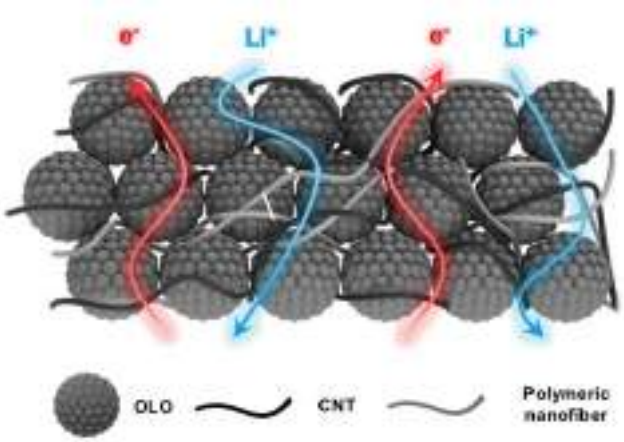


*Fig. 1. Schematic representation depicting the structural features of flexible Mn-rich cathode.*

**References:**

[1] J. M. Kim, S. H. Kim, N. Y. Kim, M. H. Ryou, H. Y. Bae, J. H. Kim, Y. K. Lee, and S. Y. Lee, iScience 23, (2020), 101739
[2] S. H. Kim, J. M. Kim, David B. Ahn, and S. Y. Lee, Small 16, (2020), 2002837

## PP-III-07

# Remote Detection of Magnetic Nanoparticles in a Biological Medium

Ichkitidze L.P.[1,2], Filippova O.V.[2], Galechian G.Yu.[2], Gerasimenko A.Yu.[1,2], Telyshev D.V.[1,2], Selishchev S.V.[1]

*1 – Institute of Biomedical Systems, National Research University of Electronic Technology, 124498 Zelenograd, Moscow, Russia*

*2 – Institute for Regenerative Medicine, Sechenov First Moscow State Medical University (Sechenov University), 119991 Moscow, Russia*

*ichkitidze@bms.zone*

In this work, we study the physicochemical properties of MNPs and the possibility of their detection at localization sites in a biological medium.MNPs were synthesized in an aqueous medium by chemical co-precipitation (Massart reaction). The main product of the reaction was $Fe_3O_4$ magnetite nanoparticles, the sizes of which were in the range of 10–25 nm. The resulting MNPs powder was mixed with microcrystalline cellulose (MCC) powder in a ratio of 3 wt. % MNPs to 97 wt. % MCC. Tablets with a diameter of 13 mm and a thickness of 2.5-5.2 mm were made from this powder (samples 1). At the same time, suspensions were prepared containing: 3 wt.% MNPs and 97 wt.% PMS (liquid polymethylsiloxane, samples 2). Sample 2 is considered a biological medium as its viscosity matches that of blood.

The magnetic field $\Delta B$, which is the difference between the fixed values of the magnetic fields without the sample and with the sample, was used to estimate the values of the magnetization $M$ and the specific magnetic moment $p_m$ inside the sample. It was believed that the measured $\Delta B$ is correlated with the values, i.e. $\Delta B \sim M$, $p_m$. It has been established that in a weak magnetic field $B_0 \leq 2$ G, all samples exhibit the properties of superparamagnetism. In fields $B_0 \approx$ 2-200 G, hysteresis was observed on the curves $M(B_0)$, from which various measured and estimated parameters were determined. With a magnetization field $B_0 \approx 200$ G for samples 1 and 2, the following values were obtained, respectively: coercive force $H_c$ – 82 G and 56 G; ratios of residual magnetization to maximum magnetization – 0.91 and 0.95; $p_m$– 0.45 emu/g and 0.15 emu/g; remanence relaxation time 81 min and 68 min (exponential scale). When vibrating for 1 min at a frequency of 2000 rpm, samples 1 and 2 lost their residual magnetization by 10-15 % and 90-95 %, respectively.

Samples were reliably recorded at a distance of up to 5-6 cm from the magnetometer sensor, which can be used for remote detection of theranostics of osteoarthritis in small animals using MNPs loaded with various ligands.

**Acknowledgement:** This work was funded by Russian Ministry of Science and Higher Education (state assignment №075-03-2023-024 from 13.01.2023). Research at Sechenov University in part of the preparation of magnetic nanoparticles was funded by the Ministry of Science and Higher Education of the Russian Federation under grant agreement No. 075-15-2021-596.

## PP-III-08

# Thin-Film Flat Superconducting Magnetic Field Concentrator

Ichkitidze L.P.[1,2], Lysenko A.Yu.[2], Savelev M.S.[1,2], Selishchev S.V.[2]

*1 – Institute of Biomedical Systems, National Research University of Electronic Technology (MIET), 124498 Zelenograd, Moscow, Russia*

*2 – Institute for Regenerative Medicine, Sechenov First Moscow State Medical University (Sechenov University), 119991 Moscow, Russia*

*ichkitidze@bms.zone*

Most magnetic field sensors (MFS) have a high resolution, i.e. low threshold sensitivity ≤1 nT, achieved through the use of superconducting film magnetic field concentrators (MFC). In this work, we study the planar structure of a superconducting film concentrator (see Figure 1), in which the MFC and magnetosensitive element (MSE) are in the same plane and do not intersect with each other. A sketch of the proposed structure is shown in Figure 1.

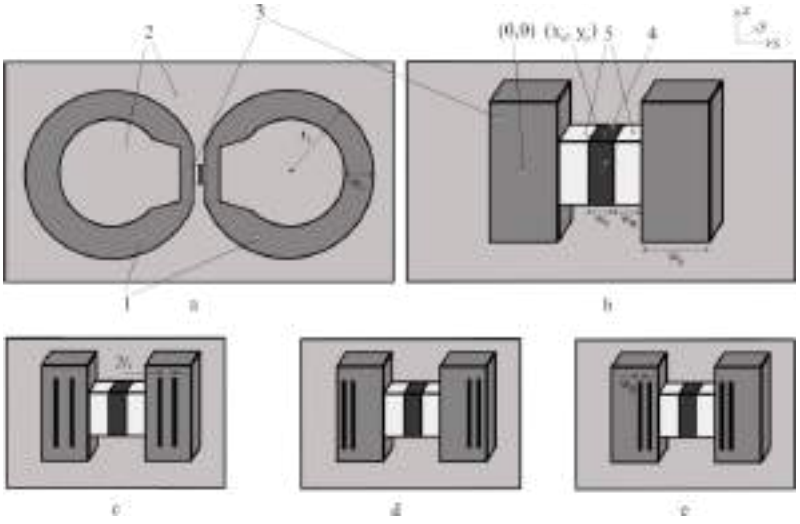

*Figure 1 Sketch of planar film superconducting magnetic field concentrator*

The concentration factor *F* of the magnetic field was determined as the ratio of the average value of the magnetic field at the MSE to the value of the external recorded field. It has been established that for a MFC containing AB without incisions (Figure 1, b), the parameter F takes values ~ from 100 to 200. The location of the incisions on the AB significantly changes *F*, in particular, its value is 20% more in Figure 1, *e* than in case *b.* The results obtained will improve the efficiency of existing magnetic field sensors in the form of a reduction in the size of the receiving antenna, which will make it possible to detect smaller magnetic objects, including magnetic nanoparticles in the biological medium.

**Acknowledgement:** This work is supported by the Ministry of Science and Higher Education of the Russian Federation (project No. 075-03-2020-216 of December 27, 2019). Research at Sechenov University in terms of computer calculation of the magnetic field concentrator was funded by the Ministry of Science and Higher Education of the Russian Federation under grant agreement No. 075-15-2021-596.

## PP-III-09

# Impact of $CO_2$ Absorption on Mobility of [EMIm][Gly] Confined in Silica Gel

Khudozhitkov A.E.[1,2], Kolokolov D.I.[1,2], Sheshkovas A.Z.[1,2], Veselovskaya J.V.[1]
*1 – Boreskov Institute of Catalysis, Novosibirsk, Russia*
*2 – Novosibirsk State University, Novosibirsk, Russia*
*alexandr.khudozhitkov@gmail.com*

The problem of the $CO_2$ capturing, despite numerous efforts still has no universal solution. Ionic liquids have been extensively investigated as promising materials for several gas separation processes, including $CO_2$ capture. Ionic liquids are known for high thermal and chemical stability as well as low vapour pressure. The use of non-volatile solvents is particularly interesting for $CO_2$ capture to prevent solvent loss and thus to mitigate the environmental concerns associated to the use of traditional volatile solvents such as ethanolamines. However, most studies focus on enhancing equilibrium capacity, and neglect to consider other properties, such as transport properties.

Amino acid ionic liquids (AAILs) based on imidazolium cations, such as [EthylMethylImidazolium][Glycinate] ([EMIm][Gly]), were recently reported to be highly attractive systems for one-pot capture and catalytic conversion of $CO_2$. AAILs have high $CO_2$ sorption capacity and low desorption temperatures. However, it has high viscosity resulting in low rates of $CO_2$ absorption and desorption. Moreover, absorption of $CO_2$ may lead to further increase of viscosity.

The promising way to overcome this problem is to disperse ionic liquid in microporous media. Several research groups showed this approach allows achieving much more rapid $CO_2$ absorption. It is supposed to be caused by higher accessibility of AAIL due to the dispersion. The influence of the host material on the mobility of ionic liquid has not been properly regarded.

In this contribution we investigate the molecular mobility of [EMIm][Gly]. With $^2H$ NMR method we characterize the dynamics and melting transition of bulk ionic liquid. The melting occurs through the dynamically heterogeneous state in the 253-283 K temperature region. Upon confinement the behaviour of ionic liquid changes only marginally indicating that guest host interaction does not alter its properties. Introduction of $CO_2$ in turn has dramatic impact on the mobility and phase transition of [EMIm][Gly]. The melting transition shifts to the higher temperatures by 40 K, which indicates that the $CO_2$ presence makes the ionic liquid more rigid with less mobile ions. Furthermore, the activation barrier of isotropic rotation of ions increases twofold (from 10 to 20 kJ/mol) and the rotation rate drops down. Since the isotropic rotation is closely related to the local viscosity, we conclude that $CO_2$ absorption leads to the ionic liquid viscosity increase inside pores.

**Acknowledgement:** This work was supported by the Russian Science Foundation, grant 21-13-00047.

## PP-III-10

# Pd-Ce-$O_x$/MWCNTs and Pt-Ce-$O_x$/MWCNTs Composite Materials for Low-Temperature Oxidation of CO and $CH_4$

Kibis L.S.[1], Zadesenets A.V.[2], Korobova A.N.[1], Kardash T.Yu.[1], Slavinskaya E.M.[1], Stonkus O.A.[1], Korenev S.V.[2], Podyacheva O.Yu.[1], Boronin A.I.[1]

*1 – Boreskov Institute of Catalysis, Novosibirsk, Russia*

*2 – Nikolaev Institute of Inorganic Chemistry, Novosibirsk, Russia*

*kibis@catalysis.ru*

The catalysts based on the combination of the noble metals and $CeO_2$ have long proven their effectiveness in various industrially important reactions, including exhaust gas after-treatment and air purification in the enclosed spaces [1,2]. One of the key factors for maintaining the high catalytic activity of the systems in the oxidation reactions at low temperature range are believed to be the size of the active metal species and their oxidation state [3,4]. The use of the carbon nanomaterials as the supports for the stabilization of the active components in a highly dispersed state can be considered as a perspective approach for the preparation of the catalytic systems with high activity and stability [5]. In this work, we studied the composite materials based on the multi-walled carbon nanotubes (MWCNTs), $CeO_2$, and Pd (Pt).

The samples were prepared by impregnation of the MWCNTs with the acetone solutions of the precursors of the active components, followed by solvent evaporation and heating of the dry residue in helium atmosphere to 350°C. A part of the samples was further heated in an oxidative atmosphere at 350°C. The physicochemical properties of the as-prepared catalysts and the catalysts after oxidative treatment were characterized by the structural ($N_2$ adsorption, XRD, TEM) and spectral (XPS) methods. The catalytic properties of the samples were studied in CO and $CH_4$ oxidation reactions in the temperature-programmed mode (TPR-CO+$O_2$ and TPR-$CH_4$+$O_2$, respectively).

The data of the structural methods showed that the Pd-based samples contained individual PdO and $CeO_2$ nanoparticles about 1–8 nm in size, as well as PdO-$CeO_2$ agglomerates. The $Pd^{2+}$ ions stabilized in $CeO_2$ lattice was also present in the samples, but their fraction was much smaller. The Pd-Ce-$O_x$/MWCNTs samples were active in CO and $CH_4$ oxidation reactions, with CO and $CH_4$ conversion starting from 0°C and 200°C, respectively (Fig. 1). The catalytic activity of the as-prepared samples and the samples after oxidative pretreatment was very similar.

In contrast to the palladium-based nanocomposites, in the Pt-Ce-$O_x$/MWCNTs samples, the platinum was mostly present in a highly dispersed state. The single $Pt^{2+}$ ions and $PtO_x$ clusters less than 1 nm in size were detected. The activity of the as-prepared Pt-Ce-$O_x$/MWCNTs sample in CO oxidation reaction was similar to the activity of the Pd-Ce-Ox/MWCNTs system (Fig. 1a). However, an additional oxidative treatment of the sample led to a significant increase in the activity in the temperature range below 0°C. The CO conversion

of about 20% was observed already at -35°C, while the CO conversion curve demonstrated a U-shaped behavior at temperatures below 100°C. This result points to the presence of the several types of the active centers on the catalyst surface, the reaction on which proceeds by different mechanisms. Based on the results of the physicochemical methods and literature data, it can be assumed that the conversion of CO at temperatures above 80°C occurs on the single $Pt^{2+}$ sites according to the Mars-van Krevelen mechanism, while the CO oxidation at low temperatures proceeds according to the associative mechanism on the $PtO_x$ clusters. The oxidative treatment led to an increase in the relative number of the sub-nanometer $PtO_x$ clusters, which resulted in an increase in the activity of the sample at low temperature. The activity of the Pt-Ce-Ox/MWCNTs catalysts in the methane oxidation reaction was observed at temperatures higher than the ones for the palladium-based catalysts. The difference in the temperature of the 50% conversion of $CH_4$ was about 50°C (Fig. 1b).

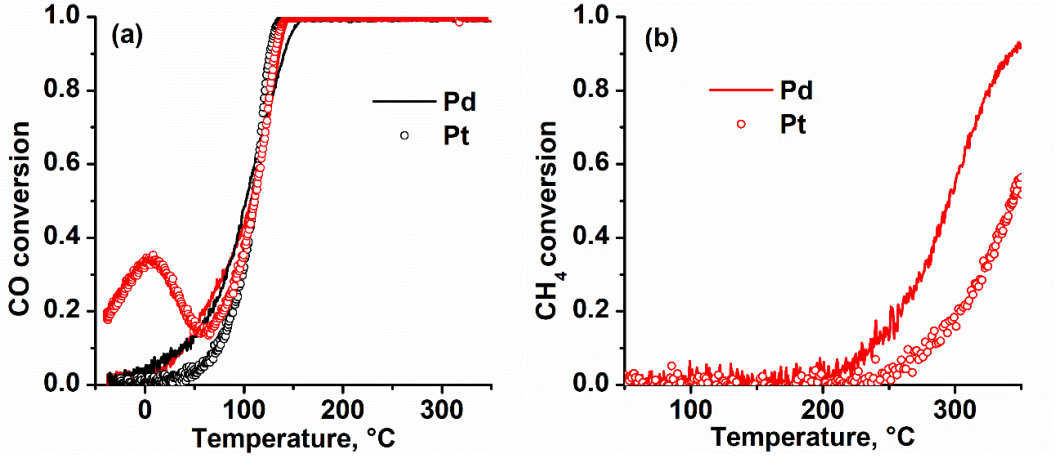


*Fig. 1. (a) TPR-CO+$O_2$ and (b) TPR-$CH_4$+$O_2$ data for the Pd- and Pt-based catalysts. Black lines – as-prepared samples, red lines – samples after oxidative pretreatment.*

Thus, the Me-Ce-$O_x$/MWCNTs composites can be considered as promising systems for various catalytic applications. In the Pd-Ce-$O_x$/MWCNTs composites the palladium species are stabilized on the surface of $CeO_2$ and/or MWCNTs as PdO nanoparticles, which demonstrate high activity in methane oxidation reaction. The highly dispersed $PtO_x$ clusters provide high activity of the Pt-Ce-$O_x$/MWNT catalysts in CO oxidation reaction in the temperature range below 0°C.

**Acknowledgement:** This work was supported by the Russian Science Foundation, grant 21-13-00094.

**References:**

[1] T. Montini, M. Melchionna, M. Monai, P. Fornasiero, Chem. Rev. 116 (2016) 5987−6041.
[2] S. Rood, S. Eslava, A. Manigrasso, C. Bannister, Proc. Inst. Mech. Eng., Part D 234 (2020) 936−949.
[3] A. Gänzler, M. Casapu, F. Maurer, H. Störmer, D. Gerthsen, G. Ferré, P. Vernoux, B. Bornmann, R. Frahm, V. Murzin, M. Nachtegaal, M. Votsmeier, J.-D. Grunwaldt, ACS Catal. 8 (2018) 4800–4811.
[4] V. Muravev, J.F.M. Simons, A. Parastaev, M.A. Verheijen, J.J.C. Struijs, N. Kosinov, E.J.M. Hensen, Angew. Chem. Int. Ed. 61 (2022) e202200434.
[5] M. Melchionna, S. Marchesan, M. Prato, P. Fornasiero, Catal. Sci. Technol. 5 (2015) 3859-3875.

## PP-III-11

# Tuning the Activity and Selectivity of $Pt/TiO_2$ Ammonia Slip Catalysts by Surface Modification

Kibis L.S.[1], Svintsitskiy D.A.[1], Ovsyuk I.Yu.[1,2], Romanenko A.V.[1], Kardash T.Yu.[1], Stonkus O.A.[1], Slavinskaya E.M.[1], Boronin A.I.[1]

*1 – Boreskov Institute of Catalysis, Novosibirsk, Russia*

*2 – Novosibirsk State University, Russia*

*kibis@catalysis.ru*

Ammonia is an important substance for nitric acid and fertilizer production, petroleum refining, *etc*. It is also used for selective catalytic reduction (SCR) of $NO_x$ from automotive exhaust. During operation of the SCR system, the excess of ammonia is dosed, resulting in its inevitable emission into the environment. Thus, the so-called ammonia slip catalysts (ASCs) oxidizing ammonia to harmless molecular nitrogen is required to control $NH_3$ emission. Although the ACSs have been used for a long time, there is still a challenge to increase their activity and selectivity towards molecular nitrogen at temperature below 300°C. In the present work, we focused on the tuning the low-temperature activity and selectivity of the $Pt/TiO_2$ catalysts by the modification of the acid-base properties of the samples surface.

For preparation of the samples, the $TiO_2$ support (P25, Degussa) was impregnated with an aqueous solution of $Pt(NO_3)_4$, followed by drying at room temperature and calcination in air at 400°C for 4h. The modification of the samples with potassium or tungsten were used to vary the acid-base properties. For modification with potassium, the $Pt/TiO_2$ sample was impregnated with a KOH aqueous solution. The resulted product was dried to an air-dry state followed by calcination in air at 200°C for 4 h. The tungsten was introduced to the catalyst before platinum deposition. The $WO_3/TiO_2$ support was synthesized by incipient wetness impregnation of titania with an ammonium paratungstate solution followed by drying and calcination in air at 400°C for 4h.

The structure of the prepared samples was analyzed with X-ray diffraction and Transmission electron microscopy. The surface composition and the oxidation state of the elements on the surface were characterized by X-ray photoelectron spectroscopy. The temperature programmed desorption of $NH_3$ was used to study the acidity of the surface. The catalytic activity measurements were performed by temperature-programmed reaction $NH_3+O_2$ with analysis of the reaction mixture with infrared spectrometer.

The performed experiments provided an opportunity to establish the correlation between the acidic properties of the surface and the activity of the catalysts in ammonia oxidation reaction together with the selectivity towards molecular nitrogen at low temperature.

**Acknowledgement:** This work was supported by the Russian Science Foundation, grant 23-23-00322.

## PP-III-12

# Eutectic Electrolytes for Low-Temperature Aqueous Lithium-Ion Batteries

Kim H.-I., Lee S.-Y.
*Yonsei University, Seoul, Republic of Korea*
*syleek@yonsei.ac.kr*

Aqueous electrolytes are promising candidates for the electrolyte of next generation energy storage devices due to their high safety and cost-effectiveness. However, the freeze of aqueous electrolyte limits their sub-zero temperature applications. Here, we designed a new class of aqueous eutectic electrolyte (AEE) based on a eutectic property of lithium bis(trifluoromethane sulfonyl)imide (LiTFSI)–water binary mixture. The eutectic property of AEE (5.2 m LiTFSI in water) enabled coordination of water molecules with $Li^+$ and $TFSI^-$, which could enhances anti-freezing phenomena and desolvation kinetics. Consequently, the AEE enables the lithium-ion hybrid supercapacitors to provide exceptional high-rate cell performance at low-temperature (−40°C) without any cell failure. This work envision the effective strategy to enhancing low-temperature performance of aqueous electrolyte via introducing the eutectic system.

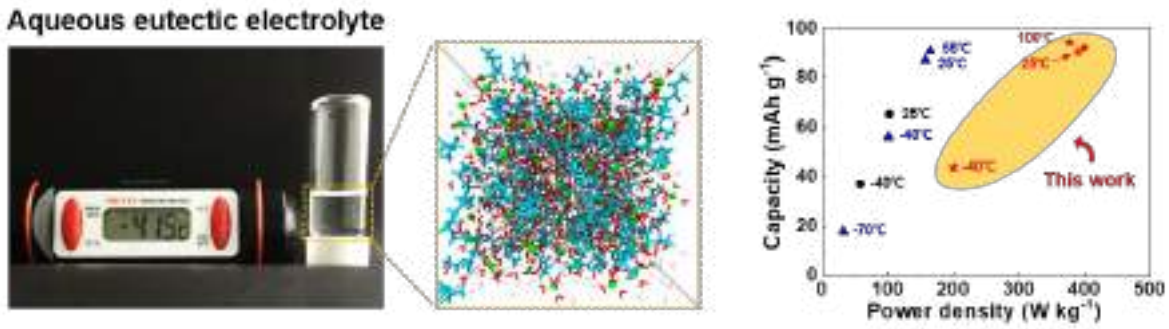


*Fig. 1. Schematic of aqueous eutectic electrolyte and the comparison in the cell performance between the eutectic HSC and previously reported wide-temperature energy storage devices.*

**Acknowledgement:** This work was supported by the Basic Science Research Program (2017M1A2A2087812, 2018R1A2A1A05019733, and 2018M3D1A1058624), Wearable Platform Materials Technology Center (2016R1A5A1009926) and Korean government (MSIP) (2014R1A5A1009799) through the National Research Foundation of Korea (NRF) funded by the Ministry of Science, ICT and future Planning. This work was also supported by Electronics and Telecommunications Research Institute (ETRI) grant funded by the Korea government (20ZB1200, Development of ICT Materials, Components and Equipment Technologies). Computational resources were from UNIST-HPC.

## PP-III-13

# Redox-Homogeneous, Gel Electrolyte-Embedded High-Mass-Loading Cathodes for High-Energy Lithium Metal Batteries

Jung-Hui Kim[1], Ju-Myung Kim[2], Sang-Young Lee[1]

*1 – Department of Chemical and Biomolecular Engineering, Yonsei University, Seoul 03722, Republic of Korea*

*2 – Energy and Environment Directorate, Pacific Northwest National Laboratory, Richland, WA 99353, United State of America*

*qaztgb1670@unist.ac.kr*

One of the main stumbling blocks in developing high-energy density Li-metal batteries is the lack of cathodes with high-mass-loading capable of delivering highly reversible redox reactions. To overcome this issue, here we report an electrode structure that incorporates a UV-cured non-aqueous gel electrolyte and a cathode where the $LiNi_{0.8}Co_{0.1}Mn_{0.1}O_2$ active material is contained in an electron-conductive matrix. This peculiar structure prevents the solvent-drying-triggered non-uniform distribution of electrode components and demonstrates redox-homogeneity in a longitudinal direction of the thick electrodes. When a cathode with a mass loading of 60 mg $cm^{-2}$ is coupled with a 100 µm thick Li-metal anode in lab-scale pouch cell configuration, a specific energy and energy density of 321 Wh $kg^{-1}$ and 772 Wh $L^{-1}$ (based on the total mass of the cell), respectively, can be delivered [1].

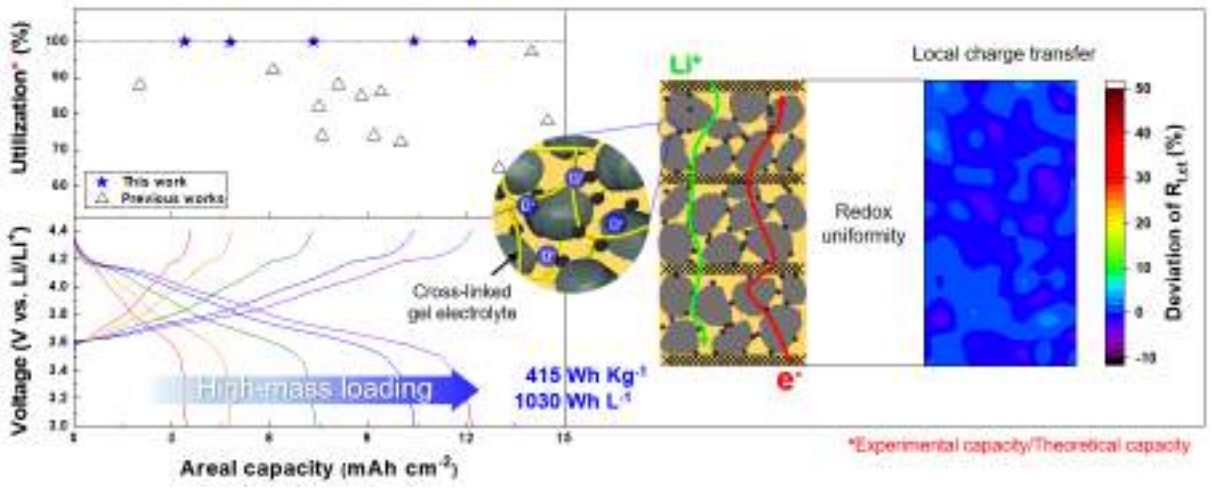


*Fig. 1. Charge/discharge profile (left, bottom) and capacity utilization of electrodes as a function of areal capacity. The schematic illustration and corresponding local charge transfer of high-areal-capacity electrode (right)*

**Acknowledgement:** This work was supported by the Basic Science Research Program (2021R1A2B5B03001615 and 2018M3D1A1058744) through the National Research Foundation of Korea (NRF) grant by the Korean Government (MSIT). This research was also supported by the Technology Innovation Program (20010960) funded by the Ministry of Trade, Industry & Energy (MOTIE, Korea) and the Yonsei University Research Fund of 2020-22-0536.

**References:**

[1] Jung-Hui Kim, Ju-Myung Kim, Seok-Kyu Cho, Nag-Young Kim & Sang-Young Lee, Nat. Commun. 13 (2022) 2541.

## PP-III-14

# Transparent and Multi-Foldable Nanocellulose Paper Microsupercapacitors

Sang-Woo Kim[1], Kwon-Hyung Lee[1], Yong-Hyeok Lee[3], Won-Jae Youe[2], Jae-Gyoung Gwon[2], Sang-Young Lee[3]

*1 – Department of Energy Engineering, School of Energy and Chemical Engineering, Ulsan National Institute of Science and Technology (UNIST), Ulsan, 44919, Republic of Korea*

*2 – Department of Forest Products, National Institute of Forest Science, Seoul, 02455, Republic of Korea*

*3 – Department of Chemical and Biomolecular Engineering, Yonsei University, 50 Yonsei-ro, Seodaemun-gu, Seoul, 03722, Republic of Korea*

*syleek@yonsei.ac.kr*

Despite the ever-increasing demand for transparent power sources in wireless optoelectronics, most of them have still relied on synthetic chemicals, thus limiting their versatile applications. We demonstrate a class of transparent nanocellulose paper microsupercapacitors (TNP-MSCs) as a beyond-synthetic-material strategy. Onto semi-IPN network structured, thiol-modified TNP, a thin layer of AgNWs and a conducting polymer are consecutively introduced through microscale-patterned masks to produce a transparent conductive electrode (TCE) with interdigitated structure. This TNP-TCE, in combination with solid-state gel electrolytes, enables on-demand cell configurations in a single body of TNP-MSC. Driven by this structural uniqueness and scalable microfabrication, the TNP-MSC exhibits high optical transparency (T = 85%), areal capacitance (0.24 mF $cm^{-2}$), controllable voltage (7.2 V), and foldability, which exceed those of previously reported transparent MSCs based on synthetic chemicals.

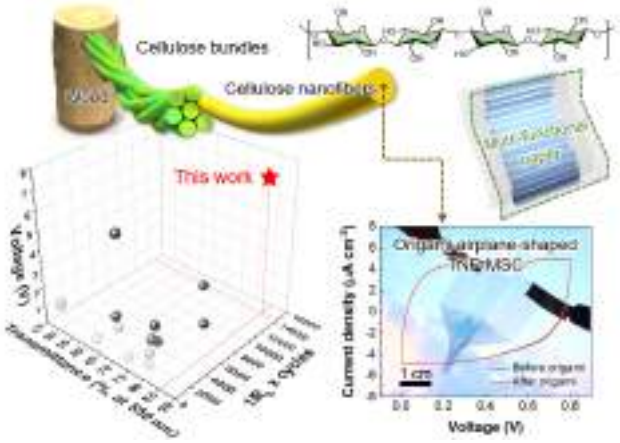


*Fig. 1. Comparison of the optical transparency, operating voltage, and mechanical flexibility (expressed as $R_b^{-1}$ × bending cycles) of the TNP-MSC to those of previously reported transparent MSCs.*

**Acknowledgement:** This work was supported by the National Research Foundation of Korea (NRF) grant funded by the Korean government (MSIT) (2021R1A2B5B03001615, 2021M3D1A2043791, and 2021M3H4A1A02099355). This work was also supported by the R&D Program for Forest Science Technology (Project No. FTIS 2021354D10-2123-AC03) provided by the Korea Forest Service (Korea Forestry Promotion Institute) and the Yonsei University Research Fund of 2020-22-0536.

## PP-III-15

# Flexible Lithium Metal Batteries Based on Polymeric Hosts

Kim S.H., Kim N.Y., Lee S.Y.
*Yonsei University, Seoul, Republic of Korea*
*seunghyeok94@gmail.com*

Despite extensive studies on lithium-metal batteries that have garnered considerable attention as a promising high-energy-density system, their application to flexible power sources is staggering due to the difficulty in simultaneously achieving electrochemical sustainability and mechanical deformability [1-3]. To address this issue, herein, we fabricated flexible lithium metal anodes based on polymeric hosts (PHs). Lithium is impregnated into nickel/copper-deposited conductive poly(ethylene terephthalate) nonwovens via electrochemical plating, resulting in self-standing flexible lithium anodes. The flexible Li anodes exhibit stable Li plating/stripping cyclability and mechanical deformability. The structural features of Li-plated polymeric host (Li@PH) and the comparison with a Li-plated Cu foil (Li@Cu) selected as a control sample are schematically illustrated in Fig. 1. Driven by the attractive characteristics of the flexible lithium anodes, the resulting lithium metal full cells provide improvements in the cyclability, rate performance, and gravimetric/volumetric energy density along with the exceptional mechanical flexibility.

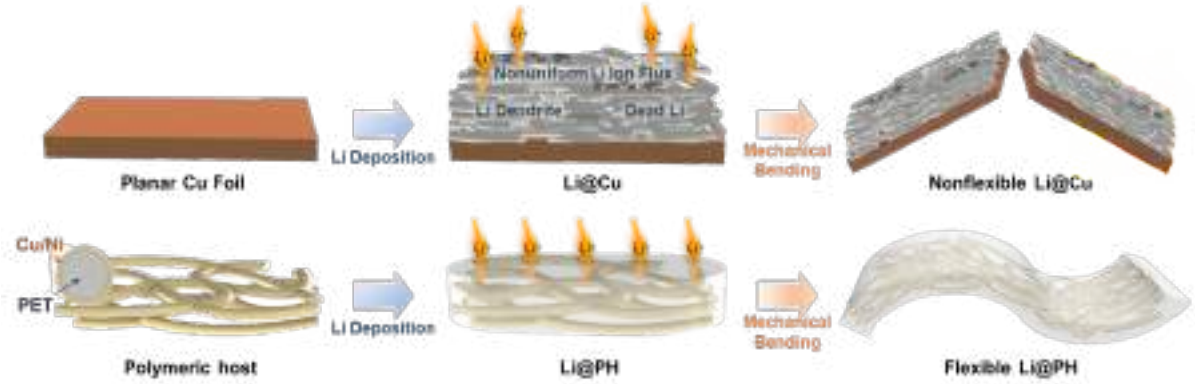


*Fig. 1. Schematic representation depicting the structural features of flexible Li@PH and nonflexible Li@Cu.*

**References:**

[1] H. J. Peng, J. Q. Huang, Q. Zhang, Chem. Soc. Rev. 46 (2017) 5237.
[2] S. Chen, C. Niu, H. Lee, Q. Li, L. Yu, W. Xu, J. G. Zhang, E. J. Dufek, M. S. Whittingham, S. Meng, J. Xiao, J. Liu, Joule 3 (2019) 1094.
[3] S. Wang, P. Xiong, J. Zhang, G. Wang, Energy Storage Mater. 29 (2020) 310.

## PP-III-16

# Demixing the Miscible Liquids: Toward Biphasic Battery Electrolytes Based on the Kosmotropic Effect

Won-Yeong Kim[1], Hong-I Kim[1], Kyung Min Lee[2], Stefano Passerini[3], Sang Kyu Kwak[2], Sang-Young Lee[1]

*1 – Department of Chemical and Biomolecular Engineering, Yonsei University, 50, Yonsei-ro, Seodaemun-gu, Seoul, Republic of Korea*

*2 – Department of Energy Engineering, School of Energy and Chemical Engineering, Ulsan National Institute of Science and Technology (UNIST), Ulsan 44919, Republic of Korea*

*3 – Helmholtz Institute Ulm (HIU), Helmholtzstraße 11, 89081, Ulm, Germany*

*kwy0744@yonsei.ac.kr*

Exploring new electrolyte chemistry beyond conventional single-phase battery electrolytes is needed to fulfill the heterogeneous requirements of anodes and cathodes [1]. Here, we report a biphasic liquid electrolyte (BLE) based on the kosmotropic effect. The key underlying technology for the BLE is phase separation of its electrolyte couples using a principle of "demixing the miscible liquids". Kosmotropic/chaotropic anions affect the ion coordination structures and the intermolecular interactions of electrolyte couples, enabling on-demand control of their immiscibility/miscibility. Despite the intrinsic miscibility of water (in aqueous electrolytes) and acetonitrile (in nonaqueous electrolytes), the structural change of the aqueous electrolyte induced by kosmotropic anions allows demixing with the nonaqueous electrolyte. The resultant BLE facilitates redox kinetics at cathodes and Zn plating/stripping cyclability at anodes. Consequently, the BLE enables Zn-metal full cells to exhibit a long cyclability (86.6% retention after 3500 cycles). Moreover, Zn anode-free full cells with the BLE exhibit a higher energy density (183 W h $kg^{-1}$) than previously reported Zn batteries.

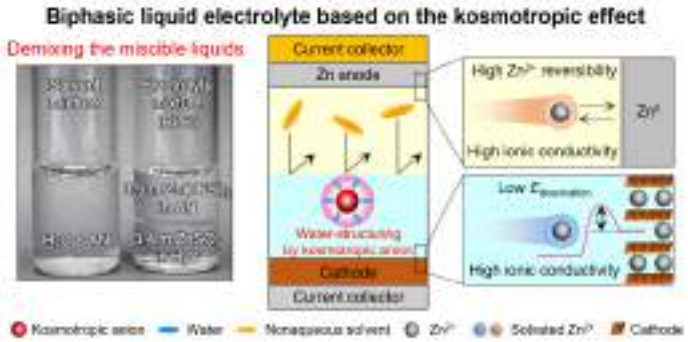


*Fig. 1. Schematic depicting the Zn metal batteries with biphasic liquid electrolyte based on the kosmotropic effect.*

**Acknowledgement:** This work was supported by the Basic Science Research Program (2021R1A2B5B03001615, 2021M3D1A2043791, and 2020R1A2C3005939) by the Korean Government (MSIT).

**References:**

[1] M. Armand and J. M. Tarascon, Nature, 2008, 451, 652–657.

## PP-III-17

# Analysis of the Product of Processing Tungsten Ore Concentrate by the Electric Arc Discharge Method in Open Air

Kokorina A.I.
*National Research Tomsk Polytechnic University, Tomsk, Russia*
*aik48@tpu.ru*

Tungsten carbide WC is a promising material for many industries due to its physical and chemical properties. Its high hardness and wear resistance, high melting point, low coefficient of friction, high electrical and thermal conductivity, as well as corrosion resistance and inertness to acids and alkalis ensure the use of tungsten carbide in the manufacturing industry, rock drilling, the manufacture of cutting tools and stamps, electronics and nuclear energy [1-2]. Tungsten carbide is also a promising catalyst carrier in hydrogen evolution reactions [2]. Electric arc synthesis is one of the methods that make it possible to obtain tungsten carbide from ore in one of the first stages [3].

The tungsten ore concentrate contained three main phases: scheelite $CaWO_4$, hubnerite $MnWO_4$, and ferberite $FeWO_4$. Processing included grinding in a vibratory mill, magnetic separation and drying in an atmospheric oven. An electric arc synthesis was carried out from a mixture of tungsten ore concentrate and siberian carbon carrier (sibunite) at a previously established mass ratio of sibunite and ore equal to 0.24. Next, the initial reagents were placed in a hollow cathode made in the form of a crucible. When an anode in the form of a cylindrical rod approached a cathode, a discharge was initiated in the cathode cavity. Synthesis was carried out for 45 s at a discharge circuit current of 220 A. These values were determined earlier. They provide the largest proportion of tungsten carbide in the synthesis product and almost complete processing of the initial ore phases. Electrical signals corresponding to the current of the discharge circuit and the voltage on the arc discharge were transmitted to a digital oscilloscope. During the synthesis an intensive release of carbon monoxide and carbon dioxide gases occurs, which can be seen on the gas analyzer. These gases close the reaction volume from atmospheric oxygen, as a result of which it is possible to implement electric arc synthesis in this system without vacuum equipment.

A X-ray analysis of the obtained sample was carried out (X-ray diffractometer Shimadzu XRD 7000s, λ=1.5406 Å). It was found that the synthesis product contains a hexagonal phase of WC, $W_2C$ and graphite. This phase composition is typical for the product of electric arc synthesis in this system in open-air environment (Fig. 1).

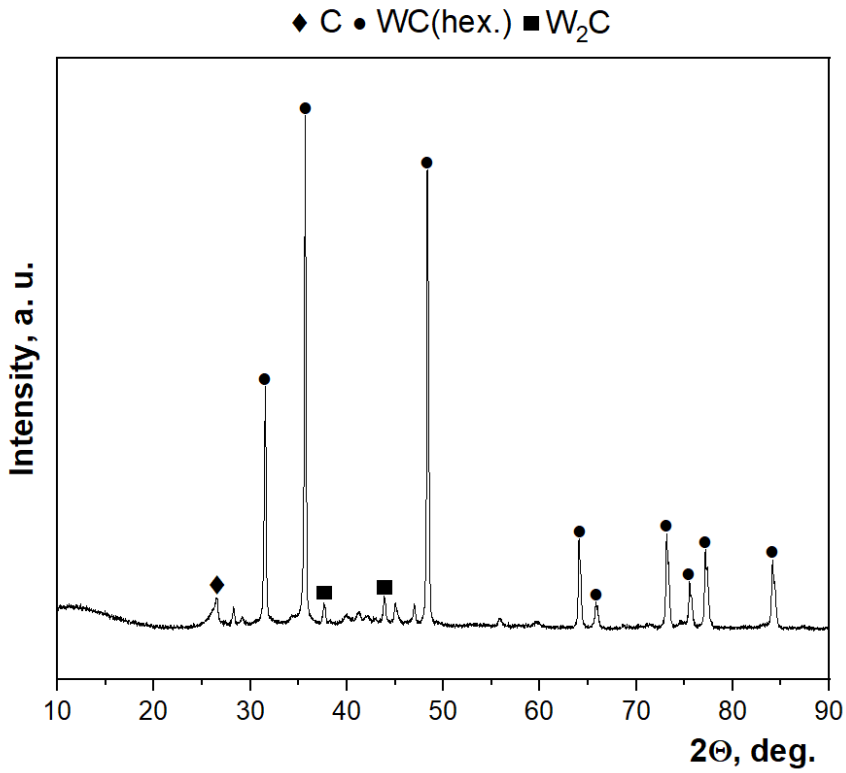


*Fig. 1. Sample X-ray diffraction pattern*

The average size of agglomerates in the obtained powder is 10 μm. The study of the catalytic properties of the resulting powder was carried out in a standard three-electrode cell in a 0.5 M solution of sulfuric acid $H_2SO_4$. Based on the results of testing the catalytic properties of the powder in electrolysis reactions, the overvoltage $\eta_{10}$ = 662 mV and the Tafel slope b = 214 mV/dec were determined.

**Acknowledgement:** This work was supported by the State Assignment for Universities (Project № FSWW-2022-0018).

**References:**

[1] Tripathy H. High temperature thermophysical properties of spark plasma sintered tungsten carbide // International Journal of Refractory Metals and Hard Materials. – 2022. – V. 104. – P. 105804.
[2] Sohail U. Role of tungsten carbide (WC) and its hybrids in electrochemical water splitting application- A comprehensive review // FlatChem. – 2022. – V. 35. – P. 100404.
[3] Pak A.Y. Vacuumless synthesis of tungsten carbide in a self-shielding atmospheric plasma of DC arc discharge // International Journal of Refractory Metals and Hard Materials – 2020. – V. 93. – P. 105343.

## PP-III-18

# Application of Silver Metal–Polymer Nanocomposites in the Analysis of Iodide Ions

Kolesnikova T.S., Uflyand I.E.
*Southern Federal University, Rostov-on-Don, Russia*
*tkol@sfedu.ru*

The creation of simple and environmentally friendly test tools for out-of-laboratory real-time analysis is one of the most important directions in the development of modern analytical chemistry. It has been proven that the most successful approach to solving this problem is the application of chemical reagents on an easy-to-use carrier. Prominent representatives of such tools are indicator powders and paper test strips. Obviously, the search for new reagents with specified chemical-analytical parameters is very important.

Currently, nanocomposite materials based on metal nanoparticles are being intensively studied. Separately, it should be noted that silver nanoparticles (AgNPs) stand out favourably due to the manifestation of a wide range of properties: outstanding plasmonic, antibacterial and catalytic activity, as well as chemical stability [1, 2]. AgNPs have a sufficiently high selectivity to halide ions, which makes it possible to use them in the development of efficient analytical methods [3].

The aim of this work was the synthesis of silver metal–polymer nanocomposites and their use for the analysis of iodide ions.

Silver metal–polymer nanocomposites were obtained by the thermolysis of silver-containing monomers based on unsaturated carboxylic acid. The obtained nanocomposites containing AgNPs are evenly distributed in a stabilizing carbon matrix. The structural characteristics and properties of the resulting nanocomposites were studied using X-ray diffraction (XRD), atomic force microscopy (AFM), scanning electron microscopy (SEM), transmission electron microscopy (TEM), and energy dispersive X-ray spectroscopy (EDS).

We have developed a method of test analysis of iodides using paper modified with the obtained silver-containing nanocomposites. The principle of the proposed approach to the determination of iodides is based on their oxidation to iodine and its subsequent dynamic extraction from the solution by an air flow with simultaneous detection. The technique includes the following steps: oxidation of iodide ions in solution ($2I^- + Ox = I_2 + Red$), gas extraction of iodine, its interaction with AgNPs fixed on the carrier surface ($I_2 + 2Ag^0 = 2AgI$), and determination of the colour intensity of the reaction zone test-strips that change depending on the concentration of iodides in the solution. The reaction of iodine with immobilized AgNPs leads to their oxidation and the appearance of a white spot on the test strip. The decrease in colour intensity can be monitored using a conventional scanner by measuring the RGB colour coordinates needed to build a calibration curve for determining the iodide content.

The working solutions were placed in a setup for dynamic gas extraction (Fig. 1), and solutions of potassium permanganate and sulfuric acid were added to them. A microcompressor was used to pump air through the jet system under laboratory conditions. The strips were removed and scanned against a white background. Scanned images were processed in a graphics editor in RGB mode by averaging the RGB colour coordinates of individual pixels within a circular reactive zone.

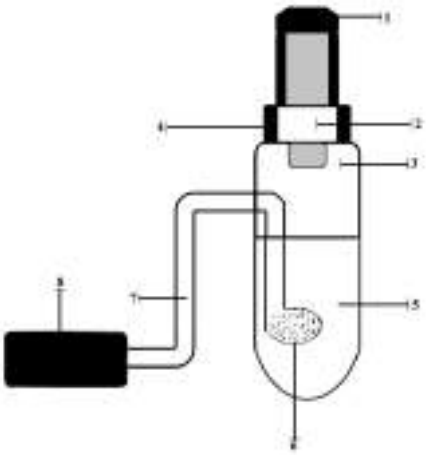

*Fig. 1. Setup for dynamic gas extraction: 1 – rubber stopper; 2 – test strip; 3 – glass vessel for the analysed solution; 4 – holder of test strips; 5 – reaction mixture; 6 – glass bubbler; 7 – polymer hose; 8 – air microcompressor*

According to the proposed method using this paper test strips, the blue colour coordinate should be chosen as an analytical signal for the colorimetric determination of iodides (iodine).

The optimal experimental conditions (reagents, their concentrations, air flow rate) were selected. The limit of detection (0.01 mg/L) and the range of determined concentrations (0.03–0.3 mg/L) of iodides were determined. Due to the high selectivity of outgassing, this method requires only minimal sample pretreatment, which simplifies analysis. In addition, the method is effective, simple and cheap.

A comparison of the proposed method with other methods described in the literature shows that it has good analytical characteristics.

**Acknowledgement:** This work was supported by the Russian Science Foundation, grant №22-13-00260.

**References:**

[1] J.R. Morones, J.L. Elechiguerra, A. Camacho, K. Holt, J.B. Kouri, J.T. Ramírez, M.J. Yacaman, *Nanotechnology 16 (*2005) 2346.
[2] P. Vasileva, B. Donkova, I. Karadjova, C. Dushkin, *Colloids Surf., A 382 (*2011) 203.
[3] T.S. Kolesnikova, A.O. Zarubina, M.O. Gorbunova, V.A. Zhinzhilo, G.I. Dzhardimalieva, I.E. Uflyand, Materials 15 (2022) 8376.

## PP-III-19

# $Ni/CeO_2$ Catalysts Synthesized by Solution Combustion Method for Steam and Aqueous-Phase Reforming of Glycerol

Matveyeva A.N., Omarov Sh.O.
*Ioffe Institute, St. Petersburg, Russia*
*anna.matveyeva@mail.ioffe.ru*

Formation and accumulation of crude glycerol is one of the disadvantages of the biodiesel industry. Therefore, the development of new and cost-effective ways for glycerol valorization are required. Steam reforming (SR) and aqueous-phase reforming (APR) are promising methods for processing glycerol to produce renewable hydrogen. Nickel is increasingly used as an active component of reforming catalysts. However, the choice of the support and the method of catalyst preparation are also important, which should provide a high dispersity of the Ni particles. For example, a high glycerol conversion was obtained for a 20 wt% Ni-based catalyst deposited on $CeO_2$ and synthesized by combustion compared to wet impregnation or co-precipitation synthesis due to the formation of smaller Ni crystallites [1]. Previously it was shown that 6.8 wt% $Ni/CeO_2$ (prepared by the solution combustion synthesis (SCS) method using urea as a fuel) in the range of 0–8.7 wt% is the minimum required amount of the active component to achieve high activity in SR of glycerol [2]. This work is aimed at conducting a comparative study of $Ni/CeO_2$ catalysts prepared by varying the SCS parameters, including fuel type (glycine, urea) and the fuel-to-oxidizer ratio, for steam and aqueous-phase reforming of glycerol.

A series of 30wt% $NiO/CeO_2$ catalysts were prepared by the SCS method, changing the fuel-to-oxidizer ratio ($\phi$=0.7–3), fuel type (glycine, urea), and oxygen access (using a covering). In some freshly prepared samples, depending on $\phi$, it was possible to detect the formation of metallic nickel. It was found that covering the beaker with a Petri dish immediately after the completion of the combustion makes it possible to retain a larger amount of metallic Ni in the samples and to increase the proportion of amorphous NiO. Thus, various forms of Ni and its interaction with $CeO_2$ were obtained, which affected activity in steam and aqueous-phase reforming of glycerol. With an increased and decreased ratio of glycine-to-oxidizer ($\phi$<1; $\phi$≥2), it is possible to avoid the formation of $CeO_2(Ni^{2+})$ solid solutions characteristic of these systems and achieve the most dispersed phases; in other cases, at $\phi$=1–1.6, trace amounts of the $CeNiO_3$-perovskite like phase were found.

Steam reforming of glycerol was carried out in a stainless steel reactor (dinner = 10 mm, L ≈ 50 cm) with a fixed catalyst bed at atmospheric pressure and 520 °C. The presence of nickel in freshly prepared samples makes it possible to exclude the stage of reductive activation of the sample before testing without loss of activity and stability. It has been shown Ce–Ni–O systems characterized by a high dispersion of phases (obtained at $\phi$<1 and $\phi$≥2) have the highest initial rate of hydrogen formation in SR (Figure 1A). In addition, these catalysts make

it possible to achieve the highest hydrogen yield and $H_2$/CO ratio, closest to the stoichiometric $H_2/CO_2$ ratio (2.33) with the complete WGS reaction.

Based on the results obtained in the SR process, the most active Ce–Ni–O system obtained at ϕ=2 with a covering (Ni:am-NiO:$CeO_2$=4:26:70 wt%; D($CeO_2$)=9.5 nm; D(Ni)= 4.8 nm) was additionally investigated in aqueous-phase reforming of glycerol at 34 bar and 231 °C using a once-through plug-flow reactor (dinner = 8 mm, L ≈ 20 cm). It has been found that such Ni–containing system makes it possible to achieve the hydrogen yield comparable to that of Pt/γ-$Al_2O_3$ at a close WHSV without undergoing noticeable deactivation (Figure 1B,C). At the same time, it is not inferior and even surpasses some other known catalysts in glycerol conversion into gas, the yield and rate of hydrogen formation, as well as the selectivity to $H_2$ and $CO_2$.

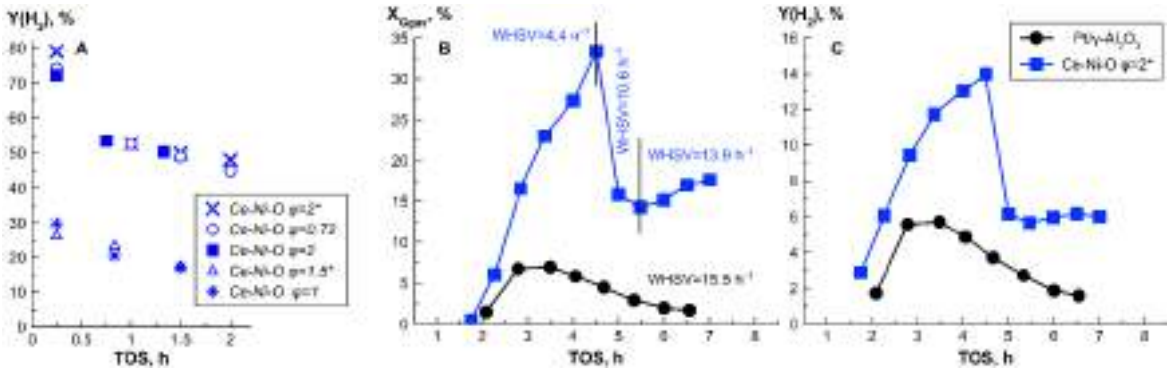


*Fig. 1. Hydrogen yield (A, C) and glycerol conversion into gas (B) versus time-on-stream obtained in SR (A) and APR (B,C) of glycerol for Ni-containing systems. *Samples were obtained by covering the beaker with a Petri dish after combustion was completed to minimize the interaction of solid products with atmospheric oxygen.*

**Acknowledgement:** This research was funded by the Russian Science Foundation (grant number 22–23–20094, https://rscf.ru/project/22-23-20094/, accessed on 03 March 2023) and the St. Petersburg Science Foundation (agreement number 26/2022 from 14 April 2022).

**References:**

[1] R.L. Manfro, A.F. da Costa, N.F.P. Ribeiro, M.M.V.M. Souza, Fuel Process. Technol. 92 (2011) 330–335.

[2] Sh.O. Omarov, K.D. Martinson, A.N. Matveyeva, M.I. Chebanenko, V.N. Nevedomskiy, V.I. Popkov, Fuel Process. Technol. 236 (2022) 107429.

## PP-III-20

# The Specifics of the Hydrodynamic Cavitation Development with the Changed of the Structural Surface of the Bodies

Skripkin S.G.[1,2], Starinskiy S.V.[1], Tsoy M.A.[1], Vasiliev M.M.[2], Kravtsova A.Y.[1,2]
*1 – Kutateladze Institute of Thermophysics, Novosibirsk, Russia*
*2 – Novosibirsk State University, Novosibirsk, Russia*
*kravtsova.alya@gmail.com*

The effect of the structural surface of the body on the emergence and development of the hydrodynamic cavitation on him was experimentally investigated in this work. The structured surface was made using the method of pulsed laser ablation. The approach allows creating the ordered structures on the surface of various materials, while varying the number of peaks, cavities, and depressions. Ablation of the sample was performed using a body-state Nd:YAG laser with a wavelength λ = 1064 nm operating in the modulated Q-factor mode [1]. The surface of the body treated by laser ablation was studied by profilometry. Based on the data obtained, the amplitude parameters of the total roughness over the area of the entire shot bit were calculated [2].

To understand of the influence of the structural surface on the occurrence and development of the cavities, two bodies were carried out in this work: the body without treatment and the body after its surface treatment. Both bodies were placed in a cavitation tunnel, and the high-speed visualization of the cavities flow at the variation of the liquid flow rate in the tunnel was performed [3].

According to the results of measurements, it was found that laser texturing delays the emerging cavitation and somewhat decreases its intensity at lower fluid flow rate. An increasing in the fluid flow rate leads to an increase in cavitation intensity for the body without treatment compared to the body after treatment, which is also expressed in an increase in the frequency of cavities. In the work was obtained a comparison of the flow regime with equal flow rates, which clearly describes the features of the development of a vapor–gas cavity for the two cases. The paper provides an explanation of the reasons for the influence of surface morphology on the development of cavities [4].

**Acknowledgement:** This work was supported by the Russian Science Foundation, grant 19-79-10217.

**References:**

[1] A. Lebedev, K. Dobroselsky, A. Safonov, S. Starinskiy, V. Sulyaeva, A. Lobasov, V. Dulin, C.N. Markides, Phys. Fluids 33 (2021) 121703.
[2] M. Kadivar, D. Tormey, G. McGranaghan, Int. J. Thermofluids 10 (2021) 100077.
[3] S.G. Skripkin, M.A. Tsoy, A.Y. Kravtsova, Sci. Rep. 12 (2022) 11182.
[4] S.G. Skripkin, S.V. Starinskiy, M.A. Tsoy, M.M. Vasiliev, A.Y. Kravtsova, Phys. Fluids 35 (2023) 025109.

## PP-III-21

# Silver-Modified ZSM-5 Zeolite for Propene Aromatization: $^{13}C$ MAS NMR and FTIR Study of Alkene Transformation Mechanism

Lashchinskaya Z.N., Gabrienko A.A., Stepanov A.G.
*Boreskov Institute of Catalysis, Novosibirsk, Russia*
*lashchinskaya@catalysis.ru*

Silver-modified zeolites are very promising materials for a number of versatile chemical technologies due to their uncommon and appealing features such as light sensitivity, stability in water, and redox properties [1,2]. Among the potential successful applications of Ag-zeolites are photocatalytic decomposition of $NO_x$ and water splitting, methane valorization, trace ethene adsorption, and antimicrobial applications.

The activity of silver-modified zeolites in light alkene aromatization was discovered by Ono et al. [3]. It was found that Ag/H-ZSM-5 displayed 99 % conversion of 1-butene and 85 % selectivity for aromatic hydrocarbons. The authors suggested that silver cations were the active sites for alkene dehydrogenation, but the reaction mechanism was not offered. Recent data on ethene aromatization on Ag/H-ZSM-5 confirmed the promoting effect of $Ag^+$ sites on alkene dehydrogenation and aromatization [4,5]. However, despite the strong interaction between ethene molecules and silver ions, the reaction was reported to occur on Brønsted acid sites (BAS) contrary to the hypothesis of Ono et al. Therefore, the rationalization of the promoting effect of silver cations is still lacking. Moreover, the absence of detailed mechanistic data on alkene aromatization on silver-modified zeolites hinders the industrial application of such materials.

In this work, the reactions of propene on H-ZSM-5 and Ag/H-ZSM-5 have been monitored by $^{13}C$ MAS NMR and FTIR spectroscopy in order to understand the effect of silver cations on propene aromatization. The pathway of propene transformation has been found to change drastically upon zeolite modification with $Ag^+$ sites. The surface species characteristic of alkene aromatization on BAS, i.e. carbocation intermediates, have not been detected for propene reaction on Ag/H-ZSM-5. Also, light alkanes are not formed alongside aromatic compounds. Thus, a different aromatization mechanism has been suggested. First, propene is stabilized on $Ag^+$ sites in the form of π-complexes at various adsorption sites which survive heating up to 623 K. Further transformation at $T \geq 623$ K has been found to proceed mainly with the assistance of silver cations via the formation of allyl-like species. Namely, propene is dissociatively adsorbed on a $Ag^+\cdots O^-$ site, and the hydrocarbon chain growth is enabled by an alkene insertion into the metal-carbon bond of an allylic intermediate (Fig. 1). The dehydrocyclization of oligomeric unsaturated intermediates can be achieved either on BAS, or with the assistance of $Ag^+$ sites. The role of BAS also consists of minor alkene oligomerization at 296–573 K and the scrambling of the selective $^{13}C$-label in the propene molecule.

Hence, the mechanism of propene aromatization on silver-modified zeolites has been established, and the efficiency of this material for light alkene aromatization has been

rationalized. The results obtained aid in understanding the mechanisms and fundamental aspects of metal-modified zeolite catalysis, while also providing valuable information for the following applied research.

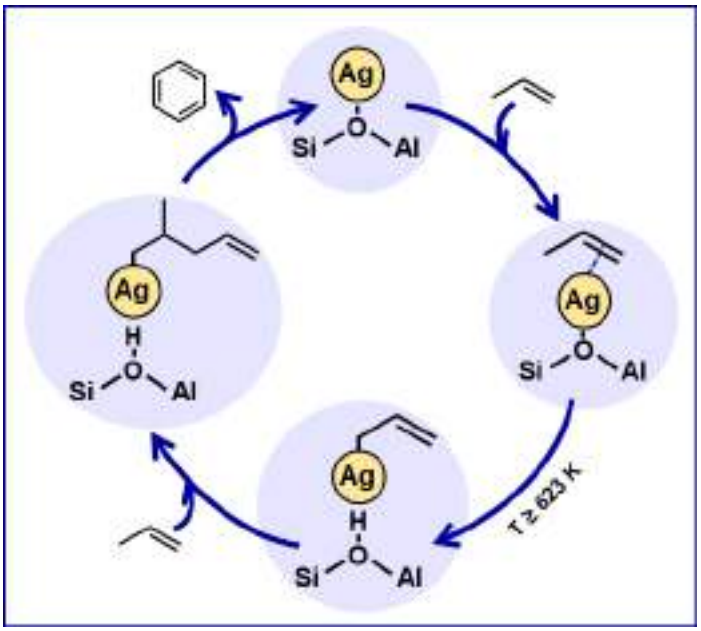


*Fig. 1. The schematic representation of propene transformation on Ag/H-ZSM-5*

**Acknowledgement:** This work was supported by the Russian Science Foundation, grant 21-73-10013.

**References:**

[1] T. Sun, K. Seff, Chem. Rev. 94 (1994) 857.
[2] Y. Ono, T. Baba, Phys. Chem. Chem. Phys. 17 (2015) 15637.
[3] Y. Ono, K. Osako, G. J. Kim, Y. Inoue, Stud. Surf. Sci. Catal. 84 (1994) 1773.
[4] M.-F. Hsieh, Y. Zhou, H. Thirumalai, L. C. Grabow, J. D. Rimer, ChemCatChem 9 (2017) 1675.
[5] E. A. Uslamin, H. Saito, N. Kosinov, E. Pidko, Y. Sekine, E. J. M. Hensen, Catal. Sci. Technol. 10 (2020) 2774.

## PP-III-22

# Nitrile Electrolyte Strategy for 4.9 V-Class Lithium-Metal Batteries Operating in Flame

H. Moon, S. -Y. Lee

*Department of chemical and Biomolecular Engineering, Yonsei University, 50 Yonsei-ro, Seodaemun-gu, Seoul, 03722, Republic of Korea*

*Hyunseok93@yonsei.ac.kr*

Challenges facing high-voltage/high-capacity cathodes, in addition to the longstanding problems pertinent to lithium (Li)-metal anodes, should be addressed to develop high-energy-density Li-metal batteries [1]. This issue mostly stems from interfacial instability between electrodes and electrolytes. Conventional carbonate- or ether-based liquid electrolytes suffer from not only volatility and flammability but also limited electrochemical stability window. Here, we report a nitrile electrolyte strategy based on concentrated nitrile electrolytes (CNEs) with co-additives. The CNE consists of high-concentration lithium bis(fluorosulfonyl)imide (LiFSI) in a solvent mixture of succinonitrile (SN)/acetonitrile (AN). The SN/AN solvent mixture is designed to ensure high oxidation stability along with thermal stability, which are prerequisites for high-voltage Li-metal cells. The CNE exhibits interfacial stability with Li metals due to the coordinated solvation structure. Lithium nitrate ($LiNO_3$) and indium fluoride ($InF_3$) are incorporated in the CNE as synergistic co-additives to further stabilize solid-electrolyte interphase (SEI) on Li metals. The resulting electrolyte (CNE + $LiNO_3$/$InF_3$) enables stable cycling performance in Li||$LiNi_{0.8}Co_{0.1}Mn_{0.1}$ and 4.9 V-class Li||$LiNi_{0.5}Mn_{1.5}O_4$ cells. Notably, the Li||$LiNi_{0.5}Mn_{1.5}O_4$ cell maintains its electrochemical activity at high temperature (100 °C) and even in flame without fire or explosion.

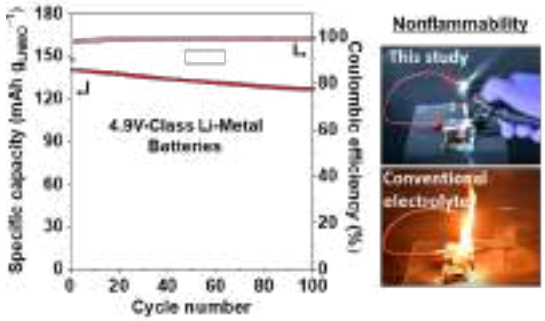


*Fig. 1. Cycling performance of the nonflammable pouch-type Li (50 µm) ||LNMO (1.5 mAh cm$^{-2}$) cell, in which the cells were cycled at charge/discharge current density of 0.1 C under an operating voltage of 3.5 −4.9 V.*

Acknowledgement: This work was supported by the U.S. Army Research Office (ARO) (W911NF-18-1-0016).

**References:**

[1] S.-J. Cho, D.-E. Yu, , T. P. Pollard, H. Moon, M. Jang, O. Borodin, S.-Y. Lee, iScience. 23 (2020) 100844.

## PP-III-23

# Enantioselective Voltammetric Sensor System Based on Mesoporous Carbon Black Carbopack X and Cyclopentadiene Derivatives for Determination of Clopidogrel Enantiomers

Nazyrov M.I., Yarkaeva Y.A.
*Ufa University of Science and Technology, Ufa, Russia*
*mnazyrov@list.ru*

For the recognition and determination of clopidogrel (Clp) enantiomers sensor system based on a glassy carbon electrode (GCE) modified by mesoporous carbon black Carbopack X (CpX) and cyclopentadiene derivatives - (1S)-2-cyclopenta-2,4-dien-1-yl-1,7,7-trimethylbicyclo[2.2.1]heptane (CPD1), (1S, 2S, 4R)-2-cyclopenta-1,3-dien-1-yl-1-isopropyl-4-methylcyclohexane (CPD2); 9-[(1S,2S,5R)-2-isopropyl-5-methylcyclohexyl]-9H-fluorene (CPD3) is developed. The electrochemical and morphological characteristics of the sensors are studied. Due to the unique properties of CpX, such as a large surface area and superconductivity, it was possible to achieve a mechanically stable and analyte-sensitive sensor layer from a combination of CpX and cyclopentadiene derivatives as chiral selectors [1]. Figure 1 shows differential pulse voltammograms (DPV) of clopidogrel enantiomers solutions. It can be seen that, the use of GCE/CpX/CPD1 makes it possible to obtain R- and S-Clp DPV's differing from each other both in peak currents and potentials ($I_{pR}/I_{pS}$=1.15, $\Delta E_p$= 20 mV). Similar results have been achieved on GCE/CpX/CPD2 ($I_{pR}/I_{pS}$=1.17, $\Delta E_p$= 18 mV) and GCE/CpX/CPD3 ($I_{pR}/I_{pS}$=1.22, $\Delta E_p$= 21 mV), what indicates the presence of cross-sensitivity to Clp enantiomers between sensors. It allows us to make a sensor system based on them with chemometric processing of analytical signals. The use of the sensor system leads to an increase in the probability of correctly recognized samples.

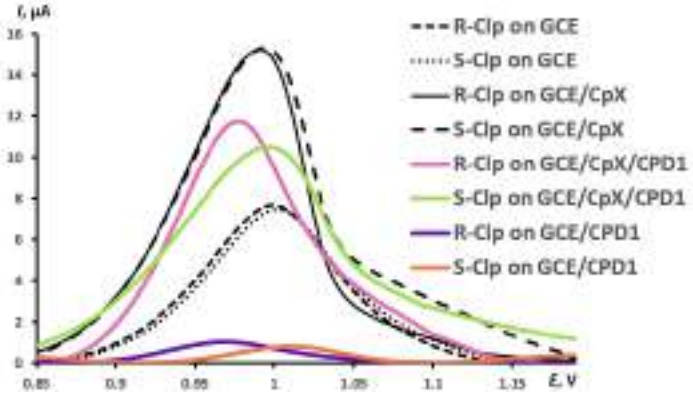


*Fig. 1. DPV's of R- and S-Clp on GCE, GCE/CpX, GCE/CpX/CPD1, GCE/CPD1.*

**Acknowledgement:** This work was supported by the Russian Science Foundation, grant 21-13-00169.

**References:**

[1] Y. Yarkaeva, M. Nazyrov, Y. Abdullin, P. Kovyazin, V. Maistrenko. Enantioselective voltammetric sensor based on mesoporous graphitized carbon black Carbopack X and fulvene derivative. Chirality. 2023; 1–12; DOI: 10.1002/chir.23563.

## PP-III-24

# Composite Material Based on Oriented Nickel Oxide Networks in a Polymer Matrix as an Active Element of a Conductometric Greenhouse Gas Sensor

Nizameeva G.R.[1,2], Lebedeva E.M.[1], Gainullin R.R.[1], Nizameev I.R.[1,3], Kadirov M.K.[1], Sinyashin O.G.[1]

*1 – Arbuzov Institute of Organic and Physical Chemistry, FRC Kazan Scientific Center of RAS, Kazan, Russia*

*2 – Kazan National Research Technological University, Kazan, Russia*

*3 – Kazan National Research Technical University named after A.N. Tupolev - KAI, Kazan, Russia*

*guliya.riv@gmail.com*

Air pollution with greenhouse gases is a widely discussed topic as one of the biggest risks to human health and the environment. Gaseous pollutants in focus include oxidizing gases such as nitrogen oxides ($NO_2$, NO, $N_2O$, $CO_2$, $SO_2$), and reducing gases such as carbon oxides (CO). These gases are either of the industrial origin or are produced by burning fossil fuels and biomass. Highly sensitive and selective gas sensors are needed to detect even small amounts of these harmful gases [1].

Gas sensors operate on different principles and various gas-sensing elements have been developed over the years. Conductometric sensors are among the simplest chemical sensors that are widely used to detect chemicals and greenhouse gases [2]. In recent years, organic semiconductors have been widely studied as active elements in such sensors.

Due to good electrical conductivity, high transparency, low redox potential, and commercial availability, poly(3,4-ethylene dioxythiophene):poly(styrene sulfonate) (PEDOT: PSS) is one of the most promising polymers for the development of active elements of gas sensors. Sensor materials based on PEDOT: PSS, in combination with low-dimensional metal structures, show promising results for various types of gases [3-5]. Composite materials can become promising elements in gas sensors since such combinations increase the sensitivity and selectivity with respect to target gases [6].

In this work, a pure PEDOT: PSS film and a PEDOT: PSS/oriented nickel fibers composite film were studied as the active element of a conductometric greenhouse gas sensor. Pure PEDOT: PSS films were spin-coated onto the surface of a glass substrate in a thin layer. And the application of the PEDOT: PSS/oriented nickel fibers composite film consisted of two stages. First, nickel fibers were deposited on the surface of a pre-cleaned glass substrate in the presence of a magnetic field to obtain an oriented network of fibers. Next, a thin film of PEDOT: PSS is deposited on the surface of the resulting network. As a result, a material was obtained consisting of a polymer matrix and oriented nickel fibers dispersed in this matrix.

The surface resistance of the obtained films, which indicates the sensitivity of the films to various gases, was studied by the Van der Pauw four-probe method in air and in an environment saturated with carbon dioxide. Pure PEDOT: PSS films in air showed a surface resistance value of 40 Ohm/sq., which increased to 70 Ohm/sq., that is, increased by 1.5 times

after exposure to carbon dioxide. The surface resistance of composite films PEDOT: PSS/oriented nickel fibers after exposure to carbon dioxide increased 4.4 times, from 3.15 Ohm/sq. to 14 Ohm/sq. The research results show a good response of composite films to carbon dioxide and the possibility of using these films as an active element in conductometric gas sensors.

**Acknowledgement:** The reported study was funded by the government assignment for FRC Kazan Scientific Center of RAS.

**References:**

[1] M. Farea, H. Alhadlaq, Z. Alaizeri, A. Ahmed, M. Sallam, M. Ahamed. 7 (2022) 22492-22499.
[2] M. Kitsara, D. Goustouridis, S. Chatzandroulis, M. Chatzichristidi, I. Raptis, T. Ganetsos, R. Igreja, C.J. Dias. 127 (2007) 186-192.
[3] Y. Seekaew, S. Lokavee, D. Phokharatkul, A. Wisitsoraat, T. Kerdcharoen, C. Wongchoosuk. 15 (2014) 2971-2981.
[4] Y. Zheng, D. Lee, H.Y. Koo, S. Maeng. 81 (2015) 54-62.
[5] B. Shiu, Y. Liu, Q. Yuan, C. Lou, J. Lin. 14 (2022) 1780.
[6] C. Tseng, Y. Chou, T. Hsieh, M. Wang, Y. Shu, M. Ger. 402 (2012) 45-52.

## PP-III-25

# Cathode Catalysts on Cobalt Coordination Bis-Diphosphine Complexes

Nizameeva G.R.[1,2], Nizameev I.R.[1,2], Kadirov D.M.[2], Strel'nik I.D.[1], Kadirov M.K.[1,2], Budnikova Yu.H.[1], Karasik A.A.[1], Sinyashin O.G.[1]

*1 – Arbuzov Institute of Organic and Physical Chemistry, Kazan, Russia*

*2 – Kazan National Research Technological University, Kazan, Russia*

*guliya.riv@gmail.com*

Cobalt complexes (Fig. 1) were obtained in situ by mixing the cobalt salt Co $(BF_4)_2$ with a non-coordinating tetrafluoroborate anion with the corresponding ligand in a ratio of 1:2.

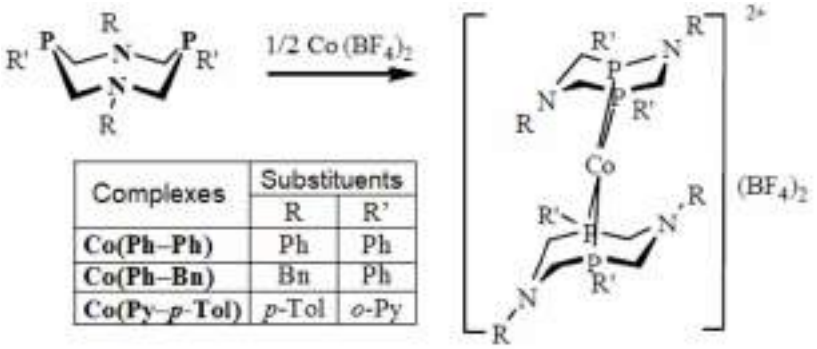


| Complexes | Substituents | |
|---|---|---|
| | R | R' |
| **Co(Ph–Ph)** | Ph | Ph |
| **Co(Ph–Bn)** | Bn | Ph |
| **Co(Py–*p*-Tol)** | *p*-Tol | *o*-Py |

*Fig. 1. Brief designations of cobalt complexes with cyclic aminomethylphosphines: 1 - $[Co(P^{Ph}{}_2N^{Ph}{}_2)_2](BF_4)_2$, 2 - $[Co(P^{Ph}{}_2N^{Bn}{}_2)_2](BF_4)_2$, 3 - $[Co(P^{Py}{}_2N^{p\text{-}Tol}{}_2)_2](BF_4)_2$*

Fig. 2A shows the results of an AFM study of the morphology of Co(Ph-Ph) aggregates on the surface of atomically smooth pyrolytic graphite. It can be seen that two types of structures are formed - flat disk-shaped ones with sizes from 50 to 300 nm and larger irregularly shaped associates with sizes of more than a micron (1 μm), which, apparently, are more complex systems formed from small aggregates. The Co(Ph-Bn) complex is characterized (Fig. 2B) by formations in the form of vesicles, including smaller particles. Vesicles are on average 2 μm in size, while internal particles are 200 nm in size. The surface aggregates of the Co(Py-*p*-Tol) complex (Fig. 2C) are individual particles whose sizes range from 20 to 50 nm.

The activity of the catalyst and the number (in brackets) of electrons transferred in one catalytic cycle increases in the series Co(Ph-Ph)/C (2.0 electrons), Co(Ph-Bn/C (2.1 electrons) and Co(Py-p-Tol)/C (2.7 electrons) This increase also correlates with the increase in the maximum power density observed in the diagnostic characteristics of proton-exchange membrane fuel cell (PEMFC) with cathodes based on Co (Ph-Ph) (5.69 mW), Co(Ph-Bn) (9.01 mW) and Co(Py - *p*-Tol) (10.17 mW) on carbon black (Vulcan XC-72) and Pt anodes on carbon black (Fig. 3).

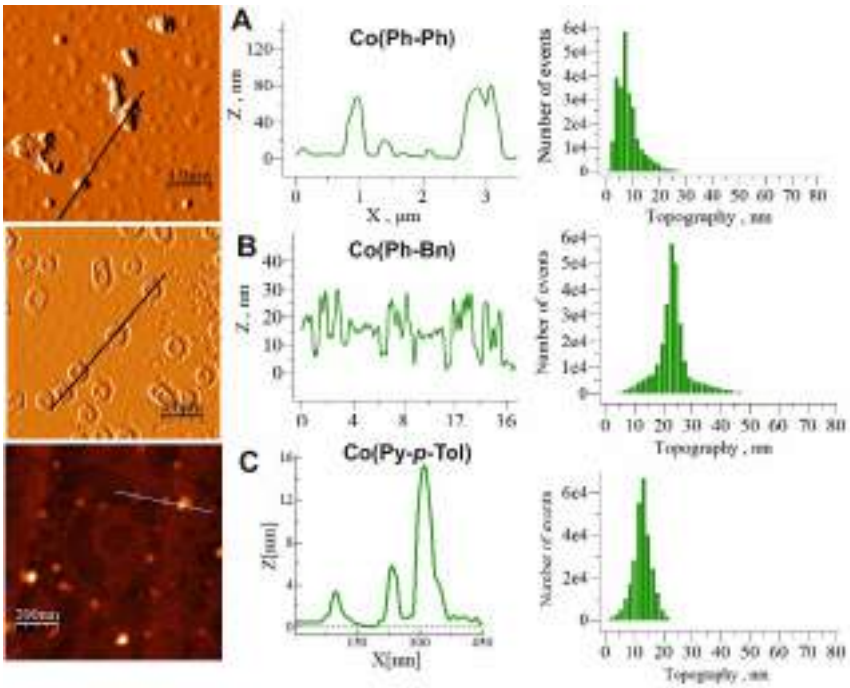


*Fig. 2. AFM images of morphologies on the surface of pyrolytic graphite (left), sections along black straight lines (in the center) and particle size distribution histograms (right) of cobalt complexes Co(Ph-Ph) (A), Co(Ph-Bn) ( B) and Co(Py-p-Tol) (C)*

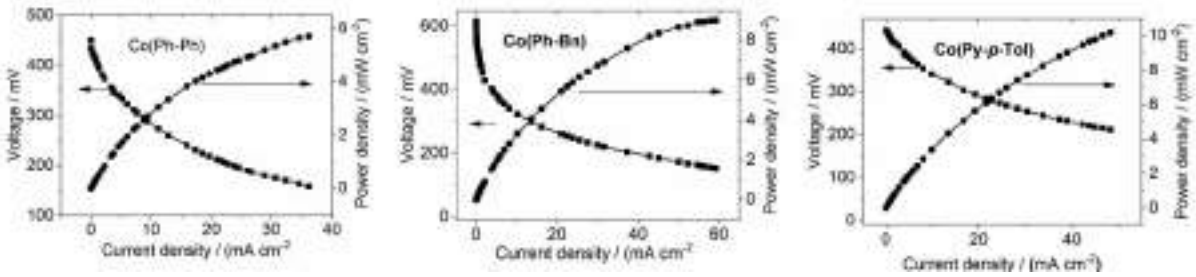


*Fig. 3. Diagnostic curves of PEMFC with cathodes based on Co (Ph-Ph) (A), Co (Ph-Bn) (B) and Co (Py - p-Tol) (C) on carbon black (Vulcan XC-72) and anodes on Pt on carbon black*

## PP-III-26

# Scalable Semi-Solid Batteries Based on Hybrid Polymer-Liquid Electrolytes

Kyeong-Seok Oh[1], Jung-Hui Kim[2], Se-Hee Kim[2], Dongrak Oh[2], Sun-Phil Han[2], Kwangeun Jung[3], Zhuyi Wang[4], Liyi Shi[4], Yongxiang Su[4], Taeeun Yim[3,*], Shuai Yuan[4,*], Sang-Young Lee[1]

*1 – Department of Chemical and Biomolecular Engineering, Yonsei University, 50 Yonsei-ro, Seodaemun-gu, Seoul 120-749, Republic of Korea*

*2 – Department of Energy Engineering, School of Energy and Chemical Engineering, Ulsan National Institute of Science and Technology (UNIST), Ulsan 44919, Korea*

*3 – Department of Chemistry, Incheon National University, 119 Academy-ro, Yeonsu-Gu, Incheon, 406-772 Republic of Korea*

*4 – Research Centre of Nanoscience & Nanotechnology, Shanghai University, 99 ShangDa Road, 200444 Shanghai, China*

*okc10@yonsei.ac.kr*

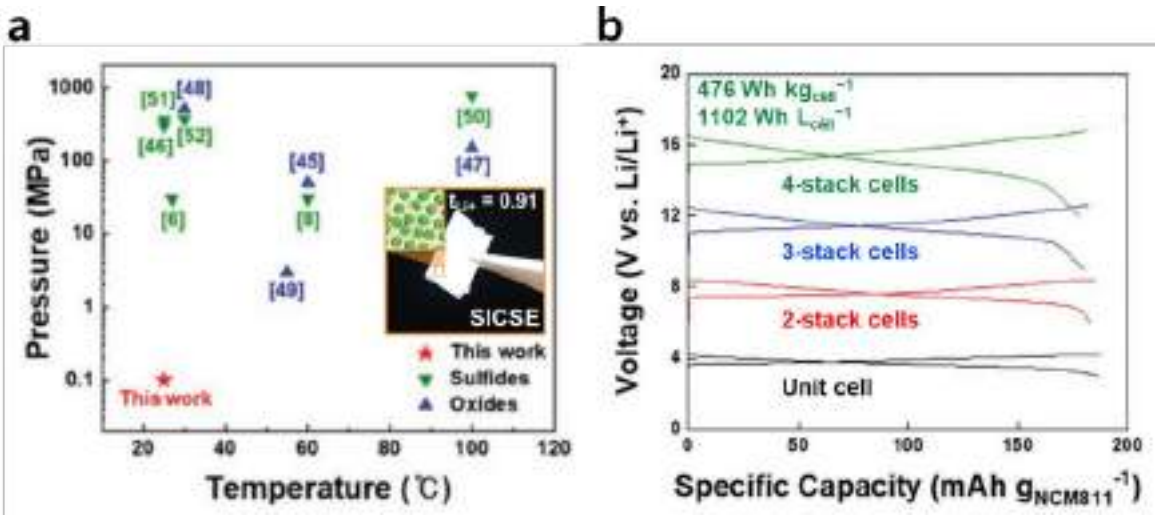


*Fig. 1. (a) Comparison in the cell operating conditions (pressure and temperature) between the SSLMBs and previously reported solid-state LMBs. (b) Bipolar configuration: charge/discharge voltage profiles of the bipolar SSLMBs with SICSE*

Despite their potential as post lithium-ion batteries, solid-state Li-metal batteries are struggling with insufficient electrochemical sustainability and ambient operation limitations. These challenges mainly stem from lack of reliable solid-state electrolytes. Here, a new class of single-ion conducting quasi-solid-state soft electrolyte (SICSE) for practical semi-solid Li-metal batteries (SSLMBs) is demonstrated. The SICSE consists of an ion-rectifying compliant skeleton and a nonflammable coordinated electrolyte. Rheology-tuned SICSE pastes, in combination with UV curing-assisted multistage printing, allow fabrication of seamlessly integrated SSLMBs (composed of a Li-metal anode and $LiNi_{0.8}Co_{0.1}Mn_{0.1}$ cathode) without undergoing high-pressure/high-temperature manufacturing steps. The single-ion conducting capability of the SICSE plays a viable role in stabilizing the interfaces with the electrodes. The resulting SSLMB full cell exhibits stable cycling performance and bipolar configurations with tunable voltages and high gravimetric/volumetric energy densities (476 Wh $kg_{cell}^{-1}$/1102 Wh

$L_{cell}^{-1}$ at four-stacked cells with 16.656 V) under ambient operating conditions, along with low-temperature performance, mechanical foldability, and nonflammability.

**Acknowledgement:** This work was supported by the Basic Science Research Program (2016R1A5A1009926, 2017M1A2A2087812, 2018M3D1A1058744, and 2021R1A2B5B03001615) through the National Research Foundation of Korea (NRF) grant by the Korean Government (MSIT) and Yonsei University Research Fund of 2020-22-0536.

**References:**

[1] R. Schmuch, R. Wagner, G. Hörpel, T. Placke, M. Winter, Nat. Energy 3 (2018) 267.
[2] M. Winter, B. Barnett, K. Xu, Chem. Rev. 118 (2018) 11433.
[3] J. Janek, W. G. Zeier, Nat. Energy 1 (2016) 16141.
[4] A. Manthiram, X. Yu, S. Wang, Nat. Rev. Mater. 2 (2017) 16103.

## PP-III-27

# $ZrO_2 \cdot nH_2O$ Prehistory: Regularities of the $ZrO_2$ Formation and the Influence on the Ni/$ZrO_2$ Catalyst Performance in Glycerol Steam Reforming

Omarov Sh.O.
*Ioffe Institute, Saint Petersburg, Russia*
*somarov@mail.ioffe.ru*

Zirconia is attracting attention as a potential catalyst support, which is already implemented in industry and promising processes. Precipitation of $ZrO_2 \cdot nH_2O$ is the most common way to obtain $ZrO_2$. A wide range of variable precipitation parameters requires the search and selection of the best conditions that allow to develop the porosity and functional composition of the surface, as well as to control the $ZrO_2$ phase composition. Therefore, studying the role of the $ZrO_2 \cdot nH_2O$ synthesis prehistory in the formation of $ZrO_2$ and catalysts based on it is still relevant. In particular, the prospect of replacing exhaustible natural gas with renewable feedstocks such as alcohols (glycerol or others) for obtaining $H_2$ or syngas during steam reforming requires a detailed study of the influence of support properties due to the more complex chemistry of catalytic process.

In continuation of previous works [1-3], the influence of the $ZrO_2 \cdot nH_2O$ precipitation conditions (precipitation with various bases; synthesis by thermal hydrolysis; aging of precipitated $ZrO_2 \cdot nH_2O$ under the mother liquor at elevated temperature and vessels made of various materials; different concentration of the $ZrOCl_2$ solution) on the formation of the above properties of $ZrO_2$ was studied. Ni catalysts were obtained on the basis of the synthesized $ZrO_2 \cdot nH_2O$, and their phase composition, reducibility, porosity, $Ni^0$ dispersion, as well as catalyst performance in the steam reforming of glycerol were studied.

Synthesis method, precipitation and aging pH and temperature have a fundamental effect on the $ZrO_2$ phases formed during subsequent heat treatment and the porosity of $ZrO_2 \cdot nH_2O$ and $ZrO_2$. Aging at pH=10 and 90 °C leads to the formation of m-$ZrO_2$ after heat treatment at 500 °C, as well as an increase in SSA (specific surface area) and pore volume of $ZrO_2 \cdot nH_2O$ (up to 400–420 $m^2/g$, 0.3–0.44 $cm^3/g$) and $ZrO_2$ (up to 140 $m^2/g$), which is associated with $ZrO_2 \cdot nH_2O$ dehydration and decomposition of dense aggregates of primary flat-like nanoparticles and micron-sized secondary $ZrO_2 \cdot nH_2O$ agglomerates. The size of t-$ZrO_2$ crystallites does not exceed 10 nm, which corresponds to the critical size of the t-$ZrO_2$–m-$ZrO_2$ transition in the absence of deformations and stresses in crystallites. The influence of the aging conditions developed with time and increased in the presence of the $Si^{4+}$ impurity. A change in the concentration of the $ZrOCl_2$ solution leads to the formation of a porous structure of $ZrO_2 \cdot nH_2O$ and $ZrO_2$ with different degrees of pore openness and width of their mouths. An extremal character of the dependence of the phase composition of $ZrO_2$ and the parameters of the porous structure on the $ZrOCl_2$ solution concentration with an extremum at 0.2–0.35 M was found. $ZrO_2 \cdot nH_2O$ was also synthesized by the thermal hydrolysis of the $ZrOCl_2$ solution with the subsequent sol neutralization to pH=9.5. A mixture of poorly

crystallized m-$ZrO_2 \cdot nH_2O$ (2.1–3.4 nm) in the form of spheroid agglomerates of 200 nm and X-ray amorphous $ZrO_2 \cdot nH_2O$ in the form shells depending on the duration of hydrolysis was obtained. For m-$ZrO_2$ crystallites, oriented intergrowth was observed, since the (-111) reflection was more intense than the (111) reflection. This method makes it possible to obtain m-$ZrO_2$ with developed porosity, as well as increased SSA up to 155 $m^2/g$. The study of the acid-base properties of the $ZrO_2$ surface by TPD of $NH_3$ and $CO_2$ made it possible to establish the predominant basicity of the surface, as well as a decrease in the specific amount of sorbed probe molecules with an increase in the content of t-$ZrO_2$.

Testing of synthesized Ni/$ZrO_2$ catalysts in glycerol steam reforming (T=600 °C, p=1 bar, glycerol/water=20/80 wt%, VHSV=72000 $h^{-1}$) showed that the observed activity and stability of these systems are determined by the combination of characteristics of porosity, surface acid-base properties, and dispersity of support crystallites and $Ni^0$, determined by the conditions for obtaining $ZrO_2 \cdot nH_2O$. Catalysts with a predominance of t-$ZrO_2$ in the phase composition after heat treatment due to the formation of a t-$ZrO_2$($Ni^{2+}$) solid solution, providing a high and stable $H_2$ yield, were obtained on the basis of $ZrO_2 \cdot nH_2O$ aged under the mother liquor at 90 °C (Fig. 1). An increase in the catalyst stability based on m-$ZrO_2$ was achieved by increasing the dispersity of the phase by varying the conditions for obtaining $ZrO_2 \cdot nH_2O$. The revealed effects are due to both the developed porosity of the support (better accessibility of metal nanoparticles, preventing blocking of pores by coke deposits) and the main properties of the surface, as well as an increase in the defectiveness of the $ZrO_2$ surface, which enhances the resistance to coking. The latter is similar to the effect of the introduction of alkaline earth or rare earth promoters.

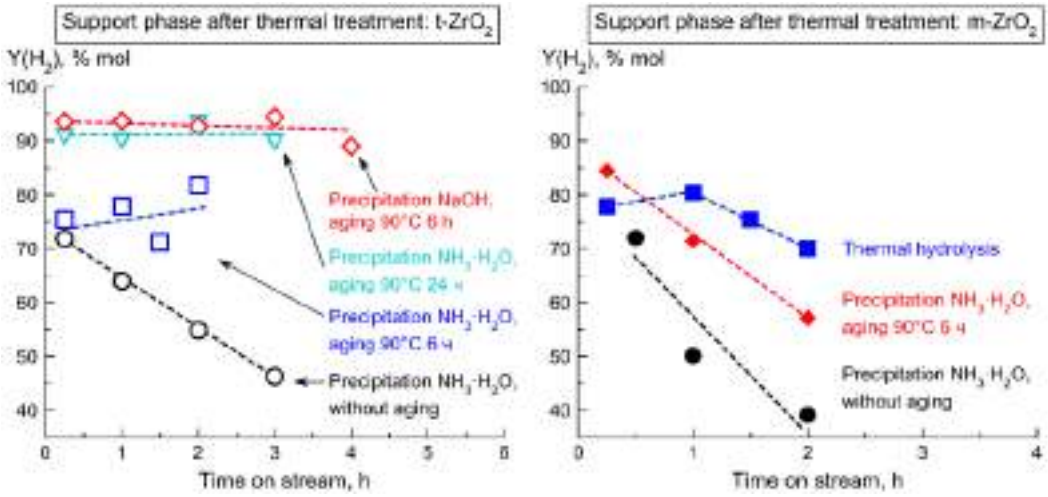


*Fig. 1. Comparison of $H_2$ yield stability over Ni catalysts supported on $ZrO_2$*

**References:**

[1] Sh.O. Omarov, N.A. Pakhomov, Catalysis in industry 13 (2021) 12–20.

[2] Sh.O. Omarov, Nanosystems: physics, chemistry, mathematics 12 (2021) 472.

[3] Sh.O. Omarov, D.A. Sladkovskiy, K.D. Martinson, M. Peurla, A. Aho, D.Yu. Murzin, V.I. Popkov, Appl. Catal. A 616 (2021) 118098.

## PP-III-28

# The Optimization of Ultrasonic Welding of PEEK Plates with CF Fabric Reinforcement by Neural Network Simulation

Panin S.V., Stepanov D.Yu., Alexenko V.O., Byakov A.V., Bogdanov A.AV.
*Institute of Strength Physics and Materials Science SB RAS, Tomsk, Russia*
*svp@ispms.ru*

The optimal mode for ultrasonic welding (USW) [1] of the "PEEK–ED (PEEK)–prepreg (PEI impregnated CF fabric)–ED (PEEK)–PEEK" lap joint was determined by artificial neural network (ANN) simulation (fig. 1), based on the sample of the experimental data expanded with the expert data set. The experimental verification of the simulation results showed that mode 10 (t = 900 ms, P = 1.7 atm, $\tau$ = 2000 ms) ensured the high strength properties and preservation of the structural integrity of the carbon fiber fabric (CFF). Additionally, it showed that the "PEEK–CFF prepreg–PEEK" USW lap joint could be fabricated by the "multi-spot" USW method with the optimal mode, which can resist the load per cycle of 50 MPa (the bottom HCF level). The USW mode, determined by ANN simulation for the neat PEEK adherends, did not provide joining both particulate and laminated composite adherends with the CFF prepreg reinforcement. The USW lap joints could be formed when the USW durations (t) were significantly increased up to 1200 and 1600 ms, respectively. In this case, the elastic energy is transferred more efficiently to the welding zone through the upper adherend.

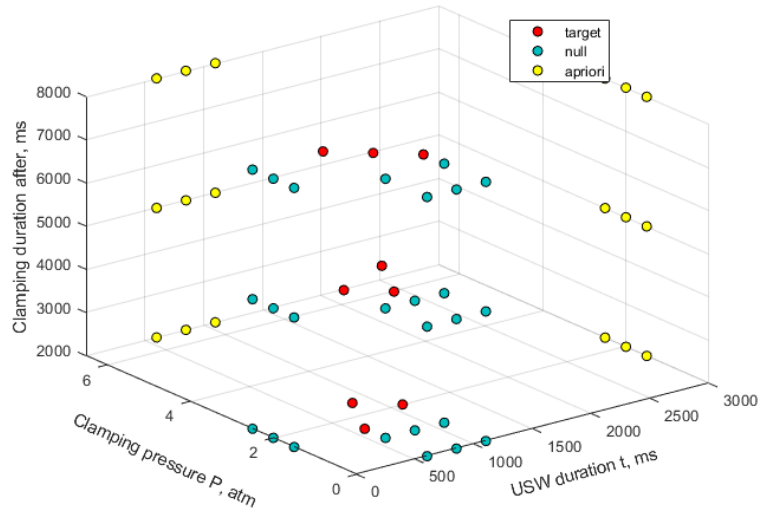


*The distribution of experimental parameters and selected priors for the USW results. The USW parameters used in the training sample: ● the experimental parameters; ● lap joints are not formed; ● the parameters when the prepreg is fractured.*

**Acknowledgement:** This work was supported by the Russian Science Foundation, grant 21-19-00741.

**References:**

[1] I.F. Villegas, I.F. Ultrasonic Welding of Thermoplastic Composites. Front. Mater. 2019, 6, 291.

## PP-III-29

# Double Perovskite Oxide $La_2NiMnO_6$ and $Sm_2NiMnO_6$ Thin Films as Promising Materials for Photovoltaics Applications

Kozlov S.S., Petrova V.I., Alexeeva O.V., Nikolskaia A.B., Karyagina O.K., Shevaleevskiy O.I.
*Emanuel Institute of Biochemical Physics, Moscow, Russia*
*balagur.sh@yandex.ru*

Perovskite solar cells (PSCs) have attracted significant research interest during the last decade due to their high power conversion efficiency (PCE) and simple fabrication process [1, 2]. In conventional PSCs, hybrid organic-inorganic materials with perovskite $ABX_3$ structure (A - $CH_3NH_3^+$, $HC(NH_2)_2^+$, $Cs^+$; B - $Pb^{2+}$, $Sn^{2+}$, X - I-, Br-, Cl-) are used as a light absorbing layers. State-of-the-art PSCs show power conversion efficiencies (PCE) over 25%, which makes them a possible alternative to conventional crystalline silicon solar cells [3]. At the same time, aforementioned hybrid perovskite materials are not stable and quickly degrade under high humidity conditions, light irradiation and increased temperatures [4]. Another issue is the presence of toxic lead, which could hamper the large-scale commercial application of hybrid PSCs [5]. Therefore, it is important to develop new stable, easily synthesizable and environmentally friendly perovskite materials used as the light absorbers in photovoltaic applications.

Recently it was reported that the rare earth based double perovskite oxides $R_2NiMnO_6$ (R = rare earth element) could be used as photoactive material in photovoltaics [6-8]. Such inorganic compounds as $La_2NiMnO_6$ (LNMO) and $Sm_2NiMnO_6$ (SNMO) are characterized by a narrow band gap, long carrier lifetime and good stability under increased temperatures [9]. However, the attempts to fabricate LNMO-based PSCs resulted in poor photovoltaic parameters, mostly due to the inferior morphology of $La_2NiMnO_6$ thin films and bad energy alignment between the photoactive layer and charge extracting layers in the PSC structure [8].

In this study, double perovskite oxide LNMO and SNMO thin films have been successfully prepared on glass substrates using the low cost sol-gel method. UV-Vis spectroscopy, scanning electron microscopy (SEM), X-ray diffraction (XRD) were used to examine the structural and optical characteristics of synthesized thin films. The optical band gap, crystalline structure and morphology of double perovskite oxide thin films have been studied to check the possibility of photovoltaic applications. It was shown that the band gap value for the LNMO films could be successfully tuned by varying the annealing conditions (temperature, heat duration).

The combination of the XPS and UPS methods was used to determine the positions of the energy bands for the LNMO film and construct energy diagrams for the $TiO_2$/LNMO interface. The obtained results showed that the conduction band (CB) of the LMNO perovskite at the $TiO_2$/LNMO interface is located 0.35 eV below the CB of the $TiO_2$ ETL. Such band energy structure reduces the efficient charge transfer across the LNMO/$TiO_2$ interface to the front FTO electrode and leads to the significant decrease of the solar cell performance. Therefore,

novel solar cell architectures should be provided in order to develop high-performance LNMO-based PSC.

In addition, double-perovskite LNMO and SNMO films were used as light absorbing layers in inorganic PSCs with the glass/FTO/NiO/LNMO(SNMO)/$SnO_2$/Ag cell architecture. Photovoltaic properties of developed PSCs were studied under standard AM1.5G illumination (1000 W/$m^2$) and LNMO-based PSCs showed PCE values above 1%. Obtained results on the structural and photoelectronic properties of LNMO and SNMO thin films will offer new opportunities to develop novel double perovskite oxide materials for photovoltaic applications.

**Acknowledgement:** This work was supported by the Russian Science Foundation, grant № 20-69-47124.

**References:**

[1] Y. Li, H. Xie, E. L. Lim, A. Hagfeldt, D. Bi, Adv. Energy Mater. 12 (2022) 2102730.
[2] A. Tejeda, W. C. H. Choy, E. Deleporte, M. Graetzel, J. Phys. D: Appl. Phys. 53 (2020) 070201.
[3] M. A. Green, E. D. Dunlop, G. Siefer, M. Yoshita, N. Kopidakis, K. Bothe, X. Hao, Prog Photovolt Res Appl. 31 (2023) 3–16.
[4] G. Schileo, G. J. Grancini, Mater. Chem. C. 9 (2021) 67-76.
[5] P. Su, Y. Liu, J. Zhang et al., J. Phys. Chem. Lett. 11 (2020) 2812-2817.
[6] Sheikh M.S., Ghosh D., Dutta A. et al. Mater. Sci. Eng. B. 2017, 226, P. 10-17.
[7] M. Kumar, A. Raj, A. Kumar, A. Anshul, Opt. Mater. 111 (2021) 110565.
[8] M.S. Sheikh, A.P. Sakhya, A. Dutta, T.P. Sinha, J. Alloy. Comp. 27 (2017) 238-245.
[9] X. Xu, Y. Zhong, Z. Shao, Trends Chem. 1 (2019) 410-424.

## PP-III-30

# Study of the Impact of the Lignite Carbonization Conditions on Mineral Phase Transformations

Popova A.N., Fyodorova N.I., Sozinov S.A., Ismagilov Z.R.
*Federal State Budget Scientific Centre «The Federal Research Center of Coal and Coal-Chemistry of Siberian Branch of the Russian Academy of Sciences», Kemerovo, Russia*
*h991@yandex.ru*

Nowadays, along with alternative energy sources, coal is still used to produce coke and as a fuel for coal-fired power plants despite the advancement of high technologies in the field of carbon materials. The main drawback of the burning coal is the formation of large quantities of ash requiring disposal. Moreover, ash mineral composition causes a high-temperature the corrosion of metals, resulting in the destruction of the heating surfaces, sealing surfaces of the exhaust valves, and gas turbine blades. Fly ash can, however, be used to extract materials for use in superior absorbers, structural, or dielectric materials.

The effect of the lignite carbonization conditions on mineral phase changes was investigated through an experimental study. It has been established that the carbonization process's temperature and gaseous atmosphere have an impact on the ash's component composition. We heated the lignite samples in the atmosphere air as well air/argon mixtures in a temperature range of 700 - 1000 °C. Such minerals as quartz ($SiO_2$), kaolinite ($Al_4Si_4O_{10}(OH)_8$), calcite ($CaCO_3$), and pyrite ($FeS_2$) are found in the mineral composition of lignite samples. In addition to pyrite, a hematite phase ($Fe_2O_3$) is observed when samples heated to a temperature of 700 °C. Further increase of heating temperature results in component composition transformation, pyrite transforms completely into hematite, while calcite transforms into lime (CaO). Kaolinite was found in carbonised samples up to a heating temperature of less than 900 °C, but it disappeared completely at higher temperatures, like 1000 °C. The phase of quartz is stable during all heat treatment modes. Kaolinite transforms into mullite when lignite samples heated at temperatures up to 1000 °C.

Also it was found that the mineral composition is unaffected when the air atmosphere is changed to an air/argon mixture during the carbonization process. The mineral components of samples studied undergo changes similar to the carbonization process that occurs in the atmosphere. The primary distinction is the appearance of the magnetite ($Fe_3O_4$) phase when lignite samples were heated to a temperature of 700 °C. Subsequent temperature increases results magnetite converted into hematite ($Fe_2O_3$).

## PP-III-31

# Applications of Detonation Nanodiamonds in the Design of Sensor Composites and Biosensors

Ronzhin N.O.[1], Posokhina E.D.[1], Mogilnaya O.A.[1], Baron A.V.[1], Puzyr A.P.[1], Baron I.J.[1,2], Burov A.E.[1], Bondar V.S.[1]

*1 – Institute of Biophysics SB RAS, Krasnoyarsk, Russia*

*2 – Voino-Yasenetsky State Medical University, Krasnoyarsk, Russia*

*roniol@mail.ru*

Nanomaterials are bringing significant advantages in the design of new analytical sensors or improvements of the existing devices. Nanomaterial application in environmental monitoring and biomedical analysing are demonstrating great potential in enhancing sensitivity, stability and in general performance of (bio)sensor devices. Detonation nanodiamonds (DNDs) possessing the chemically inert diamond core, mechanical strength, large specific surface area with the abundance of different chemically active groups and traces of metals [1] are an attractive nanomaterial applicable as structural, catalytic, and enzyme carrier element for the development of new (bio)sensing systems.

The report summarizes the results of many years of studies carried out at the Institute of Biophysics SB RAS (Krasnoyarsk) with modified DNDs possessing high colloidal stability in dispersion media [2,3] and aimed at studying their properties and applicability in the design of new (bio)sensing systems.

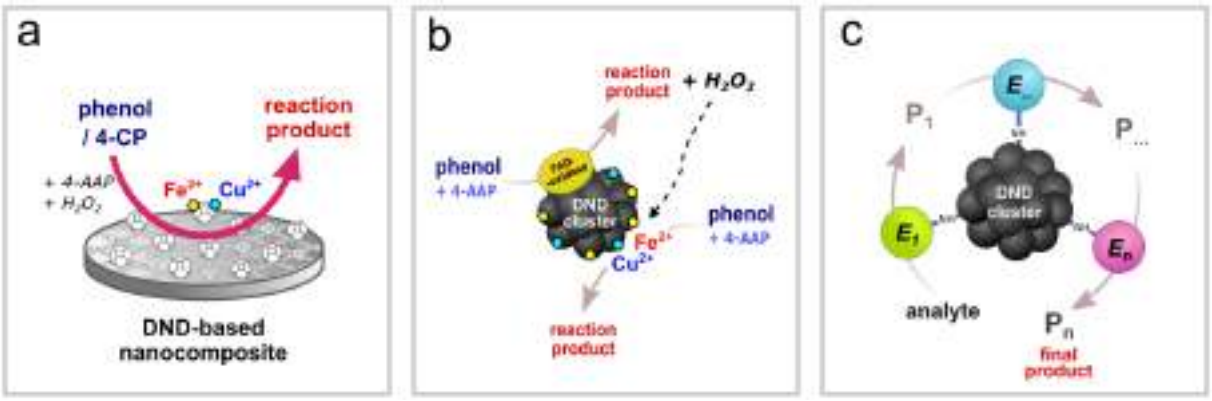


*Fig. 1. DND applications in the design of sensing and biosensing systems: DNDs as a structural and catalytic element of non-enzymatic sensor (a), DNDs as enzyme carrier and enhancer of catalytic effect (b), DNDs as a carrier for covalent immobilization of enzymes (c).*

DNDs can serve simultaneously as a structural element and as a catalyst with enzyme-like activity in the design of nanocomposites for analytical purposes. We have fabricated a novel composite material based on alumina nanofibers and DNDs for non-enzymatic detecting phenol in aqueous medium [4]. DNDs in the composite catalyse the co-oxidation reaction of phenol with 4-aminoantipyrine (4-AAP) in the presence of hydrogen peroxide to form a colored product (Fig. 1a). The catalytic effect of DNDs is realized due to the presence of copper and iron impurities on their surface [5]. The proposed composite ensures an easy-to-perform

colorimetric analysis for qualitative and quantitative determination of phenol in aqueous samples with linear response over a wide range of concentrations (0.5–106 μM). The composite is reusable sensor and retains its catalytic function for at least 1 year during storage at room temperature.

In further studies, we proposed a nanobioconjugate for the detection of phenol in aqueous medium based on the reaction of its co-oxidation with 4-AAP, but without the need to add exogenous $H_2O_2$ [6]. The nanobioconjugate was obtained by adsorption of FAD-containing enzyme from fungus *Neonothopanus nambi* onto DNDs. The enzyme of *N. nambi* is an oxidase with a mixed function: in the presence of phenol in an aqueous medium it first generates hydrogen peroxide, which is then used in the reaction of phenol co-oxidation with 4-AAP. In this case, the rate of formation of a colored reaction product in the presence of the DND–oxidase conjugate increases by an order of magnitude, compared with the reaction with a free enzyme. More effective product formation when the DND–oxidase complex is used proceeds in two ways: enzymatic (due to immobilized oxidase) and non-enzymatic (with the involvement of iron and copper ions on the DND surface) (Fig. 1b).

Our other studies demonstrated the application of DNDs in designing test-systems for determination of physiologically important blood substances. One (urease), two (glucose oxidase and peroxidase) and three (cholesterol esterase, cholesterol oxidase and peroxidase) enzymes have been covalently immobilized onto the surface of DNDs to construct nanobioconjugates for biochemical detection of urea, glucose, and total cholesterol, respectively (Fig. 1c) [7]. The experiments revealed that the obtained nanobioconjugates demonstrated a linear output of the reaction product over a wide concentration range of all analytes. The model biosensors were found to be suitable for repeated use and retain most of their activity after storage at 4 °C in deionized water for several months. Practical applicability of the designed testing systems was successfully demonstrated during determine glucose and cholesterol concentrations in human blood serum in comparative experiments with clinical biochemical analyzer as a reference tool.

**References:**

[1] N. Gibson, O. Shenderova, T.J.M. Luo, et al., Diam. Relat. Mater. 18 (2009) 620.
[2] V.S. Bondar, A.P. Puzyr, Phys. Solid State. 46 (2004) 716.
[3] A.P. Puzyr, V.S. Bondar, RU Patent № 2252192 (2005).
[4] N.O. Ronzhin, E.D. Posokhina, E.V. Mikhlina, et al., J. Nanopart. Res. 23 (2021) 199.
[5] N.O. Ronzhin, A.P. Puzyr, V.S. Bondar, J. Nanosci. Nanotechnol. 18 (2018) 5448.
[6] N.O. Ronzhin, O.A. Mogilnaya, E.D. Posokhina, et al., Dokl. Biochem. Biophys. 499 (2021) 220.
[7] N. Ronzhin, A. Baron, A. Puzyr, et al., Mod. Clin. Med. Res. 2 (2018) 7.

## PP-III-32

# Effect of Nb Doping on the Hydrophilicity of $TiO_2$ Thin Films

Rudakova A.V.[1], Bakiev T.V.[1], Mikheleva A.Yu.[1], Emeline A.V.[1,2], Bulanin K.M.[1,2]

*1 – Laboratory "Photoactive nanocomposite materials", Saint Petersburg State University, Saint Petersburg, Russia*

*2 – Department of Physics, Saint Petersburg State University, Saint Petersburg, Russia*

*aida.rudakova@spbu.ru*

Self-cleaning materials have considerable attention for both their unique properties and practical applications in energy and environmental areas. Since the effect of surface photoinduced superhydrophilicity was discovered in 1997 (Fig. 1) the $TiO_2$ based photocatalysts have gained considerable attention [1-2]. Here we report the results of a study of the wettability of Nb-doped $TiO_2$ thin films.

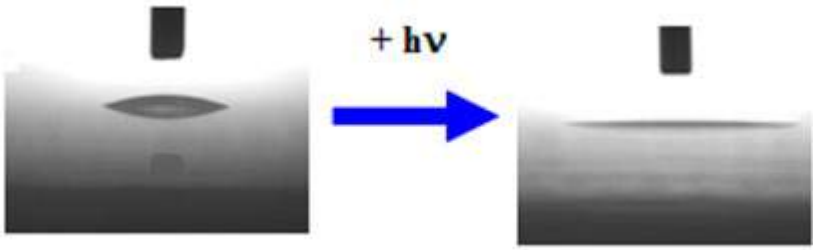


*Fig. 1. $TiO_2$ nanocoating: UV-induced superhydrophilic conversion*

The x-Nb-$TiO_2$ films were prepared by dip-coating method from x-Nb-$TiO_2$ sols where the niobium content (x) was taken as 0.0, 0.2, 0.4, 0.6, 0.8, and 1.0 at.%. The chemical and phase composition and surface morphology of the synthesized films were characterized by XRD, XPS, AFM, EDX, and SEM methods. No additional microstrain was detected in the doped films compared to the undoped film. The hydrophilicity of the surface and surface free energy of films were studied using an optical tensiometry. The work function characteristics were measured by Kelvin probe method for all nanocoatings in the ambient conditions. The composition of the hydroxyl-hydrated layer depending on the dopant concentration was studied for the corresponding x-Nb-$TiO_2$ powders by IR spectroscopy. The acidity of films' surfaces was evaluated by pH-metry methods and IR spectroscopic study of CO adsorption. During the photoinduced hydrophilicity study, the x-Nb-$TiO_2$ thin films were photoexcited in the $TiO_2$ intrinsic absorption region using a Hg lamp with a water filter and a UFS-2 filter (irradiance at 365 nm was 0.5 mW/cm$^2$).

Figure 2 presents dependences of hydrophilic and electronic properties of x-Nb-$TiO_2$ thin films and UV-induced hydrophilic conversion on dopant concentration. The results obtained are discussed in terms of changes in the Fermi level position and composition of hydroxyl-hydrated layer.

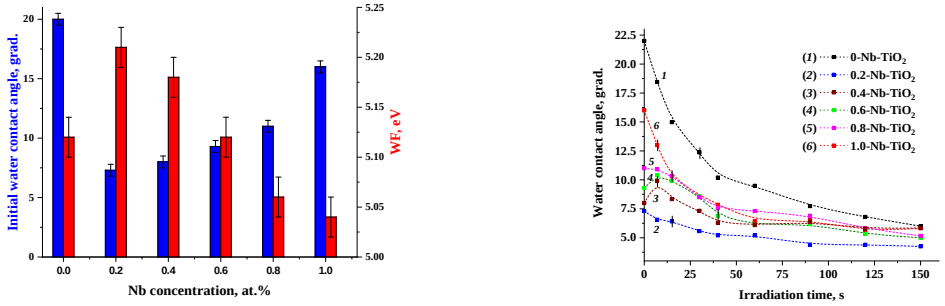


*a* *b*

*Fig. 2. x-Nb-$TiO_2$ thin films: (a) Initial water contact angle vs. work function; (b) UV-induced water contact angle alteration*

**Acknowledgement:** This work was financially supported by the Russian Science Foundation, grant 23-22-00161. The authors are also thankful to the Research Park at the Saint Petersburg State University for helpful assistance in the preparation and characterization of the samples.

**References:**

[1] R. Wang, K. Hashimoto, A. Fujishima, *et al.*, Nature 388 (1997) 431.
[2] A.V. Rudakova, A.V. Emeline, Colloid J. 83 (2021), 20.

## PP-III-33

# Enantioselective Voltammetric Sensors Based on Functionalized Fullerene for Antibiotics Determination

Zagitova L.R., Abramov I.A., Gainanova S.I.
*Ufa University of Science and Technology, Ufa, Russia*
*kabirova.lian@yandex.ru*

Enantioselective analysis of compounds is of great importance for understanding the processes occurring in living organisms, since many of them, including amino acids, proteins, and sugars, are involved in chiral interactions. The problem of recognition and determination of optical isomers is relevant because many drug compounds exist in the form of two or more spatial isomers, the pharmacological activity of which is often associated with the action of only one of them. Clinical trials show that the use of enantiopure drugs reduces side effects and thus increases their effectiveness. There is a growing interest in the chiral analysis of antibacterial compounds, especially in the determination of trace amounts of an analyte in animal source foods, which provides valuable information about their safety [1]. Unlike chiral chromatography and capillary electrophoresis, enantioselective voltammetric sensors can be easily adapted to analyze a wide range of substances and included in portable devices that allow screening of biological samples of complex composition.

The enantioselectivity of the response signal is achieved by including a chiral selector in the sensitive layer of the sensor. There are many available compounds and materials of natural or synthetic origin that can be used as chiral selectors: amino acids, metal amino acid complexes, derivatives of polysaccharides, polymers with molecular imprints, chiral electrically conductive polymers, supramolecular and self-assembling structures, cyclodextrins, crown-ethers, calixarenes and others [2-5]. Also, proteins and polypeptides have been used as selectors. The researchers attribute the chiral properties of these compounds to their structure, consisting of L-amino acids and an active center programmed by evolution for exclusively natural L-molecules. The processes of chiral recognition of enantiomers using proteins are accompanied by electrostatic and hydrophobic interactions, hydrogen bonds with the formation of diastereomeric complexes. In this case, the binding specificity is due to the interaction of enantiomers with the receptor sites of proteins immobilized on the sensor surface. Among the factors determining the success or failure of the analysis are the steric loading of the chiral center of the protein molecule and the flexibility of its structure near the chiral center. Currently, our study is aimed at design new sensors based on functionalized fullerenes with active centers for the chiral analysis of levofloxacin and chloramphenicol. The structure of the active center will be similar to protein binding sites, however, in terms of the number of active centers to the molecular weight, the proposed material will be many times superior to natural polymers. Researchers also note the special properties of fullerene as a sensor material, such as high surface to volume ratio,

biocompatible, insoluble in aqueous medium, a large number of equivalent reaction centers, easy functionalization [6].

It is assumed that the methods of organic synthesis will make it possible to program the selector for a certain configuration of the optical center of the analytes, which will ensure high selectivity and sensitivity of the sensors. The implementation of this idea will provide fundamental information about the features of the synthesis of new chiral sensor materials based on functionalized fullerenes and the design of sensors, evaluate the possibilities of their using in the determination of antibiotics in biological fluids and animal source foods.

**Acknowledgement:** This work was supported by the Russian Science Foundation № 22-73-00073, https://rscf.ru/en/project/22-73-00073/.

**References:**

[1] V.N. Maistrenko, G.A. Evtyugin. Enantioselective sensors / M.: Laboratoriya znanij, 2022. – 259 p. ISBN 978-5-93208-324-6.
[2] L.R. Zagitova, V.N. Maistrenko, Y.A. Yarkaeva, V.V. Zagitov, R.A. Zilberg, P.V. Kovyazin, L.V. Parfenova, Novel chiral voltammetric sensor for tryptophan enantiomers based on 3-neomenthylindene as recognition element, J. Electroanal. Chem. 880 (2021) 114939.
[3] R.A. Zilberg, V.N. Maistrenko, L.R. Zagitova, V.Y. Guskov, D.I. Dubrovsky, Chiral voltammetric sensor for warfarin enantiomers based on carbon black paste electrode modified by 3,4,9,10-perylenetetracarboxylic acid, J. Electroanal. Chem. 861 (2020) 113986.
[4] L. Zagitova, Y. Yarkaeva, V. Zagitov, S. Gainanova, V. Maistrenko. Voltammetric chiral recognition of naproxen enantiomers by N-tosylproline functionalized chitosan and reduced graphene oxide based sensor// J. Electroanal. Chem. 922 (2022) 116744.
[5] Y. Yarkaeva, V. Maistrenko, D. Dymova, L. Zagitova, M. Nazyrov. Polyaniline and poly(2-methoxyaniline) based molecular imprinted polymer sensors for amoxicillin voltammetric determination // Electrochim. Acta. 433 (2022) 141222.
[6] N.P. Shetti, A. Mishra, S. Basu, T.M. Aminabhavi. Versatile fullerenes as sensor materials// Mater. Today Chem. 20 (2021) 100454.

## PP-III-34

# A Microgrid-Patterned Silicon Electrode as an Electroactive Lithium Host

Myeong-Hwa Ryou, Sang-Young Lee
*Department of Chemical and Biomolecular Engineering, Yonsei University, Seoul, Republic of Korea*
*rmh902@yonsei.ac.kr*

Lithium (Li) hosts, which can electrochemically accommodate Li in preformed pores of three-dimensional frameworks, have been investigated as an advanced electrode architecture for high-energy-density Li-metal batteries [1]. However, most of the previous studies on Li hosts utilized electrochemically inert materials for their framework constituents, resulting in the undesired loss of gravimetric/volumetric energy densities of the resulting batteries [2]. Here, we present an electroactive Li host based on a microgrid-patterned Si electrode (denoted as MPS host). The MPS host is fabricated using a microscale direct ink writing technique. The lithiophilicity, electronic conductivity, and porous structure of the MPS host are customized to ensure the preferential direction of Li-ion flux and electron conduction into the ordered pore space, while providing the redox capacity. The resulting MPS host enables a stepwise sequential Si lithiation/delithiation (from the Si in the microgrid frameworks) and Li plating/stripping (inside the pore space between the microgrids) reaction, verifying its unique behavior as an electroactive Li host. In addition, a full cell assembled with the MPS host and $LiNi_{0.8}Co_{0.1}Mn_{0.1}O_2$ (NCM811) cathode (areal capacity = 3.8 mAh $cm^{-2}$) exhibits high cell energy densities (644 Wh $kg_{cell}^{-1}$/1,538 Wh $L_{cell}^{-1}$) and reliable cyclability.

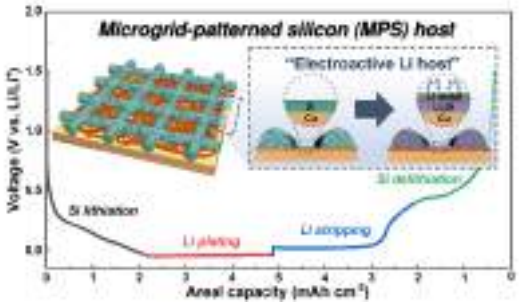


*Fig. 1. Schematic illustration depicting the structural and electrochemical features of the microgrid-patterned silicon (MPS) host.*

**Acknowledgement:** This work was supported by the Basic Science Research Program (2021R1A2B5B03001615 and 2021M3D1A2043791) through the National Research Foundation of Korea (NRF) funded by the Ministry of Science, ICT and future planning, and the Technology Innovation Program (20012216) funded by the Ministry of Trade, Industry & Energy (MOTIE).

**References:**

[1] J. Liu, Z. Bao, Y. Cui, E. J. Dufek, J. B. Goodenough, P. Khalifah, Q. Li, B. Y. Liaw, P. Liu, A. Manthiram, Y. S. Meng, V. R. Subramanian, M. F. Toney, V. V. Viswanathan, M. S. Whittingham, J. Xiao, W. Xu, J. Yang, X. Q. Yang, J. G. Zhang, Nat. Energy 4 (2019) 180—186.
[2] J. Pu, J. Li, K. Zhang, T. Zhang, C. Li, H. Ma, J. Zhu, P. V. Braun, J. Lu, H. Zhang, Nat. Commun. 10 (2019) 1896.

## PP-III-35

# Electrode-Customized Separator Membranes Based on Self-Assmbled Chiral Nematic Liquid Crystalline Cellulose Nanocrystals as a Natural Material Strategy for Sustainable Li-Metal Batteries

Ji Young Seo, Sang-Young Lee
*Department of Chemical and Biomolecular Engineering, Yonsei University 50 Yonsei-ro, Seodaemun-gu, Seoul 120-749, Republic of Korea*
*2021313105@yonsei.ac.kr*

Despite their enormous potential as a high-energy-density power source, practical applications of Li-metal batteries have been plagued mainly by poor electrochemical longevity. Here, we present an electrode-customized separator (EC separator) based on self-assembled chiral nematic liquid crystalline cellulose nanocrystal (LC–CNC) as a natural material strategy to simultaneously address the electrochemical reversibility issues of both Li-metal anodes and high-capacity cathodes in Li-metal full cells. The EC separator (thickness ~ 10 mm) comprises a 3-glycidyloxypropyl trimethoxysilane (GPTMS)-modified LC–CNC layer on a polyethylene (PE) separator support layer. The LC–CNC layer enables facile/uniform $Li^+$ flux toward Li-metal anodes owing to its ordered nanoporous channels and nanofluidic ion migration effect, thus improving Li plating/stripping cyclability. The GPTMS of the LC–CNC layer chelates heavy metal ions dissolved from high-capacity $LiNi_{0.8}Co_{0.1}Mn_{0.1}O_2$ (NCM811) cathodes, thereby enhancing structural stability of the cathodes. The resulting EC separator enables a Li-metal full cell to improve the volumetric energy density (1016 Wh $L_{cell}^{-1}$), cycling retention (84% after 100 cycles vs. 0% for the pristine PE separator), and dimensional stability of the Li-metal anode under constrained cell conditions (thin Li-metal anode (20 mm)/high-capacity NCM811 cathode), which outperform those of previously reported synthetic material-based separators for Li-metal full cells.

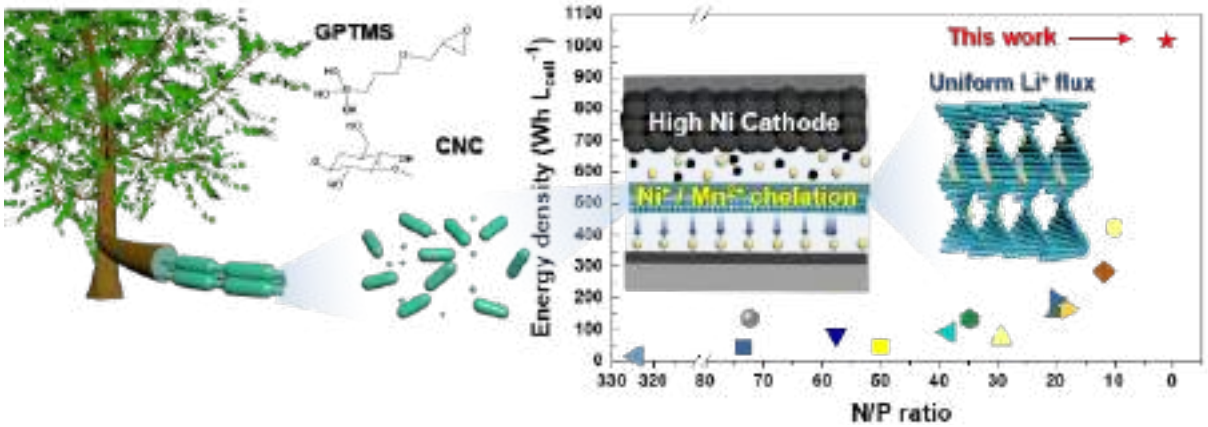


*Fig. 1. Schematic illustration depicting the fabrication of LC-CNC separator (left) and volumetric cell energy density (Wh $L_{cell}^{-1}$) as a function of the N/P ratio (EC separator Vs. previsously reported separators for Li-metal full cells)*

**Acknowledgement:** This work was supported by the National Research Foundation of Korea (NRF) grant funded by the Korea government (MSIT) (2021R1A2B5B03001615 and 2021M3D1A2043791). This work was supported by Electronics and Telecommunications Research Institute (ETRI grant funded by the Korea government (21ZB1200), the development of the technologies for ICT Material, components and Equipment) and the R&D Program for Forest Science Technology (Project No. "FTIS 2021354D10-2123-AC03) provided by Korea Forest Service (Korea Forestry Promotion Institute) and Technology Innovation Program (20010960) funded by the Ministry of Trade, Industry & Energy (MOTIE, Korea).

## PP-III-36

# Effect of Ag/$TiO_2$ Core/Shell Nanostructures on the Photocatalytic Activity of the $TiO_2$/rGO Nanocomposite Material

Seliverstova E., Serikov T., Sadykova A., Ibrayev N.
*Institute of Molecular Nanophotonics, Buketov Karaganda University, Karaganda, Kazakhstan*
*genia_sv@mail.ru*

Titanium dioxide ($TiO_2$), due to its physicochemical properties, is one of the most accessible and attractive photocatalysts [1, 2]. In order to improve its photocatalytic properties, nanocomposite materials with graphene derivatives are synthesized [3]. The problem of limited absorption of $TiO_2$ in the visible region can be solved by addition of metal nanoparticles (NPs) with localized plasmon resonance effect.

In the present work, we studied the effect of Ag/$TiO_2$ core/shell plasmonic nanostructures on the photocatalytic activity of a nanocomposite material based on $TiO_2$ and reduced graphene oxide (rGO).

The nanocomposite was obtained by hydrothermal synthesis according to the procedure of Ref. [3]. Ag/$TiO_2$ nanostructures are consisted of Ag NPs with an average diameter of 26 nm and a $TiO_2$ shell of 10 nm thick, which were obtained by the method described in [4]. Ag/$TiO_2$ NPs were added to the prepared nanocomposite at concentrations of 0.1, 0.3 and 0.5 wt%.

The photocatalytic activity of the samples was evaluated by measuring the magnitude of the photoinduced current in a standard three-electrode cell using a CS350 potentiostat/galvanostat with the determination of an EIS analyzer (Corrtest Instr.). Measurements have shown that the presence of Ag/$TiO_2$ nanostructures leads to the increase in photocurrent values in 2.8 times compared to films without plasmon NPs. The highest values were recorded for $TiO_2$/rGO films with an Ag/$TiO_2$ concentration of 0.3 wt%. From the impedance spectroscopy data (potential/galvanostat CS350, Corrtest Instr.), it was found that nanocomposite films doped with Ag/$TiO_2$ have a lower values of resistance to charge carrier transport, as well as resistance associated with recombination processes. In addition the lifetime of charge carriers was increased in the presence of plasmon NPs.

**Acknowledgement:** This research was funded by the Science Committee of the Ministry of Education and Science of the Republic of Kazakhstan, grant no. AP14871956.

**References:**

[1] Fujishima A., Honda K., Nature 238 (1972) 37.
[2] Gadgil T., Ibrayev N., Nuraje N., Eds: Colmenares JC and Xu Y-J. Photocatalytic Water Oxidation, Springer (2016) 33.
[3] Zhumabekov A., Ibrayev N., Seliverstova E., Theoret. Experiment. Chem. 55 (2020) 6.
[4] Afanasyev D., Ibrayev N., Alikhaidarova E., Bull. Karaganda- Univ. Phys. Series., 3(2019) 8.

## PP-III-37

# The Manufacturing of Fire-Extinguishing Powder Materials with Specific Morphology and Hydrophobicity of Ammonium Phosphates Particles

Shamsutdinov A.S.[1], Valtsifer I.V.[1], Huo Y.[2]
*1 – Institute of Technical Chemistry UB RAS, Perm, Russia*
2 – *College of Aerospace and Civil Engineering, Harbin Engineering University, Harbin, China*
*shamsutdinov.a@itcras.ru*

Fire-extinguishing powders (FEP) are the most effective and versatile extinguishing materials which have high specific fire-extinguishing efficiency and capable to extinguish all classes of fire. Nowadays, the main extinguishing component of FEP are ammonium phosphate salts. Their main disadvantages are high hygroscopicity and caking. In addition, powder materials of these salts are obtained by grinding granules that leads to an irregular and angular shape of microsized particles and strong cohesion between them.

Within the framework of this research, we used the spray drying method for the synthesis of FEP extinguishing components. Ammonium phosphates emulsion was obtained using heat-resistant (up to 200 °C) surfactants and a hydrophobizing agent based on polysiloxanes, the aqueous emulsions of which make it possible to impart hydrophobic properties to the surface of synthesized particles. The process of spraying drops of emulsion with hot air at a certain temperature and pressure is combined with the subsequent rapid evaporation of water and the formation of powder material particles.

This method makes it possible to obtain polyfunctional ammonium phosphate particles having a spherical shape (Fig. 1A) and a given size distribution (Fig. 1B). The use of synthesized particles of the extinguishing component in the manufacturing of FEP will enhance their flowability and efficiency of combustion processes inhibition, increase the ability to water repellency and extend the shelf life.

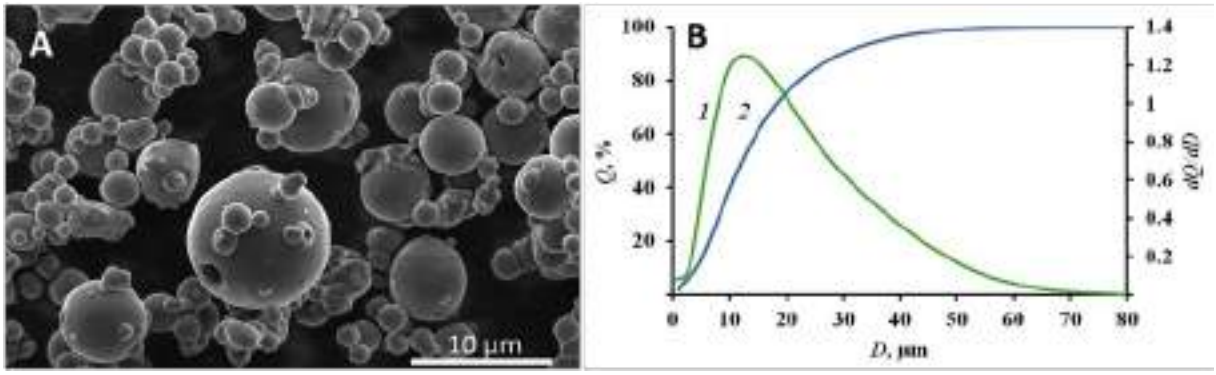


*Fig. 1. SEM images of synthesized ammonium phosphates particles (**A**) and their size distribution (**B**), where 1— differential distribution, 2—integral distribution.*

**Acknowledgement:** The reported study was supported by the Government of Perm Krai, research project No C-26/543.

## PP-III-38

# Coproduction of Hydrogen and Carbon Nanomaterials by Catalytic Decomposition of Methane-Hydrogen Mixtures: Experimental and Simulation Results

Shelepova E.V., Maksimova T.A., Bauman Yu.I., Mishakov I.V., Vedyagin A.A.
*Boreskov Institute of Catalysis, Novosibirsk, Russia*
*shev@catalysis.ru*

Hydrogen production rises up continuously due to its growing demand. Methane is the main component of natural gas, which makes it a promising source of hydrogen. The existing hydrogen production technologies are associated with a number of hardship and disadvantages. Thus, the steam reforming of natural gas is characterized by a relatively low hydrogen yield and a poor quality of the produced hydrogen, which requires an additional treatment and purification from sulfurous gas and $CO_2$ [1-2]. The thermal pyrolysis of methane is an alternative approach to producing hydrogen without the $CO_2$ formation, but this process requires high temperatures (800–900 °C), which makes it energy-intensive [3]. The process of methane catalytic pyrolysis permits one to obtain the hydrogen along with nanostructured carbon at significantly lower temperatures. In this case, the yield of both the target products can be increased by using various catalysts [4].

In the present research, the kinetics of catalytic decomposition of methane–hydrogen mixture over NiO-CuO/$Al_2O_3$ catalyst was studied using a flow-through quartz reactor equipped with McBain balances. It was shown that the presence of an excess of hydrogen in the composition of the reaction mixture is necessary to provide the long-term activity and the stable operation of the catalyst. A temperature range of 600–625 °C was found to be an optimum in terms of the higher methane decomposition rate and the higher carbon yield (Fig. 1). Within this range, the latter exceeds 30 $g/g_{cat}$ [5]. Note that the maximum carbon yield was reached with a hydrogen inlet concentration of 13 vol.%. According to the results of electron microscopy, the solid product is mainly represented by carbon filaments of different lengths and diameters. The material possesses the high values of specific surface area (120–170 $m^2/g$) along with relatively low porosity (0.16–0.18 $cm^3/g$).

In order to describe the methane decomposition process correctly, the search of an appropriate kinetic model is of primary importance. Here, the kinetic model based on the dissociative adsorption of methane was used for the mathematical modeling [6]. The kinetic constants providing the best fitting of the experimental points were obtained and the verification of the kinetic model was performed. Thus, in order to optimize the process parameters for catalytic decomposition of methane–hydrogen mixture, the mathematical modelling was carried out using the kinetic model along with the defined constants. The non-

stationary mathematical model was for this purpose. To solve the system of equations, a COMSOL Multiphysics® package, version 5.4 was applied.

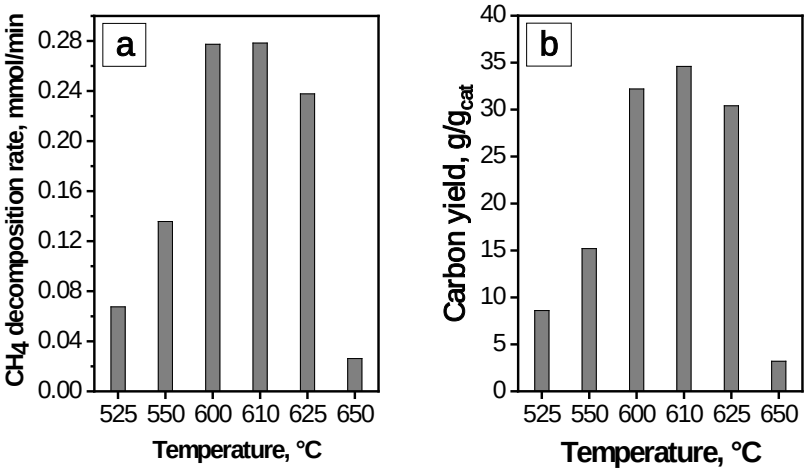


*Fig. 1. Catalytic decomposition of methane-hydrogen mixture over NiO-CuO/$Al_2O_3$ catalyst at different temperatures: (a) methane decomposition rates; (b) carbon yields*

**Acknowledgement:** This work was supported by the Ministry of Science and Higher Education of the Russian Federation within the governmental order for Boreskov Institute of Catalysis (project AAAA-A21-121011390054-1).

**References:**

[1] G. Franchi, M. Capocelli, M. De Falco, V. Piemonte, D. Barba, Membranes 10 (2020) 10.
[2] D. Pashchenko, Energy 251 (2022) 123854.
[3] G. Fau, N. Gascoin, J. Steelant, J. Anal. Appl. Pyrolysis 108 (2014) 1-11.
[4] A.M. Amin, E. Croiset, W. Epling, Int. J. Hydrogen Energ. 36 (2011) 2904–2935.
[5] E. V. Shelepova, T. A. Maksimova, Y. I. Bauman, I. V. Mishakov, A. A. Vedyagin, Hydrogen 3 (2022) 450–462.
[6] M. Borghei, R. Karimzadeh, A. Rashidi, N. Izadi, Int. J. Hydrogen Energ. 35 (2010) 9479-9488.

## PP-III-39

# Stress-Effect of Adsorption-Induced Deformation of the Carbon Adsorbent within a Range of Low Adsorption Values

Shkolin A.V., Men'shchikov I.E., Khozina E.V., Fomkin A.A.
*Frumkin Institute of Physical Chemistry and Electrochemistry, Russian Academy of Sciences, Moscow, Russia*
*shkolin@phyche.ac.ru*

Large-scale implementation of the high-pressure adsorption-based technologies is impossible without considering the effect of adsorption-induced deformation of an adsorbent both for predicting its resistance to cyclic adsorption loadings and for evaluating the thermal effects arising during the adsorption/desorption process [1, 2]. Investigations, which had started by Meechan and Bangham one hundred years ago [3] and continue today, revealed that an adsorbent is not only a source of adsorption force field but it is also affected by an adsorbing substance. On the basis of discoveries made to date, it is stated that the adsorption-induced deformation phenomenon is manifested both as a contraction and expansion of adsorbent depending on the ratio of micropore sizes and dimensions of adsorbing molecules, and thermodynamic state of the adsorption system [4]. This variability in the manifestation of adsorption-induced deformation leads to difficulties in describing and predicting the changes in the state of adsorbent during adsorption. Therefore, further development of approaches to the description of adsorption-induced effects needs new experimental data on this effect within wide ranges of temperatures and pressures and their in-depth thermodynamic analysis.

As a step towards achieving this goal, we have carried out the measurements of deformation of microporous peat-derived carbon adsorbent Sorbonorit-4 during carbon dioxide adsorption within a temperature range of 216.6 to 393 K and at a pressure up to 5 MPa. According to the analysis of standard low-temperature nitrogen adsorption data by the theory of volume filling of micropores, the micropore structure of Sorbonorit-4 is represented mainly by slit-like pores with an average half-width $x_0$ = 1.1 nm and specific micropore volume $W_0$ = 0.49 $cm^3/g$

Deformation of the adsorbent granules during $CO_2$ adsorption was measured using macroscopic dilatometry on a custom-made setup [5]. The granules of Sorbonorit-4 were stabilized via the cyclic adsorption of carbon dioxide, after which the reversibility of deformation effects was checked [6]. On average, the measurement uncertainty of the relative linear deformation $\Delta l/l_0$ of the adsorbent was $u_c(\eta)$=2,0 %, and the expanded measurement uncertainty was $U(\eta)$ = 6.0 % at the confidence level of 95 %.

It was found that the first adsorbed $CO_2$ molecules changed the overall balance of forces, which led to the noticeable jump-like deformation of the adsorbent. These initial jump-like adsorption effects can be attributed to the specific features of the transition from a unicomponent thermodynamic system "adsorbent" to a two-component system "adsorbent

+ adsorbate". At the $CO_2$ adsorption value of $a \leq 0.3$ mmol/g, which corresponds to ~one $CO_2$ molecule per micropore [5], we observed a region of the jump-like deformation of Sorbonorit-4 and inversion of temperature-dependent deformation isotherms. At low temperatures ranging from 213 to 300 K, the adsorbent contracted, while elevated temperatures of 300–393 K, it expanded abruptly. Under isosteric conditions, when $a$=0.3 mmol/g, the magnitude of adsorption-induced deformation $\Delta l/l_0$ of Sorbonorit-4 represented as a plot of reverse temperature $1/T$ is well fitted by a linear function.

The temperature-dependent effects of initial jump-like deformation of Sorbonorit-4 were interpreted as a result superposition of competing factors: changes in the compressibility of the adsorbent with rising temperature and changes in the total energy of the adsorption system depending on the features of the interactions of $CO_2$ molecules with heterogeneous centers of adsorption on the opposite walls of the narrowest micropores. Both factors affected the behaviors of the isosteric differential molar heat of $CO_2$ adsorption during the adsorption process. An abrupt decrease in the heat of $CO_2$ adsorption by 1.0 kJ/mol was observed within the range of $CO_2$ uptake $a \leq 0.3$ mmol/g. The observed correlation of this abrupt decrease in the heat of adsorption and the jump-like adsorption-induced deformation can be a result of the endothermic contribution of the deformation of the adsorbent. As the amount of adsorbed $CO_2$ molecules increased, the decrease of the heat of adsorption became slower due to the equalization of the energy of interactions between the adsorbing molecules and the adsorbent, which also affected the behaviors of the adsorption-induced deformation.

The inversion of the adsorption-induced deformation of Sorbonorit-4 represented as a function of pressure was found within a pressure range of 1 to 5 bar. At higher pressures of $CO_2$, the value of $\Delta l/l_0$ at the same pressure increased with decreasing temperature. In the indicated range of pressures, the deformation magnitude grew smoothly with pressure. These behaviors of the adsorption-induced deformation of the adsorbent resulted from a decrease in the amount of adsorbed carbon dioxide with rising temperature. At saturation pressure, the maximum linear expansion of the Sorbonorit-4 granules did not exceed 0.44 % at 293 K.

**Acknowledgement:** The work was carried out within the framework of the State Assignment no. 0081-2019-0018.

**References:**

[1] I. Men'shchikov, A. Shkolin, E. Khozina, A. Fomkin, Nanomaterials. 11, (2021) P. 971.
[2] I. E. Men'shchikov, A. V. Shkolin, E. M. Strizhenov et al., Nanomaterials. 10 (2020) P. 2243.
[3] F. T. Mechan, Proc. R. Soc. A115, (1927) P. 199.
[4] J. E. Lane, T. H. Spurling, Aust. J. Chem. 33 (1980) P.231.
[5] A. V. Shkolin, I. E. Men´shchikov, A. A. Fomkin, Nanobiotechnology Reports. 17 (2022) P.916.
[6] A. V. Shkolin, I. E. Men'shchikov, E. V. Khozina, V. Yu. Yakovlev, A. A. Fomkin, Adsorption (2022) https://doi.org/10.1007/s10450-022-00370-y.

## PP-III-40

# Photocatalytic Properties of Titanium Dioxide Doped with La in Dye Oxidation Reactions

Shmelev A.A., Filimonov N.S., Shafigulin R.V., Bulanova A.V.
*Samara University, Samara, Russia*
*Shmelsasha@yandex.ru*

In recent years, semiconductor photocatalysts have been widely used to clean the environment from various pollutants. Titanium dioxide has many positive characteristics, making it one of the most widely used photocatalysts. However, the use of $TiO_2$ as a photocatalyst is limited due to its spectral absorption region ($\lambda < 380$ nm), and therefore it can only operate in the UV region of the spectrum. One of the methods for extending the absorption spectrum of $TiO_2$ into the visible region is its doping with metal or nonmetal atoms [1, 2].

Titanium dioxide was synthesized by the sol-gel template method. Cetyltrimethylammonium bromide (CTAB) and 1-butyl-3-methylimidazolium bromide ([Bmim]Br) were used as templates. A weighed amount of the template was dissolved in a water–alcohol mixture. After that, acetic acid, titanium ethoxide, and an aqueous solution of lanthanum nitrate were successively added to the resulting solution with constant stirring. Then the solution was kept in air for 10 days until a xerogel formed and the resulting xerogel was calcined for three hours in a muffle furnace. A lanthanum-doped titanium dioxide ($La/TiO_2$) samples were obtained. Undoped titanium dioxide was synthesized by the same method, but without the addition of lanthanum nitrate.

The photocatalytic activity of the obtained samples was studied using the photodegradation reactions of methyl orange and alizarin red C. A portions of the investigated photocatalysts were placed in aqueous solutions of dyes (the concentration of methyl orange was 2 ppm, alizarin red C 25 ppm). The resulting mixture was stirred in a glass beaker using a magnetic stirrer under the action of two white light fluorescent lamps. Sampling was carried out after 1; 1.5; 2; 3 hours. The samples were filtered on a cellulose filter. The change in the concentration of the substance used was determined using a Unico 2800 spectrophotometer.

The lanthanum-doped samples showed higher photocatalytic activity in the oxidation of methyl orange and alizarin red C than the undoped titanium dioxide sample. The highest photocatalytic activity was shown by the $La/TiO_2$ sample with the applied CTAB as a template, both in relation to methyl orange and alizarin red C. After 1.5 hours, the degradation of methyl orange on the $La/TiO_2$ sample was 67%, alizarin red C - 100 %.

**References:**

[1] G.K. Sukhadeve, S.Y.Janbandhu et al., Ceram. Int. 48 (2022) 29121-29135.
[2] N. Kovalevskiy, D. Svintsitskiy et al., Nanomaterials 12 (2022) 4146.

## PP-III-41

# The Highly Active $MoVSbNbGdO_x/SiO_2$ Catalysts for Oxidative Dehydrogenation of Ethane to Ethylene

Shutilov A.A., Zenkovets G.A., Bondareva V.M., Sobolev V.I., Marchuk A.S., Tsybulya S.V., Ishchenko A.V., Prosvirin I.P., Suprun E.A.
*Boreskov Institute of Catalysis, Novosibirsk, Russia*
*alshut@catalysis.ru*

Oxidative dehydrogenation of ethane (ODE) is one of the most perspective routes for ethylene production using the natural gas feedstock that can offer a significant advantage in energy efficiency over the conventional steam pyrolysis and fluid catalytic cracking processes [1,2]. Today MoVTe(Sb)$NbO_x$ catalysts are the most promising in the ODE to produce ethylene. The$MoVTeNbO_x$ catalysts are more active compared to MoVSbNbOx catalysts. The best of the $MoVTeNbO_x$ catalysts at 350–450 °C showed the ethylene yield of 72 – 76 %. The main disadvantage of using the $MoVTeNbO_x$ catalysts is the Te volatility during the calcination and catalytic reaction. Therefore, substitution of Te by Sb which is not volatile and is more eco-friendly is beneficial. Subsequently, $MoVSbNbGdO_x$ catalysts may be considered as an alternative to replace $MoVTeNbO_x$ catalysts without altering their catalytic properties.

In this study we synthesized and investigated new multicomponent MoVSbNbGdOx/$SiO_2$ catalysts depending on the Gd content characterized by the high catalytic activity in ODE.

The catalysts with the compositions of 50 wt. % ($Mo_1V_{0.24}Sb_{0.23}Nb_{0.08}O_x$)/50 wt. % $SiO_2$ and 50 wt. % ($Mo_1V_{0.24}Sb_{0.23}Nb_{0.08}Gd_{0.01–0.02}O_x$)/ 50 wt. % $SiO_2$ were synthesized by the spray dry method. The dried precursor was then heated stepwise in flowing argon at 350 °C and then at 600 °C for 2 h. XRD, HRTEM, SEM, XPS, adsorption methods were used to reveal the phase composition, morphology and the structure of the catalysts. The catalytic properties were studied at 400 °C in a flow setup at atmospheric pressure with on-line chromatographic analysis of the reaction mixture components in a fixed catalyst bed of 0.25 – 0.50 mm catalysts fraction and the reaction mixture:$C_2H_6$:$O_2$:$N_2$ =10:10:80 (vol. %).

It was shown that the introduction of gadolinium additives into the$MoVSbNbO_x/SiO_2$ catalyst in optimum amounts (Gd/Mo = 0.01–0.015) leads to an increase in the activity and ethylene selectivity and an increase in the ethylene yield to 72 %, which is comparable with the parameters of Te-containing catalysts. The synthesized catalyst exhibits a stable on stream behavior in the reaction mixture during long term 36-h tests, while maintaining high activity and ethylene selectivity.

XRD analysis data show the presence of M1 and M2 phases in the active component of both $MoVSbNbO_x/SiO_2$ and $MoVSbNbGdO_x/SiO_2$ catalysts. With the introduction of Gd into the catalyst with Gd/Mo ratio of 0.015 – 0.02, a slight increase in the M1 phase content in the active component from 77 to 82 % is observed. After testing the catalysts in the reaction mixture, their phase composition does not change. The value of "*a*" and "*b*" crystal lattice parameters of the M1 phase in the $MoVSbNbGdO_x/SiO_2$ catalysts slightly increase with an

increase in the Gd/Mo ratio from 0 to 0.02. It may be deal with the incorporation of Gd atoms into the lattice of the $MoVSbNbO_x$ compound. According to XPS data, the introduction of gadolinium into a $MoVSbNbO_x/SiO_2$ catalyst up to a Gd/Mo ratio of 0.015 leads to an increase in the surface $V^{5+}/V^{4+}$ ratio. A correlation between an increase in the activity and selectivity to propylene and an increase in the surface concentration of $V^{5+}$ ions is due to increase in the acceptor properties of active sites capable of activating the ethane molecule [3].

It is interesting to note that the morphology of the M1 phase particles in the multicomponent catalyst containing Gd and catalyst without Gd is some different. In catalyst containing Gd M1 phase particles with a needle-like morphology are formed. In catalyst without Gd M1 phase particles with plate-like morphology formed on the surface of catalyst particles which exhibit different activity in ODE. This finding is attributed to the fact that, in the M1 phase particles with a needle-like morphology, the most developed plane emerging to the surface is the [001] plane; this feature is responsible for the higher activity of these particles in the ODE reaction than the activity of the M1 phase particles with a plate-like morphology, in which the most developed is the [010] plane, which is less active [4,5].

Therefore, it can be assumed that the promoting role of gadolinium in the catalyst at an optimum Gd content consists in increasing the amount of the M1 active phase with a needle-like morphology and increasing the surface concentration of $V^{5+}$ ions. Thus, the addition of gadolinium to the $MoVSbNbCeO_x/SiO_2$ system apparently changes the plate-like morphology of the M1 phase particles to a needle-like morphology and increases the $V^{5+}/V^{4+}$ ratio, which leads to an increase in the catalyst activity showing the ethylene yield of 72 %.

**Acknowledgement:** This work was supported by the Ministry of Science and Higher Education of the Russian Federation under a state task to Boreskov Institute of Catalysis of the Siberian Branch of the Russian Academy of Sciences (project AAAA-A21-121011390054-1).

**References:**

[1] B.Chu, L. Truter, T. Nijhuis,Y. Cheng, Appl.Catal. A. 498 (2015) 99.
[2] C.Barai, A.M. Gaffney, R. Fushimi, Catal. Today.298 (2017) 138.
[3] C. Xin, F. Wang,Q.Xu, Appl.Catal. A.610(2021) 117949.
[4] D. Melzer, P. Xu, D.Harimann, Y. Zhu, N.D. Browning, M. Sanchez-Sanchez, J. A. Lercher, Angew. Chem., Int. Ed. 55 (2016). 8873.
[5] D. Melzer, G.Mestl, K.Wanninger, Y. Zhu, D. Browning, M. Sanchez-Sanchez, J.A.Lercher, Nat.Commun., 10. (2019) 4012.

## PP-III-42

# Influence of the Cation Structure on the Physico-Chemical Properties of Solid Composite Electrolytes Based on Organic Ammonium Salts and Nanodiamonds

Stebnitskii I.A.[1,2], Mateyshina Yu.G.[1,2]
*1 – Institute of Solid State Chemistry and Mechanochemistry SB RAS, Novosibirsk, Russia*
*2 – Novosibirsk State University, Novosibirsk, Russia*
*i.stebnitskii@g.nsu.ru*

In recent years, there has been a trend to move from liquid electrolytes to solids to improve the performance and safety of electrochemical devices such as batteries and supercapacitors. A promising class of solid-state electrolytes are organic salts of substituted ammonium. Their features are a wide window of electrochemical stability, as well as plastic mechanical properties, due to which it is possible to solve the problem of poor contact between electrodes and electrolyte [1]. However, the values of ionic conductivity of organic salts are not so high for practical applications (for $(C_2H_5)_3CH_3NBF_4$ $\sigma=1.8*10^{-5}$ S/cm at T=200 $^oC$ [2]).

One way to improve the transport properties of ionic salts is heterogeneous doping with highly dispersed oxide additives (for example, MgO, $Al_2O_3$, $SiO_2$, $TiO_2$). The increase in ionic conductivity values in such composite electrolytes is due to the formation of an amorphous layer near the phase contact enriched with defects. Recently it has been shown that nanosized diamonds can be used as an additive instead of oxides. For example, heterogeneous doping of $(C_2H_5)_3CH_3NBF_4$ salt with nanodiamonds allows increasing the ionic conductivity by two orders of magnitude [2]. Nanodiamonds are characterized by high thermal, chemical, and electrochemical stability; therefore, so they can act as a promising additive to electrolytes.

At the moment, there are no works that systematically study the properties of solid composite electrolytes based on various organic salts and nanodiamonds. In this work, we studied the influence of the structure of the cation of salts of the form $(n\text{-}C_4H_9)_{(4-x)}(CH_3)_xNBF_4$ on the properties of composites using a complex of physicochemical methods: differential scanning calorimetry, X-ray phase analysis, and impedance spectroscopy.

**Acknowledgement:** This work was supported by the Russian Science Foundation, grant 20-13-00302.

**References:**

[1] Zhu H., MacFarlane D.R., Pringle J.M., Forsyth M., Trends in Chem. 1 (2019) 126.
[2] Alekseev, D.V., Mateyshina, Yu.G., N. F. Uvarov, N.F., Russ. J. Electrochem. 58 (2022) 594.

## PP-III-43

# Lignin Valorisation in the Presence of $SiO_2$@Polymer Supported Catalysts

Stepacheva A.A., Markova M.E., Manaenkov O.V., Sulman M.G.
*Tver State Technical University, Tver, Russia*
*a.a.stepacheva@mail.ru*

Lignin is considered as one of the prospective green sources for producing valuable aromatic and phenolic compounds [1]. The lignin structure is mainly presented by the covalently linked phenylpropanoid units. The selective cleavage of the C-C and C-O bonds in the lignin network is one of the ways to obtain the aromatic and oxygen-containing monomers [2].

The catalyst is one of the key factors in the hydrogenolysis of lignin controlling the lignin conversion, the yield of the product and the nature of the product. Metals and their binary compounds were reported to be effective catalysts. It was found that different metals such as Ru, Rh, Cu, Ni, Pt and Pd were capable of breaking different bonds in the lignin, resulting in up to 60 by wt. % yield of monomers [3].

The catalytic support plays an important role in depolymerization processes. Strong Brønsted and Lewis sites on the surface of the support promote activation of C-O bonds and facilitate their cleavage. In addition, the acid support can serve as a structural and energetic promoter that facilitates the reducibility of the active phase [4].

In this work, the catalysts supported on $SiO_2$@hypercrosslinked polymer were studied in the lignin depolymerisation to aromatic and phenolic monomers. The synthesis of the $SiO_2$@HPS was carried out by the hydrolytic precipitation of $SiO_2$ on the hypercrosslinked polystyrene (MN-100) in the medium of subcritical water with the following heating in a nitrogen flow at 300 °C for 5 h. The active phase deposition was performed by the impregnation of the resulted support with the solution of the metal precursor salt in the complex solvent containing water, methanol, and tetrahydrofurane. The catalysts were analyzed by low-temperature nitrogen physisorption (BET), X-Ray photoelectron spectroscopy (XPS), ammonia chemisorption, temperature programmed reduction (TPR), and transmission electron microscopy (TEM).

Lignin hydrogenolysis experiments were carried out in a stainless steel batch reactor Parr Series 5000 Multiple Reactor System (Parr Instrument, USA). In a typical procedure, 1.0 g of lignin, a calculated amount of catalyst, and 30 mL of isopropanol were loaded into the reactor cell. The catalyst loading was calculated as 2000 g of lignin per 1 g of metal in the catalyst. The reactor was heated up to 260°C under a nitrogen pressure of 2.0 MPa. After the temperature reached 260°C, nitrogen was replaced by hydrogen. The hydrogenolysis was performed for 3 h at a constant stirring (1200 rpm).

All the synthesised catalysts showed lignin conversion into liquid and gaseous products over 70 wt. %. The highest conversion (over 85 wt. %) was observed when using bimetallic Ni-Ru-$SiO_2$@HPS sample. For monometallic Ni, and Ru catalysts the conversion was also

sufficiently high (75 ant 78 wt. % respectively). The lignin hydrogenolysis resulted in the formation of a wide range of products including monophenols (phenol, anisole, guaiacol, syringol, eugenol, p-ethylphenol, p-hydroxyphenol), arenes (toluene, benzene), and cyclohexanes (cyclohexane, methylcyclohexane) and soluble oligomers (See Fig. 1). The yield of monophenols was over 20 wt. % for Ni-containing catalyst, and even exceed 32 wt. % for Ni-Ru-$SiO_2$@HPS. The chosen catalyst seems to provide a proper monophenol yield in comparison with the literature data for bimetallic Ni-based catalysts showed ca. 20-35 wt. % of monophenols at 50-80 wt. % of lignin conversion [5, 6].

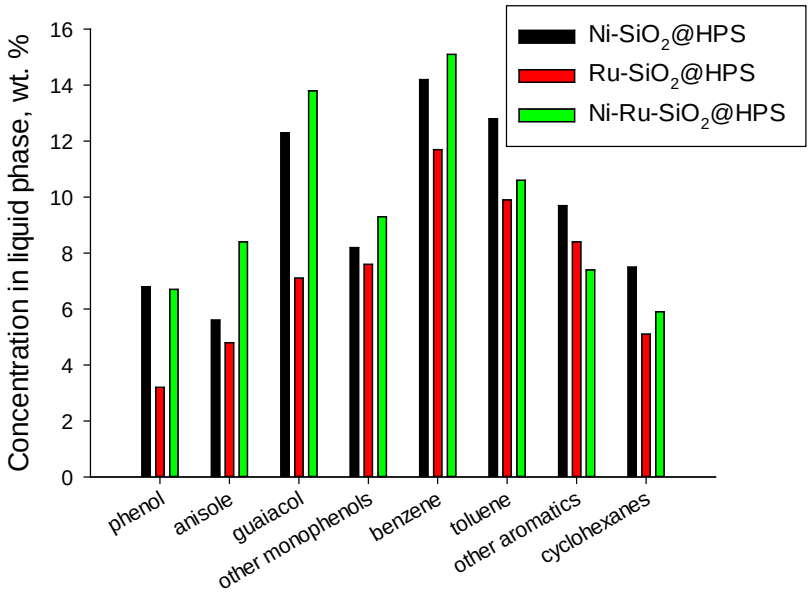


*Fig. 1. Lignin monomer yield over different catalysts*

**Acknowledgement:** This work was supported by the Russian Science Foundation, project 22-79-10096.

**References:**

[1] Zhang C., Wang F. Acc. Chem. Res. 53 (2020) 470.
[2] Roy R., Rahman M.S., Amit T.A., Jadhav B. Biomass 2 (2022) 130.
[3] Ye K., Liu Y., Wu S., Zhuang J. Ind. Crops and Products 172 (2021) 114008.
[4] Yan S., Ding W., Lin X., Cai Q., Zhang S. Fuel. 320 (2022) 123732.
[5] Zhao W., Li X., Li H., Zheng X., Ma H., Long J., Li X. ACS Sust. Chem. Eng, 7 (2019) 19750.
[6] Song Q., Wang F., Cai J., Wang Y., Zhang J., Yu W., Xu J. Energy Environ. Sci. 6 (2013) 994.

## PP-III-44

# $CO_2$ Hydrogenation Reaction over Biochar-Based Catalysts

Svidersky S.A., Dementeva O.S., Kulikova M.V.
*Topchiev Institute of Petrochemical Synthesis, Russian Academy of Sciences, Moscow, Russia*
*sviderskysa@ips.ac.ru*

The $CO_2$ hydrogenation reaction on mono- and bimetallic biochar based catalysts has been studied. It is shown that bimetallic iron-cobalt catalysts in the process of $CO_2$ hydrogenation are more effective then monometallic iron and cobalt, while the best combination of process parameters is achieved for a sample with a ratio of iron: cobalt = 3:1. The composition of the active phase of a bimetallic iron-cobalt catalyst, the genesis of its formation and the proposed mechanism of the $CO_2$ hydrogenation process on a bimetallic iron-cobalt catalyst with a predominance of iron in the composition are determined.

Currently, processes aimed at limiting the impact of greenhouse gas emissions on the climate, including carbon dioxide, whose contribution to the greenhouse effect is about sixty percent, are relevant. One of the options for involving $CO_2$ in chemical transformations is its hydrogenation to produce synthetic hydrocarbons [1].

The use of iron and cobalt catalysts are two main directions in the development of the processes of catalytic hydrogenation of carbon oxides, and combining the active sites formed by iron and cobalt in the composition led to an iron-cobalt catalyst. The authors [2] believe that the introduction of metallic cobalt increases the sorption of $CO_2$ and promotes the formation of active iron carbides, which, in turn, promotes the formation of C–C bonds occurring in the iron carbide phase. Another current trend in the development of catalysis is the use of biochar as a supports [3]. The authors [4] studied nanoscale iron catalysts showed high activity and selectivity for $C_{5+}$ hydrocarbons. Based on the above, it was advisable to study bimetallic iron-cobalt catalysts supported on biochar in the $CO_2$ hydrogenation process.

Biochar used as a catalyst support prepared by hydrothermal carbonation of cellulose. The active components supported by impregnation with subsequent heat treatment. The metal (Fe+Co) loading in finished samples was 20 %mas. Physical-chemical studies of catalysts were carried out by X-ray diffraction (XRD) using a Rotaflex D/MAX-RC diffractometer (Rigaku). The catalytic tests carried out in a flow-through fixed-bed catalytic reactor. Before the catalytic tests, the samples activated in the $H_2$ flow.

The genesis of the formation of the active phase of a bimetallic catalyst determined by a sequential study of freshly prepared, activated and catalytically tested samples. The freshly prepared sample characterized by a low content of well-crystallized phases. In the composition of the activated sample, the dominant phase is an iron-cobalt alloy, and by the lattice period in the alloy, the ratio of these components is about 60-40 in favor of iron. The composition of the sample surface after catalysis represented by phases of iron and cobalt carbides, as well as iron oxide. The average sizes of active phase crystallites for $Fe_3O_4$ was

10 nm, for $Fe_5C_2$ and $Co_2C$ - 20 nm. Thus, the formation of the active phase of the iron-cobalt catalyst occurs directly at the initial stage of the $CO_2$ hydrogenation process.

The effect of the ratio of active components on the yield of $C_{5+}$ hydrocarbons and oxygenates was significant (Fig. 1). The highest yield of both $C_{5+}$ hydrocarbons and total hydrocarbons and oxygenates was achieved in the presence of an iron-cobalt sample with a metal ratio of 3:1.

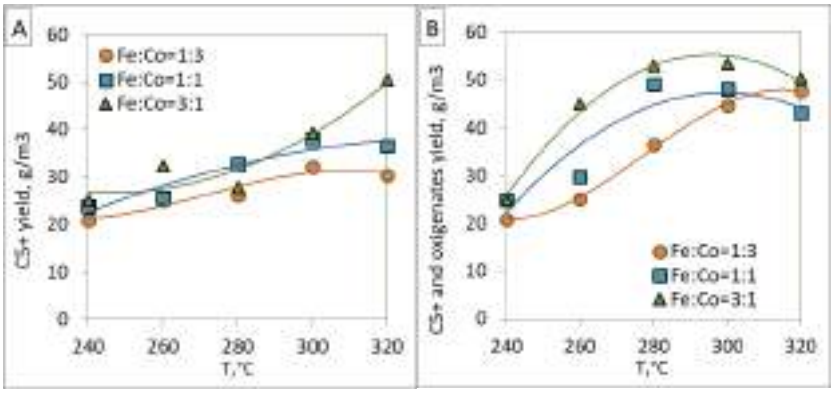


*Fig. 1. The effect of iron:cobalt ratio in the catalyst composition on the yield of $C_{5+}$ hydrocarbons (A) and the total yield of $C_{5+}$ hydrocarbons and oxygenates (B)*

Therefore, the study of the genesis of bimetallic catalysts of the $CO_2$ hydrogenation process has shown that the use of biochar as a support contributes to the synergy of iron and cobalt active sites. Unlike oxide supports, when iron and cobalt compounds bonded to it, biochar does not contribute to the formation of a massive phase of mixed oxides. The use of a carbon support during activation ensures the formation of a fundamentally different active phase – an iron-cobalt alloy, which, in turn, when starting the $CO_2$ hydrogenation process, turns into catalytically active iron and cobalt carbides. Metallic cobalt, characterized by high activity in methane formation, not formed at the same time. Moreover, the features of biochar, such as the absence of a complicated porous structure, and the binding of metal atoms to the surface through hydroxyl groups, are favor for the formation of iron-cobalt alloy crystallites with a size of 10-20 nm, passing into appropriately sized clusters of carbides. Iron and cobalt atoms, due to the formation of carbides from the alloy, are close to each other, which provides synergy in their catalytic activity. Changing the ratio of active components introduced into the composition of the catalyst allows to control the catalytic properties of the resulting catalyst in order to change the yield and composition of the products obtained.

**Acknowledgement:** This work carried out with financial support from the Russian Science Foundation (RSF Grant no. 17-73-30046P).

**References:**

[1] *Steinberg M.* Fuel. 1978. V. 57. № 8. P. 460–468.
[2] *Guo L., et al.* ChemistrySelect. 2018. V. 3. № 48. P. 13705–13711.
[3] *Kumar M., et al.* Adv. Sustain. Syst. 2020. V. 4. P. 1900149.
[4] *Maksimov A.L.,* et al. Journal of Catalysis. 2019. V. 380. P. 32-42.

## PP-III-45

# Polysaccharide Macromolecules as Transport Matrices of Nano-Size Compositions, Candidates for Diagnostics, Therapy and Theranostics of Cancer Diseases

Tantsyrev A.P., Titova Yu.Yu., Ivanov A.V.
*A. E. Favorsky Irkutsk Institute of Chemistry, Siberian Branch of the Russian Academy of Sciences, Irkutsk, Russia*
*ytitova60@gmail.com*

Currently, cancer is one of the leading causes of mortality both in economically developed and underdeveloped countries. Despite the recent advances in cancer therapy, a number of oncological diseases, due to their localization, are still difficult to be timely diagnosed and treated. First of all, these are brain diseases. Blood supply of the brain proceeds through the blood-brain barrier that protects the brain against foreign compounds and objects from the bloodstream. Moreover, the brain cancer is also hard to cure surgically, since operative intervention often leads to the brain dysfunctions.

Today, one of the most prospective ways to overcome the blood-brain barrier today is the application of nano-sized particles with a certain diameter [1], namely, 3-10 nm. Unfortunately, most of similar compounds, which can be considered as candidates for the diagnostics and therapy of malignant neoplasms, do not possess high solubility in water and colloidal stability, and the synthesis of such particles is rather sophisticated. On the other hand, it is known that such molecules as arabinogalactan (AG) of Siberian larch can both penetrate the brain through the blood-brain barrier and act as a polymer matrix transporting metal nanoparticles into the brain as well as stabilize these particles [2].

Here we report on new results of the study on new iodine-, boron- and gadolinium-containing arabinogalactan nanocomposites, including those obtained by a mechanochemical method. The nanocomposites obtained are promising candidates for parallel multichannel diagnostics and therapy of brain cancer.

**Acknowledgement:** The authors are grateful to the Baikal Analytical Centre for Collective Uses, SB RAS.

**References:**
[1] V. Ceña, P. Játiva, Nanomedicine (Lond). 13 (2018)1513.
[2] Patent RU 2778928.

## PP-III-46

# The Preparation of Zeolite Containing $MoS_2$ Catalysts for Hydrodeoxygenation/Hydroisomerization of Aliphatic Esters

Vlasova E.N.[1], Zhao Y.[2], Aleksandrov P.V.[1], Suprun E.A.[1], Gerasimov E.Y.[1], Pakharukova V.P.[1], Bukhtiyarova G.A.[1]

*1 – Boreskov Institute of Catalysis, Novosibirsk, Russia*

*2 – Novosibirsk National Research University, Novosibirsk, Russia*

*evgenia@catslysis.ru*

Modern trends in the design of catalytic systems for the industrial implementation are aimed at creating catalysts with a specific set of desired properties. In the modern scientific literature concerning of the study of bifunctional catalysts activity in the hydrodeoxygenation of fatty acid triglycerides (FATs), aluminosilicate and zeolite materials are most used in the form of powders, on which the active component is supported, while in industry granular catalysts are used. The use of a one-stage process the hydroprocessing of FATs (hydrodeoxygenation and hydroisomerization/hydrocracking, simultaneously) for into bio-jet fuel components will reduce capital and operating costs, avoid intermediate purification, simplify process control, and reduce energy and hydrogen consumption.

For this purpose we synthesized several composite supports $Al_2O_3$-zeolite differing in the zeolite material (ZSM-5, ZSM-12, ZSM-22 and silicoaluminophosphate SAPO-11). Pseudo-boehmite powder was mixed with a zeolite material in a Z-shaped blade mixer followed by peptization by nitric acid solution and extrusion. All composite supports contained 30 wt.% of zeolite on the calcined basis.

Mo catalysts were prepared by incipient wetness impregnation of synthesized $Al_2O_3$-zeolite extrudates by aqua solution containing the precursors of active component. Mo content was about 7 wt.% (after calcination of the catalysts at 550°C for 4 hours).

A comparative study of the prepared catalysts in the reactions of methyl palmitate (MP) conversion in a flow reactor was performed at temperatures of 230–350°C (with an interval of 20°C), at hydrogen pressure of 3.0 and 5.0 MPa, a $H_2$/feedstock ratio of 600, and LHSV of 36 $h^{-1}$.The liquid and gases products were quantified using gas chromatographs, Vario EL Cube was used to follow total O content.

Supports and catalysts were characterized by XRD, HRTEM and SEM. According to XRD data structure of zeolites was preserved in synthesized supports and catalysts. Uniform distribution of zeolite crystallites in composite materials was confirmed by SEM. According to TEM data, the average size of sulfide nanoparticles was 4.5–5.5 nm. At the same time, it was found that sulfide nanoparticles were localized on the surface of alumina, such particles could not be found on the surface of zeolites.

A comparative study of sulfide Mo catalysts showed that the introduction of zeolites leads to an increase in MP conversion by 10–15% in all temperature range (due to a rate increase of the acid-catalyzed ester hydrolysis reaction) and a decrease in the selectivity of the

formation of $C_{16}$ alkanes due to decarbonylation reaction. 100% conversion of oxygen-containing compounds is achieved at a temperature of 310°C. The highest yield of *iso*-alkanes was observed for ZSM-22 containing catalyst.

**Acknowledgement:** This work was supported by the Russian Science Foundation (grant no. 22-13-00371).

## PP-III-47

# Sodium Chloride as an Active Medium in the Solid Phase Redox Transformations of Organic Substances

Vol'eva V.B.[1], Ovsyannikova M.N.[1], Ryzhakova A.V.[1], Zhorin V.A.[2]

*1 – N.M. Emanuel Institute of Biochemical Physics of Russian Academy of Sciences, Moscow, Russia*

*2 – N.N. Semenov Federal Research Center for Chemical Physics* Russian Academy of Sciences, *Moscow, Russia*

*violetta.voleva@gmail.com*

When NaCl is used as a medium for the solid-phase oxidation of hindered phenols, its chemical participation in the process, including homolysis with the formation of Na˙ and Cl˙ atoms was found. It was evidenced by the registration of paramagnetic particles during the transformation of the redox pair 3,6-di-tert-butylcatechol (Cat) – 3,6-di-tert-butyl-ortho-benzoquinone (Q) in NaCl under pressure and shear deformations (P + SD) in screw devices and on Bridgman rotary anvils. Paramagnetic particles were identified by EPR as sodium 3,6-di-tert-butyl-ortho-benzosemiquinolate (SQNa) (a triplet from two equivalent ring protons $a_H$ 3.3 Oe, each component of the triplet contains a quadruplet from the magnetic nuclei of the sodium cation $J$ 3/2). The chlorine atom was identified as its paramagnetic adduct with orthosilicic ether $(Cat)_2Si$ as the radical $(Cat)_2SiCl$˙. The number of detected paramagnetic particles is small ~ 0.1% due to the reversibility of their formation.

Additional evidence for the participation of Na˙ in the solid-phase redox process was the formation of 3,5-di-tert-butylcatechol (3,5-Cat) under the action of P + SD on 2,4-di-tert-butylphenol (2,4-DTBP) in NaCl medium. Similar ortho-hydroxylation was observed earlier in the 2,4-DTBP-CuCl·Py-$O_2$-DMSO coordination-catalytic system [1], and was also carried out by the interaction of 2,4-DTBP with $Cu_2O$ as an oxygen donor under P + SD action on Bridgman anvils [2]. With this in mind, the only possible mechanism for the formation of 3,5-Cat from 2,4-DTBP in the NaCl medium involves the formation of Na adduct with adsorbed in NaCl oxygen, NaOO˙, and hydroxylation in its coordination complex with 2,4-DTBP.

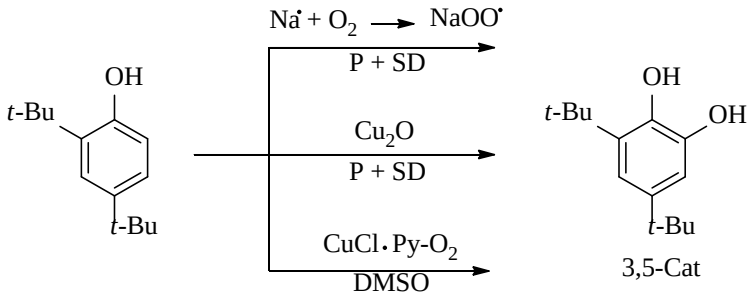


The formation of adducts of Na˙ atom with the components of reaction mixtures in NaCl apparently performs a catalytic function in solid-state transformations under P + SD conditions. Thus, the participation of SQNa as an intermediate stimulates the formation of

semiquinolate complexes during the interaction of Q with metal powders. A number of 2- and 3-ligand complexes $(SQ)_2M$ (M = Cu, Zn) and $(SQ)_3M$ (M = Cr, Al, W, V) were obtained, wich are spectrally identical to those obtained from Cat and metal salts.

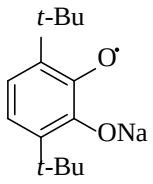


SQNa

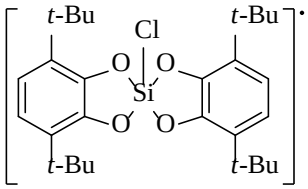


$(Cat)_2SiCl^{\bullet}$

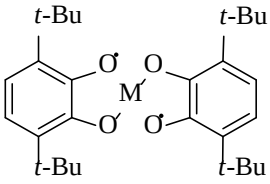


$(SQ)_2M$, M = Cu, Zn

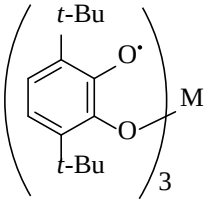


$(SQ)_3M$, M = Cr, Al, W, V

**References:**

[1] Battaini J., De Carolis M., Monzani E., Tuczer F., Casella L. *Chem.Commun*. **2003**, 726-727.
[2] Vol'eva V.B., Zhorin V.A., Komissarova N.L., Ovsyannikova M.N., Ryzhakova A.V., Kurkovskaya L.N. Solid-phase ortho-hydroxylation of 2,4-di-tert-butylphenol and its derivatives, *Russ. J. Org. Chem.*, **2020**, *56* (2), 350-352.

## PP-III-48

# Study of the Hydrothermal Treatment Process on the Stability of Acrylate Copolymers for the Development of Energy-Saving Drag Reduction Additives

Voronina N.S., Nechaev A.I., Strelnikov V.N., Valtsifer V.A.
*Institute of Technical Chemistry Ural Branch Russian Academy of Sciences, Perm, Russia*
*voronina.n@itcras.ru*

Efficient and rational use of energy resources is one of the main tasks of many technological processes. One of the ways to reduce energy consumption when drilling oil and gas wells is to reduce the power consumption of drive systems of pumping units through the use of special additives that can significantly reduce the hydrodynamic resistance of turbulent flows of drilling fluid (Toms effect [1]). For water-based drilling fluids, high molecular weight ionic flexible-chain linear polymers based on acrylamide (AA) and its derivatives are widely used as such additives.

Recently, there has been an increase in the share of hard-to-recover oil reserves, so the drilling of deep and ultra-deep exploration and production oil and gas wells is actively developing in difficult mining and geological conditions. With increasing depth, both the probability of the presence of hardness salts and acid gases and the temperature increase. Such harsh environmental conditions adversely affect the performance of the polymer components of drilling fluids. At the same time, polyacrylamide molecules are subject to several types of degradation [2], the most significant of which is thermal. This leads to a sharp decrease in the hydrodynamic efficiency of polymers, which is a serious problem in the oil industry, since degradation of more than 20% is considered critical for many processes and jeopardizes the performance of technological operations [3, 4]. However, the study of degradation pathways is a complex problem due to the almost infinite variety of reaction conditions to which a polymer can be subjected. Therefore, it is important to establish the influence of the process of thermal hydrolysis of copolymers of acrylamide and sodium salt of 2-acrylamide-2-methylpropanesulfonic acid (AMPS) on their physicochemical properties, composition and structure of acrylate copolymers and, as a result, on their ability to reduce the hydrodynamic resistance of turbulent water flows at temperatures above 100 °C.

Previously, a team of authors carried out studies to establish the effect of the composition of a ternary acrylate copolymer on its resistance to elevated temperatures [5, 6]. However, the process of thermohydrolysis has not been studied both from the point of view of changing the chemical composition and colloidal characteristics, which have the main effect on the effect of reducing hydrodynamic resistance, and from the point of view of the process occurring at intermediate temperatures up to 180 °C.

In the course of a comprehensive study involving a set of physicochemical methods, the effect of hydrothermal exposure up to 200 °C on the stability of AA-AMPSNa copolymers was studied. An increase in the stability and a decrease in the degree of hydrolysis of acrylate ionic copolymers during thermal hydrolysis associated with the presence of sulfonate substituents

in the side groups of the polymer chain was revealed. It has been shown that with an increase in the temperature of thermohydrolysis up to 160°C, no new chemical compounds are formed from the synthesized AA-AMPSNa copolymer, except for the replacement of amide groups by carboxyl groups with the simultaneous release of nitrogen in the form of ammonia. It has been established that under the influence of thermal hydrolysis, partial thermal degradation of the copolymer also occurs. It has been determined that with an increase in the temperature of hydrothermal treatment, there is a decrease in the intrinsic viscosity and average size of the solvated macromolecular coils of the AA-AMPSNa copolymers (Fig. 1).

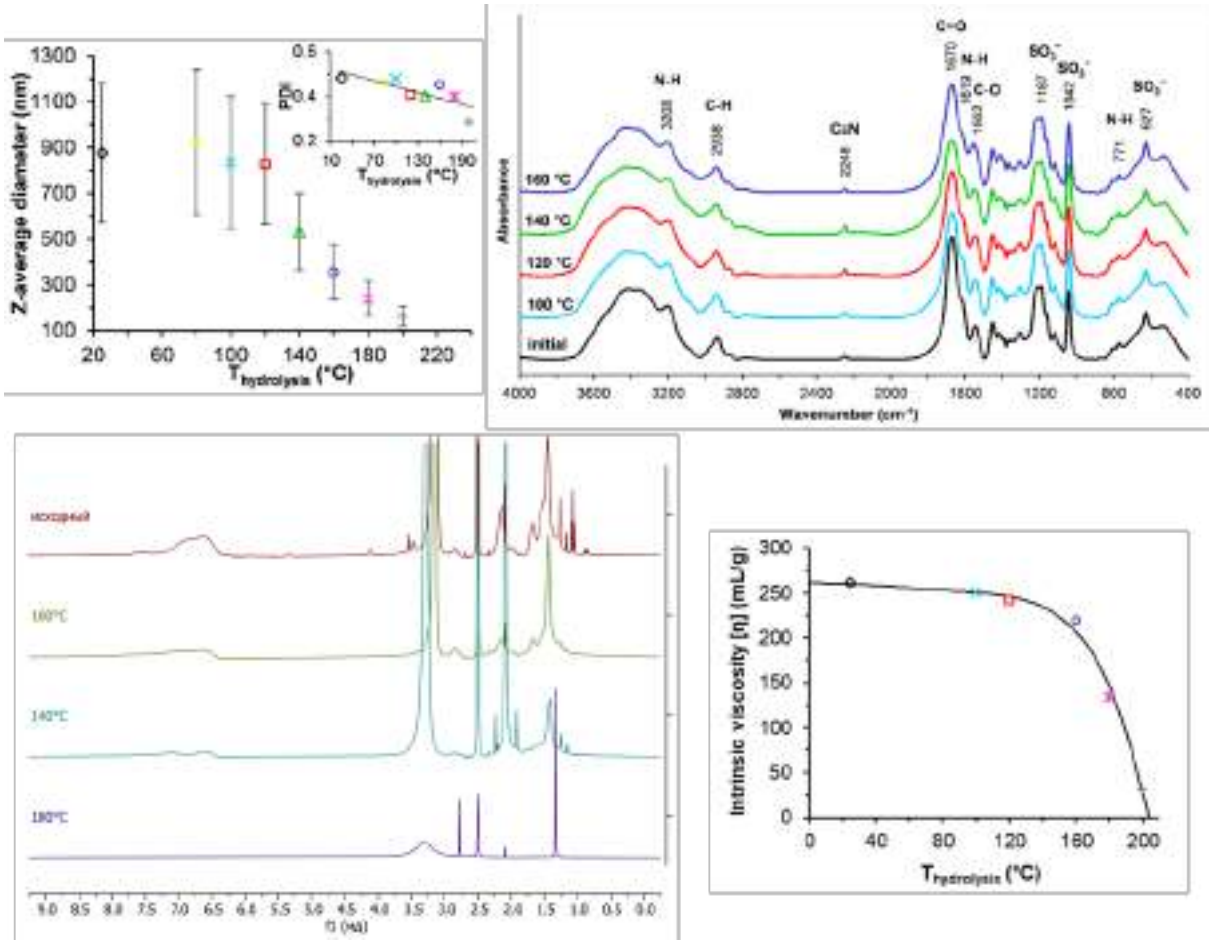


*Fig. 1. The effect of hydrothermal treatment temperature on the composition and structure (IR and NMR spectra), as well as on the intrinsic viscosity and size of polymer coils of an acrylate copolymer*

**Acknowledgement:** The reported study was funded by RFBR and Perm Territory, project number 20-43-596014; The work was carried out using the equipment of The Core Facilities Center «Research of materials and matter» at the PFRC UB RAS.

**References:**

[1] B. Toms. Proc. 1st Int. Congr. Rheol., North Holland, Amsterdam, 1948: cc. 135–141.
[2] M.J. Caulfield, G.G. Qiao, D.H. Solomon. Chem. Rev. 102 (2002) 3067–3084.
[3] A.M. Mansour, R.S. Al-Maamari, A.S. Al-Hashmi, et al. J. Pet. Sci. Eng. 115 (2014) 57–65.
[4] A.R. Al Hashmi, R.S. Al Maamari, I.S. Al Shabibi, et al. J. Pet. Sci. Eng. 105 (2013) 100–106.
[5] A.I. Nechaev, I.I. Lebedeva, V.A. Val'tsifer, V.N. Strel'nikov. Russ. J. Appl. Chem. 89 (2016) 1296–1301.
[6] A.I. Nechaev, N.S. Voronina, V.N. Strel'nikov, V.A. Val'tsifer. Polym. Sci. Ser. B. 64 (2022) 287-293.

## PP-III-49

# Pine Nut Shell Derived Activated Carbons for Non-Aqueous Electrolyte Based EDLCs: An Effect of Surface Oxygen Functional Groups

Yeletsky P.M.[1,2], Mozyleva M.A.[1,2], Kozlov D.V.[1,2], Lebedeva M.V.[1,2]
*1 – Boreskov Institute of Catalysis SB RAS, Novosibirsk, Russia*
*2 – Novosibirsk State University, Novosibirsk, Russia*
*yeletsky@catalysis.ru*

Currently, the world demand of energy accumulating devices is increasing very intensively. Among such devices, supercapacitors (SCs) take a special place due to the very fast charge-discharge rates, high power density, long cycle life as well as simplicity. Due to higher operating voltage (2 – 3 V) SC based on non-aqueous electrolytes are of a high interest since they exhibit much higher energy and power densities [1]. Mostly used materials for SC electrodes are activated carbons (ACs), which are the accessible and environmentally friendly compared to other porous carbon materials. They can be produced from both renewable and fossil feedstocks.

In this work, as a feedstock, pine nut shell (PNS) was selected. It represents a quite attractive AC precursor, since shell of various nuts and fruit stones has a high lignin content together with a high density and mechanical strength, which can be inherited by the produced activated carbon [2]. Herewith, a series of pine nut shell derived activated carbons was synthesized via a two-step procedure: 1) oxidative carbonization in a reactor with fluidized catalyst bed at 460 °C to obtain biochar; 2) activation by KOH to produce activated carbon. Furthermore, the AC samples were calcined in the Ar atmosphere at 900 °C to remove oxygen functional groups that affect capacitive properties of supercapacitors and their stability. The obtained ACs appeared to have BET specific surface area (SSA) of ~1000 – 2000 $m^2 \cdot g^{-1}$ increasing with the temperature, and microporous structure (Table).

Table – Texture characteristics and oxygen content of PNS derived activated carbons.

| Sample | $T_{act}$, °C | $A_{BET}$, $m^2 \cdot g^{-1}$ | $A_{DFT}$, $m^2 \cdot g^{-1}$ | $V_\Sigma/V_\mu$, $cm^3 \cdot g^{-1}$ | $<d_{pore}>$, nm | O-content, wt. %* |
|---|---|---|---|---|---|---|
| PNS-biochar | - | 137 | 163 | 0.08/0.04 | 2.4 | 19.9 |
| Original ACs | | | | | | |
| AC60 | 600 | 1145 | 826 | 0.52/0.44 | 1.8 | 16.3 |
| AC70 | 700 | 1482 | 1305 | 0.65/0.57 | 1.8 | 8.9 |
| AC80 | 800 | 1718 | 1423 | 0.82/0.67 | 1.9 | 6.9 |
| AC90 | 900 | 2036 | 1730 | 1.02/0.76 | 2.0 | 4.7 |
| AC100 | 1000 | 1952 | 1674 | 0.99/0.70 | 2.0 | 2.4 |
| ACs treated in Ar flow at 900 °C (1 h) | | | | | | |
| AC60-90 | 600 | 1046 | 989 | 0.46/0.40 | 1.8 | 0.7 |
| AC70-90 | 700 | 1342 | 1238 | 0.58/0.51 | 1.7 | 3.4 |
| AC80-90 | 800 | 1608 | 1370 | 0.75/0.58 | 1.9 | 4.2 |
| AC90-90 | 900 | 1820 | 1469 | 0.97/0.67 | 2.1 | 0.5 |

* – by difference. $T_{act}$ – activation temperature, $A_{BET}$, $A_{DFT}$ – specific surface area according to BET or DFT model, $V_\Sigma/V_\mu$ - total pore volume/micropore volume, , $<d_{pore}>$ - mean pore diameter.

At the same time, the oxygen content drops with the temperature and does not exceed ~5 % at 900 and 1000 °C including all the calcined samples.

The obtained carbons were tested on their ability to store energy using 1 M $BMIMBF_4$/ACN electrolyte. In the Figure, dependencies of their gravimetric and surface specific capacitance on ACs activation temperature are provided. As can be seen, the gravimetric capacitance of non-treated ACs is weakly varied, while those of the calcined ACs increases and reaches 116 $F \cdot g^{-1}$ at 1000 °C. Specific surface capacitance dependencies exhibit another trends: the surface capacitance of original ACs drops with the temperature up to ~900 °C while those of calcined samples varies weakly having a mean value of ~ 0.7 $F \cdot m^{-2}$. This value is typical for biomass-derived activated carbons in non-aqueous electrolytes [1] and associated mainly with an electric double layer mechanism of charge accumulation. High capacitance values for the samples prepared at the low activation temperatures (600 and 700 °C) are associated with a significant contribution of faradaic processes (up to 30%) in energy accumulation due to high content of O-containing functional groups.

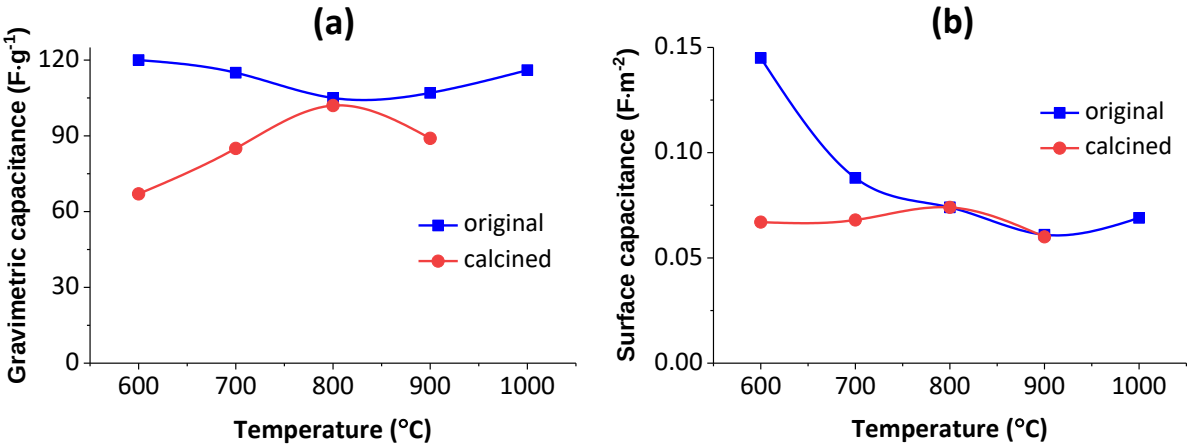


*Fig. Gravimetric (**a**) and surface (**b**) capacitance of PNS-derived ACs in 1 M $BMIMBF_4$/ACN electrolyte at a discharge current density of 0.6 $A \cdot g^{-1}$ in a three electrode cell*

Tests performed in CR2032 coin cell revealed that removing O-groups results in the stability increase. The capacitance decay of the calcined samples is 20% less compared to those of the non-treated ones.

**Acknowledgement:** This work was supported by the Ministry of Science and Higher Education of the Russian Federation within governmental order for the Boreskov Institute of Catalysis SB RAS (project AAAA-A21-121011390007-7) and Novosibirsk State University (project № FSUS-2022-0022).

**References:**

[1] P.M. Yeletsky, M.V. Lebedeva, V.A. Yakovlev. J. Energy Storage. 50 (2022) 104225.
[2] J. Alcañiz-Monge, M. del C. Román-Martínez, M.Á. Lillo-Ródenas. Molecules. 27 (2022) 1630.

## PP-III-50

# Effect of Microadditives on Morphology, Stability and Number of Charge Carriers in a Solar Cell Based on $P_3DDT/PC_{61}$ BM

Yudanova E.I., Denisov N.N., Krinichnyi V.I.
*Federal Research Center of Problems of Chemical Physics and Medicinal Chemistry, RAS*
*Acad.Semenov av. 1, Chernogolovka, Moscow region, 142432 Russian Federation*
*yudan@icp.ac.ru*

The paper presents the results of the light-induced EPR and optical absorption study of spin charge carriers photoexcited by light photons with an energy in the range of 1.34 – 4.52 eV in composites of regioregular poly(3-dodecylthiophene) (P3DDT) with methyl ether [6,6]-phenyl-$C_{61}$-butyric acid ($PC_{61}BM$) modified by various molecular nanoadditives. The morphology of the polymer matrix suggests the presence of two structural polymorphs - a chaotically structured α-polymorph and a more crystalline β-polymorph. Light irradiation leads to the formation in these polymorphs of spin charge carriers, polarons and methanofullerene radical anions. Magnetic resonance, relaxation and dynamic parameters of such carriers depend on the energy of exciting light photons, as well as on the balance between the α-polymorph of the polymer with spin traps and its more structured β-polymorph [1]. These parameters can be changed by adding to the system small quantity (3-6% by weight) of 2D molecules with an extended π-structure, for example, acenes. During the preparation of the composite this initiates its structuring process which efficiency is proportional to the acene band gap. It was found that small flat acene molecules introduced into the initial composite solution indirectly bring the nearest macromolecules of the polymer matrix together. The concentration and other properties of charge carriers photoinitiated in modified composites correlate with the band structure of the introduced acene too. The calculations of the zone structure of acenes allowed us to indicate a close relationship between their band gap energy and the stimulated properties of spin charge carriers in so modified composites. The amplification of the π–π interaction of small molecules was supposed to cause a greater overlap of the wave functions of polymer chains and nearby additives, which accelerates the electronic relaxation of all spin ensembles formed in the systems under study, reduces the number of spin traps and widens their high-energy optical absorption band. It has been shown that charge carriers photoinitiated in the α-polymorph are characterized by an extreme dependence of their main parameters on the energy of exciting photons. The concentration and stability of both mobile charge carriers were observed to be increased in both polymorphs of acene-modified polymer:methanofullerene solar cells. The maximum effect was registered for a composite weakly doped with naphthalene and other molecules. Ultimately, the addition of small 2D molecules increases the stability of spin charge carriers photoinitiated in a composite doped with anthracene or naphthalene molecules by more than 2 and 5 times, respectively. This eliminates the selectivity of spin charge carriers to photon energy and changes the mechanism of their transfer to the electrodes. If in the amorphous α-phase of the

composite charge transfer is carried out mainly by polarons along polymer chains, whereas the charge hopping between 2D layered stacks prevails in its more crystalline β-polymorphs. Polymorphism and modification of the organic polymer:fullerene composite allow shifting the balance of their metastable amorphous α-phase towards a more stable and crystalline β-polymorph. This can be realized either by irreversible trigger modification of the composite by small flat molecules with an extended π–π structure, or/and its episodic processing by certain light photons. The results obtained confirm the universal proposal for the use of polymers optimally doped with small 2D molecules and their composites modified with fullerenes to create electronic and spintronic devices with spin-assisted parameters.

**Acknowledgement:** This work was done by the State Assignment No. AAAA-A19-119032690060-9.

**References:**

[1] V.I. Krinichnyi, E.I. Yudanova, N.N. Denisov, V.R. Bogatyrenko, Synth. Metals. 267 (2020) 116462.

# List of Participants


**Abakumov Artem**
Skolkovo Institute of Science and Technology
Moscow, Russia
A.Abakumov@skoltech.ru

**Abdulmenova Anastasia**
Tomsk Polytechnic University
Tomsk, Russia
ava75@tpu.ru

**Abyzova Elena**
Tomsk Polytechnic University
Tomsk, Russia
abyzovaeg@gmail.com

**Afonnikova Sofya**
Boreskov Institute of Catalysis
Novosibirsk, Russia
afonnikova@catalysis.ru

**Aga-Tagiyeva Sayara**
Immanuel Kant Baltic Federal University
Kaliningrad, Russia
agatagiyewas@gmail.com

**Ahn Suk-kyun**
Pusan National University
Busan, Republic of Korea
skahn@pusan.ac.kr

**Akhmetov Nikita**
Skolkovo Institute of Science and Technology
Moscow, Russia
nikita.akhmetov@skoltech.ru

**Akimov Albert**
Institute of Petroleum Chemistry SB RAS
Tomsk, Russia
akimov149@yandex.ru

**Aleksandrova Galina**
A.E. Favorsky Irkutsk Institute of Chemistry of SB RAS
Irkutsk, Russia
alexa@irioch.irk.ru

**Alekseev Dmitriy**
Institute of Solid State Chemistry
and Mechanochemistry SB RAS
Novosibirsk, Russia
D.alekseev1@list.ru

**Alekseev Roman**
Mendeleev University of Chemical Technology
Moscow, Russia
alexeev-roma@mail.ru

**Alikin Evgeny**
Ecoalliance LLC
Novouralsk, Russia
alikin@eco-nu.ru

**Almaeva Daria**
Boreskov Institute of Catalysis
Novosibirsk, Russia
almaeva@catalysis.ru

**Andryushchenko Vladimir**
Kutateladze Institute of Thermophysics of SB RAS
Novosibirsk, Russia
vladimir.andryushchenko@gmail.com

**Antipov Evgeny**
Lomonosov Moscow State University
Moscow, Russia
evgeny.antipov@gmail.com

**Arefina Irina**
ITMO University
Saint Petersburg, Russia
irina-arefina97@mail.ru

**Babaev Anton**
ITMO University
Saint Petersburg, Russia
a.a.babaev1@gmail.com

**Baksheev Evgeny**
Ecoalliance LLC
Novouralsk, Russia
rzmetall102@gmail.com

**Baldin Egor**
Semenov Federal Research Center for Chemical Physics
Moscow, Russia
baldin.ed16@physics.msu.ru

**Baranov Evgeniy**
Kutateladze Institute of Thermophysics of SB RAS
Novosibirsk, Russia
itpbaranov@gmail.com

**Bauman Yury**
Boreskov Institute of Catalysis
Novosibirsk, Russia
bauman@catalysis.ru

**Bedilo Alexander**
Boreskov Institute of Catalysis
Novosibirsk, Russia
abedilo@bk.ru

**Beloborodov Dmitry**
Skolkovo Institute of Science and Technology
Moscow, Russia
Dmitry.Beloborodov@skoltech.ru

**Belskaya Olga**
Center of New Chemical Technologies BIC
Omsk, Russia
obelska@ihcp.ru

**Bikyashev Envyar**
Southern Federal University
Rostov-on-Don, Russia
eabikyashev@yandex.ru

**Bokarev Dmitry**
N.D. Zelinsky Institute of Organic Chemistry RAS
Moscow, Russia
bokarev_d@mail.ru

**Borisov Vadim**
Center of New Chemical Technologies BIC
Omsk, Russia
bva13011986@gmail.com

**Borodaevskiy Maxim**
Boreskov Institute of Catalysis
Novosibirsk, Russia
maxim.borodaevskiy@gmail.com

**Borodina Anastasia**
Insitute of Macromolecular Compounds RAS
Saint Petersburg, Russia
anastasi2998@gmail.com; Anastasia_2998@mail.ru

**Boroznin Sergey**
Volgograd State University
Volgograd, Russia
boroznin@volsu.ru

**Boroznina Natalia**
Volgograd State University
Volgograd, Russia
boroznina.natalya@volsu.ru

**Botin Andrei**
Gubkin Russian State Univercity of oil and gas
Moscow, Russia
botin-andrey@mail.ru

**Bragina Alina**
Boreskov Institute of Catalysis
Novosibirsk, Russia
bragina@catalysis.ru

**Bukhtiyarov Valerii**
Boreskov Institute of Catalysis
Novosibirsk, Russia
vib@catalysis.ru

**Bukhtiyarova Marina**
Boreskov Institute of Catalysis
Novosibirsk, Russia
mvb@catalysis.ru

**Bykov Alexey**
Tver State Technical University
Tver, Russia
bykovav@yandex.ru

**Chepenko Dmitriy**
A.E. Favorsky Irkutsk Institute of Chemistry of SB RAS
Irkutsk, Russia
Chepenko@irioch.irk.ru

**Cherevkov Sergei**
ITMO University
Saint Petersburg, Russia
s.cherevkov@gmail.com

**Chetyrkina Margarita**
Skolkovo Institute of Science and Technology
Moscow, Russia
margarita.chetyrkina@skoltech.ru

**Choi Jihye**
Pusan National University
Busan, Republic of Korea
wisdom1jang@gmail.com

**Choi Soojeong**
Pusan National University
Busan, Republic of Korea
soojeong9901@pusan.ac.kr

**Choi Subi**
Pusan National University
Busan, Republic of Korea
subi.choii@gmail.com

**Chung Ildoo**
Pusan National University
Busan, Republic of Korea
idchung@pusan.ac.kr

**Chzhou Valeriya**
Institute of Strength Physics and Materials Science SB RAS
Tomsk, Russia
Valeriya_chzhou99@mail.ru

**Danilova Irina**
Boreskov Institute of Catalysis
Novosibirsk, Russia
danig@catalysis.ru

**Davletkildeev Nadim**
Omsk Scientific Center of SB RAS
Omsk, Russia
dna_mail@mail.ru

**Dmitrieva Anastasia**
ITMO University
Saint Petersburg, Russia
dmitrieva@scamt-itmo.ru

**Dmitruk Kirill**
Boreskov Institute of Catalysis
Novosibirsk, Russia
k.dmitruk@g.nsu.ru

**Dorofeeva Nataliya**
Tomsk State University
Tomsk, Russia
nv-dorofeeva@yandex.ru

**Dryuchkov Evgeniy**
Volgograd State University
Volgograd, Russia
dryuchkov@volsu.ru

**Dubkov Konstantin**
Boreskov Institute of Catalysis
Novosibirsk, Russia
dubkov@catalysis.ru

**Dubovtsev Dmitry**
Vyatka State University
Kirov, Russia
d.dubovtzev@yandex.ru

**Emeline Alexei**
Saint Petersburg State University
Saint Petersburg, Russia
alexei.emeline@spbu.ru

**Ershov Kirill**
Voevodsky Institute of Chemical Kinetics and Combustion SB RAS
Novosibirsk, Russia
KErshov93@gmail.com

**Evtushenko Diana**
Tomsk State University
Tomsk, Russia
edn29@mail.ru

**Evtushok Vasily**
Boreskov Institute of Catalysis
Novosibirsk, Russia
evtwas93@mail.ru

**Fakhrutdinova Elena**
Tomsk State University
Tomsk, Russia
fakhrutdinovaed@gmail.com

**Fedorov Andrey**
Institute of oil and gas problems SB RAS
Yakutsk, Russia
gelvirb@mail.ru

**Fedorova Zaliya**
Boreskov Institute of Catalysis
Novosibirsk, Russia
sabirova@catalysis.ru

**Gabrienko Anton**
Boreskov Institute of Catalysis
Novosibirsk, Russia
gabrienko@catalysis.ru

**Garyntseva Natalya**
Institute of Chemistry and Chemical Technology SB RAS
Krasnoyarsk, Russia
garyntseva@icct.ru

**Gavriljuk Oksana**
Federal Research Center of Coal and Coal-Chemistry of SB RAS
Kemerovo, Russia
o.m.gavriljuk@mail.ru

**Gerasimov Evgeny**
Boreskov Institute of Catalysis
Novosibirsk, Russia
gerasimov@catalysis.ru

**Gerasimova Daria**
Immanuel Kant Baltic Federal University
Kaliningrad, Russia
dst-678677g@mail.ru

**Gerus Yury**
Boreskov Institute of Catalysis
Novosibirsk, Russia
yurygerus@yandex.ru

**Glyaznetsova Yuliya**
Institute of oil and gas problems SB RAS
Yakutsk, Russia
glyaz1408@mail.ru

**Gnedenkov Andrey**
Institute of Chemistry FEB RAS
Vladivostok, Russia
asg17@mail.com

**Golovanova Olga**
Dostoevsky Omsk State University
Omsk, Russia
golovanoa2000@mail.ru

**Goloveshkin Alexander**
A.N. Nesmeyanov Institute of Organoelement
Compounds RAS
Moscow, Russia
golov-1@mail.ru

**Golubev Evgeny**
Enikolopov Institute for Synthetic Polymer
Materials RAS
Moscow, Russia
gek_fin@rambler.ru

**Golubtsov Georgii**
Novosibirsk State University
Novosibirsk, Russia
ggv@catalysis.ru

**Gong Jian Ping**
Hokkaido University
Sapporo, Japan
gong@sci.hokudai.ac.jp

**Gorbunov Yaroslav**
N.D. Zelinsky Institute of Organic Chemistry RAS
Moscow, Russia
yaroslavgor1710@gmail.com

**Gorkusha Aleksandr**
Novosibirsk State University
Novosibirsk, Russia
Deepforesttt922@gmail.com

**Gorlova Anna**
Boreskov Institute of Catalysis
Novosibirsk, Russia
gorlova@catalysis.ru

**Grabchenko Maria**
Tomsk State University
Tomsk, Russia
marygra@mail.ru

**Grigorieva Veronika**
Nikolaev Institute of Inorganic Chemistry of SB RAS
Novosibirsk, Russia
grigoryeva@niic.nsc.ru

**Gryaznova Marina**
FSBI Technological Institute for Superhard
and Novel Carbon Materials
Troitsk, Russia
mig@tisnum.ru

**Gulyaev Roman**
National Research Tomsk Polytechnic University
Tomsk, Russia
guliaev.g2016@yandex.ru

**Gurevich Sergey**
Ioffe Physical Technical Institute
Saint Petersburg, Russia
gurevich@quantel.ioffe.ru

**Ha Chang-Sik**
Pusan National University
Busan, Republic of Korea
csha@pusan.ac.kr

**Hong Young-Kuk**
Yonsei University
Seoul, Republic of Korea
Youngkuk95@yonsei.ac.kr

**Ibrayev Niyazbek**
Karaganda Buketov University
Karaganda, Kazakhstan
niazibrayev@mail.ru

**Ichkitidze Levan**
Institute of Biomedical Systems, National Research University of Electronic Technology
Zelenograd, Russia
ichkitidze@bms.zone; leo101@inbox.ru

**Ilyina Ekaterina**
Boreskov Institute of Catalysis
Novosibirsk, Russia
evi@catalysis.ru

**Imae Toyoko**
National Taiwan University of Science and Technology
Taipei, Taiwan
imae@mail.ntust.edu.tw

**Ivanova Yuliya**
Boreskov Institute of Catalysis
Novosibirsk, Russia
ivanova@catalysis.ru

**Ivantsov Mikhail**
A.V. Topchiev Institute of Petrochemical Synthesis RAS
Moscow, Russia
ivantsov@ips.ac.ru

**Jeon Chaeyoung**
Pusan National University
Busan, Republic of Korea
pnu83285@pusan.ac.kr

**Jing Liqiang**
Heilongjiang University
Harbin, China
jinglq@hlju.edu.cn

**Kamenshikov Aleksandr**
RCC LABTEST
Moscow, Russia
alexkam@lab-test.ru

**Kapishnikov Aleksandr**
Novosibirsk State University
Novosibirsk, Russia
a.kapishnikov@g.nsu.ru

**Kashin Alexander**
Institute of Strength Physics and Materials Science SB RAS
Tomsk, Russia
kash@ispms.ru

**Kazakov Maksim**
Boreskov Institute of Catalysis
Novosibirsk, Russia
kazakov@catalysis.ru

**Kazakova Eva**
Boreskov Institute of Catalysis
Novosibirsk, Russia
eva@catalysis.ru

**Kharchenko Nadezhda**
Boreskov Institute of Catalysis
Novosibirsk, Russia
n.kharchenko@g.nsu.ru

**Kharlamova Tamara**
Tomsk State University
Tomsk, Russia
kharlamova83@gmail.com

**Khlebnikova Tatiana**
Boreskov Institute of Catalysis
Novosibirsk, Russia
khleb@catalysis.ru

**Khovental Peter**
Skolkovo Institute of Science and Technology
Moscow, Russia
petr.khovental@skoltech.ru

**Khramtsova Daria**
V.S. Sobolev Institute of Geology and Mineralogy of SB RAS
Novosibirsk, Russia
d.khramtsova@g.nsu.ru

**Khudozhitkov Alexander**
Boreskov Institute of Catalysis
Novosibirsk, Russia
alexandr.khudozhitkov@gmail.com

**Kibis Lidiya**
Boreskov Institute of Catalysis
Novosibirsk, Russia
kibis@catalysis.ru

**Kim Hong-I**
Yonsei University
Seoul, Republic of Korea
hikimzz95@gmail.com

**Kim Il-Doo**
Korea Advanced Institute of Science and Technology (KAIST)
Daejeon, Republic of Korea
idkim@kaist.ac.kr

**Kim Jung-Hui**
Yonsei University
Seoul, Republic of Korea
qaztgb1670@unist.ac.kr

**Kim Sang-Woo**
Yonsei University
Seoul, Republic of Korea
sangwoo949@unist.ac.kr

**Kim Seung-Hyeok**
Yonsei University
Seoul, Republic of Korea
seunghyeok94@gmail.com

**Kim Won-Yeong**
Yonsei University
Seoul, Republic of Korea
kwy0744@yonsei.ac.kr

**Kirik Nadezhda**
Institute of Chemistry and Chemical Technology SB RAS
Krasnoyarsk, Russia
kiriknp@icct.ru

**Kiselev Evgeniy**
Institute of Biophysics SB RAS
Krasnoyarsk, Russia
evgeniygek@gmail.com

**Klimenko Inna**
Emanuel Institute of Biochemical Physics of RAS
Moscow, Russia
inna@deom.chph.ras.ru

**Kogolev Dmitry**
Tomsk Polytechnic University
Tomsk, Russia
kogolev@tpu.ru

**Kokorina Aleksandra**
Tomsk Polytechnic University
Tomsk, Russia
aik48@tpu.ru

**Kolesnikova Tatiana**
Southern Federal University
Rostov-on-Don, Russia
tkol@sfedu.ru

**Kolokolov Daniil**
Boreskov Institute of Catalysis
Novosibirsk, Russia
kdi@catalysis.ru

**Kolosov Valery**
Tananaev Institute of Chemistry - Subdivision of the Federal Research Centre «Kola Science Centre of the Russian Academy of Sciences»
Apatity, Russia
v.kolosov@ksc.ru

**Komarov Ivan**
JSC Research Institute «Graphite»
Moscow, Russia
master_kom@mail.ru

**Komarova Ekaterina**
Institute of Strength Physics and Materials Science SB RAS
Tomsk, Russia
katerina@ispms.ru

**Komayko Alena**
Skolkovo Institute of Science and Technology
Moscow, Russia
Alena.Komayko@Skoltech.ru

**Konon Marina**
Institute of Silicate Chemistry RAS
Saint Petersburg, Russia
marina-konon@mail.ru

**Koroleva Olga**
Institute of Mineralogy SU FRC MG UB RAS
Miass, Russia
olgankoroleva@gmail.com

**Korotaev Evgeniy**
Nikolaev Institute of Inorganic Chemistry of SB RAS
Novosibirsk, Russia
korotaev@niic.nsc.ru

**Kosivtsov Yury**
Tver State Technical University
Tver, Russia
kosivtsov@science.tver.ru

**Kotov Andrey**
Tomsk State University
Tomsk, Russia
asdfec01@yandex.ru

**Kovalenko Elizaveta**
Boreskov Institute of Catalysis
Novosibirsk, Russia
lizavetakovalenko@mail.ru

**Kovalenko Galina**
Boreskov Institute of Catalysis
Novosibirsk, Russia
galina@catalysis.ru

**Kozadaeva Maria**
Tomsk Polytechnic University
Tomsk, Russia
mariakoz71@gmail.com

**Kozhunova Elena**
Lomonosov Moscow State University
Moscow, Russia
kozhunova@polly.phys.msu.ru

**Kozlov Denis**
Boreskov Institute of Catalysis
Novosibirsk, Russia
kdv@catalysis.ru

**Krasnoborodko Sergey**
MTEON
Moscow, Russia
krasnoborodko@mteon.ru

**Kravtsova Aleksandra**
Kutateladze Institute of Thermophysics of SB RAS
Novosibirsk, Russia
Kravtsova.Alya@gmail.com

**Krivonogov Artem**
Boreskov Institute of Catalysis
Novosibirsk, Russia
akriv@catalysis.ru

**Krivoshapkin Pavel**
ITMO University
Saint Petersburg, Russia
krivoshapkin@scamt-itmo.ru

**Krivoshapkina Elena**
ITMO University
Saint Petersburg, Russia
kef@scamt-itmo.ru; elena.krivoshapkina@itmo.ru

**Kruglyakov Vasiliy**
Boreskov Institute of Catalysis
Novosibirsk, Russia
krugl@catalysis.ru

**Kruglyakova Olga**
Boreskov Institute of Catalysis
Novosibirsk, Russia
voroshin@catalysis.ru

**Krupnin Arthur**
NRC Kurchatov Institute
Moscow, Russia
artkrupnin@gmail.com

**Krysanova Kristina**
A.V. Topchiev Institute of Petrochemical Synthesis RAS
Moscow, Russia
vermont.content@gmail.com

**Kubanova Marina**
Platov South-Russian State Polytechnic
University (NPI)
Novocherkassk, Russia
kubanova_mc@mail.ru

**Kulikova Maya**
A.V. Topchiev Institute of Petrochemical Synthesis RAS
Moscow, Russia
m_kulikova@ips.ac.ru

**Kurbanova Bayan**
International Science Complex "Astana"
Astana, Kazakhstan
kurbanovabaan@gmail.com

**Kurkin Tikhon**
Enikolopov Institute for Synthetic Polymer
Materials RAS
Moscow, Russia
t.kurkin@gmail.com

**Kurmanova Maria**
Tomsk State University
Tomsk, Russia
froggylandy@gmail.com

**Kurtsevich Ekaterina**
Tomsk Polytechnic University
Tomsk, Russia
katyacha95@mail.ru

**Kuzmin Anton**
A.E. Favorsky Irkutsk Institute of Chemistry of SB RAS
Irkutsk, Russia
kuzmin2000av@gmail.com

**Kuznetsov Artem**
V.S. Sobolev Institute of Geology and
Mineralogy of SB RAS
Novosibirsk, Russia
ku.artemy@gmail.com

**Kuznetsova Irina**
Boreskov Institute of Catalysis
Novosibirsk, Russia
cuznets01@yandex.ru

**Laletina Svetlana**
Institute of Chemistry and Chemical
Technology SB RAS
Krasnoyarsk, Russia
shkulepo@rambler.ru

**Lashchinskaya Zoya**
Boreskov Institute of Catalysis
Novosibirsk, Russia
lashchinskaya@catalysis.ru

**Lebedev Oleg**
Enikolopov Institute for Synthetic Polymer
Materials RAS
Moscow, Russia
oleg.lebedev@phystech.edu

**Lebedeva Elgina**
A.E. Arbuzov Institute of Organic and Physical
Chemistry KazRC RAS
Kazan, Russia
elgina.lebed@mail.ru

**Lebedeva Marina**
Novosibirsk State University
Novosibirsk, Russia
lebedeva@catalysis.ru

**Lee Chaijun**
Pusan National University
Busan, Republic of Korea
leecj0928@pusan.ac.kr

**Lee Jaejun**
Pusan National University
Busan, Republic of Korea
Jlee-pse@pusan.ac.kr

**Lee Jihyun**
Pusan National University
Busan, Republic of Korea
jh11369@pusan.ac.kr

**Lee Jin-Hyeong**
Pusan National University
Busan, Republic of Korea
dy8897@gmail.com

**Lee Sang-Young**
Yonsei University
Seoul, Republic of Korea
syleek@yonsei.ac.kr

**Levin Vadim**
Emanuel Institute of Biochemical Physics of RAS
Moscow, Russia
levin1943@gmail.com

**Lobinsky Artem**
Ioffe Physical Technical Institute
of Russian Academy of Sciences
Saint Petersburg, Russia
lobinski.a@mail.ru

**Logunova Svetlana**
Boreskov Institute of Catalysis
Novosibirsk, Russia
logunova@catalysis.ru

**Lokteva Alina**
ITMO University
Saint Petersburg, Russia
lokteva@scamt-itmo.ru

**Lopatkin Vladimir**
Boreskov Institute of Catalysis
Novosibirsk, Russia
v.lopatkin@g.nsu.ru

**Makarova Svetlana**
Institute of Solid State Chemistry
and Mechanochemistry SB RAS
Novosibirsk, Russia
makarova@solid.nsc.ru

**Maksimova Tatiana**
Boreskov Institute of Catalysis
Novosibirsk, Russia
maksimova@catalysis.ru

**Markova Mariia**
Tver State Technical University
Tver, Russia
mashulikmarkova@gmail.com

**Markovskaya Dina**
Boreskov Institute of Catalysis
Novosibirsk, Russia
chimik17@mail.ru

**Matsko Mikhail**
Boreskov Institute of Catalysis
Novosibirsk, Russia
Matsko@catalysis.ru

**Matus Ekaterina**
Boreskov Institute of Catalysis
Novosibirsk, Russia
matus@catalysis.ru

**Matveeva Valentina**
Tver State Technical University
Tver, Russia
matveeva@science.tver.ru

**Matveyeva Anna**
Ioffe Physical Technical Institute of Russian Academy of Sciences
Saint Petersburg, Russia
ann.matveyeva@yandex.ru

**Mel'gunov Maksim**
Boreskov Institute of Catalysis
Novosibirsk, Russia
max@catalysis.ru

**Menshchikov Ilya**
A.N. Frumkin Institute of Physical Chemistry and Electrochemistry RAS
Moscow, Russia
i.menshchikov@gmail.com

**Mishakov Ilya**
Boreskov Institute of Catalysis
Novosibirsk, Russia
mishakov@catalysis.ru

**Moon Hyunseok**
Yonsei University
Seoul, Republic of Korea
hyunseok93@yonsei.ac.kr

**Moshkin Mikhail**
The Federal Research Center Institute of Cytology and Genetics SB RAS
Novosibirsk, Russia
mmp@bionet.nsc.ru

**Motorzhina Anna**
Immanuel Kant Baltic Federal University
Kaliningrad, Russia
motorzhina.anna@yandex.ru

**Murashkina Anna**
Saint Petersburg State University
Saint Petersburg, Russia
a.murashkina@spbu.ru

**Nashivochnikov Aleksandr**
Boreskov Institute of Catalysis
Novosibirsk, Russia
mataiassaiatam17@gmail.com

**Navrotskaya Anastasiya**
ITMO University
Saint Petersburg, Russia
navrotskaya@scamt-itmo.ru

**Nazyrov Marat**
Ufa University of Science and Technology
Ufa, Russia
mnazyrov@list.ru

**Nevolina Lyubov**
Institute of Mineralogy SU FRC MG UB RAS
Miass, Russia
nevolina@mineralogy.ru

**Nikoshvili Linda**
Tver State Technical University
Tver, Russia
nlinda@science.tver.ru

**Nikulaichev Semyon**
Tomsk State University
Tomsk, Russia
lenenskiwedonot@mail.ru

**Nizameeva Guliya**
A.E. Arbuzov Institute of Organic and Physical Chemistry KazRC RAS
Kazan, Russia
guliya.riv@gmail.com

**Novikov Mikhail**
East-Siberian Institute of Medical and Ecological Research
Angarsk, Russia
novik-imt@mail.ru

**Oh Kyeong-Seok**
Yonsei University
Seoul, Republic of Korea
okc10@yonsei.ac.kr

**Oh Seungjoon**
Pusan National University
Busan, Republic of Korea
Seungjoon312@gmail.com

**Okhlopkova Lyudmila**
Boreskov Institute of Catalysis
Novosibirsk, Russia
mila65@catalysis.ru

**Okulov Artem**
M.N. Mikheev Institute of Metal Physics UB RAS
Ekaterinburg, Russia
okulovartem@imp.uran.ru

**Omarov Shamil**
Ioffe Physical Technical Institute of Russian Academy of Sciences
Saint Petersburg, Russia
somarov@mail.ioffe.ru

**Orlova Ekaterina**
Lomonosov Moscow State University
Moscow, Russia
agapova@polly.phys.msu.ru

**Ouarab Nouredine**
Semiconductor Technology Research Center for Energetic (CRTSE)
Algiers, Algeria
ouarab_nourdine@yahoo.fr

**Ozerova Anna**
Boreskov Institute of Catalysis
Novosibirsk, Russia
ozerova@catalysis.ru

**Pakharukov Yuri**
Tyumen State University
Tyumen, Russia
ruslan.safargaliev@mail.ru

**Pakharukova Vera**
Boreskov Institute of Catalysis
Novosibirsk, Russia
verapakh@catalysis.ru

**Panin Alexey**
Institute of Strength Physics and Materials Science SB RAS
Tomsk, Russia
pav@ispms.ru

**Panin Sergey**
Institute of Strength Physics and Materials Science SB RAS
Tomsk, Russia
svp@ispms.ru

**Pantyukhov Petr**
Emanuel Institute of Biochemical Physics of RAS
Moscow, Russia
pantyukhov@mail.ru

**Parfenov Mikhail**
Novosibirsk State University
Novosibirsk, Russia
parfenov@catalysis.ru

**Parfenova Lyudmila**
Institute of Petrochemistry and Catalysis UFRC RAS
Ufa, Russia
luda_parfenova@mail.ru

**Park Sung Soo**
Dong-Eui University
Busan, Republic of Korea
pss@deu.ac.kr

**Parmon Valentin**
Siberian Branch of the Russian Academy of Sciences
Novosibirsk, Russia
parmon@sb-ras.ru

**Parshina Anastasia**
Northern (Arctic) Federal University named after M.V. Lomonosov
Arkhangelsk, Russia
a.parshina@narfu.ru

**Pavlova Svetlana**
Boreskov Institute of Catalysis
Novosibirsk, Russia
pavlova@catalysis.ru

**Petropavlovskaya Viktoria**
Tver State Technical University
Tver, Russia
victoriapetrop@gmail.com

**Petrova Vasilisa**
Emanuel Institute of Biochemical Physics of RAS
Moscow, Russia
balagur.sh@yandex.ru; listentojanacheck@gmail.com

**Petrukhin Denis**
Immanuel Kant Baltic Federal University
Kaliningrad, Russia
denisrussia2000@gmail.com

**Philippov Alexey**
Boreskov Institute of Catalysis
Novosibirsk, Russia
philippov@catalysis.ru

**Plyusnin Pavel**
Nikolaev Institute of Inorganic Chemistry of SB RAS
Novosibirsk, Russia
plus@niic.nsc.ru

**Popova Anna**
Federal Research Center of Coal and Coal-Chemistry of SB RAS
Kemerovo, Russia
h991@yandex.ru

**Porukova Iuliana**
A.V. Topchiev Institute of Petrochemical Synthesis RAS
Moscow, Russia
porukova@ips.ac.ru

**Potemkin Dmitriy**
Boreskov Institute of Catalysis
Novosibirsk, Russia
potema@catalysis.ru

**Potylitsyna Arina**
Boreskov Institute of Catalysis
Novosibirsk, Russia
arina231299@mail.ru

**Preman Anjali Nagapadi**
Pusan National University
Busan, Republic of Korea
anjaligcm94@gmail.com

**Pribytkov Gennady**
Institute of Strength Physics and Materials Science SB RAS
Tomsk, Russia
gapribyt@mail.ru

**Prokhorova Tatiana**
Tananaev Institute of Chemistry - Subdivision of the Federal Research Centre «Kola Science Centre of the Russian Academy of Sciences»
Apatity, Russia
t.prokhorova@ksc.ru

**Prosolov Konstantin**
Institute of Strength Physics and Materials Science SB RAS
Tomsk, Russia
konstprosolov@gmail.com

**Psyanchin Artur**
Ufa University of Science and Technology
Ufa, Russia
Artps96@yandex.ru

**Rachkovskaya Lubov**
Research Institute of Clinical and Experimental Lymphology
Novosibirsk, Russia
noolit@niikel.ru

**Rachkovskii Edmund**
Research Institute of Clinical and Experimental Lymphology
Novosibirsk, Russia
reed@academ.org

**Rasmetyeva Alexandra**
Ural Federal University
Ekaterinburg, Russia
a.v.rasmetieva@urfu.ru

**Reutova Olesia**
Tomsk State University
Tomsk, Russia
reutovaolesya@mail.ru

**Rogovenko Elena**
Institute of Chemistry and Chemical Technology SB RAS
Krasnoyarsk, Russia
Rogovenko_elena1989@mail.ru

**Ronzhin Nikita**
Institute of Biophysics SB RAS
Krasnoyarsk, Russia
roniol@mail.ru

**Rostovshchikova Tatiana**
Lomonosov Moscow State University
Moscow, Russia
t.rost50@mail.ru

**Rudakova Aida**
Saint Petersburg State University
Saint Petersburg, Russia
aida.rudakova@spbu.ru

**Rudneva Yuliya**
Nikolaev Institute of Inorganic Chemistry of SB RAS
Novosibirsk, Russia
rudneva@niic.nsc.ru

**Rymzhina Anastasiia**
Samara National Research University
Samara, Russia
nastya.rymzhina.98@mail.ru

**Ryou Myeong-Hwa**
Yonsei University
Seoul, Republic of Korea
rmh902@yonsei.ac.kr

**Sabirova Aigul**
A.E. Arbuzov Institute of Organic and Physical Chemistry KazRC RAS
Kazan, Russia
aisafa84saf@gmail.com

**Sadykov Vladislav**
Boreskov Institute of Catalysis
Novosibirsk, Russia
sadykov@catalysis.ru

**Sagun Anton**
Institute of Strength Physics and Materials Science SB RAS
Tomsk, Russia
ais43@yandex.ru

**Salanov Aleksei**
Boreskov Institute of Catalysis
Novosibirsk, Russia
salanov@catalysis.ru

**Sankova Natalya**
Boreskov Institute of Catalysis
Novosibirsk, Russia
natalya@catalysis.ru

**Satonkina Nataliya**
Lavrentyev Institute of Hydrodynamics of SB RAS
Novosibirsk, Russia
snp@hydro.nsc.ru

**Seliverstova Evgeniya**
Karaganda Buketov University
Karaganda, Kazakhstan
genia_sv@mail.ru

**Seo Ji Young**
Yonsei University
Seoul, Republic of Korea
2021313105@yonsei.ac.kr

**Serebrennikova Polina**
Novosibirsk State University
Novosibirsk, Russia
ps.serebrennikova@yandex.ru

**Sergeev Artem**
Semenov Federal Research Center for Chemical Physics
Moscow, Russia
sergeev@polly.phys.msu.ru

**Serikov Timur**
Karaganda Buketov University
Karaganda, Kazakhstan
serikov-timur@mail.ru

**Shalygin Anton**
Boreskov Institute of Catalysis
Novosibirsk, Russia
shas@catalysis.ru

**Shamanaev Ivan**
Boreskov Institute of Catalysis
Novosibirsk, Russia
i.v.shamanaev@catalysis.ru

**Shamsutdinov Artem**
Institute of Technical Chemistry UB RAS
Perm, Russia
literus12@gmail.com

**Shchipunov Yury**
Institute of Chemistry, Far East Branch, Russian Academy of Sciences
Vladivostok, Russia
yury.shchipunov@googlemail.com

**Shelepova Ekaterina**
Boreskov Institute of Catalysis
Novosibirsk, Russia
shev@catalysis.ru

**Sheshkovas Andrey**
Boreskov Institute of Catalysis
Novosibirsk, Russia
sheshckowas@yandex.ru

**Shestakova Daria**
Boreskov Institute of Catalysis
Novosibirsk, Russia
shestakova@catalysis.ru

**Shilina Marina**
Lomonosov Moscow State University
Moscow, Russia
mish@kinet.chem.msu.ru

**Shilov Nikolai**
Immanuel Kant Baltic Federal University
Kaliningrad, Russia
nikolayshilov2002@gmail.com

**Shivtsov Danil**
Boreskov Institute of Catalysis
Novosibirsk, Russia
danil@catalysis.ru

**Shkolin Andrey**
A.N. Frumkin Institute of Physical Chemistry and Electrochemistry RAS
Moscow, Russia
shkolin@phyche.ac.ru

**Shlyakhtina Anna**
Semenov Federal Research Center for Chemical Physics
Moscow, Russia
annashl@inbox.ru

**Shlyapin Dmitry**
Center of New Chemical Technologies BIC
Omsk, Russia
dmitryshlyapin@yandex.ru

**Shmelev Aleksandr**
Samara University
Samara, Russia
Shmelsasha@yandex.ru

**Shubin Yury**
Nikolaev Institute of Inorganic Chemistry SB RAS
Novosibirsk, Russia
shubin@niic.nsc.ru

**Shutilov Aleksey**
Boreskov Institute of Catalysis
Novosibirsk, Russia
alshut@catalysis.ru

**Shuvarakova Ekaterina**
Boreskov Institute of Catalysis
Novosibirsk, Russia
katerina.shuv@gmail.com

**Sidorov Alexander**
Tver State Technical University
Tver, Russia
Sidorov_science@mail.ru

**Sidorov Oleg**
FCDT “Soyuz”
Dzerzhinsky, Russia
sidorov.o.i@mail.ru; soyuz@fcdt.ru

**Simentsova Irina**
Boreskov Institute of Catalysis
Novosibirsk, Russia
sii@catalysis.ru

**Snegirev Andrey**
A.V. Rzhanov Institute of Semiconductor Physics of SB RAS
Novosibirsk, Russia
komrad.snegirev2017@gmail.com

**Sotnikova Anastasia**
A.V. Topchiev Institute of Petrochemical Synthesis RAS
Moscow, Russia
sotnikova.anast@ips.ac.ru

**Stakheev Aleksandr**
N.D. Zelinsky Institute of Organic Chemistry RAS
Moscow, Russia
st@ioc.ac.ru

**Stebnitskii Ivan**
Novosibirsk State University
Novosibirsk, Russia
i.stebnitskii@g.nsu.ru

**Stepacheva Antonina**
Tver State Technical University
Tver, Russia
a.a.stepacheva@mail.ru

**Stepanenko Sergei**
Boreskov Institute of Catalysis
Novosibirsk, Russia
stepanenko@catalysis.ru

**Stepanidenko Evgeniia**
ITMO University
Saint Petersburg, Russia
stepanidenko.e@mail.ru; eastepanidenko@itmo.ru

**Sulman Aleksandrina**
Tver State Technical University
Tver, Russia
alexsulman@mail.ru

**Sulman Mikhail**
Tver State Technical University
Tver, Russia
sulmanmikhail@yandex.ru

**Sushnikova Anna**
Institute of Metallurgy of the UB RAS
Ekaterinburg, Russia
sushnikova.ann@gmail.com

**Suvorova Marina**
Boreskov Institute of Catalysis
Novosibirsk, Russia
ms-suvorova@yandex.ru

**Svidersky Sergey**
A.V. Topchiev Institute of Petrochemical Synthesis RAS
Moscow, Russia
SviderskySA@ips.ac.ru

**Syrokvashin Mikhail**
Nikolaev Institute of Inorganic Chemistry of SB RAS
Novosibirsk, Russia
syrokvashin@niic.nsc.ru

**Tang Yun**
Fudan University
Shanghai, China
yuntang@fudan.edu.cn

**Taratayko Aleksey**
Tomsk State University
Tomsk, Russia
taratayko1997@mail.ru

**Tikhonov Boris**
Tver State Technical University
Tver, Russia
tiboris@yandex.ru

**Tikhov Serguei**
Boreskov Institute of Catalysis
Novosibirsk, Russia
tikhov@catalysis.ru

**Timkina Yulia**
ITMO University
Saint Petersburg, Russia
timkina.yu.a@gmail.com

**Timofeev Konstantin**
Tomsk State University
Tomsk, Russia
kvintkl@gmail.com

**Timofeeva Maria**
Boreskov Institute of Catalysis
Novosibirsk, Russia
timofeeva@catalysis.ru

**Titova Yuliya**
Irkutsk State University
Irkutsk, Russia
ytitova60@gmail.com

**Tokranov Alexander**
Samara University
Samara, Russia
grekopop181@gmail.com

**Tracey Chantal Talena**
ITMO University
Saint Petersburg, Russia
traceychantal@gmail.com

**Tsyganova Tatyana**
Institute of Silicate Chemistry RAS
Saint Petersburg, Russia
Tsyganova2@yandex.ru

**Tudupova Biligma**
Ioffe Physical Technical Institute
of Russian Academy of Sciences
Saint Petersburg, Russia
biligma0201@gmail.com

**Tyubaeva Polina**
Plekhanov Russian University of Economics
Moscow, Russia
polina-tyubaeva@yandex.ru

**Udoratina Elena**
Institute of Chemistry of the Komi Science Centre UB RAS
Syktyvkar, Russia
udoratina-ev@chemi.komisc.ru

**Ushakova Elena**
ITMO University
Saint Petersburg, Russia
elena.ushakova@itmo.ru

**Usmanov Ruslan**
A.E. Favorsky Irkutsk Institute of Chemistry of SB RAS
Irkutsk, Russia
usa.arslan@bk.ru

**Uvarov Mikhail**
Voevodsky Institute of Chemical Kinetics and Combustion SB RAS
Novosibirsk, Russia
uvarov@kinetics.nsc.ru

**Varyan Ivetta**
Emanuel Institute of Biochemical Physics of RAS
Moscow, Russia
ivetta.varyan@yandex.ru

**Varygin Andrey**
Nikolaev Institute of Inorganic Chemistry of SB RAS
Novosibirsk, Russia
a.varygin@g.nsu.ru

**Vedyagin Aleksey**
Boreskov Institute of Catalysis
Novosibirsk, Russia
vedyagin@catalysis.ru

**Verevkina Kseniya**
Volgograd State University
Volgograd, Russia
verevkina@volsu.ru

**Veselov Grigory**
Boreskov Institute of Catalysis
Novosibirsk, Russia
g.veselov@catalysis.ru

**Vinogradov Kirill**
Samara National Research University
Samara, Russia
winkir1997@yandex.ru

**Vinu Ajayan**
University of Newcastle
Newcastle, Australia
Ajayan.Vinu@newcastle.edu.au;
gican@newcastle.edu.au; vinu.ajayan@gmail.com

**Vlasenko Nikita**
Institute of Physiologically Active Compounds RAS
Chernogolovka, Russia
gmxten@yandex.ru

**Vlasov Maxim**
Institute of High Temperature Electrochemistry UB RAS
Ekaterinburg, Russia
maxim.vlsv@yandex.ru

**Vlasova Evgeniya**
Boreskov Institute of Catalysis
Novosibirsk, Russia
evgenia@catalysis.ru

**Vodyankina Olga**
Tomsk State University
Tomsk, Russia
vodyankina_o@mail.ru

**Vol'eva Violetta**
Emanuel Institute of Biochemical Physics of RAS
Moscow, Russia
violetta.voleva@gmail.com

**Volodin Alexander**
Boreskov Institute of Catalysis
Novosibirsk, Russia
volodin@catalysis.ru

**Vorobyeva Ekaterina**
Boreskov Institute of Catalysis
Novosibirsk, Russia
catherina.vorobieva@gmail.com

**Voronina Natalia**
Institute of Technical Chemistry UB RAS
Perm, Russia
voronina.n@itcras.ru

**Vorontsov Pavel**
Immanuel Kant Baltic Federal University
Kaliningrad, Russia
pavel.voroncov.a@gmail.com

**Vysokikh Yury**
MTEON
Moscow, Russia
yv@mteon.ru

**Wang Yazhou**
Boreskov Institute of Catalysis
Novosibirsk, Russia

**Xiang Xu**
Beijing University of Chemical Technology
Beijing, China
xiangxu@mail.buct.edu.cn

**Yarkaeva Yulia**
Ufa University of Science and Technology
Ufa, Russia
julijajarkaeva05@gmail.com

**Yeletsky Petr**
Boreskov Institute of Catalysis
Novosibirsk, Russia
yeletsky@catalysis.ru

**Yu Long**
South China University of Technology
Guangzhou, China
felyu@scut.edu.cn

**Yudanova Evgeniya**
Federal Research Center of Problems of Chemical Physics and Medicinal Chemistry RAS
Chernogolovka, Russia
yudan@icp.ac.ru

**Yurpalova Daria**
Center of New Chemical Technologies BIC
Omsk, Russia
omsk-glyzdova@mail.ru

**Zagitova Liana**
Ufa University of Science and Technology
Ufa, Russia
Kabirova.lian@yandex.ru

**Zakharov Yuriy**
Federal Research Center of Coal and Coal-Chemistry of SB RAS
Kemerovo, Russia
h991@ya.ru

**Zarubina Anastasia**
Southern Federal University
Rostov-on-Don, Russia
karginova@sfedu.ru

**Zavorin Alexey**
Boreskov Institute of Catalysis
Novosibirsk, Russia
zavorin@catalysis.ru

**Zelentsov Dmitry**
Surgut State University
Surgut, Russia
zelentsov_do@surgu.ru

**Zenkovets Galina**
Boreskov Institute of Catalysis
Novosibirsk, Russia
zenk@catalysis.ru

**Zhao Dongyuan**
Fudan University
Shanghai, China
dyzhao@fudan.edu.cn

**Zhao Yiheng**
Boreskov Institute of Catalysis
Novosibirsk, Russia

**Zhidkov Ivan**
Ural Federal University
Ekaterinburg, Russia
i.s.zhidkov@urfu.ru

**Zhirov Nikita**
Institute of Petroleum Chemistry SB RAS
Tomsk, Russia
krigsnu@gmail.com

**Zhou Gang**
Fudan University
Shanghai, China
zhougang@fudan.edu.cn

**Zhuzhgov Aleksey**
Boreskov Institute of Catalysis
Novosibirsk, Russia
faleks2010@gmail.com

**Zvonareva Daria**
Volgograd State University
Volgograd, Russia
zvonareva@volsu.ru

# Content

# Content

# Content

# Content

# Content

# Content

# Content

# Content

# Content

# Content

# Content



## III. Applications

# Content

# Content

# Content

# Content

# Content

# Content

# Content

# Content

# Content

# Content

# Content

# Content

# Content

# Content

# Content

# Content

# Content

# Content

# Content

# Content

# Content

# Content

*Компания «НКЦ «ЛАБТЕСТ» имеет 20-летний опыт работы в сфере поставок и обслуживания аналитического оборудования для исследования свойств структурированных пористых материалов газо-адсорбционными методами.*

## АДСОРБЦИОННОЕ ОБОРУДОВАНИЕ

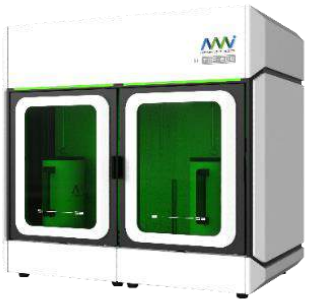

- Анализаторы удельной поверхности и пористости;
- Анализаторы газовой сорбции под высоким давлением;
- Гравиметрические анализаторы адсорбции;
- Анализаторы сорбционной емкости и кривых прорыва.

## ХЕМОСОРБЦИОННОЕ ОБОРУДОВАНИЕ

- Анализаторы динамической хемосорбции;
- Полупромышленные реакторные установки;
- Лабораторные микрореакторы.


**ПРОВЕДЕНИЕ ДЕМОНСТРАЦИОННЫХ АНАЛИЗОВ ВАШИХ ОБРАЗЦОВ В НАШЕЙ ЛАБОРАТОРИИ!**

КОНСУЛЬТАЦИИ СПЕЦИАЛИСТОВ | МЕТОДИЧЕСКАЯ ПОДДЕРЖКА | ОПЕРАТИВНАЯ ПОСТАВКА | ТЕХНИЧЕСКОЕ ОБСЛУЖИВАНИЕ



119071, Москва, Ленинский пр. 19, стр.1, +7 495 256-24-84, info@lab-test.ru, www.lab-test.ru

ЭМТИОН

О компании: ЭМТИОН – это российская инновационная компания, специализирующаяся на производстве и поставках аналитического и технологического оборудования. Ведущие специалисты компании имеют 15-летний опыт работы в области приборостроения. ЭМТИОН предлагает Заказчикам как отдельные решения, так и комплексное оснащение лабораторий, начиная с этапов проработки концепции и предпроектных работ и заканчивая вводом оборудования в эксплуатацию. Опытные инженеры осуществляют сервис в течении всего срока эксплуатации Оборудования.

## Рентгеновская дифрактометрия

- Порошковые и монокристальные дифрактометры
- Высокопроизводительные детекторы Mythen
- Вращение образца 360°
- Автосменщик до 12 образцов
- Высокоточный гониометр
- Угловой диапазон сканирования -110°/161°
- Минимальный шаг сканирования 0,0001°
- Температурный диапазон от -196°C до 1600°C
- База данных спектров, программа обработки

## КР (рамановская) спектроскопи и микроскопия

- До 5ти автоматически выбираемых лазеров
- Пространственное разрешение до 0,2мкм
- Спектральный диапазон 350-1100 нм
- Спектральное раазрешение 0.25 $см^{-1}$
- Четыре автоматизированные дифракционные решетки
- Возможность комбинации с жидкостными, газовыми, охлаждающими и вакуумными ячейками

## Атомно-силовая микроскопия

- Поддержка всех существующих АСМ методик
- Прыжковая микроскопия для количественного нано-механического анализа
- Измерение линейной ВАХ в диапазоне токов от 50пА до 100мкА
- Диапазон сканирования 100x100x10мкм
- Разрешение по оси Z – 0,05 нм
- Опции нагрева, охлаждения, измерения в жидкости, в вакууме, в магнитном поле и др.

## Электронная микроскопия

- Термоэмиссионный катод
- Катод с полевой эмиссией типа Шоттки
- Ускоряющее напряжение от 0.1кВ до 30кВ
- Увеличение от 6 до 1 000 000х
- Разрешение до 1 нм
- Опции низкого вакуума и низкого ускоряющего напряжения
- Система энергодисперсионного микроанализа
- Опции EBSD, CL, AFM, Tensile stage и др.

## Двухколонный (FIB SEM) электронный микроскоп

- Электронная пушка с катодом Шоттки (FEG)
- Жидкометаллический источник ионов галлия (LMI)
- Разрешение FEG: 0.8нм@30кВ/1.5нм@1кВ
- Разрешение LMI: 30нм@30кВ
- Ускоряющее напряжение до 30кВ
- Приставка для работы на просвет (STEM)
- Моторизированный по 5 осям предметный стол: XYZ 140x140x60мм, поворот 360°, наклон -10 ... 80°

## Комбинированные АСМ-Раман системы

- Одновременные АСМ/Раман исследование
- Нано-раман (TERS, TEFS, TERFS)
- Одновременное использование до 5-ти лазеров, полная автоматизация
- Быстрое сканирование (1000x1000 точек за 3 сек.)
- Опции нагрева, охлаждения, измерения в жидкости, в вакууме, в магнитном поле и др.

ООО НТЦ "ЭМТИОН" / ИНН 7735195944/ тел. +7-499-390-90-81
Адрес: РФ, Москва, Зеленоград, Савелкинский проезд, д 4
www.mteon.ru / info@mteon.ru

ЭМТИОН

ЭМТИОН также предоставляет услуги «Внешнеторгового Агента», позволяющие Заказчикам получить сложное научное оборудование иностранного производства с поставкой «до двери» в РФ. Наша команда выполняет анализ технического задания Заказчика, поиск возможных поставщиков, анализ коммерческих предложений и спецификаций, согласование условий внешнеэкономического контракта, логистику "под ключ", организацию пусконаладочных работ, а также обучение персонала Заказчика.

## Лазерная литография

- От настольных лабораторных систем до приборов промышленного применения
- Диаметр обрабатываемых подложек до 300мм
- Минимальный топологический размер ≤110нм
- Минимальный размер по вертикали ≤400нм
- Неравномерность края ≤30нм
- Максимальная скорость 50000мм/с
- Максимальная высота образца 70мм
- Максимальная область экспонирования 300×300×70мм

## Спектральные эллипсометры

- От 190нм до 25000нм (серия приборов)
- Двойной компенсатор вращения (DRC) для одновременного измерения всех 16 элементов матрицы Мюллера
- Пятипозиционная автоматическая платформа управления образцами
- Обширная база данных и библиотека моделей геометрической структуры

## Технологическое оборудование

- Настольные и стационарные технологические установки
- Размер обрабатываемых подложек до 200мм
- Магнетронное и газофазное осаждение металлов и диэлектриков
- Электронно-лучевое напыление металлов (Au, Al, Pd, Ni, Cr, Pt, Mo и др.)
- Плазмохимическое травление и очистка
- Синтез углеродных наноструктур
- Пробоподготовка (напыления покрытий, шлифовка, полировка, ионное утонение и др.)

## Электронно-лучевая литография

- Проектирование 2D/3D структур произвольной сложности
- Импорт из форматов: GDS, DXF, CSF, ELM, TIF, BMP
- Автоматическое и полуавтоматическое совмещение слоев
- Моделирование результатов экспонирования
- Активная компенсация ошибок
- PCI карта для управления из компьютера
- Управление быстрым бланкером луча в колонне
- Возможно экспонирование без бланкера

## Оптические профилометры

- Быстрое бесконтактное сканирование 2D профиля образца и 3D топографии.
- Измерение шероховатости образца, кривизны поверхности, толщины пленок, анализ дефектов (микротрещины, сколы, царапины) и др.
- Вертикальное z разрешение до 0.1 (PSI)
- Возможность изменения поля зрения за счет использования разных объективов.
- Высокая повторяемость и воспроизводимость измерений

## Вибромагнитометры (VSM)

- Вибромагнетометры с охлаждением жидким азотом
- Диапазон магнитных полей до 9 Тл
- Широкий выбор опций
- Измерение кривой намагниченности, петли гистерезиса и множества других параметров
- Безжидкостные низкотемпературные вибромагнетометры 1.5-400 K

ООО НТЦ "ЭМТИОН" / ИНН 7735195944/ тел. +7-499-390-90-81
Адрес: РФ, Москва, Зеленоград, Савелкинский проезд, д 4
www.mteon.ru / info@mteon.ru

Scientific edition

**ASAM-8**
**The 8th Asian Symposium on Advanced Materials**
July 3 – 7, 2023, Novosibirsk, Russia

Book of Abstracts

Editors:
Prof. A.A. Vedyagin, Prof. A.M. Volodin, Prof. Yu.V. Shubin,
Dr. M.O. Kazakov, Dr. M.S. Melgunov, Dr. D.A. Shlyapin

Научное издание

**Восьмой азиатский симпозиум по современным материалам**

3 – 7 июля 2023 года, Новосибирск, Россия

Сборник тезисов докладов

Под общей редакцией:
д.х.н. Ведягин А.А., д.х.н. Володин А.М., д.х.н. Шубин Ю.В.,
к.х.н. Казаков М.О., к.х.н. Мельгунов М.С., к.х.н. Шляпин Д.А.

Составители: М.С. Суворова, С.С. Логунова
Компьютерная обработка: Ю.В. Климова, Т.О. Барсуков
Обложка: Е.К. Казакова

**Издатель:**
Федеральное государственное бюджетное учреждение науки
«Федеральный исследовательский центр «Институт катализа им. Г.К. Борескова
Сибирского отделения Российской академии наук»
630090, Новосибирск, пр-т Академика Лаврентьева, 5, ИК СО РАН
http://catalysis.ru
E-mail: bic@catalysis.ru Тел.: +7 383 330 67 71

**Электронная версия: адрес сайта конференции**
Издательский отдел Института катализа СО РАН
E-mail: pub@catalysis.ru Тел.: +7 383 326 97 15

Объём: 54 МБ. Подписано к размещению: 22.06.2023.
Адрес размещения:

Системные требования: i486; Adobe® Reader® (чтение формата PDF)

**ISBN** 978-5-906376-49-7